The Characterisation and Interactions of Biomedical Polymers

By

Fiona E. Black,
BSc. (Hons), DIS.

Thesis submitted to
The University of Nottingham
for the degree of
Doctor of Philosophy.

October, 1999.

Abstract

As the world population grows and the standard of living increases a need for better health care is an important consideration. Over the latter half of this century the use of polymeric materials within the field of medicine has grown considerably.

This thesis investigates a variety of novel polymers whose applications within the medical field are both important and varied. In the cases studied, as with other polymeric materials intended for medicinal uses, the interaction with their surfaces is important, as when placed in the body the surface is the first place of contact and hence interaction with the system. Because of the importance of these surface interactions, which can elicit both beneficial and detrimental effects, this thesis is concerned with the surface chemistry and the relationship of this property to the interfacial interactions of the polymeric systems investigated.

Chapter 1 will concentrate on providing a historical overview of the field of polymers, especially the applications in the biomedical field. The surface analytical techniques of surface plasmon resonance (SPR), atomic force microscopy (AFM), X-ray photoelectron spectrometry (XPS) and secondary ion mass spectrometry (SIMS) utilised in this thesis to investigate the surface properties of the materials of interest will also be introduced.

The demand for organ transplants far outweighs the supply of donor organs. Therefore, many patients with a variety of disease die each year. If new organs could be grown utilising the patients own cells, the supply of organs could be increased to meet the demand and these custom grown organs would not have the problems of rejection as observed with donor ones. This is what tissue engineering aims to do. By utilising polymer matrices, to provide a scaffold for the tissue to grow in the correct configuration and a variety of growth factors and cell signalling agents to ensure the correct differentiation and function of the cells, it is hoped in the future new organs for example lungs and livers will be able to be grown on demand. Chapter 3 and 4 concentrate on the in depth study of a polymer intended for such an application. Chapter 3

concentrates on determining the surface chemistry of this polymer system. XPS and SIMS are used to identify the type of chemical groups present at the surface and quantify their contribution to the overall surface layer. Chapter 4, probes the interactions, both specific and non specific with this system using a variety of complementary techniques. SPR is utilised to quantify the extent and rate of the interactions, whilst AFM in force distance mode the strength of these. AFM was also utilised to visualize the absorbed molecules on the polymer surfaces.

In Chapter 5 the area of gene therapy is introduced. It is hoped that in the future, gene therapy may form the basis of a cure for inherited genetic diseases, such as hemophilia and other conditions such as AIDS and some cancers. The main problems which need to be overcome before this aim can be realised are firstly, isolating the correct genes to cure the diseases, and secondly, delivery of these genes. Cationic polymers and cationic lipids are two of the three main areas of research being investigated to find a potential carrier system for the DNA. In Chapter 5, the effect of PEG molecular weight on the condensation of plasmid DNA into a particles by poly(L-lysine)s for gene therapy is investigated. SPR was utilised to investigated the rate and extent of DNA binding and condensation by the various polymers, and utilising AFM the effect of PEG molecular weight on the structure of the observed particles was probed.

The gene therapy theme is continued in Chapter 6 where the surface interactions of a cationic lipid / DNA gene therapy complex is investigated by both AFM and SPR. There are two main aims to the studies in this chapter. Firstly, to provide an understanding of the interactions between the DNA and lipid components of the delivery system. It is hoped this will supply further information on its stability, formation and structure and secondly, to provide a knowledge of the interactions of the complex with model surfaces. This may provide an insight into the gene therapy vectors possible mode of interaction with the cell.

Chapter 7, is concerned with a family of dendrimeric polymers. The family of interest are the poly(amidoamine) (PAMAM) dendrimers. These have shown potential not only as drug delivery vehicles in the field of cancer

chemotherapy and gene therapy, but also in enhancing medical imaging. The investigations performed in Chapter 7 form a basis for understanding the factors effecting the PAMAM's interaction with cell membranes and hence, provide information for optimising their formulation into drug delivery vehicles. The studies undertaken utilised both AFM and SPR as well as a range of model surface. These surfaces possess differing characteristics and were utilised in conjunction with AFM and SPR to study the effect of dendrimer size, shape, surface charge and charge density on the interaction of these molecules.

The final chapter, Chapter 8 discusses the progress made towards the aims of this thesis as outlined in section 1.8 and addresses the avenues for future investigations exposed by experimental work in chapters 3 - 7. Overall it is hoped that the work described in this thesis shows that a multi technique approach, as well as the collaborations of chemists, materials engineers, biophysicist, biologists and clinicians may, in the future lead to a better understanding of the materials utilised in the medical setting and hence provide a systematic design of systems for treating specific disease conditions.

Content

ABSTRACT i

CONTENT iv

FIGURE LIST xiv

TABLE LIST xxvi

APPENDICES xxviii

ABBREVIATIONS xxix

CHAPTER 1 : INTRODUCTION 1

1.1 : Polymer revolution 1

1.2 : The use of polymers in medical applications 5

1.3 : The need for surface characterisation 12

1.4 : X-ray photoelectron spectroscopy : Theory and applications 17

1.5 : Secondary ion mass spectrometry : Theory and application 23

1.6 : Atomic force microscopy : Imaging theory 28

1.6.1 : Atomic force microscopy : Biological applications . . 35

1.6.2 : Atomic force microscopy : Materials applications . . 37

1.6.3 : AFM Force distance : theory and application 40

1.7 : Surface plasmon resonance : Theory 47

1.7.1 : SPR : Materials applications 51

1.7.2 : SPR : Biological applications 54

1.8 : Aims of thesis 56

CHAPTER 2 : EXPERIMENTAL PROCEDURES 58

2.1 : Materials 58

2.2 : SPR analysis 58

2.3 : AFM imaging 59

2.4 : AFM force-distance measurements 60

2.5 : ToF-SIMS analysis 61

2.6 : XPS analysis 61

CHAPTER 3 : POLYMERS FOR TISSUE ENGINEERING : SURFACE CHARACTERISATION 63

3.1 : Introduction 63

3.1.1 : The need for tissue engineering 63

3.1.2 : The use of polymers in tissue engineering 64

3.1.3 : The need for surface analysis of tissue engineering scaffolds 66

3.1.4 : Introduction to the PLA-PEG-biotin system 69

3.2 : Materials and methods 73

3.2.1 : Polymers 73

3.2.2 : Characterisation of film continuity and thickness 73

3.2.3 : Static contact angle measurements 75

3.2.4 : XPS 75

3.2.5 : AFM 76

3.2.6 : ToF-SIMS 76

3.3 : Results and discussion 77

3.3.1 : Characterisation of film continuity 77

3.3.2 : Static contact angle measurements 79

3.3.3 : XPS 81

3.3.4 : AFM 85

3.3.5 : TOF-SIMS 89

3.3.5.1 : Co-polymer composition 89

3.3.5.2 : Image analysis of patterned protein 101

3.4 : Conclusions and Future work 114

CHAPTER 4 : POLYMERS FOR TISSUE ENGINEERING : SURFACE INTERACTIONS 120

4.1 : Introduction 120

4.1.1 : The study of protein interactions with biomaterial surfaces 120

4.1.2 : Cell adhesion molecules 120

4.1.3 : Aim of work 122

4.2 : Materials and Methods 126

4.2.1 : SPR : Effect of PLA-PEG ratio on interactions with avidin and HSA 126

4.2.2 : System Stability 127

4.2.3 : Biotin-peptide immobilisation 129

4.2.4 : AFM : Effect of PLA-PEG ratio on interactions with avidin and HSA 131

4.2.5 : SPR : Effect of surfactants on degree of surface modification 131

4.2.6 : AFM force-distance : Effect of PLA-PEG ratio on interactions with avidin and BSA 133

4.2.7 : AFM force-distance : Effect of surfactant on the interaction between streptavidin and the PLA-PEG-biotin 134

4.3 : Results and discussion 135

4.3.1 : SPR : Effect of PLA : PEG ratio on protein binding 135

4.3.2 : System stability 149

4.3.3 : Biotin-peptide immobilisation 150

4.3.4 : AFM :Effect of PLA : PEG ratio on protein binding 150

4.3.5 : SPR : Effect of surfactants on the degree of surface modification 153

4.3.6 : AFM force-distance 166

4.3.7 : Effect of surfactant on the interaction between streptavidin and the PLA-PEG-biotins as determined by AFM force-distance 174

4.4 : Conclusion 176

4.4.1 : Effect of PLA : PEG ratio on protein binding 176

4.4.2 : Effect of surfactant on the degree of surface engineering of PLA-PEG-biotin polymers by avidin 181

CHAPTER 5 : POLYMERS IN GENE THERAPY 184

5.1 : Introduction 184

5.1.1 : Background to gene therapy 184

5.1.2 : Background to investigations 191

5.2 : Materials and Methods 191

5.2.1 : Polymers 191

5.2.2 : DNA 192

5.2.3 : SPR 198

5.2.4 : AFM imaging studies 199

5.2.5 : AFM force-distance studies 199

5.3 : Results and Discussion 201

5.3.1 : SPR analysis of the interaction between DNA and immobilised PLL-PEGs 201

5.3.2 : SPR analysis of the interaction of PLL-PEGs with immobilised DNA 209

5.3.3 : Liquid AFM imaging of DNA / PLL complexes . . 214

5.3.4 : Effect of PEG on the strength of interaction between DNA and PLL probed by AFM force-distance 222

5.3.5 : SPR : Effect of cationic polymer density on DNA binding 233

5.4 : Conclusions 236

CHAPTER 6 : CATIONIC LIPIDS AN ALTERNATIVE APPROACH TO GENE THERAPY 239

6.1 : Introduction 239

6.1.1 : Use of cationic lipids in gene therapy 239

6.1.2 : Characterisation of DNA / cationic lipid complexes 242

6.1.3 : Introduction to self-assembled monolayers 245

6.1.4 : Aims of investigations performed in this chapter . 247

6.2 : Materials and Methods 249

6.2.1 : General 249

6.2.2 : SPR 249

6.2.3 : AFM 252

6.3 : Results and Discussion 253

6.3.1 : SPR - interactions of cationic liposomes with model SAM surfaces 253

6.3.2 : SPR - interactions of DNA with model SAM surfaces 263

6.3.3 : SPR - interactions of cationic liposomes / DNA complexes with model SAM surfaces 263

6.3.4 : AFM - imaging and force-distance studies of cationic liposomes on SAM surfaces 266

6.3.5 : AFM - imaging and force-distance studies of DNA on SAM surfaces 276

6.3.6 : AFM - imaging and force-distance studies of DNA / cationic lipid complex on amino SAM surface 279

6.3.7 : SPR - interactions between complex components . 284

6.4 : Conclusions 286

6.4.1 : Imaging of gene therapy constructs under pseudo-physiological conditions 286

6.4.2 : Investigations into interactions with model surfaces 287

CHAPTER 7 : POLYMERS AS DRUG DELIVERY VEHICLES - DENDRIMERS 290

7.1 : Introduction 290

7.1.1 : Dendrimer synthesis and uses 293

7.1.2 : Characterisation of PAMAM dendrimers 297

7.1.3 : Applications of the PAMAM dendrimers 300

7.1.4 : Aims of work 301

7.2 : Materials and methods 302

7.2.1 : SPR 302

7.2.1.1. : Interactions with SAMs 302

7.2.1.2. : Characterisation and interactions with cell membranes 304

7.2.1.3. : Interactions with DNA 306

7.2.2 : AFM Imaging 306

7.2.3 : AFM force-distance studies 307

7.2.3.1 : Dendrimer Biotinylation 307

7.2.3.2 : Experimental Procedure for interactions between dendrimers and SAMs 309

7.2.3.3 : Experimental procedure for interactions between dendrimers and cell membranes 310

7.2.3.4 : Experimental procedure for interactions between dendrimers and DNA 310

7.3 : Results and discussion 311

7.3.1 : SPR 311

7.3.1.1 : Interaction with Dodecanethiol SAM 311

7.3.1.2 : Interaction with 11-MUA SAM 316

7.3.1.3 : Interaction with 2-aminoethanethiol SAM ... 321

7.3.1.4 : Interaction with polymer brushes Lan-1 and Lan-2. 323

7.3.1.5 : Characterisation of lipid surface 327

7.3.1.6 : Interaction with model membrane surface 339

7.3.1.7 : Dendrimer interactions with DNA 342

7.3.2 AFM imaging 345

7.3.2.1 : AFM imaging in air 345

7.3.2.2 : AFM liquid imaging - effect of generation ... 349

7.3.2.3 : Effect of SAM terminal group on the images obtained of the dendrimers 354

7.3.3 : AFM force-distance studies 357

7.3.3.1 : Biotinylation of dendrimers and characterisation 358

7.3.3.2 : Effect of dendrimer type on the force of interaction with a range of surfaces 365

7.3.3.3 : Effect of pH on the interaction of the dendrimers with model surfaces 369

7.3.3.4 : Effect of ionic strength on the interaction of the dendrimers with model surfaces 373

7.3.3.5 : Interaction of dendrimers with a cell membrane fraction 377

7.3.3.6 : Interaction of dendrimers with immobilised DNA 380

7.4 : Conclusions 382

CHAPTER 8 : OVERALL CONCLUSIONS 384

ACKNOWLEDGEMENTS 388

APPENDICES 390

Appendix 1 : Charge ratio calculations 390
Appendix 2 : Preparation of cell membrane fractions 393

REFERENCES 394

Figure List

CHAPTER 1 : INTRODUCTION

Figure 1.1 : Concept of polymer-drug conjugates 8

Figure 1.2 : The EPR effect 9

Figure 1.3 : A surface 14

Figure 1.4 : Schematic representation of a typical XPS instrument 18

Figure 1.5 : Effect of emission angle on sampling depth in XPS 20

Figure 1.6 : Schematic representation of a basic SIMS setup 24

Figure 1.7 : Collision cascade as observed in SIMS 25

Figure 1.8 : A schematic representation of an STM 29

Figure 1.9 : A schematic representation of an AFM
(a) early
(b) present day 32

Figure 1.10 : Schematic representation of the different imaging modes in AFM
(a) contact
(b) non-contact
(c) tapping 34

Figure 1.11 : Schematic representation of the acquisition of a phase image 39

Figure 1.12 : A schematic representation of typical AFM force distance curve 43

Figure 1.13 : Schematic representation of an the SPR effect 48

Figure 1.14 : A typical setup for a SPR instrument 50

CHAPTER 3 : POLYMERS FOR TISSUE ENGINEERING : SURFACE CHARACTERISATION

Figure 3.1 : Structure of PLA-PEG-biotin and scheme of use as a tissue engineering scaffold 70

Figure 3.2 : Effect of polymer concentration on integrity of film formed 78

Figure 3.3 : Typical XPS scans of the C1s envelope for
(a) PLA
(b) PEG
(c) PLA-PEG-biotin(**3**.64)
(d) PLA-PEG-biotin(1.49)
(e) PLA-PEG-biotin(0.53) 82

Figure 3.4 : AFM images of the biotin-PLA-PEGs before and after incubation in buffer 87

Figure 3.5 : A typical positive ion ToF-SIMS spectra for the biotin -PLA-PEG(1.49) polymer 90

Figure 3.6 : A typical negative ion ToF-SIMS spectra for the biotin -PLA-PEG(1.49) polymer 91

Figure 3.7 : PEG oligomer distribution 99

Figure 3.8 : Correlation between theoretical PLA : PEG ratio calculated from NMR and experimental values determined from XPS and ToF-SIMS 100

Figure 3.9 : Images of an avidin patterned biotin-PLA-PEG polymer showing protein distribution 111

Figure 3.10 : Images of an avidin patterned biotin-PLA-PEG polymer showing PDMS distribution 112

Figure 3.11 : Schematic representation of interaction of PDMS and avidin with the biotin-PLA-PEG 115

Figure 3.12 : Image of avidin distribution showing leaching and topography 116

CHAPTER 4 : POLYMERS FOR TISSUE ENGINEERING : SURFACE INTERACTIONS

Figure 4.1 : Schematic representation of the surface engineering strategy 125

Figure 4.2 : Sequence of biotinylated peptide used 130

Figure 4.3 : A typical SPR trace for the interaction of avidin with the biotinylated PLA-PEG(3.63) polymer 136

Figure 4.4 : Effect of PLA : PEG ratio on the extent of surface engineering by avidin on the biotinylated-PLA-PEGs. 137

Figure 4.5 : Effect of mixing biotinylated and non-biotinylated PLA-PEGs on the extent of avidin binding
(a) different ratios of polymers with similar molecular weight
(b) 1 : 1 ratios of polymers with varying molecular weights 139

Figure 4.6 : Effect of PLA : PEG ratio on the extent of non-specific binding of avidin to the non-biotinylated polymers 141

Figure 4.7 : Effect of biotinylation and PLA : PEG ratio on the rate of avidin binding to the PLA-PEG polymers 142

Figure 4.8 : Effect of PLA : PEG ratio on the interaction of HSA with the biotinylated PLA-PEG polymers 144

Figure 4.9 : Rate of binding of HSA and avidin after HSA incubation to biotinylated polymers 145

Figure 4.10 : Extent of avidin binding to biotinylated polymers before and after incubation with HSA 146

Figure 4.11 : Interaction of avidin preincubated with biotin with the biotinylated-PLA-PEGs
(a) Extent of interaction
(b) rate of interaction 148

Figure 4.12 : Effect of PLA : PEG ratio on the binding of biotinylated RGD peptide 151

Figure 4.13 : Effect of PLA : PEG ratio on avidin coverage of PLA-PEG-biotins 152

Figure 4.14 : Effect of PLA : PEG ratio on HSA coverage of biotinylated PLA-PEGs 154

Figure 4.15 : A typical SPR trace for the interaction of PVA with a PLA-PEG-biotin 155

Figure 4.16 : Summary of the extent of interaction of PVA with
(a) the biotinylated PLA-PEGs
(b) the non-biotinylated PLA-PEGs 157

Figure 4.17 : Effect of PVA on the specific interaction between the PLA-PEG-biotins and avidin 158

Figure 4.18 : Effect of PVA on the non-specific interaction between the PLA-PEGs and avidin 160

Figure 4.19 : Effect of low concentration of PVA on extent of avidin binding to PLA-PEG-biotin(1.49) 162

Figure 4.20 : Extent of binding of pluronic to biotinylated polymer surfaces
(a) Pluronic F68
(b) Pluronic F108
(c) Pluronic F127 164

Figure 4.21 : Extent of avidin binding to biotinylated polymer surfaces after pluronic incubation
(a) Pluronic F68
(b) Pluronic F108
(c) Pluronic F127 165

Figure 4.22 : Effect of PLA : PEG ratio on the strength of interaction between a BSA coated tip and the biotinylated polymers 167

Figure 4.23 : Effect of PLA : PEG ratio on the strength of interaction between a streptavidin coated tip and the biotinylated polymers 169

Figure 4.24 : Effect of PLA : PEG ratio on the strength of interaction between a streptavidin coated tip and the non-biotinylated polymers 170

Figure 4.25 : Effect of incubating a streptavidin coated tip with excess biotin on the interaction with the biotinylated polymers 172

Figure 4.26 : Effect on incubating polymer samples with BSA on the interaction with a streptavidin coated tip 173

Figure 4.27 : Effect of PVA surfactant on the interaction between a streptavidin coated tip and the biotinylated polymers 175

CHAPTER 5 : POLYMERS IN GENE THERAPY : CATIONIC POLYMERS

Figure 5.1 : Examples of cationic polymers used for gene therapy 189

Figure 5.2 : Plasmid DNA restriction map 193

Figure 5.3 : Typical gel of extracted plasmid 196

Figure 5.4 : Non specific interactions of non-biotinylated cationic polymers with streptavidin
(a) Typical SPR trace for interaction between PLL and streptavidin
(b) Summary of interactions of PLL-PEGs 202

Figure 5.5 : Effect of concentration on degree of binding
(a) PLL binding to streptavidin
(b) DNA binding to PLL 204

Figure 5.6 : A typical SPR Trace for the interaction of DNA with the cationic polymers 205

Figure 5.7 : Summary of SPR shifts for
(a) biotinylated cationic polymer binding to streptavidin
(b) Binding of DNA to cationic polymer
(c) DNA cationic polymer structure reorganisation 207

Figure 5.8 : Schematic representation of the effect of PEG molecular weight on complex formation with DNA 208

Figure 5.9 : A typical SPR trace for the interaction between DNA and streptavidin 210

Figure 5.10 : Effect of degree of biotinylation on binding of biotin-DNA to streptavidin 211

Figure 5.11 : A typical SPR trace for the interaction of cationic polymers with immobilised DNA 213

Figure 5.12 : Schematic representation on the effect of PLL-PEG orientation on binding to DNA 215

Figure 5.13 : Effect of charge ratio on the structure of the complex formed between DNA and PLL
(a) charge ratio 1.00 :0.27 DNA/PLL
(b) charge ratio 1.00 :1.35 DNA/PLL
(c) charge ratio 1.00 : 2.70 DNA/PLL
(d) high resolution image of 'bead-on-string' structure observed for high DNA : PLL ratios 218

Figure 5.14 : Effect of PEG molecular weight on DNA / PLL-PEG complex structure 220

Figure 5.15 : Complexation of DNA with polycations and effect of PEG molecular weight
(a) Effect of DNA / polycation ratio
(b) Effect of PEG molecular weight 221

Figure 5.16 : Schematic representation of curve shapes due to varying phenomena
(a) Attractive force
(b) Repulsive forces
(c) Sample rigidity (c(i)) hard (c(ii)) soft
(d) Multiple interaction
(e) Molecular stretching 223

Figure 5.17 : Typical force distance curves for interactions between cationic polymers and (a) streptavidin and (b) DNA
(i) PLL
(ii) PLL-PEG(5 kDa)
(iii) PLL-PEG(12 kDa) 225

Figure 5.18 : Effect of PEG molecular weight on strength of interactions
(a) interactions between cationic polymers and streptavidin
(b) interactions between cationic polymers and DNA 229

Figure 5.19 : Schematic diagram of the effect of PEG molecular weight on the interaction
(a) with streptavidin
(b) with DNA 231

Figure 5.20 : Effect of cationic polymer density on the binding of DNA 235

CHAPTER 6 : CATIONIC LIPIDS AN ALTERNATIVE APPROACH TO GENE THERAPY

Figure 6.1 : Schematic representation of suggested DNA cationic lipid complex structure 243

Figure 6.2 : Structure of (a) plasmid DNA, (b) cholesterol and EDMPC 250

Figure 6.3 : Interaction of cationic liposomes with a C12Me surface
(a) Typical SPR trace
(b) Schematic representation of mechanism of adsorption 256

Figure 6.4 : Typical SPR traces for the interaction of liposomes with SAMs
(a) 11-MUA SAM
(b) $C2NH_2$ SAM 257

Figure 6.5 : Relative rates of interaction of liposomes with SAMs 259

Figure 6.6 : Comparison of SPR traces for cationic liposomes interacting with C12Me and C3Me surfaces 261

Figure 6.7 : Relative rates of adsorption of liposomes, DNA and complex on $C2NH_2$ SAM 265

Figure 6.8 : AFM images of template stripped gold and SAMs 267

Figure 6.9 : AFM images of liposomes adsorbed to SAMs 268

Figure 6.10 : Typical force-distance curves of a dodecanethiol surface :
(a) before cationic liposome deposition
(b) after cationic liposome deposition 270

Figure 6.11 : Size distribution of liposomes on 11-MUA SAM 271

Figure 6.12 : Images of liposomes on amino terminated SAM. Effect of time on structure observed 273

Figure 6.13 : Size distribution of liposomes on $C2NH_2$ SAM 274

Figure 6.14 : Images of DNA
(a) adsorbed to $C2NH_2$ surface
(b) on mica in 20 mM Tris, 2.5 mM, $MgCl_2$ (pH 8.0) 277

Figure 6.15 : Force-distance curves of a 2-aminoethanethiol surface :
(a) before DNA deposition
(b) after DNA deposition 278

Figure 6.16 : Images of the complex on the 2-aminoethanethiol surface after varying periods of time. 280

Figure 6.17 : Size distribution for complex structures from early time point images
(a) Distribution from images as Figure 5.15 (a)
(b) Distribution from images as Figure 5.15 (b) . . . 281

Figure 6.18 : Schematic representation of proposed interaction of complex with 2-aminoethanethiol surface over time 283

CHAPTER 7 : POLYMERS AS DRUG DELIVERY VEHICLES - DENDRIMERS

Figure 7.1 : Summary of polymer groups 291

Figure 7.2 : The effect of core, repeat group and generation number on the architecture of dendrimers 292

Figure 7.3 : Conformational isomerism of dendrimers 294

Figure 7.4 : Schematic representation of a PAMAM dendrimer 299

Figure 7.5 : Structure of Lan-1 and Lan-2
(a) Lan-1 structure
(b) Lan-2 structure
(c) Idealised surface structure of Lan-1 and Lan-2 when bound to silver SPR slide 303

Figure 7.6 : A typical SPR trace for the interaction between the Generation 8.0 PAMAM dendrimers and a dodecanethiol SAM 312

Figure 7.7 : (a) Interaction of amino terminated dendrimers with a dodecanethiol SAM
(b) Interaction of carboxyl terminated dendrimers with a dodecanethiol SAM 314

Figure 7.8 : (a) Interaction of amino terminated dendrimers with a 11-MUA SAM
(b) Interaction of carboxyl terminated dendrimers with a 11-MUA SAM 317

Figure 7.9 : Schematic interpretation of low generation amino terminated dendrimers binding to the dodecanethiol and 11-MUA SAMs 318

Figure 7.10 : Effect of pH on interaction of dendrimers with an 11-MUA surface 320

Figure 7.11 : (a) Interaction of amino terminated dendrimers with a 2-aminoethanethiol SAM
(b) Interaction of carboxyl terminated dendrimers with a 2-aminoethanethiol SAM 322

Figure 7.12 : (a) Interaction of amino terminated dendrimers with a Lan-1
(b) Interaction of carboxyl terminated dendrimers with a Lan-1 324

Figure 7.13 : (a) Interaction of amino terminated dendrimers with a Lan-2
(b) Interaction of carboxyl terminated dendrimers with a Lan-2 325

Figure 7.14 : A typical SPR trace for the generation 7.5 dendrimer interacting with a Lan-1 surface 326

Figure 7.15 : Effect of dendrimer generation on depth and density of adsorbed layer 328

Figure 7.16: Schematic representation of the membrane fraction adsorbed to dodecanethiol and 11-MUA SAMs 332

Figure 7.17: Typical SPR trace for the adsorption of the cell membrane fraction to a SAM 333

Figure 7.18 : Typical Adsorption Profiles for phosphatidylcholine and Fibrinogen to the dodecanethiol SAM 334

Figure 7.19 : Interaction between PAMAM Dendrimers and CACO2 membrane fraction 340

Figure 7.20 : Interaction between PAMAM Dendrimers and DNA 343

Figure 7.21 : AFM images of Dendrimers in air
(a) methyl SAM on gold
(b) generation 4.0 dendrimer 347
(c) generation 9.5 dendrimer
(d) generation 6.0 dendrimer 348

Figure 7.22 : AFM images of Dendrimers in buffer 350

Figure 7.23 : Height distribution taken from both liquid and air images of dendrimers 352

Figure 7.24 : Effect of dendrimer generation on packing as observed from phase images 353

Figure 7.25 : Close packed generation 8.0 dendrimers observed by AFM 355

Figure 7.26 : Schematic representation of the effect of dendrimer surface interaction on the degree of sweeping 356

Figure 7.27 : Effect of biotinylation on interaction of dendrimers with streptavidin (1)
(a) Effect of degree of substitution
(b) Effect of linker length
(c) Schematic representation of effect of linker length 359

Figure 7.28 : Effect of biotinylation on interaction of dendrimers with streptavidin (2)
(a) Amino terminated dendrimers
(b) Carboxyl terminated dendrimers 361
(c) Rate 364

Figure 7.29 : Effect of dendrimer type on the extent interaction with model surfaces
(a) amino terminated surface
(b) carboxyl terminated surface 366
(c) methyl terminated surface 368

Figure 7.30 : Effect of pH on the interaction of PAMAM dendrimers with model surfaces
(a) Interaction between 11-MUA and the generation 9.5 dendrimer
(b) Interaction between the 2-aminoethanethiol and the generation 9.0 dendrimer. 370
(c) Interaction between 11-MUA and the generation 9.0 dendrimer.
(d) Interaction between 11-MUA and the generation 5.0 dendrimer 372
(e) Interaction between dodecanethiol and the generation 3.5 dendrimer 374

Figure 7.31 : Effect of ionic strength on interactions between dendrimers and model surfaces
(a) Interaction between 11-MUA and the generation 9.0 dendrimer
(b) Interaction between 11-MUA and generation 5.0 dendrimer 376
(c) Interaction between the dodecanethiol surface and generation 9.5 dendrimer 378

Figure 7.32 : Effect of dendrimer type on the interaction with a membrane mimicking surface 379

Figure 7.33 : Effect of dendrimer type on the interaction with DNA ... 381

Table list

CHAPTER 1 : INTRODUCTION

Table 1.1 : Parameters contributing to the unique properties of surfaces 15

Table 1.2 : "Wish list" for the perfect surface analytical technique 16

CHAPTER 3 : POLYMERS FOR TISSUE ENGINEERING : SURFACE CHARACTERISATION

Table 3.1 : Summary of PLA and PEG content of tested polymer 74

Table 3.2 : Effect of PLA molecular weight in contact angles for biotinylated polymers 80

Table 3.3 : Summary of peak contributions and PLA peak ratios for biotinylated and non-biotinylated PLA-PEG polymers 84

Table 3.4 : Carbon : oxygen ratios for the biotinylated and non-biotinylated PLA-PEG polymers 86

Table 3.5 : Summary of surface roughnesses for PLA-PEG-biotin's before and after incubation in buffer 88

Table 3.6 : Summary of ToF-SIMS peaks observed for PLA and PEG in the biotin-PLA-PEG polymers
(a) positive peaks
(b) negative peaks 93

Table 3.7 : Summary of ToF-SIMS peaks observed for PLA and PEG in the PLA-PEG polymers
(a) positive peaks
(b) negative peaks 95

Table 3.8 : Summary of peaks observed for PDMS in PLA-PEG-biotin ToF-SIMS image 103

Table 3.9 : Summary of peaks observed for protein in PLA-PEG-biotin ToF-SIMS image
(a) positive spectra
(b) negative spectra 104

Table 3.10 : Summary of distribution of peaks over 6,000 counts
(a) Positive spectra
(b) negative spectra 108

CHAPTER 4 : POLYMERS FOR TISSUE ENGINEERING : SURFACE INTERACTIONS

Table 4.1 : Ratio of biotinylated to non-biotinylated polymers used to investigate the minimum avidin coverage possible . . . 128

Table 4.2 : Structure of surfactants used in SPR studies 132

CHAPTER 5 : POLYMERS IN GENE THERAPY : CATIONIC POLYMERS

Table 5.1 : Summary of SPR results investigating the effect of PEG molecular weight on the extent of interaction of PLL-PEG with immobilised DNA 216

CHAPTER 6 : CATIONIC LIPIDS AN ALTERNATIVE APPROACH TO GENE THERAPY

Table 6.1 : Effect of flow rate and liposome concentration on liposome coverage as measured by SPR 254

Table 6.2 : Summary of SPR data for interaction of liposomes, DNA and complex SAMs 254

Table 6.3 : Summary of SPR results for interaction between complex fractions 285

CHAPTER 7 : POLYMERS AS DRUG DELIVERY VEHICLES - DENDRIMERS

Table 7.1 : Summary of lipid membrane SPR characterisation studies ... 330

Table 7.2 : Summary of interaction of phosphatidylcholine, BSA, IgG and fibrinogen with the dodecanethiol and 11-MUA surfaces 335

Table 7.3 : Effect of lipid : protein ratio on adsorption profile observed on dodecanethiol SAM with SPR 338

Appendices

Appendix 1 : Charge ratio calculations 390

Appendix 2 : Preparation of cell membrane fraction 393

Abbreviations

ADA	Adenosine deaminase
AFM	Atomic force microscopy
AIDS	Aquired immune difficency syndrome
APTES	3-aminopropyltriethoxyl silane
biotin-HPDP	N-([3-biotinamido]hexyl)-3'-[2'pyridyldithiol]propamide
BSA	Bovine serum albumin
CEMA	Carboxyethylmethacylamide
DMPE	Dimyristoylphospatidylethanolamine
DMSO	Dimethyl sulfoxide
DNA	Deoxyribonucleic acid
DOPE	1,2-dioleoyl-3-trimethylammonium-propane also known as 1,2-dioleoyl-*sn*-glycero-3-phosphoethanolamine
DOGSDSO	1,2-dioleoyl-sn-glycero-3-succinyl-2-hydroxyethyl disulfide ornithine
DOTAP	*N*-(1-(2,3-dioleoyloxy)-propyl)-*N*,*N*,*N*-trimethylammonium chloride
EDTA	Ethylenediaminetetraacetic acid
EDMPC	p-ethyldimyristoylphosphatidylcholine also known as 1,2-dimyristoyl-sn-glycero-3-ethylphosphocholine
EPR	Enhanced permeability and retention
HSA	Human serum albumin
HEPES	(N-[2-hydroxyethyl]piperazine-N'-2-ethanesulphonic acid])
HPMA	N-(2-hydroxypropyl methacrylamide)
KE	Kinetic energy
LB	Langmuir-Bloggett
LS-AFM	Large scanning - AFM

PALS	Phase analysis light scattering
PAMAM	Poly(amido amine)
PC	Phosphatidylcholine
PCS	Photon correlation spectroscopy
PE	Poly(ethylene)
PEG	Poly(ethylene glycol)
PEI	Poly(ethylene imine)
PEO	Poly(ethylene oxide)
PHEMA	Poly(hydroyethylmethacrylate)
PLG	Poly(lactide-co-glycolide)
PLL	Poly(L-lysine)
POPC	1-palmitoyl, 2-oleoyl phosphatidylcholine
POS	Poly(n-octyl-styrene)
PPO	Poly(propylene oxide)
PS	Poly(styrene)
PVA	Poly(vinyl alcohol)
PVP	Poly(vinyl pyrrolidone)
RES	Reticuloendotheilal system
RGD	Arginine-Glycine-Aspartic acid (Arg-Gly-Asp)
RNA	Ribonucleic acid
SAM	Self assembled monolayer
SAXS	Small-angle X-ray scattering
SCID	Severe Combined Immune Deficiency
SIMS	Secondary ion mass spectrometry
SMANCS	Styrene-maleic anhydride coupled to neocarzinostatin
SPM	Scanning probe microscope
SPR	Surface plasmon resonance
STE	Saline buffered Tris EDTA
STM	Scanning tunneling microscope
TAE	Tris acetate EDTA

TE	Tris EDTA
TFE	Trifluoroethanol
T_m	Melting temperature
ToF	Time of flight
Tris	Tris(hydroxymethyl)aminomethane
TSG	Template stripped gold
XPS	X-ray photo electron spectroscopy

Chapter 1 : Introduction

1.1 : Polymer revolution

The use of polymers within our everyday life is so common, for the majority of the time it does not even cross our minds that we are utilising them. Their use affects every aspect of our daily lives from the clothes we wear and the transport we use, to the way we communicate and the foods we eat.

The term polymer was first coined in 1833 by Jons Jacob Berzelius in his book "Jahres Bericht". In this book he noted with respect to the $(C_2H_2)n$ series, which includes benzene, acetylene and styrene that a molecule may have the same chemical composition but different molecular weights. He classified this 'polymerism' as a type of isomerism, although he did not appreciate the significance of this term to high molecular weight materials. Although the knowledge of the existence of what we now know as polymers had been documented centuries earlier.

The first known documentation about the naturally occurring polymer rubber, was in 1511. Even as late as 1920 the existence of the high molecular weight polymer molecule was still being debated. Staudinger, the first dedicated "polymer chemist" in his paper "Uber Polymerisation" proposed long linear chain structures for poly(styrene) and poly(oxymethylene). He and his followers argued for the existence of polymers where "many single molecules are held together by normal valency bonds". However, other powerful scientists such as the Noble prize winning Heinrich Wieland stated that "their are no organic molecules with molecular weights greater than 5,000. Purify your products eg. rubber, then it could be crystallised and it would be found that it is a low molecular weight product" and other comments such as;

"we are shocked, like zoologists would be if they were told that somewhere in Africa an elephant was found who was 1,500 feet long and 300 feet high" were thrown at Staudinger in response to his talk on polymer structure at the 1926 symposia "Gesellschaft Deutscher Naturforscher und Arzte" (Misra (1993)). This was even after a multitude of polymers had been synthesised and the lower molecular weight ones characterised. For example, the ethylene glycol / ethylene dihalide ($HO\text{-}[C_2H_4O]n\text{-}H$) products of Lourenco which were purified by distillation up to $n = 6$, as well as, the osmotic pressure studies of Rodewald on starch where molecular weights of up to 39,700 were identified, and the controlled synthesis of polypeptides by Emil Fischer in 1906.

Finally in 1953 Staudinger received the Nobel prize for his work in macromolecule (a term he first coined) chemistry. In his address on presenting the award to Staudinger, Frega said " It is no secret that for a long time many colleagues rejected your view .....Perhaps this was understandable. In the world of high polymers almost everything was new and untested. Long standing, established concepts had to be revised or new ones created."

Whilst the academic were still arguing over the existence of the polymers structure, industrialists were already making their fortunes from them. Early entrepreneurs utilised derivatives of horn and hooves, for making combs and produced viscose rayon from cotton cellulose. The first chemically synthesised, commercially available, polymers were the product of the phenol and formaldehyde polymerisation developed by the Belgian Bakeland and known as Bakerlite. It wasn't until the logical chemical synthesis approach of Carothers, who joined DuPont in 1928, did the synthesis and commercial development of polymeric materials of known chemical composition emerge. His work, for example on reactivity ratio, viscosity, molecular weight ratios and the discovery that poly(hexamethylene adipamide) could be spun from a

melt to form a strong fibre - Nylon and J. Hills work on cold drawing techniques which gave DuPont the monopoly on the production of synthetic textile fabrics (Stahl (1981)).

As eluded to above, polymers have played an important role in the industrial development of many countries. In this century there have been three significant industries launched as a result of the development of new families of polymers. The first of these were the thermoplastics of Carothers and other researchers of the time. This linear, spaghetti-like family of polymers such as, poly(ethylene) (PE), poly(styrene) (PS) and nylon, emergence as a commercially viable set of materials became established in the 1920-30's. The second family, whose origins date from the 1940's are commonly known as the thermosets. These comprise of crosslinked or vulcanized forms of the spaghetti-like thermoplastics to produce epoxies, urethanes and solvent resistant elastomers and rubbers. The final family of polymers are the randomly branched polymers. These can form amorphous, low density structures an their appearance arose in the 1960's.

Since the late 1970's and early 80's a new family of synthetic polymers has been developed. These are now coming into the stage of commercial viability. Known as the dendrimers, their branched structure emanates from a central core forming a ball-like structure (Tomalia (1997)). As well as the development of new synthetic polymers, exploitation of naturally occurring polymers such as the polysaccharides, proteins, DNA, and derivatives of these has also played a crucial role in the social development of the world population over the last century. Each of these families of polymers have specific architectures and these can be related to their properties and hence their applications.

In 1973 the British Plastics Federation produced a pamphlet titled "Plastics their Contribution to Society and Considerations of their Disposal" (Fergusson (1973)). In this source of information they quote the main uses of plastics to be in the following areas.

(1) Building - pipes, flooring, window frames, work surfaces and built in furniture

(2) Packaging - especially for food

(3) Electrical - due to their insulating properties

(4) Consumer products, utensils such as buckets and durables such as fridges and hoovers

(5) Furniture, both for structure ie frames, as well as components eg. Imitation leather covers and foam padding

(6) Transport components ie car dashboards

(7) Other applications - uses in chemical plants, protective clothing, transport pipes eg. for gas and liquids and agriculture eg. feeding troughs and greenhouses.

However the medical applications of polymers were not mentioned, even though their application in this field had been progressing for at least 20 years.

However, in the 1981 publication of the American Chemical Society titled "Polymer Science Overview", a very polarised view of polymer applications is observed. Bakers view is bias was toward the use of polymers in the "age of information and communication" rather than that of a building material as suggested in the previous reference. However, in one short paragraph he highlights the use of polymeric films in the medical field, discussing the areas of contact lenses and prosthetics, as well as controlled release from capsules, drugs for cancer chemotherapy and the advantage of

controlled release in the agrochemical market. He finishes by saying that the "wonderful spiral conformation of collagen and the subtle information content of its peptide components in muscle action are qualities to be sought in the polymers made by people" in the future. This chapter is in stark contrast to another in this book by Hupfer and Ringsdorf who centre their whole discussion on the application of "Polymer Monolayers and Liposomes as Model Biomembranes and Cells" (Stahl (1981)).

1.2 : The use of polymers in medical applications

When the potential of utilising polymers in the medical field was first realized the majority of work was performed on materials whose characteristics had already been proven in other applications. For example, materials utilised in the first artificial hearts were the same as those utilised in women's girdles (Peppas (1994)). The problem with many 'off-the-shelf' polymers is that they erode from the bulk leading to complex dose kinetics, the possibility of dose dumping and hence, toxic side effects when utilised as drug delivery systems. Therefore, polymers specifically designed for the application of drug delivery have been synthesised whose erosion occurs from the surface providing more controllable delivery kinetics. These polymers include the poly(anhydrides), poly(ortho esters) and poly(phosphazenes) (Lemmouchi (1998), Leong (1985), Ng (1997)). One such system utilises poly(anhydrides) and the cancer chemotherapy drug carmustine. The polymer / drug blend is formed into wafers. These are placed at the tumour site after its removal in patients suffering from brain tumors (Valtonen (1997)). This was the first new treatment for 20 years to be approved by the Food and Drug Administration in the United States for the treatment of recurring glioblastoma.

The use of polymer systems within the field of drug delivery can be

divided into three main categories. Firstly, passive diffusion from or through a polymer system. Secondly, the use of polymers which can be degraded either enzymatically or chemically, releasing the trapped therapeutic agent. Finally, a system which is activated by an external stimuli releasing its carried moiety (Langer (1998)). These approaches can be used on their own or in combination. The approach taken depends not only on the therapeutic which is to be delivered, but also on the target site and changes in the body function which may have occurred due to the disease state.

Early polymer drug delivery systems were formed from the drug physically trapped within a solid polymer matrix. This system was either injected or implanted into the patient. These included the use of silicone rubber, which allowed the release of low molecular weight lipidic drugs over a long period of time (Folkman (1964)). However, this approach is limited in its potential applications, due to the fact that it cannot be used for drugs which posses molecular weights of greater than 400 or are charged. Therefore, systems were developed in which the drug concentration within the polymer in which it was physically imbedded was high enough to produce micro or nano holes which allowed diffusion of the drug out of the polymer matrix to perform its therapeutic benefit (Langer (1998)). Early systems utilised hydrogels and ethylene-vinyl polymers whilst more recent systems have utilised biodegradable polymer matrices.

The addition of antibodies to polymers is a novel method for the controlled release of therapeutic agents. The drug is only released in the presence of the antigen. This type of mechanism has been utilised in a system under development for treating narcotic addicts. The implantable system releases naltrexone, a narcotic antagonist on the binding of morphine, a heroin metabolite to a receptor on the system (Heller (1997)).

When considering macromolecular drugs such as polypeptides, the stability of the molecule within the polymer matrix is an important consideration (Costantino (1994)). The major problem is the presence of enzymes and aqueous moisture in the body. These causes hydrolysis of these highly labile molecules and hence their deactivation. Work is ongoing into ways to minimize this (Johnson (1996)).

The concept of polymer drug conjugates where drugs are chemically bonded rather than physically entrapped to a polymer vehicle was first introduced by Ringsdorf in 1975 (Ringsdorf (1975)). Many examples of this approach, which also allows for the incorporation of targeting moieties have been investigated. This approach is depicted in Figure 1.1. The main area of this concepts success has been that of cancer chemotherapy due to the enhanced permeability and retention (EPR) effect first proposed by Maeda and co-workers in 1986 (Matsumura (1986)). The EPR theory proposes that as a consequence of the leaky vascular system and poor lymph drainage found in many cancer types, the drug accumulates at the tumour site (Putman (1995) Duncan (1996), Matthews (1996)). This theory is schematically represented in Figure 1.2. This passive targeting mechanism has been shown to be effective in the PK1 system. In this case doxarubicin was conjugated via a peptide linker to N-(2-hydroxypropyl) methacrylamide)) (HPMA) (Duncan (1996)). Whereas the use of styrene-maleic anhydride coupled to neocarzinostatin (SMANCS) has been shown by Maeda and co-workers to be a successful treatment for liver cancer (Maeda (1991)).

By adding a targeting moiety the efficiency of this type of systems can be improved. However, finding suitable candidates for the target moiety is difficult. The targeting moiety must show a significant degree of specificity, to

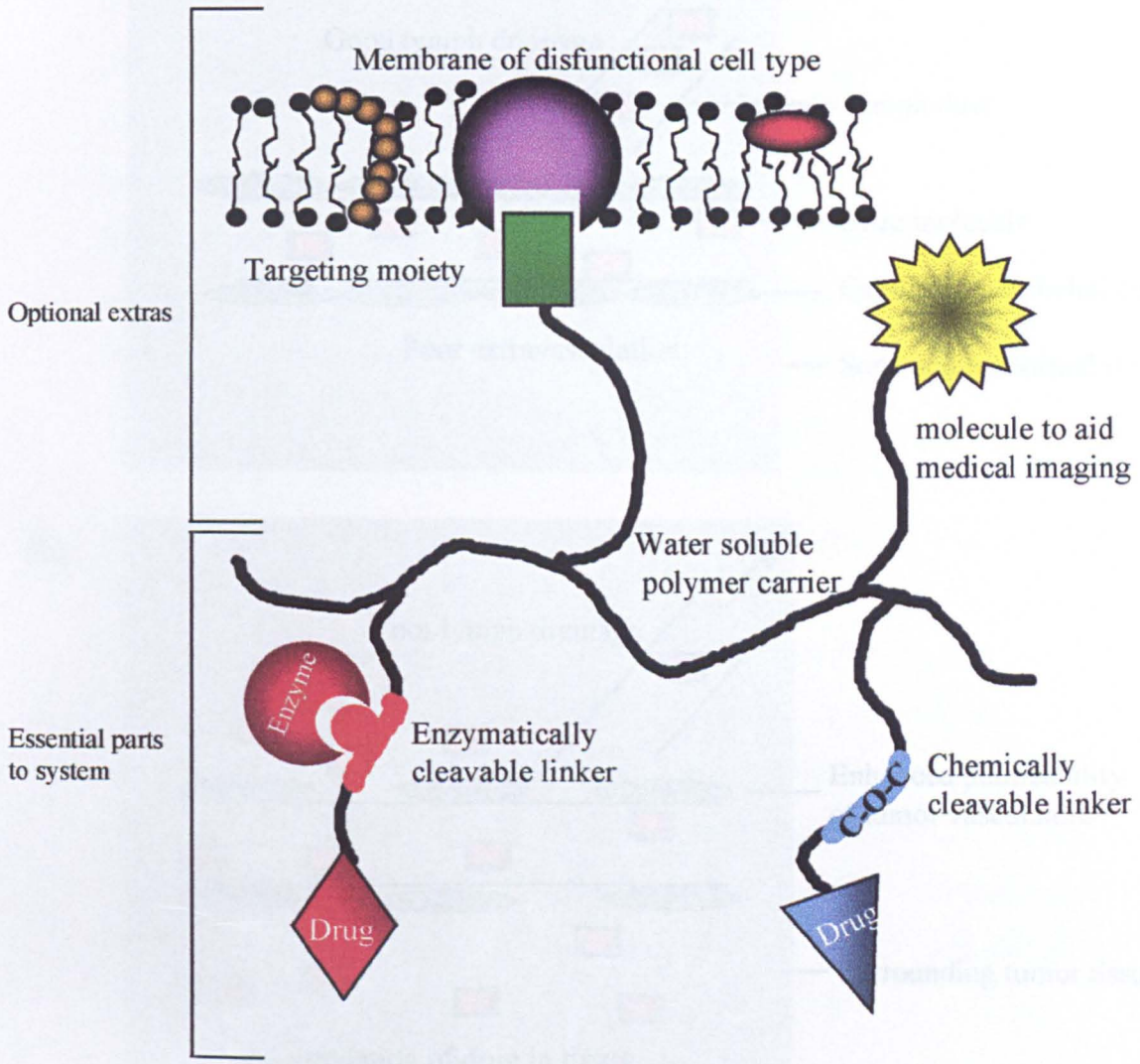

Figure 1.1 : Concept of polymer-drug conjugates

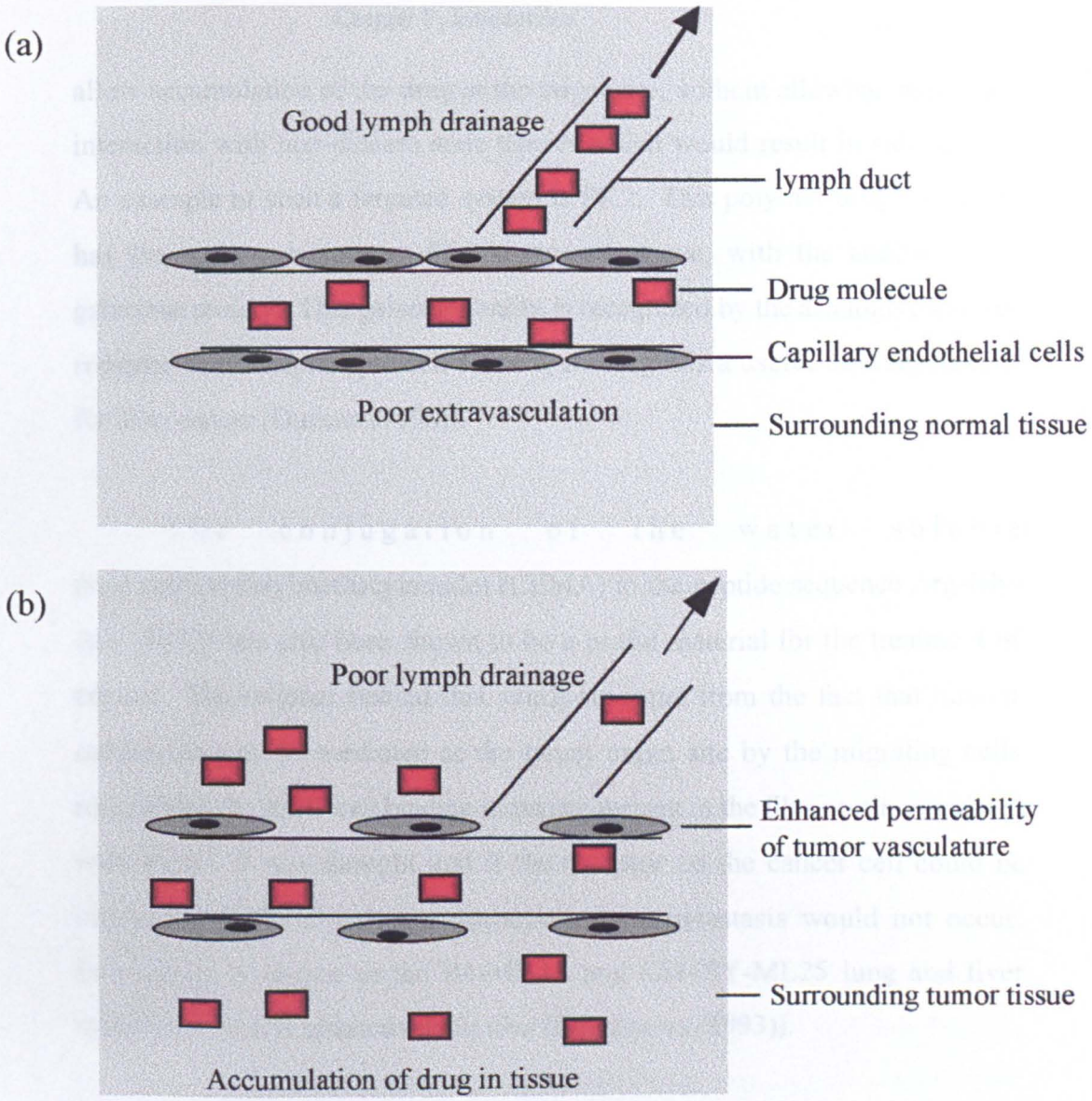

Figure 1.2 : The EPR effect
(a) Normal tissue
(b) Tumor tissue

In normal tissue the polymeric drugs are too large to pass through the capillary walls in significant numbers and tissue accumulation does not occur due to the effective lymph system. However, in tumor tissue the capillary walls are 'leaky' so the polymeric drugs can pass easily into the surrounding tissue and the drug is able to accumulate here due to the poor lymph drainage.

allow accumulation of the drug at the target site, without allowing significant interaction with non-disease state tissues which would result in side effects. An example of such a targeted system is PK2. This polymer drug conjugate has the same structure as PK1 discussed above, with the addition of a galactose moiety. This galactose entity is recognized by the asialoglycoprotien receptor of the hepatocyte cell surface, making this a useful delivery system for liver cancer (Duncan (1996)).

The conjugation of the water soluble poly(carboxyethylmethacylamide) (CEMA) to the peptide sequence Arg-Gly-Asp (RGD) has also been shown to be a useful material for the treatment of cancer. The rational behind this synthesis came from the fact that tumour metastasis may be mediated at the target organ site by the migrating cells recognising the RGD cell binding sequence present in the fibronectin associated with them. It was thought that if the receptor on the cancer cell could be blocked by a RGD-polymer sequences then metastasis would not occur. Indeed this held true in the B16-B116 and L5178Y-ML25 lung and liver metastasis models respectively *in vivo* (Komazawa (1993)).

Bioadhesive polymers are those which can attach to biological surfaces and hence be retained for prolonged periods of time (Yang (1992)). The use of this type of polymer for controlled drug delivery is another area of major research. The major polymers of interest are derivatives of naturally occurring polymers. For example, chitosan is a deacetylated version of chitin found in insects hard shells, alginates are extracted from seaweed and lectins are normally derived from the bean family or tomatoes (Illum (1998), Peppas (1996)). The main application of this type of system has been buccal patches (Veillard (1987), Ishida (1981)), ointments (Nagai (1985)), tablets, such as the system in which the bioavailability of diltiazem was increased from 30.4 to

69.6% (Miyazaki (1995)) and topical ocular delivery (Hui (1985), Greaves (1993), Davies (1992)).

Charged polymers such as the poly(ethyleneimine) (PEI), chitosan and PAMAM dendrimers have been utilised to deliver DNA successfully *in vitro* and *in vivo* to a number of cell lines (Boussif (1995), Tang (1997), Leong (1998)). The delivery of DNA has the potential for controlling or curing inherited genetic diseases, as well as some cancers and AIDS. These cationic polymers are able to condense the oppositely charged DNA into small enough particles to allow successful delivery and also protect the DNA from degradation so it still maintains its therapeutic attributes. This area of polymer therapeutics will be discussed further in Chapter 5.

Smart, intelligent delivery systems, possess characteristics which change due to a stimuli or a alteration in their local environment. These polymers provide a potential advantage over standard therapeutic regimes where the dose of a therapeutic agent needs to change such as the delivery of insulin to diabetics. An examples of such smart systems are, polymer matrices which include magnetic beads. On application of an alternating magnetic field to these systems the material size increases allowing an increase in the rate of drug release. This effect was shown to be reversible and sustainable over the period of several months by Edelman and co-workers (Edelman (1987)). The use of ultra-sound and electric currents are two other stimuli under investigation for the control of drug delivery from polymer vehicles (Lavon (1998), Kwon (1991)) as are pH and temperature. An example of a pulsatile polymer whose stimuli is pH is the a co-polymer of poly(hydroxyethyl methacrylate) and poly(N,N-dimethylaminoethyl methacrylate), whereas poly(-N-isopropylacrylamide)'s stimuli is temperature (Goldraich (1993), Chen (1995)).

1.3 : The need for surface characterisation

In all the examples given above, the systems comprise of more than one component. When utilising anything in the medical setting, strict guidelines are set down about the knowledge needed of a systems stability and efficacy before it can be put on the market. Much of a systems stability and efficacy can be attributed to the interaction of molecules with the systems surface. For example, a polymeric materials surface energetics and morphology have been shown to effect cellular adhesion and protein conditioning of the materials on exposure to body fluids (Absolom (1984), Schakenraad (1984), Missirilis (1991), Horbett (1995), Davies (1997)). Therefore, if we can understand a materials surface interactions, which in turn are governed by its surface chemistry, we may be able to predict the systems suitability for a chosen application and hence reduce the extent of testing needed to find a new candidate for the chosen biomedical application.

Understanding the surface chemistry and hence interactions of a systems requires a prerequisite of understanding what a surface is. Figure 1.3 shows an idealised structure of a crystalline material. It can be observed that the atom A at is surrounded on all sides by atomic neighbours, and therefore can be termed to be in the bulk of the material. Minimisation of forces, both attractive and repulsive felt on this atom and the stabilisation of its unfilled valencies can be achieved by interactions with its neighbouring atoms. However, atom B is not surrounded by neighbouring atoms on all sides and is known to be at the surface. Unlike the bulk atoms, this atom is unable to balance the attractive and repulsive forces felt by it due to its inhomogeneous environment. This means the atoms below this surface atom will be able to electrostatically push or pull it towards the bulk of the material. Due to this

distortion of electronic energy, which is also contributed to by the fact that the surface atoms valencies may not be filled, a surface will always try to minimise its interfacial energy. This requires a change in surface composition or geometry. Other special attributes of surface atoms such a B in Figure 1.3 is that they have an increased probability of reacting with external entities and by interacting with contaminants found in the external environment can potentially change the surface properties of the material in a uncontrolled manner in an attempt to reduce their interfacial energy. The depth to which these inhomogeneities in electronic distribution are felt depends on the type of material of interest. In a crystalline material such as that depicted in Figure 1.3, by the time the fourth level of atoms is reached approximately 1.5 nm into the sample the atoms no longer possesses properties associated with surface atoms (Ratner (1998)). Whereas in polymeric material the 'surface layer' may extend up to tens of nm into the bulk depending on the materials molecular weight. The distorted electronic distribution in the surface region provides it with a range of properties different from that of the bulk of the material. These are important in its interaction with biomolecules and are summarised in Table 1.1.

To characterise these defined parameters (Table 1.1) which cause a surfaces unique properties, techniques which can measure them have been developed. The perfect instrument to measure the surface properties and interactions of materials would have the distinguishing features described in Table 1.2, however no such technique exists. Therefore a range of complementary techniques which posses a selection of these criteria are used to build up information on a certain aspect of the surfaces attributes. When used in a complementary fashion these individual pictures, like pieces in a jigsaw puzzle can fit together to provide an overall definitive knowledge of the system of interests surface.

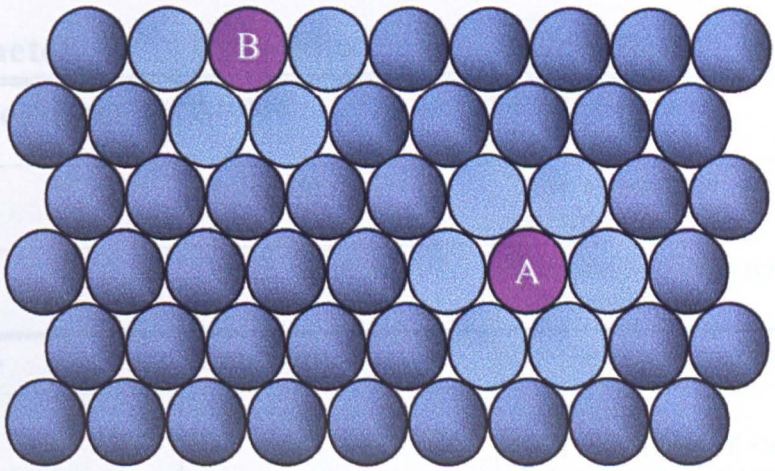

Figure 1.3 : The surface

A monocrystalline material showing the homogeneous distribution of neighboring atoms  around a bulk atom  and inhomogeneous distribution around a surface atom 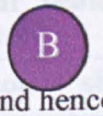 leading to the asymmetrical interactions on the surface atoms and hence providing their unique properties

Parameter	Examples	Variables
Composition	**Atomic**	Type of atom Ratio to others
	Molecular	Type and number of functional groups
	Depth profile	Composition with respect to distance from surface
Order	**Chirality**	Pure or racemic mixture
	Crystallinity	Space lattice % of total material structure
	Orientation	Crystal plane molecular
	Supramolecular assemblies	
Heterogeneity	**Crystal boundaries**	
	Dislocations	
	Domains	Eg. Phase separation
	Vacancies and inclusions	
Texture	**Atomic**	Atomic steps and defects
	Molecular scale roughness	
	Macroscopic shape	
Energetics	**Wettability**	
	Adsorptivity	

Table 1.1 : Parameters contributing to the unique properties of surfaces
Adapted from Ratner (1998)

Property	Details
Discrimination	(1) Surface from bulk (2) Material from contamination
High signal to noise ratio	Mass of material of interest is small typically 10^{-8} g / cm^2
Analytical sensitivity	As high as possible
Spatial resolution	Atomic, if not, a minimal of molecular resolution
Cheap / Easy to use	Allows use as routine analytical method

Table 1.2 : "Wish list" for the perfect surface analytical technique

Adapted from Ratner (1998) and Davies (1999)

The list of such techniques used to investigate surface properties is long and varied, therefore the following sections will only introduce those utilised in the experimental chapters of this thesis. Sections 1.4 and 1.5 will concentrate on secondary ion mass spectrometry (SIMS) and X-ray photoelectron spectroscopy (XPS) respectively, these two techniques provide information on a systems surface chemistry. Atomic force microscopy (AFM) (section 1.6), can be utilised to produce images of a materials surface structure and probe dynamic molecular recognition events, where as surface plasmon resonance (SPR), which is introduced in section 1.7 can be utilised to investigate dynamic processes at the material surface.

1.4 : X-ray photoelectron spectroscopy : Theory and applications

X-ray photoelectron spectroscopy (XPS) is utilised to measure the kinetic energy of electrons expelled from a materials surface by a monochromatic X-rays. This kinetic energy is related to the nature of the surface atoms and their chemical environment, and hence provides quantitative information of the chemical bonding at the surface. The technique is surface sensitive, non-destructive and requires little sample preparation. However, it does require relatively large samples which need to be analysed under an ultra high vacuum, with results which are only spatially resolved to 8-150 μm (Duc (1995)). A schematic representation of the instrument setup is shown in Figure 1.4.

In essence X-rays, normally from a Mg Kα or Al Kα source, are fired at the surface of the sample of interest under vacuum. The energy of these X-rays is great enough to remove the 1s electrons from atoms such as carbon,

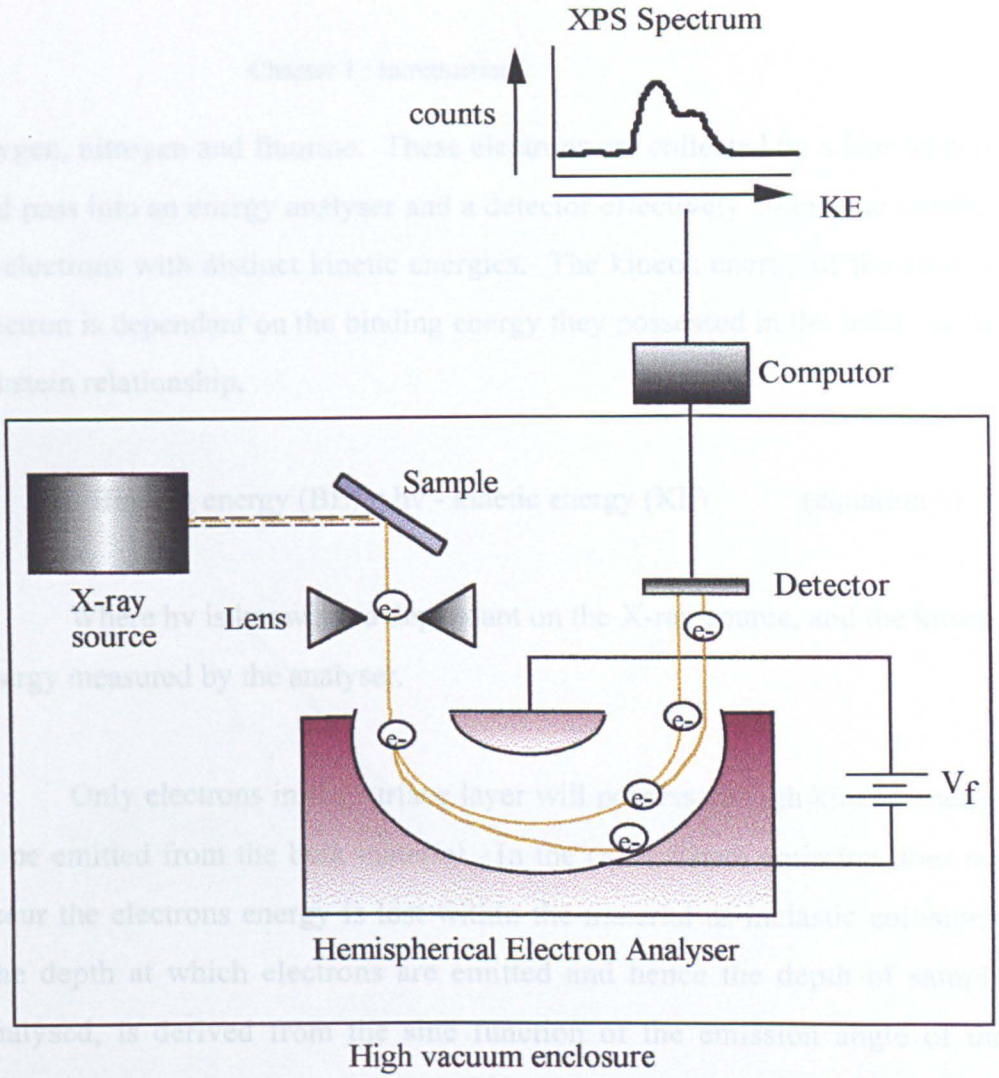

Figure 1.4 : Schematic representation of a typical XPS instrument

oxygen, nitrogen and fluorine. These electrons are collected by a lens system and pass into an energy analyser and a detector effectively counts the number of electrons with distinct kinetic energies. The kinetic energy of the emitted electron is dependant on the binding energy they possessed in the solid via the Einstein relationship,

$$\text{Binding energy (BE)} = h\nu - \text{kinetic energy (KE)} \qquad \text{(equation 1)}$$

Where hv is known and dependant on the X-ray source, and the kinetic energy measured by the analyser.

Only electrons in the surface layer will possess enough kinetic energy to be emitted from the bulk material. In the cases where emission does not occur the electrons energy is lost within the material as inelastic collisions. The depth at which electrons are emitted and hence the depth of sample analysed, is derived from the sine function of the emission angle of the photoelectrons from the sample relative to its surface plane (Ratner (1998)). This is depicted schematically in Figure 1.5. For example, a spectrum recorded at a normal emission (90°) to the surface would sample from a three times deeper surface region to that of a spectrum recorded at 20° to the sample plane. In general the sampling depth range of XPS is between 1 and 25 nm (Ratner (1998)). In an XPS spectra, the data output takes the form of a plot of KE versus number of counts. As discussed earlier the BE is related to the chemical environment of the electron, this provides a 'fingerprint' of the sample surface.

As discussed above, XPS provides information not only on the atoms present at the surface of the sample of interest, but also their chemical bonding. This is because the core (1s) electrons local environment is altered depending on the binding of the valency electrons. For example, a carbon

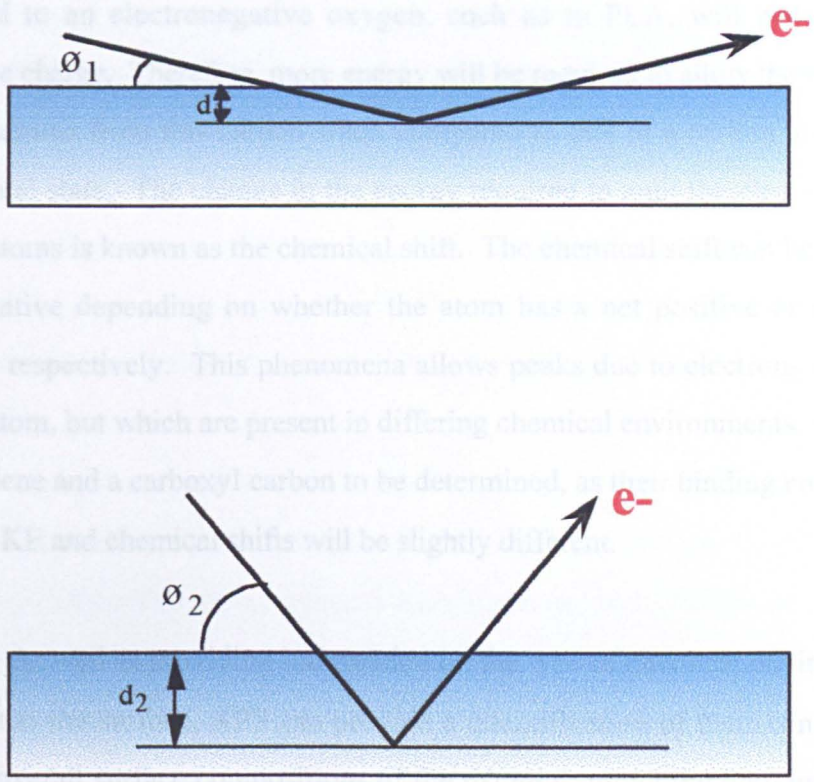

Figure 1.5 : Effect of emission angle on sampling depth in XPS

emission angle (ø)
sampling depth (d)

bonded to an electronegative oxygen, such as in PLA, will posses a net positive charge. Therefore, more energy will be required to allow the escape of the electrons from this carbon when compared to that of a carbon atom in its elemental state. The change in the energy required to emit the electrons from these atoms is known as the chemical shift. The chemical shift can be positive or negative depending on whether the atom has a net positive or negative charge respectively. This phenomena allows peaks due to electrons from the same atom, but which are present in differing chemical environments, such as a methylene and a carboxyl carbon to be determined, as their binding energy and hence, KE and chemical shifts will be slightly different.

As well as providing information on the type of chemical environments present at the surface, XPS can provide a quantification of their contribution to the overall surface compositions of the material, providing a knowledge of the sensitivity factors for the instrument are available. Sensitivity factors are governed by a variety of mathematical components including the photoionisation cross section.

In the field of biomedical polymers, XPS has a range if useful applications. In the field of block co-polymers, Black et al. showed that XPS could be utilised to measure the change in surface contribution of PLA and PEG in a range of PLA-PEG block co-polymers with varying molecular weight of PLA blocks (Black (1999)), whereas, the surface contribution of the lactide and glycolide components of PLGA polymers were distinguished by Davies and co-workers in their studies. They also showed the degradation processes of such biodegradable biomaterials can also be followed (Davies (1990), (1996)). Results such as these are useful as they provides information on how the material may degradation in the body and hence, give an indication of the metabolites formed.

The degree of surface modification of a material can be followed by XPS, as has been shown by Gombotz and co-workers in their studies probing the functionalisation of poly(ethylene terphthalate) polymer films by the plasma polymerisation of PEO. Migonney and co-workers also investigated by XPS the derivatisation of silicones by 4-hydroxybutyric acid sodium salts for use as contact lenses (Gombotz (1989), Migonney (1995)).

As well as providing information on the surface chemistry and the extent of surface derivatisation of a material, XPS can provide information on the extent of biomolecules interactions with these surfaces (Ratner (1987)). The measurement of the extent of contamination of polymeric surfaces has been carried out. For example, Paynter et al. in addition to characterising the surface chemistry of commercially available polyester arterial prostheses also looked at protein adsorption to these (Paynter (1989)). Biofouling and attempts to minimise this have also been followed by XPS (Lopez (1992), Sheu (1993)). Advantageous interactions that have been studied include cell adhesion and the effect of protein interactions with respect to the biocompatibility of the system (Gilding (1980), Ertel (1990)).

Advances in the technology of the XPS instrument now mean that XPS can be utilised in an imaging mode. However, the resolution is not as good as that of the imaging SIMS as discussed later in section 1.5 (Munro (1993)). Advances in sample preparation now allows sample analysis to be performed by a freeze-etch method. In this type of analysis samples are prepared in a cryogenic mode, allowing polymers surfaces can be analysed in their hydrated state (Lewis (1993)). Using this method, Ratner and co-workers investigated a tri-block polymer comprised of poly(hydroyethylmethacrylate) (PHEMA) and poly(n-octyl-styrene) (POS). They found that in the dry state the

hydrophobic POS was dominant at the surface where as in the hydrated state the polymer surface possessed a dominant amount of PHEMA (Ratner (1995)).

1.5 : Secondary ion mass spectrometry : Theory and application

Secondary ion mass spectrometry (SIMS) is a technique which measures the mass of surface ion fragments produced from bombarding a surface with an ion or atom beam. The basic setup of a SIMS instrument is shown in Figure 1.6. Primary ions or atoms, usually from a noble gas are fired at the surface of the sample of interest. These ions penetrate the sample to a depth of between 30 - 100 Å from the surface. The energy of these ions breaks interatomic and intermolecular bonds of the material via a collision cascade as depicted in Figure 1.7 and releases mass fragments characteristic of the sample. These fragments, be they positive or negative are accelerated up to a mass spectrometer by the application of a negative or positive bias respectively to a quadrupole or time-of-flight (ToF) detector. The mass spectrometer calculates the mass / charge (m / z) ratio of these fragments and data output is in the form of mass versus frequency. Neutral molecular fragments may also be obtained by directing them into a ionising area and then collecting the resultant ionic fragments. By applying the knowledge obtained from conventional mass spectrometry a detailed identification of the surface chemistry of the sample can be obtained. When operating in static mode (SSIMS), by limiting the number of atoms interacting with the surface to less than 10^{13} only the top 10 Å of the material of interest are analysed showing the surface sensitivity of this technique (Hearn (1987)). However, molecular weights of only up to approximately 800 are measurable by quadrupole SSIMS instruments for higher m / z ratios, a time of flight SIMS (ToF-SIMS)

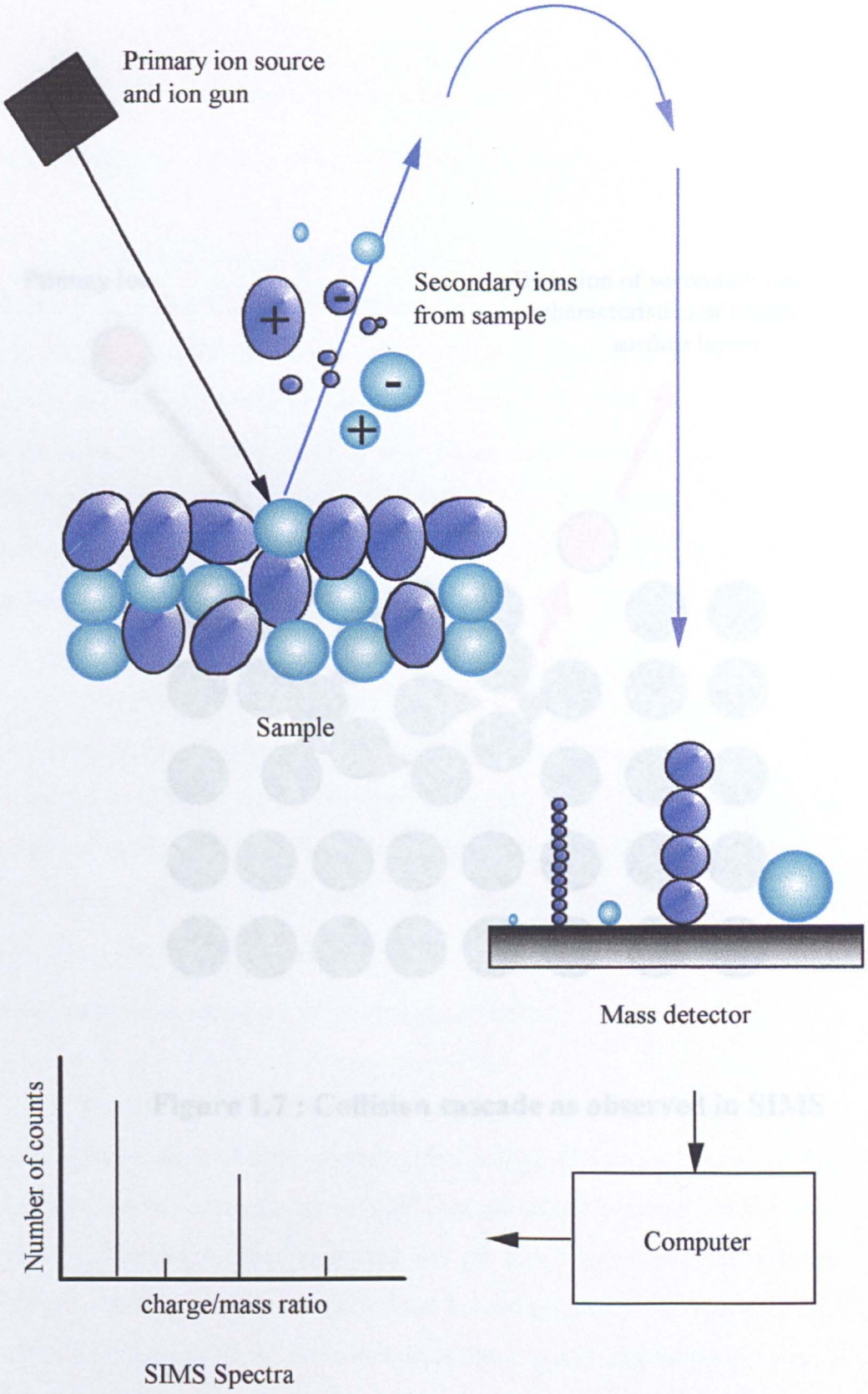

Figure 1.6 : Schematic representation of a basic SIMS setup

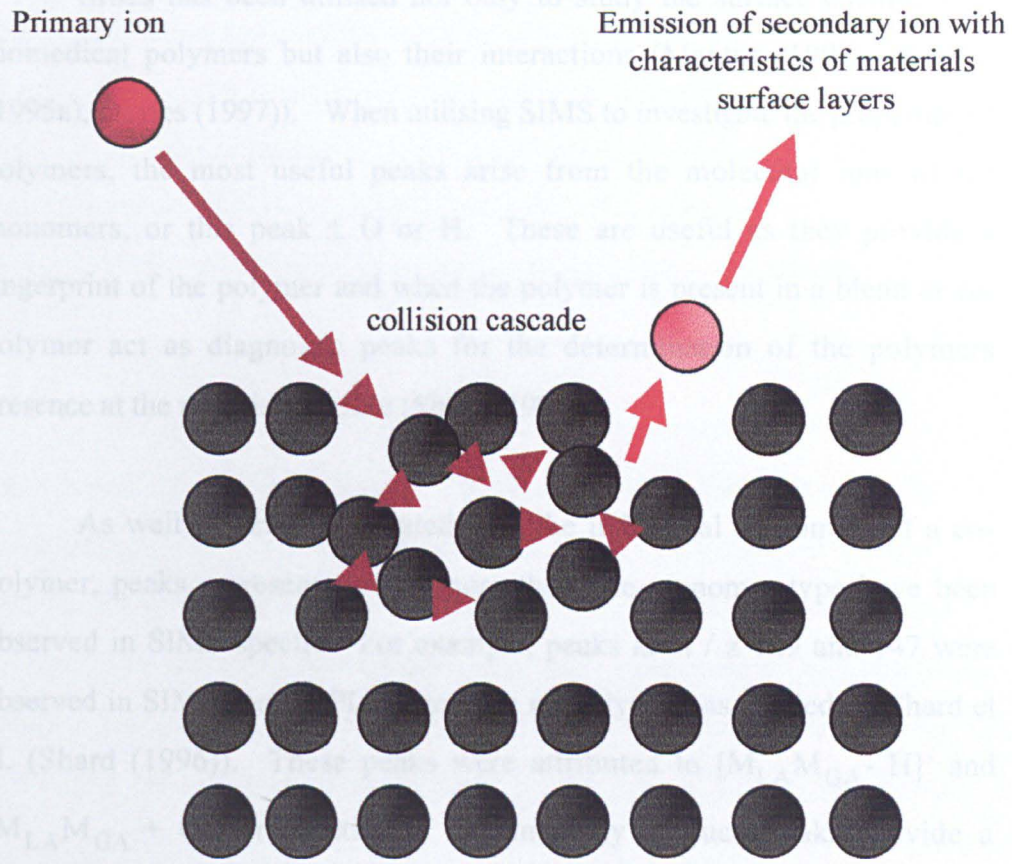

Figure 1.7 : Collision cascade as observed in SIMS

is needed and this can provide a range up to 10,000 m / z.

SIMS has been utilised not only to study the surface chemistry of biomedical polymers but also their interactions (Mantus (1993), Chilkoti (1995a), Davies (1997)). When utilising SIMS to investigate the properties of polymers, the most useful peaks arise from the molecular ions of the monomers, or this peak ± O or H. These are useful as they provide a fingerprint of the polymer and when the polymer is present in a blend or co-polymer act as diagnostic peaks for the determination of the polymers presence at the materials surface (Shard (1996b)).

As well as peaks associated with the individual monomers of a co-polymer, peaks representative of more than one monomer type have been observed in SIMS spectra. For example, peaks at m / z 129 and 147 were observed in SIMS spectra PLGA random co-polymers as studied by Shard et al. (Shard (1996)). These peaks were attributed to $[M_{LA}M_{GA}- H]^-$ and $[M_{LA}M_{GA} + OH]^-$ respectively. The intensity of such peaks provide a measure of the randomness of the co-polymerisation.

The theory of the surface composition and phase separation of polyurethanes derived from results obtained from XPS and other techniques, was significantly altered after detailed analysis of SIMS spectra of the same system. The earlier data suggested that the soft segments of the polymer formed a surface covering layer of the harder segments. However, SIMS analysis of the top 10 Å of the materials found peaks characteristic of both segments. This suggested that the surface interface of the polymeric materials was more complicated than originally thought. It was also found that the contribution of the soft segment to the surface of the polymer was related to its molecular weight (Hearn (1987), (1988)).

SIMS, has been shown to be a particularly useful technique for determining the presence of low molecular weight drugs at or near the surface of polymer films and colloids containing them (Davies (1987) (1988)). The adsorption of proteins on to materials surfaces is another surface interaction followed by SIMS. Mantus et al. utilising homopolymers of 16 amino acids to determine peaks unique to these amino acids. These peaks were then utilised to identify the presence of proteins on fouled sensor membranes (Mantus (1993)).

As with XPS determination of the surface contamination of polymer films is also obtainable by SIMS. The presence of bis-ethylene steramide the lubricating oil has been determined on the surface of poly(etherurethane) by Feast and Munro (Feast (1987); whilst in the evaluation of clean methods for colloidal particles using both the complementary techniques of XPS and SIMS. Kooha, Weng and their co-workers were able to identify the presence of surfactants (Kooha (1989) Weng (1994)).

SIMS can be utilised to calculate the ratio of chemical groups present at the surface of materials. However, unlike XPS where quantitative results can be obtained, results from SIMS are only semi-quantitative due to matrix effects. Matrix effects arise due to the ease at which the material of interest produces secondary ions (Werner (1980)). This can vary significantly between materials. However, many semi-quantitative investigations can be found in the literature such as those by Weng and co-workers on styrene butadiene amongst others (Weng (1995), Davies (1991), Lub (1987)).

SIMS can also be used to obtain a chemical picture of the surface of a material. Images are obtained where each pixel point of the image contains a SIMS spectrum. This approach has been utilised to probe the distribution of

drugs within nanoparticulate systems (Davies (1987)) and image biological samples (Burns (1986), Davies (1993)). For example, Briggs and Hearn have imaged proteins immobilised to conducting surfaces (Briggs (1988)).

1.6. : Atomic force microscopy : Imaging theory

In March 1986 a paper appeared in Physical Review Letters introducing a new type of microscope for " investigating surfaces of insulators on an atomic scale". The paper was written by Binnig, Quate and Gerber and the microscope was the atomic force microscope (Binnig (1986)). This paper has subsequently launched many careers in the high resolution imaging of materials as diverse as carbon graphite to DNA and PE to semiconductors as well as those concerned with the measurement of intermolecular forces (Goh (1995), Shao (1996), Hansma (1997),Giancarlo (1998)).

The atomic force microscope or AFM is a member of the family of microscopes known as the scanning probe microscopes (SPM). As their name suggests, these microscopes construct images of a surface from a probe scanning across the surface, where some form of interaction between the probe and the surface is measured. This family, as well as including the AFM, also includes the magnetic force, electrostatic force and frictional force microscopes (Meyer (1992)).

The first member of the SPM family was the scanning tunneling microscope (STM), as depicted in Figure 1.8. In this case, the interaction measured between the probe, usually constructed of platinum-iridium and the sample, is a current of electron movement. This current is induced by applying a voltage bias to the tip. By maintaining the level of electron flow at

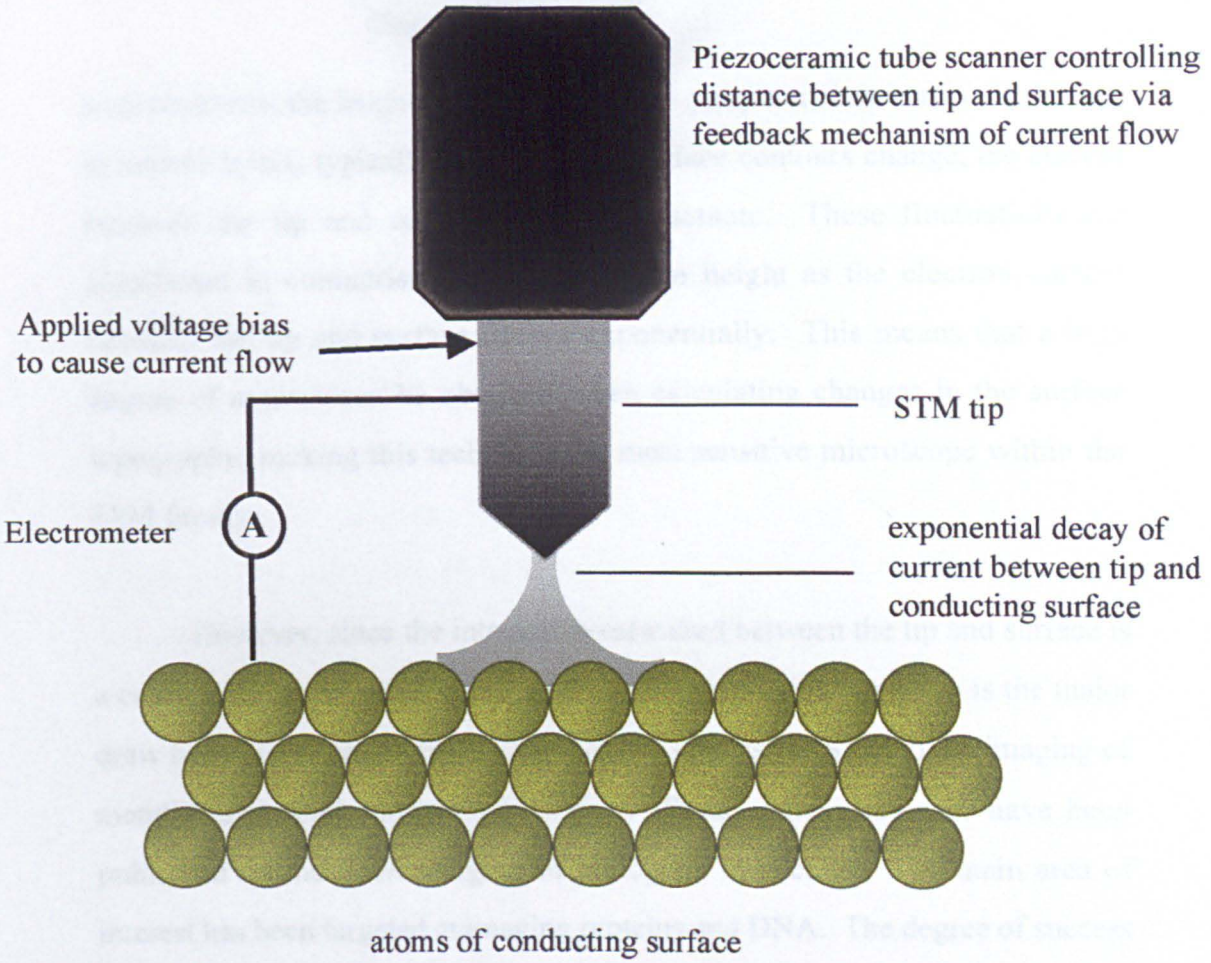

Figure 1.8 : A schematic representation of an STM

a constant rate, the height of the tip above the sample surface can be controlled to atomic levels, typically 10 Å. As the surface contours change, the current between the tip and surface will also fluctuate. These fluctuations are significant in comparison to the change in height as the electron current between the tip and surface decays exponentially. This means that a high degree of control can be obtained when calculating changes in the surface topography, making this technique the most sensitive microscope within the SPM family.

However, since the interaction measured between the tip and surface is a current, this means that the sample must be conductive and this is the major draw back of this technique. In the main this limits the STM to the imaging of metallic and semi-conductor materials. Some papers however have been published on the STM imaging of biological molecules. The main area of interest has been targeted at imaging proteins and DNA. The degree of success in the imaging of proteins can be attributed to their molecular folding, as both models and experimental investigations suggest that electron transport occurs down the peptide backbone, through hydrogen and sulfides bonds and through the hydration layer (Hopfield (1974), Beratan (1989), Amrein (1989), Gukenberger (1989), Stemmer (1989), Patel (1997)). Images of DNA have also been obtained utilising STM, where the phosphate backbone is suggested as the route of electron transport. However, the topographies of these images, obtained by various groups have been contradictory (Engel (1991)) and features which may be part of the adsorbed molecule on a surface, could just as likely be due to the surface itself as opposed to the biomolecule (Roberts (1994)).

The way in which the AFM overcomes this problem is by measuring the tip deflection as it scans over the surface, in a similar way to which a

record player needle scans over a record. The deflections in this case however are converted to an image of the surface. In early AFM instruments the tip deflections as it scanned over the sample surface were detected by the changes in current between the AFM tip and a STM tip positioned above the cantilever, as depicted in Figure 1.9 (a). Whilst being a very sensitive method of detection, severe difficulties were found in lining the STM tip directly above the AFM cantilever (Digital Instruments (1996)). Subsequently, an optical system of detection was invented as depicted in Figure 1.9 (b). By utilising a segmented photodiode both the up and down, and left and right movements of the laser beam reflected off the back of the tip containing cantilever can be monitored. The up and down movement is related to the topography, height changes of the surface; whereas the left \ right changes are characteristic of the frictional forces between the AFM tip and sample surface.

These early AFM instruments worked in contact mode, where the tip is in continuous contact with the surface of the sample. The feedback mechanism in contact mode is controlled in one of two ways. The first of these is known as constant height or variable deflection mode. In this system, the height of the cantilever above the surface remains constant, therefore as the topography of the surface goes up and down the deflection of the tip is either increased or decreased. The change in the reflection angle of the laser is recorded and converted to an image of the surface contours. In constant deflection or constant force mode, the deflection of the tip and hence the force felt between it and the sample are kept constant by moving either the tip or sample up or down. In this mode, it is these movements which are converted into the topography image (Lal (1994)).

Whilst useful for producing high resolution images of hard surfaces such as silicon and graphite, both theoretical calculations and experimental

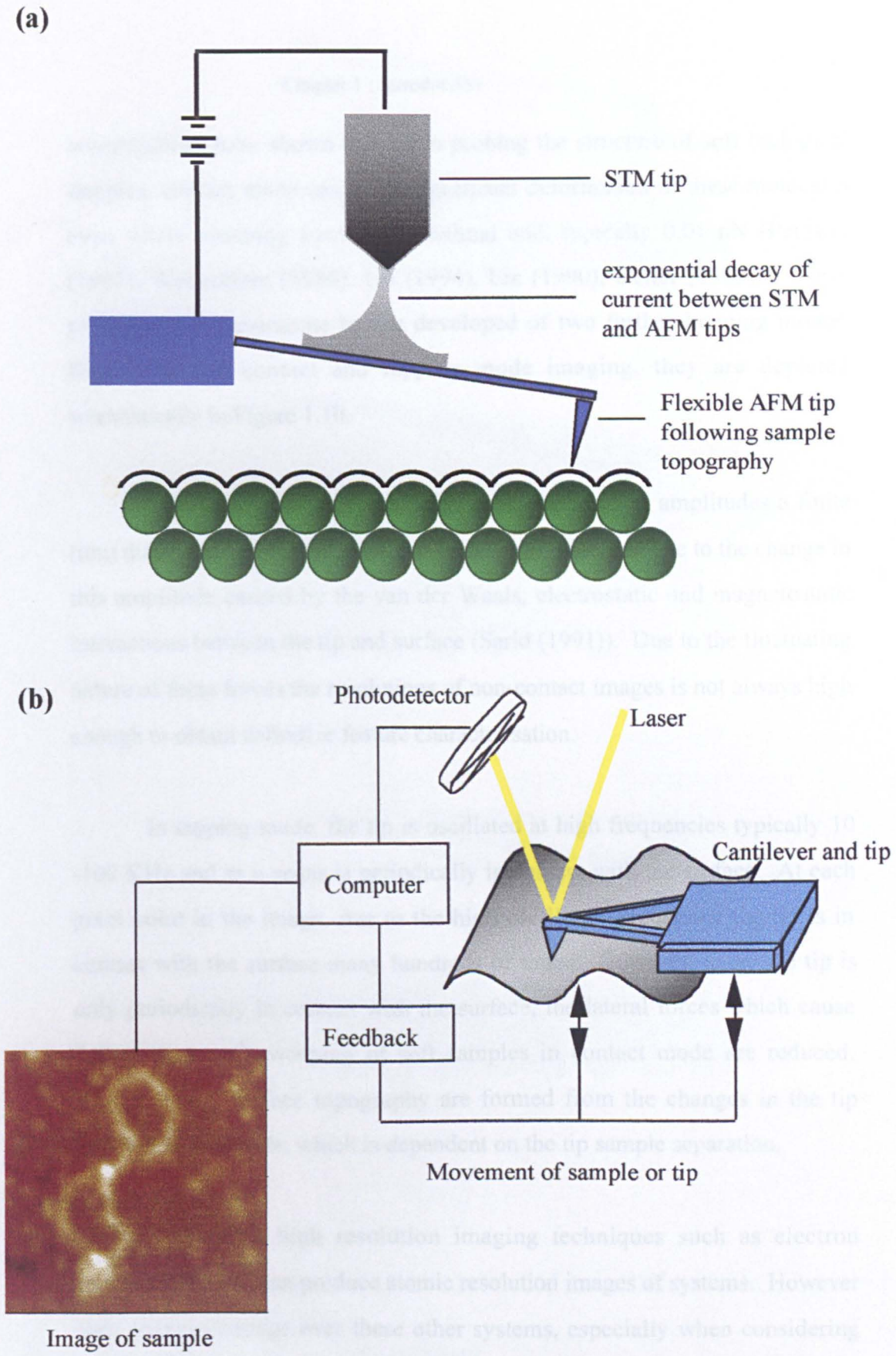

Figure 1.9 : A schematic representation of AFMs
(a) early
(b) present day

investigations have shown that when probing the structure of soft biological samples, contact mode can cause significant deformation of these molecules even where scanning forces are minimal and, typically 0.01 nN (Persson (1987), Weisenhorn (1989), Lal (1994), Lin (1990), Keller (1993)). These problems were overcome by the developed of two further imaging modes. Known as non-contact and tapping mode imaging, they are depicted schematically in Figure 1.10.

In non-contact mode, the tip is oscillated at small amplitudes a finite (nm) distance away from the surface. Images are obtained due to the change in this amplitude caused by the van der Waals, electrostatic and magnetostatic interactions between the tip and surface (Sarid (1991)). Due to the fluctuating nature of these forces the resolutions of non-contact images is not always high enough to obtain definitive feature characterisation.

In tapping mode, the tip is oscillated at high frequencies typically 10 -100 KHz and as it scans is periodically in contact with the surface. At each pixel point in the image, due to the high oscillation frequency the tip is in contact with the surface many hundreds of times. However, since the tip is only periodically in contact with the surface, the lateral forces which cause deformation and sweeping of soft samples in contact mode are reduced. Images of the surface topography are formed from the changes in the tip oscillation amplitude, which is dependent on the tip sample separation.

Like other high resolution imaging techniques such as electron microscopy, SPM can produce atomic resolution images of systems. However their main advantage over these other systems, especially when considering biological and medical samples, is that they can be performed at atmospheric pressure and temperature and under liquid. This means, biological samples can

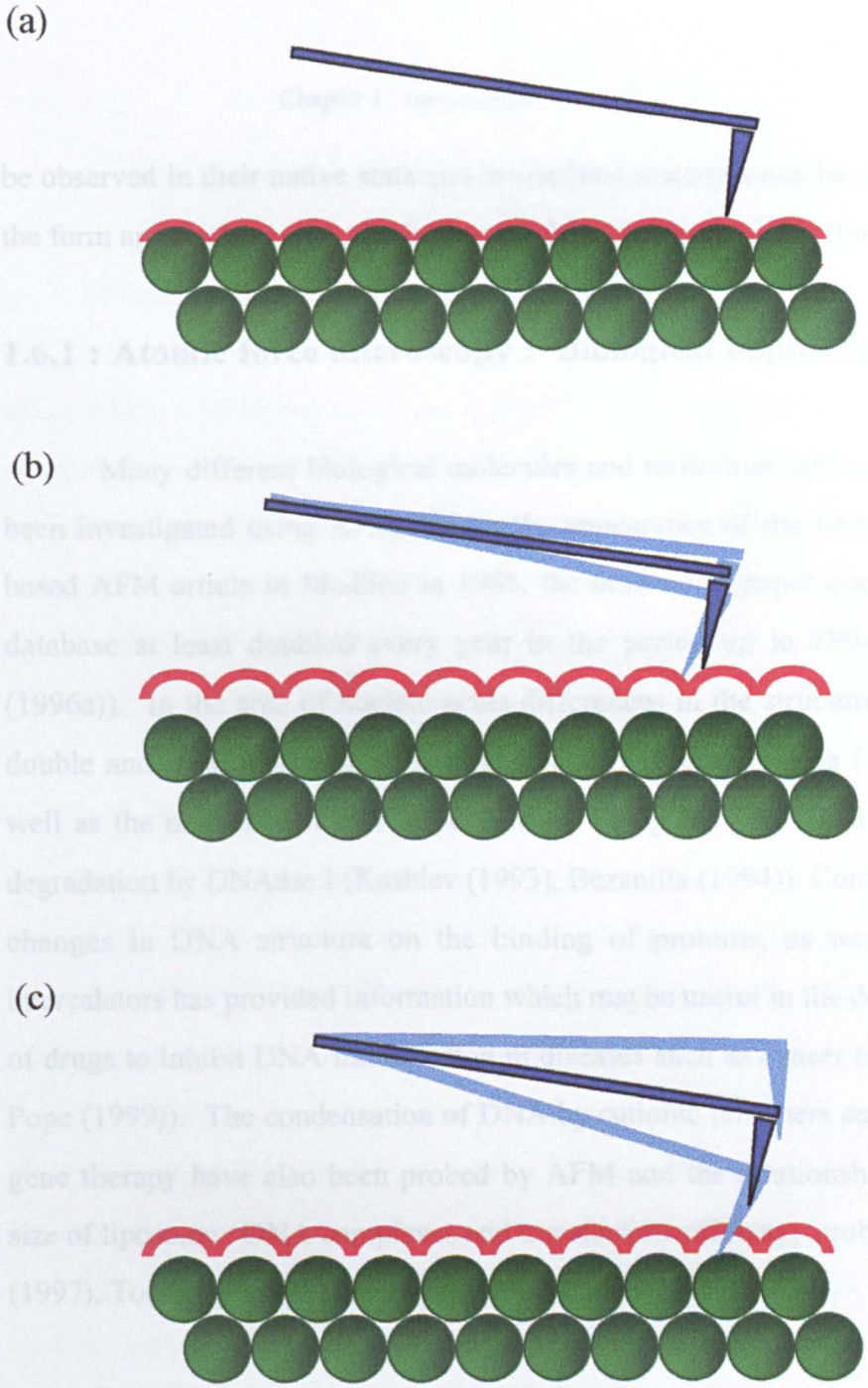

Figure 1.10 : Schematic repesentation of the different imaging modes in AFM

(a) contact
(b) non-contact
(c) tapping

be observed in their native state and biomedical materials can be observed in the form approaching that which they would be present in in the body.

1.6.1 : Atomic force microscopy : Biological applications

Many different biological molecules and molecular interactions have been investigated using AFM. Since the appearance of the first biological based AFM article in Medline in 1988, the number of paper quoted in this database at least doubled every year in the period up to 1994 (Hansma (1996a)). In the area of nucleic acids differences in the structure of single, double and triple stranded DNA have been observed (Hansma (1996b)), as well as the movement of RNA polymerase along its length and enzymatic degradation by DNAase I (Kashlev (1993), Bezanilla (1994)). Conformational changes in DNA structure on the binding of proteins, as well as DNA intercalators has provided information which maybe useful in the development of drugs to inhibit DNA transcription in diseases such as cancer (Erie (1994) Pope (1999)). The condensation of DNA by cationic polymers and lipids for gene therapy have also been probed by AFM and the relationship between size of liposome / DNA complexes and transfection efficiency probed (Dunlap (1997), Toncheva (1998) Kawaura (1998), Hart (1998)).

In the area of proteins, both soluble and membrane bound, their structure and interactions have been investigated using AFM. In 1994 Yang and co-workers showed a pentimeric structure of the pertussis toxin B subunit (Yang (1994)). It is interesting to note however, that the X-ray crystallographic structure of the same subunit depicts a seven domain triangle (Stein (1994)). These structural differences may have significant effect on the function of this molecule. This example shows that AFM can provide vital information on protein solutions structure which may help us understand the

function of these macromolecules more clearly (Shao (1996)).

Results from papers by Radmacher (1994) and Thomson (1996) suggest that the conformational changes in enzymatic proteins can be measured using AFM. For example, on the addition of a tetrasaccharide substrate for lysozyme to a monolayer of this protein, height fluctuations were observed to increase significantly. The conformational changes of another protein Laminin, have also been observed both in air and liquid. Laminin is a major basement membrane protein which possesses a crucifix like structure. The flexibility of the crucifix arms have been observed by the AFM (Chen, C. (1998)).

On the larger scale, imaging of a variety of cells have been obtained. Fixed or dried ethryocytes, neurons, cardiac myocytes and bacterial cells have been imaged (Gould (1990), Butt (1991a)). Imaging of these structures may in the future allow AFM to be used as a diagnostic tool for the identification of pathological conditions of tissues or cells (Hoh (1992)). The imaging of living cells is more difficult, as the resolution obtained is significantly dependent on cell type and its stage in the cell cycle. However, in some cases it has been reported that the imaging of these live cells does not, up to the resolution of the AFM appear to alter the integrity of the cell and intracellular components such as actin filaments and granula motion can be observed (Haberle (1991), Henderson (1992), Fritz (1994)).

A major interest to both the biologist and the drug delivery expert is the cell membrane. AFM imaging could provide significant information on the structure of this complex material, as well as providing an incite into the interaction of molecules with it. Lipid bilayers which mimic the cell membrane have been studied under aqueous conditions. Bilayers of dimyristoylphosphatidylethanolamine (DMPE) were showed by Zasadzinski

and co-workers to posses ridged structures with 0.7-0.9 nm spacings (Zasadzinski (1991)). Whereas, Yang and co-workers showed that the imaging force utilised to study langmiur-bloggett bilayer of phospholipids is important. The imaging force must be high enough to overcome the hydration force so the actual lipid surface is being probed, but not be so high that the delicate structure of the bilayer is disturbed and the layer swept away so only the underlying subtract is imaged (Yang (1994)). Images of streptavidin on biotinylated lipid monolayers were observed by Scheuring an co-workers at resolutions greater than 1 nm. The crystal structure of the streptavidin was also seen (Scheuring (1999)).

1.6.2 Atomic force microscopy : Materials applications

Many different polymers have been studied and molecular and sub-micron features resolved. The effect of processing on these polymers structure has also been elucidated.

The dynamic processes of the interaction of biomedical polymers has also been probed. Platelet attachment onto PE with resolution of the pseudopodia has obtained, along with the hydration of dextran monolayers and investigations into time dependence of fibrinogen adsorption to polystyrene films utilising a combined AFM-SPR instrument (Chen (1996), Frazier (1997b) Siedlecki (1998)). Shakesheff et al. showed that release of a model protein, albumin, from poly(ortho ester) films in an aqueous environment could be followed using AFM (Shakesheff (1995)).

A study by Lee and co-workers, utilised AFM in conjunction with scanning electron microscopy to follow the calcification process on porin bioprosthetics for implantation into the human heart. They showed that the

alteration of the surface structure of the valve is an important factor in the occurrence of calcification, as the calcific deposits were located in the surface defects of the valve (Vansteenkiste (1998)).

Thomson and co-workers showed the time dependence of the degradation of starch granules by α-amylase. The focal point for the degradation occurred at a site where the granule was already damaged (Thomson (1994)). Investigations such as these show the potential of AFM for following the release profile of macromolecular drugs from their polymeric transport vehicle, and time dependant biocompatibility of materials.

As well as being utilised to provide information on the surface topography and dynamic processes occurring at these surfaces, AFM can also be utilised to investigate the changes in the materials viscoelastic properties and the strength of interactions with other molecules gaining further information on the materials suitability for its intended purpose.

With the emergence of tapping mode AFM came the ability to produce phase images of surfaces. The theory behind phase imaging is represented schematically in Figure 1.11. In simple terms, phase images are produced when the tip feels an interaction with the surface as it scan. Depending on the strength of this interaction, there will be a varying degree of change when comparing the phase at which the tip is being resonated and the phase of the oscillation being detected by the feedback mechanism. The lag in the phase detected when compared to that of the applied resonance can be related to the interaction between the tip and the surface. This technique has been utilised to distinguish between polymers in a poly(sebasic anhydride) / poly(lactic acid) blend by Chen and co-workers where as Kaiyama et al. investigated the phase separation of a polystyrene / poly(vinyl methyl ether) system and the

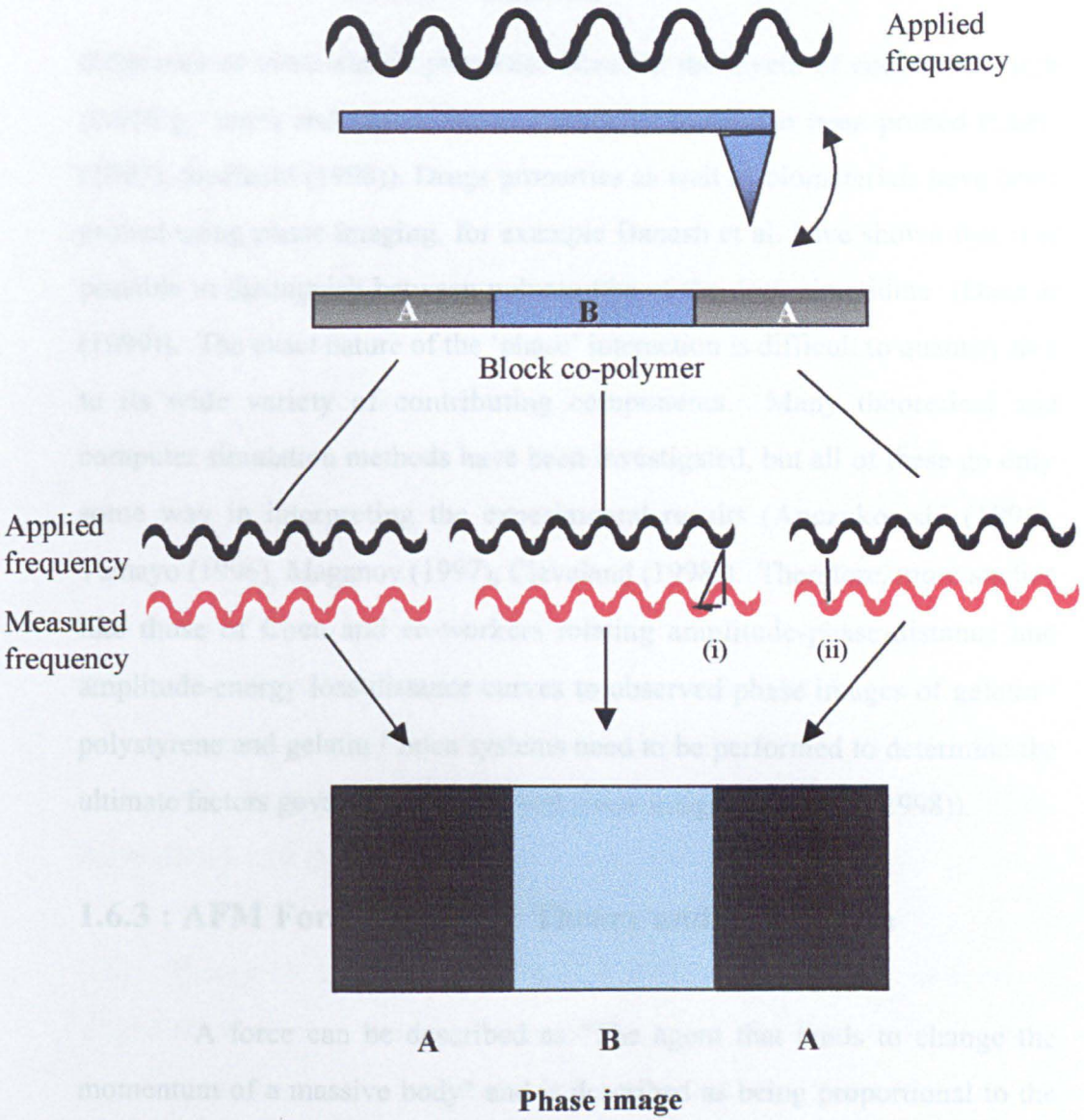

Figure 1.11 : Schematic representation of the acquisition of a phase image

(i) Significant interaction is observed between the tip and polymer B, therefore a large lag is observed when comparing the applied and measured frequencies. This is manifested as region of significant phase difference in the image

(ii) Minimal interaction is observed between the tip and polymer B, therefore only a small lag is observed when comparing the applied and measured frequencies. This is manifested as region of minimal phase difference in the image

difference of visco-elastic properties between the layers of coextruded high (0.956 g / cm^3) and low (0.922 g / cm^3) PE have also been probed (Chen (1997), Siedlecki (1998)). Drugs properties as well as biomaterials have been probed using phase imaging, for example Danesh et al. have shown that it is possible to distinguish between polymorphs of the drug cimetidine (Danesh (1999)). The exact nature of the 'phase' interaction is difficult to quantify due to its wide variety of contributing components. Many theoretical and computer simulation methods have been investigated, but all of these go only some way in interpreting the experimental results (Anczykowski (1996), Tamayo (1996), Maganov (1997), Cleveland (1998)). Therefore, more studies like those of Chen and co-workers relating amplitude-phase-distance and amplitude-energy loss-distance curves to observed phase images of gelatin / polystyrene and gelatin / mica systems need to be performed to determine the ultimate factors governing the observed phase images (Chen, X. (1998)).

1.6.3 : AFM Force-distance : Theory and application

A force can be described as "The agent that tends to change the momentum of a massive body" and is described as being proportional to the rate of increase of momentum. According to Newton

$$F = m.a$$

Force = Mass . acceleration

(Equation 2)

(Minidictionary of Physics (1988))

When considering forces at the molecular level, molecules can be thought of as springs, and their intra-molecular vibrations as oscillations of the

spring. As such they approximate to the laws of harmonic motion and any force which displaces them from their equilibrium state can be defined in terms of Hookes law which states that

$$F = -d \cdot k$$

Force = - displacement . spring constant

(Equation 3)

The spring constant is a constant of proportionality and is related to the rigidity of the molecule. The displacement is signified as a negative value this can be attributed to the fact that for every action there is an equal and opposite reaction. For example, if the molecule is displaced to the right, a force pulling the molecule to the left back to its equilibrium position will be felt by the molecule (Atkins (1990)).

Forces are important at all levels, from maintaining atoms within a crystal structure to ensuring aeroplanes stay in the air. For example, a cells structure and function is regulated by the interaction of different materials. Its cytoskeleton is formed from a multitude of proteins whose interactions regulate a cells mechanical an topological properties. The cells movement within the body is regulated by the formation and breaking of interactive forces between adhesion molecules (Humer (1999), Murray (1999)). On binding these and other molecules to receptors, a cascade of events which alter the cellular processes and are comprised of the interaction of differing molecules is initiated. Indeed, it was quoted by Creighton that "the biological function of proteins almost invariably depend on their direct physical interactions with other molecules" (Creighton (1993)).

To experimentally measure the force of interactions between molecules a range of techniques have been utilised. These include immunoassay based methods (Phizicky (1995), X-ray crystallography (Perutz (1992)), NMR (Wüthrich (1992)), surface force apparatus and (Tabor (1969), Claesson (1996), optical traps (Svoboda (1994) Grier (1997), pipette suction (Leckband (1994)) and as elucidated to above, AFM. However, most of these techniques are limited by either sensitivity or spatial resolution. The AFM on the other hand can measure forces as low as 10^{-15} N and due to the sharpness of the AFM tip employed, contact areas can be as low as 10 nm^2 (Butt (1991b)).

In AFM force measurements the deflections of a soft cantilever (typically with a spring constant of approx. 100 mN / m) to which the molecule of interest is attached, is directly proportional to the force felt by the molecule on unbinding from its interaction with the surface. The relationship between the force of the unbinding process and the deflection of the cantilever as introduced above is Hookes law (equation 3). In this case the constant of proportionality is the spring constant of the tip, which can be determined experimentally by a variety of methods (Hutter (1994), Butt (1993), Florin (1995)).

Figure 1.12 provides a schematic representation of the results obtained from a single force distance curve. In such an investigation, as can be observed from this figure the tip and sample are brought into contact at a constant velocity. The point of contact between the two is signified by a sharp change in the deflection of the cantilever, which whilst the tip and sample are separate remains constant. The constant tip deflection whilst the tip and sample are separate is known as the rest position or zero cantilever deflection and the point of contact occurs when the attractive (electrostatic and / or Van der

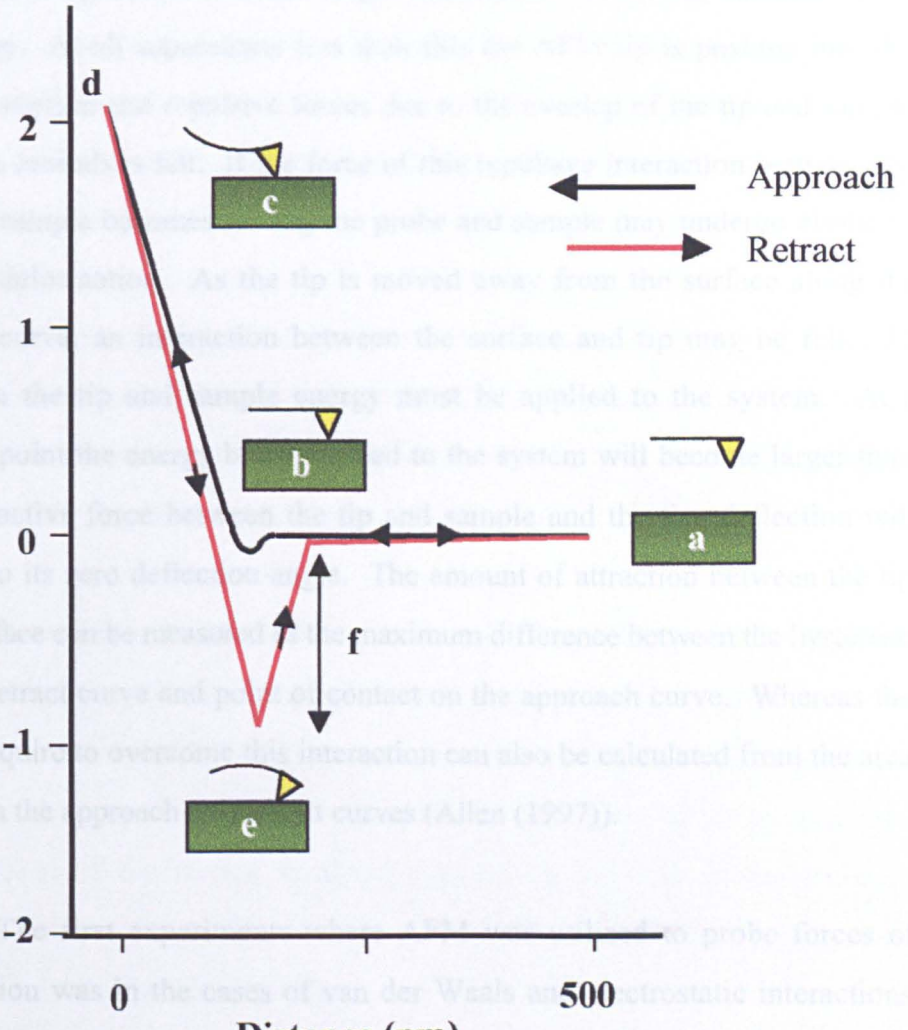

Figure 1.12 : A schematic representation of typical AFM force distance curve

(a) Tip and sample separate - zero deflection
(b) Point of contact between tip and surface
(c) Contact region of curve
(d) Maximum contact force
(e) Attraction between tip and surface
(f) Maximum adhesion force

Waals) force gradient becomes larger than that of the spring constant of the AFM tip. At all separations less than this the AFM tip is pushing into the sample surface and repulsive forces due to the overlap of the tip and sample electron orbitals is felt. If the force of this repulsive interaction between the tip and sample becomes too big the probe and sample may undergo elastic or plastic deformation. As the tip is moved away from the surface along the retract curve, an interaction between the surface and tip may be felt. To separate the tip and sample energy must be applied to the system. At a certain point the energy being applied to the system will become larger than the attractive force between the tip and sample and the tips deflection will return to its zero deflection angle. The amount of attraction between the tip and surface can be measured as the maximum difference between the hysteresis of the retract curve and point of contact on the approach curve. Whereas the work require to overcome this interaction can also be calculated from the area between the approach and retract curves (Allen (1997)).

The first experiments where AFM was utilised to probe forces of interaction was in the cases of van der Waals and electrostatic interactions (Ducker (1991)). The first measurement of a discrete force was by Hoh and co-workers in 1993 where they describe the measurement of discrete forces of 10 pN (Hoh (1993)). They attribute this to the breaking of a single hydrogen bond. The measurement of force, especially discrete ones has now developed into a field of its own, complementing both AFM imaging studies and results obtained from other techniques such as SPR.

The majority of papers published on measuring specific interactions utilising the AFM have been centred on the interaction between the tetrameric protein streptavidin and vitamin K, which is also known as biotin. This interaction will be dealt with in more detail in Chapter 4. The biotin avidin

bond is the strongest known naturally occurring non-covalent bond and has been studied in detail both structurally and thermodynamically (Tao (1992), Radmancher (1995)). The first AFM force-distance experiments performed utilising the streptavidin biotin interaction were performed independently by Lee and Florin. Lee and co-workers utilised biotin functionalised beads and streptavidin coated surfaces, where as Florin et al. utilised biotinylated agrose beads and avidin coated AFM tips (Florin (1994), Lee (1994a)). More recent investigations have shown that AFM force distance measurements can distinguish between interaction of different biotin and streptavidin analogues (Chilkoti (1995b), Dammer (1995)).

GroEL is a protein whose function is to stabilise partially unfolded proteins during the early stages of biosynthetic pathways. The forces of interaction between this molecule and proteins in unfolded and native states was found by Vinckier et al. to be significantly dependent on the protein state. In the case of the citrate synthase enzyme an increase in the force of interaction from 420 to 770 pN was observed when comparing the native and denatured form (Vinckier (1998)).

As well as the binding of substrates to proteins, the interaction between individual DNA base pairs and complementary and non-complementary DNA strands have been investigated (Boland (1995), Ikai (1997)). The unfolding, as well as rupturing of bonds can be measured by AFM. The large protein titin was reversibly unfolded using AFM by Rief and co-workers. They observed multiple interactions being broken, the separation of these in the retract curve was 25 nm. This saw-tooth like retract curve was attributed to the denaturing of successive immunoglobulin domains (Rief (1998)).

The stiffness of surfaces can also probed by AFM force-distance analysis. The slope of the contact area of the force distance curve becomes shallower as the samples surface becomes softer. Frazier et al. utilised theory to follow the change in stiffness of a dextran monolayer as it was hydrated (Frazier (1997)).

As well as being used to gather point information on the extent of interaction between the tip and surface, maps of the extent of interaction can be obtained. Allen et al. showed that utilising a biotin coated probe the surface coverage of an immunoassay well by streptavidin could be probed (Allen (1998)). Hinterdorfer utilised AFM probes attached to antibodies via relatively long molecular tethers to determine the spatial distribution of immobilised antigens (Hinterdorfer (1996)). The use of AFM to map forces of interactions has many potential applications, such as the high throughput screening of combinatorial drug libraries.

Because of the biomedical bias of this thesis, the examples of AFM applications shown here have been of the biological nature. However, the SFM family have applications in a wide variety of fields. Examples, of their uses include the movement of atoms, with the potential of actually building arrays of atoms or molecules for the next generation of computers (Hansma (1989), Clery (1992)), chemically mapping the distribution of functional groups on a surface (Frisbie (1994)). As well as many investigations into the effects of friction, wear and lubrication on a variety of material surfaces. These type of investigations are equally important to those in the biological field as they provide information into the mechanical failure of materials, which can cost, and potential improvement of these materials, which could save significant amounts of money in the industrial sector per annum (Bhushan (1995)).

1.7 : Surface plasmon resonance : Theory

Surface plasmon resonance, or SPR is a surface analytical technique which provides the opportunity to characterise many surface dynamic phenomena *in situ,* without the need for additional parameters such as the labelling molecules.

The SPR instrument is based on the interaction of a laser bean with a noble metal film. A schematic representation of the interaction between the laser and metal film is depicted in Figure 1.13. A metal can be thought of as an array of nuclei surrounded by a sea of electrons. The electrons at the metal surface are free to oscillate and do so at a specific frequency. If the wave vector of an incoming laser beam is the same as that of the oscillation of these surface electrons, instead of the laser energy being either totally or partly internally reflected, depending on whether the incidental angle is less than or greater than the critical angle respectively, it will be adsorbed by these surface electrons so they can resonate. The energy of these resonating electrons is propagated along the surface forming a so called surface plasmon wave (Salamon (1996a)). It is from this effect that the technique derives its name, the **surface** electrons or **plasmons** are being caused to **resonate**. The frequency at which the surface electrons resonate is not only a property of the metal, but also of the dielectric properties of material in contact with the metal surface. However, the energy of the surface plasmon wave decays exponentially away from the surface of the metal film. Therefore, only those materials in the direct proximity to the film (a few 100 nm) can influence the frequency of the electrons oscillations making this surface, not bulk sensitive technique. In general, the metal of choice for SPR is silver or gold, a film of which, typically 20-50 nm thick is coated on to either glass or mica support (Davies (1994)).

Incoming laser light is the same energy and phase as that of the free oscillation of the surface plasmons, therefore light energy is converted into movement and surface plasmons resonate. Energy is dissipated by causing neighbouring atoms to resonate and hence forming a surface plasmon wave

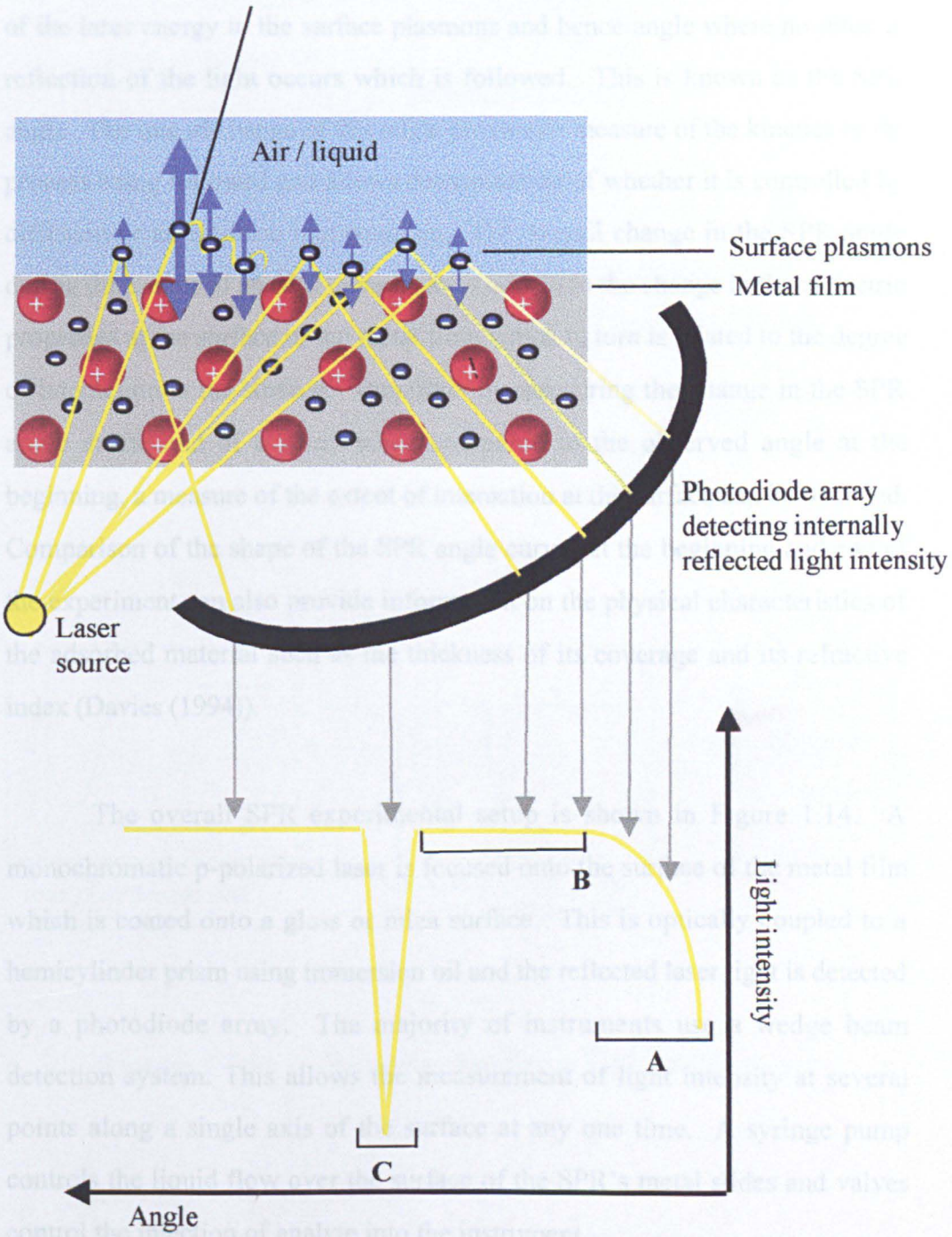

Figure 1.13 : Schematic representation of an the SPR effect

A : internally reflected light intensity increase with angle
B : Critical angle above which all light is totally internally reflected
C : SPR angle

During the course of an SPR experiment, it is the angle where coupling of the laser energy to the surface plasmons and hence angle where no internal reflection of the light occurs which is followed. This is known as the SPR angle. The rate of change of this angle provides a measure of the kinetics of the process being followed and allows determination of whether it is controlled by diffusion or an intrinsic rate equation. The overall change in the SPR angle during the course of an SPR experiment is related to the change in the dielectric properties at the surface of the metal film, which in turn is related to the degree of interaction at the surface. Therefore, by measuring the change in the SPR angle at the end of a study when compared to the observed angle at the beginning, a measure of the extent of interaction at the surface can be obtained. Comparison of the shape of the SPR angle curves at the beginning and end of the experiment can also provide information on the physical characteristics of the adsorbed material such as the thickness of its coverage and its refractive index (Davies (1994)).

The overall SPR experimental setup is shown in Figure 1.14. A monochromatic p-polarized laser is focused onto the surface of the metal film which is coated onto a glass or mica surface. This is optically coupled to a hemicylinder prism using immersion oil and the reflected laser light is detected by a photodiode array. The majority of instruments use a wedge beam detection system. This allows the measurement of light intensity at several points along a single axis of the surface at any one time. A syringe pump controls the liquid flow over the surface of the SPR's metal slides and valves control the injection of analyte into the instrument.

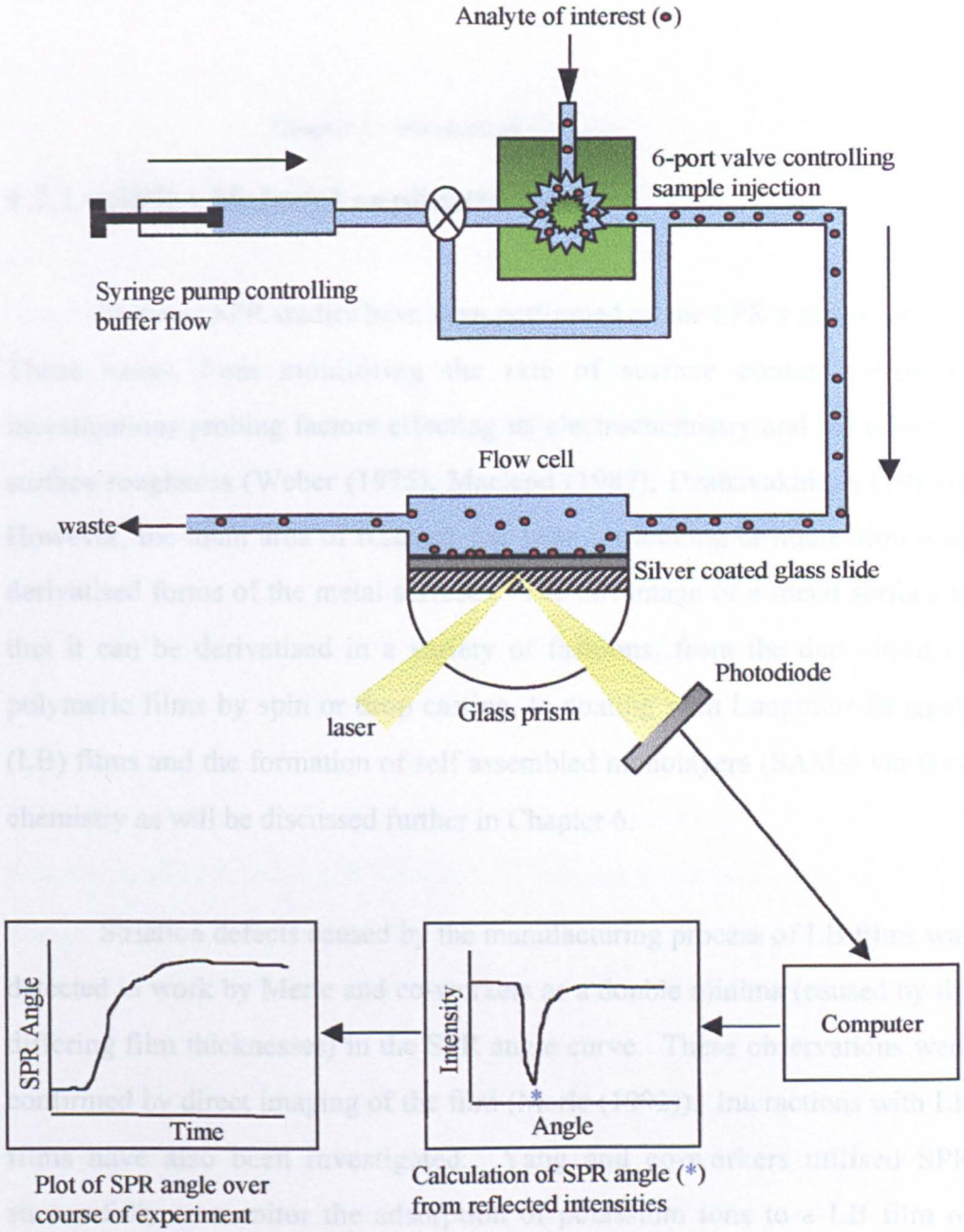

Figure 1.14 : A typical setup for a SPR Instrument

1.7.1 : SPR : Material applications

Previous SPR studies have been performed on the SPR's metal surface. These range from monitoring the rate of surface contamination to investigations probing factors effecting its electrochemistry and the effect of surface roughness (Weber (1975), Macleod (1987), Dzahavakhidze (1989)). However, the main area of research has been on looking at interaction with derivatised forms of the metal surfaces. The advantage of a metal surface is that it can be derivatised in a variety of fashions, from the deposition of polymeric films by spin or drop casting, to coating with Langmuir-Bloggett (LB) films and the formation of self assembled monolayers (SAMs) via thiol chemistry as will be discussed further in Chapter 6.

Striation defects caused by the manufacturing process of LB films was detected in work by Merle and co-workers as a double minima (caused by the differing film thicknesses) in the SPR angle curve. These observations were confirmed by direct imaging of the film (Merle (1992)). Interactions with LB films have also been investigated. Yang and co-workers utilised SPR successfully to monitor the adsorption of potassium ions to a LB film of valinomycin (Yang (1992)).

In the field of polymeric materials, SPR has been used to investigate polymer adsorption (Green (1997)), self assembly (Advincula (1996)), as well as the degradation and hydration properties of polymeric interfaces (Chen (1995), (1996), Green (1996), Frazier (1997a) (1997b)). During the hydration of a polymer, water absorption results in a reduction in the refractive index of the polymer film and an increase in polymer film thickness. Green et al., have shown that the net effect of these two processes results in a reduction in the SPR angle shift upon hydration. This work showed that for segmented

polyurethanes containing poly(ethylene oxide) (PEO) / poly(propylene oxide) (PPO) of varying PEO / PPO ratios, that as the PEO content of the polymer increases (ie. as the hydrophilicity increases) the extent of polymer hydration increases also (Green (1996)). In addition to studies in a liquid environment, film swelling dynamics for the incorporation of methanol into poly(methyl methacrylate) films have been investigated within a gaseous environment (Drake (1995)).

SPR can be used in conjunction with AFM to provide complementary information on a polymeric system. In Shakesheff and co-workers investigations, an SPR was interfaced to an AFM forming a combined SPR/AFM instrument. This instrument could measure both the kinetics of a polymer surface erosion and visualise the structural changes occurring to the film surface at the same time. This allows the inter-relationship between these two variables to be directly analyzed (Chen (1995), (1996)).

Heparin binding polymers have the potential to be used as extracorporeal filters to remove heparin from blood following therapeutic use. The interaction of model plasma proteins with heparinized surfaces of such polymeric materials has been investigated (Frazier (1996), Van Delden (1997)).

Non-specific protein interactions with a biomaterial can lead to its failure in its role due to poor biocompatibility. Of late, there has been increased documentation of the use of SPR to monitor non-specific protein adsorption. Zenhausern et al. have looked at the adsorption of fibronectin to titanium dioxide surfaces, using SPR as a complementary technique to AFM (Zenhausern (1993)).

Mrksich et al. have illustrated the use of SPR to probe the protein

resistance of SAMs of alkanethiols with oligo(ethylene glycol) end groups. Utilising mixed SAMs comprised of alkanethiols terminated in either oligo(ethylene glycol) or methyl groups, they showed that by increasing the mole fraction of oligo(ethylene glycol) terminated alkanethiols a decrease in non-specific protein adsorption occurred (Mrksich, (1995)).

The factors effecting protein adsorption at polymer interfaces was investigated by Green and co-workers on a model PS substrate. In their investigations they studied the effects of protein type, solution flow rate and protein solution concentration on adsorption. Furthermore, they showed that the thickness of an adsorbed monolayer of protein is dependent on the size and shape of the protein, as well as the ordering of the protein layer at the interface. In more recent investigations the same group have probed the competitive adsorption of proteins from complex protein solutions, such as plasma and used specific antibodies to detect the surface concentration of particular proteins (Green (1997a)).

The efficiency of the Pluronic™ polymers (PEO/PPO/PEO triblock copolymers) which are specifically designed to inhibit protein adsorption have also been investigated, utilising AFM as a complementary tool to SPR (Green (1997b), (1998)). When investigating the effect of both PPO and PEO molecular weight, it was found that the amount of protein adsorbed to the surfaces could be related to, firstly the strength of binding of the co-polymer to the underlying hydrophobic polystyrene surface (related to the PPO block size) and secondly, to the length of the extending PEO chain.

The application of SPR to determine levels of gases via adsorption to modified slides has been shown by Liedberg and O'Donnell for halothane and NO_2 respectively (Liedberg (1983), O'Donnell (1991)). Experiments of this

type suggest that SPR maybe useful as a technique for monitoring environmental levels of dangerous gases.

1.7.2 : SPR : Biological applications

In the biological field, the main use of SPR is to study interactions, for example antibody-antigen, DNA hybridization, and interactions with cell adhesion molecules (Van der Merwe (1996), Bates (1995), Buckle (1996), Schuck (1997), Bondeson (1993), Fisher (1994)). The relative affinity constants of a variety of viral antibodies has been determined by SPR, and this technique was shown to be a quicker and as efficient as conventional immunoassay methods (Pellequer (1993)). Monoclonal antibodies immobilised on the SPR surface have been utilised by Brigham-Burke et al. as a rapid method for determining the optimum conditions for immunoaffinity chromatography (Brigham-Burke (1993)).

The two main methods for synthesising lipidic surfaces is either transfer of LB films or the production of SAMs comprised of either thiol-lipids or a hybrid SAM bilayer (Tamm (1985), Plant (1995)). The lipidic surfaces studied by Plant and co-workers were synthesised utilising the hybrid SAM bilayer technique. Surfaces were formed from an octadecanethiol SAM surface, with a 1-palmitoyl, 2-oleoyl phosphatidylcholine (POPC) lipid layer on top of this. They found these lipidic layers were stable under the flow conditions of the SPR experiments for at least 15 h and minimal nonspecific binding of proteins to them was observed. On the addition of a biotinylated lipid to the vesical from which the lipidic layer is formed, whilst non specific binding remained low, on the addition of neutra-avidin, a protein which has specific binding sites for biotin, a significant level of binding to the lipid surface occurred. This shows that specificity can be built into these lipidic

surfaces (Plant (1995)).

Bunjes and co-workers formed their lipid surfaces on a thiolated peptide layer, which had been previously deposited as a SAM on the metal surface of the SPR slide. The carboxyl termini of these peptide chains were then activated and coupled to dimyristoylphospatidylethanolamine (DMPE) to form a phospholipid-like surface. This surface was then interacted with phosphatidylcholine (PC) liposomes to form a lipid bilayer. Results for the increase in layer thickness on the addition of DMPE obtained from SPR corresponded well with X-ray reflectometry data. On addition of the PC liposomes an increase in layer thickness of 2.6 nm was observed. This is in close correlation to the theoretical value of 2.5 nm for a monolayer of PC. This suggests a discrete lipid layer, with minimal nonspecific binding or binding of closed vesicles has occurred. When PC liposomes containing ATPase were deposited on the DMPE surface proton transport across the membrane could be detected (Bunjes (1997)).

A significant amount of the investigations into lipidic membranes and the use of SPR to study them has been carried out by Salamon and co-workers. The have shown that altering the ratio of lipid types in a lipidic surface can alter its conformation as well as the association of lipid membrane proteins to the layer (Salamon (1997)). They have also studied the effect of protein concentration, bilayer composition and ionic strength on the binding isotherms of cytochrome c an essential protein in the mitochondria respiratory electron chain to such surfaces (Salamon (1996a)). The interaction of cytochrome c with cytochrome oxidase and rhodopsin and transducin were probed by this group as examples of a membrane bound enzyme-substrate interaction and receptor ligand interaction respectively (Salamon (1996b), Salamon (1996c)).

Kai and co-workers have shown that a specific double stranded DNA product of PCR, which possesses a single stranded 3' terminus can be selectively and quantitatively identified by SPR. The gene they utilised for their target DNA was that of the verotoxin from E. coli. They suggest that this method maybe useful as a rapid detection system for the presence of this toxin (Kai (1999)).

1.8 : Aims of thesis

As discussed in the above sections surface analytical techniques can be utilised to build up a detail picture of both biomaterials and biological systems. This thesis aims to obtain information on a range of biomedical material systems surfaces by using the techniques described in sections 1.5 - 1.8 in a complementary fashion. A further aim is to relate the information obtained from techniques probing the surface chemistry of the biomedical material to those results obtained from techniques which probe the materials interactions with other biomolecules and in turn, these interactions to the materials potential efficiency within a chosen application.

The experimental chapters 3 and 4 will concentrate on a range of polymeric materials which have been proposed as candidates for producing scaffolds for tissue engineering applications. Chapter 3 summarises a detailed analysis of the surface chemistry of these polymers obtained from XPS and ToF-SIMS. In Chapter 4, both the specific and non-specific interactions of these polymer systems as determined by SPR and AFM is discussed and results obtained related to those seen in Chapter 3.

The structure of drug delivery vehicles when associated with their carrier drug is an important factor in the efficiency of the system in delivering

the active moiety successfully. In Chapters 5 and 6 the interaction between DNA and polymeric and lipid carriers respectively are investigated. The work in Chapter 5 probes the interactions between a cationic polymer and DNA. The effect of adding varying molecular weight PEG to the cationic polymer on the formation and structure of the resultant gene delivery complex was also probed by AFM and SPR.

Chapter 6 's work forms a basis for understanding the interactions of a lipidic based gene therapy vector with the cell membrane. As a first step towards this goal self assembled monolayers (SAMs), whose structure and formation will be discussed further in this chapter were utilised to immobilise the gene therapy complex. This provides an opportunity to investigate the effect of differing surface chemistries on the gene therapy complexes and its constituent parts (DNA and cationic liposomes) bound conformation.

The final experimental chapter, Chapter 7 follows a similar rational to that of Chapter 6, however, the delivery system under investigation this time is a range of dendrimeric polymers. The investigations summarised in this chapter again uses SAMS to probe the factors influencing the dendrimers surface interactions. This work which utilises SPR and AFM in both imaging and force-distance modes to provide a basis for understanding these polymeric materials interactions with both drugs and the cell surface.

The examples of biomedical polymeric systems and the range of techniques described in this thesis, aim to provide not only an overview of the detailed picture that can be formed of a systems surface utilising the discussed surface analytical techniques, but also highlight the wide range of applications of polymers in the biomedical setting and the relevance of studies such as those described herein to their development.

Chapter 2 : Experimental procedures

2.1 : Materials

All materials, unless otherwise stated where purchased from Sigma-Aldrich (Poole, England) and used without further purification. Solvents utilised were of HPLC quality and obtained from Fisher (Loughborough, Leicestershire, UK). Buffer solutions were made from salts purchased from sources as stated at 99.9% purity and deionized water obtained from a Elga Maxim system (Lane End, High Wycombe, Bucks., UK.) with water of conductivity on average 15 Ωcm.

2.2 : SPR analysis

The SPR instrument utilised in all investigations was of a Kretschmann configuration with a monochromatic laser source of 780 nm wavelength (Ortho-Clinical Diagnostics, Chalfont St. Giles, Bucks, UK.). Glass SPR sensor slides coated with an approximately 50 nm silver layer on one surface were used as a basis for all experiments (Ortho-Clinical Diagnostics, Buckinghamshire, UK.). In cases, where these were to be utilise to investigate the interactions with polymeric films, films were cast on using a home-built spin-coater formed from a modified drill. The spin speeds of the spin coater were calibrated and a speed of 2,000 rpm was used to cast the films onto the silver surface of the slides.

Four pixel points were identified in each of the channels in the SPR head from which the stable minima in light intensity, termed the SPR angle (in millidegrees; mDA) was determined by a photodiode array. This angle was recorded at each of the pixel points throughout each SPR experiment by computer software controlling the instrument (Ortho-Clinical Diagnostics, Bucks, UK.) and a plot of SPR angle versus time produced for each

experiment.

In-house software electronically regulated rheodyne type 6-port valves, which were employed to inject samples and regulate fluid flow. At the beginning of each SPR experiment a stable baseline reading of the liquid media was obtained, by flowing it across the SPR sensor slide surface. 1 ml injection volumes of the analyte whose interactions were to be investigated were used and analyte samples were prepared in the same buffer as that used for the liquid media. The media flow rate remained constant at 0.240 ml / min unless otherwise stated. After each completed injection, a buffer wash period of 300 sec (unless otherwise stated) was carried out to remove all analyte molecules not strongly adsorbed to the surface. All experiments were carried out at ca. 34.4 °C and temperature was controlled by a heated block integral to the instrument.

Each experiment was repeated a minimum of two times and average and standard deviation for SPR angle change of the period of the experiment as well as the rate of SPR angle change was calculated by software supplied by Ortho-Clinical Diagnostics (Ortho-Clinical Diagnostics, Bucks, UK.). A minimum of 12 pixel points were utilised to calculate the average and standard deviations.

2.3 : AFM imaging

All AFM images shown in this thesis were obtained from a multimode SPM, with a Nanoscope IIIa controller (Digital Instruments, Santa Barbara, CA, USA) utilising a vertical engage E scanner (10 x 10 x 2.5mm). Unless otherwise stated Tapping mode™ was utilised to obtain the images. In air, single beam TESP silicon cantilevers with integrated tips (Digital Instruments, Santa Barbara, CA, USA) with resonant frequencies between 250 - 278 kHz

were employed. However, in liquid 100 mm long triangular silicon nitride with a nominal spring constant of 0.38 N/m and integrated oxide sharpened tips were utilised. These cantilever was acoustically excited at approximately 10 kHz, close to its resonant frequency in aqueous conditions to obtain images.

2.4 : AFM force-distance measurements

AFM adhesion force measurements were obtained using a home built instrument known as a large scanning - AFM (LS-AFM) (Lomas (1999)). Sharpened (NP-S) nanoprobe tips (Digital Instruments, Santa Barbara, CA, USA) were utilised as derivatised as described in Chapters 4, 5 and 7. All force measurements were performed in an aqueous environment in media which had been filter through 2 μm filters (Sartorius AG, Gothiger, Germany). Measurements were performed at a constant speed of 1μm / s unless otherwise stated. In all experiments, probe integrity was checked before each stage of the experiments in control procedures described in the text of chapters 3, 5 and 7. Within the same study, the probe-sample contact forces were maintained at a constant level (typically 2-3 nN), with the aim of reducing errors due to differences in probe-sample contact area and minimising damage to tip or sample. Samples were held in position during the experiment by magnetic disks, to which they were attached by Tempfix™ (Agar Scientific, Stanstead, Essex, UK.).

Raw force data was obtained as cantilever deflection (nA) versus displacement of the z-piezo (nm). Cantilever deflection (nÁ) was first converted to a deflection distance (nm) using the gradient of the linear portion of the retract trace (Lee (1994)). Using the cantilever spring constant (k), and Hooke's Law (F = kd), the cantilever deflection was converted to force (nN). The spring constants of individual cantilevers were determined using software on a Dimensions 3000 instrument with Nanoscope IIIa controller (Digital

Instruments, Santa Barbara, CA, USA). The horizontal distance axis (nm) was converted from z-piezo displacement to probe-sample separation by subtracting the cantilever deflection distance (nm) from the z-piezo displacement for every data point in each force curve. In some cases this calculation was carried out by hand and in others, in-house software written by A. Moore and S. Kitching was utilised. The consistency of results obtained from the two techniques was checked by analysing randomly selected data by both methods. In all cases, the results obtained were not significantly different.

2.5 : ToF-SIMS analysis

ToF-SIMS analysis was undertaken using a Phi 7,200 instrument (Physical electronics, Eden Prairie, MN. USA) utilising a Cesium as the primary ion source. The total dose per sample did not exceed 1.6×10^{12} ions / cm^2. The polymeric samples for SIMS analysis were cast onto aluminium foil coated sample studs as described in Chapter 3.

ToF-SIMS analysis of patterned polymer samples prepared as described in Chapter 3 were performed on the same instrument. However in this case the primary ion used was Gallium, step size was 2.2 ns and the ion dose over a 100 μm scan was no greater than 4.9×10^{12} ions / cm^2.

2.6 : XPS analysis

XPS analysis of polymeric materials was performed on a VG Escalab Mk 2 electron spectrometer (VG scientific, East Grinsted, Sussex, UK) utilising a monochromatic Al Kα (1486.7 eV) X-ray source. The electron gun was operated at 200 W and the take-off angle to the spectrometer was 35°

from the surface plane. Wide scans over 500 eV were obtained to check for contamination of the polymer surfaces. Whilst narrow scans of 10 eV were obtained over the regions of the C1s and O1s envelopes to determine the contribution of the different chemical environments of these electrons to the materials surface composition.

Silicon wafers coated in the polymeric materials as described in Chapter 3, were attached to sample studs using double sided tape. The resulting spectra peak areas were determined using the instruments software. Carbon / Oxygen ratios were derived taking into consideration the relative intensities of the elements using F1s as a standard mark (relative intensity = 1). The relative intensities of the peak of interest C1s and O1s are 0.25 and 0.66 respectively.

Chapter 3 : Polymers for tissue engineering : Surface characterisation

3.1 : Introduction

3.1.1 : The need for tissue engineering

Through the collaboration of engineers and life scientists, a new field of research has been developed. Known as tissue engineering the aim of scientists within this field is to improve, maintain, or restore tissue function. This area of research may provide solutions to many of the social and economic problems associated with tissue transplants and reconstructive surgery. These problems include cost, which in the USA., exceeds $400 billion per annum for the health care of people with tissue failure and the shortage of donor organs. In the USA., only approximately 3,000 livers are donated per year and demand for these is in excess of 30,000 people (Cima (1993)).

The most publicised areas of tissue transplantation are those of organs such as the heart, liver, lungs, and bones, as in hip replacements. Much research is progressing to develop alternatives to present procedures with the aim of providing efficiency equal to or better than transplanted organs, but without the problems of rejection and ethics associated with such surgery (Michalopoulos (1997)). Other areas of research in the tissue engineering field are the areas of skin replacements for burns patients (2,150,000 people per annum in the US), replacement pancreases for diabetics, cartilage and tendon, nerve and dental replacements (Langer (1993), Martin (1997), McKay (1997)).

3.1.2 : The use of polymers in tissue engineering

The field of tissue engineering can be divided into three main areas, the use of isolated cells or cell substituents, the use of tissue inducing substances such as growth hormones and finally, the use of matrices containing cells. This last area is that of interest within the context of this thesis and can be divided into two further groups; the open and closed systems. In the closed system cells are surrounded by a semi-permeable membrane which allows the influx of nutrients and outflux of waste but does not allow passage of immune system constituents, to reduce the risk of rejection.

In open systems, the cells are seeded onto a scaffold formed from either a natural or synthetic polymer and the construct is transplanted into the patient. There a many advantages of transplanting cells / polymer matrix systems rather than fully grown mature tissue, some of which are summarised below.

(1) Donor tissue may not be available, whereas a supply of most cell lines exist as *in vitro* culture.

(2) When transplanting large tissues, difficult surgery is required to join the multitude of tiny blood vessels; whereas the transplantation of cells or tissue, less than 1 mm thick requires no such vascularisation.

(3) Cells can be significantly expanded in number in a polymer matrix, so on transplantation they can grow into a tissue to fit the defect, whereas tissue transplants posses a limited potential for growth as they are normally transplanted in a mature state.

(4) Cells can be genetically engineered far easier than intact tissue.

(5) On removal of cells from the donor tissue unwanted cell types can be removed prior to seeding onto the polymer matrix to decrease the chance of rejection when implanted back into the patient (Cima (1993)).

Both natural and synthetic materials have been utilised as the scaffold material for tissue engineering. Whilst natural materials are useful as they are easily degraded by naturally occurring enzymes and mimic the bodies natural environment, they are limited by the control the tissue engineer has on their physico-chemical properties such as, hydrophilicity, rate of degradation, mechanical properties and surface chemistry. Control over such properties in synthetic materials is much easier. However, such polymers are not always as accepted by the bodies immune system. Therefore, ultimately a material which has the controllable characteristics of the synthetic polymers but the biocompatibility of the natural polymers is required.

Many examples of the opens system or polymer scaffold approach to tissue engineering exist. For example, in bone and dental reconstruction, poly(lactic acid) (PLA) is seen as a versatile material being strong and hard but also biodegradable (Ishaug (1994)). When fashioned into bone plates and screws, this material has been observed to successfully aid the healing of osteotomies in dogs, and be totally degraded 4 years after the original surgery (Lehman (1994)). When used either on its own or in conjunction with poly(glycolic acid) (PGA), PLA has been observed to allow osteoblast proliferation and these cells were observed to produce levels of collagen similar to normal tissue. The shape and size of these vascularised bone flaps can also be controlled (Peter (1998), Ishaug (1994)). The above example requires surgery to implant the scaffold which can cause stress to the patient. Elisseeff and co-workers have investigated a polymer / chondrocyte system which can be injected subcutaneously and polymerized *in situ* by photopolymerisation. The implants were shown to produce collagen and proteoglycans at similar levels to native neocartiledge. They suggest this approach may be useful for plastic and orthopaedic surgery (Elisseeff (1999)).

Whilst biodegradability is a useful property for a scaffold matrix, a material which provides stimuli for the cells to grow, spread and differentiate would increase their efficiency in this role. This type of stimuli can be achieved simply by controlling the topography, porosity and surface chemistry of the material (Ma (1999), (Harris (1998)). For example, Gao and co-workers showed that by hydrolysing the surface ester groups of PGA fibres to alcohols and acids, increased cell adhesion was observed via the interaction of serum proteins with the material (Gao (1998)).

A more adventurous manner for controlling cellular processes on the polymer scaffold is by the incorporation of growth factors and / or adhesive protein (Whang (1995)). The use of such molecules to provide a stimuli for cell growth and differentiation will be discussed in Chapter 4. The presence of these molecules at the matrix surface can be controlled by the biodegradation rate of the polymeric matrix and hence provide a time-dependent influence on the function of the surrounding cells.

3.1.3 : The need for surface analysis of tissue engineering scaffolds

In tissue engineering, as well as drug delivery a knowledge of a materials surface structure provides vital information to develop structure activity relationships. The two most popular techniques for quantifying a surfaces chemical composition are X ray-photoelectron spectroscopy (XPS) and secondary ion mass spectrometry (SIMS). These techniques were introduced in 1.2.3 and 1.2.4 respectively and have been widely utilised in the characterisation of polymeric surfaces and determination of factors which effect these and hence their efficacy as tissue engineering scaffolds or drug delivery systems. These factors include such things as molecular weight,

segregation of blocks in co-polymer systems and casting solvent (Deslandes (1998), Chen (1998), Lang (1998), Davies (1995), Davies (1994)).

As well as the chemical composition of a materials surface being important, its topography can also play a significant role in its viability as a biomaterial. Many research groups have utilised AFM to obtain information on polymer structure at both sub-micron and molecular levels .

Sub-micron studies of polymer surfaces are important as they provide an understanding of the organisation of polymer molecules into macro-assemblies. This work is typified by the studies of Shakesheff et al. who looked at poly(ethylene oxide) and poly(sebatic anhydride) (PSA) solvent cast films, as well as melt-crystalline PSA. AFM images showed spherulites and the radiating fibres of the polymer within theses structures (Shakesheff (1995), (1994(a), (1994(b)).

Sub-micron AFM imaging is also useful for investigating the distribution of polymer types in blends or when present as co-polymers. The distribution of the contributing polymer types is important as it can significantly effect the efficiency of a material in a chosen application. The study of Davies et al. showed that in a polymer blend of PSA and PLA, the PSA was present as islands within a network of the PLA at the materials surface (Davies (1996)). These AFM studies were performed in parallel with XPS and SIMS investigations which showed a surface excess of PLA in all cases, independent of whether the polymers were miscible or not. The degradation profile of these polymer films was also followed by AFM and morphological changes in the polymer films identified.

As well as being utilised *in situ* to study the degradation profiles of

biodegradable polymers, AFM can be used to study the hydration of polymers. Frazier et al. showed the effect of hydration on thiolated dextran monolayers morphology using AFM in its imaging mode. By utilising it in its force-distance mode changes in the elasticity of the polymer over varying hydration times were also shown. The reversibility of the process was also investigated by dehydrating the polymer monolayer.

As discussed above, the grafting of materials to a polymers surface can change its interfacial properties and hence increase it efficiency as potential tissue engineering scaffold candidate. Uchia and Ikada utilised AFM to study the effect of grafting 2-(dimethylamino)ethyl methacrylate onto poly(ethylene terephthalate) (PET). They found that a brush-like structure was formed on the underlying PET. However this layer was inhomogeneous and clusters of the grafted chains were formed. The clusters were observed to tilt in the direction of the AFM scanning under liquid. However, this tilting was observed to be reversible on the removal of the load from the scanning AFM tip. The degree of tilting was dependant on the chain length of the grafted polymer and was not observed in air imaging (Uchida (1997)).

The use of polymers whose surface characteristics change with the application of an external stimuli are useful in the field of tissue engineering as they provide a method of detaching cells from the polymer scaffold (Chen, C. (1998)). One such polymer is N-isopropylacrylamide (NIPA) whose stimulus is a change in temperature. The structure of this polymer has been probed using AFM imaging in liquid. It was found that the surface domain structure of this polymer was not only altered by temperature, but also by the degree of homogeneity within the polymer. The domain size was observed to be far smaller in those polymers prepared at temperatures below the polymers cloud point. Changes in surface structure and roughness were reproducible on

cycling of temperature above and below the volume phase transition temperature (Suzuki (1997)).

Independent of the polymer chosen to form the basis of the tissue engineering scaffold it must be processed to provide the required shape for the tissue to grow into. This processing may alter the interfacial properties of the material. The effect of processing on the molecular arrangement in polymer films has been investigated by Motomatsu and co-workers. They showed that increasing annealing temperature of PEO films increased the degree of orientation in the fibril-like lamellae (Motomatsu (1996)). Whereas, Wawkushewski et al. showed various levels of morphological orientation in gel drawn PE ranging from molecules forming nanofibrils which associate into microfibrils and in turn aggregate to form micron fibres (Wawkushewski (1994) (a) & (b)).

3.1.4 : Introduction to the PLA-PEG-biotin system

The next two chapters will concentrate on studies which investigate the surface characteristics and interactions of a polymer which has been proposed as a material for forming tissue engineering scaffolds. This polymer is a tri-block material formed from poly(lactic acid) (PLA), poly(ethylene glycol) (PEG) and biotin; its structure is depicted in Figure 3.1. This polymer has several properties which are attractive for materials to form tissue engineering scaffolds.

The hydrophobic PLA acts as a rigid backbone giving the scaffold physical integrity and form. PLA is also a biodegradable polymer which aids breakdown and removal of the polymer scaffold from the body at the end of

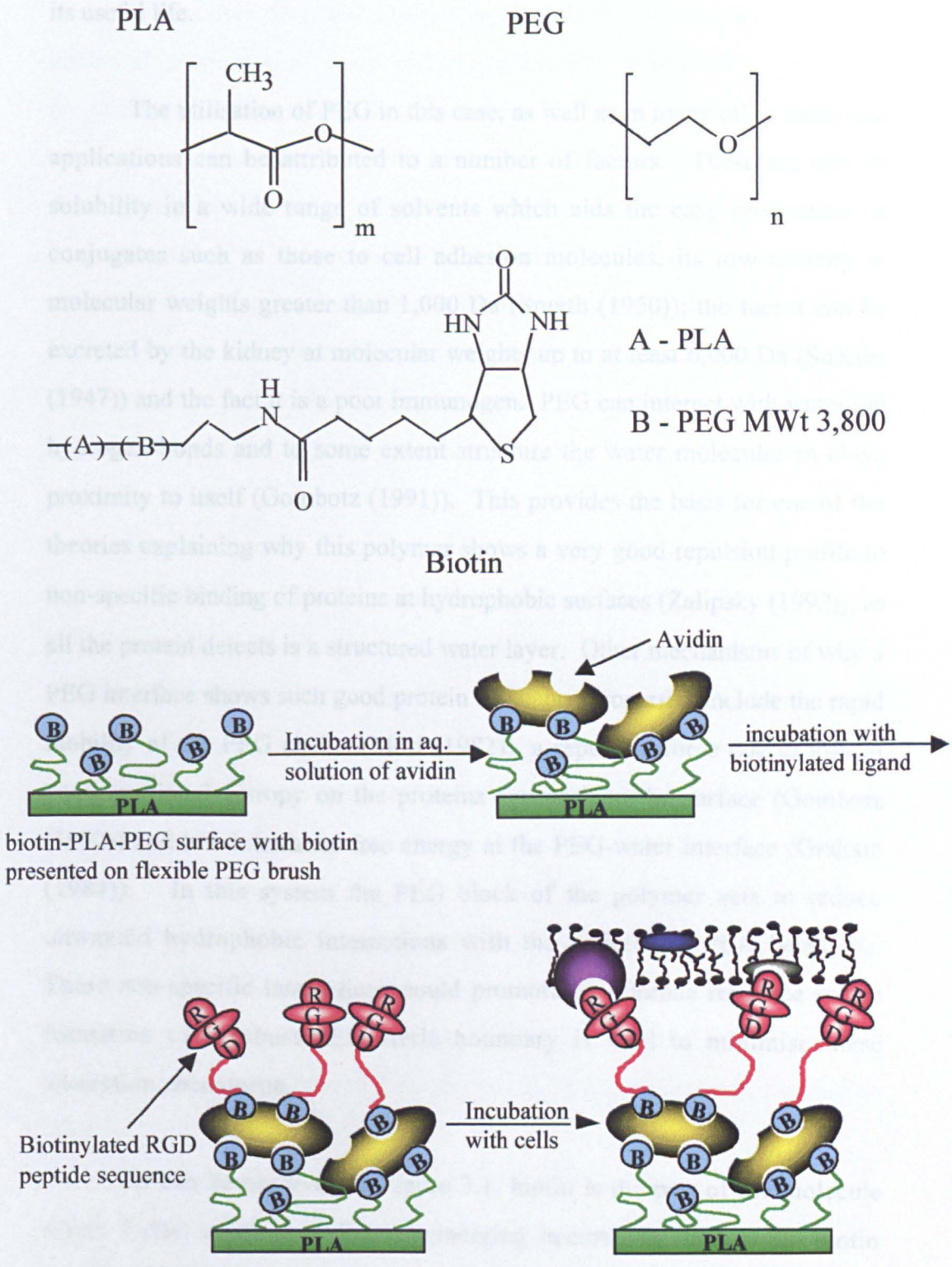

Figure 3.1 : Structure of PLA-PEG-biotin and scheme of use as a tissue engineering scaffold

its useful life.

The utilisation of PEG in this case, as well as in many other medicinal applications can be attributed to a number of factors. These include its solubility in a wide range of solvents which aids the easy production of conjugates such as those to cell adhesion molecules, its low toxicity at molecular weights greater than 1,000 Da (Smyth (1950)); the fact it can be excreted by the kidney at molecular weights up to at least 6,000 Da (Shaffer (1947)) and the fact it is a poor immunogen. PEG can interact with water via hydrogen bonds and to some extent structure the water molecules in close proximity to itself (Gombotz (1991)). This provides the basis for one of the theories explaining why this polymer shows a very good repulsion profile to non-specific binding of proteins at hydrophobic surfaces (Zalipsky (1992)), as all the protein detects is a structured water layer. Other mechanisms of why a PEG interface shows such good protein resistance properties include the rapid mobility of the PEG chains (Mori (1982)), a repulsive force due to loss of conformational entropy on the proteins approach to the surface (Gombotz (1992)) and low interfacial free energy at the PEG-water interface (Graham (1984)). In this system the PEG block of the polymer acts to reduce unwanted hydrophobic interactions with the underlying PLA backbone. These non-specific interactions could promote an immune response so the formation of a robust PEG steric boundary is vital to minimise these adsorption phenomena.

As can be observed in Figure 3.1, biotin is the part of the molecule where facile, aqueous surface engineering occurs via streptavidin-biotin interactions. Once bound to the polymer surface, the free binding sites of the streptavidin allow further surface modification of the polymer via the addition of biotinylated cell adhesion molecules such as RGD-peptides.

The studies described in the next two chapter investigate the surface chemical properties of three different PLA-PEG-biotin polymers. The polymers possess varying molecular weight PLA blocks. Experiments were performed to investigate if a difference in the PEG and hence biotin surface density could be obtained by varying the PLA block molecular weight. Studies have shown that for the promotion of cell adhesion and spreading, a defined density of cell adhesion molecules on the surface is required (Massia (1991)). Using this series of polymers it is hoped that the optimum density of biotin on the polymer and hence RGD sequence could be determined for different cell types adhesion and spreading.

In this chapter, a range of surface sensitive chemical analysis techniques were used to determine the interfacial chemical structure of the PLA-PEG-biotin polymers introduced above. For surface engineering to occur, the biotin and hence the PEG portion of the polymer needs to be located within the surface layer of the polymer. Investigations were performed by XPS and ToF-SIMS to quantify the contribution of PLA and PEG to the surface layer.

Surface topography is another important consideration when a material is considered for tissue engineering applications, as surface roughness may effect cell adhesion and spreading on the polymer surfaces. AFM investigations were performed to distinguish if PLA : PEG ratio had any effect on the surface topology of the material.

Patel et al. have shown that this polymer system can be used to grow both neuronal and endothelial cells patterned in lines (Patel (1998)). Imaging ToF-SIMS was utilised to quantify the distribution of streptavidin binding to the polymer surface, when patterned in 50 μm wide lines.

3.2 : Materials and methods

3.2.1 : Polymers

Polymers were kindly prepared by Dr. S. Cannizzaro, by the method described in Cannizzaro et al (1998). Four biotinylated polymers were investigated in this study where a constant PEG block of molecular weight 3,800 Da is used with PLA blocks ranging from 22,562, to 3,242 Da as determined by NMR. Three analogous non-biotinylated polymers were prepared of similar structures, formed from PEG blocks of 3,000 Da and PLA blocks of 17,861, 10,591 and 4,219 Da. The structural details and PLA : PEG ratios of the biotinylated and non-biotinylated polymers are summarised in Table 3.1 and Figure 3.1. All polymers prior to use were stored at 0 - 3 °C in powder form and used without further purification.

3.2.2 : Characterisation of film continuity and thickness

SPR experiments were performed to determine the minimal concentration of polymer in a chloroform solution which would give a complete film when spun cast at ~2,000 rpm. Proteins are known to bind to the silver slides utilised in SPR (Green (1997)), therefore control experiments were initially performed on SPR slides to determine the background levels of avidin binding to silver. Various concentrations (1.0 - 10.0 mg / ml) of both the biotinylated (biotin-PLA-PEG(0.53), PLA MWt. 3,242) and non-biotinylated (PLA-PEG(0.86), PLA MWt. 4,219) polymers were then investigated to determine the maximal and minimal binding of avidin to the biotinylated polymer and non-biotinylated polymers respectively.

Polymer name	PLA-PEG-biotin (3.63)	PLA-PEG-biotin (3.45)	PLA-PEG-biotin (1.49)	PLA-PEG-biotin (0.53)
PEG WMt. (from NMR)	3,800	3,800	3,800	3,800
PLA MWt. (from NMR)	22,562	25,240	9,261	3,242
PLA : PEG ratio	3.63 : 1	3.45 : 1	1.49 : 1	0.53 : 1

Polymer name	PLA-PEG- (3.64)	PLA-PEG- (2.17)	PLA-PEG- (0.86)
PEG WMt. (from NMR)	3,000	3,000	3,000
PLA MWt. (from NMR)	17,861	10,591	4,219
PLA : PEG ratio	3.64 : 1	2.17 : 1	0.86 : 1

Table 3.1 : Summary of PLA and PEG content of tested polymers

Experiments were performed on SPR slides which had been cast with 100 µl of the polymers from chloroform solutions at 1.0 - 10.0 mg /ml concentrations at 2,000 rpm. Buffer flow of 10 mM phosphate buffer at pH 7.4 was allowed to obtain a stable baseline. 1 ml of avidin (5×10^{-7} M) was then injected and a further buffer wash performed to remove excess avidin which was only loosely associated with the surface.

3.2.3 : Static contact angle measurements

Samples for contact angle measurements were prepared on SPR slides. A 100 µl aliquot of a 3 mg / ml solution of the polymers in chloroform was spun cast at a speed of 2,000 rpm onto the SPR slide. Static contact angles were determined using a Vickers Ealing contact angle goniometer (Good (1992)). Phosphate buffer was utilised as the liquid phase. A 2 µl drop was added to the polymer surface using a microsyringe and readings taken immediately, using the rotating telescope part of the instrument. This telescope lens possessed an engraved cross hair and angle measuring grid for determining the angle the buffer drop made with the polymer film. Measurements were repeated at least 20 times on a minimum of 4 different films for each polymer.

3.2.4 : XPS

Polymer samples for XPS studies were cast directly onto silicon wafers (Exsil, Alfreton, Derbyshire, UK.). 200 µl of a 3 mg / ml solution of the polymer in chloroform solution was cast at ~2,000 rpm to give a continuous film. Samples were analysed using a VG Escalab Mk. 2 electron spectrometer (VG scientific, East Grinsted, Sussex, UK) utilising a monochromatic Al Kα (1486.7 eV) X-ray source. The electron gun was

operated at 200 W and the take-off angle to the spectrometer was 35° from the surface plane. Wide scans over 500 eV were obtained to check for contamination of the polymer films. Narrow scans of 10 eV were obtained over the regions of the C1s and O1s envelopes to determine the contribution of PLA and PEG to the polymer surface layer.

Experiments were also performed casting the polymer from both chloroform or trifluoroethanol (TFE). This was performed as the polycarbonate base used for analysis of cell adhesion to the cast polymer films dissolves in chloroform, therefore TFE was utilised as a solvent for polymer film casting in cell culture experiments. XPS was performed to check that the choice of casting solvent did not alter the ratio of PLA to PEG at the surface significantly.

3.2.5 : AFM

Samples of the polymer films were cast from 3 mg / ml solutions in chloroform onto glass coverslips (Chance Propper Ltd., Warley, UK) or 3 mg / ml solutions in TFE onto Hybrislips™ (Sigma Chemical Company, Poole, UK). Polymer films were imaged in tapping mode in air, both before and after exposure to 10 mM phosphate buffer pH 7.4. Single beam, TESP silicon nitride tips were utilised on a multimode SPM with Nanoscope IIIa controller. The AFM tips utilised had resonant frequencies between 250-278 KHz.

3.2.6 : ToF-SIMS

Polymer samples for ToF-SIMS analysis were prepared from either 0.1 or 2.5 % w / w solutions in chloroform. 200 µl was spun cast onto silicon wafers. ToF-SIMS analysis of the samples was performed on a Phi 7200

instrument (Physical electronics, Eden Prairie, MN., USA) utilising Cesium as the primary ion source. The ion dose for each sample did not exceed 1.6 x 10^{12} ions / cm^2.

To determine the distribution of avidin on the polymer surface of the patterned polymer samples imaging ToF-SIMS was performed. Patterned samples were prepared following the method of Patel et al. (1998). In summary, a PLA-PEG-biotin(3.45) polymer film was spun cast from a 3 mg / ml solution of the polymer in chloroform onto a silicon surface. A PDMS mould containing 50 μm wide grooves was plasma etched in an oxygen plasma and then placed directly onto the polymer surface. 1 ml of avidin-rhodamine in distilled water was placed at the open end of the mould capillaries allowing the flow of solution by capillary action down the capillary. After 1 h the avidin-rhodamine solution was removed by blotting and replaced with water. After a further 5 min, this solution was also blotted away. The washing procedure was repeated a further 4 times. The mould was then carefully removed under an aqueous environment and the whole polymer sample rinsed in excess water. These samples were mapped by ToF-SIMS with Gallium as the primary ion, step size was 2.2 ns and the ion dose over a 100 μm scan was no greater than 4.9 x 10^{12} ions / cm^2.

3.3 : Results and discussion

3.3.1 : Characterisation of film continuity

When investigating a polymeric materials surface it is important that the film is a continuous layer and thick enough to prevent contributions from the properties of the underlying substrate. This is important as if the film was discontinuous, misleading results in both surface characterisation and surface

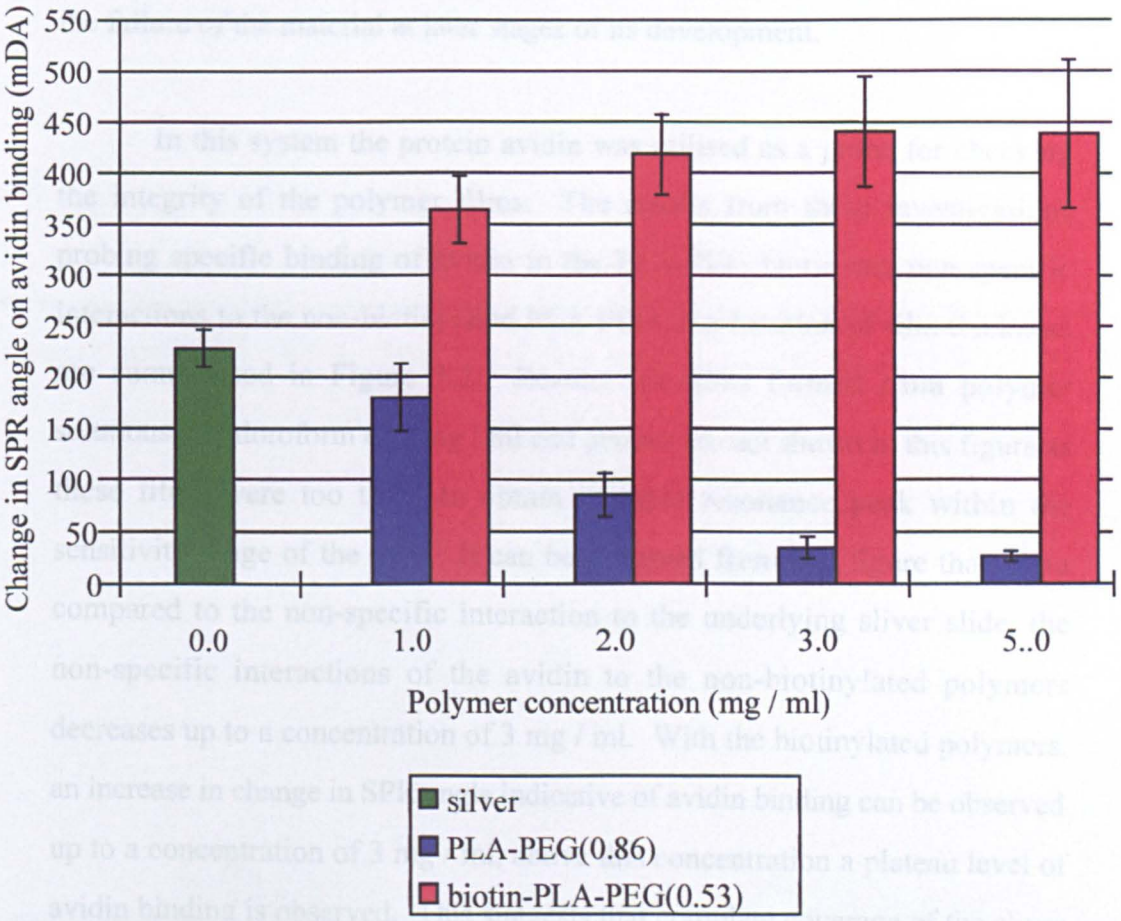

Figure 3.2 : Effect of polymer concentration on integrity of film formed

SPR experiments utilised avidin as a probe to determine the minimum concentration of polymer which gave a continuous film coverage

bars = average ± 1 standard deviation ($n \geq 8$)

interactions of the polymeric material could occur. This in turn may lead to the failure of the material at later stages of its development.

In this system the protein avidin was utilised as a probe for checking the integrity of the polymer films. The results from these investigations probing specific binding of avidin to the PLA-PEG-biotin and non-specific interactions to the non-biotinylated PLA-PEG as a function of film thickness are summarised in Figure 3.2. Results for films formed from polymer solutions in chloroform of 7 mg / ml and greater are not shown in this figure as these films were too thick to obtain a stable resonance peak within the sensitivity range of the SPR. It can be observed from this figure that when compared to the non-specific interaction to the underlying sliver slide, the non-specific interactions of the avidin to the non-biotinylated polymers decreases up to a concentration of 3 mg / ml. With the biotinylated polymers, an increase in change in SPR angle indicative of avidin binding can be observed up to a concentration of 3 mg / ml, above this concentration a plateau level of avidin binding is observed. This suggests that complete coverage of the sliver SPR slide by the polymer is obtained at a concentration of 3 mg / ml since no significant difference in specific or non-specific binding of avidin to the polymer films is observed above this concentration. Therefore, all further experiments were performed with films formed from a 3 mg / ml polymer solution.

3.3.2 : Static contact angle measurements

From Table 3.2 it can be observed that as the PLA : PEG ratio decreases from 3.64 : 1 to 0.53 : 1 a corresponding decrease in static contact angle from 74.5° ± 2.5° to 62.4° ± 1.8° is observed. This table also shows reference values for PS and PLGA of 87° and 63° respectively (McGurk

Polymer	PS	PLA-PEG-biotin(3.64)	PLA-PEG-biotin(1.49)	PLA-PEG-biotin(0.53)	PLGA
Contact angle (°)	87	74.5 ± 2.5	69.5 ± 2.4	62.4± 1.8	63

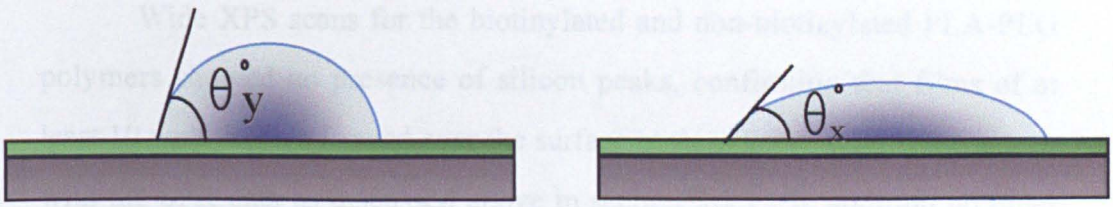

The larger the angle the more hydrophobic the surface

Table 3.2 : Effect of PLA molecular weight in contact angles for biotinylated polymers

Ref : Good (1992), McGurk (1998)

(1998)). PS is a hydrophobic polymer being a saturated hydrocarbon and hence unable to form hydrogen bonds. As such it has a high contact angle. The surface energy of this polymer system is high, hence it resists movement of the water droplet from its application point. On the other hand PLGA is a relatively hydrophilic polymer which is able to form hydrogen bonds through its carboxyl moiety and as such possesses a lower surface energy (Good (1992)). This means that it is energetically favourable for the liquid to spread over the surface. The contact angle of the biotin-PLA-PEGs decreases with PLA-PEG ratio. This suggests as the PEG content of the polymer increases, its surface contribution also increases. This leads to a more hydrophilic surface and hence the observed decrease in contact angle.

3.3.3 : XPS

Wide XPS scans for the biotinylated and non-biotinylated PLA-PEG polymers showed no presence of silicon peaks, confirming that films of at least 10 nm thick are formed over the surface of the silicon wafer. This agrees with the SPR data as discussed above in section 3.3.1. In addition no other peaks except for those indicative of the polymer were present. This shows that there was minimal contamination of the films from common contaminants such as poly(dimethylsiloxane).

Figure 3.3 shows typical XPS scans of the C1s envelopes obtained from pure PLA (a) and PEG (b) and the three biotinylated PLA-PEG block co-polymers with PLA-PEG ratios of 3.64 : 1 (c), 1.49 : 1 (d), and 0.53 : 1 (e) respectively. From the Figures 3.3 (a) and (b) the contributions from the four different carbon environments present in the PLA and PEG can be observed. From Figure 3.3 (a) deconvoluted within the C1s envelope are three peaks at binding energies of 285.0, 286.98 and 289.06 eV for the peaks labelled 1, 2 and

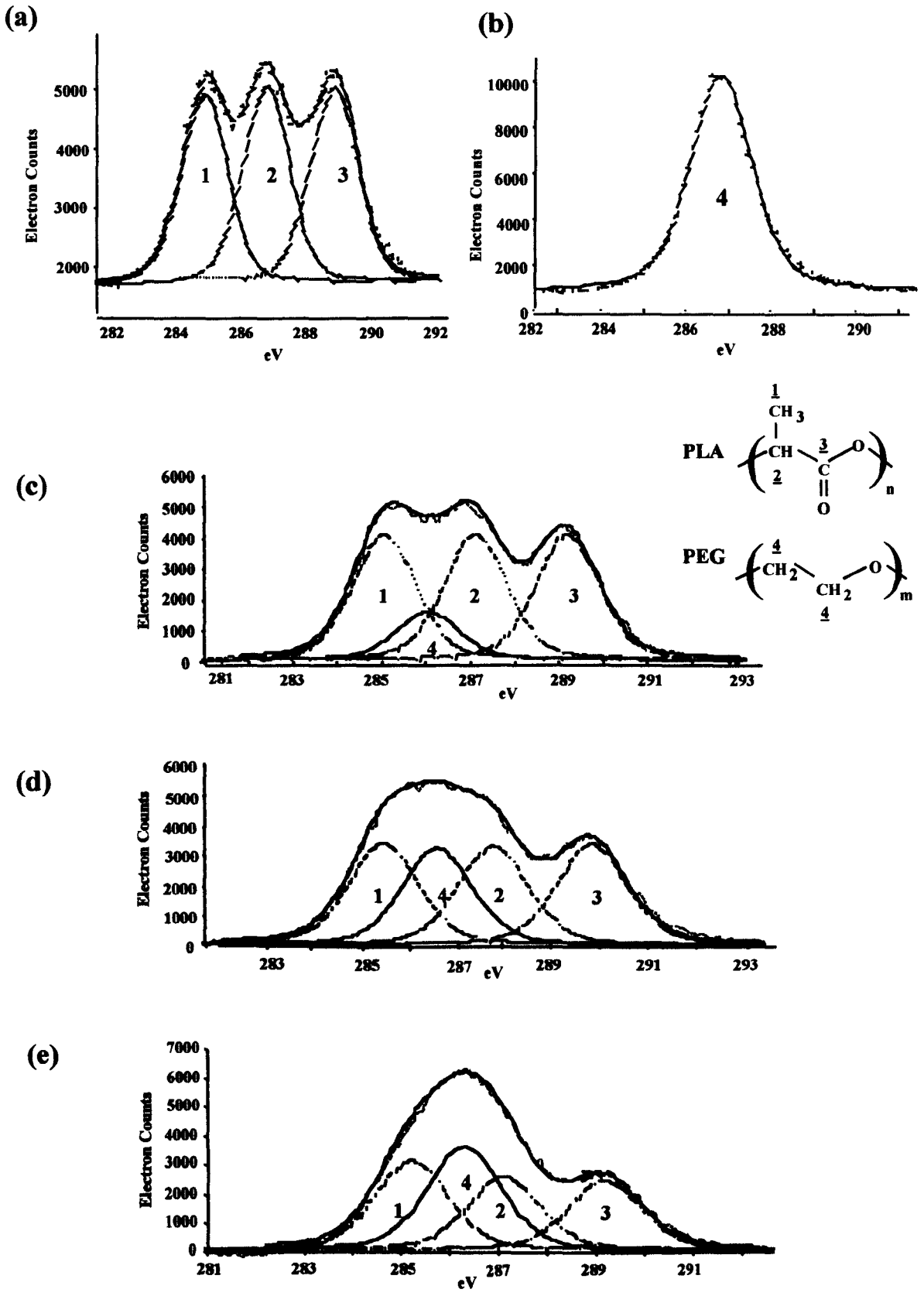

Figure 3.3 : Typical XPS scans of the C1s envelope for:

(a) PLA **(b) PEG**

(c) biotin-PLA-PEG(3.64) **(d) biotin-PLA-PEG(1.49)**

(e) biotin-PLA-PEG(0.53)

3 respectively which are associated with PLA. They correspond to the methyl, CH and carbonyl carbon environments within the PLA structure as labelled in Figure 3.3 (a) and as described previously (Davies (1989)). In the PEG C1s spectrum only one peak at a binding energy of 286.45 eV is observed this is due to the $\underline{C}H_2$-O in the ether environment (Beamson (1992)).

On deconvolution of the C1s envelop for the PLA-PEG-biotin polymers contributions from both the PLA and PEG carbons are observed. The ratios of the different carbon environments for the three PLA portions of the polymer series are shown in Table 3.3. The ratios in all the PLA-PEG-biotin systems shows a close correlation to the theoretical 1 : 1 : 1, ratio. This provides evidence that there is minimal hydrocarbon contamination of the polymers. As the PLA : PEG ratio decreases, it can be observed from Figure 3.3 (c), (d) and (e) respectively that a significant increase in the contribution from the PEG peak is observed. Table 3.3 summaries the contribution of the different peaks to the overall spectra for both the biotinylated and non-biotinylated PLA-PEGs. An increase in PEG at the surface is observed for both the biotinylated and non-biotinylated PLA-PEGs as PLA : PEG ratio decreases. In the case of the biotinylated polymers the increase is from 12.8 % to 32.2 % to 54.1 % of C1s envelope, as PLA : PEG ratio changes from 3.64 to 1.49 and finally 0.54. This suggests that the biotin content at the surface will also have increased, as it is bound at the PEG block termini. An increase from 14.9-36.2 % of counts was attributed to the PEG peak as PLA : PEG ratio decreased from 3.63-0.86 % for the non-biotinylated polymers. These results are similar to those observed for the biotinylated polymer which suggests that biotinylation of the polymer has little effect on the surface orientation of the material. As shown in Table 3.3 also, the PLA peak ratios deviated no more than 4% from the theoretical ratio of 1 : 1 : 1. This provides further evidence that hydrocarbon contamination is minimal.

Polymer	PLA-PEG(3.64)			PLA-PEG(2.17)			PLA-PEG(0.86)		
Contribution of PLA peaks (1,2,3) (%)	29.4	29.3	29.1	27.6	27.6	27.3	24.1	25.0	24.3
Ratio of PLA peaks	1.00 : 1.00 : 0.99			1.00 : 1.00 : 0.99			0.96 : 1.00 : 0.97		
Contribution of PEG peak (%)	12.2			17.5			26.6		
% of PEG at surface	13.9			21.1			36.2		
PLA : PEG ratio	2.41 : 1			1.57 : 1			0.92 : 1		

Polymer	PLA-PEG-biotin(3.63)			PLA-PEG-biotin(1.49)			PLA-PEG-biotin(0.53)		
Contribution of PLA peaks (1,2,3) (%)	29.4	29.7	29.6	25.5	24.9	25.3	22.5	21.8	20.6
Ratio of PLA peaks	0.99 : 1.00 : 1.00			1.00 : 0.98 : 0.99			1.00 : 0.97 : 0.92		
Contribution of PEG peak	11.3			24.3			35.1		
% of PEG at surface	12.8			32.2			54.1		
PLA : PEG ratio	2.61 : 1			1.03 : 1			0.70 : 1		

Table 3.3 : Summary of peak contributions and PLA peak ratios for biotinylated and non-biotinylated PLA-PEG polymers

This table shows that the peak ratio for the PLA peaks is close to the theoretical value of 1.0 : 1.0 : 1.0 suggesting minimal hydrocarbon contamination. It can also be observed that as the PLA MWt. decreases the contribution of the counts characteristic of the PEG increase.

Table 3.4 summarises the carbon to oxygen (C : O) ratios for the biotinylated and non-biotinylated polymers. In pure PLA the C : O ratio is 3:2 whereas in PEG it is 2 : 1. Therefore, the higher the value of C : O ratio for the PLA-PEG polymers the greater the surface presence of PEG. From Table 3.4 it can be observed that the C : O ratio increases, as the PLA : PEG ratio decreases, suggesting that the surface becomes more PEG like as the molecular weight of PLA decreases. The same trend is observed for both the biotinylated and non-biotinylated polymers systems. For example on decreasing the PLA : PEG ratio of the biotinylated polymers from 3.63 : 1 to 0.53 : 1 an increase in the C : O ratio from 1.73 : 1 to 1.88 : 1 is observed. These values are similar to the theoretical values of 1.61 : 1 and 1.83 : 1 for PLA-PEG-biotin(3.63) and PLA-PEG-biotin(0.53) respectively. The slightly higher values could be due to a preferential orientation of PEG at the surface when compared to the bulk.

No differences were observed when comparing the XPS wide scans for the polymers cast from either chloroform and TFE. The presence of chlorine or fluorine, marking the presence of residual casting solvent was not detected. The elemental C : O ratios and ratios of PLA : PEG C1s environments were also not significantly different for these systems. This suggests that the casting solvent has little effect on the surface composition of the films formed, prepared using the method described in this thesis.

3.3.4 : AFM

Figure 3.4 shows the three biotinylated PLA-PEG films before and after incubation in buffer. The cast polymer films (Figure 3.4 (a) - (c)) are continuous, free from exposed substrate defects and extremely flat, with a typical z range of 5 nm over a 1 μm^2 area. There was no evidence of phase separation of the components. Table 3.5 summarises the surface roughness of

Polymer	C : O ratio		% of total counts	
	Theoretical	Experimental	C	O
PLA-PEG-biotin(3.63)	1.61 : 1	1.72 : 1	63.2	36.8
PLA-PEG-biotin(1.49)	1.70 : 1	1.76 : 1	63.8	36.2
PLA-PEG-biotin(0.53)	1.83 : 1	1.88 : 1	65.3	34.7

Polymer	C : O ratio		% of total counts	
	Theoretical	Experimental	C	O
PLA-PEG (3.64)	1.61 : 1	1.66 : 1	61.3	38.7
PLA-PEG-(2.17)	1.66 : 1	1.70 : 1	62.9	37.1
PLA-PEG-(0.86)	1.77 : 1	1.90 : 1	65.5	34.5

Table 3.4 : Carbon : oxygen ratios for the biotinylated and non-biotinylated PLA-PEG polymers

For both the biotinylated and non-biotinylated PLA-PEGs it can be observed that as PLA molecular weight decreases, the C : O ratio moves from a predominately PLA (C : O = 1.5) to a more PEG-like (C : O = 2.0) one.

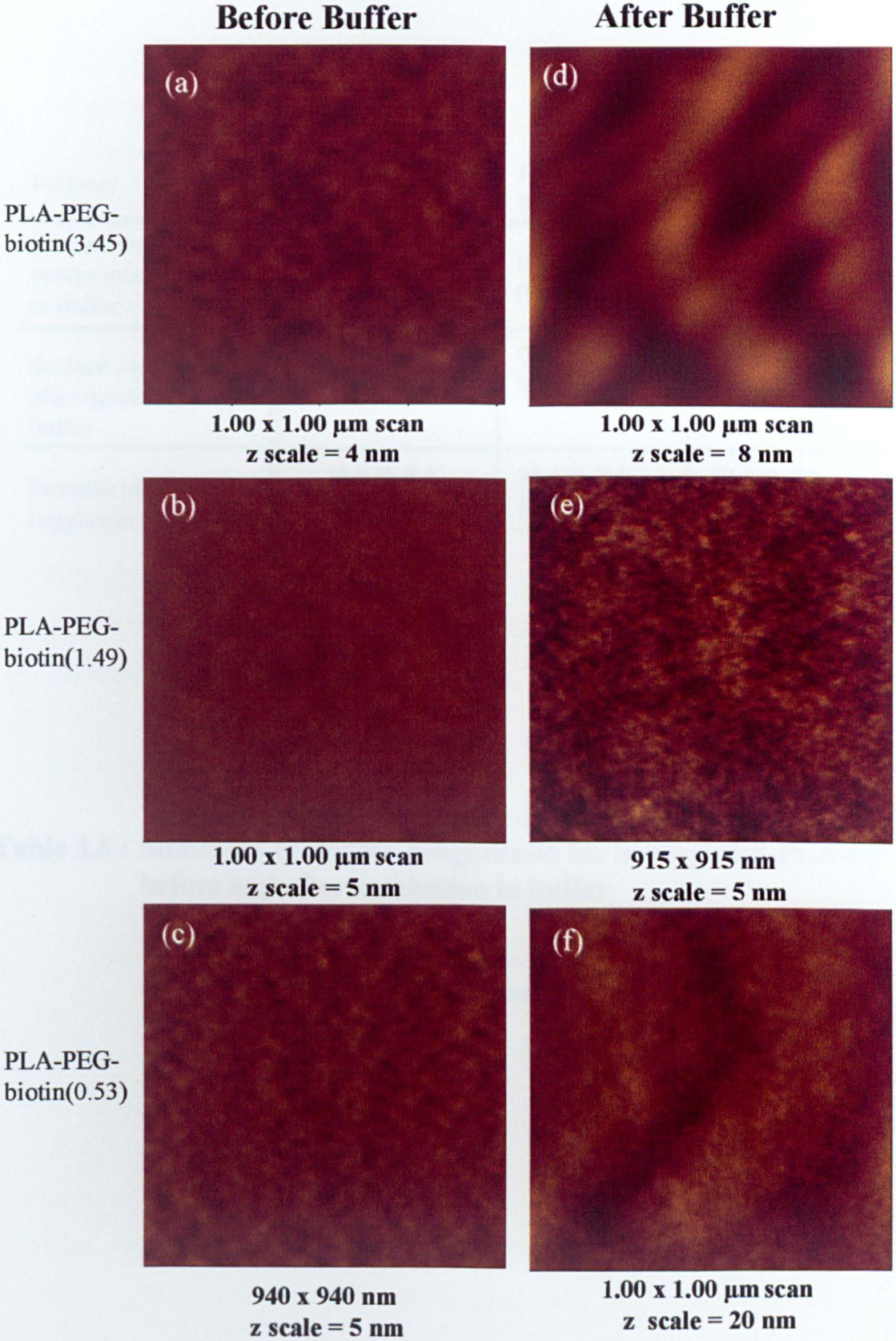

Figure 3.4 : Images of biotinylated polymers before and after incubation in buffer

Polymer	PLA-PEG-biotin(3.63)	PLA-PEG-biotin(1.49)	PLA-PEG-biotin(0.53)
Surface roughness before incubation in buffer	0.237 RA 0.300 RMS	0.293 RA 0.400 RMS	0.741 RA 0.923 RMS
Surface roughness after incubation in buffer	0.324 RA 0.392 RMS	0.437 RA 0.601 RMS	1.490 RA 1.922 RMS
Increase in surface roughness (%)	26.9 % RA 23.5 % RMS	33.4 % RA 33.0 % RMS	50.3 % RA 61.5 % RMS

Table 3.5 : Summary of surface roughnesses for biotinylated-PLA-PEGs before and after incubation in buffer

RA = roughness analysis
RMS = route mean square

these samples. Images of the polymer surface after incubation in buffer are shown in Figure 3.4 (d) - (e). Although the surfaces remain extremely flat with a typical z scale of 11 nm, a slight increase in the surface roughness of the polymer films as determined by the Nanoscope IIIa roughness analysis software does occur. The increase in surface roughness appears to be related to PLA : PEG ratio. As the PLA : PEG ratio decreases more PEG becomes present at the surface. This increase in PEG results in a slightly higher surface roughness. After incubating with buffer the degree of increase in surface roughness again appears to be related to the amount of PEG present at the polymer surface. This could be attributed to the higher density of the PEG at the surface as PLA : PEG ratio decreases. This will lead to a larger association of water on incubation and hence allow for a larger rearrangement of the PEG chains on drying, producing a rougher surface.

3.3.5 : TOF-SIMS

3.3.5.1 : Co-polymer composition

Typical ToF-SIMS spectra in positive and negative ion modes for the biotinylated PLA-PEG(1.49) polymer are depicted in Figures 3.5 and 3.6. As can be observed from these images the majority of the major peaks could be attributed to peaks associated with either PLA or PEG. A summary of these peaks for the biotinylated and non-biotinylated polymers are shown in Tables 3.6 and 3.7 respectively, along with the counts and fragment associated with them. Peaks for the PLA and PEG agree with previous work by Davies et al., Scholes and co-workers and Briggs (Briggs (1989), Davies (1989), Scholes (1999)).

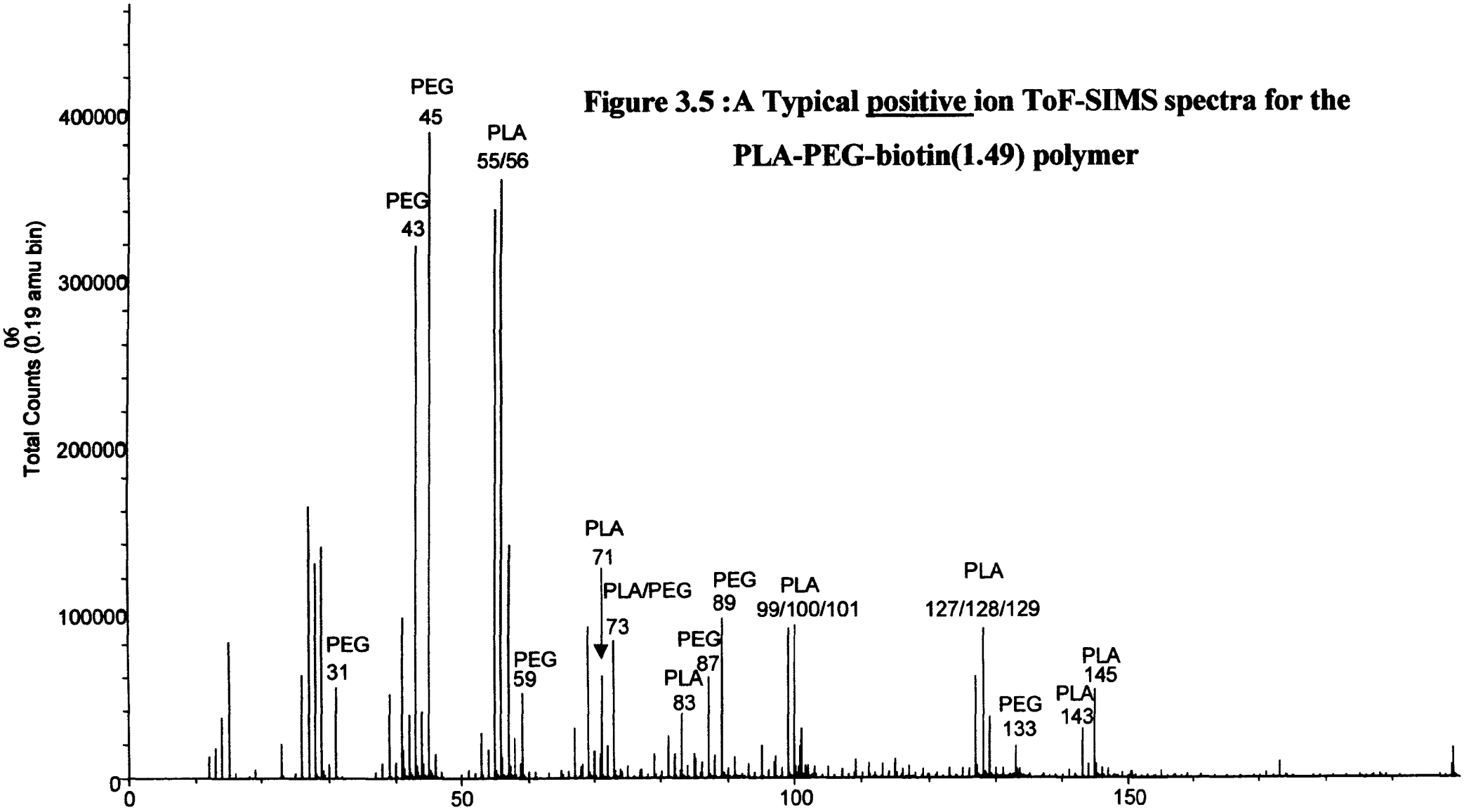

Figure 3.5 :A Typical positive ion ToF-SIMS spectra for the PLA-PEG-biotin(1.49) polymer

Figure 3.6 : A Typical <u>negative</u> ion ToF-SIMS spectra for the PLA-PEG-biotin(1.49) polymer

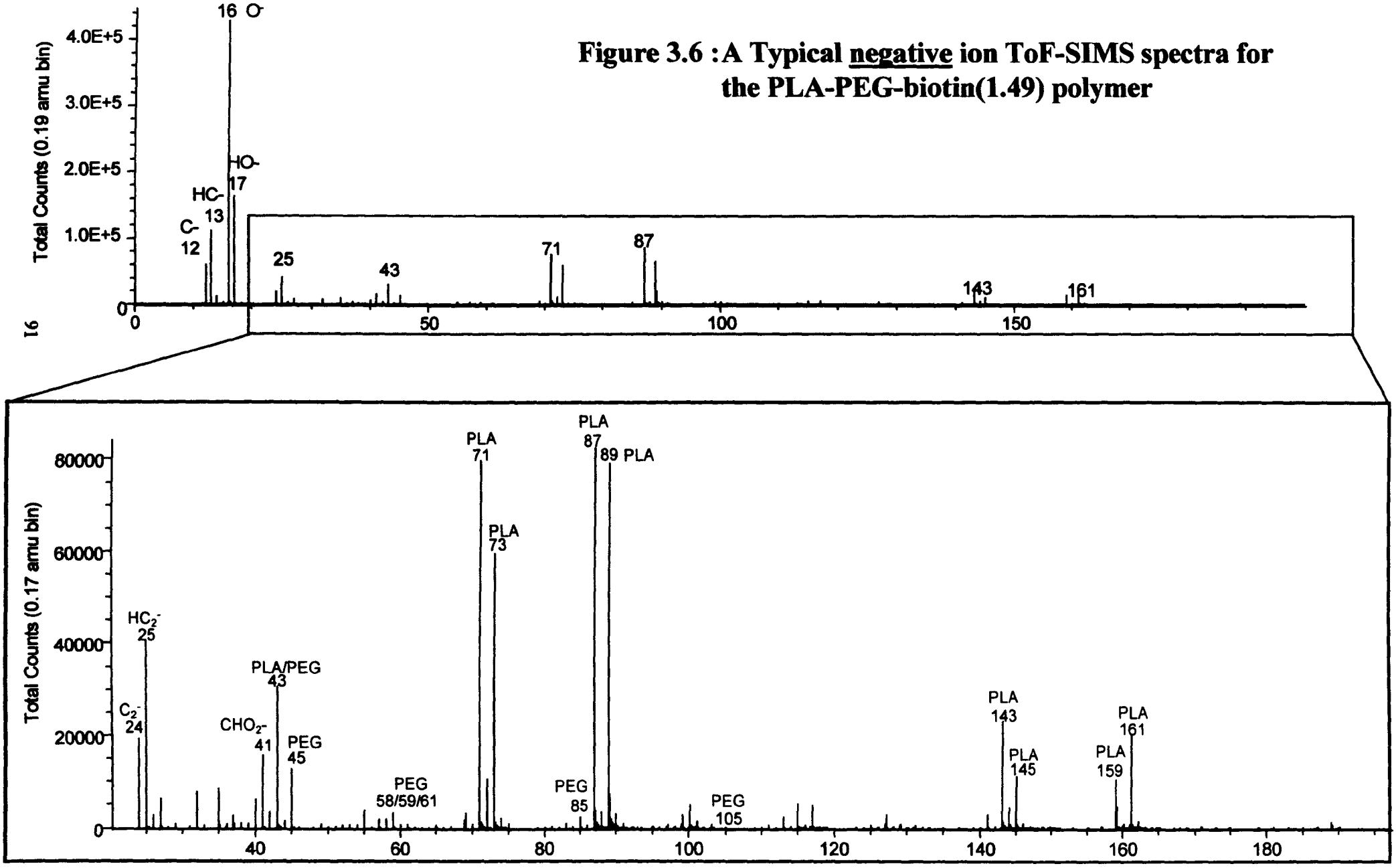

In the positive spectrum mass range of 0 - 150, there are several characteristic peaks for PLA as previously described namely those at m / z 55, 71, 73, 99, 100, 101, 127, 128, 129, 143 and 145 (Davies (1989)). The most intense of these is the peak at 55 which correspond to $[M_{PLA} - OH]^+$, as in previous studies by Davies and co-workers, the molecular ions for PLA $[M_{PLA} \pm H]^+$ at m / z 71 and 73 are less intense than this peak. For example, for the PLA-PEG-biotin(3.45), the m / z 55 peak has 450,615 counts whereas the 71 peak has only 32,398 counts. Care must be taken when assessing the m/ z 73 peak as this will also have contributions from the PEG $[CH_3 OCH{=}COH]^+$ ion. A cluster of peaks is observed at m / z 99, 100 and 101 these are attributed to the mass fragments of the PLA of $[2M_{PLA} - CO_2 - H]^+$, $[2M_{PLA} - CO_2 - H]^{\bullet+}$ and $[2M_{PLA} - CO_2 + H]^+$ respectively. Another radical ion is detected at m / z 128 which corresponds to $[2M_{PLA} - O]^{\bullet+}$, this peak again is the middle one of a cluster of three the other two being $[2M_{PLA} - O H]^+$ and $[2M_{PLA} H - O]^+$ for m /z 127 and 129 respectively. The peak at m / z 83 has been assigned an interesting cyclic structure as shown in Table 3.6.

Peaks representative of the PEG portion of the PLA-PEG molecules both biotinylated and not, are also present in the spectra for all the polymers. Namely the molecular ion at m / z = 43 $[CH_2 = COH]^+$, m / z = 45 $[CH_3CH = OH]^+$, m / z = 59 $[HOCH = C = OH]^+$, as well as m / z = 87 / 89, $[2M_{PEG} \pm H]^+$ and m / z = 133, $[3M_{PEG} + H]^+$.

In the negative spectrum a number of prominent ions occur, at m / z < 44 peaks corresponding to $[C]^-$ (m / z = 12) $[CH]^-$ (m / z = 13) $[O]^-$ (m / z = 16) $[OH]^-$ (m / z = 17), $[C_2]^-$ (m / z = 24), $[C_2H]^-$ (m / z = 25), $[C_2HO]^-$ (m / z = 41) and $[C_2H_3O]^-$ (m / z = 43) arising from either PLA or PEG. Above this

Peak mass	Counts biotin-PLA-PEG (3.45)	Counts biotin-PLA-PEG (1.49)	Counts biotin-PLA-PEG (0.53)
PEG			
31 $[H_2C{=}OH]^+$	28,465	52,994	132,630
43 $[H_2C{=}C{=}OH]^+$	52,945	60,236	106,666
45 $[H_3C\text{-}CH{=}OH]^+$	363,635	369,729	571,279
59 $[H_3C\text{-}CH_2\text{-}O{=}CH_2]^+$	38,532	54,480	18,552
87 $[CH_2{=}CH{=}O\text{-}CH_2CH{=}O\text{-}H]^+$	1,398	3,822	22,583
89 $[CH_3CH_2\text{-}O\text{-}CH_2CH{=}O\text{-}H]^+$	114,712	94,001	127,391
133 $[(CH_2CH_2O)_3H]^+$	7,281	7,625	11,355
PLA			
55 $[H_2C{=}CH\text{-}C{=}O]^+$	450,615	288,832	81,300
56	519,238	357,197	235,430
71 $[CH_2{=}C\text{-}CO_2H]^+$	32,398	27,111	17,774
83 Cyclic product see bottom of table	7,346	12,268	8,720
99 $[H_3C\text{-}CH\text{-}O\text{-}CO\text{-}C\text{-}CH_3]^+$	166,270	86,931	66,974
100 $[H_3C\text{-}CH\text{-}O\text{-}CO\text{-}CH\text{-}CH_3]^+$	164,244	91,998	61,072
101 $[H_3C\text{-}CH\text{-}O\text{-}HCO\text{-}CH\text{-}CH_3]^+$	36,274	24,752	11,886
127 $[H_2C{=}CH\text{-}CO_2\text{-}CH(CH_3)CO]^+$	145,417	65,039	36,067
128 $[H_3C\text{-}CH_2\text{-}CO_2\text{-}CH(CH_2)CO]^+$	173,814	88,038	47,119
129 $[H_3C\text{-}CH_2\text{-}CO_2\text{-}CH(CH_3)CO]^+$	32,156	22,868	14,282
143 $[H_2C{=}C\text{-}CO_2\text{-}CH(CH_3)\text{-}CO_2H]^+$	62,561	29,458	16,209
145 $[H_3C\text{-}CH\text{-}CO_2\text{-}CH(CH_3)\text{-}CO_2H]^+$	89,769	58,568	57,133
PLA and PEG			
73 $[H_3C\text{-}CH\text{-}CO_2H]^+$ OR $[H_3C\text{-}CH_2\text{-}O\text{-}CH_2\text{-}CH_2]^+$	72,011	83,528	86,944

Table 3.6 (a) : Summary of ToF-SIMS peaks and associated counts for <u>positive</u> peaks characteristic of PLA and PEG for the biotin-PLA-PEG polymers

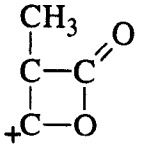

PLA m/z = 83

Peak mass	Counts biotin-PLA-PEG(3.45)	Counts biotin-PLA-PEG(1.49)	Counts biotin-PLA-PEG(0.53)
PEG			
58 $[O=C=CH_2\text{-}O]^-$	2,544	2,068	7,498
59 $[HO\text{-}CH=CH\text{-}O]^-$	1.395	2,085	7,332
61 $[HOCH_2CH_2O]^-$	270	505	797
85 $[H_2C=CHOCH=CH\text{-}O]^-$	5347	2570	3,846
105 $[HOCH_2CH_2OCH_2CH_2O]^-$	302	341	418
PLA			
45 $[H\text{-}CO_2]^-$	21,936	17,204	12,763
71 $[H_2C=CH\text{-}CO_2]^-$	154,667	77,721	46,117
73 $[H_3C\text{-}CH_2\text{-}C\text{-}O_2]^-$	46,038	36,445	25,822
87 $[O\text{-}C(CH_2)\text{-}CO_2H]^-$	179,581	83,510	92,652
89 $[O\text{-}CH(CH_3)\text{-}CO_2H]^-$	7810	82,922	123,026
143 $[H_2C=CH\text{-}CO_2\text{-}CH(CH_3)\text{-}CO_2]^-$	57,142	23,963	26,480
145 $[H_3C\text{-}CH_2\text{-}CO_2\text{-}CH(CH_3)\text{-}CO_2]^-$	12,958	6,661	5,587
159 $[H_3C\text{-}CH_2\text{-}CO_2\text{-}CH(CH_3)\text{-}CO_2\text{-}CH_2]^-$	36,244	15135	16,307
161 $[O\text{-}H_2C\text{-}CH_2\text{-}CO_2\text{-}CH(CH_3)\text{-}CO_2H]^-$	37,181	21,172	36,767
PLA/PEG			
43 $[H_2C=CH\text{-}O]^-$	1,679	1,078	1,826

Table 3.6 (b) : Summary of ToF-SIMS peaks and associated counts for negative peaks characteristic of PLA and PEG for the biotin-PLA-PEG polymers

Peak mass	Counts PLA-PEG (3.64)	Counts PLA-PEG(2.17)	Counts PLA-PEG(0.83)
PEG			
31 $[H_2C{=}OH]^+$	23,386	43,898	69,909
43 $[H_2C{=}C{=}OH]^+$	86,521	302,892	274,894
45 $[H_3C\text{-}CH{=}OH]^+$	324,522	387184	439,113
59 $[H_3C\text{-}CH_2\text{-}O{=}CH_2]^+$	44,243	79,773	20,173
87 $[CH_2{=}CH{=}O\text{-}CH_2CH{=}O\text{-}H]^+$	2,350	7,584	5,117
89 $[CH_3CH_2\text{-}O\text{-}CH_2CH{=}O\text{-}H]^+$	96,659	103,945	112,256
133 $[(CH_2CH_2O)_3H]^+$	8,048	6,855	9,699
PLA			
55 $[H_2C{=}CH\text{-}C{=}O]^+$	401,902	387,149	292,766
56	474,825	468,192	362,667
71 $[CH_2{=}C\text{-}CO_2H]^+$	47,173	34,109	41,813
83 Cyclic product see bottom of table	21,046	18,216	13,726
99 $[H_3C\text{-}CH\text{-}O\text{-}CO\text{-}C\text{-}CH_3]^+$	128,764	123,524	91,104
100 $[H_3C\text{-}CH\text{-}O\text{-}CO\text{-}CH\text{-}CH_3]^+$	132,209	125,855	2,592
101 $[H_3C\text{-}CH\text{-}O\text{-}HCO\text{-}CH\text{-}CH_3]^+$	29,288	27,929	27,034
127 $[H_2C{=}CH\text{-}CO_2\text{-}CH(CH_3)CO]^+$	107,249	98,750	64,943
128 $[H_3C\text{-}CH_2\text{-}CO_2\text{-}CH(CH_2)CO]^+$	138,700	126,102	3,707
129 $[H_3C\text{-}CH_2\text{-}CO_2\text{-}CH(CH_3)CO]^+$	37,482	22,418	24,990
143 $[H_2C{=}C\text{-}CO_2\text{-}CH(CH_3)\text{-}CO_2H]^+$	49,058	42,908	1,176
145 $[H_3C\text{-}CH\text{-}CO_2\text{-}CH(CH_3)\text{-}CO_2H]^+$	70,476	70,213	68,350
PLA and PEG			
73 $[H_3C\text{-}CH\text{-}CO_2H]^+$ OR $[H_3C\text{-}CH_2\text{-}O\text{-}CH_2\text{-}CH_2]^+$	53,414	75,874	75,578

Table 3.7 (a) : Summary of ToF-SIMS peaks and associated counts for <u>positive</u> peaks characteristic of PLA and PEG for the PLA-PEG polymers

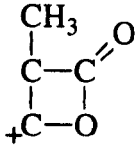

PLA m/z = 83

Peak mass	Counts PLA-PEG (3.64)	Counts PLA-PEG (2.17)	Counts PLA-PEG (0.83)
PEG			
58 $[O=C=CH_2\text{-}O]^-$	1,700	73	115
59 $[HO\text{-}CH=CH\text{-}O]^-$	4,320	5,511	5,949
61 $[HOCH_2CH_2O]^-$	1,218	1,495	2,042
85 $[H_2C=CHOCH=CH\text{-}O]^-$	3,802	257	3,890
105 $[HOCH_2CH_2OCH_2CH_2O]^-$	391	451	532
PLA			
45 $[H\text{-}CO_2]^-$	18,820	20,013	15,295
71 $[H_2C=CH\text{-}CO_2]^-$	112,974	3,122	115,365
73 $[H_3C\text{-}CH_2\text{-}C\text{-}O_2]^-$	56,071 / 32,267	38,347 / 64,803	32,484
87 $[O\text{-}C(CH_2)\text{-}CO_2H]^-$	124,722	142,443	98,745
89 $[O\text{-}CH(CH_3)\text{-}CO_2H]^-$	108,203	127,134	124,324
143 $[H_2C=CH\text{-}CO_2\text{-}CH(CH_3)\text{-}CO_2]^-$	36,631	41,980	35,157
145 $[H_3C\text{-}CH_2\text{-}CO_2\text{-}CH(CH_3)\text{-}CO_2]^-$	9,778	9,767	7,658
159 $[H_3C\text{-}CH_2\text{-}CO_2\text{-}CH(CH_3)\text{-}CO_2\text{-}CH_2]^-$	24,147	26,348	21,671
161 $[O\text{-}H_2C\text{-}CH_2\text{-}CO_2\text{-}CH(CH_3)\text{-}CO_2H]^-$	24,792	30,174	32,771
PLA/PEG			
43 $[H_2C=CH\text{-}O]^-$	37,749	49,043	46,613

Table 3.7 (b) : Summary of ToF-SIMS peaks and associated counts for <u>negative</u> peaks characteristic of PLA and PEG for the PLA-PEG polymers

mass, a number of anions corresponding to only each of the polymer blocks can be distinguished. For the PLA these peaks include m / z = 45 $[CHO_2]^-$, and $[nM_{PLA} \pm H]$ at m / z = 71 / 73 (n =1) and for $[M_{PLA} + O \pm H]$ m / z = 143 / 145 (n = 2) and m / z = 87 / 89.

Peaks for the PEG block of the polymers in the negative spectra are significantly less intense than those for the PLA portion of the molecule. The main peaks are m / z 58, 59, 61 and 85 which correspond to $[CH_2{=}CHOCH_3]^-$, $[HOCH{=}CHO]^-$, $[HOCH_2CH_2O]$- and $[CH_2{=}CHOCH{=}CHO]^-$ respectively.

From Tables 3.6 and 3.7 for the biotinylated and non-biotinylated polymers respectively, it can be observed that as the PLA : PEG ratio decreases in most cases the counts attributed to PLA peaks also decrease. For example, in the negative spectra, the PLA peak intensity at m / z = 71 which is equivalent to $[M_{PLA} - H]$ or $[M_{PLA}H - 2H]^-$ decreases from 46,038 to 25,822 counts with a corresponding decrease in the PLA : PEG ratio from 3.45 : 1 to 0.53 : 1 for the biotinylated polymers. In the positive spectra, a similar picture is observed. For example for the m / z = 127 peak a decrease from 107,249 to 64,943 is observed on decreasing the PLA :PEG ratio from 3.64 : 1 to 0.83 : 1.

In contrast, the intensity of the PEG peaks in general for both the positive and negative spectra are observed to increase as PLA : PEG ratio decreases. In the positive spectra this is typified by the PEG positive ion peak at m / z = 43 $[CH_2CO^+H]$. The ion count increases from 52,945 to 106,666 counts when the PLA : PEG ratio decreases from 3.45 to 0.53 : 1 for the biotinylated polymers. In the negative spectra for the non biotinylated PLA-PEGs, the same trend is observed, i.e. the m / z peak at 59 shows an increase in the number of counts from 4,320 to 5,945 as the PLA : PEG ratio

decreases from 3.64 to 0.83 : 1.

The decrease in intensity of the PLA peaks and corresponding increase in intensity of the PEG peaks can be attributed to the increase in the proportion of PEG in the polymer and hence its increased availability at the surface. These results agree well with those from XPS which also showed an increase in the PEG contribution to the surface layer with decreasing PLA : PEG ratio.

For both the biotinylated and non-biotinylated PLA-PEGs the distribution of PEG oligomers which was observed in the spectrum of biotin-PEG(3,800 Da) in Figure 3.7 as intense peaks at a separation of m / z = 44 is difficult to distinguish even in the polymer PLA-PEG-biotin(0.53). This can be attributed the lower surface density of PEG on addition of the PLA block and to the intensity of PLA peaks in the block co-polymer masking the PEG peak distribution. Peaks due to biotin were not distinguished in the spectra of the PLA-PEG-biotin polymers and this may again be attributed to their low surface concentration, as well as the intensity of the polymer peaks masking their presence.

Figure 3.8 shows the relationship between the theoretical bulk ratio of PLA : PEG calculated from NMR and experimental values from XPS and ToF-SIMS for both the biotinylated (3.8 (a)) and non-biotinylated (3.8 (b)) polymers. For both polymer series and both techniques there is a linear correlation between experimental PLA : PEG ratios and calculated ones with R^2 values of 0.982 and 0.978 or greater for the biotinylated and non-biotinylated polymers respectively. Deviations of the experimental PLA : PEG ratios from those calculated from NMR can be attributed to preferential

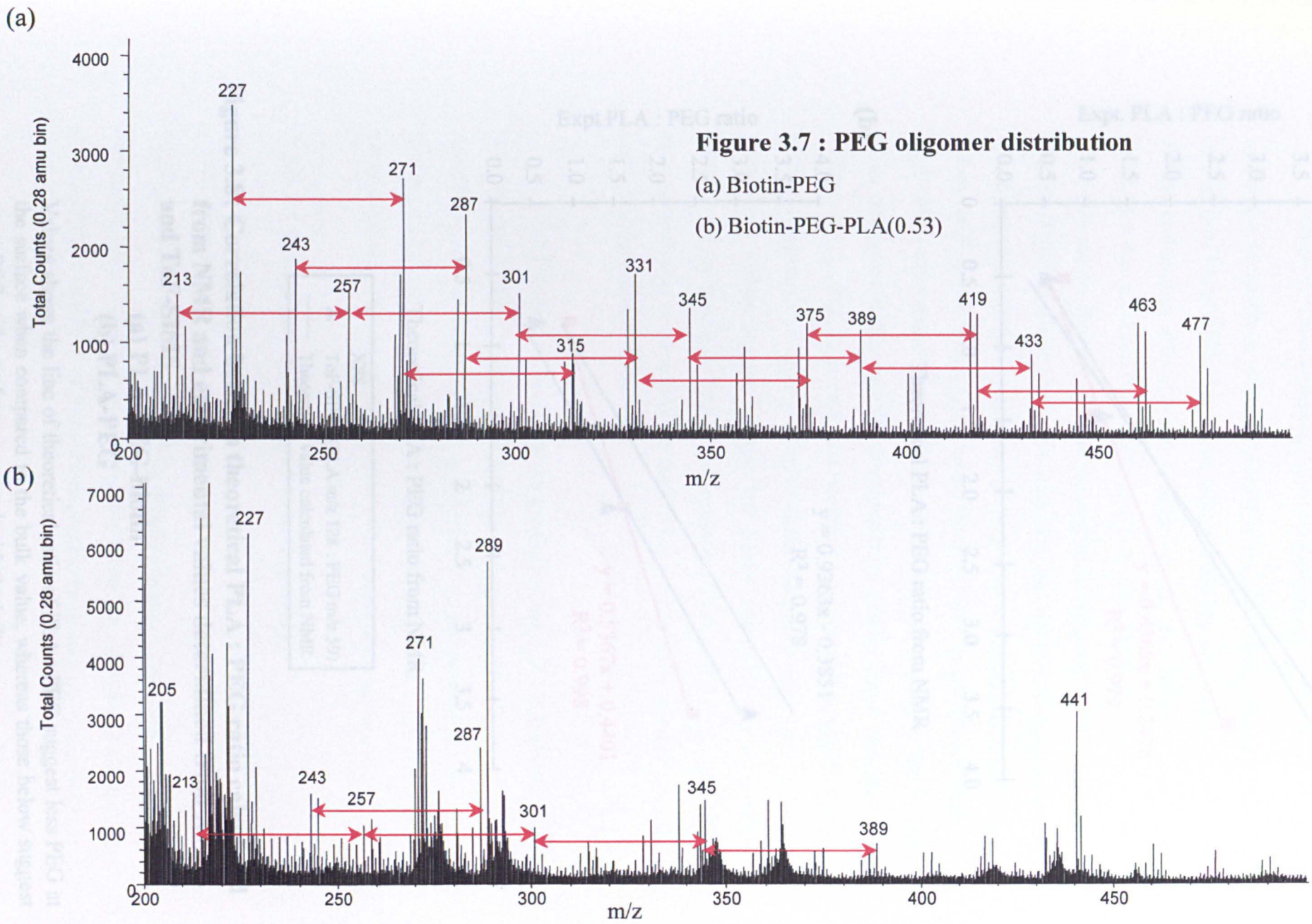

Figure 3.7 : PEG oligomer distribution

(a) Biotin-PEG

(b) Biotin-PEG-PLA(0.53)

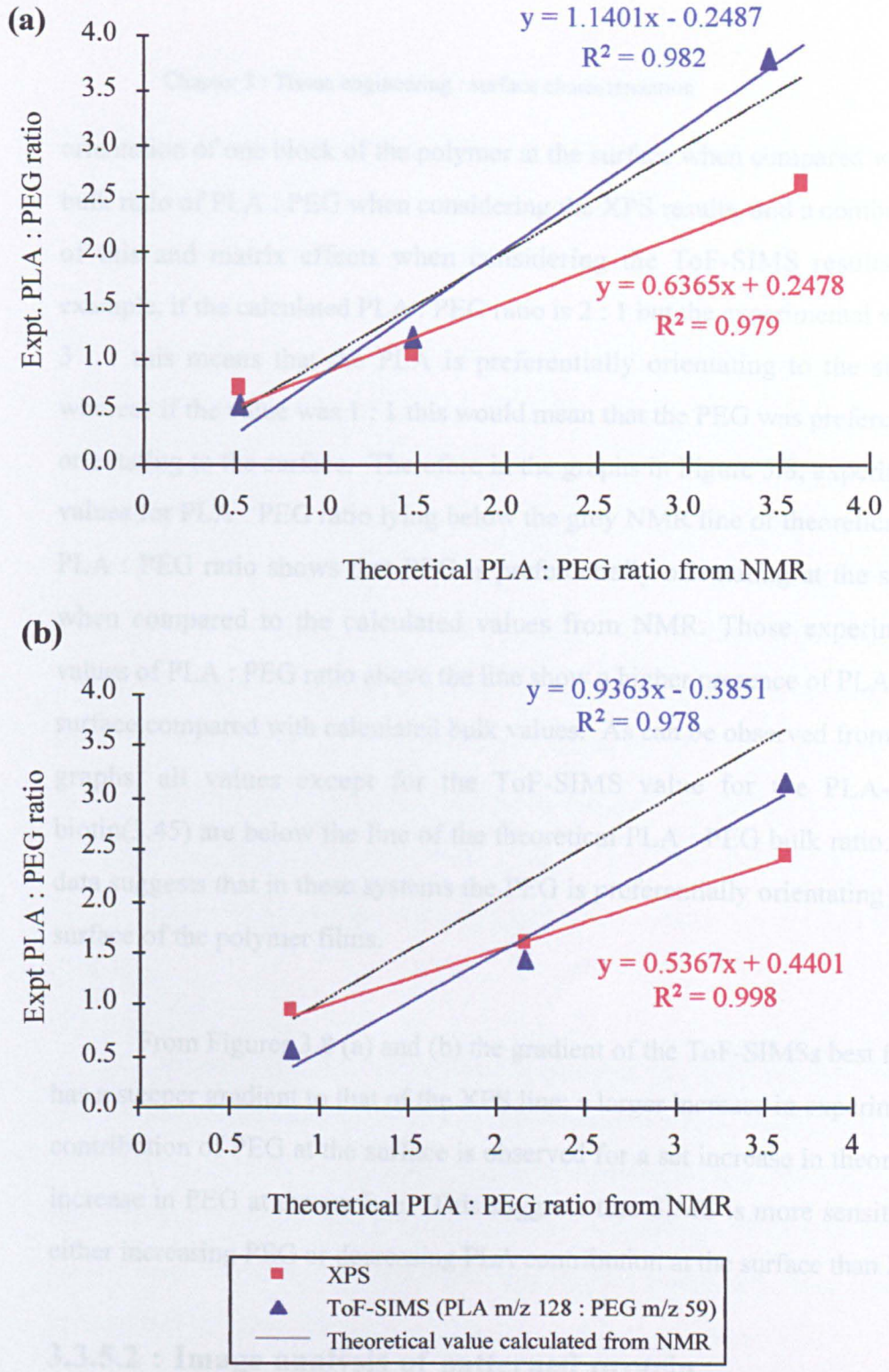

Figure 3.8: Correlation between theoretical PLA : PEG ratio calculated from NMR and experimental values determined from XPS and ToF-SIMS

(a) PLA-PEG-biotin

(b) PLA-PEG

Values above the line of theoretical ratio of PLA : PEG suggest less PEG at the surface when compared to the bulk value, whereas those below suggest more PEG at the surface compared with the bulk.

orientation of one block of the polymer at the surface when compared with the bulk ratio of PLA : PEG when considering the XPS results, and a combination of this and matrix effects when considering the ToF-SIMS results. For example, if the calculated PLA : PEG ratio is 2 : 1 but the experimental value is 3 : 1 this means that the PLA is preferentially orientating to the surface, whereas if the value was 1 : 1 this would mean that the PEG was preferentially orientating to the surface. Therefore in the graphs in Figure 3.8, experimental values for PLA : PEG ratio lying below the grey NMR line of theoretical bulk PLA : PEG ratio shows that PEG is preferentially orientating at the surface when compared to the calculated values from NMR. Those experimental values of PLA : PEG ratio above the line show a higher presence of PLA at the surface compared with calculated bulk values. As can be observed from these graphs, all values except for the ToF-SIMS value for the PLA-PEG-biotin(3.45) are below the line of the theoretical PLA : PEG bulk ratio. This data suggests that in these systems the PEG is preferentially orientating at the surface of the polymer films.

From Figures 3.8 (a) and (b) the gradient of the ToF-SIMSs best fit line has a steeper gradient to that of the XPS line; a larger increase in experimental contribution of PEG at the surface is observed for a set increase in theoretical increase in PEG at the surface. This suggests that SIMS is more sensitive to either increasing PEG or decreasing PLA contribution at the surface than XPS.

3.3.5.2 : Image analysis of patterned protein

As discussed in 3.2.6, microfluidic flow techniques can be utilised to form lines of avidin on the PLA-PEG-biotin surface. After incubating with biotinylated RGD-peptides and cells, this technique allows the controlled growth of cells in lines where the RGD-peptide is present as shown by Patel

et al. in their 1998 paper investigating the patterning of nerve and endothelial cells (Patel (1998)). Using imaging ToF-SIMS, the surface of such a avidin patterned polymer surface was investigated.

Surprisingly, it was found that the PLA-PEG-biotin spectra were dominated by PDMS transferred from the microfluidic flow mould. A summary of the peaks from the total ion count spectra associated with residues of PDMS are summarised in Table 3.8. The main peaks of interest for PDMS are the molecular ion $[(CH_3)_3\text{-}Si]^+$ and the multiples of this $[(CH_3)_3\text{-}Si\text{-}(O\text{-}Si\text{-}(CH_3)_2)n]^+$ i.e. n = 1 m/z = 147, and the cyclic product as depicted in Table 3.9 with m /z = 133. Other peaks of interest in the positive spectra are m / z 117, $[(CH_3)_3\text{-}Si\text{-}O\text{-}Si]+$ and m / z 103, $[H.(CH_3)_2\text{-}Si\text{-}O\text{-}Si]$. In the negative spectra the peaks of interest arising from PDMS in the m / z < 150 region are $[CH_3SiO]^-$ m / z = 59, $[SiO_2]^-$ m / z = 60, $[CH_3SiO_2]^-$ m / z = 75, $[CH_3Si\text{-}O\text{-}SiO_2]^-$ m / z = 119 and $[(CH_3)_3Si\text{-}O\text{-}SiO_2]^-$ m / z = 149 (Briggs (1989)).

Characteristic peaks associated with amino acids taken from Mantus and co-workers investigation into the fractionation of poly amino acids and protein as studied by SIMS were utilised to determine the avidin location on the patterned polymer film (Mantus (1993)). A summary of these peaks, the amino acid fragment they represent and counts associated with them are summarised in Table 3.9.

The characteristic peaks for PLA and PEG have been discussed in 3.3.5.1 (Davies (1989), Briggs (1989)). Table 3.10 summarises the distribution of the counts for the PDMS, protein and polymers taken from the total ion count spectra. The distribution of the counts shows the location of the peaks representative of the protein, PDMS and polymer on the avidin patterned

Positive Spectra		Negative Spectra	
Peak mass	**Counts**	**Peak mass**	**Counts**
73 $[(CH_3)\text{-}Si]^+$ (also contributions from protien, PLA,PEG)	523,101	59 $[H_3C\text{-}Si\text{-}O]^-$ (also contributions from protien)	57,127
103	8,926	60 $[SiO_2]^-$ (also contributions from protien)	27,349
117	20,336	75 $[H_3C\text{-}SiO_2]^-$	24,165
133 $[(CH_3)_2Si(O)\text{-}O\text{-}Si\text{-}CH_3]+$	31,383	119 $[H_3C\text{-}Si\text{-}O\text{-}SiO_2]^-$	2,254
147 $[(CH_3)_3\text{-}Si\text{-}O\text{-}Si\text{-}(CH_3)_2]^+$	164,238	149 $[(CH_3)_3Si\text{-}O\text{-}SiO_2]^-$	5,783

Table 3.8 : Summary of peaks observed for PDMS in PLA-PEG-biotin ToF-SIMS image. Counts taken from total ion spectra
Peaks taken from Briggs (1989)

Positive Spectra

Peak mass	Amino acid	Counts
28 $[HNCH]^+$	Gly	874,697
30 $[H_2N{=}CH_2]^+$	Gly,Leu,Phe, Tyr,Trp, His,Ser,Met, Lys, Arg,Orn. Asp, Glu	42,125
42 $[HNC\text{-}CH_3]^+$	Ala, Phe, Met	43,445
44 $[H_2\text{-}N{=}C\text{-}CH_3]+$	Ala,Leu,Phe, Tyr,Trp,His,Ser,Met,Lys, Arg,Orn.Asp, Glu	37,226
56 $[O{=}C{=}N{=}CH_2]^+$	Phe, Met, Gly, Lys	144,225
58 $[O{=}C(H)\text{-}NH{=}CH_2]^+$	Phe, Ser	26,941
60 $H_2N{=}CH\text{-}CH_2\text{-}OH]^-$ (Ser)	Ser, Arg	5,014
61 $[CH_2{=}S\text{-}CH_3]^+$	Met	5,552
62	Asp	462
68	Pro, Lys	4,143
70	Val, Pro, Arg, Orn	6,441
72 $HC(O)\text{-}NH{=}C(H)CH_3$	Val, Asp	13,951
73 (PLA / PEG / PDMS)	Arg	522,626
77	Phe, Tyr, Trp	2,755
81 see below	His	6,257
82	His	6,505
84 $[C_4H_6NO]^+$ (Glu) see below Lys	Leu, Lys, Glu	3,128
86 $[OHC\text{-}NH{=}CH\text{-}CHO]^+$	Leu, Asp	5,754
88 $[HO\text{-}CH_2\text{-}CH{=}NH\text{-}CHO]^+$	Asp	6,663
91 $H_2C{=}(C_6H_6)$ (Phe)	Phe, Tyr, Met	2,731
97	Arg	7,734
102 $[HN{=}C\text{-}CH_2)_2\text{-}S\text{-}CH_3]^+$ (Met) $[H_2N{=}CH\text{-}(CH_2)_2\text{-}CO_2H]^+$ (Glu)	Met, Glu	4,664
104 $[H_2N{=}CH\text{-}CH_2)_2\text{-}S\text{-}CH_3]^+$	Met	1,455

Table 3.9 (a) : Summary of positive peaks observed in ToF-SIMS image of avidin patterned on biotin-PLA-PEG which are characteristic of the protein
Peaks taken from Mantus (1993)

Positive Spectra

Peak mass	Amino acid	Counts
108 SEE BELOW	His	652
110 SEE BELOW	His	1103
118 $[HN.C\text{-}CH_2\text{-}(C_6H_6)]^+$	Phe	4,897
120 $[H_2N{=}CH\text{-}CH_2\text{-}(C_6H_6)]^+$	Phe	3,190
127 (PLA)$[HN{=}C\text{-}(CH_2)_3\text{-}NH\text{-}C(NH_2)NH]^+$	Arg	42,252
128 (PLA)	Arg	47,096
129 (PLA) $[H_2N{=}CH\text{-}(CH_2)_3\text{-}NH\text{-}C(NH_2)NH]^+$	Arg	21,379
130	Tyr	3,130
134 [NH.C-CH2-(C_6H_6)-*p*OH]+	Tyr	4,808
136 [NH2=CH-CH2-(C_6H_6)-*p*OH]+	Tyr	699

Table 3.9 (a) cont.: Summary of positive peaks observed in ToF-SIMS image of avidin patterned on biotin-PLA-PEG which are characteristic of the protein

Peaks taken from Mantus (1993)

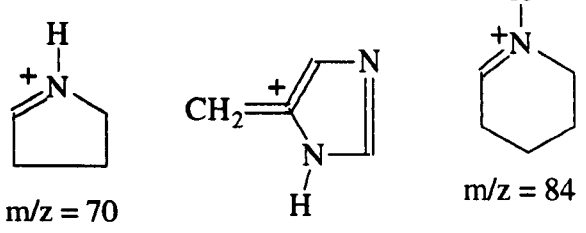

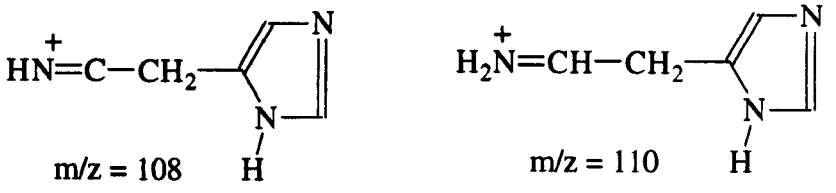

Negative Spectra

Peak mass	Amino acid	Counts
16 [O]-	Tyr	1,852,657
25 [C_2H]-	Phe, Tyr	164,047
26 [OCN]-	Gly,Leu,Phe, Tyr,Trp, His,Ser,Met, Lys, Arg,Asp, Glu	7,442
32 [S]-	Met	10,882
33 [HS]$^-$	Met	1,398
42 [CN]-	Gly,Leu,Phe, Tyr,Trp, His,Ser,Met, Lys, Arg,Asp, Glu	6,160
47 [H_3C-S]-	Met	381
58 (PEG)[H_2C-C(O)=NH]$^-$	Ser, Gly	7,461
59 (PDMS)[$C_3H_3O_2$]$^-$	Ser	22,664
60 (PDMS)	Phe, Tyr	27,323
62	Pro	1,396
66 See below	Pro	202
68	Pro	245
72	Ala	7,487
73 [H_2N-CH_2-C(O)=NH]$^-$	Gly	49,109
76	Phe	2490
77 [C_6H_5]$^-$	Phe	2,570
80	Trp	359
84	Ser	579
87 (PLA)	Ala	67,558
91 See below	Phe	4,891
98	Ala	464
100	Val	4,121
101[OHC-NH-CH_2-CO-NH]	Gly	2,291
108	Trp	38
114 [HN=C(0)-CH_2-CH_2-$CH(CH_3)_2$]$^-$	Leu	465
115 [OHC-NH-$C(CH_3)$H-C(O)=NH]$^-$	Ala, Val	5,153

Table 3.9 (b) : Summary of negative peaks observed in ToF-SIMS image of avidin patterned on biotin-PLA-PEG which are characteristic of the protein

Negative Spectra

Peak mass	Amino acid	Counts
116 $[H_2N\text{-}CH(CH(CH_3)_2)\text{-}C(O)=NH]^-$	Val	506
119 (PDMS) See below	Tyr	2,240
129 $[H_2N\text{-}CH(CH_2\text{-}CH(CH_3)_2)\text{-}C(O)=NH$	Leu	1,340
134	Tyr, Trp	275
137	Pro	372
139	Pro	368
140	Leu	128
141[$O=C=N\text{-}CH(CH(CH_3)_2)\text{-}CO=NH]^-$	Val	3,115
143 (PLA) $OHC\text{-}NH\text{-}CH(CH(CH_3)_2)\text{-}CO=NH]^-$	Val	23,366
144 $[C_{10}H_{20}N]^-$	Trp	4,679
155 $[C_8N_2H_{15}O]^-$	Val, Leu	472
157 $[C_8N_2H_{17}O]^-$	Leu	969
162	Trp	1,187
165	Pro	2,463
169	Leu	346
189 $[C_{11}H_{13}N_2O]^-$	Trp	1577

Table 3.9 (b) cont.: Summary of negative peaks observed in ToF-SIMS image of avidin patterned on biotin-PLA-PEG which are characteristic of the protein

Peaks taken from Mantus (1993)

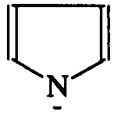

m/z = -66

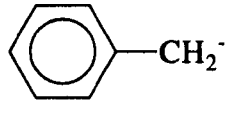

m/z = -91

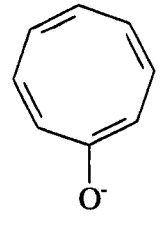

m/z = -119

Mass	Compound	Distribution	Max intensity	Peak counts from spectra
Total	All	Stripe	127	
135	PDMS	All	4	4,635
117	PDMS	All	4	20,336
103	PDMS	All	3	8,926
147	PDMS	Rest	11	164,238
133	PDMS	Rest	5	31,383
89	PEG	Stripe	7	40,248
87	PEG	Stripe	6	35,442
73	PEG/PLA/PDMS/Protein	Rest	25	523,101
59	PEG	All	8	57,127
45	PEG	Stripe	14	186,795
43	PEG	Stripe	19	339,968
83	PLA	Stripe	7	18,519
101	PLA	Stripe	6	22,895
100	PLA	Stripe	8	41,186
99	PLA	Stripe	8	49,285
145	PLA	Stripe	6	31,447
127	PLA	Stripe	8	42,423
143	PLA	Stripe	5	17,510
129	PLA	Stripe	5	21,232
71	PLA	Stripe	6	31,454
28	Protein	Rest	27	874,697
30	Protein	Rest	8	42,125
42	Protein	All	8	43,445
44	Protein	All	6	37,226
56	Protein	Stripe	14	144,225
58	Protein	All	5	26,941
70	Protein	Stripe	4	6,441
72	Protein	All	5	13,951
81	Protein	Stripe	4	6,257
82	Protein	Stripe	4	6,505
88	Protein	Stripe	5	6,663
97	Protein	Stripe	4	7,734
127	Protein / PLA	All	7	42,252
128	Protein / PLA	Stripe	9	47,096
129	Protein / PLA	Stripe	6	21,379

Table 3.10 (a) : Summary of the distribution for peaks over 6,000 counts from positive total ion ToF-SIMS image of avidin patterned onto biotin-PLA-PEG by microfluidic flow using a PDMS mould

Counts taken from total ion spectra. For assignment of peaks see table 3.6 and 3.7 for PLA and PEG, and 3.8 and 3.9 for PDMS and protein respectively
All = even distribution over all of surface
Stripe = microfluidic flow channel
Rest = area where mould was in contact with surface

Mass	Compound	Distribution	Max intensity	Peak counts from spectra
Total	All	Same	132	
43	PEG/PLA	Same	13	16,321
45	PLA	Same	4	10,481
71	PLA	Stripe	7	51,426
73	PLA	Stripe	8	48,913
89	PLA	Stripe	8	64,440
87	PLA / protein	Stripe	8	67,676
143	PLA / protein	Stripe	5	23,422
145	PLA	Stripe	4	12,653
58	PEG / protein	Rest	4	7,545
59	PEG/PDMS /protein	Stripe	5	22,714
61	PEG	Stripe	3	6,946
60	PDMS / protein	Rest	5	27,349
75	PDMS	Rest	5	24,165
16	protein	All		1,852,657
25	protein	All		164,047
26	protein	All		7,442
32	protein	Stripe		10,882
42	protein	Rest		6,160
72	protein	Stripe		7,487
73	protein	Stripe		49,109
115	protein	Stripe		5,153

Table 3.10 (b) : Summary of the distribution for peaks over 6,000 counts from negative total ion ToF-SIMS image of avidin patterned onto biotin-PLA-PEG by microfluidic flow using a PDMS mould

For assignment of peaks see table 3.6 and 3.7 for PLA and PEG, and 3.8 and 3.9 for PDMS and protein respectively

All = even distribution over all of surface

Stripe = microfluidic flow channel

Rest = area where mould was in contact with surface

surface, where 'all' means peaks were evenly distributed over all of the surface, 'stripe' refers to the area of the microfluidic mould channels and 'rest' where the mould was in contact with the polymer surface.

Figure 3.9 shows images of the patterned PLA-PEG-biotin polymer showing the distribution of peaks associated with amino acids along with a total ion spectrum arising from the region marked on the image. From this figure and Table 3.10 and it can be observed that the majority of the peaks which represent fragments from amino acids are located in the "stripe" area of the image (Mantus (1993)). The spectrum in Figure 3.10 is taken from the "stripe" area of the ToF-SIMS image and shows the intensity of positive peaks which are representative of the amino acid fragments. When comparing the intensities of those peaks in the "stripe" area to those for the "rest" area, the "stripe" area intensities are higher. For example, the peak at m / z = 30 which is found in most amino acids is observed to increase from 262 counts to 1356 in the area of the stripe, where as m / z = 56 present in phenylalanine, lysine, methionine and glycine is attributed to 3,457 in the "rest" area and 6,461 in the "stripe" area. This data correlates well to published fluorescent and AFM images of the same system which shows that the protein is restricted to the area of capillaries in the PDMS mould (Patel (1998)).

Table 3.10 shows the distribution of the peaks associated with PDMS, whereas Figure 3.10 illustrates images representative of the patterned polymer surface using peaks associated with PDMS. It can be observed that the majority of PDMS peaks are located in the area of the image where PDMS mould was in contact with the polymer surface ("rest"). Figure 3.10 depicts spectra representative of the "stripe" and "rest" areas of the ToF-SIMS image. These show the relative intensities of the PDMS peaks in these areas. It can be observed that the negative peaks associated with PDMS are present in both

Figure 3.9 : Images of avidin patterned PLA-PEG-biotin polymer showing protein distribution

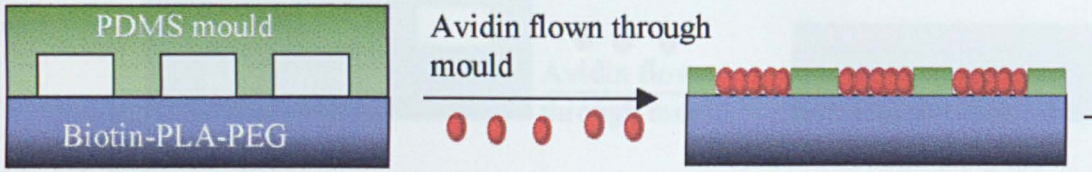

ToF-SIMS

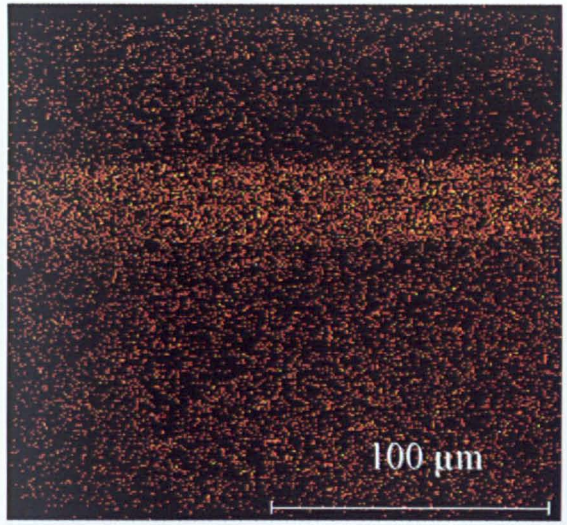

Protein peak images for mass 32(met),72 (ala) and 115 (ala) added together (negative spectra)

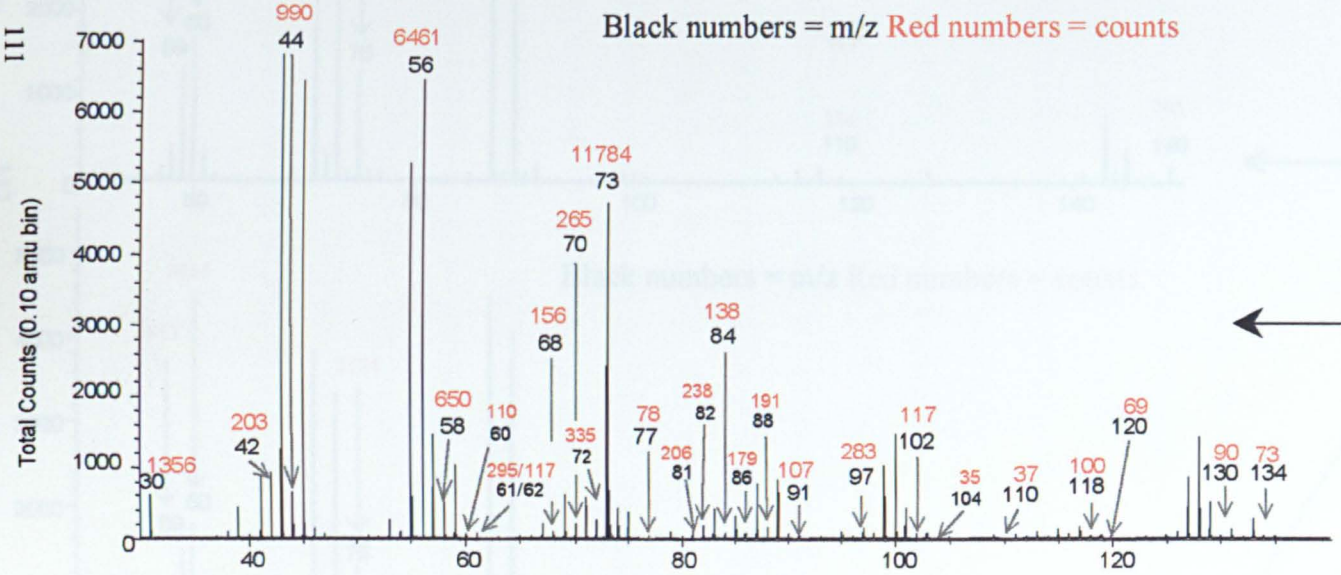

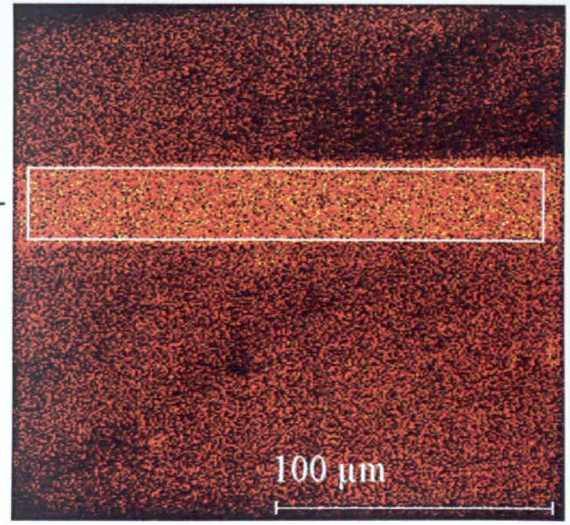

Protein peak images for mass 56(phe, gly, lys,met),70 (val, pro, arg, orn) and 81 (his) added together (positive spectra)

Figure 3.10 : Images of avidin patterned biotin-PLA-PEG polymer showing PDMS distribution

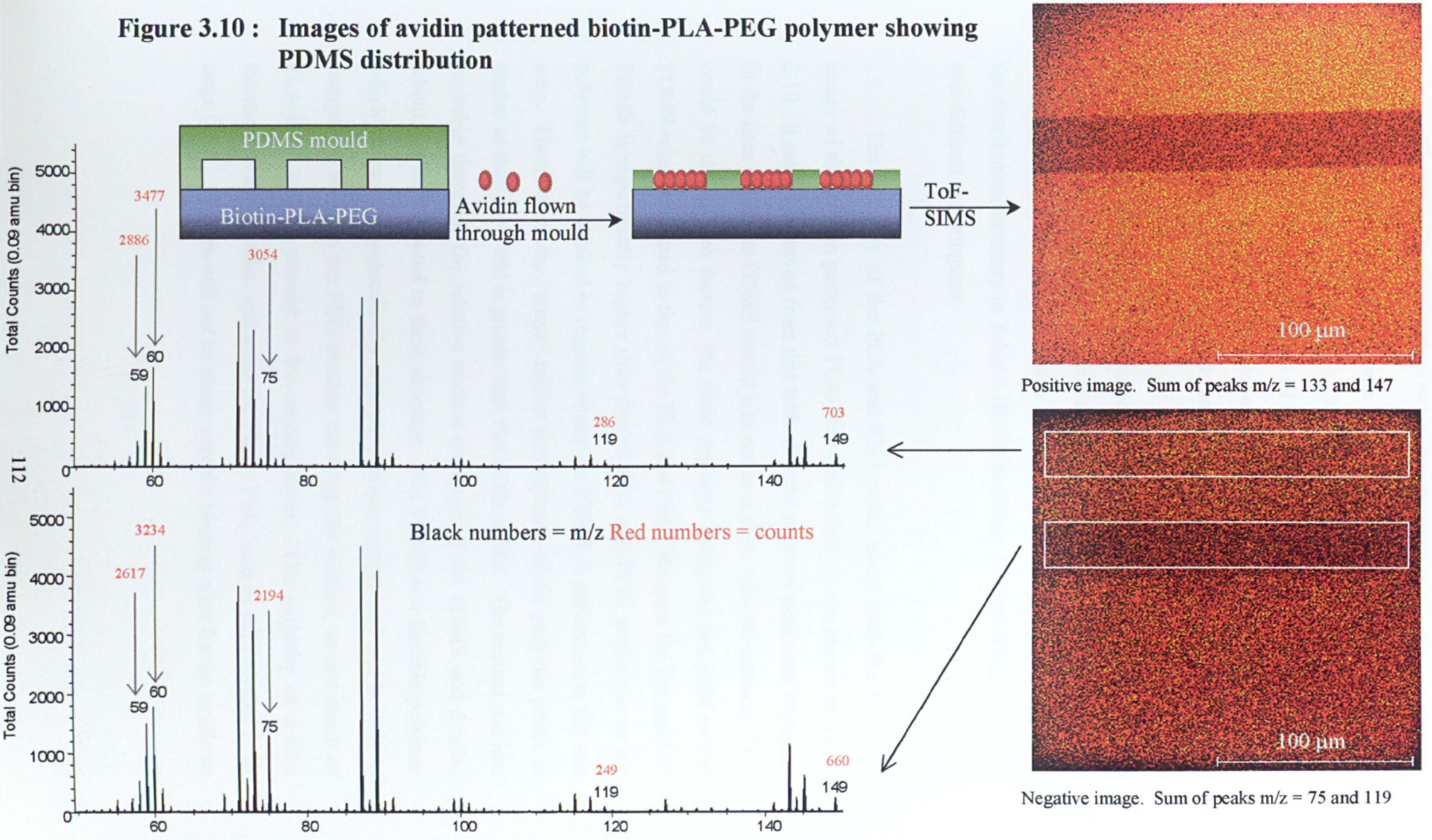

areas, however they are more intense in the "rest" area, for example, the peak at m / z -60 increases from 3234 to 3477 counts. This suggests that although some PDMS leaching occurs from all the underneath surface of the mould onto the PLA-PEG-biotin or protein covered PLA-PEG-biotin more leaching occurs where the mould is in contact with the polymer surface i.e. in the "rest" area.

It should be noted that the peaks chosen for the images depicted in Figure 3.9 and 3.10 where chosen as they gave the best resolution of the "stripe" and "rest' areas. When other peaks were chosen, as is suggested from the distribution summary in Table 3.10, the boundary between these two areas was difficult to distinguish.

The intensity of the PLA and PEG peaks taken from the total ion image of the protein patterned PLA-PEG-biotin surface are shown in Table 3.10. It can be observed from this table that the polymer peaks are strongest in the area where the PDMS mould was not in contact with the surface. This could be due to two factors, the most probable being the ion yield of the PDMS when compared to that of the PLA and PEG. Because the ion yield of PDMS is significantly higher than that of PLA and PEG, peaks due to the polymer will be masked in regions where the PDMS is present ie. in the rest area. Therefore in the "stripe" region the intensity of the polymer peaks is higher as their ion yield is greater than that of the avidin. The second and less probable theory is the relative surface coverage of the PDMS and avidin, which can be attributed to their structure. The PDMS is a flexible polymer which interacts non-specifically with the polymer surface and will be able to interpolate between the PEG brushes covering the surface, so not much of PLA-PEG will be present at the surface layer. The majority of avidin interactions are specific, and since the PLA : PEG ratio of the polymer is so large (3.45 : 1), there will not be many specific binding sites for the avidin to

attach to. Therefore, a significant proportion of the surface may be not coated in protein (This is discussed in more detail in Chapter 4). This is represented schematically in Figure 3.11.

From Figure 3.12 the effect of poor plasma treatment of the mould can be observed. If not plasma etched for long enough the surface of the mould will not be hydrophilic enough for a strong seal with the polymer surface. This in turn will allow the protein solution to leak from the capillary channels. This phenomena is observed in Figure 3.12 as peaks associated with amino acids as detailed in Table 3.8 can be observed at the lower edge of the capillary mould interface. Figure 3.12 also illustrates that as well as determining the spatial distribution of components on a surface, the surface topology of a sample can be followed to some extent by imaging ToF-SIMS. As denoted by arrows on the figure significant differences in the intensity of the polymer peaks can be observed in the region where avidin is not present. These could be attributed to the topography of the polymer film.

3.4 : Conclusions and future work

As discussed in the introduction to this chapter (3.1.4), for cells to grow and spread efficiently a optimal density of cell adhesion molecules is required (Massia (1991)). However, this density will vary with cell type. Therefore, in tissue engineering, a polymer scaffold system where the degree of surface modification by cell adhesion molecules can be controlled would be of significant benefit. To try and realise this aim the PLA-PEG-biotin system was developed. It was hoped that by varying the PLA molecular weight the density of PEG and hence biotin at the surface could be varied. The investigations in this chapter probed the surface characteristics of such materials to distinguish the relative contribution of the three different entities

(a)

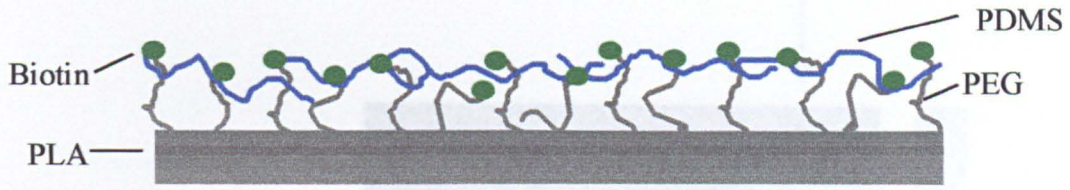

PDMS is flexible and therefore can form a relatively complete layer over the polymer surface masking the PLA and PEG

(b)

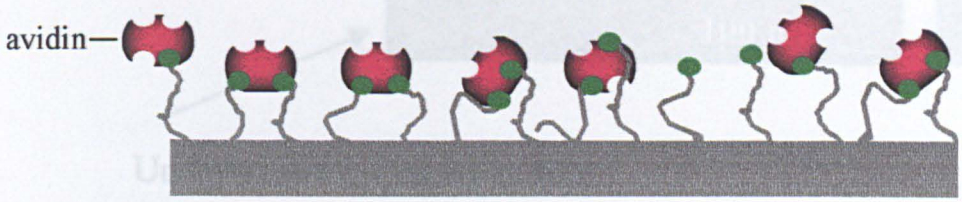

The globular avidin can not alter its conformation significantly and because it only binds specifically to the polymer surface a significantly proportion of the polymer surface is uncovered

Figure 3.11 : Schematic representation of the interaction of (a) PDMS and (b) avidin with the PLA-PEG-biotin

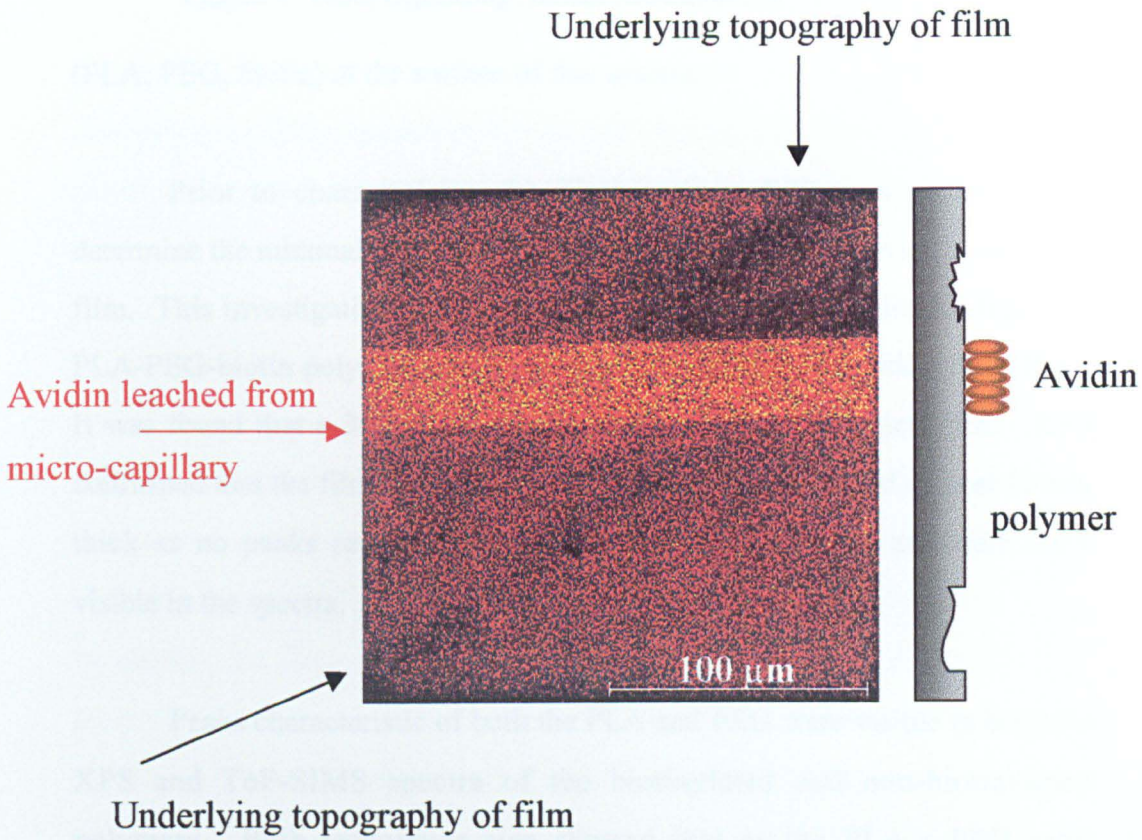

Figure 3.12 : Total ion ToF-SIMS image of avidin patterning on biotin-PLA-PEG, showing leaching of avidin from capillary and topography of underlying polymer film

(PLA, PEG, biotin) at the surface of this system.

Prior to characterising the films surface, SPR was performed to determine the minimal concentration of polymer needed to provide a complete film. This investigation monitored the extent of specific avidin binding to a PLA-PEG-biotin polymer and its non-specific interactions with a PLA-PEG. It was found that a 3 mg / ml solution cast to form a complete film. XPS confirmed that the films cast in this manner were complete and at least 10 nm thick as no peaks representative of the underlying silicon substrate were visible in the spectra.

Peaks characteristic of both the PLA and PEG were visible in both the XPS and ToF-SIMS spectra of the biotinylated and non-biotinylated polymers. Both techniques also showed that as the PLA : PEG ratio decreased ie. molecular weight of PLA decreased, an increase in the surface contribution of the PEG portion of the molecule occurred. From XPS, for both the biotinylated and non-biotinylated PLA-PEG polymers a higher carbon : oxygen ratio was observed at the surface than that calculated for the bulk from NMR investigations. Since the C : O ratio for PLA and PEG is 3 : 2 and 2 : 1 respectively this suggests that the PEG is preferentially orientating to the surface.

Although peaks characteristic of both PLA and PEG were determined by XPS and SIMS, the presence of biotin was not. However, since biotin is only located at the termini of the PEG portion of the molecule these results suggest that as PLA : PEG ratio deceases the density of biotin at the surface will increase.

Static contact angle measurements demonstrated that as PLA : PEG

ratio decreased a reduction in the contact angle from 74.5° ± 2.5° to 62.4° ± 1.8° also occurred. This means that the surface became more hydrophilic. This in addition to results from XPS and ToF-SIMS suggest that more PEG was locating at the surface.

From AFM imaging of the complete PLA-PEG-biotin films it could be observed that their surface structure was constant and extremely flat, with z scales no greater than 20 nm even after incubating in buffer. On performing roughness analysis of the surfaces it was observed that the PLA-PEG-biotin(0.53) was rougher than the other two polymers. After incubating the films in buffer this sample also had the largest percentage increase in surface roughness. These results suggested that the roughness of the film could be related to the PLA : PEG ratio of the polymer.

These results show that by altering the molecular structure of this PLA-PEG-biotin material its surface characteristics in terms of PLA and PEG content can be controlled. This in turn suggests that the presence of biotin at the surface can be manipulated in a controlled fashion. Therefore by surface engineering of the system by avidin and biotinylated cell adhesion molecules, their density at the PLA-PEG-biotin interfaces may be controlled so the optimum concentration of cell adhesion molecules for cell growth and spreading can be determined.

However, these results also show that care must be taken as the bulk composition of the material is not always representative of the chemical composition of the surface as shown by carbon : oxygen ratios calculated from XPS data. AFM also showed that by altering the chemical composition of the materials its surface structure can also be altered. This also has implications for the proliferation of cells on this biomaterials surface.

In tissues in the body different cell types grow along side each other in a complementary fashion. For tissue engineering to be a successful pursuit as an alternative for tissue transplant, this must be able to occur in these systems. By the use of micro-fluidic flow techniques narrow lines typically in the tens of micrometers range can be formed. By isolating cell adhesion molecules specific to different cell types onto these different lines it may be possible to encourage the co-culture of differentiated cell types on a biomaterials surface.

In this investigation, imaging ToF-SIMS was utilised to map the distribution of avidin patterned on the surface of a PLA-PEG-biotin surface by micro-fluidic flow. Peaks representative not only of the underlying PLA-PEG-biotin polymer were characterised but also those representative of PDMS residues from the micro-fluidic flow mould and amino acid fragments representative of the patterned avidin. The presence of the peaks corresponding to the PDMS and avidin were mainly located in two separate regions. The PDMS was located where the mould had come in contact with the polymer surface and the protein where the mould micro-capillaries were. However, the sharpness of the boundary between these two regions was dependant on the PDMS and protein peaks chosen. These results although not quantitative show that ToF-SIMS imaging is a useful technique for visualising the qualitative distribution of differing chemical groups present at a surface of biomedical polymers of interest.

Chapter 4 : Polymers for Tissue Engineering : Surface Interactions

4.1 : Introduction

In the last chapter, the importance of the characterisation of a materials surface was discussed. This chapter will focus on understanding how this surface structure will influence the material's interactions with biological macromolecules. In the case of a tissue engineering scaffold, the primary function of the material is to provide a basis for successful growth and differentiation of the cells seeded onto it, ultimately forming a functional tissue. However, equally important is its role in ensuring the implant is not rejected by an immune response once in the body. The immune response is a complex process, incorporating both antibody and cellular activity. Antibodies are proteins with specific receptors for the foreign material and once bound make it easier for the phagocytic cells to ingest the foreign material or the blood complement proteins to 'kill' it (Alberts (1989)). The immune response could act as a major route for failure of the tissue engineering scaffold, therefore the study of the interaction between proteins and the biomaterial is very important.

4.1.1 : The study of protein interactions with biomaterial surfaces

The study of the interactions of proteins with biomaterials has been carried out using a wide range of techniques on a variety of materials. For example SPR has been utilised by many groups to study the rate and extent of protein interactions with biomaterials. Utilising this technique Bousquet and co-workers showed results which suggest human serum albumin's (HSA) interactions with methylidene malonate nanoparticles to be mainly

electrostatic, with hydrophobic force stabilisation (Bousquet (1999)), whereas Garrett and Milthorpe showed it is a useful technique from monitoring the time and pH dependence of HSA adsorption to a range of contact lens materials (Garrett (1996)).

In a study combining AFM and SPR, Green et al. studied the adsorption kinetics of a range of proteins to polystyrene surfaces. The adsorption kinetics obtained from SPR for the different proteins could be related to their molecular architecture, whereas AFM showed the different monolayer structures for the various proteins. The final layer thickness of the protein monolayer on polystyrene, as determined by SPR, was observed to correlate well with ellipsometry results (Green (1997)). Other techniques such as H^1 NMR, theoretical modelling, 2D electrophoresis and radiolabelling have been successfully utilised to investigate the factors which effect the non-specific interactions of proteins with biomedical polymers and hence provide information on their biocompatibility (Furness (1998), Luck (1998), McPherson (1998), Szleifer (1997)).

4.1.2 : Cell adhesion molecules

The above examples, highlight the research interest in improving biomaterials protein resistivity and hence making them more acceptable to the immune system. However, a biomaterials interaction with certain proteins can be favourable. In recent years, an emphasis has been put on the potential gains of using cell adhesion molecules. This is a very diverse family of molecules including, the Ig super family, selectins, cadherins and integrins. These molecules are found on cell membranes and in the extracellular matrix. They promote cell adhesion, spreading, migration and cell differentiation into various tissue types (Horwitz (1997)). Their roles in a variety of other cellular

mechanisms has also been identified. These include the tyrosine phosphorylation signalling pathway, control of intracellular calcium ion fluctuations and programmed cell death (Ojaniemi (1997), Juliano (1993) Meredith (1993)). These cell adhesion molecules act by either binding to themselves as observed with the cadherins, binding to carbohydrates such as the lectins and selectins or binding specific peptides sequences such as the integrins.

The binding of integrins to molecules to cause cellular events requires two components. Firstly, the presence of extracellular divalent cations, and secondly, a peptide sequence in the molecule to which the integrin binds, which contains an acidic amino acid. Two examples of such peptide sequences are the RGD (arginine-glycine-aspartic acid) and TIGSR (tyrosine-isoleucine-glycine-serine-arginine) peptide sequences (Jones (1996)). Because of the wide variety of integrins and their presence on the majority of cell types, the potential use for this binding relationship provides many avenues for its applications.

The two main areas of research into the exploitation of integrins and RGD-like peptides are chemotherapy and tissue engineering. Within the field of preventing or curing disease states, the blocking integrin mediated binding may be useful. Some disease state have been shown to be mediated by integrin proteins. These include, infection by certain microbes causing meningitis and diarrhoea which use the integrins as a pathway to enter cells and some cancer types where normal integrins are no longer produced, their distribution altered or integrins not normally associated with the cell type are expressed (Horwitz (1997)).

In tissue engineering it is hoped that the inclusion of integrins or RGD-

like peptides into tissue engineering scaffolds will promote cell adhesion, spreading and differentiation, (Shakesheff (1998)) so in the future the production of organs containing multiple cell types with differentiated functions will be possible rather than the production of tissue with singular cell types as is observed at the present time.

Many groups have discussed the addition of such peptides and proteins to a polymer chain. The advantages of polymer-protein conjugates include increased solubility and plasma half-life and reduced immunogenicity (Wilkinson (1987)). The uses of this type of system range from diagnostic tools and materials which could be used in the separation of biological cells to polymer systems for lysosomal drug release (Lowndes (1994)). The use of polymer RGD conjugates within the field of tissue engineering has been highlighted in recent papers.

Dai and Saltzman have shown fibroblast aggregation can be induced by PEG conjugated to RGD containing peptides in fibroblasts transformed to produce nerve growth factor (NGF). The PEG peptide conjugate aggregated cells produced significantly larger quantities of NGF compared to those in normal cell culture. This type of approach could prove advantageous in large scale cell culture and tissue engineering applications (Dai (1996)).

The adhesion strength and number of focal points on bone cells was observed by Rezania and co-workers to be significantly greater on quartz surfaces grafted with RGD containing peptides when compared to those coated in RGE containing peptides sequences. The RGE peptide was used as a control peptide as it is known not to interact with bone sialoprotein. They suggest that this immobilisation strategy has applications in the fields of implants, biosensors and diagnostic devices, where specific cell adhesion is

required (Rezania (1997)).

4.1.3 : Aim of work

As discussed in Chapter 3, the polymer investigated in this study is a block co-polymer of poly(lactic acid) (PLA) and poly(ethylene glycol) (PEG), whose PEG terminus is biotinylated. The structure of this material was depicted in Figure 3.1. All parts of this material are essential to its success as a polymer for the construction of tissue engineering scaffolds. The hard, hydrophobic PLA gives the material structural integrity. Being biodegradable it aids removal of the polymer scaffold from the body at the end of its useful life. The PEG as discussed above, acts to minimise non-specific interactions of proteins and hence increase the biocompatibility of the system. The biotin is the functional part of the molecule and via avidin-biotin interactions allows the surface engineering of this material by biotinylated RGD-peptides. The strategy for surface modification is depicted in Figure 4.1. Avidin a tetrameric protein binds to the polymer surface via avidin-biotin interactions. As the protein has four binding sites three are potentially still available for binding biotinylated RGD-peptide sequences. These sequences in turn promote cell adhesion and spreading via integrin interactions.

The streptavidin-biotin interaction has been widely studied. It is the strongest naturally occurring non-covalent interaction with an affinity constant of 10^{15} L / mol (Diamandis (1991)). Because of its high affinity constant this interaction has been used in many medical applications including pretargeting methods for cancer chemotherapy (Sharkey (1997), Casalini (1997)), systems for increased resolution imaging, including that for deep venous thrombosis (Rosebrough (1996)) immunoassays (Allen (1996), Viera (1998), Ding (1999)), staining in immunocytochemistry (Ferri (1999)) and assessing cardiovascular

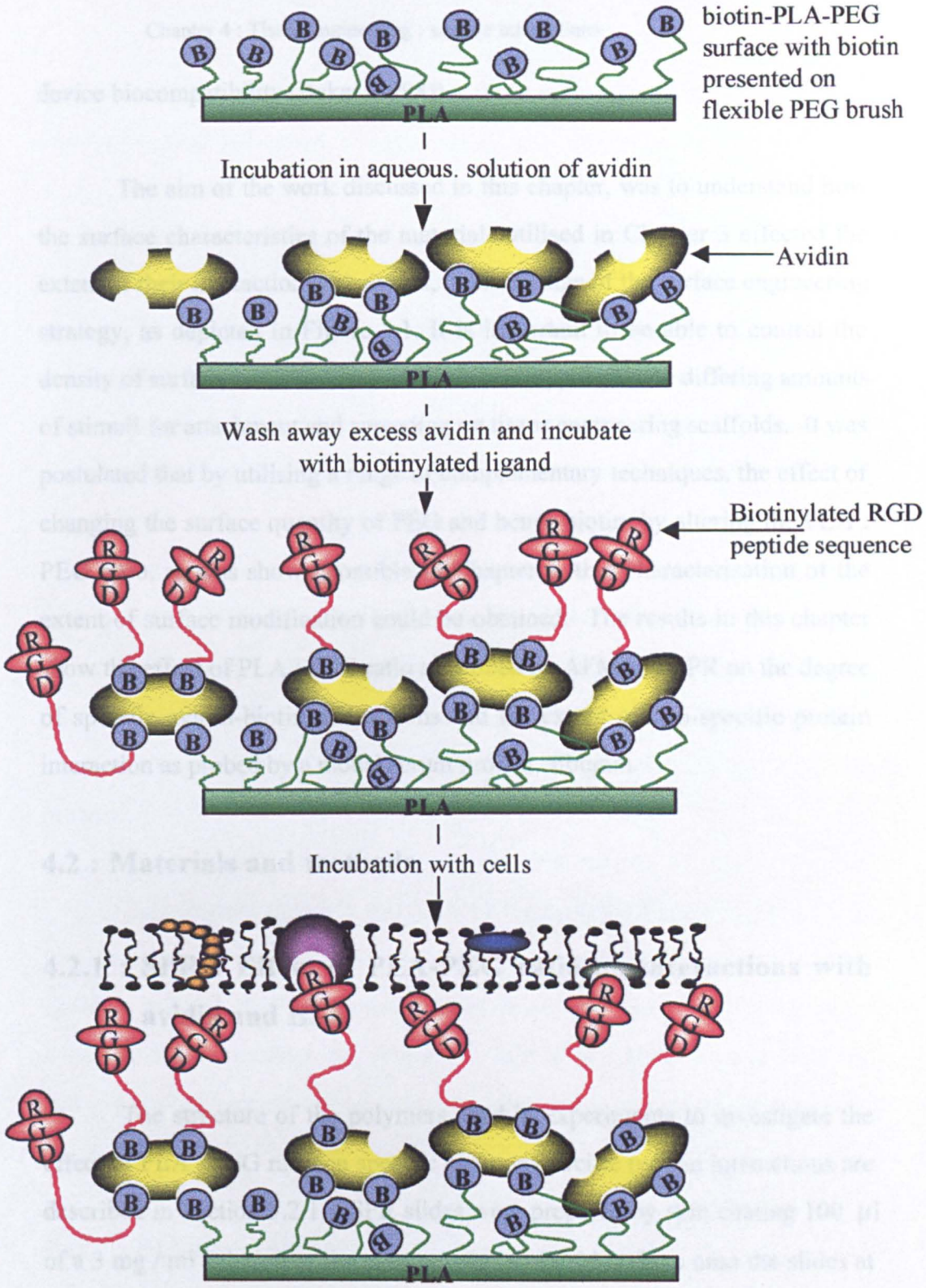

Figure 4.1 :Schematic representation of the surface engineering strategy

device biocompatibility (Baker (1998)).

The aim of the work discussed in this chapter, was to understand how the surface characteristics of the materials utilised in Chapter 3 effected the extent of their interaction with avidin, the first stage of the surface engineering strategy, as depicted in Figure 4.1. It is important to be able to control the density of surface modification as different cell types require differing amounts of stimuli for attachment and spreading on tissue engineering scaffolds. It was postulated that by utilising a range of complementary techniques, the effect of changing the surface quantity of PEG and hence biotin, by altering the PLA : PEG ratio, as was shown possible in Chapter 3, that characterisation of the extent of surface modification could be obtained. The results in this chapter show the effect of PLA : PEG ratio as probed by AFM and SPR on the degree of specific avidin-biotin interactions and the extent of non-specific protein interaction as probed by a model serum protein, albumin.

4.2 : Materials and methods.

4.2.1 : SPR : Effect of PLA-PEG ratio on interactions with avidin and HSA

The structure of the polymers used in experiments to investigate the effect of PLA : PEG ratio on specific and non-specific protein interactions are described in Section 3.2.1. SPR slides were prepared by spin coating 100 μl of a 3 mg / ml solution of the chosen polymer in chloroform onto the slides at ~2,000 rpm. After a stable baseline of buffer flow (phosphate buffer, 10 mM, pH 7.4) had been obtained 1 ml of a 5 x 10^{-7} M avidin solution, in the same buffer was injected over the polymer surface. The change in SPR angle obtained after a buffer wash following the injection provides a measure of the

specific and non-specific avidin binding to the biotinylated and non-biotinylated polymers.

To determine the extent of non-specific interaction with the PLA-PEG-biotin polymers two sets of control experiments were performed. In the first, the same procedure as above was utilised but instead of using avidin, human serum albumin (HSA), 0.5 mg / ml in phosphate buffer was utilised. This protein possesses no specific binding site for biotin and is often used as a model protein to study the biocompatibility of polymeric materials.

In the second control experiment, avidin which had been pre-incubated with a 5 fold molar excess of biotin was utilised. Each mole of avidin possesses four moles of biotin binding sites, therefore by using a 5 fold molar excess of biotin the binding sites should all be blocked. Therefore only non-specific interactions between the avidin and polymer surface could be probed.

Experiments utilising mixtures of biotinylated PLA-PEG and PLA-PEG were also investigated to probe the level to which the avidin binding could be reduced. SPR slides were coated in polymer films cast from polymer solutions as summarised in Table 4.1. SPR experiments to determine the extent of avidin binding were performed as described for the single biotinylated polymers.

4.2.2 : System stability

When utilising this polymer system for tissue culture experiments, samples of avidin coated polymer may be prepared a few days before the cells are seeded on to the polymer scaffold. Therefore it is important to ensure that

Polymer 1 / Polymer2	biotin-PLA-PEG(1.49)	biotin-PLA-PEG(1.49)	biotin-PLA-PEG(1.49)	biotin-PLA-PEG(1.49)
PLAPEG (0.96)	0.8 : 0.2	0.6 : 0.4	0.4 : 0.6	0.2 : 0.8
PLAPEG (3.64)	0.5 : 0.5			
PLAPEG (2.17)	0.5 : 0.5			
PLAPEG (0.86)	0.5 : 0.5			

Table 4.1 : Ratios of bioti ylated to non-biotinylated polymers used to investigate the minimal avidin coverage possible

the polymer / avidin surface is stable over time. To test the stability of this polymer system, coated slides were prepared as described above. These were incubated for 5 min in a 5 x 10^{-7} M solution of avidin in phosphate buffer (pH 7.4, 10 mM). Then the polymer slides with avidin specifically bound to them were washed with deionised water and dried under a nitrogen stream. The slides were then either used immediately or stored under ambient conditions in a glass petri dish for 48 h prior to use. The SPR experiment consisted of buffer flow, to obtain a stable baseline and then a 1 ml injection of biotinylated ferritin 3 x 10^{-7} M. A buffer wash was performed after the injection to check for removal of loosely bound ferritin. This experiment determined the proportion of active avidin that was still able to bind biotinylated species, compared with freshly prepared slides. Control experiments were performed using the same protocol but utilising ferritin which was not biotinylated, to check for non-specific interactions between the ferritin and avidin.

4.2.3 : Biotin-peptide immobilisation

The second, and most important stage of the surface engineering of the biotinylated PLA-PEG is the binding of the biotinylated peptide sequences to the avidin. Experiments were performed to assess if the PLA : PEG polymer ratio had any effect on the amount of biotinylated RGD binding to the avidin at the polymer interface. The biotinylated RGD sequence utilised is depicted in Figure 4.2. These experiments were performed on the SPR. After obtaining a stable baseline, avidin (5 x 10^{-7} M) was injected to bind to the biotinylated polymer. Following a buffer wash, 1 ml of biotinylated-RGD peptide (0.1 mg / ml) was injected, and the experiment concluded by another buffer wash to remove any loosely bound peptide.

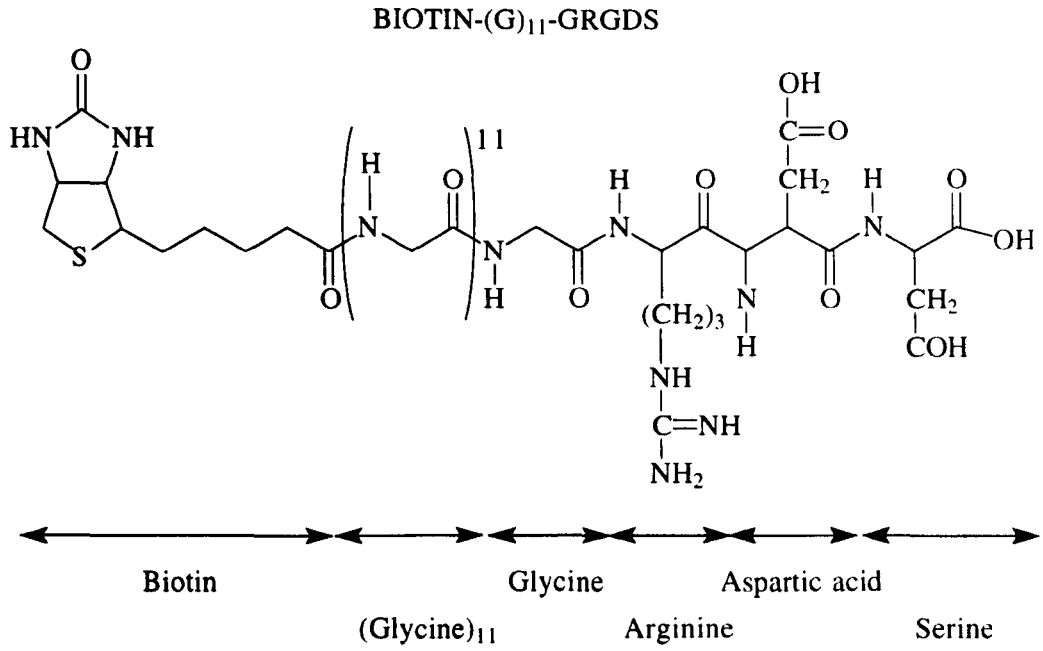

Figure 4.2 : Sequence of biotinylated peptide used

4.2.4 : AFM : Effect of PLA-PEG ratio on interactions with avidin and HSA

Polymer samples utilised to investigate the extent of protein interaction with varying PLA-PEG ratios were cast from a 200 µl portion of a 3 mg /ml solution of the polymer in TFE onto polycarbonate Hybrislips™. Samples were incubated for 5 min with either 0.5 mg / ml HSA or 5 x 10^{-7} M avidin, both in phosphate buffer. After the incubation period, samples were rinsed with deionised water and dried under a nitrogen stream. Samples were imaged in tapping mode in air as described in Chapter 2.3.

4.2.5 : SPR : Effect of surfactants on degree of surface modification

When processing polymers into scaffolds for tissue engineering purposes, surfactants are often used to stabilise the newly formed surfaces. It was a concern that this process may effect the degree of surface modification of the biotinylated PLA-PEGs by avidin. Therefore a variety of surfactants, at varying concentrations, were investigated to determine the what to which they limited the avidin surface modification of the biotinylated polymers. The surfactants utilised in these studies were poly(vinyl alcohol) (PVA) (88% hydrolyzed, 85 kDa) at concentrations between 0.005 and 1.00% (w / v) and the Pluronic surfactants F68, F108 and F127 at concentrations of 0.1 and 1.0% (BASF Corp., Parsippany, NJ. USA.). The molecular weights for the PEO and PEG blocks of the Pluronics are shown in Table 4.2. All dilutions were performed in phosphate buffer (10 mM, pH 7.4). The protocol for the SPR investigations was as follows. A stable buffer baseline (phosphate, 10 mM, pH 7.4) was obtained on the chosen polymer coated slide (4.2.1). 1 ml of the chosen surfactant and concentration was injected over the surface and a buffer

Pluronic	Total MWt	Monomer units MWt.		
		PEO	PPO	PEO
F68	8,350	75	30	75
F108	14,000	128	54	128
F127	11,500	98	67	98

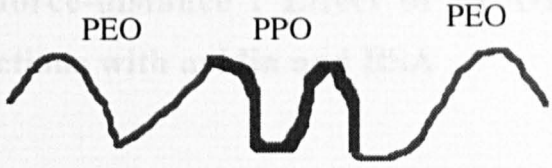

Schematic representation of the pluronics structure

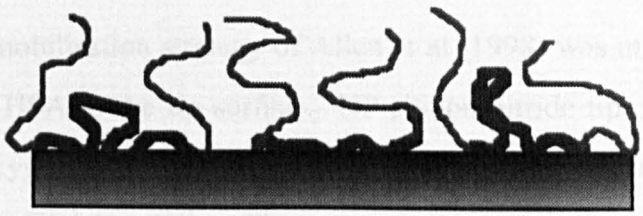

loops chains and tails conformation of the pluronics adsorbed at a hydrophobic interface

Table 4.2 : Structure of Pluronic™ surfactants used in SPR studies

wash followed to remove the excess which was not strongly associated with the surface. This was followed by an avidin injection (5 x 10^{-7} M in phosphate buffer) to quantify the extent of interaction still obtainable with the PLA-PEG-biotin. A buffer wash finished the SPR run, to remove loosely bound avidin. Experiments were also performed utilising the same protocol, on the non-biotinylated PLA-PEGs to observe the effect of surfactants on the non-specific binding of avidin to the polymers.

4.2.6 : AFM force-distance : Effect of PLA-PEG ratio on interactions with avidin and BSA

Force-distance experiments were performed with both avidin and BSA coated probes to measure the strength of specific and non-specific interactions with the PLA-PEG-biotin polymers.

The immobilisation strategy of Allen et al (1998) was utilised to bind streptavidin or HSA to the tip surface. NP silicon nitride tips were plasma etched using oxygen as the plasma gas for 30 sec at forward power of 20 W (Biorad, Polaron Division, UK.). They were then incubated in 3-aminopropyl dimethyl ethoxy silane (ABCR, Germany 4 % v / v) in toluene for 1 h. After washing in isopropanol, ethanol and phosphate buffer (pH 7.0, 100 mM) the tips were transferred to a 10% solution of glutaraldehyde in phosphate buffer for 2 h. After washing in buffer, samples were incubated overnight in either 0.1 mg /ml BSA or streptavidin solutions in buffer (phosphate, 10 mM, pH 7.4). Prior to use, the tips were rinsed in excess buffer.

Protein coated silicon wafer samples were prepared by the same method, except they were plasma etched at maximum power of 100 W for 1 min and sonicated for 10 sec in washing solutions between incubations. The

protein coating on the tips was confirmed by performing force distance curves on protein coated silicon samples. Only tips showing minimal adhesion were utilised for experiments to test the effect of PLA : PEG ratio on the extent of protein interaction.

Polymer samples (200 µl) were cast on to Hybrislips™ from a 3 mg / ml solution in TFE. The extent of interaction with both BSA and streptavidin coated probes was performed on the biotinylated polymers. Non-biotinylated polymer samples of similar PLA : PEG ratios were employed to determine the extent of non-specific streptavidin interactions with the polymers and a minimum of 60 curves were measured on each of the polymer surfaces.

Two control experiments were performed. Firstly, force-distance curves were performed before and after incubating the polymer surfaces with BSA. This was performed to theoretically block the hydrophobic binding sites on the PLA portion of the polymer, so only specific binding phenomena would be measured. Secondly, utilising fresh polymer samples, force-distance curves were obtained before and after incubating the streptavidin coated tip in a 5 molar excess of biotin. This theoretically would block the specific binding sites of the streptavidin so only the non-specific interactions of the streptavidin with the polymer could be probed. Incubation of the tip was performed whilst it was mounted on the AFM to ensure that the contact area between the tip and surface remained constant.

4.2.7 : AFM force-distance : Effect of surfactant on the interaction between streptavidin and the PLA-PEG-biotin

The effect of surfactants on the strength of the interaction between

streptavidin coated tips and the biotinylated PLA : PEGs as a function of PLA : PEG ratio was determined as follows. Force-distance measurements were performed on the three PLA-PEG-biotins with PLA : PEG ratios 3.45 : 1, 1.49 : 1 and 0.53 : 1 before and after incubating the polymers in 1% (w / v) solution of PVA for 30 min and washing the samples in excess phosphate buffer (pH 7.0, 100 mM).

4.3 : Results and discussion

4.3.1 : SPR : Effect of PLA : PEG ratio on protein binding

Figure 4.3 shows a typical SPR trace for avidin binding to the PLA-PEG-biotin(3.63). It can be observed that the interaction is rapid, completed within 90 sec. It is also stable, no decrease in SPR angle, which is indicative of removal of avidin from the polymer surface, is observed during the buffer wash.

Figure 4.4 shows the effect of PLA : PEG ratio on the extent of surface modification. It can be observed that as the PLA : PEG ratio decreases from 3.63 : 1 to 0.53 : 1 an increase from 180 ± 14 to 440 ± 54 mDA is observed on avidin binding to the polymer surface. This can be explained in that, as the PLA molecular weight decreases, there is an increase in the density of the biotinylated PEG sections of the polymer at the surface as shown by XPS and ToF-SIMS as described in Chapter 3 sections 3.3.3 and 3.3.4. Therefore, there is a larger number of available biotin molecules for binding to avidin, leading to the larger SPR shift observed with higher PEG levels. It is interesting to compare these values to those obtained for avidin interacting with a planar self-assembled monolayer of biotin formed from N-([3-biotinamido]hexyl)-3'-[2'pyridyldithiol]propamide (Biotin-HPDP) where a shift of only 198 ± 16 mDA is observed. This suggests that the

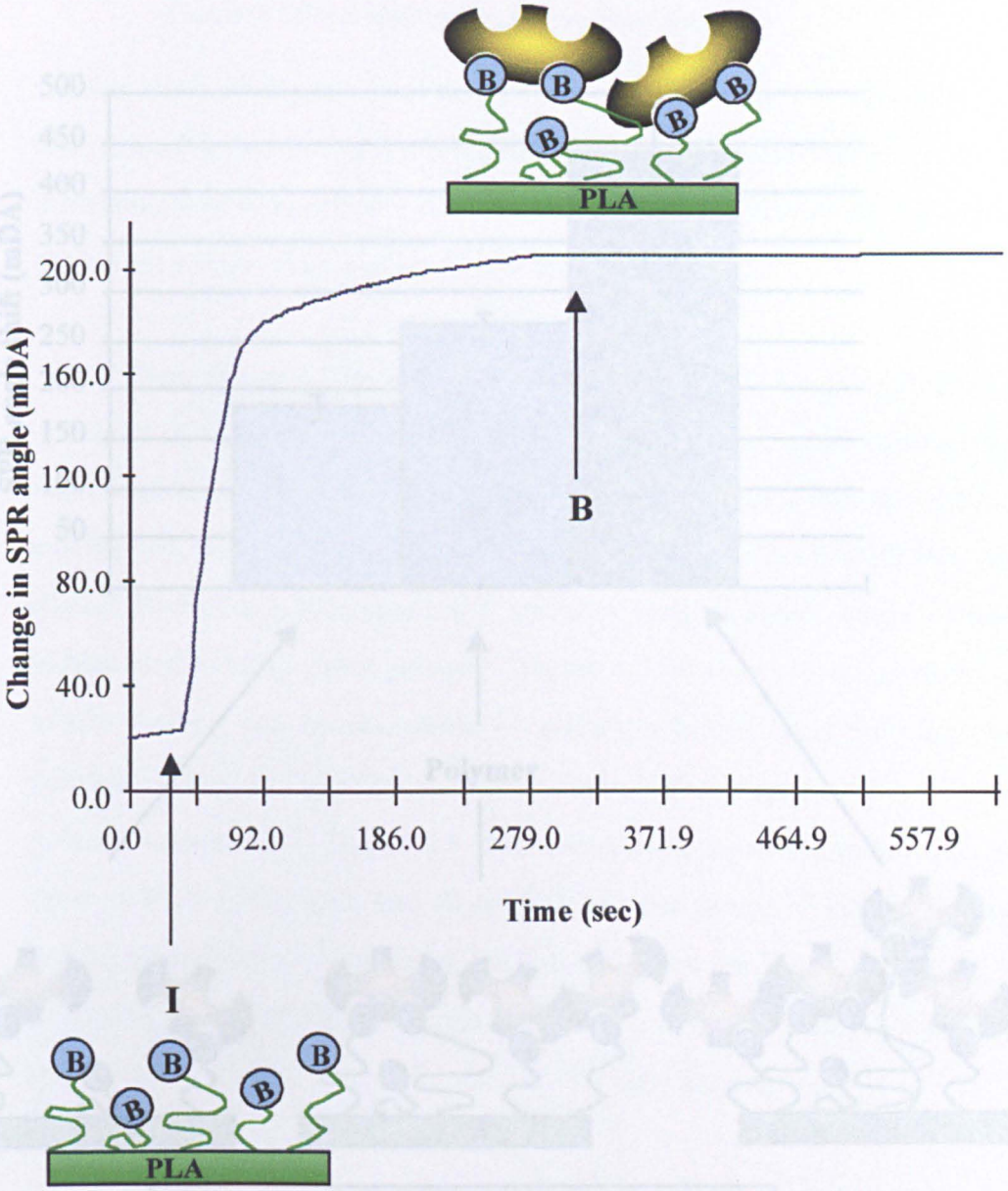

Figure 4.3 : A typical SPR trace for the interaction of avidin with the PLA-PEG-biotin(3.63) polymer

I = Time of avidin injection
B = Start of buffer wash

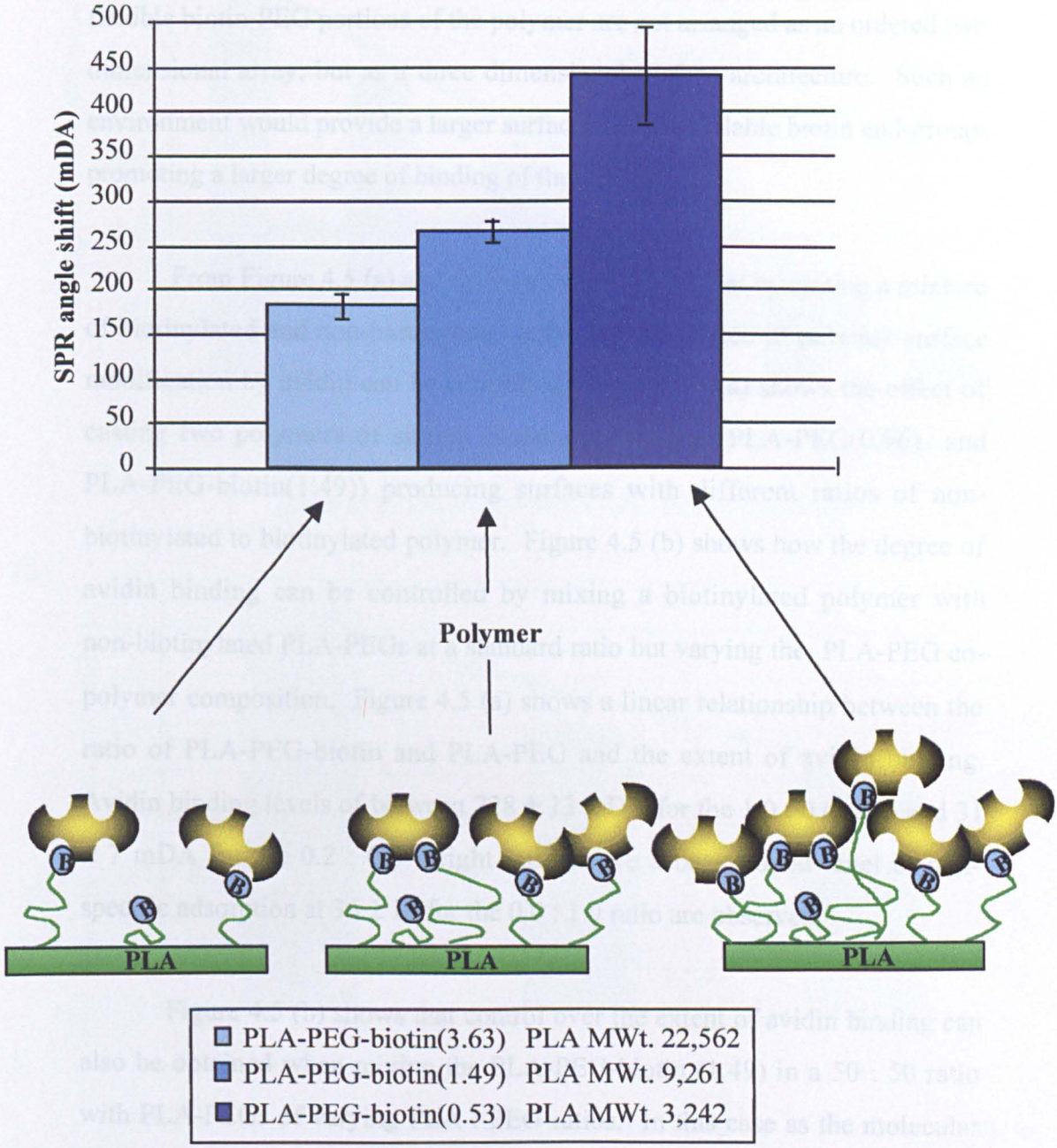

Figure 4.4 : Effect of PLA : PEG ratio on the extent of surface engineering by avidin on the biotinylated-PLA-PEGs.

As the PLA molecular weight decreases, the density of PEG chains with biotin end-groups increases, therefore, an increase in avidin binding is observed.

bars = average ± 1 standard deviation ($n \geq 21$)

flexible biotin-PEG portions of the polymer are not arranged as an ordered two dimensional array, but as a three dimensional surface architecture. Such an environment would provide a larger surface area of available biotin end-groups promoting a larger degree of binding of the streptavidin.

From Figure 4.5 (a) and (b) it can be observed that by casting a mixture of biotinylated and non-biotinylated polymers the degree of polymer surface modification by avidin can be controlled. Figure 4.5 (a) shows the effect of casting two polymers of similar molecular weights (PLA-PEG(0.96) and PLA-PEG-biotin(1.49)) producing surfaces with different ratios of non-biotinylated to biotinylated polymer. Figure 4.5 (b) shows how the degree of avidin binding can be controlled by mixing a biotinylated polymer with non-biotinylated PLA-PEGs at a standard ratio but varying the PLA-PEG co-polymer composition. Figure 4.5 (a) shows a linear relationship between the ratio of PLA-PEG-biotin and PLA-PEG and the extent of avidin binding. Avidin binding levels of between 228 ± 13 mDA for the 1.0 : 0.0 ratio and 31 ± 7 mDA for the 0.2 : 0.8 weight ratio above a background level of non-specific adsorption at 36 ± 14 for the 0.0 : 1.0 ratio are observed.

Figure 4.5 (b) shows that control over the extent of avidin binding can also be obtained when mixing the PLA-PEG-biotin (1.49) in a 50 : 50 ratio with PLA-PEGs of varying PLA : PEG ratios. In this case as the molecular weight of the PLA in the non-biotinylated polymer decreases less biotin is observed to bind to the surface. This decrease could be attributed to the decrease in the contribution of the hydrophobic PLA at the surface. Proteins are known to interact with hydrophobic surfaces, so when utilising the polymers with less PLA then less non-specific adsorption will occur so a lower SPR shift comprising of the specific biotin-avidin interactions will be observed.

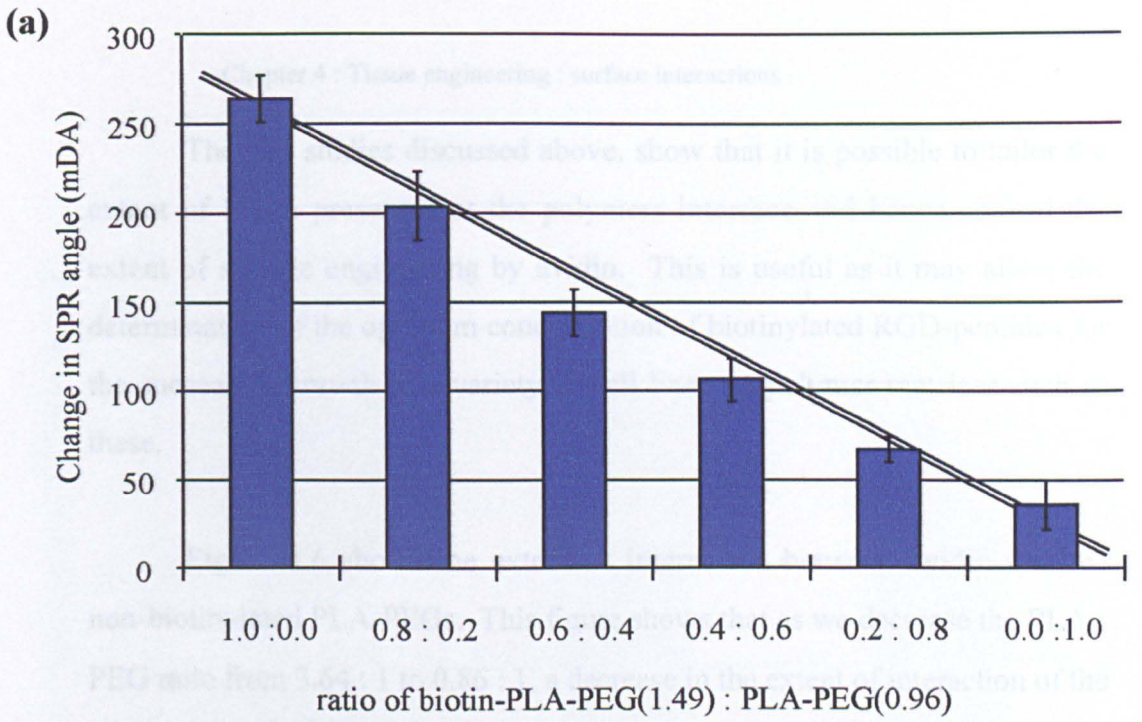

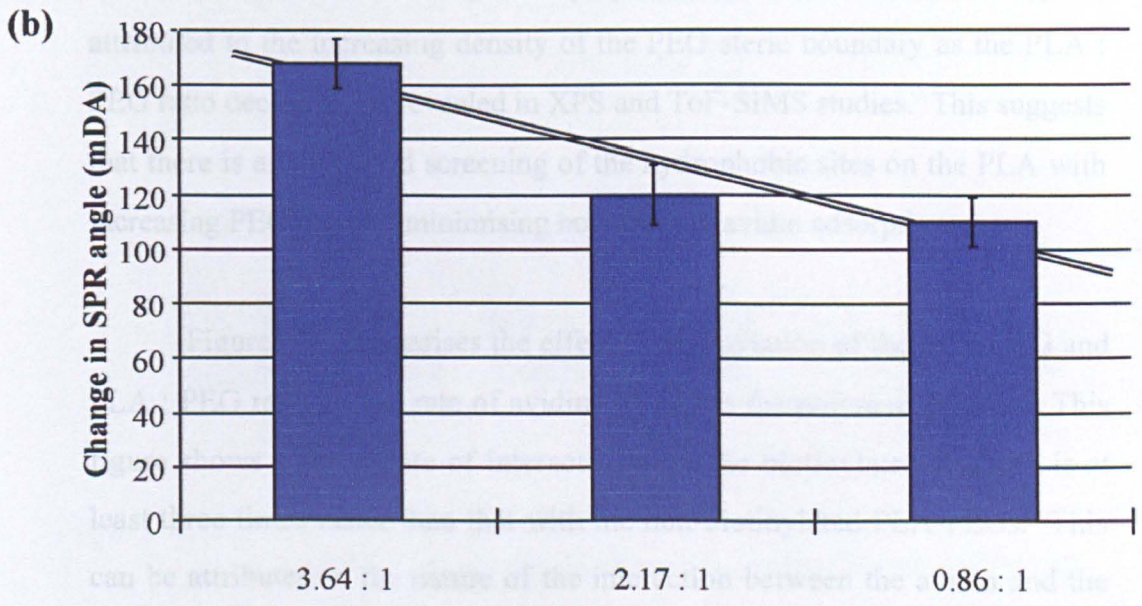

Trendline showing that avidin binding decreases with density of biotinylated PEGs

Figure 4.5 : Effect of mixing biotinylated and non-biotinylated PLA-PEGs on extent of avidin binding

(a) different ratios of polymers with similar molecular weights

(b) 1 : 1 ratios of polymers with varying molecular weights

bars = average ± 1 standard deviation ($n \geq 8$)

The two studies discussed above, show that it is possible to tailor the extent of biotin presented at the polymers interface and hence control the extent of surface engineering by avidin. This is useful as it may allow the determination of the optimum concentration of biotinylated RGD-peptides for the successful growth of a variety of cell lines on polymer matrices such as these.

Figure 4.6 shows the extent of interaction between avidin and the non-biotinylated PLA-PEGs. This figure shows that as we decrease the PLA : PEG ratio from 3.64 : 1 to 0.86 : 1, a decrease in the extent of interaction of the avidin with the non-biotinylated polymers is observed. This may be attributed to the increasing density of the PEG steric boundary as the PLA : PEG ratio decreases, as revealed in XPS and ToF-SIMS studies. This suggests that there is an increased screening of the hydrophobic sites on the PLA with increasing PEG density, minimising non-specific avidin adsorption.

Figure 4.7 summarises the effect of biotinylation of the PLA-PEG and PLA : PEG ratio on the rate of avidin binding to the polymer surfaces. This figure shows that the rate of interaction with the biotinylated surfaces is at least three times faster than that with the non-biotinylated PLA-PEGs. This can be attributed to the nature of the interaction between the avidin and the PEG polymer end group. The avidin binding to the PLA-PEG-biotin is a specific molecular recognition event, whereas the interaction with the non-biotinylated PLA-PEG is solely due to adsorption of the protein to the exposed hydrophobic PLA sites at the surface. These two adsorption mechanisms are naturally significantly different, the favoured binding event is the avidin-biotin complex which promotes a significantly higher rate of interaction to the PLA-PEG-biotin.

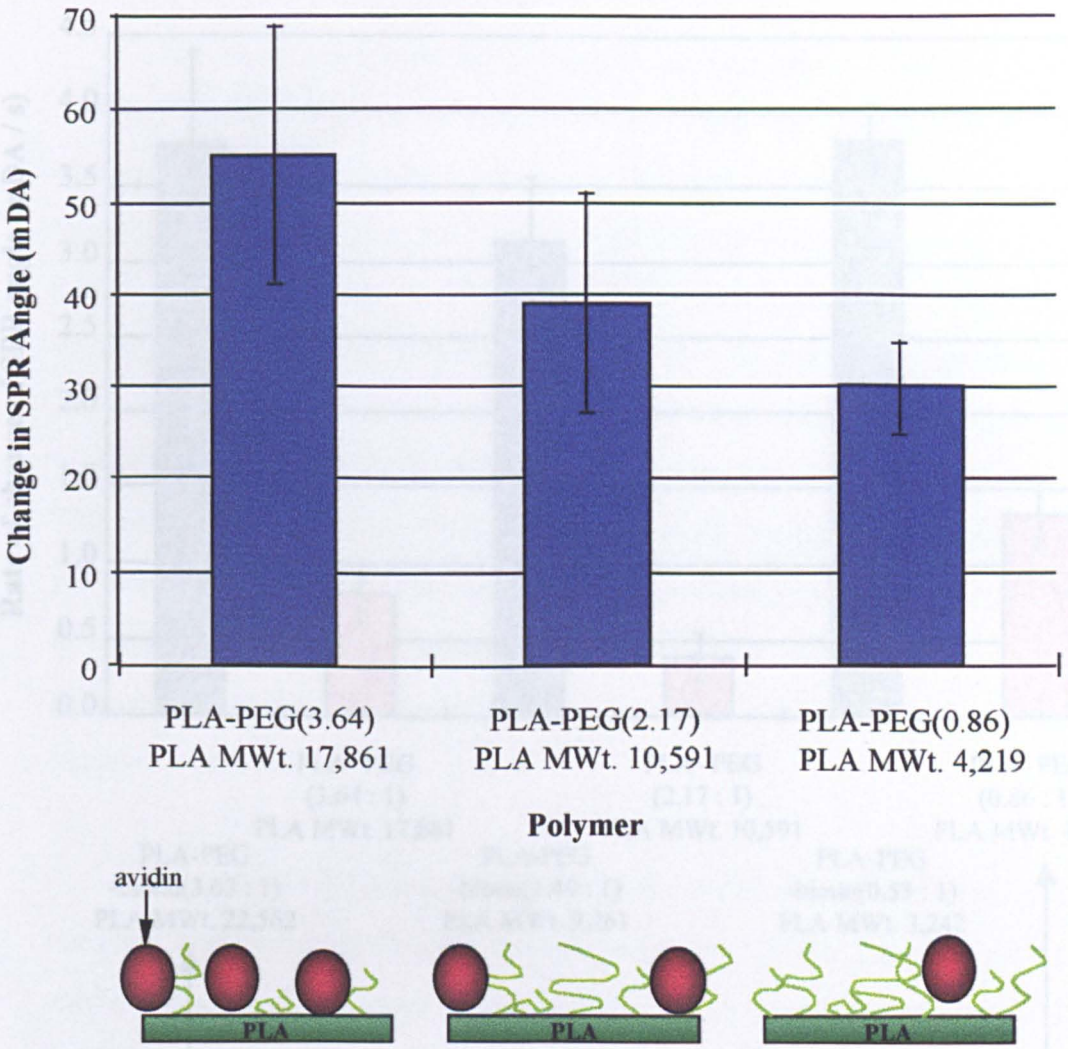

Figure 4.6 : Effect of PLA : PEG ratio on the extent of non-specific binding of avidin to the non-biotinylated polymers.

bars = average ± 1 standard deviation ($n \geq 13$)

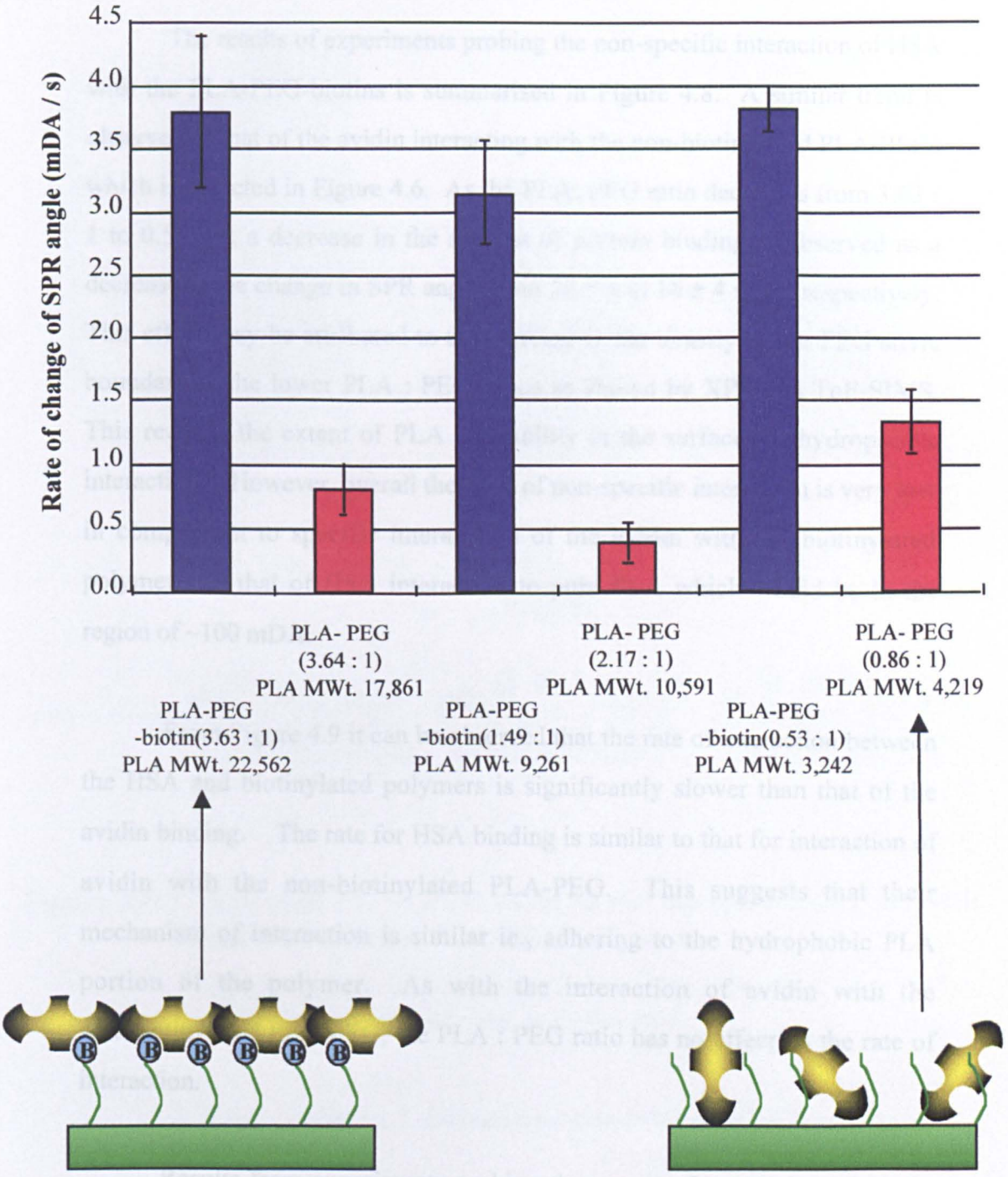

Figure 4.7 : Effect of biotinylation and PLA : PEG ratio on the rate of avidin binding to the PLA-PEG polymers

bars = average ± 1 standard deviation (n ≥ 14)

The results of experiments probing the non-specific interaction of HSA with the PLA-PEG-biotins is summarised in Figure 4.8. A similar trend is observed to that of the avidin interacting with the non-biotinylated PLA-PEGs which is depicted in Figure 4.6. As the PLA: PEG ratio decreases from 3.63 : 1 to 0.53 : 1, a decrease in the amount of protein binding is observed as a decrease in the change in SPR angle from 26 ± 4 to 16 ± 4 mDA respectively. This effect may be attributed to the increase in the density of the PEG steric boundary at the lower PLA : PEG ratios as shown by XPS and ToF-SIMS. This reduces the extent of PLA availability at the surface for hydrophobic interactions. However, overall the level of non-specific interaction is very low in comparison to specific interactions of the avidin with the biotinylated polymer and that of HSA interaction to pure PLA which would be in the region of ~100 mDA.

From Figure 4.9 it can be observed that the rate of interaction between the HSA and biotinylated polymers is significantly slower than that of the avidin binding. The rate for HSA binding is similar to that for interaction of avidin with the non-biotinylated PLA-PEG. This suggests that their mechanism of interaction is similar ie., adhering to the hydrophobic PLA portion of the polymer. As with the interaction of avidin with the non-biotinylated PLA-PEG, the PLA : PEG ratio has no effect on the rate of interaction.

Results from experiments probing the extent of interaction of avidin with the biotinylated polymers after prior incubation of the polymer with HSA are shown in Figure 4.10. The extent of interaction may be reduced, due to the HSA blocking the availability of some of the biotin sites, possibly due to steric effects. It is interesting to note that the largest drop in the degree of avidin binding to the biotinylated polymers after pre-incubation with HSA

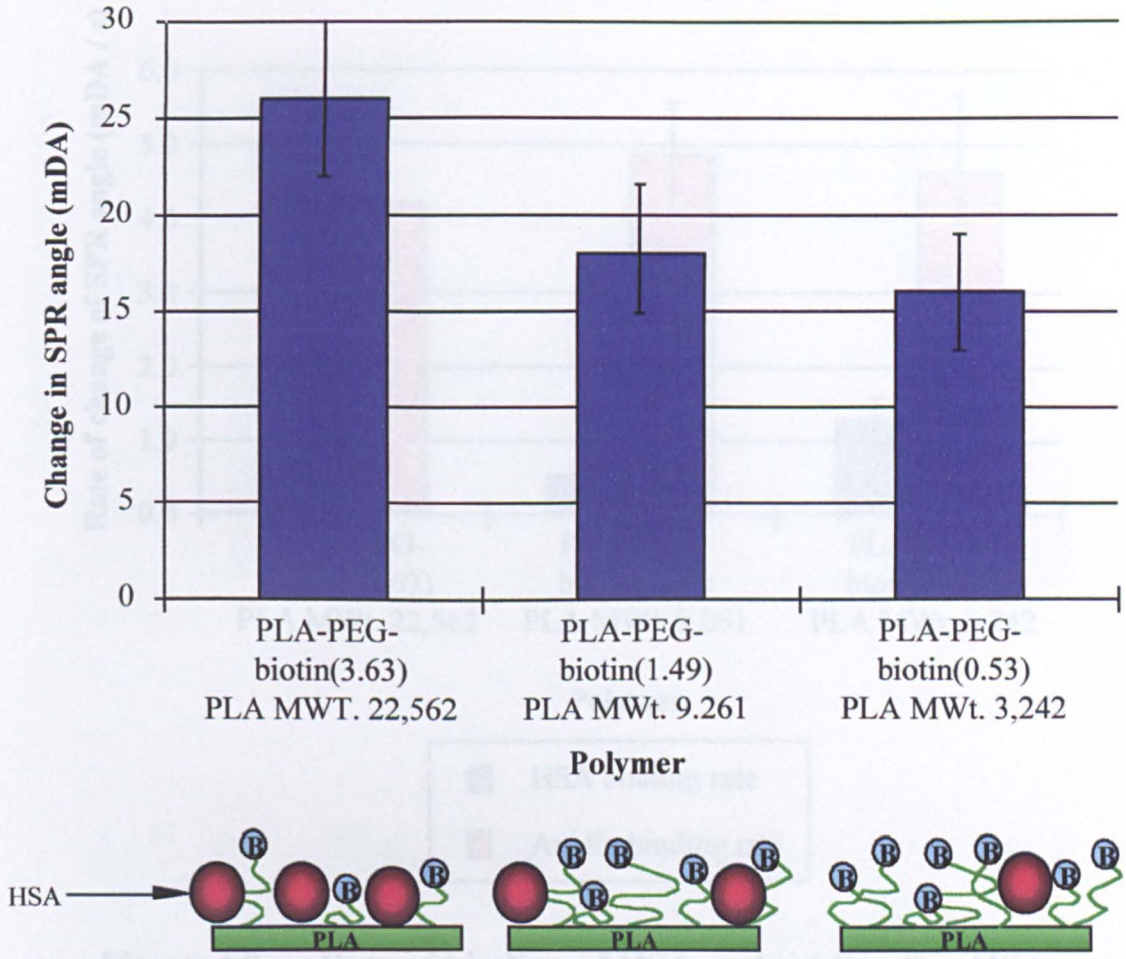

Figure 4.8 : Effect of PLA : PEG ratio on the interaction of HSA with the biotinylated PLA-PEG polymers

Due to the increase in the effectiveness of the PEG steric layer as PLA molecular weight decreases, less HSA bind.

bars = average ± 1 standard deviation ($n \geq 12$)

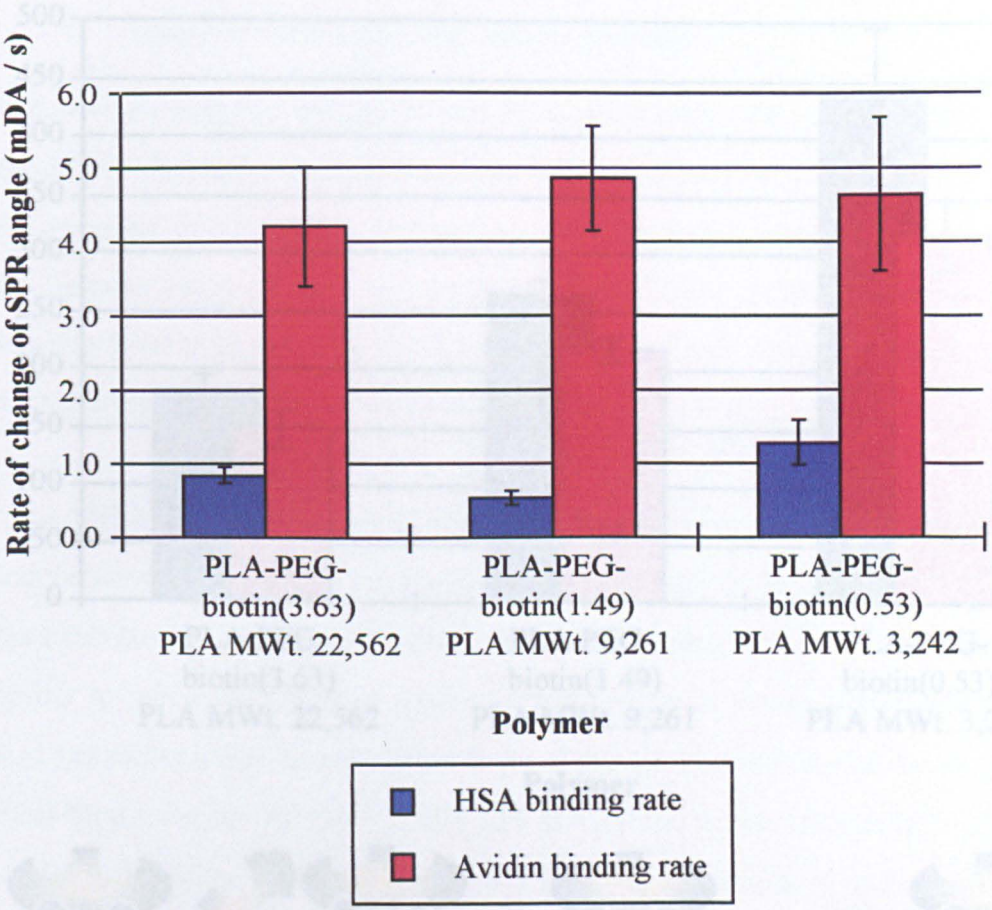

Figure 4.9 : Rate of binding of HSA and avidin after HSA incubation to biotinylated polymers

Independent of PLA : PEG ratio the interaction of HSA and avidin with the biotinylated polymers occurs at a constant rate. The specific molecular recognition process of the avidin-biotin binding is significantly faster than the hydrophobic interaction of the HSA.

bars = average ± 1 standard deviation ($n \geq 11$)

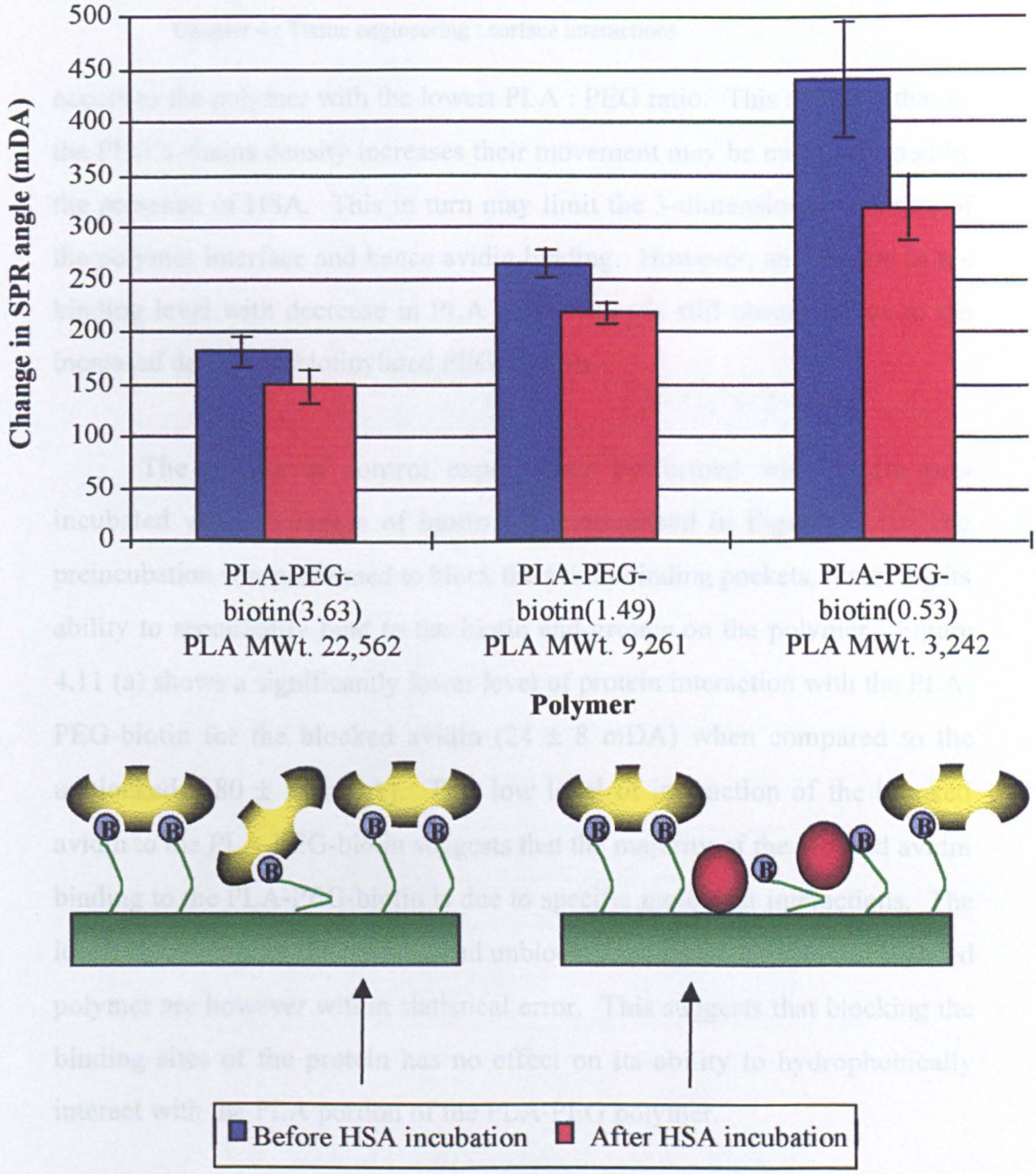

Figure 4.10 : Extent of avidin binding to biotinylated polymers before and after incubation with HAS

Bars = average ± 1 standard deviation (n ≥ 12)

occurs to the polymer with the lowest PLA : PEG ratio. This suggests that as the PEG's chains density increases their movement may be more confined by the presence of HSA. This in turn may limit the 3-dimensional structure of the polymer interface and hence avidin binding. However, an increase in the binding level with decrease in PLA : PEG ratio is still observed due to the increased density of biotinylated PEG brushes.

The results of control experiments performed with avidin pre-incubated with an excess of biotin are summarised in Figure 4.11. The preincubation was performed to block the avidin binding pockets, removing its ability to specifically bind to the biotin end-groups on the polymer. Figure 4.11 (a) shows a significantly lower level of protein interaction with the PLA-PEG-biotin for the blocked avidin (24 ± 8 mDA) when compared to the unblocked (180 ± 14 mDA). This low level of interaction of the blocked avidin to the PLA-PEG-biotin suggests that the majority of the blocked avidin binding to the PLA-PEG-biotin is due to specific molecular interactions. The levels of binding for the blocked and unblocked avidin on the non-biotinylated polymer are however within statistical error. This suggests that blocking the binding sites of the protein has no effect on its ability to hydrophobically interact with the PLA portion of the PLA-PEG polymer.

Figure 4.11 (b) summaries the rate of the interaction of the blocked and unblocked avidin interacting with the PLA-PEG-biotin and PLA-PEG polymers. It can be observed that the rate of interaction for the blocked avidin compared with the unblocked is significantly slower. The binding rate is reduced from approximately 3.76 to 0.75 mDA / s when the avidin binding pockets are blocked. The rate of interaction for the blocked avidin on the PLA-PEG-biotin is similar to that for the interaction of the unblocked avidin on the non-biotinylated polymers (0.85 ± 0.1 mDA / s). This suggests that

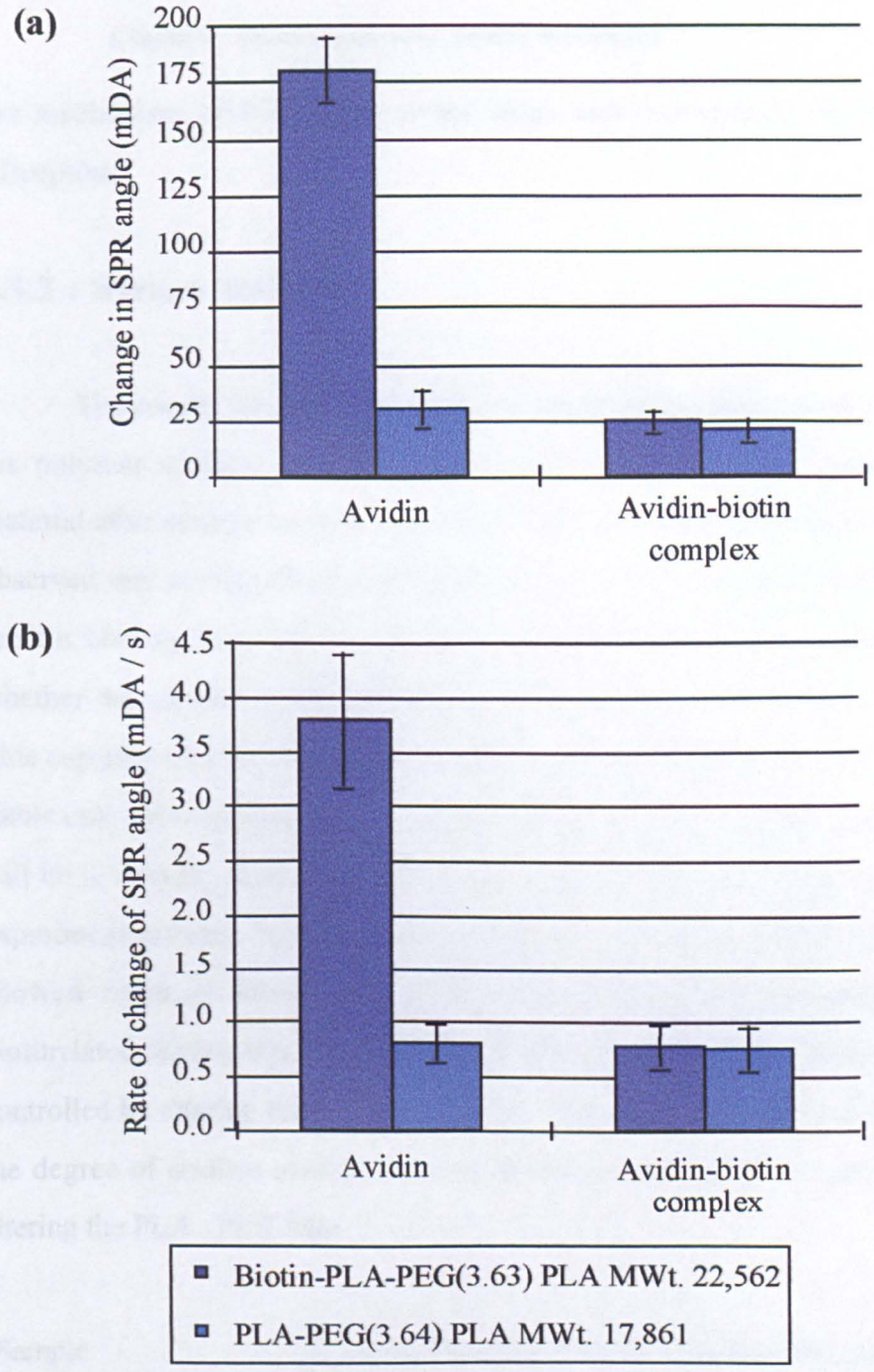

Figure 4.11 : Interaction of avidin preincubated with biotin with the biotinylated-PLA-PEGs

(a) Extent of interaction

(b) rate of interaction

Both the rate and extent of avidin binding is significantly reduced when its binding pockets are blocked as the binding mechanism changes from a molecular recognition process to a hydrophobic interaction

Bars = average ± 1 standard deviation ($n \geq 14$)

the mechanism of interaction is the same and non-specific hydrophobic adsorption.

4.3.2 : System stability

The results for the experiments to determine if avidin immobilized on the polymer surface could still bind significant amounts of biotinylated material after storage are summarised in Table 4.3. From this table it can be observed that no significant difference is seen in the extent of biotinylated-ferritin binding to avidin coated PLA-PEG-biotin polymers, regardless of whether the samples were used immediately or stored for 48 h prior to use. This suggests that the surface engineering of the polymer system by avidin is stable over this time period. This means that the scaffolds surface engineering will be in a steady state whilst the cells adhere and bind to the interface. The experiment probing the non-specific interaction between ferritin and avidin showed minimal interactions. This suggests that the majority of the biotinylated ferritin binding is specific and hence its surface concentration is controlled by altering the PLA : PEG ratio. This result provides evidence that the degree of surface modification by biotin-peptide could be controlled by altering the PLA : PEG ratio.

Sample	Extent of binding of biotinylated ferritin (mDA)
Freshly prepared	214 ± 29
Stored for 48 h	209 ± 18

Table 4.3 : Effect of storage on the ability of avidin immobilised on biotinylated polymers to bind biotinylated ferritin

4.3.3 Biotin-peptide immobilisation

Figure 4.12 summaries the effect of the PLA : PEG ratio on the extent of biotinylated peptide binding to avidin immobilised on the PLA-PEG-biotin co-polymer series. This figure shows that an increase in SPR shift, which is indicative of more material binding to the surface, is observed on decreasing the PLA : PEG ratio. Once again, this effect may be rationalized in terms of the denser surface coverage of avidin on the polymer surfaces with decreasing PLA : PEG ratio as depicted in Figure 4.4. It is evident that the change in SPR angle observed for the binding of the biotinylated RGD-peptide is not as significant as that observed for avidin binding. This is due to the significantly different molecular weights of the materials. Avidin has a molecular weight of approximately 60 -70 kDa (Diamandis (1991)), whereas the peptide is only a few 1,000 Da. Therefore the change in SPR angle corresponding to the extent of peptide binding, will be less than that for the avidin as the increase in density of material on the polymer surface will be less for the peptide.

4.3.4 : AFM : Effect of PLA : PEG ratio on protein binding

Figure 4.13 shows the three biotinylated polymers before and after incubation with avidin. Before incubation the polymer surfaces are featureless with topological z axis variation typically of less than 10 nm as shown in Figure 4.13 (a), (b) and (c) for the polymers 3.63 : 1, 1.49 : 1 and 0.53 : 1 respectively. After incubation both individual avidin molecules of sizes 7 - 9 nm and small molecular aggregates (11 - 40 nm) are observed on the surface. Figures (d) (e) and (f) reveal that as the PLA molecular weight decreases from 22,562 to 9,261 and 3,242 respectively, the number and size of both the avidin molecules and molecular aggregates increases with decreasing PLA : PEG ratio. This again can be attributed to the increase in density of the PEG brushes and

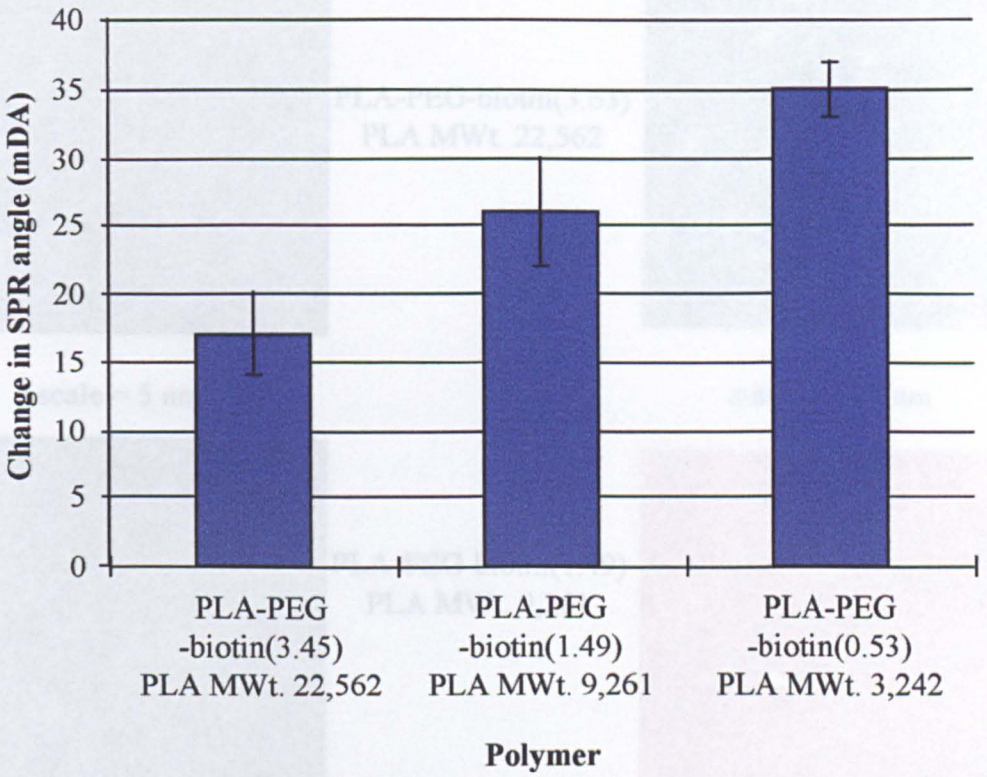

Figure 4.12 : Influence of PLA : PEG ratio on the binding of the biotinylated RGD peptide

As PLA : PEG ratio decrease the density of biotinylated-PEGs increases and hence, so does the bound avidin. This means the number of free avidin binding site is greater providing the opportunity for a higher degree of surface engineering by the biotinylated peptide as observed from the increased SPR angle.

Bars = average ± 1 standard deviation ($n \geq 17$)

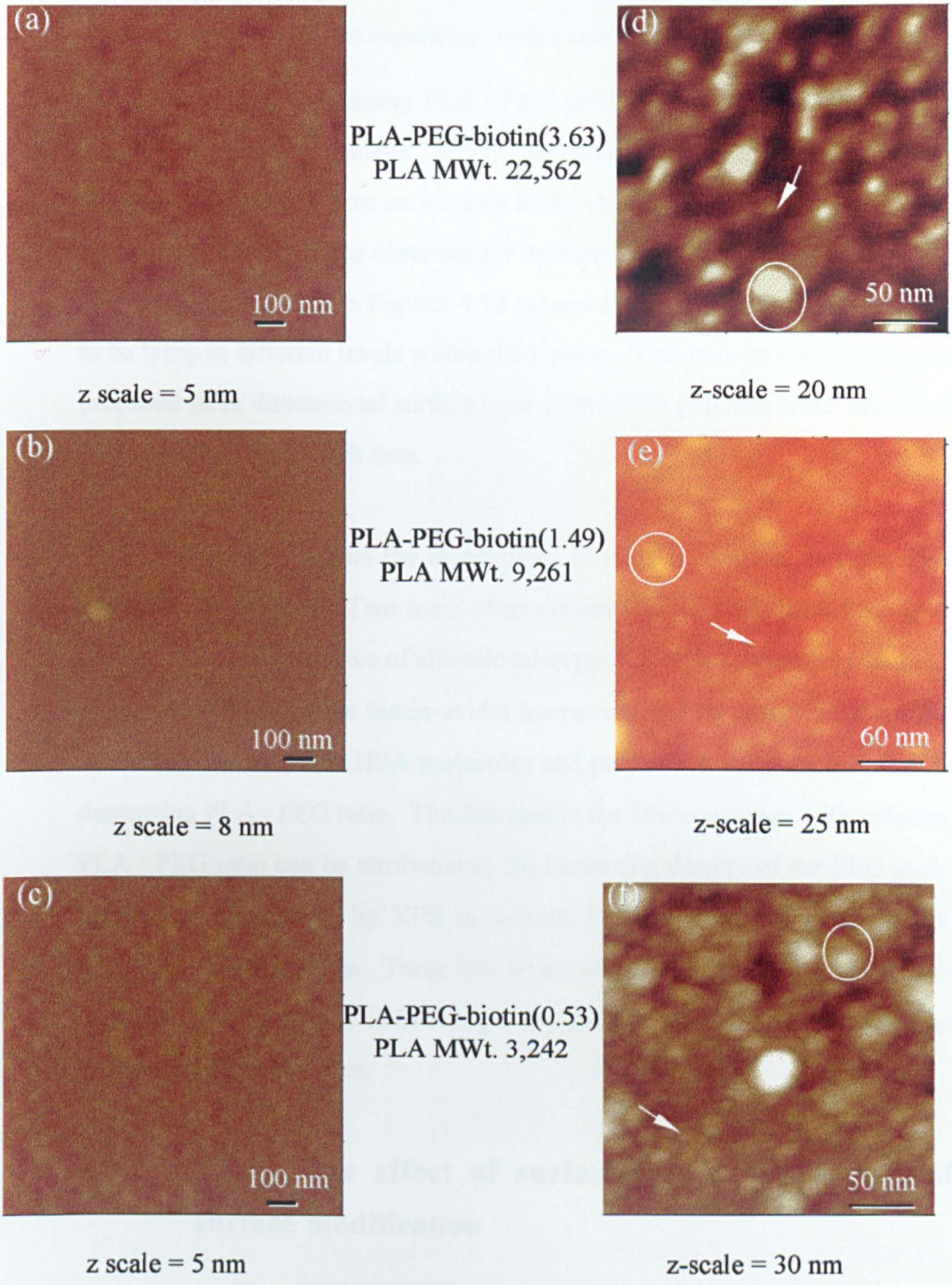

Figure 4.13 : Effect of PLA : PEG ratio on avidin coverage of PLA-PEG-biotins

Images a-c depict the biotinylated polymers prior to incubation with avidin, whereas d-e show the same polymers surfaces after incubation. In images d-f individual avidin molecules (marked →) and small molecular aggregate (⬭) are observed.

hence biotin, with decreasing PLA : PEG ratio, providing more sites for the binding of avidin molecules. This data corresponds well with the results obtained using SPR where an increase in the change in SPR angle from 180 ± 14 to 440 ± 54 mDA was observed for the same series of polymers. It is also interesting to note that in Figures 4.13 (e) and (f) the avidin molecules appear to be lying in different levels within the z plane. This may be attributed to the proposed three dimensional surface layer of the PEG polymer brush discussed with reference to the SPR data.

Figure 4.14 shows the biotinylated PLA-PEG polymer surfaces after incubation with HSA. Two main observations can be made from this set of images. Firstly, the degree of albumin adsorption is significantly less than that observed for the specific biotin-avidin interaction and secondly, the extent of interaction between the HSA molecules and polymer surface decreases with decreasing PLA : PEG ratio. The decrease in the HSA coverage with reducing PLA : PEG ratio can be attributed to the increasing density of the PEG steric barrier (as determined by XPS in section 3.3.3), minimising non-specific hydrophobic interactions. These low levels of HSA surface coverage also fit well with the low change in SPR angle observed for the adsorption of HSA on to these polymer surfaces.

4.2.5 : SPR : The effect of surfactants on the degree of surface modification

Figure 4.15 shows a typical trace for the interaction of PVA at concentrations of 1.0 and 0.1 % (w / v) with the PLA-PEG-biotin(3.63). Both concentrations produce similar levels of interaction at the end of the buffer wash of 127 ± 19 mDA. However, the trace for the 1.0 % (w / v) PVA solution shows a maximum increase of approximately 200 mDA prior to the

PLA-PEG-biotin(3.63)
PLA MWt. 22,562

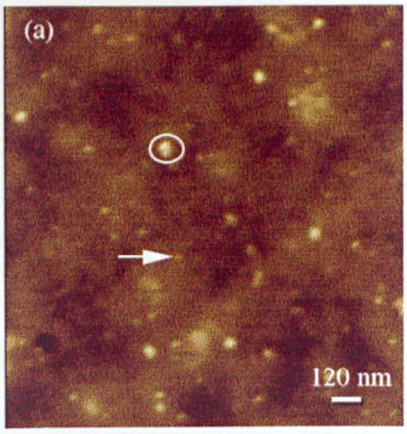

z scale = 15 nm

PLA-PEG-biotin(1.49)
PLA MWt. 9,261

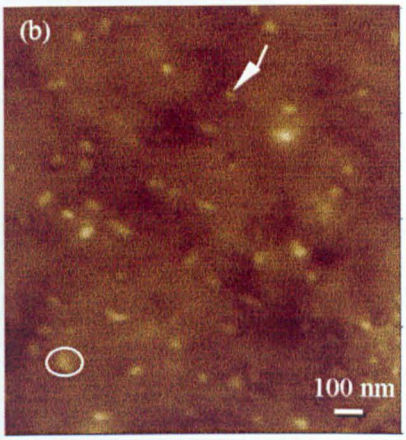

z scale = 15 nm

PLA-PEG-biotin(0.53)
PLA MWt. 3,242

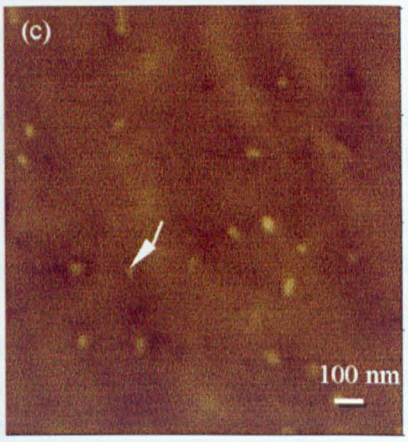

z scale = 12 nm

Figure 4.14 : Effect of PLA : PEG ratio on HSA coverage of biotinylated PLA-PEGs

Images a-c depict the non-biotinylated polymers after incubation with avidin. In the images individual avidin molecules (marked →) and small molecular aggregate (⬭) are observed. The number of these decreases with PLA : PEG ratio. This can be attributed to the increased density of the PEG steric boundary with decreasing PLA molecular weight. This steric layer protects against hydrophobic interactions of the avidin with the PLA portion of the polymer

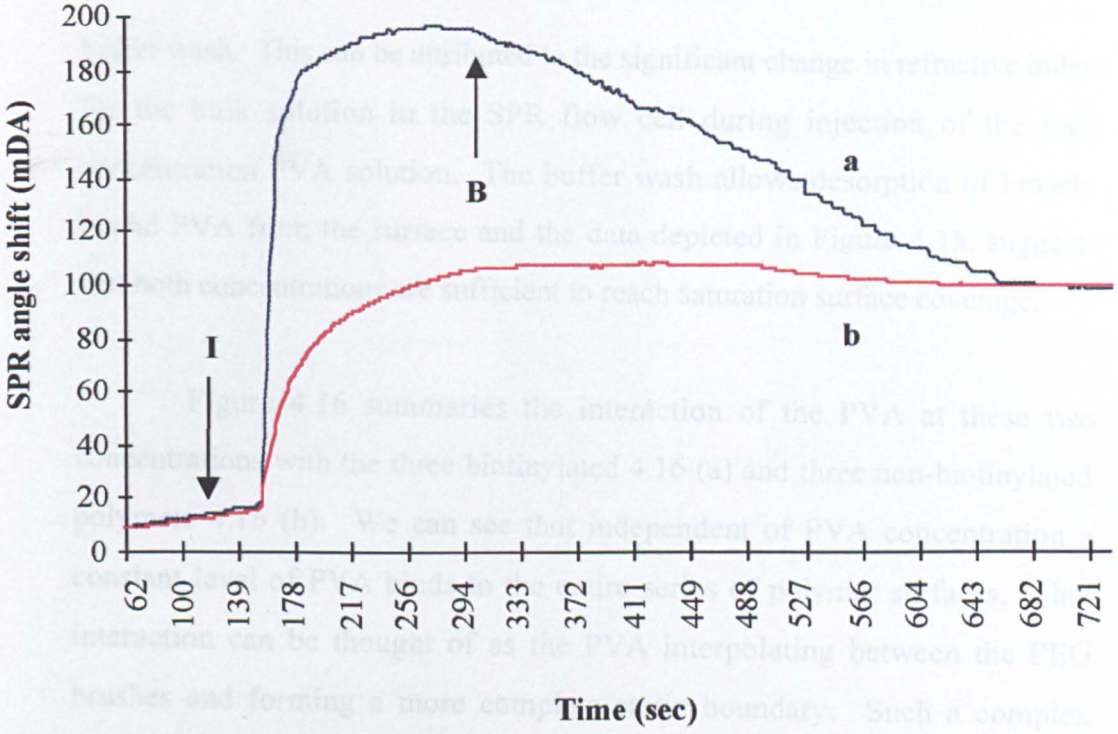

Figure 4.15 : A typical SPR trace for the interaction of PVA with PLA-PEG-biotin

(a) Trace for 1.0% (w / v) PVA
(b) Trace for 0.1% (w / v) PVA

I = injection of PVA
B = start of buffer wash

The significant higher maximum for the 1.0 (w / v) PVA can be attributed to the refractive index change of the PVA bulk solution. On washing with buffer, loosely bound PVA is removed from the biotin-PLA-PEG surface. Since both the 0.1 and 1.0 % (w / v) PVA solutions produce the same change in SPR angle at the end of the buffer wash suggests that a saturated surface coverage of PVA has been obtained.

buffer wash. This can be attributed to the significant change in refractive index for the bulk solution in the SPR flow cell during injection of the high concentration PVA solution. The buffer wash allows desorption of loosely bound PVA from the surface and the data depicted in Figure 4.15, suggests that both concentrations are sufficient to reach saturation surface coverage.

Figure 4.16 summaries the interaction of the PVA at these two concentrations with the three biotinylated 4.16 (a) and three non-biotinylated polymers 4.16 (b). We can see that independent of PVA concentration a constant level of PVA binds to the entire series of polymer surfaces. This interaction can be thought of as the PVA interpolating between the PEG brushes and forming a more complete steric boundary. Such a complex interface may yield a number of properties. Firstly, it may reduce non-specific interactions with the underlying PLA substrate and secondly, it may mask some of the polymer biotin end groups and hence may reduce the bioaffinity of the surface assembly.

Figure 4.17 shows the effect of PVA on the degree of surface engineering by avidin on the PLA-PEG-biotins. In all cases PVA causes a reduction in the extent of avidin binding to the biotinylated polymers. This decrease ranges from 26.7 to 34.2 % of the overall amount of avidin binding as observed for the PLA-PEG-biotin(3.63) and PLA-PEG-biotin(0.53) respectively. However, the overall amount of binding is still significantly larger than that observed for the non-biotinylated PLA-PEGs which show avidin binding at levels no greater than 54 ± 14 mDA.

In the case of the PLA-PEG-biotin(3.63) and PLA-PEG-biotin(1.49), there is no significant difference between the results for the avidin binding after incubation of the polymer with 0.1 and 1.0% (w / v) PVA solution. This

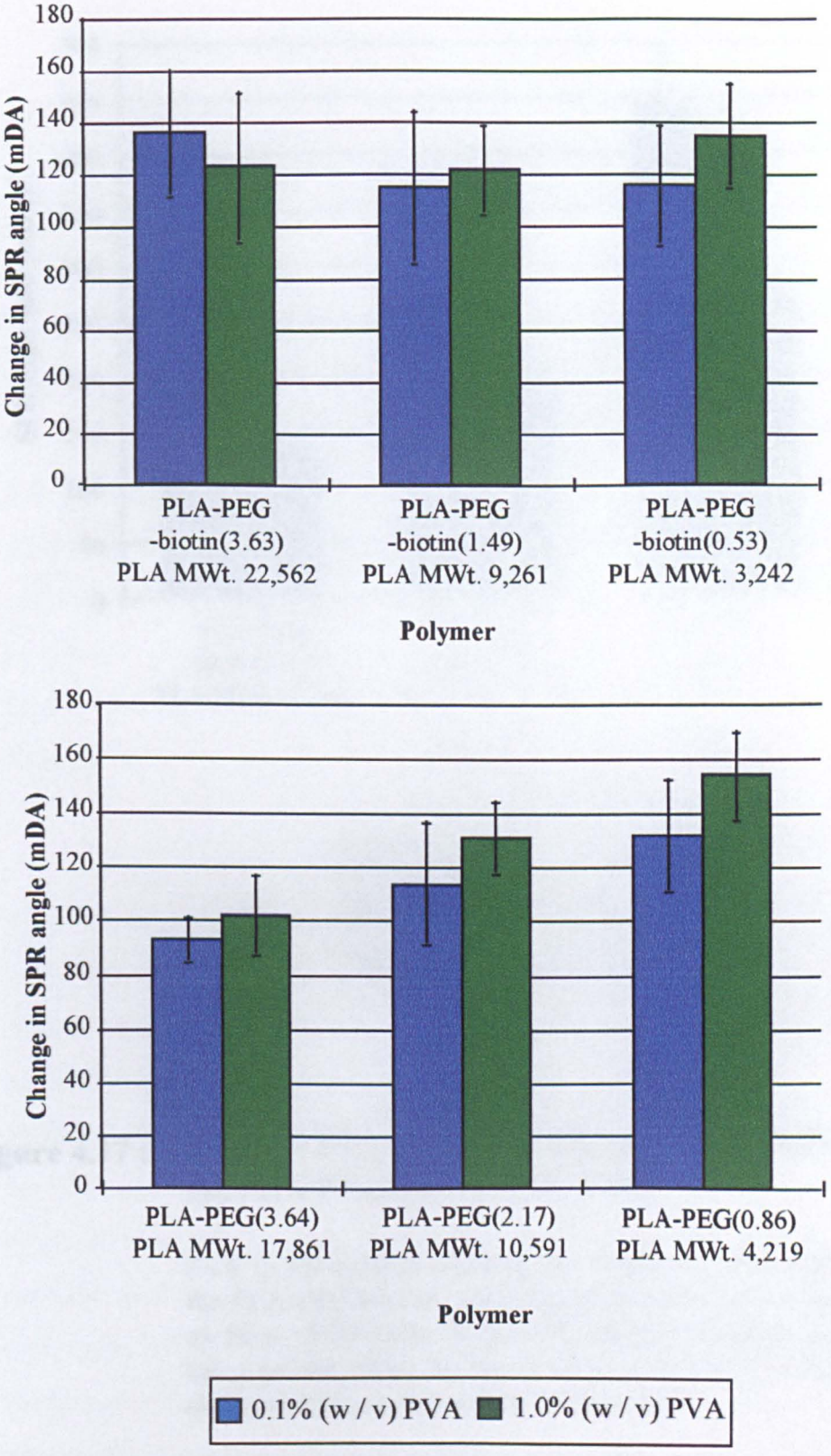

Figure 4.16 : Summary of the extent of interaction of PVA with
(a) biotinylated PLA-PEGs
(b) non-biotinylated PLA-PEGs

Bars = average ± 1 standard deviation ($n \geq 22$)

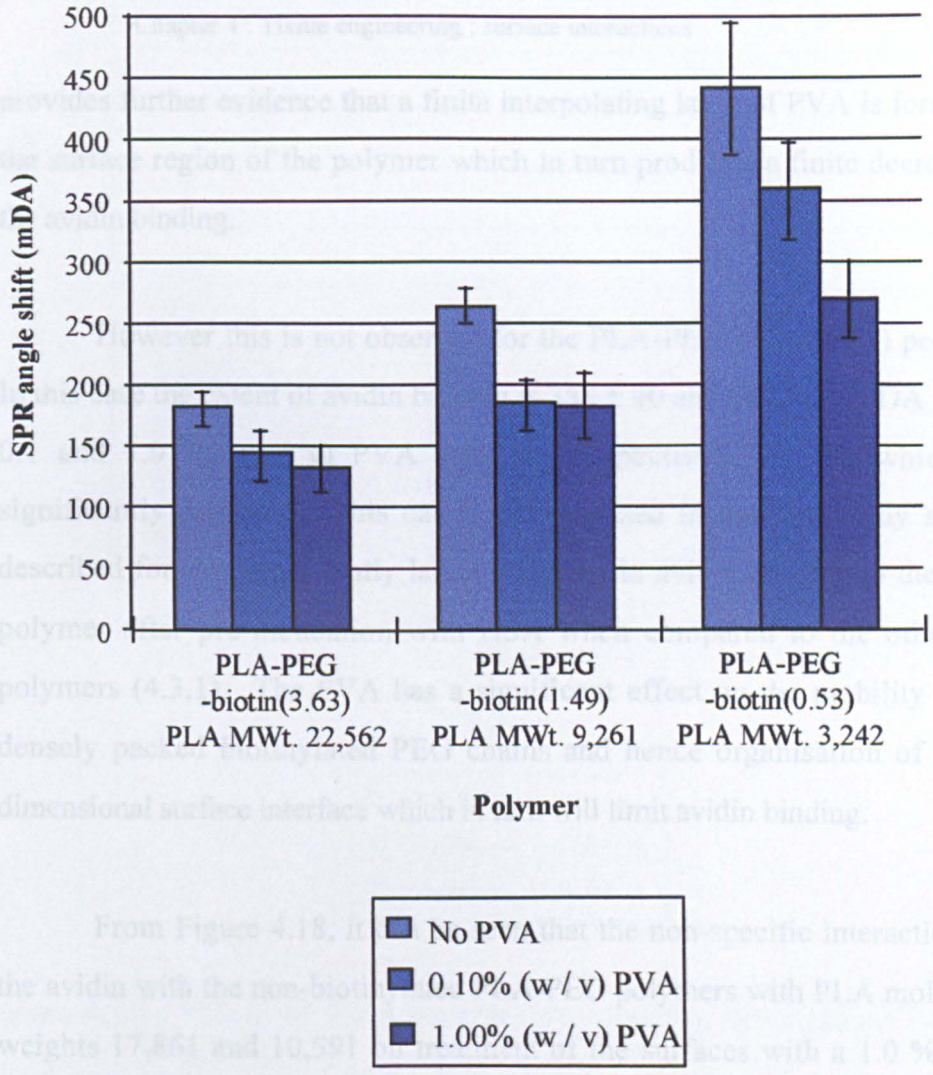

Figure 4.17 : Effect of PVA on the specific interaction between the PLA-PEG-biotins and avidin

PVA is observed to decrease the extent of avidin binding to the PLA-PEG-biotins. The degree of reduction is dependent on PLA : PEG ratio. As the PEG density increases the PVA has a greater effect on the mobility of the biotinylated PEG chains and hence their ability to bind avidin.

Bars = average ± 1 standard deviation ($n \geq 21$)

provides further evidence that a finite interpolating layer of PVA is formed in the surface region of the polymer which in turn produces a finite decrease in the avidin binding.

However this is not observed for the PLA-PEG-biotin(0.53) polymer. In this case the extent of avidin binding is 358 ± 40 and 285 ± 29 mDA for the 0.1 and 1.0 % (w / v) PVA solutions respectively, results which are significantly different. This can be rationalized in the same way as that described for the significantly larger decrease in avidin binding to the same polymer after pre-incubation with HSA when compared to the other two polymers (4.3.1). The PVA has a significant effect on the mobility of the densely packed biotinylated PEG chains and hence organisation of the 3-dimensional surface interface which in turn will limit avidin binding.

From Figure 4.18, it can be seen that the non-specific interactions of the avidin with the non-biotinylated PLA-PEG polymers with PLA molecular weights 17,861 and 10,591 on treatment of the surfaces with a 1.0 % PVA solution are significantly reduced, ie. the standard error bars of avidin adsorption before and after washing the polymer surfaces with PVA do not overlap. This may be attributed to the interpolating layer of PVA between the PEG brushes masking the hydrophobic binding sites on the PLA so less avidin is able to bind non-specifically. In the case of the PLA-PEG(0.86) a reduction in HSA adsorption to the polymer surface is observed, but as can be seen from Figure 4.18 the standard errors for the SPR shifts due to avidin binding before and after the PVA wash overlap and therefore the decrease is not significant.

Further experiments were undertaken to investigate the lowest concentration of PVA which produced a change in SPR angle. These

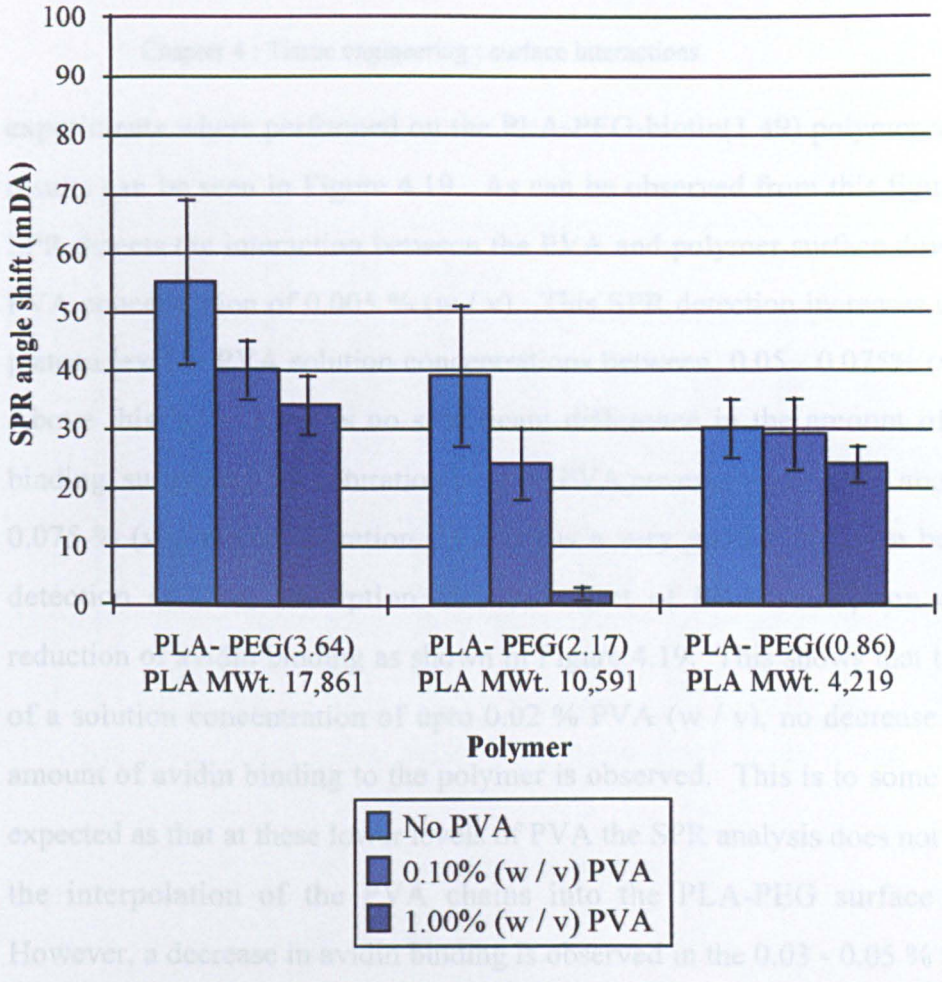

Figure 4.18 : Effect of PVA on the non-specific interaction between the PLA-PEGs and avidin

Bars = average ± 1 standard deviation (n ≥ 18)

experiments where performed on the PLA-PEG-biotin(1.49) polymer and the results can be seen in Figure 4.19. As can be observed from this figure, the SPR detects the interaction between the PVA and polymer surface down to a PVA concentration of 0.005 % (w / v). This SPR detection increases up to a plateau level at PVA solution concentrations between 0.05 - 0.075% (w / v). Above this value there is no significant difference in the amount of PVA binding, suggesting the saturation level of PVA coverage is attained above the 0.075 % (w / v) concentration. There is a very good correlation between detection of PVA adsorption and the effect of PVA adsorption on the reduction of avidin binding as shown in Figure 4.19. This shows that the use of a solution concentration of upto 0.02 % PVA (w / v), no decrease in the amount of avidin binding to the polymer is observed. This is to some extent expected as that at these lower levels of PVA the SPR analysis does not detect the interpolation of the PVA chains into the PLA-PEG surface layer. However, a decrease in avidin binding is observed in the 0.03 - 0.05 % (w / v) PVA solution range, corresponding to the detected increase in PVA deposition suggesting the masking of specific avidin and non-specific binding sites of the PLA-PEG-biotin system.

The Pluronic™ polymers are known in many cases to significantly reduce non-specific binding of proteins to polymers. Therefore, they would be a useful surfactant to use when forming new surfaces with polymers for tissue engineering scaffolds. However, to be an effective choice they should have minimal effect on the biotin-avidin interaction which is the basis for the PLA-PEG surface engineering. Because of this concern their effect on the specific interaction between avidin and the PLA-PEG-biotin polymers was investigated. Three pluronics were chosen for these investigation namely F68, F108 and F127 (Table 4.2) which have previously shown on both polymer colloids and planar surfaces to maximise the reduction in protein adhesion

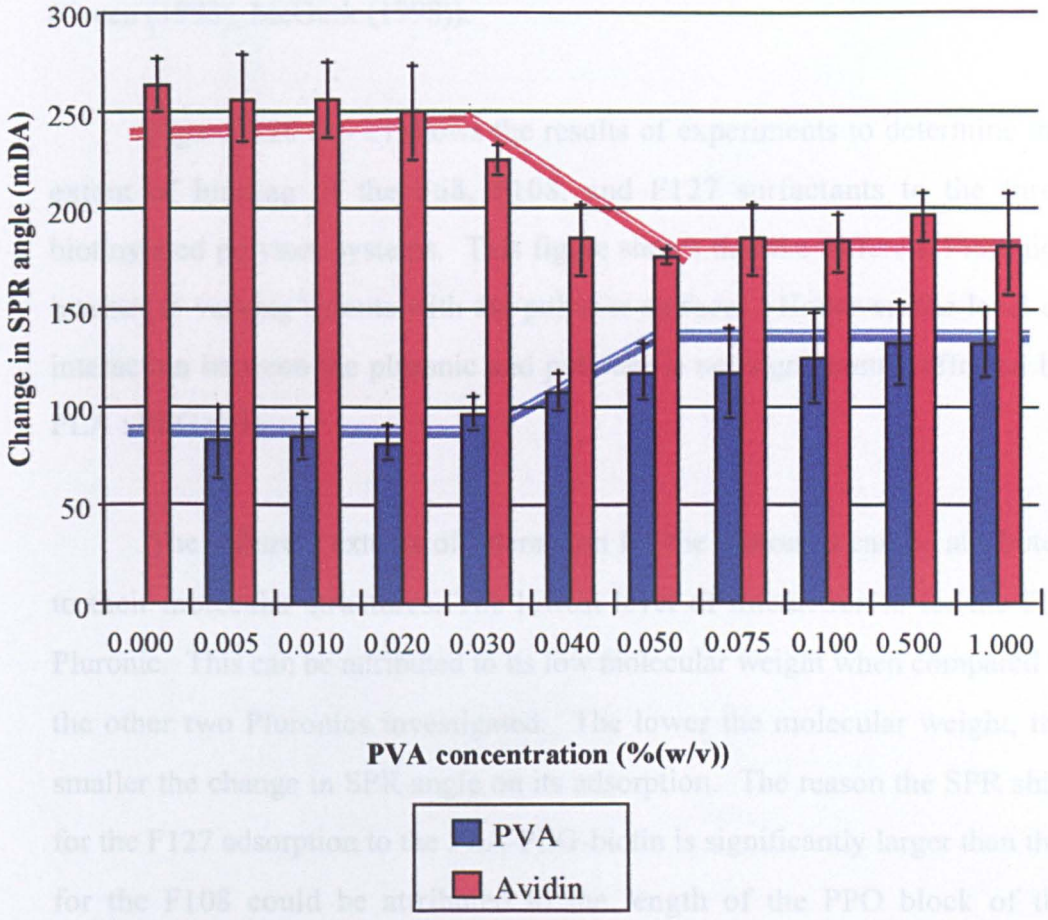

Figure 4.19 : Effect of low concentration of PVA on extent of avidin binding to biotin-PLA-PEG(1.49)

Up to a concentration of 0.02 % (w / v), PVA has no effect on the extent of avidin interaction with the polymer surface. Between 0.02 and 0.075 % (w / v) PVA as the PVA coverage increases a complementary decrease in avidin interaction is observed. Above this PVA concentration no further increase in PVA adsorption or decrease in avidin binding is observed.

Bars = average ± 1 standard deviation ($n \geq 15$)

(Green (1998), McGurk (1998)).

Figure 4.20 (a - c) shows the results of experiments to determine the extent of binding of the F68, F108, and F127 surfactants to the three biotinylated polymer systems. This figure shows that the different Pluronics interact to varying extents with the polymer surfaces. However, the level of interaction between the pluronic and polymer is not significantly effected by PLA : PEG ratio

The different extents of interaction for the pluronics can be attributed to their molecular structures. The lowest level of interaction is for the F68 Pluronic. This can be attributed to its low molecular weight when compared to the other two Pluronics investigated. The lower the molecular weight, the smaller the change in SPR angle on its adsorption. The reason the SPR shift for the F127 adsorption to the PLA-PEG-biotin is significantly larger than that for the F108 could be attributed to the length of the PPO block of the polymer. The F127 has a PPO block of 67 monomer units whereas the F108 block is only 54 units long. On adsorption of the Pluronics to the PLA-PEG-biotin surface the PPO probably interacts with the hydrophobic PLA. The longer this portion of the Pluronic, the larger the change in the PLA-PEG-biotin interface characteristics and therefore the higher the change in SPR angle. This has been observed previously by Green (1996) who studied the effect of PPO block length on the extent of Pluronic adsorption to polystyrene.

From Figure 4.21 it can be observed that the three different pluronic surfactants effect binding of avidin to the PLA-PEG-biotins to varying extents. This again can be attributed to their structure. Pluronic F68 has the lowest molecular weight and has the least effect on avidin binding. Its low molecular weight means it will have minimal effect on the surface characteristics of the

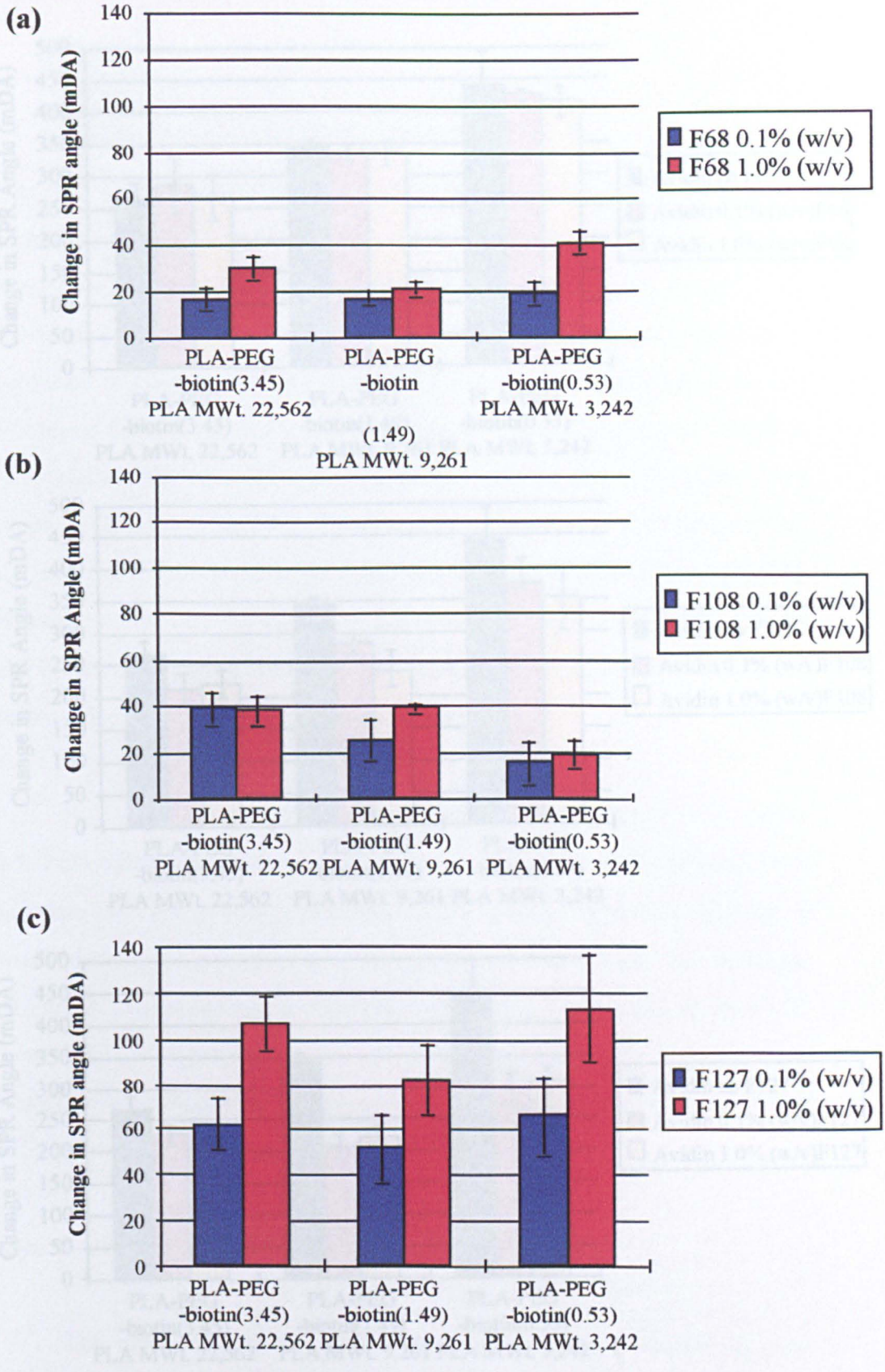

Figure 4.20 : Extent of binding of Pluronics to biotinylated polymer surfaces

The extent of Pluronic binding can be attributed to it molecular structure. F68 has the lowest MWt. so the SPR shift is the least. The PPO block for F127 is larger than that of F108 leading to the higher observed change in SPR angle.

Bars = average ± 1 standard deviation ($n \geq 14$)

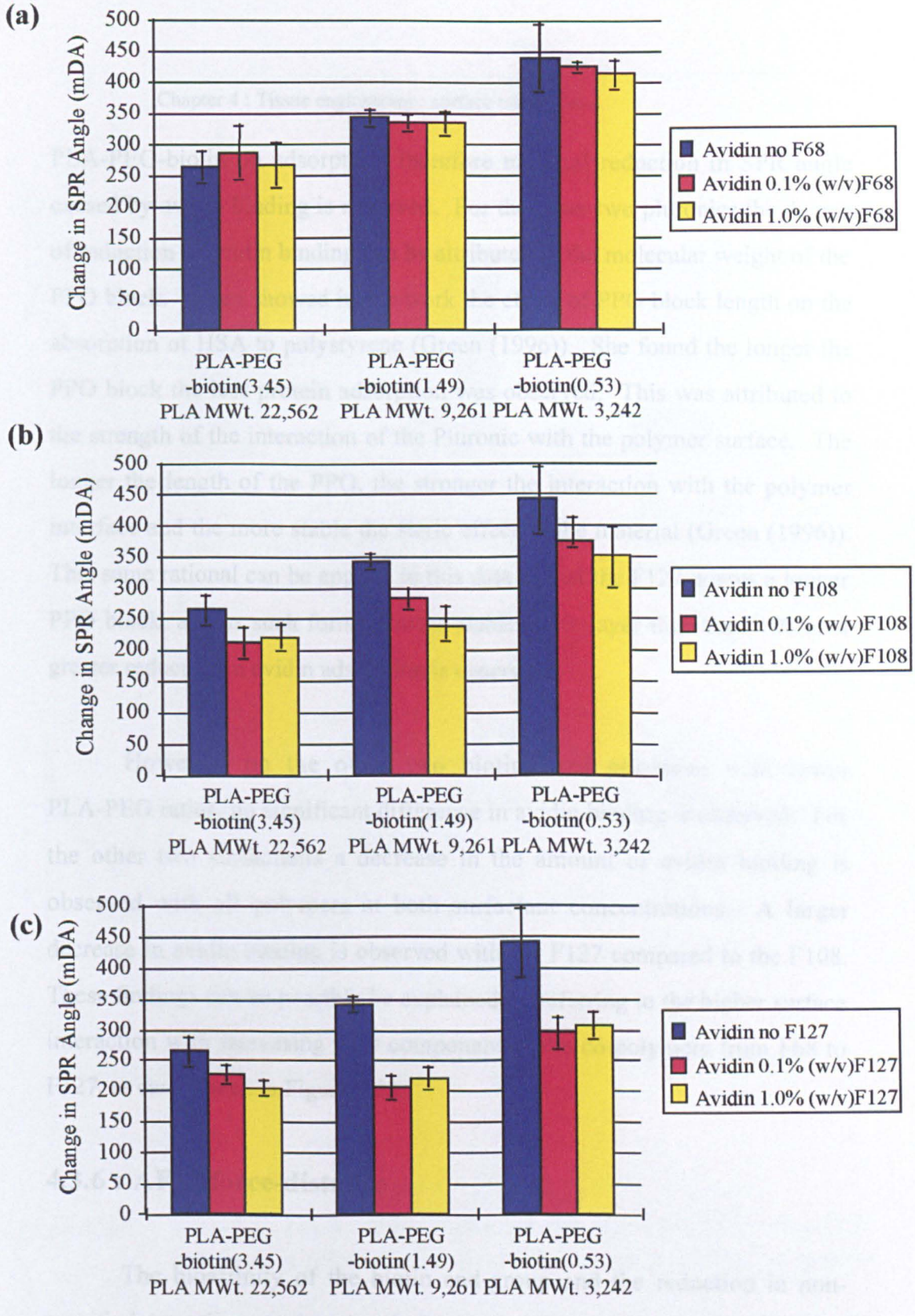

Figure 4.21 : Extent of avidin binding to biotinylated polymer surfaces after Pluronic incubation

The extent of reduction in avidin binding can be attributed to the surface characteristics of the polymer as altered by the Pluronics. The largest degree of reduction is for F127 and smallest for F68. This can be related to the Pluronics degree of interaction with the PLA-PEG-biotin (Figure 4.20).

Bars = average ± 1 standard deviation ($n \geq 12$)

PLA-PEG-biotin on adsorption, therefore minimal reduction in SPR angle caused by avidin binding is observed. For the other two pluronics the degree of reduction in avidin binding can be attributed to the molecular weight of the PPO block. Green showed in her work the effect of PPO block length on the absorption of HSA to polystyrene (Green (1996)). She found the longer the PPO block the less protein adsorption was observed. This was attributed to the strength of the interaction of the Pluronic with the polymer surface. The longer the length of the PPO, the stronger the interaction with the polymer interface and the more stable the steric effect of the material (Green (1996)). This same rational can be applied to this data in that the F127 posses a longer PPO block, and as such forms a more stable steric layer than the F108 so a greater reduction in avidin adsorption is observed.

However, on the other two biotinylated polymers with lower PLA-PEG ratios, no significant difference in avidin binding is observed. For the other two surfactants a decrease in the amount of avidin binding is observed with all polymers at both surfactant concentrations. A larger decrease in avidin binding is observed with the F127 compared to the F108. These findings can be possibly be explained by referring to the higher surface interaction with increasing PPO component of the co-polymers from F68 to F127, as can be seen in Figure 4.20.

4.3.6 : AFM force-distance

The bioaffinity of the biotin end-group and the reduction in non-specific interactions on changing the PLA : PEG ratio of the PLA-PEG-biotins was studied by AFM in its force-distance mode. Figure 4.22 shows the effect of PLA-PEG ratio on the non-specific interactions of a BSA coated tip with the PLA-PEG-biotin polymers. It can be seen from this figure that as the

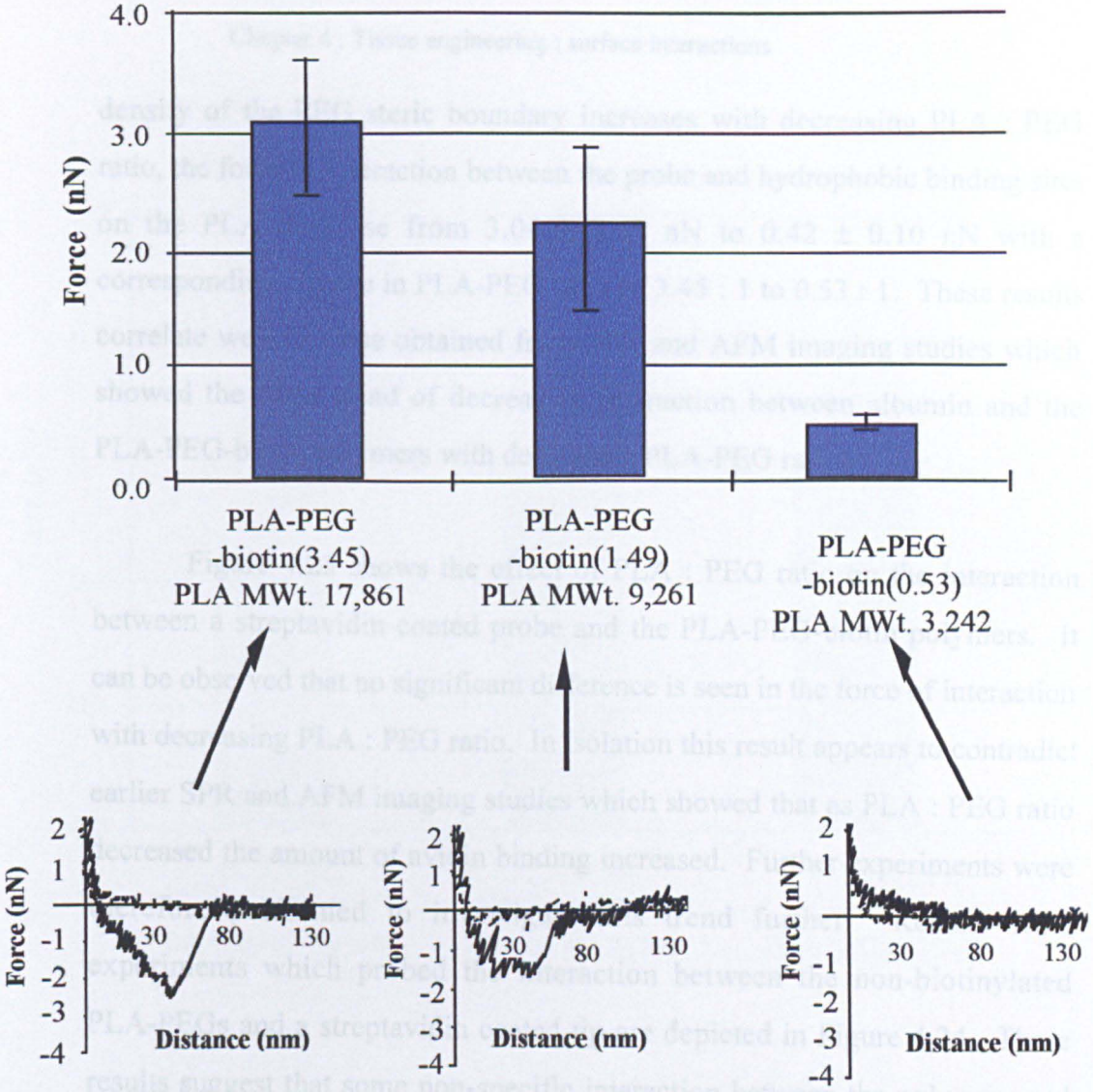

Typical force curves on each of the polymer surfaces prior to tip calibration

Figure 4.22 : Effect of PLA : PEG ratio on the strength of interaction between a BSA coated tip and the biotinylated polymers

As the molecular weight of PLA decreases, the density of the PEG steric layer increases. Therefore the extent of non-specific interaction with the underlying PLA decreases

Bars = average ± 1 standard deviation ($n \geq 128$)

density of the PEG steric boundary increases with decreasing PLA : PEG ratio, the force of interaction between the probe and hydrophobic binding sites on the PLA decrease from 3.04 ± 0.63 nN to 0.42 ± 0.10 nN with a corresponding change in PLA-PEG ratio of 3.45 : 1 to 0.53 : 1. These results correlate well to those obtained from SPR and AFM imaging studies which showed the same trend of decreasing interaction between albumin and the PLA-PEG-biotin polymers with decreasing PLA-PEG ratios.

Figure 4.23 shows the effect of PLA : PEG ratio on the interaction between a streptavidin coated probe and the PLA-PEG-biotin polymers. It can be observed that no significant difference is seen in the force of interaction with decreasing PLA : PEG ratio. In isolation this result appears to contradict earlier SPR and AFM imaging studies which showed that as PLA : PEG ratio decreased the amount of avidin binding increased. Further experiments were therefore performed to investigate this trend further. Results from experiments which probed the interaction between the non-biotinylated PLA-PEGs and a streptavidin coated tip are depicted in Figure 4.24. These results suggest that some non-specific interaction between the polymers and the streptavidin coated tip exists. The extent of this interaction between the tip and polymer seems to be dependent on the PLA : PEG ratio. As the PLA : PEG ratio decreases, Figure 4.24 shows that the extent of non-specific interaction with the non-biotinylated polymers decreases. This can be attributed to the increasing efficiency of the PEG steric boundary as shown in the AFM and SPR data. These results suggest that a proportion of the interaction between the biotinylated PLA-PEG and the streptavidin coated tip may be due to hydrophobic interactions with the PLA substrate. This concept was probed in two ways.

The results of the first experiment are shown in Figure 4.25. In this

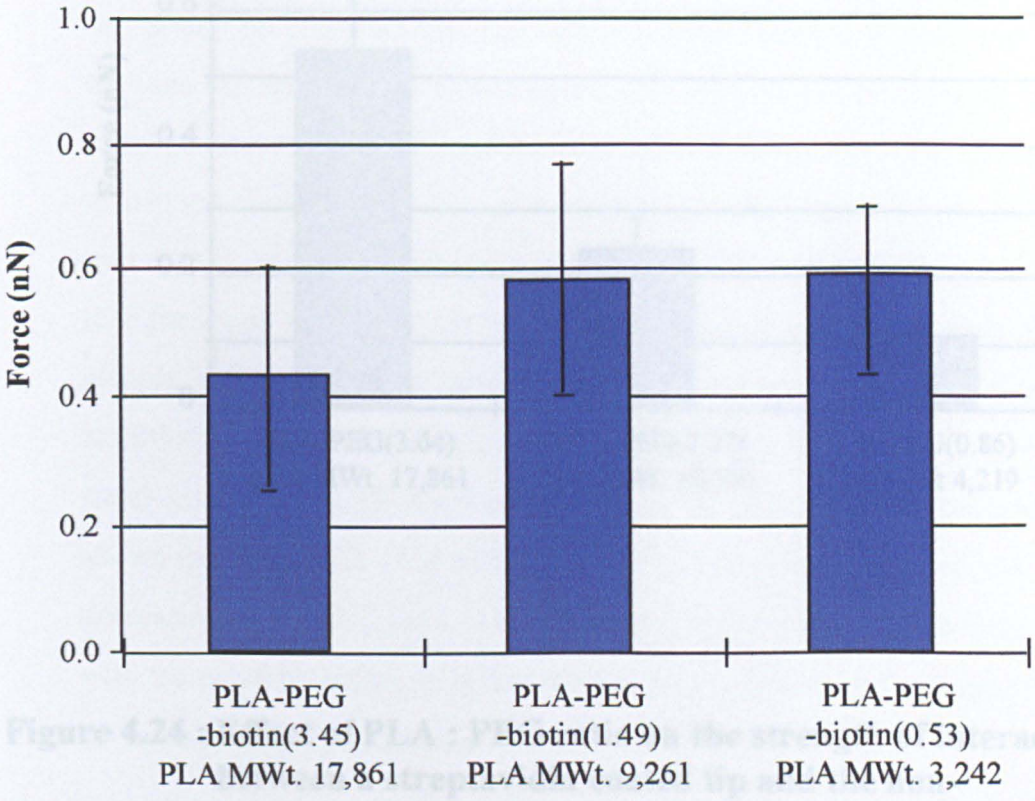

Figure 4.23 : Effect of PLA : PEG ratio on the strength of interaction between a streptavidin coated tip and the biotinylated polymers

Unlike previous SPR and AFM studies, no-significant difference is observed for the interaction of streptavidin with the PLA-PEG-biotins. This suggests that under these circumstances more than one interaction is occurring between the protein and polymer surface

Bars = average ± 1 standard deviation ($n \geq 119$).

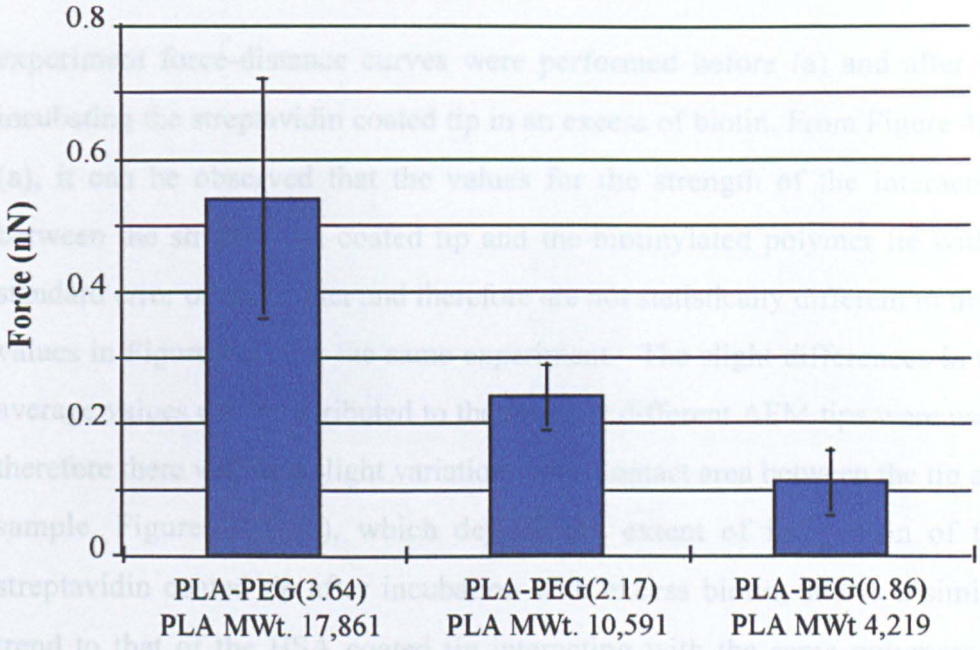

Figure 4.24 : Effect of PLA : PEG ratio on the strength of interaction between a streptavidin coated tip and the non-biotinylated polymers

As PLA molecular weight decrease, the density of the PEG steric layer increases. This results in a reduction in the extent of the hydrophobic interaction between the streptavidin and PLA.

Bars = average ± 1 standard deviation ($n \geq 117$)

experiment force-distance curves were performed before (a) and after (b) incubating the streptavidin coated tip in an excess of biotin. From Figure 4.25 (a), it can be observed that the values for the strength of the interaction between the streptavidin coated tip and the biotinylated polymer lie within standard error of each other and therefore are not statistically different to those values in Figure 4.23 for the same experiment. The slight differences in the average values can be attributed to the fact that different AFM tips were used, therefore there will be a slight variation in the contact area between the tip and sample. Figure 4.25 (b), which depicts the extent of interaction of the streptavidin coated tip after incubation with excess biotin, shows a similar trend to that of the HSA coated tip interacting with the same polymers as shown in Figure 4.22. The extent of interaction is observed to decrease with decreasing PLA : PEG ratio. This suggests that the streptavidin is interacting with the polymer surface in both a specific (to the biotin) and non specific (to the hydrophobic PLA) manner.

This theory was probed further by measuring force-distance curves before and after incubating the polymer surfaces with BSA. The incubation with BSA would hopefully block the non-specific binding sites of the PLA portion of the polymer so only the specific binding between the streptavidin and biotin end-group would occur. The results from this experiment are depicted in Figure 4.26. Figure 4.26 (a) again shows an the interaction between the streptavidin tip and biotinylated polymers which is not significantly different to those observed in Figure 4.23 and 4.25, as would be expected, as the same forces are being probed. The results in Figure 4.26 (b) show that as PLA : PEG ratio decreases the extent of specific binding due to biotin-avidin interactions now increases. This data shows the expected trend and correlates well with the SPR and AFM imaging data that as the density of biotinylated PEGs is increased, and hence the density of biotin end-groups increases, a

a)

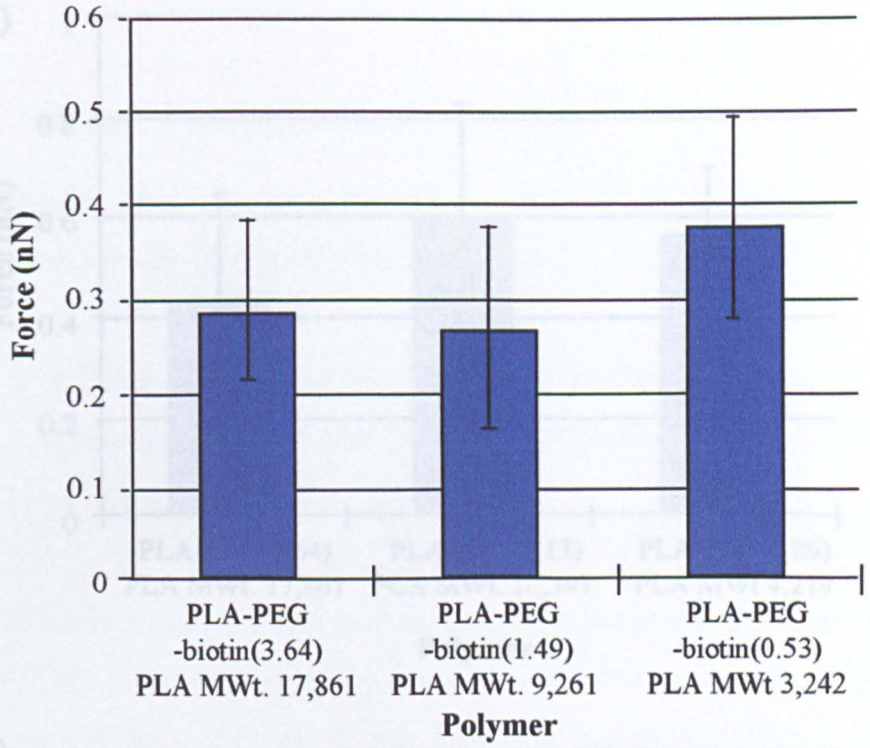

b)

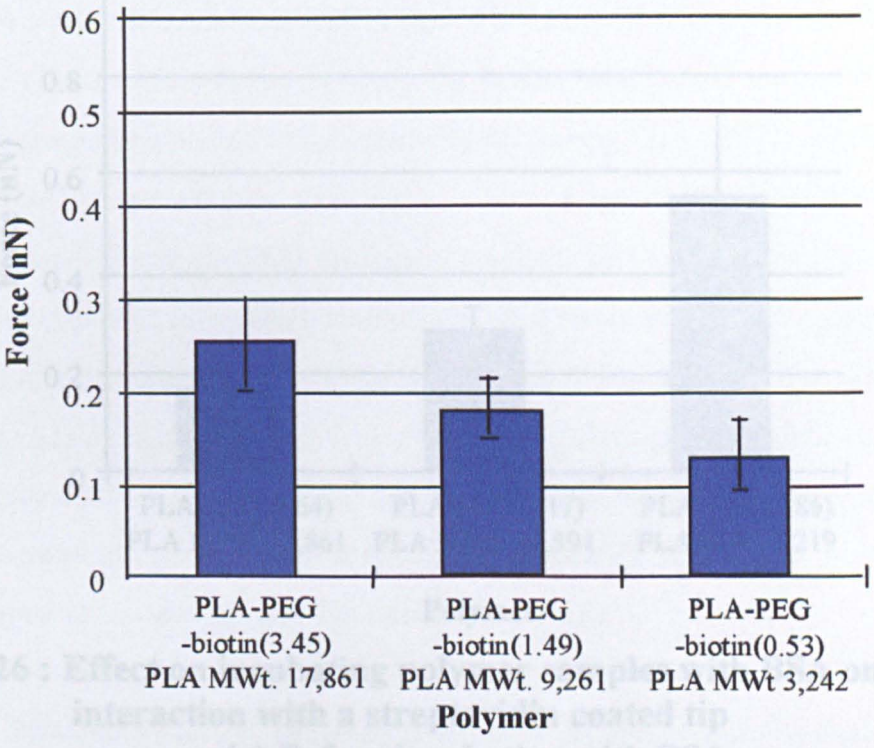

Figure 4.25 : Effect of incubating a streptavidin coated tip with excess biotin on the interaction with the biotinylated polymers
(a) Before incubation with biotin
(b) After incubation with biotin

After incubating with excess biotin the streptavidin's binding sites are blocked, therefore it is only capable of non-specific interactions with the PLA-PEG-biotins. These are observed to decrease with increasing PEG density i.e. decreasing PLA : PEG ratio.

Bars = average ± 1 standard deviation ($n \geq 114$)

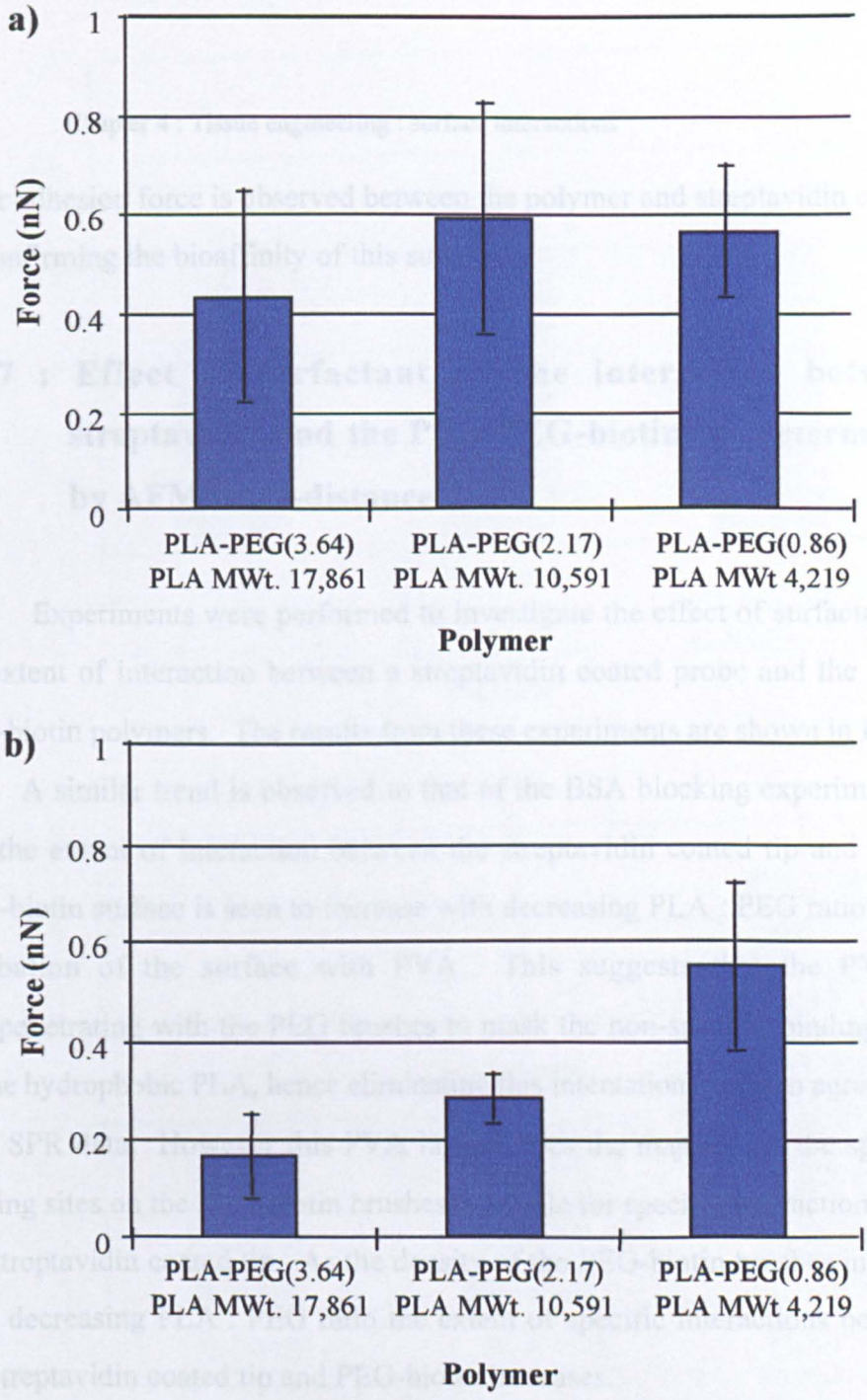

Figure 4.26 : Effect on incubating polymer samples with BSA on the interaction with a streptavidin coated tip
(a) Before incubation with BSA
(b) After incubation with BSA

The BSA interacts with the hydrophobic PLA. Therefore the streptavidin can essentially only bind specifically. This specific binding is observed to increase with decreasing PLA MWt. This can be rationalised in that as the PLA MWt. decreases, the density of biotinylated PEG chains increases. Therefore the force of interaction between the streptavidin tip and polymer surface also increases.

Bars = average ± 1 standard deviation ($n \geq 123$)

larger adhesion force is observed between the polymer and streptavidin coated tip confirming the bioaffinity of this substrate.

4.3.7 : Effect of surfactant on the interaction between streptavidin and the PLA-PEG-biotins as determined by AFM force-distance

Experiments were performed to investigate the effect of surfactant on the extent of interaction between a streptavidin coated probe and the PLA-PEG-biotin polymers. The results from these experiments are shown in Figure 4.27. A similar trend is observed to that of the BSA blocking experiment in that the extent of interaction between the streptavidin coated tip and PLA-PEG-biotin surface is seen to increase with decreasing PLA : PEG ratio, after incubation of the surface with PVA. This suggests that the PVA is interpenetrating with the PEG brushes to mask the non-specific binding sites on the hydrophobic PLA, hence eliminating this interaction, again in agreement with SPR data. However this PVA layer leaves the majority of the specific binding sites on the PEG-biotin brushes available for specific interactions with the streptavidin coated tip. As the density of the PEG-biotin brushes increase with decreasing PLA : PEG ratio the extent of specific interactions between the streptavidin coated tip and PEG-biotin increases.

Previous studies of the interaction between streptavidin, its analogue avidin and biotin have produce rupture forces between single molecules of 257 ± 25 pN, 340 ± 120 and 220-460 pN for studies performed by Florin, Lee and Allen respectively (Florin (1994), Lee (1994), Allen (1997)). The results for the interaction of the streptavidin probe and the PLA-PEG-biotin polymers with PLA molecular weights 22,562 and 9,261 after blocking of the hydrophobic PLA by either BSA or PVA correspond well with these values.

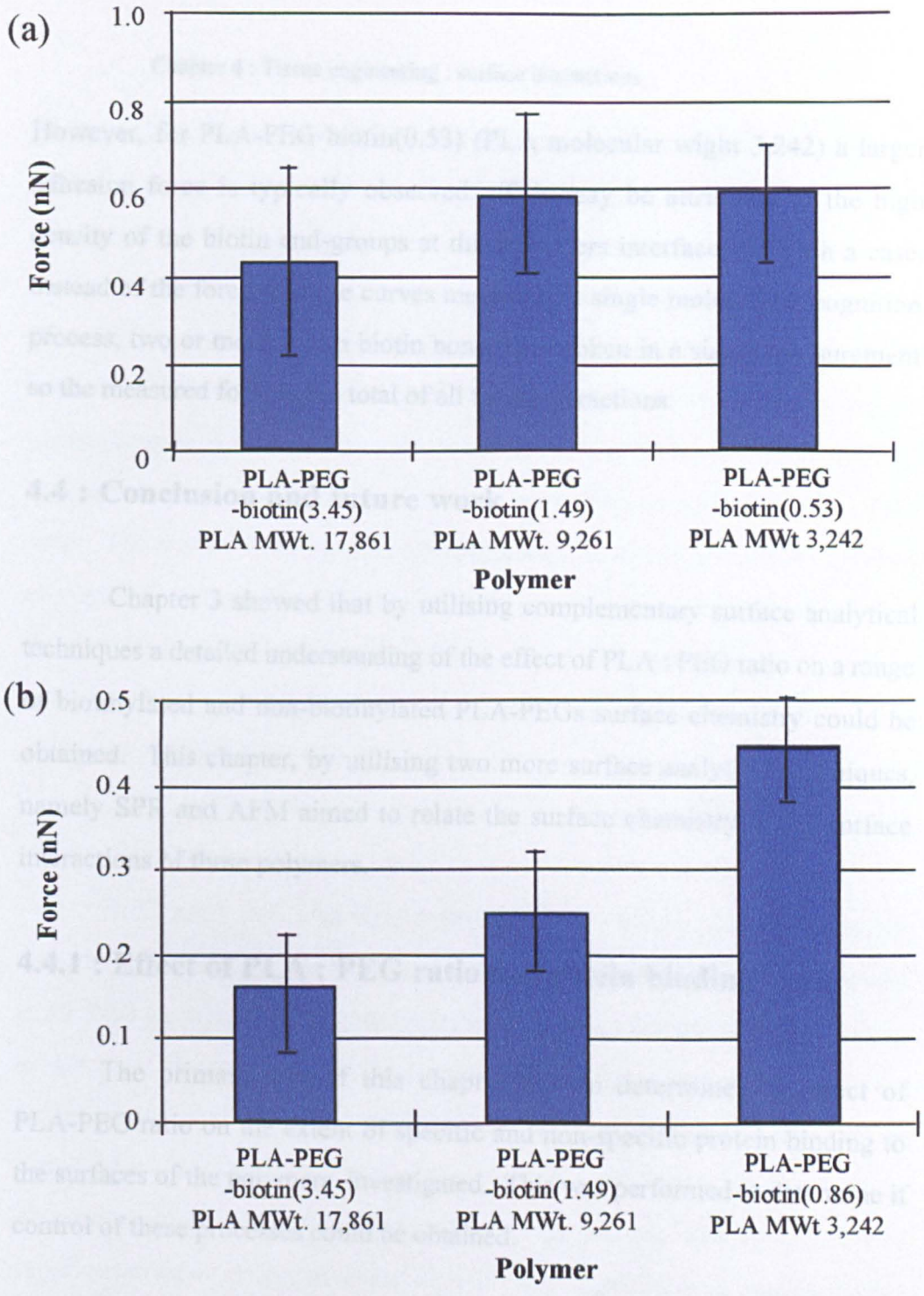

Figure 4.27 : Effect of PVA surfactant on the interaction between a streptavidin coated tip and the biotinylated polymers

The PVA appears to mask the PLA. Therefore only specific interactions between the streptavidin and polymer are observed. The interactions between the streptavidin and PLA-PEG-biotins appears to increase with decreasing PLA MWt., ie. increasing density of biotinylated PEGs.

Bars = average ± 1 standard deviation ($n \geq 97$)

However, for PLA-PEG-biotin(0.53) (PLA molecular wight 3,242) a larger adhesion force is typically observed. This may be attributed to the high density of the biotin end-groups at this polymers interface. In such a case, instead of the force distance curves measuring a single molecular recognition process, two or more avidin biotin bonds are broken in a single measurement so the measured force is the total of all these interactions.

4.4 : Conclusion and future work

Chapter 3 showed that by utilising complementary surface analytical techniques a detailed understanding of the effect of PLA : PEG ratio on a range of biotinylated and non-biotinylated PLA-PEGs surface chemistry could be obtained. This chapter, by utilising two more surface analytical techniques, namely SPR and AFM aimed to relate the surface chemistry to the surface interactions of these polymers.

4.4.1 : Effect of PLA : PEG ratio on protein binding

The primary aim of this chapter was to determine the effect of PLA-PEG ratio on the extent of specific and non-specific protein binding to the surfaces of the polymers investigated. This was performed to determine if control of these processes could be obtained.

When placed into the body non-specific binding of proteins to a materials surface is a major cause of the loss of biocompatibility. PLA is a hydrophobic polymer and as such is prone to non-specific binding of proteins. In Chapter 3 it was observed that as the PLA molecular weight decreased, its presence at the surface was also reduced. In this chapter SPR studies showed that the extent of non-specific interactions of HSA with the biotinylated

polymers also decreased with PLA : PEG ratio and this reduction is attributed to its lower surface concentration. This reduction in HSA interaction was confirmed by AFM imaging studies which showed a reduction in surface coverage of the protein molecules on the polymer surface with decreasing PLA-PEG ratio. When probing the strength of interaction between a HSA coated AFM tip and the biotinylated polymers by force-distance measurements, a statistically significant reduction in the maximal force of interaction between the two entities was observed on reducing the PLA : PEG ratio. The results from these complementary investigations into the level of non-specific interaction of proteins with the PLA-PEG-biotin polymers of varying PLA : PEG ratio show that a correlation between the extent of non-specific protein interactions and the surface concentration of PLA at the surface as determined in Chapter 3 exists.

In Chapter 3 it was shown that as PLA : PEG ratio decreased the contribution of PEG to the surface increased. As the biotin moiety is located at the PEG terminus this suggests an increase in the available biotin for binding avidin also. However, due to the low content of biotin when compared to the monomer units of the PLA and PEG this was not determined by XPS or ToF-SIMS. By using SPR the effect of PLA : PEG ratio on the specific interactions of avidin with the biotinylated polymers was investigated. These experiments showed that the extent of avidin binding did indeed increase with a decrease in the PLA : PEG ratio. The extent of avidin binding to the biotinylated polymers in the case of the PLA-PEG-biotins with PLA : PEG ratios 1.49 : 1 and 0.53 : 1 showed statistically significant more binding than that to a planar biotin SAM surface. This suggested that the polymer interface was acting as a flexible surface region with higher surface area than that of the planar SAM surface for avidin binding.

Further evidence that the surface coverage of avidin on the polymer surface was affected by PLA : PEG ratio was obtained from AFM imaging studies. These again showed an increase in the coverage of avidin on decreasing the PLA : PEG ratio. In images of the PLA-PEG-biotins with PLA : PEG ratios 1.49 : 1 and 0.53 : 1 aggregates of the avidin and avidin entities in various z planes were observed. This provided further tentative evidence that the polymer surface maybe acting as a 3-dimensional surface region rather than a 2-dimensional monolayer.

When probing the strength of interactions between a streptavidin coated tip and the biotinylated polymers, no significant difference was observed in the maximal adhesion forces for the three biotinylated polymers of varying PLA : PEG ratios. Similar studies on non-biotinylated PLA-PEG's by SPR and AFM force-distance measurements showed that there was some non-specific interaction between the polymers and streptavidin protein. This non-specific interaction was observed to decrease with PLA presence at the surface (decreasing PLA : PEG ratio) as determined by XPS and ToF-SIMS in Chapter 3. It was therefore hypothesised that the interaction between the biotinylated polymers and the streptavidin tip used in these investigations comprised not only of specific avidin-biotin interactions but also non-specific PLA protein interactions. Control experiments showed that this was indeed true.

On blocking the binding sites of the streptavidin on the tip with excess biotin so only non-specific interactions between it and the polymer surface were measured a decrease in the maximal force of interaction between the tip and polymer was observed on decreasing the PLA : PEG ratio. This was the same trend as that observed for the non-specific interaction of the BSA coated

tip with these surfaces. This control experiment showed that streptavidin did indeed interact with these polymer surfaces non-specifically. SPR was utilised to confirm this and on flowing blocked avidin over the surface of the PLA-PEG-biotins a small degree of interaction was observed. The change in SPR angle which is indicative of material adsorbing to the surface was observed to decrease on lowering the PLA : PEG ratio and hence reduced PLA at the surface.

To measure the extent of specific interactions between a streptavidin coated tip and the biotinylated polymers, the non-specific protein interactions with the polymer needed to be blocked. This was performed by incubating the PLA-PEG-biotin samples with BSA prior to probing the strength of interaction between them and the streptavidin tip. In this case results like those seen in SPR experiments were observed ie. as the PLA : PEG ratio decreased the extent of specific interactions between the avidin and polymer surface increased due to the increased density of PEG and hence biotin at the polymer surface as determined by XPS and ToF-SIMS.

Although SPR and AFM both showed that streptavidin bound non-specifically to the PLA-PEG-biotin polymers and the extent of this was governed by the polymers surface chemistry. Trends observed in initial experiments probing the total interaction between streptavidin and the polymers measured by AFM and SPR did not agree. This could be due to the nature in which the two techniques probe this interaction. In SPR the dynamic properties of the system are investigated and the biomolecules of interest, in this case avidin are flown over the surface of the material. Due to the buffer flow, any interaction which is not strong, such as the non-specific interaction between the avidin and hydrophobic portion of the polymer will not contribute significantly to the overall binding level. AFM force-distance

measurements, push the molecule whose interactions are to be measured into the surface of the material of interest unlike SPR where they are flown over the top of the surface. In this process the contributions of non-specific interactions will be more strongly felt and in this case their contribution to the overall interaction of avidin with the PLA-PEG-biotins will be greater and hence, as observed, able to mask the extent of specific interaction between the avidin and biotin

The results discussed in this section show that by altering the surface chemistry of the PLA-PEG-biotin system by varying the PLA molecular weight as discussed in Chapter 3; control can be obtained over the degree of surface modification of this system with avidin. Further investigations were performed utilising SPR to determine biotinylated peptides binding levels to the various PLA-PEG-biotin polymers. These showed that differing levels of this peptide bound to the avidin engineered surface depending on the PLA : PEG ratio. More was observed to bind to the polymer with the lowest PLA : PEG ratio, ie. most avidin, although SPR shift values were not significantly different. This can be attributed to the small shifts caused by the addition of the peptide which is a small molecule. These results from experiments probing avidin and biotinylated peptide interactions with the PLA-PEG-biotins show that controllable modification of these polymer surfaces can be obtained.

The level of surface modification of the PLA-PEG-biotin surfaces was shown to be further controlled by mixing the biotinylated polymers with non-biotinylated PLA-PEGs and hence reduce specific binding further.

In future work the effect of avidin and hence cell adhesion molecule density on cell binding and spreading on these polymer surfaces will be investigated to determine the optimal density of cell adhesion molecules for a

range of cell types.

4.4.2 : Effect of surfactant on degree of surface engineering of PLA-PEG-biotin polymers by avidin

Surfactants are often used to reduce surface tension and hence stabilising newly formed surfaces. This is a useful process in tissue engineering scaffolds formation but may have detrimental effects on the surface properties on the polymeric material. Therefore, the effect of a range of surfactants on the extent of surface modification of the PLA-PEG-biotins was investigated.

In the case of PVA, the extent of reduction in avidin binding to the polymer surface was observed to be dependant on surfactant concentration. Below a concentration of 0.03 % (w / v) no decrease in the extent of avidin binding was observed. A decrease in avidin binding was then observed. This decrease was proportional to the increasing surface coverage of the polymers with PVA. Above a concentration of 0.05 % (w / v) no further increase in PVA binding, or decrease in the polymers surface modification by avidin were observed.

A larger decrease in the extent of avidin binding to the PLA-PEG-biotin polymers was observed as the PLA : PEG ratio decreased. This was attributed to the reduction in PEG chain mobility. At high PEG densities, the interpolating PVA would elicit a higher reduction in the PEGs conformational freedom and hence its ability to bind avidin. However, in all cases independent of PVA concentration and PLA : PEG ratio the levels of specific avidin-biotin binding were significantly larger than non-specific interaction of avidin to the control PLA-PEG polymers.

As well as reducing the levels of specific binding, SPR showed that PVA reduced the levels of non-specific avidin interactions to the control PLA-PEG polymers. AFM force-distance experiments also showed that it reduces the extent of non-specific avidin interactions with the PLA-PEG-biotins.

The fact that non-specific protein interactions and hence the risk of immune response is reduced by PVA, and the extent of specific avidin binding is not vastly reduced by it suggest that PVA is a good surfactant for the application of reducing the surface tension of newly formed surfaces in tissue engineering scaffold formation.

As well as the effect of PVA a range of Pluronic surfactants tri block polymers of PEO-PPO-PEO were studied and the effect of PPO and PEO molecular weight investigated. As with previous studies by Green et al. (1996), it was observed that a larger reduction in protein binding was caused by both higher molecular weight PPO and PEO. This means that control over the extent of avidin binding to a certain PLA-PEG-biotin can also be controlled by pre-incubating the surface with Pluronics of varying PPO and PLA content.

In summary, the work in this chapter shows that the extent of both specific and non specific interactions of the biotinylated PLA-PEGs can be controlled by altering the PLA : PEG ratio of the polymers and hence, surface chemistry as discovered in Chapter 3. This provides the basis for further studies investigating the effect of the degree of surface modification by cell adhesion molecules and on cell binding and spreading on this polymer system. In addition, it has been shown that the treatment of these surfaces by surfactants is not significantly detrimental to their ability to specifically bind

avidin, and but does reduces the extent of non-specific protein interactions with their surfaces which can lead to poor biocompatibility. By using Pluronic surfactants it can be concluded that as well as acting to stabilise new surfaces, these surfactants can be, by selecting specific PPO and PEO molecular weights control the degree of surface modification of the PLA-PEG-biotins by avidin.

Chapter 5 : Polymers in gene therapy

5.1 : Introduction

5.1.1 : Background to gene therapy

Conditions caused by defective genes are widespread and often fatal. The defective genes in turn lead to defective biological function of proteins or imbalances in the homeostasis of the cells producing the observed disease state. If genes could be delivered to these cells which contained copies of the correct genetic code, inherited conditions such as haemophilia and cystic fibrosis, and other disease states such as arthritis, atherosclerosis, AIDS and cancer could be controlled or cured. Effective gene delivery also has the potential to perform as a vaccine, potentially eliminating the problems of current treatment regimes (Garnett (1999), Ledley (1996)).

However, delivering the gene or DNA to the sight of action is a significant problem. Nature has provided an excellent carrier system in the virus with its highly effective infection pathway. Many papers have been published using recombinant viruses as gene carriers. These viruses are able to infect the cell and deliver the DNA to its target, but are unable to replicate or produce viral based disease. Many viral groups have been investigated, however, the major research has been in the area of retro, adeno-associated viruses and adeno-viruses (Wivel (1998)).

Retro-viruses are RNA based viruses which can insert genes into host chromosomes. The mutants used in gene therapy are recombinant and hence have the ability to infect cells and insert their gene but have no coding for viral proteins, so cannot replicate (Miller (1990)). As the retro-virus only infects dividing cells, transformation is more efficient in the *ex vivo* situation. Cells are

removed from the patient, stimulated to divide, infected with the correct gene via the retro-virus and implanted back into the patient. *In vivo* delivery has also been performed, but rapid removal of the virus is observed by human complement. This can be reduced by modification of the virus (Rother (1995)) and is also aided by delivery directly to the sight of action i.e. in cancer to the tumour (Culver (1992)). However, retro-viruses are not observed by many to be a good choice of vector (Cornetta (1992), Temin (1990)). These doubts are attributed primarily to the random nature of the foreign RNA insertion into the DNA. This may lead to mutagenesis or oncogenesis. Secondly, the possibility of the recombinant virus becoming transformed by other viral or cellular RNA, leading to a new type of replicating virus with unknown properties is a major concern (Vanin (1994)).

These problems can be reduced by the use of adeno-associated viruses which are less prone to recombination and infect cells during all phases of the cell cycle. Their main problem however, is their production in packaging cell lines as titers are low without the aid of helper viruses (Flotte (1995)). Unlike retro and adeno-associated viruses, adeno-viruses do not insert their genetic material into the host chromosome, instead it is present as extrachromosomal elements or epitopes. Like adeno-associated viruses, they too infect dividing and non-dividing cells. Other advantages include, the fact that they can be directly administered to patients producing a high efficiency infection. Their main problem is toxicity. Unlike the retro-virus they are attenuated, not transformed. This means whilst not able to replicate they still possess several viral proteins which induce cytopathic and immunogenic responses *in vivo*. This in turn can reduce gene expression and antibodies produced to the viral vector prevents repetitive administration (Yei (1994)).

The major problems associated with viral delivery has forced the

investigation of new synthetic delivery systems. These can be divided into two major groups, the cationic polymers and cationic lipids. This chapter will concentrate on the use of cationic polymers whereas chapter six will be concerned with the use of cationic lipids.

DNA is a highly charged colloidal material that does not diffuse or cross the cell membrane well. DNA used for gene therapy is normally in the form of a circular plasmid, which codes not only the therapeutic agent but also sequences such as promoters, enhancers, introns and genes which aid mRNA translation and processing, and postranslational processing of the therapeutic agent where needed. These codes enhance the effectiveness of the host cell to produce the therapeutic agent, but also mean that the DNA to be delivered has between 5-10,000 base pairs and hence a molecular weight of in excess of a million daltons. Therefore, to produce a particulate for delivery which optimally, possesses a diameter less than 100 nm the DNA needs to be condensed to a volume 10^4-10^6 less than that of its relaxed state (Ledley (1996)). Once inside the body DNA is rapidly eliminated from the administration site. This is either by endonucleases and exonucleases degradation or receptor mediated uptake by the Kupffer cells present in the liver and spleen (Kawabata (1995)).

Because of these problems polymeric carriers need to fulfil the following criteria. Firstly, they must be able to condense the DNA so the particulate size is small enough for successful transport around the body and delivery to the target sight (Pouton (1998a)). Secondly, it must protect the DNA from degradation whilst in transit between the administration and target sites. Thirdly, increase the effectiveness of cellular uptake over that of free DNA administration and finally it must release the DNA in a form inside the cell where it can be expressed. In summary, it should present enough active

gene at the right cell type for transcription to elicit a beneficial effect.

Many different polymers families have been investigated for their effectiveness as gene therapy vectors, the majority of them have been cationic polymers but non-ionic polymers such as poly(vinyl pyrrolidone) (PVP) and poly(vinyl alcohol) (PVA) have also been investigated (Mumper (1995), (1996)). PVP has been shown to increase the retention, dispersion and uptake of many conventional drugs (Robinson (1990)). Whereas as a gene therapy vector there is evidence that it stabilises DNA against DNAases *in vitro,* whilst *in vivo,* an increase in distribution and the number of cells expressing the gene when compared to delivery of naked DNA has been observed (Mumper (1995), (1996)). It is thought that the interaction between PVP and DNA may be comprised of hydrogen bonding and hydrophobic interactions. These may also be responsible for its ability to extend dose response kinetics.

Wheeler and co-workers have shown advantages of coating liposome/DNA complexes with PEG (Wheeler (1999)). Depending of the length of the acyl chain used to anchor the PEG, the stability of the PEG coating can be altered. This is a useful phenomena as it produces a delivery system with lower hydrophobic interactions, which in turn may lead to a lower immune response. Whilst the instability of the coating allows release of the cationic liposome / DNA complex which can then fuse with the endosome releasing the DNA into the cytoplasm.

Sustained release of plasmid *in vitro* of up to a month from a poly(lactide-co-glycolide) (PLG) matrix has been shown by Shea and co-workers. Their primary interest is in release of growth factor coding genes for tissue engineering, but this system lends itself to a wide range of applications (Shea (1999)).

When considering the cationic polymers, many different monomers and architectures have been investigated to determine the best vector for gene therapy, but as yet a universal delivery system has not been discovered. Some of these polymers and architectures are shown in Figure 5.1. Particulates of DNA and the polycation form spontaneously on mixing due to a co-operative system of interchain electrostatic bonding. The physico-chemistry of the complex particulate is determined by the polymer type, its molecular weight and ratio of DNA to polymer (Van de Wetering (1998)). In all cases, the DNA is tightly packed protecting it from DNAases in the extracellular matrix (Kabanov (1991)), but competition with membranes or cellular molecules for interaction with the polycations charge allows rearrangement and release of the DNA (Kabanov (1995)).

Polycation DNA complexes have the advantage over liposomal delivery systems that they are more stable in a wider range of medias of differing pH and ionic strength. This facilitates their formulation, storage and delivery to patients (Kabanov (1995)).

Polyethyleneimines (PEI) have a high evenly distributed charge density which promotes the condensation of DNA to varying sized and charged particulates. Due to of its high charge density, it is thought to act as a ion sponge, buffering the DNA against degradation in the acidic lysosomal compartments. This theory was proposed by Behr (Boussif (1995)). The method of formulation of particulates between PEI and DNA as with other cationic polymers effects their transfection efficiency. *In vitro* experiments by Boussif and co-workers showed that complexes formed from the addition of DNA to PEI had a lower activity to those formed from the addition of PEI to DNA (Boussif (1996)).

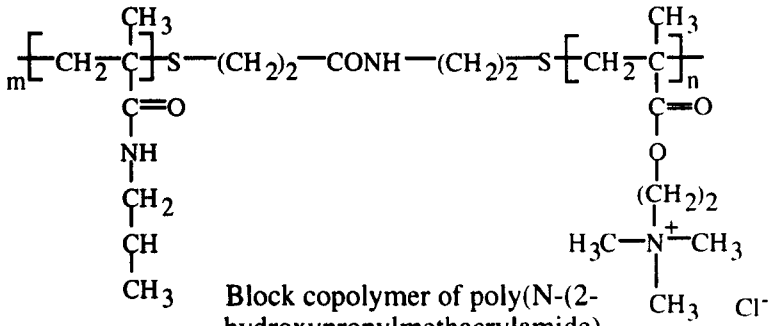

Block copolymer of poly(N-(2-hydroxypropylmethacrylamide) and 2-(trimethylamino) ethyl methacrylate chloride (Konak (1998))

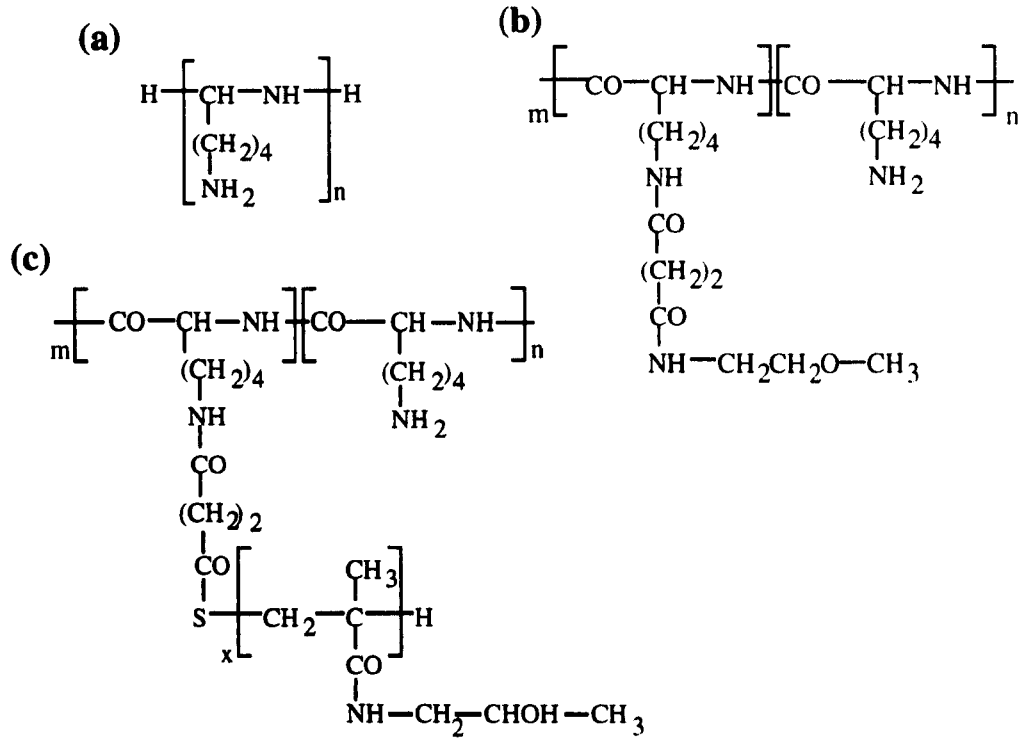

poly-l-lysine (a) and block co-polymers of PLL with (b) poly(ethylene glycol) and (c) poly(N-(2-hydroxypropyl)methacrylamide (Toncheva (1998))

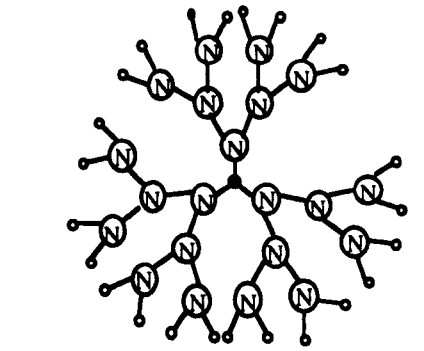

PAMAM dendrimers

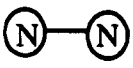

= N-CH_2-CO-NH-CH_2-CH_2-N

Full generation (n.0) = N-H +

Half generation (n.5) =N-CH_2-CH_2-CO_2^- Na^+

Figure 5.1 : Examples of cationic polymers used for gene therapy

Chitosan formed from deacetylating the naturally occurring polymer chitin and it has been shown to produce DNA complexes with varying shapes from spheres to pretzels. The size of these structures alters in relationship with the molecular weight of the chitosan (Mumper (1995), Illum (1998)). In some cell lines their transfection efficiency is observed to increase gene expression over a 24-96 h time period *in vivo*. This finding is in contrast to PEI whose transfection efficiency levels were seen to decrease. Therefore, at 96 h post addition in some cell lines, a 10 fold increase in transfection efficiency is observed for chitosan over PEI (Erbacher (1998)).

Poly(amidoamine) (PAMAM) dendrimers have been shown to complex DNA and exhibit transfection in a number of cell lines *in vitro* including human T-cells and carcinoma (Haensler (1993b)). By attaching pH sensitive endosomal lytic peptides to the terminal groups of the dendrimers the effectiveness of dendrimer mediated transport has been shown to increase approximately threefold (Haensler (1993a)). Tang and co-workers have shown that by heat treating dendrimers to break some of the peptide bonds incomplete dendrimer generations or "fractured dendrimers" are formed. These "fractured dendrimers" show an increase in transfection efficiency over complete generation dendrimers. This increase in transfection is related to the increase in dendrimer flexibility which allows the formation of a smaller DNA / dendrimer complex (Tang (1996)).

Many moieties have been added to cationic polymers to aid their successful delivery of genetic material to the correct cell type. These include oligosaccharides, intercalating agents (Haensler (1993b)), long hydrophobic (Behr (1989) Kabanov (1993)) or hydrophillic (Toncheva (1998) Konak (1998)) blocks and asialoglycoprotein or other such peptide or protein vector molecules such as RGD sequences ((Wu (1988), Plank (1992), Kabanov (1994)

Erbacher (1998)).

5.1.2 : Background to investigations

When polycation DNA complexes are formed, they possess a relatively neutral surface which leads to destabilisation and hydrophobic interaction with proteins. Hence, they are removed from circulation (Kabanov (1995)). The aim of this work is to investigate the effect of adding poly(ethylene glycol) (PEG) to the cationic polymer poly-l-lysine (PLL) on its complexation with DNA and complex structure. The rational behind adding PEG to the cationic polymer is to increase the hydrophilicity of the system by providing a steric layer around the outside of the complex, similar to that observed in STEALTH™ liposomes. This effect should increase circulation time, reduce hydrophobic interactions with proteins and hence, hopefully increase the number of cells transfected with the complexed DNA. The polymers used possess a constant content of a 20 kDa block of PLL and varying amounts of PEG from 5 to 20 kDa. SPR was utilised to investigate how PEG content effects the rate and extent of complexation to DNA. Complementary studies utilising AFM, measured the effect of PEG molecular weight on the strength of interaction between the DNA and PLL and liquid images provided information on how PEG molecular weight effected the complex structure.

5.2 : Materials and methods

5.2.1 Polymers

All cationic polymers used in this investigation were synthesised by V. Toncheva (University of Gent, Krisjlaan, Gent, Belgium) and used without further purification. Polymers used possessed a block of PLL of 20 kDa and

PEG of either 5, 12, 20 kDa and were present as bromide salts. PLL of molecular weight 20 kDa was used as a control material. Identical polymers which had been biotinylated were used in experiments where the polymer needed to be bound to a surface. Only polymers with 5 and 12 kDa PEG were available. Biotin molecules were attached at a 5% level as pendant groups from α-amino groups.

5.2.2 : DNA.

DNA was extracted by the following method which is adapted from Maniatis (1986). 500 ml of E. coli transformed with pSV-ß-galactosidase plasmid (see Figure 6.2) were grown in shaking suspension of LB broth (Gibco BRL, Paisley, UK) to a turbidity of 0.6 OD at a wavelength of 600 nm. Cells were harvested by a 15 min centrifuge at 1,300 g at 4 °C. The supernatant was removed and cells resuspended in saline buffered Tris EDTA (STE) (0.1 M NaCl, 10 mM Tris·HCl, 1 mM EDTA, pH 8.0). The spin was repeated and supernatant removed.

Cells were lysed using an alkali method. The pellet was resuspended in solution I (50 mM glucose 25 mM Tris·HCl, 10 mM EDTA pH 8.0). 2 ml of lysozyme (25 mg / ml (10 mM Tris·HCl)) was added. This was followed by an addition of 20 ml fresh solution II (0.2 N NaOH (diluted from 10 N stock) containing 1% SDS). The sample was mixed by inversion and stored at room temperature for 10 minutes. 15 ml of ice cold solution III (5 M potassium acetate (60 ml), glacial acetic acid (11.5 ml), deionised water (28.5 ml)) was then added. The sample was mixed by inversion till only one phase was observed and stored on ice until a white flocculent appeared (~ 10 min). This flocculent comprises of chromosomal DNA, high molecular weight RNA and potassium, SDS, membrane protein complexes. The sample was then

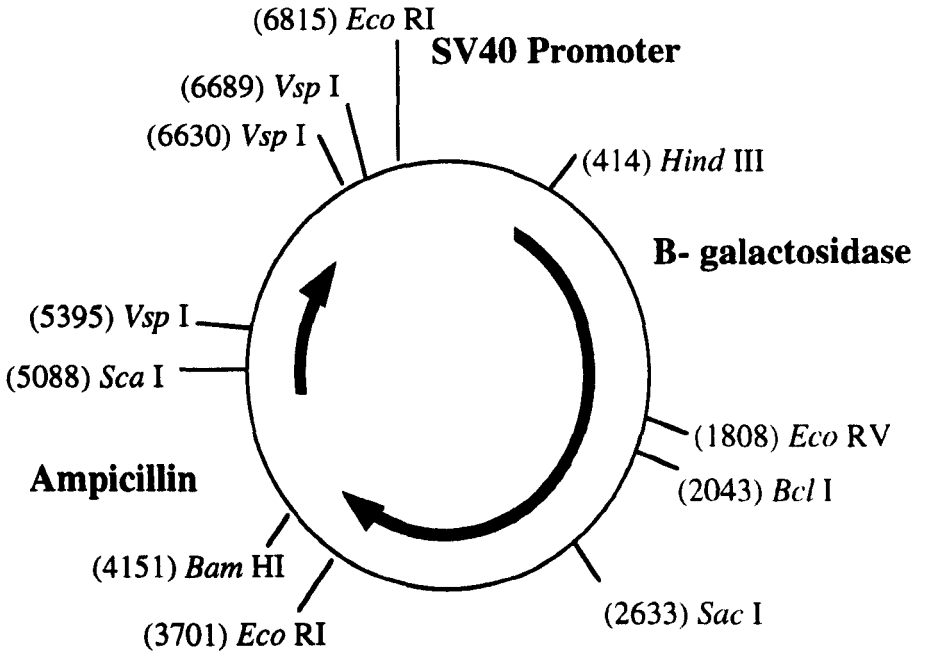

Figure 5.2 : Plasmid DNA restriction map

centrifuged at 20,000 g for 15 min and 4 °C without braking. Supernatant was transferred to a clean centrifuge tube via filtering through a four layer cheese cloth leaving viscous liquid behind. 0.6 volume of isopropyl alcohol was added and mixed with supernatant. The mixed sample was stored at room temperature for 10 min and then centrifuged at 15,000 g for 15 min at room temperature. Supernatant was removed and the pellet washed at room temperature with 70% ethanol. The ethanol was drained off the pellet by inverting the tube on a tissue and allowing the residual ethanol to evaporate in air . The pellet was redissolved in 3 ml of Tris EDTA (TE) (10 mM Tris·HCl, 1 mM EDTA, pH 8.0).

The purification of plasmid DNA was performed using a PEG precipitation method. High molecular weight RNA was removed by the addition of 3 ml of ice cold 5 M lithium chloride. The sample was mixed and centrifuged at 15,000 g for 20 min at 4 °C. An equal volume of isopropanol was then added and sample centrifuged at 15,000 g for 30 min at room temperature. The supernatant was removed and the pellet was resuspended in 500 µl of TE (10 mM Tris·HCl, 1 mM EDTA, pH 8.0) containing DNAase free pancreatic RNAase (20 µg / ml). The sample was allowed to stand at room temperature for 30 min to allow enzymatic degradation of remaining RNA. After the addition of 500 µl of 1.6 M sodium chloride containing 13 % (w/v) PEG (MWt. 8,000 Da) the sample was mixed and centrifuged at 12,000 g for 5 min at room temperature. The supernatant was removed and pellet resuspended in TE. The sample was extracted with phenol (25) : chloroform (24) : isoamyl alcohol (1) followed by chloroform. 100 µl of 10 M ammonium acetate was added to the aqueous phase and mixed. After the addition of 2 volumes of ethanol the sample was stored at -20 °C for 20 min. The sample was centrifuged at 15,000 g for 5 min and 4°C and supernatant removed by aspiration. 200 µl of ice cold 70% ethanol was added and sample vortexed and

spun at 12,000 g for 2 min at 4°C. The supernatant was removed and remaining ethanol allowed to evaporate. Pellet was redissolved in 500 µl of TE.

Recovery of plasmid DNA was quantified by carrying out an OD at 260 nm. An OD of 1.0 is equivalent to 50 µl DNA / ml. Purity of plasmid DNA was confirmed by using gel electrophoresis. A 0.7% agrose gel in Tris acetate EDTA, (TAE) (Tris. HCl 10 mM, 57.1 ml / l glacial acetic acid, EDTA 1 mM pH 7.2) with ethidium bromide at a concentration of 0.25 µg /ml. 500 µg of DNA mixed in a 2 : 1 ratio with loading buffer (10 mM Tris. Hcl, Ph 7.5, 50 mM EDTA, 10 % Ficol 400, 0.25% (w / v) bromophenol blue, 0.25 % (w / v) xylene cyanol) was added to the gel wells. The gel was run at a power of 100 V for 60 min in TAE buffer containing 0.25 µg / ml ethidium bromide. Molecular weight of DNA was checked against a lambda Hind II marker (0.5 µg / well) . Gels were visualise using a UV transilluminator and photographed using a Polaroid gel documenting system, an example of such a gel is shown in Figure 5.3.

Where DNA needed to be adhered to a surface, a biotinylated version of the extracted plasmid was used. Biotinylation was performed using a biotinylated psoralen (EZ-link™ psoralen-PEO-biotin) (Pierce and Warnier, Chester, UK). Four ratios of biotinylated agent molecules per DNA plasmid, namely 20 : 1, 40 : 1, 80 : 1 and 120 : 1 were used to establish the optimal ratio for maximal incorporation of biotin into the DNA. DNA was made to a concentration of 1 µg / µl in TE (10 mM Tris, 1 mM EDTA, pH 7.4) and biotinylated psoralen to 13.78 µg / 100 µl in the same buffer and stored under dark conditions. Enough biotinylated psoralen was added to 20 µg of DNA to give the ratios 20 : 1, 40 : 1, 80 : 1 and 120 : 1 ratios of DNA base pairs to biotinylating agent molecules. The samples were vortexed for 30 s and place in

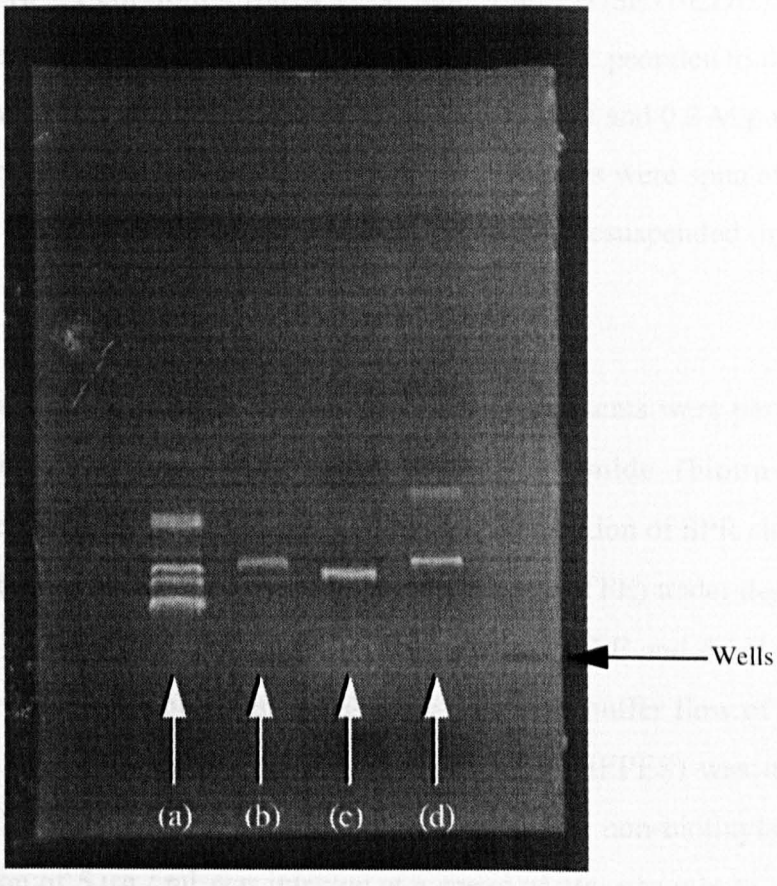

Figure 5.3 : Typical gel of extracted plasmid

(a) lambda hind III marker
(b) pSV B-gal plasmid (restriction map see Figure 5.2)
(c) plasmid + Bam H1
(d) plasmid + Vsp 1

an ice bath. All this procedure was carried out under minimal light conditions to minimise psoralen degradation. The DNA / biotinylated psoralen samples were place 10 ± 1 cm from a 100 W UVC light source (USH-102DH) (Nikon, UK.) and left for 1.5 h for irreversible intercalation of the psoralen to the DNA to occur. After this period, 2 volumes of ice cold ethanol and 0.2 M potassium acetate were added to precipitate the DNA. The samples were spun at 10,000 rpm for 15 min and excess liquid removed. DNA was resuspended in 5 ml of TE.

To check the reaction had worked, SPR experiments were performed. N-([3-biotinamido]hexyl)-3'-[2'pyridyldithiol]propamide (biotin-HPDP) SAMs were prepared on SPR slides by overnight incubation of SPR slides in a 1 mM solution of biotin-HPDP in dry trifluoroethanol (TFE) under desiccated conditions. Prior to use slides were washed with dry TFE and dried under a nitrogen stream. After obtaining a stable baseline with buffer flow of HEPES pH 7.4, 10 mM, 1 ml of streptavidin (5×10^{-7} M in HEPES) was injected. After a buffer wash 1 ml of DNA either biotinylated or non-biotinylated at a concentration of 5 μg / ml was injected at a speed of 100 μl / min to quantify the interaction with streptavidin. The experiment finished with a buffer wash to remove any loosely bound DNA.

After the optimal degree of biotinylation had been established, a concentration dependant study was performed to determine the minimal concentration of biotinylated DNA which would give maximal SPR shift. The same protocol as above was followed but DNA concentrations ranged from 1 - 10 μg / ml. Control experiments were also performed using this protocol to determine the extent of DNA and biotinylated-psoralen binding to the streptavidin.

5.2.3 : SPR

SPR experiments were performed to study the rate and extent of interaction between the DNA and cationic polymers. SAMs of biotin on SPR slides formed from biotin-HPDP as described above. These model surfaces were utilised to immobilise either the biotinylated DNA or polymer to investigate the interaction with the other. The buffer used in these experiments was 10 mM HEPES at pH 7.4.

After obtaining a stable baseline of buffer flow, 1 ml of streptavidin (5 x 10^{-7} M in HEPES) was injected followed by a buffer wash. The biotinylated DNA (5 μg / ml in HEPES) or biotinylated polycation at a 0.5 mg/ml concentration of PLL was then injected (1 ml). This corresponds to total polymer concentrations of 0.5, 0.625, 0.8 and 1.0 mg / ml for the PLL, PLL-PEG(5 kDa), PLL-PEG(12 kDa) and PLL-PEG(20 kDa) respectively. After another buffer wash, 1 ml of the other component in its non-biotinylated form was then injected to investigate at the extent of interaction. All experiments were terminated with a buffer wash. DNA and polycation injections and buffer washes were performed at 100 μl / min.

Control experiments were performed to determine the background levels of non-specific cationic polymer binding to streptavidin. These experiments again utilised biotin-HPDP coated SPR slides. 1 ml of streptavidin (5 x 10^{-7} M HEPES) was injected and followed by a buffer wash to remove loosely bound material. After the buffer wash was completed 1 ml of non-biotinylated cationic polymer at concentrations utilised above, was injected at 100 μl / min. Again a buffer wash followed.

5.2.4 : AFM imaging studies

Complexes of the DNA and polymers were formed in HEPES buffer 10 mM, pH 7.4. Initial studies were performed to investigate the effect of charge ratio on the structure of the complex formed. This study was carried out using PLL only. A 0.5 mg / ml solution of the PLL and 10 μg/ml solution of the DNA were made and an appropriate amount of DNA added to a known quantity of PLL to give charge ratios of 1.00 : 0.27, 1.00 : 1.35 or 1.00 : 2.70 DNA to PLL. After addition of the DNA, the solutions were mixed on a vortex mixer for 2 min to ensure an even distribution of PLL and DNA. 100 μl of the mixture was then placed on freshly prepared 3-aminopropyltriethoxyl silane (APTES) treated mica.

APTES mica was prepared by adding pieces of freshly cleaved mica (Agar scientific, UK) into a 5 cm diameter glass petri dish with 10 μl of APTES on the lid. The dish was then flushed with nitrogen sealed with Parafilm (American National Can, Chicago, USA) and left for 1 h.

The polymer / DNA complexes were allowed to incubate with the APTES mica for 10-15 min before imaging with a Digital Multimode AFM with Nanoscope IIIa controller (Digital Instrument, Santa Barbara, USA) in tapping mode under a HEPES pH 7.4 10 mM environment. The short thin cantilever on a Nanoprobe NP tip (Digital Instruments, Santa Barbara, CA USA) was utilised for imaging.

5.2.5 : AFM force-distance studies

Streptavidin coated silicon nitride AFM tips and silicon wafer surfaces were prepared as Section 4.2.6. All force distance work was carried out in

HEPES buffer 10 mM pH 7.4.

Prior to determining the interaction between DNA and the PLL-PEGs, several controls were performed. The streptavidin coating of the tips was confirmed by performing force-distance curves on streptavidin coated surfaces. Only tips which showed no adhesion were used. This suggesting that both the tip and surface have the same surface properties ie. Are both coated in streptavidin, so no interaction is observed (Allen (1997)). After confirming that no adhesion was seen on four similarly coated streptavidin surfaces three were incubated in biotinylated cationic polymer solution of either PLL, PLL-PEG(5 k) or PLL-PEG(12 kDa) for 30 min. The polymer solutions were present at a concentration of 0.5 mg /ml PLL, ie. total polymer concentrations of 0.50, 0.63, 0.80 for the PLL, PLL-PEG(5 kDa) or PLL-PEG(12 kDa) polymers respectively. After this period the tips were washed in buffer and the background levels of interaction between the streptavidin coated tip and cationic polymer coated surfaces were measured. The fourth streptavidin surface was used as a control to check the tip was still coated in streptavidin.

After background levels of interaction had been determined for the streptavidin coated tip and the polymer surfaces, the streptavidin coated tip was incubated in a 5 μg / ml solution of biotinylated DNA in HEPES (10 mM pH 7.4) without removal from the AFM to ensure contact area remained the same. After 30 min the tip was washed in excess buffer and force-distance curves measured on each of the polymer surfaces and the control streptavidin surface. A minimum of 60 force distance curves were performed at each stage of the experiment.

5.3 : Results and Discussion

The following section will discuss the results obtained from the experiments described in section 5.2. Initial discussion will centre on SPR investigations into the effect of PEG molecular weight on the process of DNA binding to the PEGylated cationic polymers. After discussing the formation of the complexes as probed by SPR, the second part of the discussion will concentrate on the structure of the DNA / cationic polymer complexes and the effect of PEG on this. The structure of the DNA / polycation particulates is important as this will effect their efficiency in delivery to cells. Finally, results of AFM force-distance investigations which probed the strength of interaction between the DNA and the cationic polymers are discussed in terms of molecular flexibility and PEG molecular weight.

5.3.1 : SPR analysis of the interaction between DNA and immobilised PLL-PEGs

Figure 5.4 shows the results obtained from experiments to determine the background levels of interaction between the non-biotinylated cationic polymers and streptavidin. Figure 5.4 (a) shows a typical SPR trace for the interaction of non-biotinylated PLL with streptavidin immobilised on a biotin-HPDP surface. It can be observed that a small change in SPR angle is observed. The extent of the change is also seen to reduce to approximately half its maximal level during the buffer wash This is indicative of a low level of interaction between the PLL and streptavidin surface. Figure 5.4 (b) shows a summary of the results for all the PLL-PEG block copolymers and in all cases the interaction is minimal. It can therefore be assumed that the majority of the interaction observed between the biotinylated PLL and PLL-PEGs and the streptavidin coated surface is due to specific biotin-streptavidin interactions

(a)

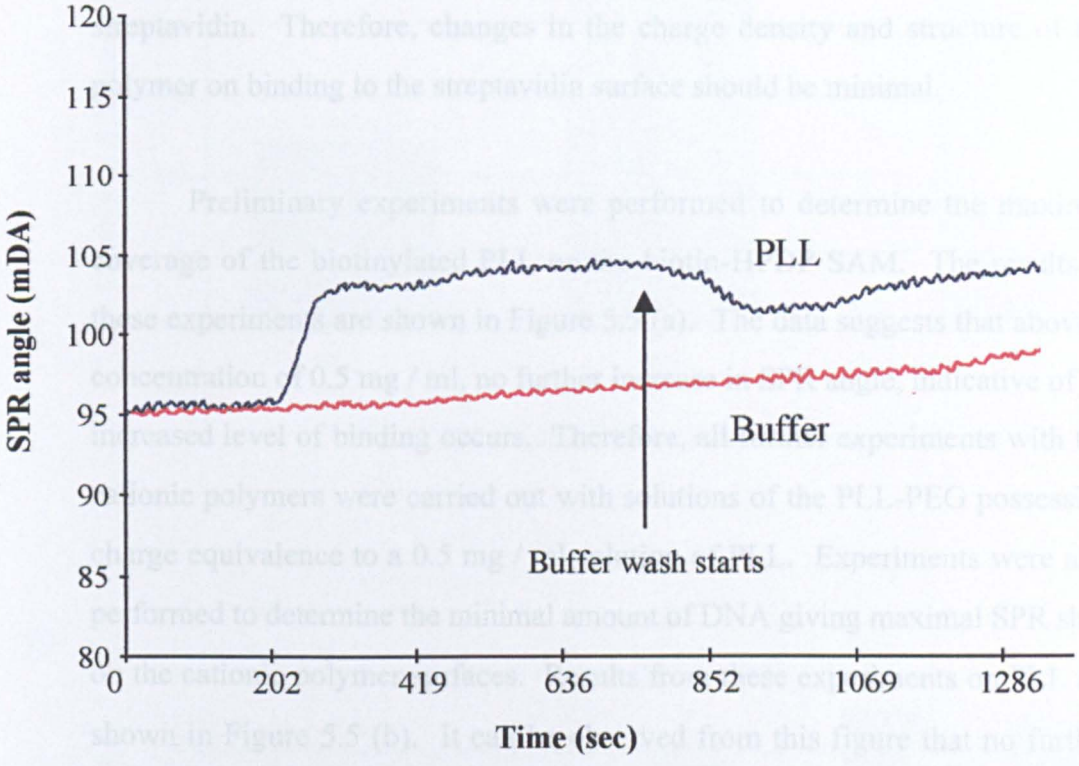

(b)

polymer	Change in SPR angle
PLL	11 ± 4
PLL-PEG(5 kDa)	9 ± 2
PLL-PEG(12 kDa)	9 ± 5
PLL-PEG(20 kDa)	5 ± 3

Figure 5.4 : Non specific interactions of non-biotinylated cationic polymers with streptavidin

(a) Typical SPR trace for interaction between PLL and streptavidin

(b) Summary of interactions of PLL-PEGs

values = average ± 1 standard deviation (n ≥ 22)

rather than interactions between the charged polymer itself and the streptavidin. Therefore, changes in the charge density and structure of the polymer on binding to the streptavidin surface should be minimal.

Preliminary experiments were performed to determine the maximal coverage of the biotinylated PLL on the biotin-HPDP SAM. The results of these experiments are shown in Figure 5.5 (a). The data suggests that above a concentration of 0.5 mg / ml, no further increase in SPR angle, indicative of an increased level of binding occurs. Therefore, all further experiments with the cationic polymers were carried out with solutions of the PLL-PEG possessing charge equivalence to a 0.5 mg / ml solution of PLL. Experiments were also performed to determine the minimal amount of DNA giving maximal SPR shift on the cationic polymer surfaces. Results from these experiments on PLL are shown in Figure 5.5 (b). It can be observed from this figure that no further increase in SPR angle was seen above a concentration of 5 μg / ml. This means that no further DNA bound to the surface above this concentration. Therefore, this concentration was used in all further experiments.

Figure 5.6 shows a typical SPR trace for the interaction of DNA with the immobilised biotinylated PLL polymer. From this trace the initial single phase binding processes of the streptavidin to the biotin-HPDP SAM can be observed, this is followed by the biotinylated PLL binding to the available binding pockets of the streptavidin. When examining at the interaction between the DNA and PLL a significantly different shaped SPR trace is produced. This shape of trace is unique, within the realms of this thesis, to this type of molecular interaction. Two distinct regions are observed in the DNA binding phase. A number of explanations may be evoked for such a response, but one possible theory is that after the initial binding of DNA to the cationic polymers, a subsequent reorganisation and condensation of the DNA

(a)

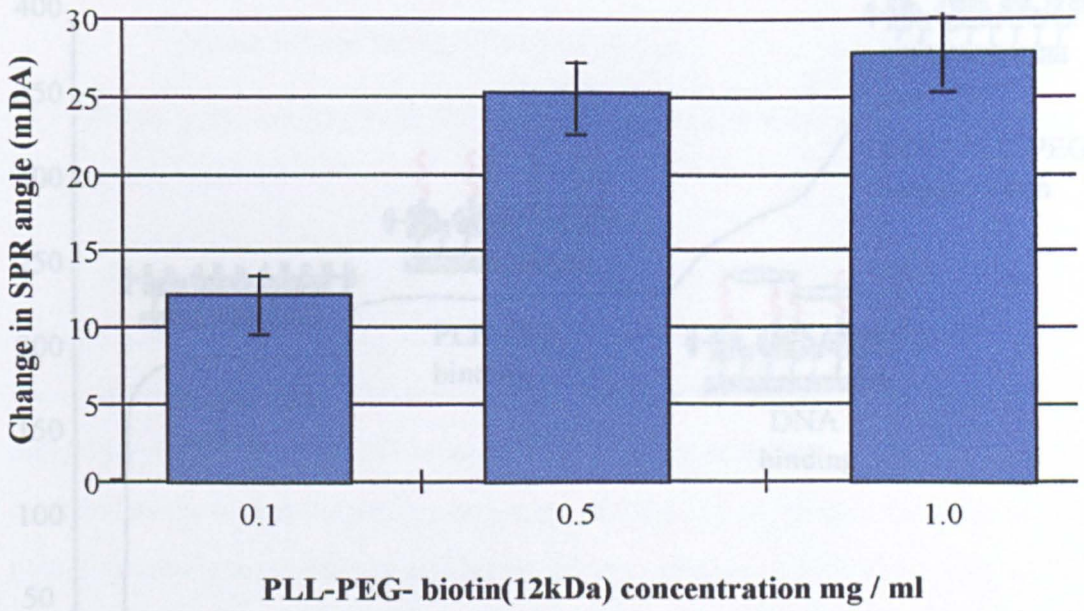

(b)

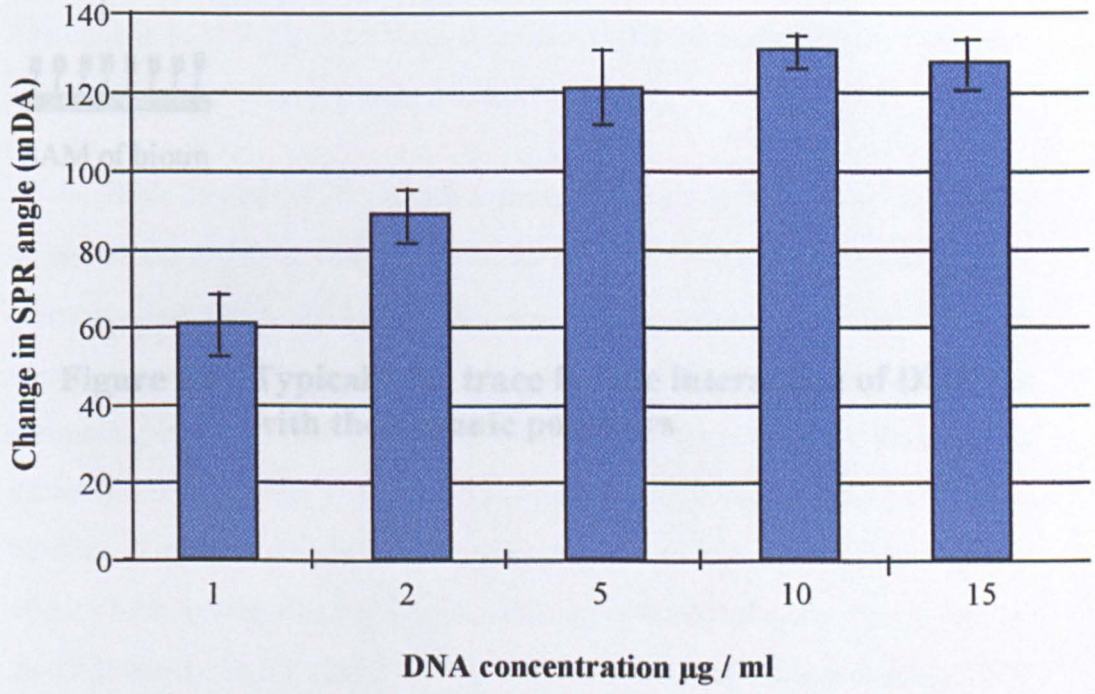

Figure 5.5 : Effect of concentration on level of binding

(a) biotinylated PLL binding to streptavidin

(b) DNA binding to PLL

bars = average ± 1 standard deviation (n ≥ 13)

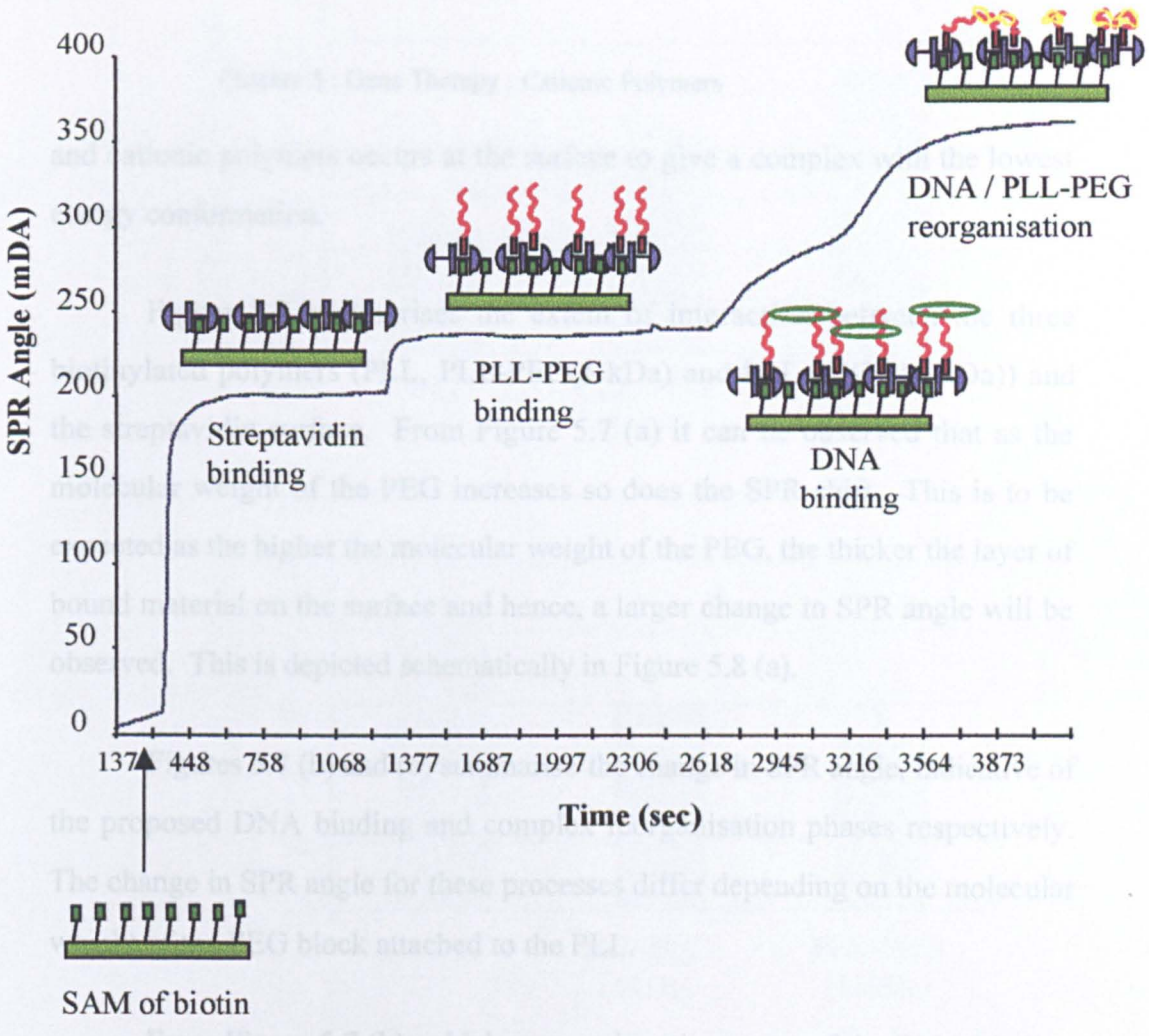

Figure 5.6 : Typical SPR trace for the interaction of DNA with the cationic polymers

and cationic polymers occurs at the surface to give a complex with the lowest energy conformation.

Figure 5.7 summarises the extent of interaction between the three biotinylated polymers (PLL, PLL-PEG(5 kDa) and PLL-PEG (12 kDa)) and the streptavidin surface. From Figure 5.7 (a) it can be observed that as the molecular weight of the PEG increases so does the SPR shift. This is to be expected as the higher the molecular weight of the PEG, the thicker the layer of bound material on the surface and hence, a larger change in SPR angle will be observed. This is depicted schematically in Figure 5.8 (a).

Figures 5.7 (b) and (c) summarise the change in SPR angle, indicative of the proposed DNA binding and complex reorganisation phases respectively. The change in SPR angle for these processes differ depending on the molecular weight of the PEG block attached to the PLL.

From Figure 5.7 (b), which summarises the extent of the DNA binding phase of the trace, it can be observed that as the PEG molecular weight increases, less DNA binds. The difference in the extent of binding is within standard error when comparing the PLL and PEG-PLL(5 kDa). However when comparing PLL and PLL-PEG(12 kDa) the errors do not overlap so it can be stated that the presence of 12 kDa PEG causes a significant reduction in DNA binding. This reduction in DNA binding can be attributed to the steric barrier effect of the hydrophilic PEG layer. This layer shields the charged groups on the PLL backbone and also promotes steric repulsion of the approaching DNA chains. The reduction in DNA binding, caused by an increase in the PEG steric layer thickness, is shown schematically in Figure 5.8 (b).

For the condensation and reorganisation phase of the DNA / cationic polymer SPR curve (Figure 5.7 (c)), a smaller change in SPR angle was

(a)

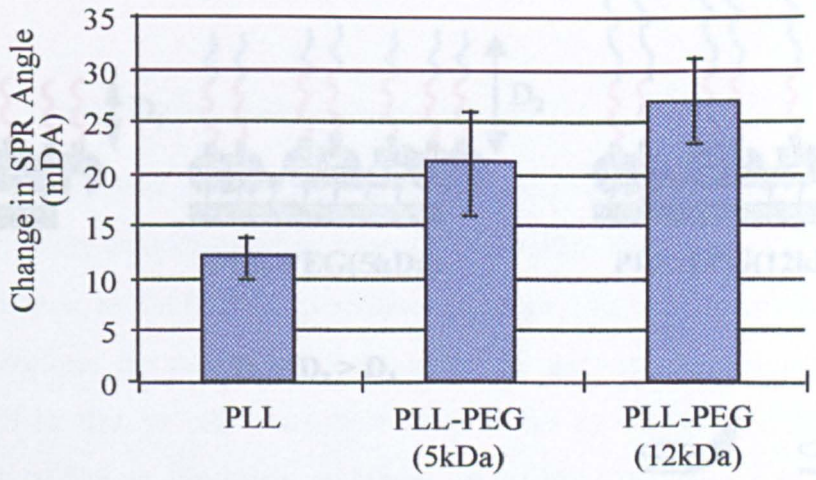

(b)

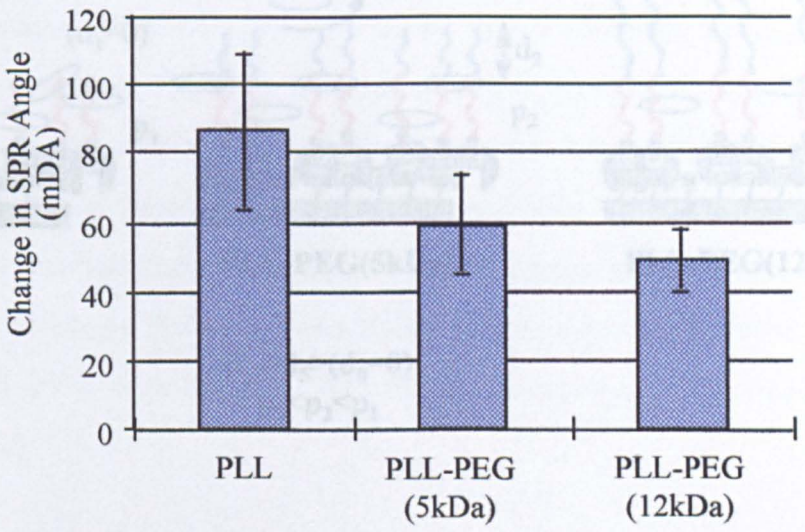

(c)

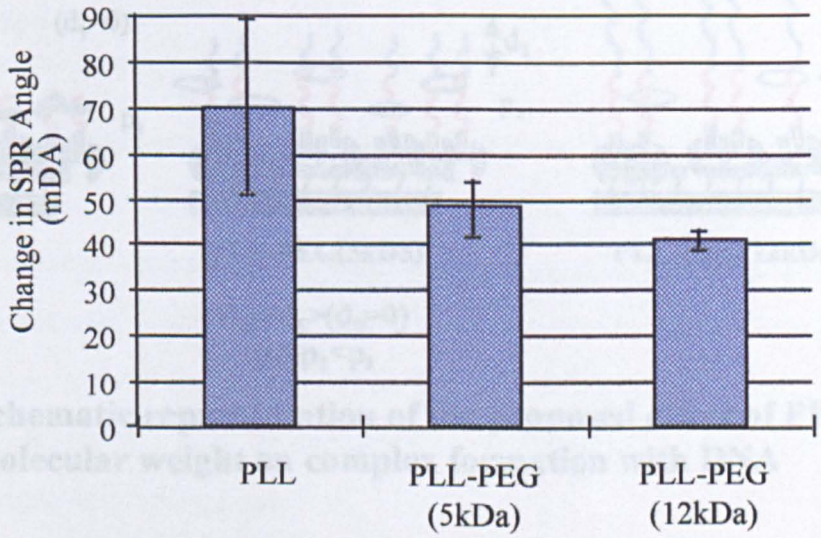

Figure 5.7 : Summary of SPR shifts for :

(a) biotinylated cationic polymer binding to streptavidin

(b) Binding of DNA to cationic polymer

(c) DNA cationic polymer structure reorganisation

bars = average ± 1 standard deviation ($n \geq 14$)

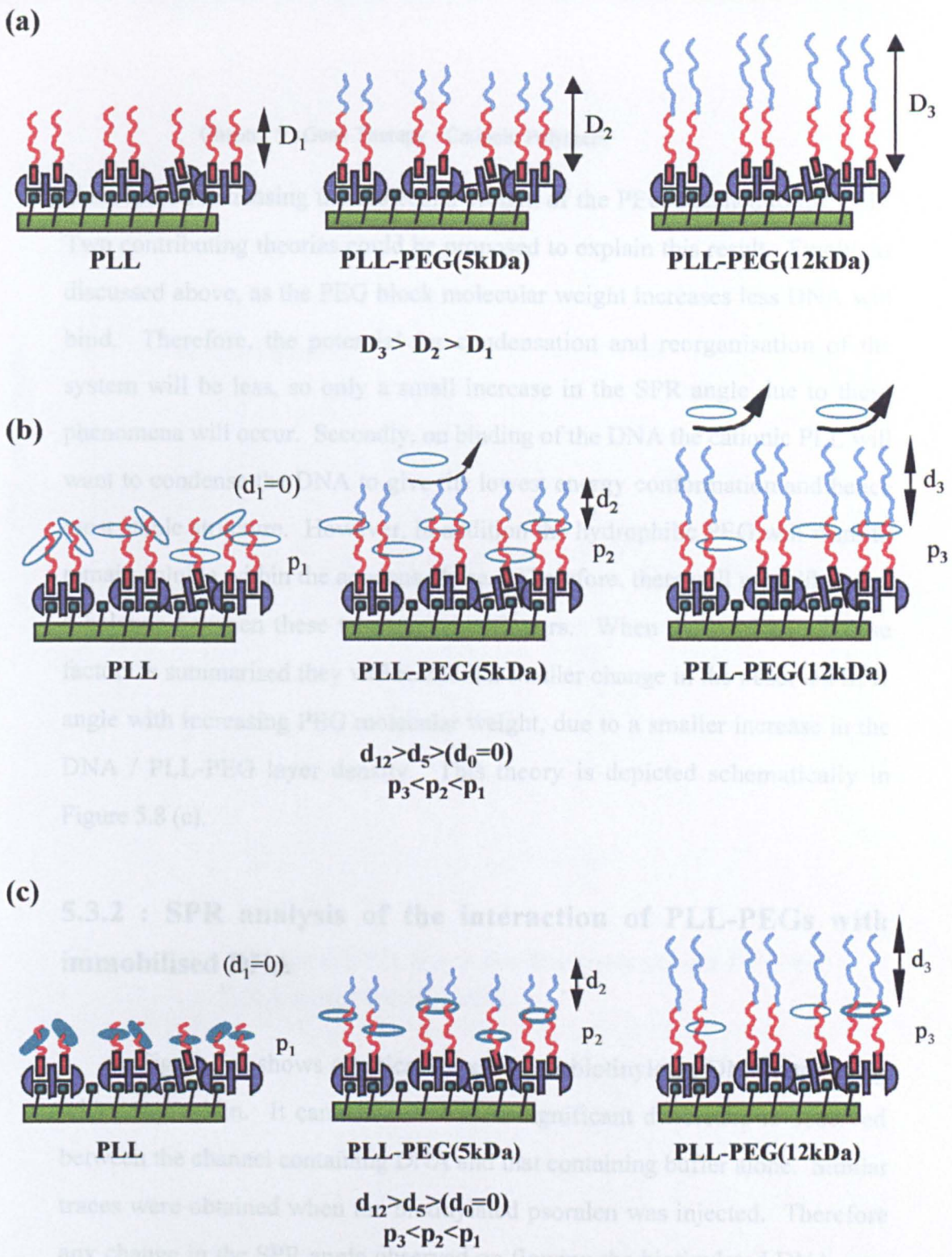

Figure 5.8 : Schematic representation of the proposed effect of PEG molecular weight on complex formation with DNA

d = thickness **p = density of DNA**

(a) Effect of PEG molecular weight on the thickness of the adsorbed polymer layer
(b) The higher the PEG molecular weight, the less DNA binds
(c) The less DNA bound and higher the PEG molecular weight, the less complexation and hence increase in SPR angle occurs

observed on increasing the molecular weight of the PEG attached to the PLL. Two contributing theories could be proposed to explain this result. Firstly, as discussed above, as the PEG block molecular weight increases less DNA will bind. Therefore, the potential for condensation and reorganisation of the system will be less, so only a small increase in the SPR angle due to these phenomena will occur. Secondly, on binding of the DNA the cationic PLL will want to condense the DNA to give the lowest energy conformation and hence most stable structure. However, in addition the hydrophilic PEG will want to remain soluble within the aqueous phase. Therefore, there will most likely be a balance between these two opposing factors. When the product of these factors is summarised they will result in a smaller change in the observed SPR angle with increasing PEG molecular weight, due to a smaller increase in the DNA / PLL-PEG layer density. This theory is depicted schematically in Figure 5.8 (c).

5.3.2 : SPR analysis of the interaction of PLL-PEGs with immobilised DNA

Figure 5.9 shows a typical trace of non-biotinylated DNA interacting with streptavidin. It can be seen that no significant difference is observed between the channel containing DNA and that containing buffer alone. Similar traces were obtained when the biotinylated psoralen was injected. Therefore any change in the SPR angle observed on flowing the biotinylated DNA over the streptavidin surface must be due to the biotinylated DNA binding to the available streptavidin binding sites.

Results for the control experiments to determine the extent of biotinylation required to give a maximal SPR shift are shown in Figure 5.10. It can be observed that no change in the SPR angle is observed up to a ratio of 40

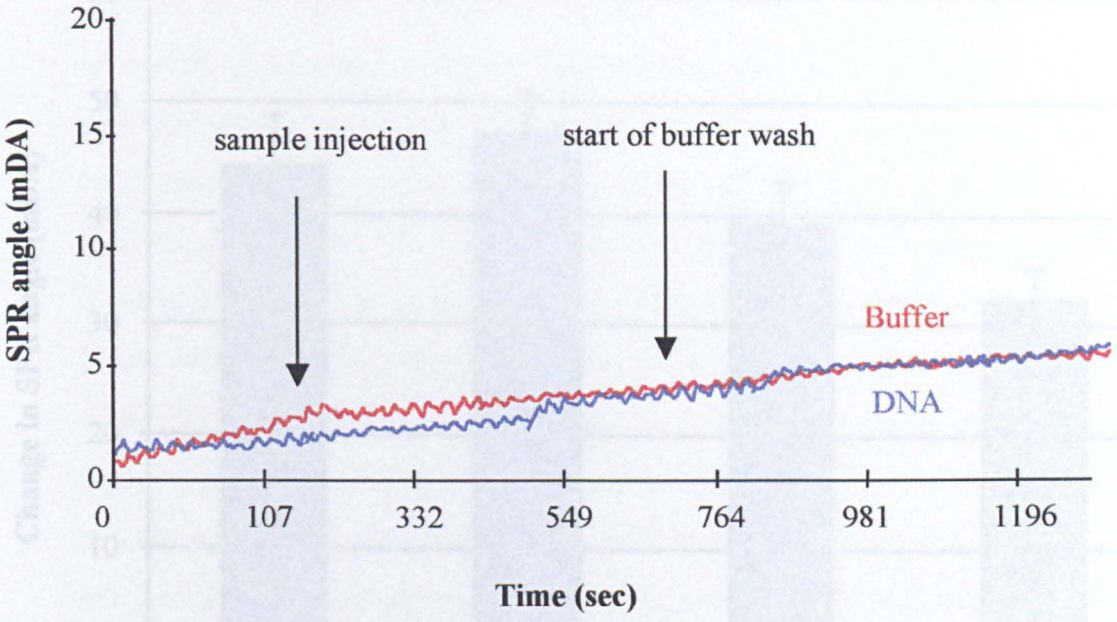

Figure 5.9 : A typical SPR trace for the interaction between DNA and streptavidin

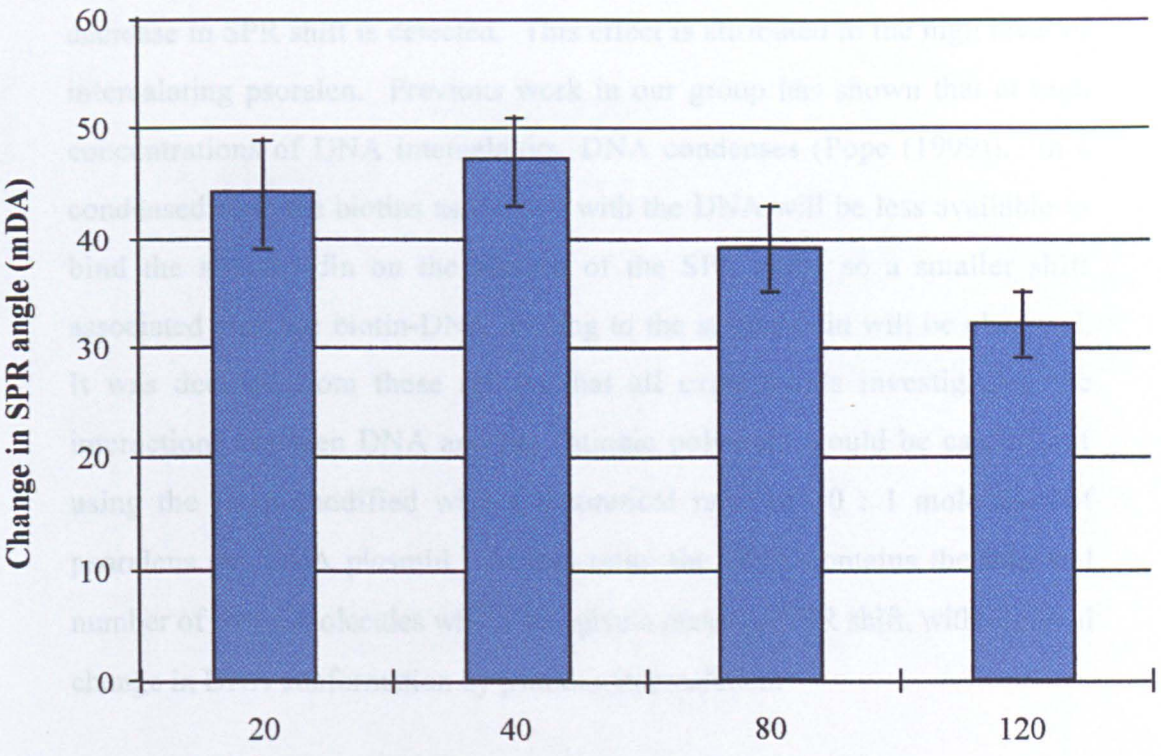

Figure 5.10 : Effect of degree of biotinylation on binding of biotin-DNA to streptavidin

This figure shows that above a theoretical loading of 40 biotins per plasmid, the maximal binding of the DNA-biotin to a streptavidin surface is reduced. This may be due to changes in the DNA conformational flexibility.

bars = average ± 1 standard deviation ($n \geq 12$)

: 1 theoretical loading of biotinylated psoralen per plasmid. Above this value a decrease in SPR shift is detected. This effect is attributed to the high level of intercalating psoralen. Previous work in our group has shown that at high concentrations of DNA intercalators, DNA condenses (Pope (1999)). In a condensed state the biotins associated with the DNA will be less available to bind the streptavidin on the surface of the SPR slide, so a smaller shift associated with the biotin-DNA binding to the streptavidin will be observed. It was decided from these results that all experiments investigating the interactions between DNA and the cationic polymers would be carried out using the DNA modified with a theoretical ratio of 20 : 1 molecules of psoralens per DNA plasmid. At this ratio, the DNA contains the minimal number of biotin molecules which will give a maximal SPR shift, with minimal change in DNA conformation by psoralen intercalation.

Experiments were repeated to check if biotinylation had any effect on the minimal concentration of DNA needed to give maximal SPR shift. The results from these experiments showed that in a similar manner to the non-biotinylated DNA, no additional increase in SPR angle is observed on binding to the polycations at DNA concentrations above 5 μg / ml. Therefore this concentration of DNA was used for all experiments investigating the DNA's interaction with the cationic polymers.

Figure 5.11 shows a typical SPR trace for the interaction of PLL with immobilised DNA. Again, we observe the one phase binding of the streptavidin to the biotin-HPDP SAM and biotinylated DNA to the free binding pockets of the streptavidin. However, in this case the interaction between the DNA and PLL also is monophasic. A possible explanation is that due to the presence of the psoralen on the plasmid DNA, and the fact the DNA is bound to the surface, the DNA may be conformationally restrained

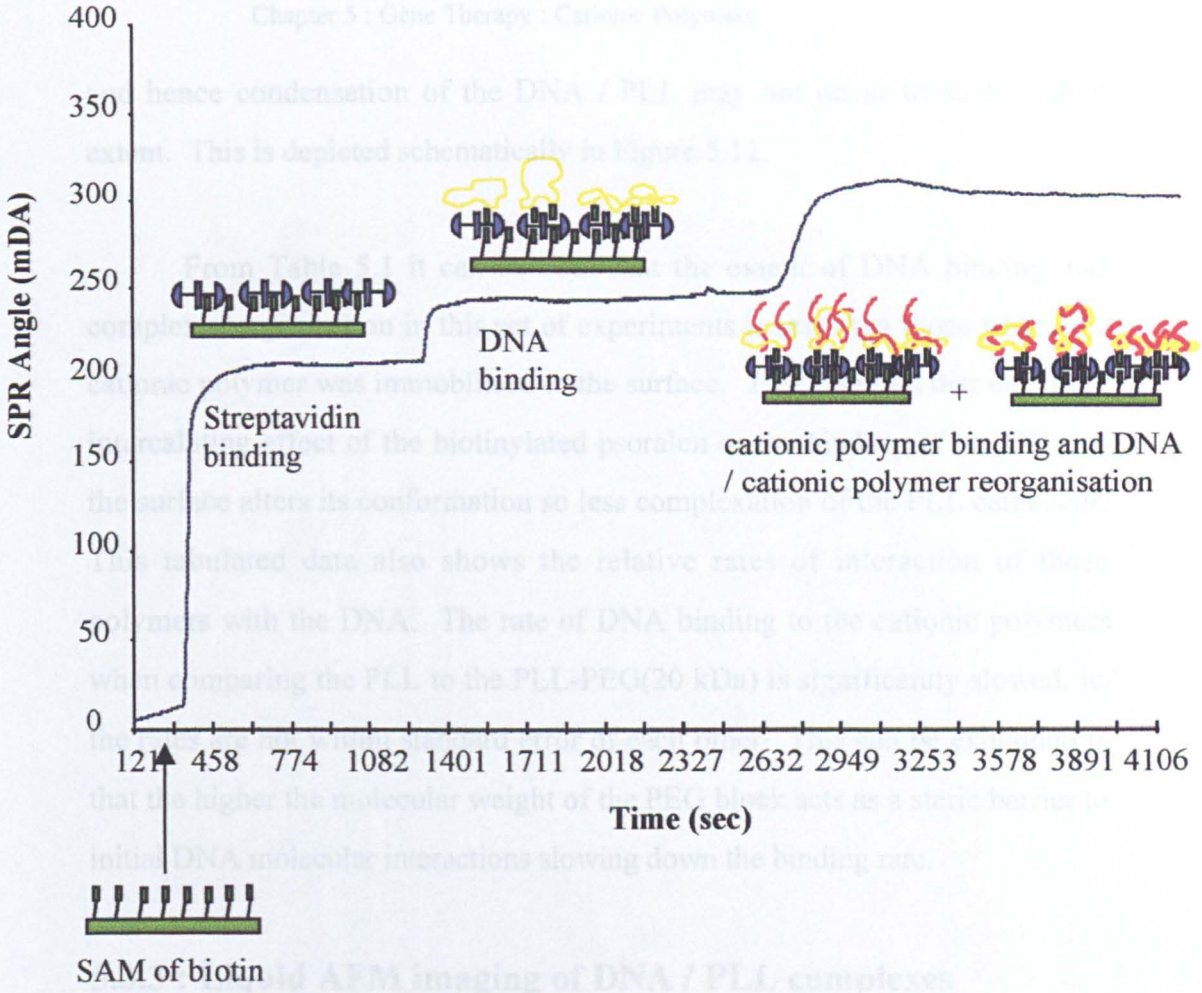

Figure 5.11 : A typical SPR trace for the interaction of cationic polymers with immobilised DNA

and hence condensation of the DNA / PLL may not occur to such a great extent. This is depicted schematically in Figure 5.12.

From Table 5.1 it can be seen that the extent of DNA binding and complex reorganisation in this set of experiments is less than those where the cationic polymer was immobilised to the surface. This suggests that either the intercalating effect of the biotinylated psoralen or the binding of the DNA to the surface alters its conformation so less complexation of the PLL can occur. This tabulated data also shows the relative rates of interaction of these polymers with the DNA. The rate of DNA binding to the cationic polymers when comparing the PLL to the PLL-PEG(20 kDa) is significantly slowed, ie. the rates are not within standard error of each other. This can be explained in that the higher the molecular weight of the PEG block acts as a steric barrier to initial DNA molecular interactions slowing down the binding rate.

5.3.3 : Liquid AFM imaging of DNA / PLL complexes

All AFM investigations were performed in liquid, so the structure of the DNA / cationic polymer complexes could be visualised under pseudo-physiological conditions. Preliminary experiments to determine the effect of charge ratio on the structure of the complex between DNA and the cationic polymers were carried out using PLL only. Figure 5.13 depicts three images of DNA / PLL complexes with ratios of 1.00 : 0.27, 1.00 : 1.35 and 1.00 : 2.70 in Figures 5.13 (a), (b) and (c) respectively. Figure 5.13 (a) shows a range of differing size globules between 15 - 142 nm at their widest diameter. The globules may be attributed to areas of DNA condensed by the cationic polymer. Many of these have string-like protrusions, marked with arrows in the image. These protrusions have diameters of 12.2 ± 2.3 nm which equates well with the diameter of free DNA, as observed in previous AFM studies

(a) DNA unlabelled

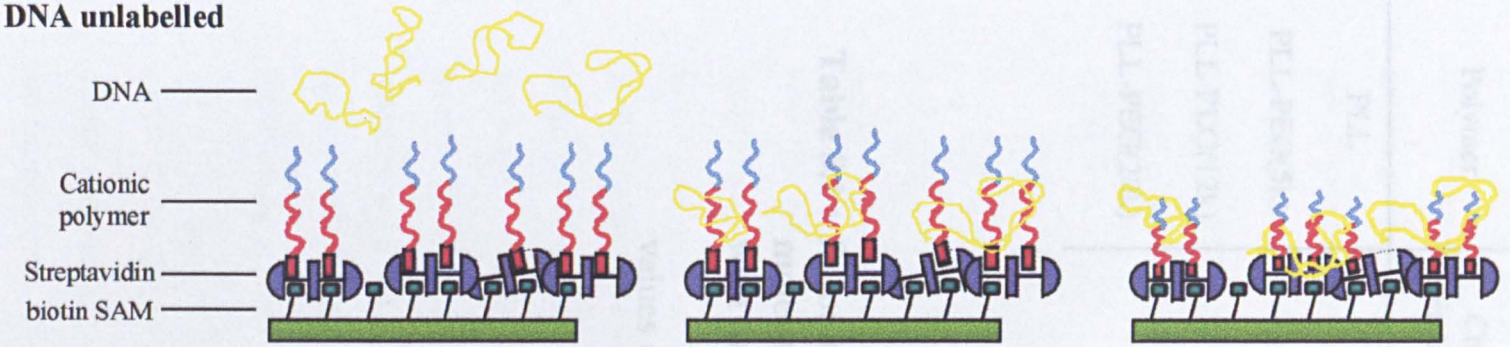

Unlabelled DNA is conformationally unperturbed, therefore it can bind to cationic polymers and condensation and reorganisation of The DNA / polymer construct can occur

(b) DNA biotin labelled

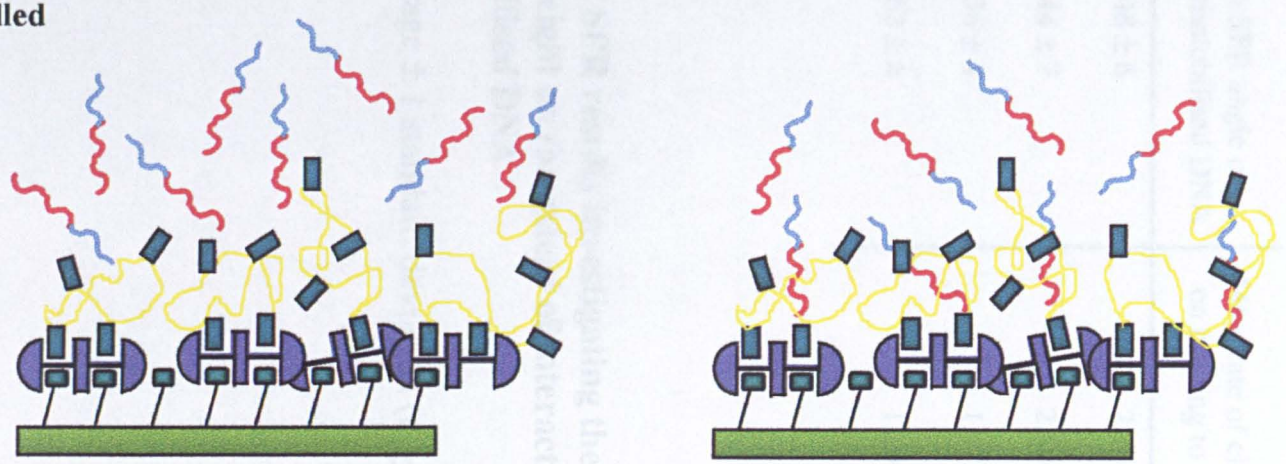

Biotin labelled DNA is conformationally restrained, therefore although the cationic polymers can ,condensation and reorganisation of the DNA / polymer construct can not occur

Figure 5.12 : Schematic representations of the effect of DNA labeling on PLL-PEG binding and DNA / cationic polymer reorganisation

(a) DNA unlabelled
(b) DNA biotin labelled

Polymer	Change in SPR angle on binding to immobilised DNA	Max. rate of change of SPR angle on binding to immobilised DNA
PLL	48 ± 6	2.760 ± 0.506
PLL-PEG(5k)	44 ± 7	2.406 ± 0.267
PLL-PEG(12k)	56 ± 4	1.972 ± 0.392
PLL-PEG(20k)	63 ± 6	1.509 ± 0.186

Table 5.1 : Summary of SPR results investigating the effect of PEG molecular weight on the extent of interaction of PLL-PEG with immobilised DNA

values = average ± 1 standard deviation ($n \geq 12$)

(Hansma (1996b)). Just below the centre of the image marked with a circle, a DNA string-like molecule can be observed with bead-like structures along its length. These features have diameters between 13 and 26 nm and are most likely comprised of PLL and condensed DNA. A higher resolution image of this is shown in Figure 5.13 (d). A possible explanation for this structure is that at low cationic polymer concentrations the DNA may condense primarily in small discrete areas along its length with the bead-like structures being comprised of areas of DNA condensed with PLL, similar to the 'bead-on-a-string' structure that has been observed in cationic lipid DNA complexes (Dan (1998)).

Figure 5.13 (b) shows the structure of particles formed from DNA and PLL at a ratio of 1.00 : 1.36. In this image, discrete regular shaped and sized entities of 79 -120 nm in diameter are observed (marked with circles). In addition, the underlying mica surface appears to have small pit like areas distributed over its surface. Similar pit-like features were also observed prior to the deposition of the DNA / cationic polymer complexes, and are attributed to the treatment of the mica with APTES. The surface of the DNA / cationic polymer entities have a rough appearance with globular like protrusions from the surface with diameters from 14 to 36 nm. This provides further evidence that the DNA / cationic polymer complex may form via a preliminary step where small areas of the plasmid condensing to give the 'beads-on-a-string' structure observed in Figure 5.13 (a) and (d) prior to collapsing to form the spherical particle observed in Figure 5.13 (b).

If the DNA : PLL ratio is increased to give a larger excess of positive charge, entities such as those in Figure 5.13 (c) are observed. These complexes are formed from a 1.00 : 2.70 ratio of DNA to PLL, and are comprised of a dense inner region (56 - 89 nm diameter) similar to the entities observed in

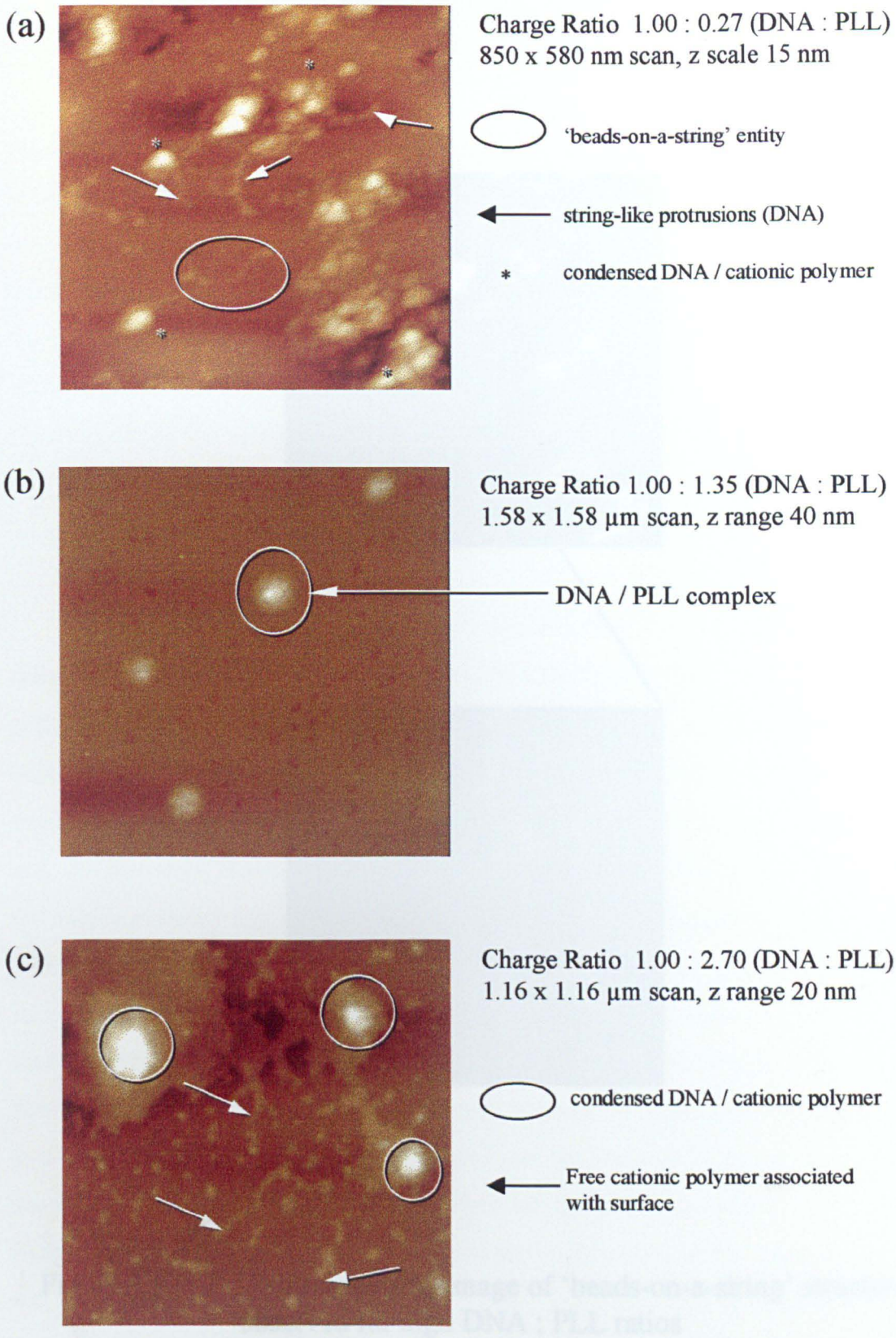

Figure 5.13 : Effect of charge ratio on the structure of the complex formed between DNA and PLL

(a) charge ratio 1.00 :0.27 DNA / PLL
(b) charge ratio 1.00 :1.35 DNA / PLL
(c) charge ratio 1.00 : 2.70 DNA / PLL

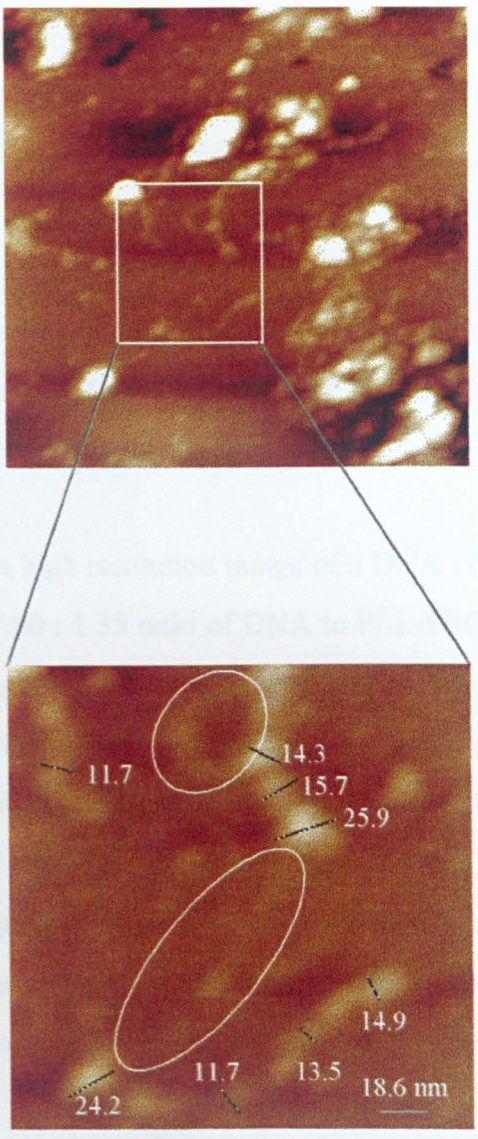

Figure 5.13 (d) : High resolution image of 'beads-on-a-string' structure observed for high DNA : PLL ratios

Diameter of bead part of structures are marked on image and areas attributed to free DNA are marked by rings.

186.2 x 186.2 nm image with 8 nm z-scale

Figure 5.13 (b). These features are surrounded by a corona of material, possibly extra PLL. These corona regions seem to follow no pattern in size or shape. Small randomly shaped regions are also observed distributed across the mica surface. In the simultaneously recorded phase image (data not shown) these regions possess the same phase shift as that for the material associated with the complexes corona. This similarity in phase shifts suggests that these regions possess the same material properties as the corona and hence these they are also thought to be comprised of PLL (Chen (1997), Siedlecki (1998)). Examples of these areas are marked with arrows in image 5.12 (c).

Figure 5.14 (a) is a high resolution image of a DNA \ cationic polymer complex formed from a 1.00 : 1.35 ratio of DNA to PLL-PEG(5 kDa) similar to those displayed in Figure 5.13 (b). Again the complex has a rough surface with irregular sized (14 - 38 nm) globular structures within the overall spherical structure. These globular structures have diameters ranging between 71 - 99 nm. As discussed above the observed substructure of these DNA / cationic polymer complexes suggests that the DNA may primarily complex in small areas along its length before collapsing in on itself to form the irregular, rough surfaced structure observed in Figure 5.13 (a). In comparison, Figure 5.14 (b) shows complexes formed with the PLL-PEG (20 kDa) at the same charge ratio. Similar sized particles are formed (diameters between 77 - 104 nm) but the surface topography is significantly changed and the contrast of the surface substructure is lost. A possible explanation for the loss of contrast at the surface of the complex is that the PEG is locating at the surface of the complex and forming a steric layer around the PLL / DNA core. Due to the hydrophilic nature of PEG, in an aqueous environment a lot of water will associate with the PEG chains making them very soft and hence difficult to image in a liquid environment, producing the poorly defined structures observed in Figure 5.14 (b). This theory and the effect of charge ratio on the observed DNA / PLL

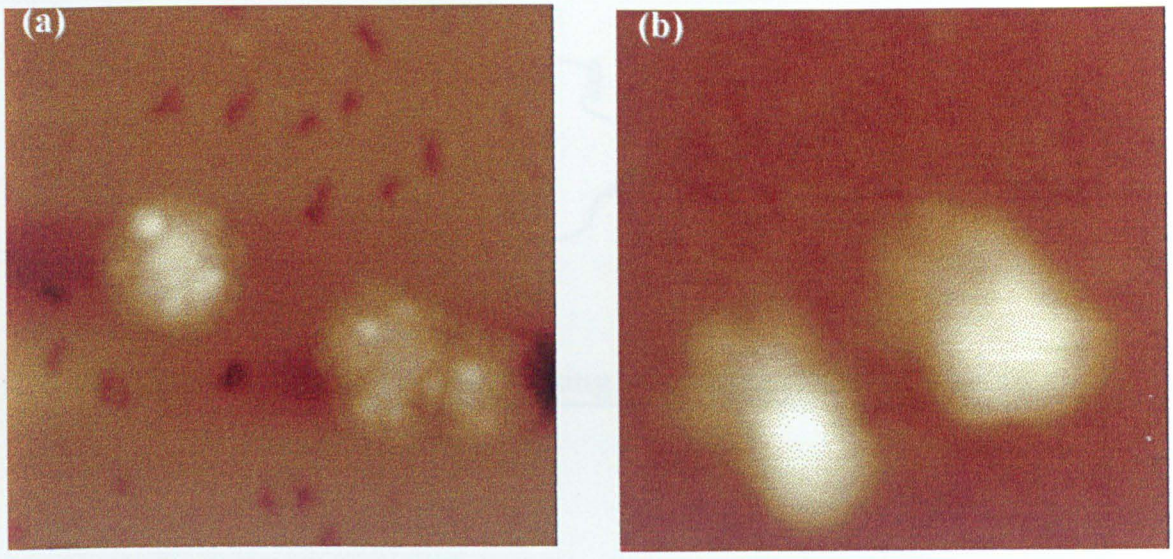

Charge Ratio 1 : 1.35
DNA:PLL-PEG(5kDa)
496 nm^2 scan, z range 30 nm

Charge ratio 1 : 1.35
DNA:PLL-PEG(20kDa)
533 nm^2 scan, z range 30 nm

Figure 5.14 : Effect of PEG molecular weight on DNA / PLL-PEG complex structure
(a) Complex formed from DNA and PLL-PEG(5 kDa)
(b) Complex formed from DNA and PLL-PEG(20 kDa)

When imaged under aqueous conditions the surface substructure of the DNA / cationic polymer complex disappears with increased PEG molecular weight. This suggests that the surface is soft and fluid in nature and therefore implies that the PEG is located at the surface.

(a)

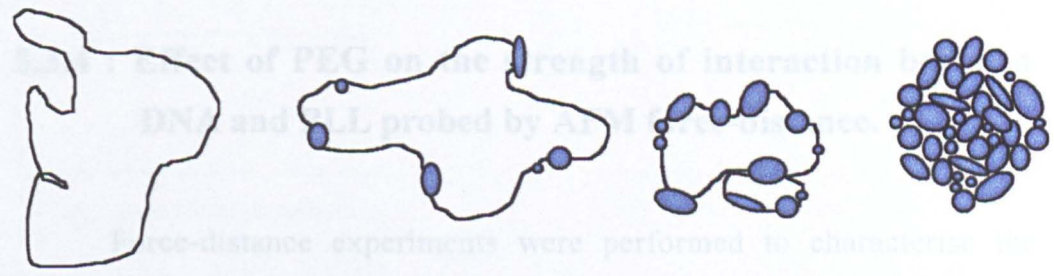

Free DNA → Increasing concentration of polycation

(b)

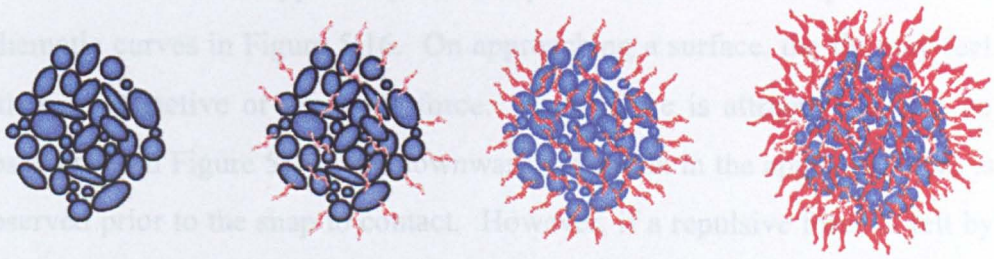

PLL → Increasing PEG molceular weight

Figure 5.15 : Complexation of DNA with the cationic polymerss and effect of PEG molecular weight

(a) Effect of DNA / polycation ratio

(b) Effect of PEG molecular weight

structure observed are depicted schematically in Figure 5.15.

5.3.4 : Effect of PEG on the strength of interaction between DNA and PLL probed by AFM force-distance.

Force-distance experiments were performed to characterise the interaction between DNA and the PLL and PLL-PEG block co-polymers. Evidence on the type of molecular processes occurring between two surfaces functionalised with the molecules of interest may be gleaned from analysing the shape of the obtained force-distance curves. Typical curves for each of the cationic polymers interacting with the streptavidin or the DNA coated tips are shown along with an idealised curves showing the phenomena of interest in Figures 5.17 and 5.16 respectively.

The five main types of probe sample interactions are depicted in the schematic curves in Figure 5.16. On approaching a surface, the tip may feel either an attractive or repulsive force. If the force is attractive as can be observed from Figure 5.16 (a) a downward deflection in the approach curve is observed prior to the snap to contact. However, if a repulsive force is felt by the tip before it snaps into contact with the surface, a curve such as that depicted in Figure 5.16 (b) is observed. This also shows that if the contact force is increased sufficiently then the tip can penetrate the layer contributing to the repulsive force.

Work by Tao and co-workers showed that the gradient of the contact area of the force-distance curve can be related to the rigidity modulus of the surface. They saw that the gradient of the contact area of the curve was greater for hard materials such as steel than that for softer ones such as rubber. Hence they were also able to use force distance measurements to distinguish the

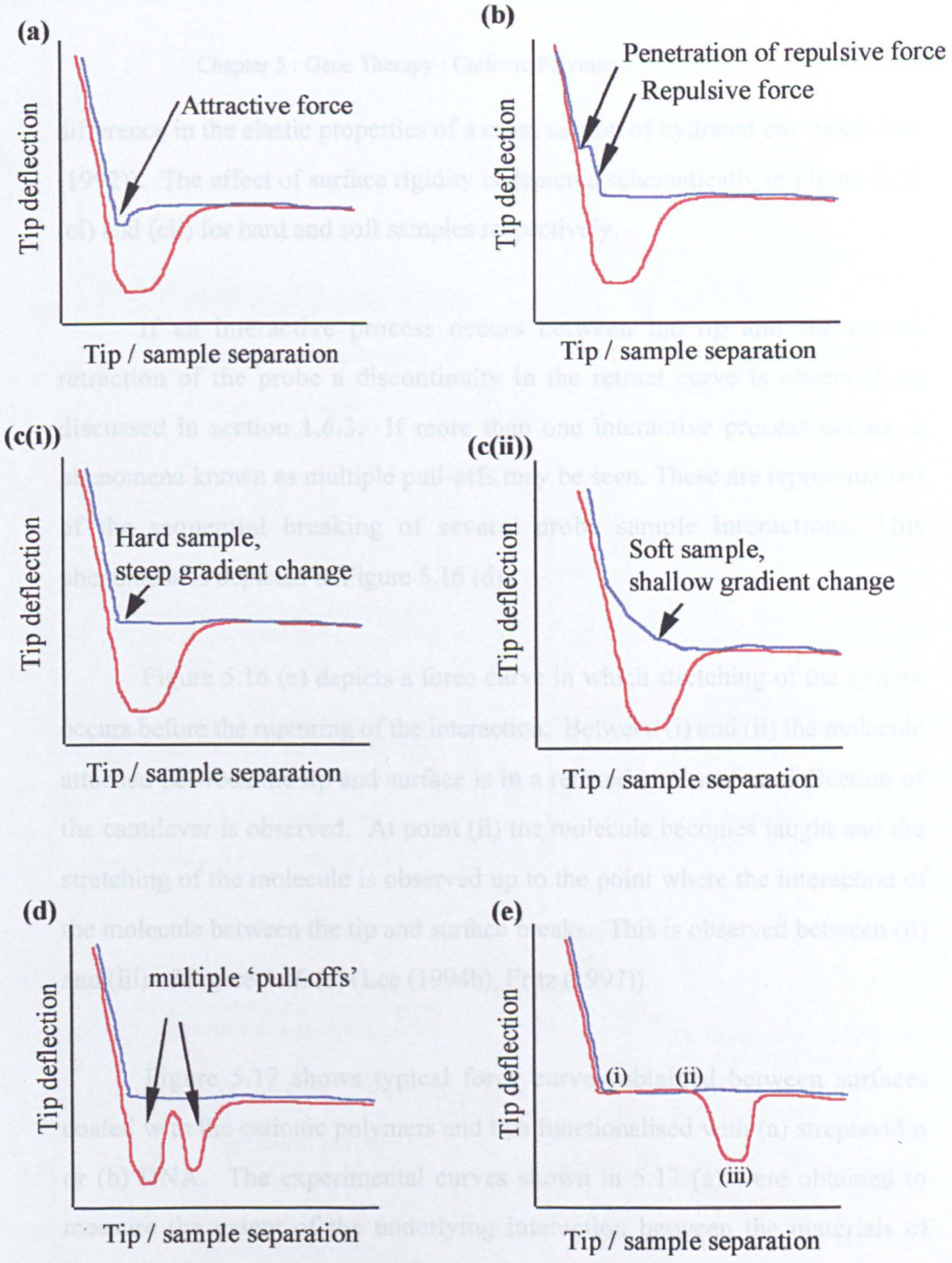

Figure 5.16 : Schematic representation of curve shapes due to varying phenomena

(a) Attractive force
(b) Repulsive forces
(c) Sample rigidity (c(i)) hard (c(ii)) soft
(d) Multiple interaction
(e) Molecular stretching

difference in the elastic properties of a cross section of hydrated cow tibia (Tao (1992)). The effect of surface rigidity is depicted schematically in Figure 5.16 (ci) and (cii) for hard and soft samples respectively.

If an interactive process occurs between the tip and surface on retraction of the probe a discontinuity in the retract curve is observed, as discussed in section 1.6.3. If more than one interactive process occurs, a phenomena known as multiple pull-offs may be seen. These are representative of the sequential breaking of several probe sample interactions. This phenomena is depicted in Figure 5.16 (d).

Figure 5.16 (e) depicts a force curve in which stretching of the system occurs before the rupturing of the interaction. Between (i) and (ii) the molecule attached between the tip and surface is in a relaxed state and no deflection of the cantilever is observed. At point (ii) the molecule becomes taught and the stretching of the molecule is observed up to the point where the interaction of the molecule between the tip and surface breaks. This is observed between (ii) and (iii) of Figure 5.16 (e) (Lee (1994b), Fritz (1997)).

Figure 5.17 shows typical force curves obtained between surfaces coated with the cationic polymers and tips functionalised with (a) streptavidin or (b) DNA. The experimental curves shown in 5.17 (a) were obtained to measure the extent of the underlying interaction between the materials of interest and the substrate to which they were immobilised. Figure 5.17 (a(i)), shows the interaction between the PLL surface and streptavidin coated tip. A simple force curve is observed with virtually no attractive force at the snap-to-contact (approach curve), and a maximum adhesion force of 0.200 ± 0.116 nN (retract curve). In this case the adhesion force is attributed to an interaction between the negatively charged streptavidin and positively charged PLL. The

(a) Interactions between cationic polymers and streptavidin

(a) Interactions between cationic polymers and DNA

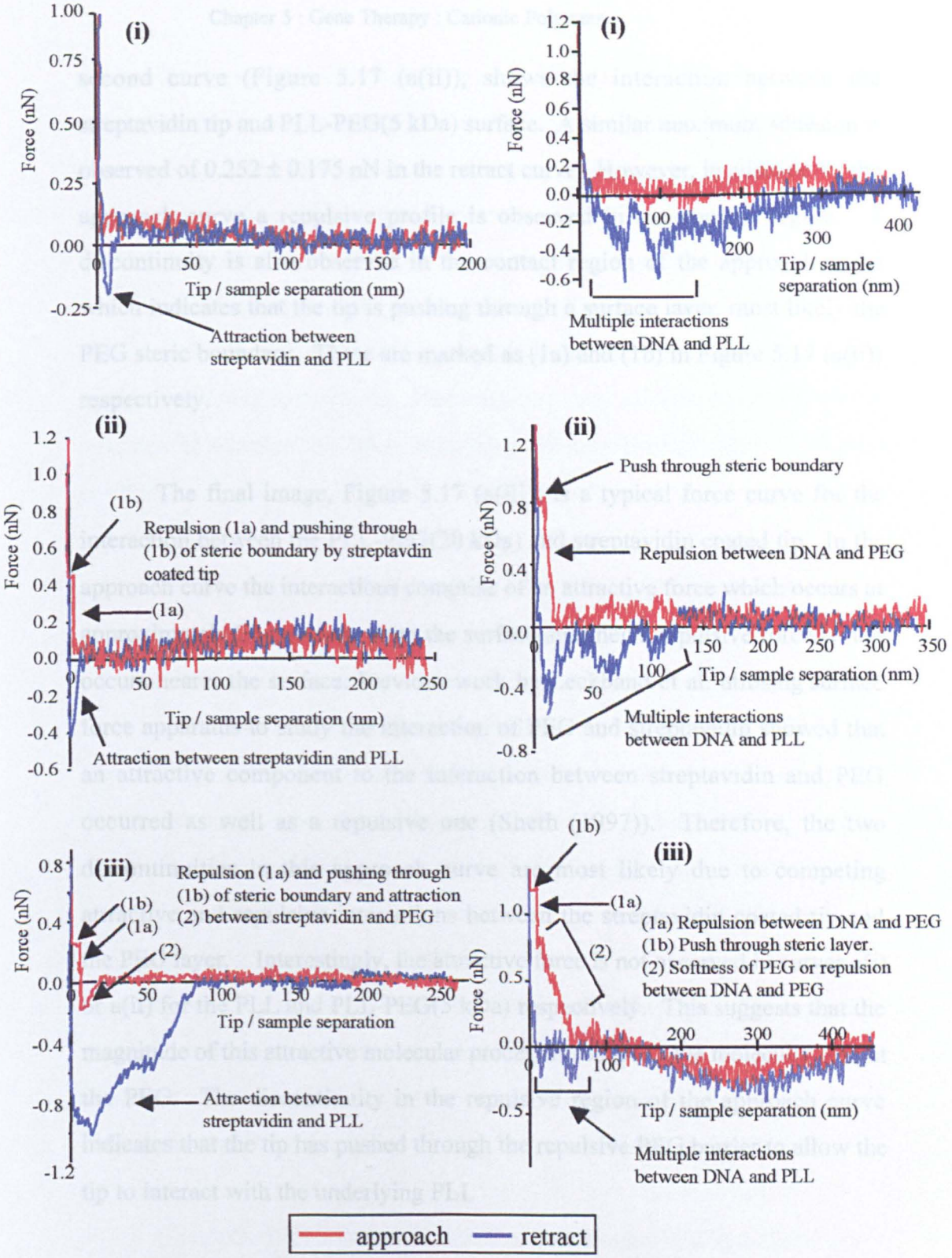

Figure 5.17 : Typical force distance curves for interactions between cationic polymers and (a) streptavidin and (b) DNA
(i) PLL
(ii) PLL-PEG(5 kDa)
(iii) PLL-PEG(12 kDa)

second curve (Figure 5.17 (a(ii)), shows the interaction between the streptavidin tip and PLL-PEG(5 kDa) surface. A similar maximum adhesion is observed of 0.252 ± 0.175 nN in the retract curve. However, in addition, in the approach curve a repulsive profile is observed in the contact region. A discontinuity is also observed in the contact region of the approach curve which indicates that the tip is pushing through a surface layer, most likely the PEG steric boundary. These are marked as (1a) and (1b) in Figure 5.17 (a(ii)) respectively.

The final image, Figure 5.17 (a(iii)) is a typical force curve for the interaction between the PLL-PEG(20 kDa) and streptavidin coated tip. In the approach curve the interactions comprise of an attractive force which occurs at approximately 20 nm away from the surface and then a repulsive force which occurs nearer the surface. Previous work by Leckband et al. utilising surface force apparatus to study the interaction of PEG and streptavidin showed that an attractive component to the interaction between streptavidin and PEG occurred as well as a repulsive one (Sheth (1997)). Therefore, the two discontinuities in this approach curve are most likely due to competing attractive and repulsive interactions between the streptavidin coated tip and the PEG layer. Interestingly, the attractive force is not observed in curves a(i) or a(ii) for the PLL and PLL-PEG(5 kDa) respectively. This suggests that the magnitude of this attractive molecular process is related to the molecular weight the PEG. The discontinuity in the repulsive region of the approach curve indicates that the tip has pushed through the repulsive PEG barrier to allow the tip to interact with the underlying PLL

Figure 5.17 (b) shows the interactions of the DNA coated tip with the cationic polymers. Figure 5.17 (b(i)) is a typical experimental curve for the interaction between DNA and PLL. Two significant differences can be

observed between this curve and Figure 5.17 (a(I)), the curve showing the interaction between the streptavidin and PLL. Firstly, the maximal adhesion force between the DNA and PLL is significantly larger (0.777 ± 0.138 nN) when compared to that of the streptavidin and PLL (0.200 ± 0.116 nN). Secondly, the final pull-off occurs much further away from the surface than that observed in Figure 5.17 (a(i)) for the PLL-streptavidin interaction and multiple adhesive pull-offs are observed. The extended and multiple 'pull-offs' may be attributed to molecular stretching and sequential rupturing of several interactions between the DNA and PLL molecules (Fritz (1997), Grandbois (1999)).

On the addition of PEG to the PLL an additional feature in the force-distance curve is observed, as can be seen from Figure 5.17 (b(ii)) which shows a force-distance curve typical of those observed between PLL-PEG(5 kDa) and DNA. In the retract trace multiple pull-offs and stretching associated with the interaction between the DNA and PLL are still present but a discontinuity in the repulsive region of the approach curve similar to that in 5.17 (a(ii)) is also observed. As with the curve typical of the interaction between the streptavidin and this cationic polymer, the discontinuity is most likely due to the tip pushing through the PEG steric boundary to the underlying PLL. Evidence that the interaction between the DNA and PLL is still occurring, despite the presence of PEG, comes from the fact that the retract curve, as discussed above, is illustrated by the presence of stretching and multiple pull-offs, in the retract curve as seen with the PLL and DNA curve (5.17 (b(i)).

Figure 5.17 (b(iii)) depicts a typical experimental force-distance curve for the interaction between DNA and PLL-PEG(12 kDa). This curve is similar to that for the PLL-PEG(5 kDa) in that it possesses a penetration discontinuity in the approach curve, attributed to the tip pushing through the

PEG steric boundary. The stretching and multiple pull-offs observed in the retract curve, indicative of an interaction between the DNA and PLL are still observed. However, an additional feature is observed in the curve for PLL-PEG(12 kDa) when compared to that of the PLL-PEG(5 kDa). This feature is denoted as (2) in Figure 5.19(b(iii)). This change in gradient in the approach curve could be explained by two factors. Firstly, the presence of a second repulsive force felt by the tip in close contact with the cationic polymer surface or secondly, it may be due to an increase in the surface compliance of the interacting materials. This increase in surface compliance could be associated with the increased molecular weight of the PEG.

Figure 5.18 (a) summarises the maximal adhesive forces observed for the control experiments. In these experiments, both immobilised biotinylated PLL-PEGs and DNA were brought into contact with streptavidin coated interfaces Figure 5.18 (b) depicts the effect of PEG molecular weight on the maximal adhesive force recorded between the biotinylated cationic polymers immobilised on a streptavidin surface, and DNA immobilised to the AFM tip by the same method.

From Figure 5.18 (a) it can be observed that the streptavidin coated tips show a minimal interaction with the PLL and PLL-PEG(5 kDa) samples. However, a much larger interaction of 0.986 ± 0.378 nN is observed with the PLL-PEG(12 kDa). This is unexpected as it would be assumed that as the PEG molecular weight increased the efficiency of the steric boundary would also increase and hence less interaction between the streptavidin coated tip and underlying PLL would be observed. However, as discussed above in relation to the shape of the force curves, the AFM tip appears to penetrate the PEG steric boundary. Therefore a possible explanation for these unexpected results could be the changing availability of the PLL charge on increasing the molecular

(a)

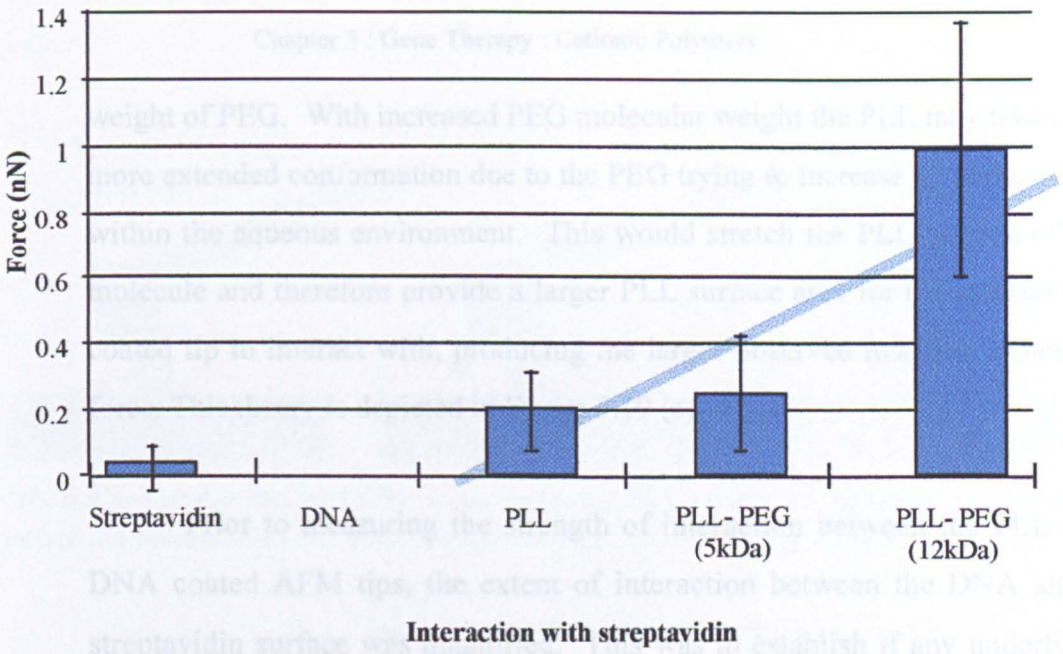

Interaction with streptavidin

(b)

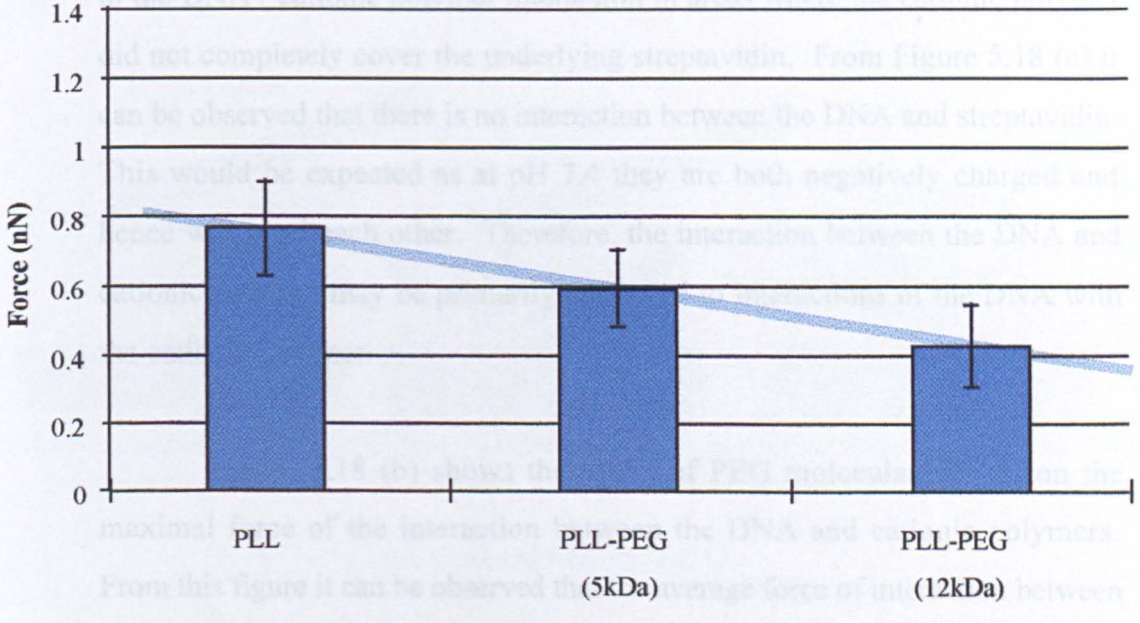

Interaction with DNA

Trendline showing effect of PEG MWt. on force-distance interactions

Figure 5.18 : Effect of PEG molecular weight on strength of interactions
(a) interactions between cationic polymers and streptavidin
(b) interactions between cationic polymers and DNA

weight of PEG. With increased PEG molecular weight the PLL may take on a more extended conformation due to the PEG trying to increase its surface area within the aqueous environment. This would stretch the PLL portion of the molecule and therefore provide a larger PLL surface area for the streptavidin coated tip to interact with, producing the larger observed maximal adhesion force. This theory is depicted in Figure 5.19 (a).

Prior to measuring the strength of interaction between the PLL and DNA coated AFM tips, the extent of interaction between the DNA and a streptavidin surface was quantified. This was to establish if any underlying interaction between the DNA and streptavidin existed, as this may contribute to the DNA / cationic polymer interaction in areas where the cationic polymer did not completely cover the underlying streptavidin. From Figure 5.18 (a) it can be observed that there is no interaction between the DNA and streptavidin. This would be expected as at pH 7.4 they are both negatively charged and hence will repel each other. Therefore, the interaction between the DNA and cationic polymer may be primarily attributed to interactions of the DNA with the cationic polymer.

Figure 5.18 (b) shows the effect of PEG molecular weight on the maximal force of the interaction between the DNA and cationic polymers. From this figure it can be observed that the average force of interaction between the DNA and PLL gradually decreases with increased molecular weight of PEG and a significant difference between the maximal forces of interaction for the PLL and PLL-PEG(12 kDa) and DNA results is observed. A probable explanation for the decrease in the maximal force between the DNA and cationic polymer is the conformation of the DNA. As the plasmid DNA is biotinylated in relatively few positions it will only be attached to the tip at minimal locations, therefore most of the plasmid will be located away from the

(a)

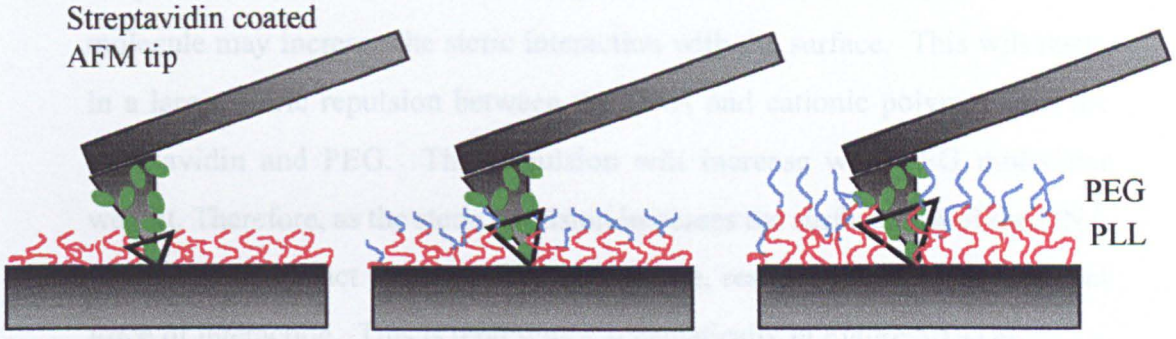

As the molecular weight of PEG increases, the PLL chains are extended, therefore a larger the contact area between the tip and PLL exists causing a larger adhesion force.

contact area between tip and PLL

(b)

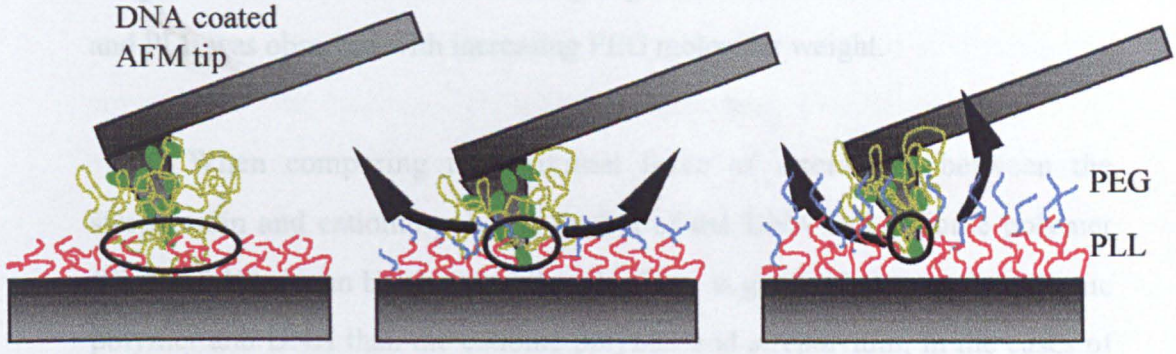

As the molecular weight of PEG increases the steric barrier becomes denser, this causes deformation of the soft DNA, so less is available to interact with the underlying PLL.

contact area between tip and PLL

steric repulsion between DNA and PEG

Figure 5.19 : Schematic diagram for a possible hypothesis explaining the effect of PEG molecular weight on the interaction
(a) with streptavidin
(b) with DNA

streptavidin coated tip. The resulting conformational flexibility of the DNA molecule may increase the steric interaction with the surface. This will result in a larger steric repulsion between the DNA and cationic polymer than the streptavidin and PEG. This repulsion will increase with PEG molecular weight. Therefore, as the steric repulsion increases the surface area of the DNA coated tip in contact with the PLL will reduce, resulting in a lower maximal force of interaction. This is represented schematically in Figure 5.19 (b).

It is interesting to note that results obtained from AFM force distance show the same trend as those observed from SPR experiments, which showed a smaller change in the SPR angle, in the region of the trace associated with DNA binding and DNA / PLL condensation with increasing PEG molecular weight. A similar trend of decreasing degree of interaction between the DNA and PLL was observed with increasing PEG molecular weight.

When comparing the maximal force of interaction between the streptavidin and cationic polymer to that of the DNA and cationic polymer (Figure 5.18), it can be observed that the force is greater between the cationic polymer and DNA than the cationic polymer and streptavidin, in the cases of PLL and PLL-PEG(5 kDa). One possible explanation for this can be attributed to differences in the charge density and conformational flexibility of the DNA and streptavidin. The DNA molecule possesses one charge per base whereas there are only 28 negatively charged amino acids on the surface of a streptavidin molecule which has a molecular weight of ~ 67,000 Da and size 5 x 5 nm, so the charge density will be far less (Bernstein (1977)). For this reason it is likely that the force of attraction between the DNA and cationic polymer will be far greater than that between the streptavidin and cationic polymer. In addition, the DNA is more conformationally flexible than the streptavidin allowing easier redistribution of its charge to interact with the cationic polymer.

Both these factors will contribute to the larger adhesion force observed in these cases.

The force of interaction between the PLL-PEG(12 kDa) and streptavidin however is not significantly different to that for the interaction between the PLL-PEG(12 kDa) and DNA. This could be attributed to the dense steric layer of PEG and the streptavidin and DNA structure when attached to the tip as discussed above. The streptavidin is firmly, covalently attached to the tip whereas the DNA is only attached to the tip at a few specific points, therefore the majority of the plasmid will be free to move. As such the plasmid may act in a similar fashion to the flexible PEG molecules, ie. as a steric boundary. Therefore, when brought into close proximity to the PEG, a larger steric repulsion will be felt between the DNA and PLL than the streptavidin and PLL. This suggests that the surface area of streptavidin in contact with the PLL will be significantly higher than that of the DNA, providing a larger area for an interaction to occur. The observed results imply that the sum of the large number of streptavidin / PLL interactions, which will be relatively weak due to the streptavidin molecules low negative surface charge are of similar strength to the few, but stronger interactions between the highly negatively charged DNA and PLL.

5.3.5 : SPR : Effect of cationic polymer density on DNA binding

The effect of the charge density of the PLL on the binding of DNA was investigated using SPR. The PLA-PEG-biotin polymers used in Chapters 3 and 4 were utilised to provide surfaces of varying densities of surface bound streptavidin and hence free biotin binding sites for the potential immobilisation of the biotinylated-PLL. The results from experiments probing the effect of

streptavidin density on the extent of biotin-PLL binding and the interaction of this with DNA are shown in Figure 5.20. These results show that the density of streptavidin effects the extent of binding of the biotinylated cationic polymer. For example, on the PLA-PEG-biotin(3.45) surface, a change of 11 ± 8 mDA is observed on biotinylated-PLL binding whereas on increasing the surface density of streptavidin by utilising PLA-PEG-biotin(0.53) an increase in the SPR shift indicative of biotin-PLL binding to 39 ± 9 mDA is observed. This suggests that increasing the density of streptavidin and hence free biotin binding sites on the surface allows more biotinylated-PLL to bind. On the addition of DNA to the SPR it can be observed from Figure 5.20 that the larger the change in SPR angle for the binding of biotin-PLL to the streptavidin surface, the higher the change in SPR angle due to the interaction with DNA.

These preliminary experiments show that the extent of biotin-PLL and hence DNA binding to the surface can be controlled. It would be interesting to repeat these SPR experiments immobilising the biotinylated DNA on the streptavidin coated PLA-PEG-biotin surfaces to try and determine the reason for the low levels of interaction observed between the cationic polymers and DNA in the experiments described in section 6.3.2. The low levels of interaction observed in that section could be due to one of the following possibilities. Firstly, only a low level of biotinylated-DNA bound to the surface. This in turn would lead to a low negative charge density at the surface and hence not much cationic polymer binding or secondly, that there was too much biotinylated-DNA bound to the surface so it could not condense effectively on PLL binding. By using different densities of bound DNA these two theories could be probed and the contribution of each to the overall interaction between DNA and PLL investigated.

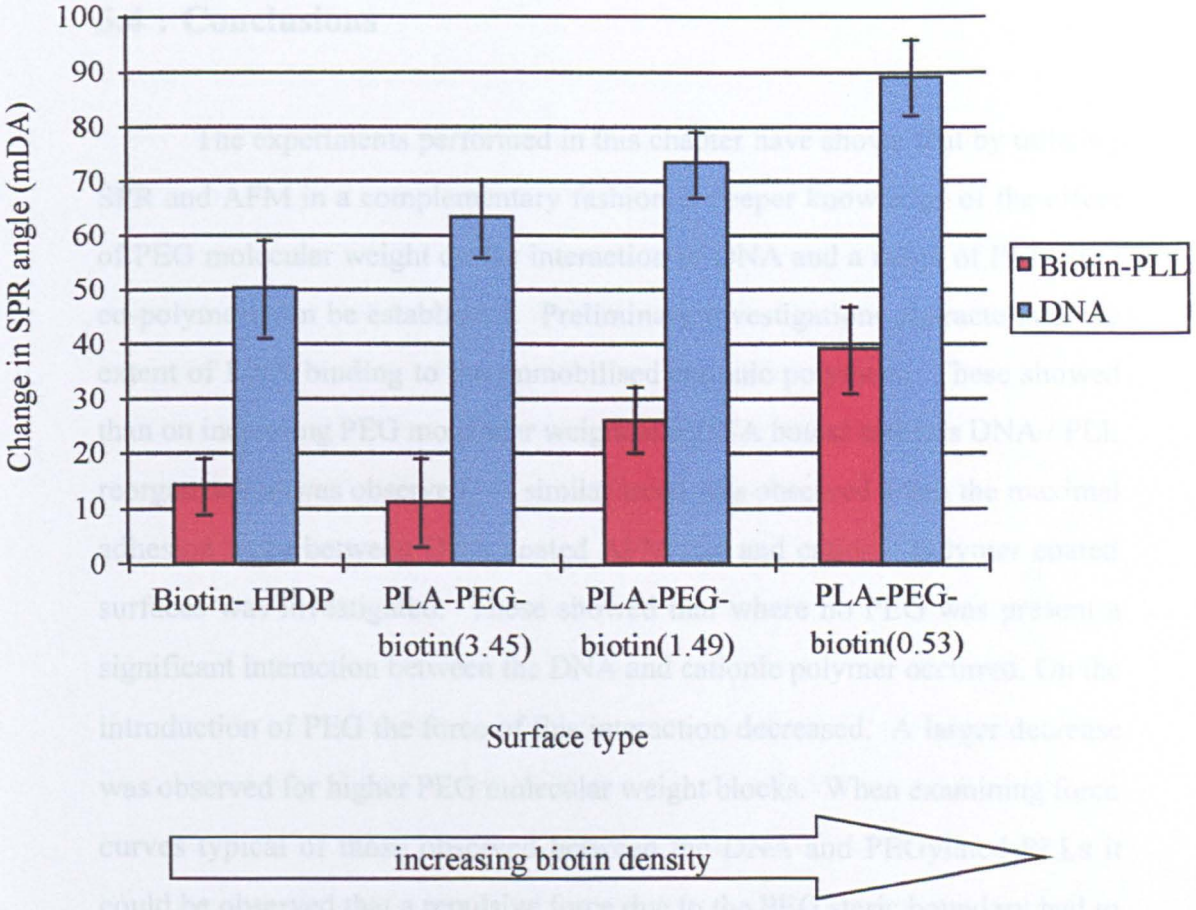

Figure 5.20 : Effect of cationic polymer density on the binding of DNA

This figure shows that the surface coverage of biotin-PLL and hence DNA can be controlled. This may be a useful property for elucidating the factors effecting the efficiency of DNA / cationic polymer complexation.

bars = average ± 1 standard deviation ($n \geq 15$)

5.4 : Conclusions

The experiments performed in this chapter have shown that by utilising SPR and AFM in a complementary fashion, a deeper knowledge of the effect of PEG molecular weight on the interaction of DNA and a range of PLL-PEG co-polymers can be established. Preliminary investigations characterised the extent of DNA binding to the immobilised cationic polymers. These showed than on increasing PEG molecular weight less DNA bound and less DNA / PLL reorganisation was observed. A similar trend was observed when the maximal adhesion force between DNA coated AFM tips and cationic polymer coated surfaces was investigated. These showed that where no PEG was present a significant interaction between the DNA and cationic polymer occurred. On the introduction of PEG the force of this interaction decreased. A larger decrease was observed for higher PEG molecular weight blocks. When examining force curves typical of those observed between the DNA and PEGylated PLLs it could be observed that a repulsive force due to the PEG steric boundary had to be overcome before binding of the DNA to the PLL could occur. The extent of this steric repulsion was observed to increase with PEG molecular weight.

In SPR experiments where DNA was immobilised to the surface and the cationic polymer introduced to measure the extent of interaction with DNA, significant binding / reorganisation was observed. This suggests that DNA conformational flexibility has a significant role to play in the formation of complexes from cationic polymers and DNA.

When images of the complexes were obtained using AFM, a variety of structures were observed. The form of these depended on the ratio of PLL to DNA (ie. positive to negative charge). In the presence of an excess of DNA 'beads-on-a-string'-like entities were observed. On increasing the PLL : DNA

ratio, spherical structures were observed. These possessed a rough / contoured surface with the individual globular particles which made up the spherical entity having similar sizes of those observed for the 'beads-on-a-string' like entities observed at lower PLL : DNA ratios. It was therefore suggested that the 'beads-on-a-string' like entities comprise of string-like DNA molecules which had been condensed in certain areas by the cationic polymer into bead-like regions. On increasing the cationic polymer content, these structure collapse in on themselves producing the rough / contoured structures observed at cationic polymer : DNA ratios in the region of 1 : 1.

When comparing images of complexes formed from the same charge ratio of PLL : DNA but differing molecular weights of PEG, it was observed that the average size of the complexes increased with PEG molecular weight. This agrees with SPR data where it was observed that the extent of the SPR trace attributed to DNA / PLL condensation and reorganisation was less as PEG molecular weight increased, suggesting a larger particulate would be formed. Liquid images also showed that on increasing the PEG molecular weight the surface substructure of the DNA / cationic polymer complexes was lost. It is suggested that this is due to the hydrophilic PEG portion of the molecule locating at the surface of the complex, whilst the substructure containing DNA / PLL core is hidden below this fluid PEG steric boundary.

In summary, SPR and AFM force-distance studies have shown that DNA flexibility and PEG molecular weight both effect the formation of complexes between DNA and PLL. In contrast AFM imaging studies of the DNA / cationic polymer complexes suggest that PEG locates at the surface of the formed complexes forming a steric boundary. This results in a particulate with a fluid-like surface which potentially will be less immunogenic than complexes formed form PLL alone, improving the biocompatibility of the gene

therapy construct.

Chapter 6 : Cationic lipids an alternative approach to gene therapy

6.1 : Introduction

6.1.1 : Use of cationic lipids in gene therapy

In the last chapter, the problems with viral gene therapy and the advantages of using cationic polymers was discussed. This chapter will centre on the study of the physicochemical properties of cationic liposomes as alternative delivery vectors for gene therapy. The first use of lipid based vehicles to deliver genes was that of using the actual cells of the patient. As described in Chapter 5 these can be removed from the patient and infected with the correct gene and transplanted back into the patient. The first clinical application of this approach according to Ledley (1996) was to treat Severe Combined Immune Deficiency (SCID) (Blaese (1995)). Peripheral blood lymphocytes or bone marrow progenitor cells were used as donor cells for the DNA encoding for the enzyme adenosine deaminase (ADA) which is deficient in the patients (Bordigon (1995)). After transplanting or transfusing these transformed cells back into the patient, low levels of ADA expression were observed over extended periods of time (Kohn (1995)). Other diseases where cell based approaches are being investigated include Arthritis (Bandara (1993)), Cancer (Dranoff (1993)) and Gaucher disease (Xu (1994)).

There are many theoretical advantages of cell based gene therapy. Since the genes are added *ex vivo*, the cells can be tested for purity and the extent of transcription before being administered back to the patient. Secondly, the genes are permanently incorporated into the cells chromosomes. On transplantation of the cells back into the patient, all daughter cells will also produce the therapeutic benefits of the corrected gene (Ledley (1996)). This approach is potentially a long term solution. However, there are also

disadvantages to cellular gene therapy. The main one is likely to be the higher cost of this approach compared to conventional biological pharmaceuticals and secondly, the lack of proven experience of transplanting cells into humans, albeit that a variety of methods have been developed in animal models. In the light of these disadvantages, liposomes which can mimic to some extent the cell membrane surface have become a large area of research (Hug (1991)).

One of the early examples of *in vivo* application of lipids as a vector for gene therapy was to target genes encapsulated in a lactosylceramide liposome to the asialoglycoprotein receptor in hepatocytes of the liver. Whilst liver targeting was observed for the gene therapy vector, as discussed in Chapter 6, the majority of the vectors ended up in the Kupffer cells not the hepatocytes (Nicolau (1983)).

Due to the low transfection efficiency observed with this type of lipid, pH sensitive lipids became a more popular choice for formulations. These lipids theoretically are taken up by endocytosis, but at acidic pHs such as those found within the endosome, they fuse with the cell membrane releasing the DNA into the cytoplasm (Wang (1989)). However, more recently, liposomes formed from cationic lipids have been shown to be more effective *in vitro* and *in vivo* at transfecting cells and the majority of research now centres on this type of system (Ledley (1996)).

Cationic lipids possesses qualities similar to cationic polymers. As they are both flexible and positively charged molecules. This allows them to condense DNA, protect it from enzymatic degradation, alter the biodistribution of the DNA and increase transfection efficiency by mechanisms such as inducing endocytosis, enhancing release from the endosome and facilitating nuclear entry (Kabanov (1995)).

Evidence for the membrane fusion of cationic lipid and cationic cholesterol derivatives has been shown by confocal laser scanning microscopy (Noguchi (1998)). Whereas Bhattacharya and Madel present evidence that the use of cationic lipids with unsaturated hydrocarbon chains give a more effective delivery of DNA than their saturated hydrocarbon relations. In the presence of anions, as would be found within the cell, DNA release is more successful at temperatures around the T_m (melting temperature) of the lipid. For the unsaturated hydrocarbon lipids this is found around body temperature (Bhattacharya (1998)). Normally, cationic lipids are combined with neutral lipids to form a mixed functional liposome. The ratio of cationic to nonionic lipid giving the best transfection results depends on the lipids and cell type used (Gorman (1997), Zhao (1997)).

The size and surface charge of the DNA / lipid complex not only depends on the ratio of neutral to cationic lipid but also the ratio of lipid to DNA. Many studies have shown that for effective transfection of a complex, an overall positive charge is required. This can be attributed to the fact that a positively charged complex will interact better with the negatively charged cell membrane due to charge attraction (Zabner (1995)). Studies by Zuidam and Barenholz using fluorescent, pH dependant probes and static light scattering techniques have also shown the importance of DNA / cationic lipid ratio on stability and degree of encapsulation of the DNA (Zuidam (1997), (1998)). Other studies have shown that surface charge can be related to hepatic uptake (Aoki (1997)) and that transfection efficiencies increase with particle size up to a certain point. This point is dependant on the system under investigation (Felgner (1994)). Zelphati and co-workers showed that serum components such as BSA and macroglobulin effect physicochemical properties and cellular uptake of liposome gene therapy vectors, but differing the ratio of cationic to neutral lipid can be used to minimise this effect (Zelphati (1998)).

Different approaches to modifying cationic liposomes have been investigated to try and increase their efficacy as a gene therapy vector. Tang and Hughes found that the addition of a disulfide bond in to a lipid, 1,2-dioleoyl-sn-glycero-3-succinyl-2-hydroxyethyl disulfide ornithine conjugate (DOGSDSO) when utilised in liposomes also containing 1,2-dioleoyl-3-trimethylammonium-propane (DOPE) increased the production of luciferase 50 times over that of non-disulfide analog in certain cell lines (Tang (1998)). Other defined entities attached to cationic lipids to try and increase their transfection efficiency include Tween-20 and recombinant retro-viruses (Porter (1998), Liu (1996)).

6.1.2 : Characterisation of DNA / cationic lipid complexes

Many theories have been proposed for the structure of the DNA / cationic lipid complex structure, which embrace not only of forces of interaction between the DNA and cationic lipid, but also hydrophobic interactions with the neutral lipid. The original structure for DNA cationic lipid complexes was suggested by Felgner and co-workers as being somewhat like 'beads on a string', where the liposomes form bead-like structures on a DNA string (Felgner (1987)). Some electron microscopy evidence backs this theory, but it also supports other structures for the complex. These include, tube like structures of DNA surrounded by a lipid bi-layer, a multilamellar type structure with alternating lipid bilayers and DNA monolayers and hexagonally packed DNA columns surrounded by cationic lipid monolayers (Gershon (1993), Sternberg (1994), Radler (1997), Koltover (1998)). These structures are schematically represented in Figure 6.1. Further evidence for the multilamellar state has been gleaned from synchrotron small-angle X-ray scattering (SAXS) investigations (Salditt (1998)) and modelling has compared

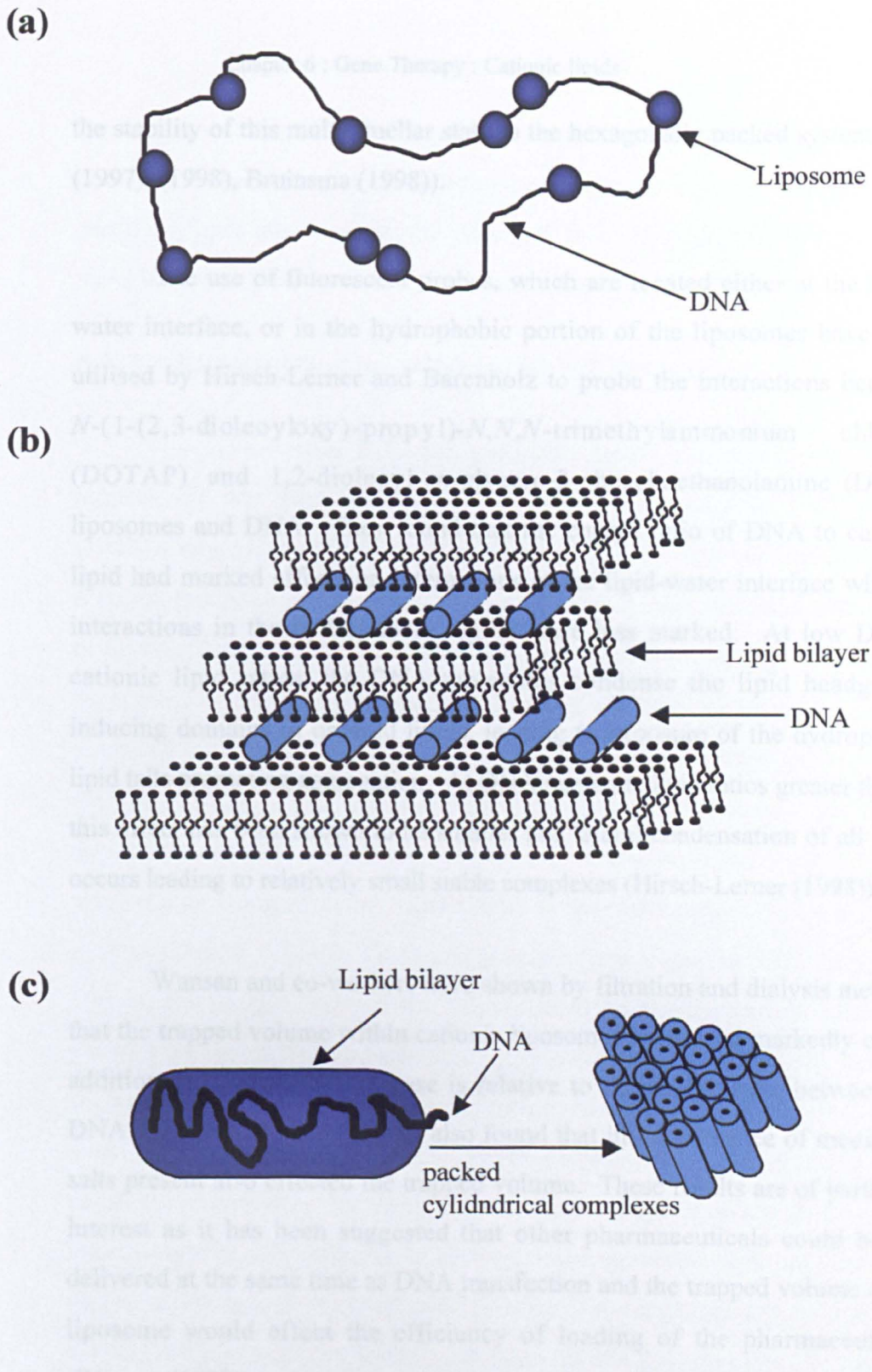

Figure 6.1 : Schematic representation of suggested DNA catioinc lipid complex structure (adapted from Dan (1998))

(a) beads on a string
(b) multi lamellar
(c) hexagonally packed tubes

the stability of this multilamellar state to the hexagonally packed system (Dan (1997), (1998), Bruinsma (1998)).

The use of fluorescent probes, which are located either at the lipid / water interface, or in the hydrophobic portion of the liposomes have been utilised by Hirsch-Lerner and Barenholz to probe the interactions between *N*-(1-(2,3-dioleoyloxy)-propyl)-*N*,*N*,*N*-trimethylammonium chloride (DOTAP) and 1,2-dioleoyl-*sn*-glycero-3-phosphoethanolamine (DOPE) liposomes and DNA. They found that the charge ratio of DNA to cationic lipid had marked effects on interactions at the lipid-water interface whereas interactions in the hydrophobic region were less marked. At low DNA / cationic lipid ratios, the DNA molecules condense the lipid headgroups inducing domains of ordered lipids, leading to exposure of the hydrophobic lipid tails promoting aggregation. At DNA / cationic lipid ratios greater than 1, this effect has been shown to be smaller and lateral condensation of all lipids occurs leading to relatively small stable complexes (Hirsch-Lerner (1998)).

Wansan and co-workers have shown by filtration and dialysis methods that the trapped volume within cationic liposomes is reduced markedly on the addition of DNA. The decrease is relative to the charge ratio between the DNA and cationic lipid. It was also found that in the presence of media, the salts present also effected the trapped volume. These results are of particular interest as it has been suggested that other pharmaceuticals could be co-delivered at the same time as DNA transfection and the trapped volume of the liposome would effect the efficiency of loading of the pharmaceuticals (Wansan (1998)).

In investigations concerned with the structure of gene therapy vehicles it is important that their structure is not significantly altered on adsorption to

the surface on which the characterisation is to be performed. The surface used must also have controlled characteristics to ensure a reproducible adsorption profile. Such surfaces can be obtained from the use of self-assembled monolayers. A brief introduction to such systems is given below.

6.1.3 : Introduction to self-assembled monolayers

The interaction between gold and thiols for the production of monolayers was first introduced by Nuzzo and Allara in 1983 (Nuzzo (1983)), and much of the early work in this area was performed by the research groups of Nuzzo and Whitesides. Termed self-assembled monolayers or SAMs, these surfaces are formed when an alkanethiol, dialkyl-disulfides or organosufides adsorb from vapour or solution. Binding occurs via the sulphur atoms of the molecules onto a metal or some semiconductor surface atoms (Sheen (1992)). The common surfaces used as substrates for SAMs deposition are gold and silver. The structure produced has trans extended alkyl chains arranged in an ordered array at approximately 30° to the surface normal (Dubois (1992)). There are primarily two stages to SAM formation. Firstly, low density crystalline islands form where the carbon chains lie parallel to the surface. Secondly, at surface saturation of this phase, a transition occurs to a structure where chains become closely aligned to the surface normal (Poirier (1996)). These surfaces, whose characteristic are primarily governed by the terminal group on the alkyl chain are stable in both aqueous or ethanolic solution or air for months, however, some self-exchange has been shown to occur (Schlenoff (1995)). This exchange can be useful for the formation of mixed monolayers (Cotton (1998), Takami (1995)). Removal of SAMs from the metal surfaces requires heating to over 70 °C, or UV irradiation in the presence of light (Mrksich (1996b)).

The structure of SAMs and their formation has been widely studied

using a range of techniques. Characterisation of the chemical content of the surface layer has primarily been achieved using XPS, infra-red spectroscopies including reflection and fourier transform modes and SIMS (Dubois (1993), Zhong (1994), Pan (1998)). Whereas SAM formation has been followed using quartz crystal microbalance (Karpovich (1994)), SPR (Mittler-Neher (1995)) and the formed SAM surface structure by AFM (Pan (1993)) and STM (Kim (1992), Takami (1995)), X-ray diffraction (Samant (1991)) and computer simulation (Sprik (1994)). SAMs have been observed to taken on either hexagonal centred rectangular lattice or oblique structure depending on thiol species used (Nelles (1998)).

It has been found that molecular sized defects can occur in a SAM surface. The size and frequency of these is dependant on not only chain length (Porter (1987)) but also SAM functional groups. Chidsey and Loiacono found that the degree of defects in SAMs is CF_3<CH_3<OH<NC<CO_2H for a group of constant alkyl chain length thiols, but as chain length is increased from C9-10 to C15, this is less pronounced (Chidsey (1990), Nuzzo (1990)). Racemic and pure enantiomeric SAMs have also been seen to possesses different electrochemical properties due to the surface organisation of the layers (Muskal (1995)).

The chemical modification of deposited SAMs is another area of interest, reactions include amine and alcohol derivatisation of 11-mercaptoundecanoic acid, amine photo-attachment to di-11-(4-azidobenzoate)-1-undecyl disulfide and derivatisation with phenyl isothiocyanate of hydroxyl and carboxyl terminated SAMs (Duevel (1992), Wollman (1994), Himmel (1997)). Whitesides and co-workers showed that inter-chain reactions in SAMs can occur. A carboxylic acid SAM of 16-mercaptohexadecanioic acid was reacted with trifluoroacetic anhydride and

alkyl amines to produce a SAM of mixed acid and amide functionalities (Yan (1997)).

Although the majority of work in the area SAMs is carried out using thiolated hydrocarbons, a wide variety of molecules have been modified with a thiol moiety to allow the production of this type of monolayer surface. These include DNA (Rabke-Clemmer (1994)), saccharides (Fritz (1996)), lipids (Lang (1994), (Duschl (1996)) and polymers (Lenk (1993), Nakayama (1998)).

By patterning SAMs using micro-contact printing as introduced in Chapter 3, surface topology and functionality can be controlled. This may be useful for the orientated growth of cells (Mrksich (1996a)). Because of their controllable and characterisable surfaces many other applications for SAMs and modified SAMs have been proposed. These include, surfaces for the production of "cells" performing biochemical functions, biomimicing surfaces to allow control over cellular activity (Mrksich (1996b), immunosensing (Caruso (1997)), a basis for combinatorial drug synthesis and screening (Jacobs (1994)), electrontransfer agents (Willner (1992), Cotton (1998)), corrosion passivators (Zamborini (1998)) and microelectronics (Gardner (1995)).

6.1.4 : Aims of investigations performed in this chapter

The efficiency of a gene therapy vector is controlled partly by its interactions with other materials. As introduced in Chapter 1, by understanding the surface chemistry of a system, its interactions with other materials can be interpreted. As the system under investigation in this chapter is a multi-phase one, the contribution of the different components to the systems interface is a major consideration to understanding its surface interactions and hence efficiency. To obtain images of a cationic lipid, (1 : 1 molar ratio of 1,2-dimyristoyl-sn-glycero-3-ethylphosphocholine chloride salt

(EDMPC)) and Cholesterol / DNA gene therapy complex and hence determine the contribution of the DNA and lipid components to the surface was the first aim of this chapter.

To visualise a drug delivery system such as this gene therapy complex it needs to be associated with a surface. The interaction between it and the surface must be strong enough to allow well-defined and reproducible images of the material to be obtained but not so strong that it significantly alters the vectors structure. The surfaces used in this case to immobilise the gene therapy vectors for imaging were SAMs. As discussed above there are many favourable properties of SAMs which make them useful tools for studying a variety of molecules interactions under controlled conditions. These include the interactions of proteins (Muller (1993), Silin (1996)), lipids (Sakmann (1996)) and cell membranes (Rao (1997)). Therefore, their use in this study was advantageous as they provided a controlled surface structure on which the cationic lipid / DNA complexes could be imaged under physiological conditions using the AFM.

Surfaces were formed from either 11-mercaptoundecanoic acid (11-MUA), dodecanethiol (C12Me), propanethiol (C3Me) and 2-aminoethanethiol ($C2NH_2$). These SAMs provided three different surface functionalities with which to probe both the charge and hydrophobic interactions of the gene therapy complex. Both the DNA and cationic liposomes were imaged prior to the formulated complex to distinguishes any alteration formulation of the gene therapy vector had on both the DNA and liposome structure.

The second aim of this chapter was to try and determine the extent of interaction of these liposomal gene therapy vectors with different types of surfaces to provide a preliminary understanding of how they may interact with

the cell membrane and hence determine their mechanisms of transfection. Knowledge of the gene therapy system at this level may also aid improvement in the design of such systems (Pouton (1998b)). SPR studies provided the opportunity to characterise the rate and extent of interaction of the complex as well as its constituent parts with the variety of surface chemistries investigated and each other.

6.2 Materials and methods.

6.2.1 : General

All DNA, liposomes and complexes were provided by Glaxo-Welcome Research and Development, Ware, UK and were used with out further modification. Stock solutions of the liposomes and complex were stored at 0-3 °C and DNA at -20 °C. DNA is a pMB113 plasmid as depicted in Figure 6.2 (a). This contains expression vectors for CFTR and the human cytomegalovirus enhancer and promoter gene to direct transcription of the assayed gene. A tetracycline resistance marker in also coded for. The liposome comprises of a 1 : 1 molar ratio of 1,2-dimyristoyl-sn-glycero -3-ethylphosphocholine chloride salt (EDMPC) and Cholesterol. The complex possesses a 3 : 1 ratio of DNA (mg) to lipid (mM). The structure of EDMPC and cholesterol are shown in Figure 6.2 (b).

6.2.2 : SPR

Silver SPR slides were coated in self assembled monolayers of either 11-mercaptoundecanoic acid (11-MUA), dodecanethiol (C12Me), propanethiol (C3Me) and 2-aminoethanethiol ($C2NH_2$), by overnight incubation in 1mM ethanolic solutions of these materials. Prior to use, slides were washed with ethanol and dried under a nitrogen stream. Problems arose with 2-aminoethanethiol SAMs on occasions due to this material being very

(a)

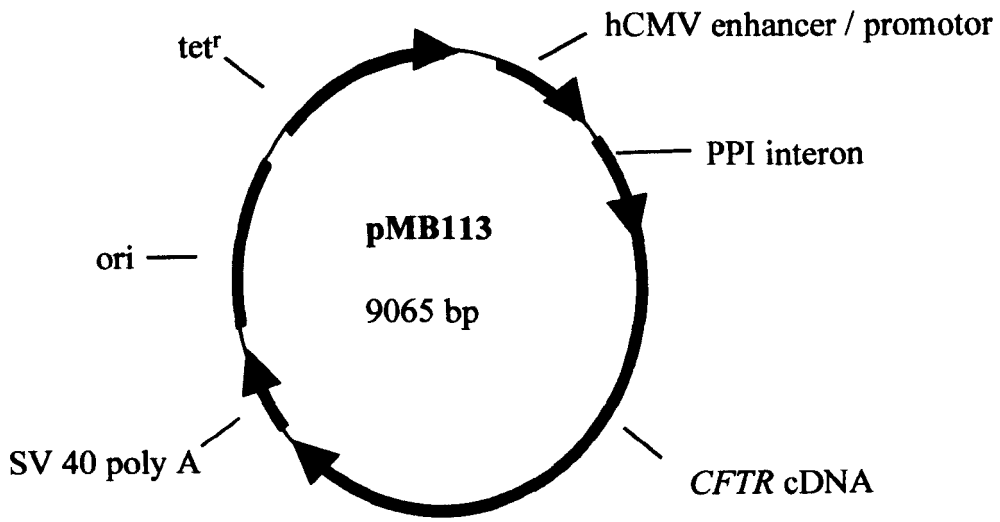

(b)

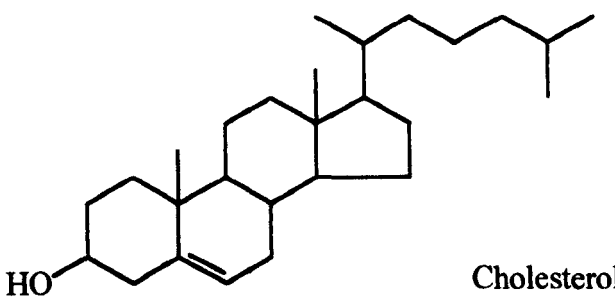

Cholesterol

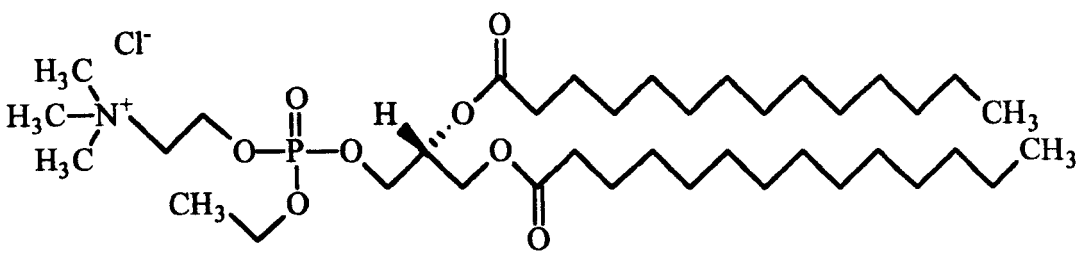

1,2-dimyristoyl-sn-glycero-3-ethylphosphocholine
(EDMPC)

Figure 6.2 : Structure of (a) plasmid DNA and (b) EDMPC and cholesterol

deliquescent leading to poor solubility in ethanol and marking of silver on SPR slides. If this occurred a new batch of material was used to ensure the integrity of the SAM. The buffer in all SPR experiments was Tris buffer (10 mM, pH 8.0).

SPR experiments were performed to determine the extent of interaction of the DNA, cationic liposomes and complex with the four SAMS. Preliminary experiments were performed to determine the minimal concentration of the cationic liposomes giving maximal SPR shift on the dodecanethiol SAM, concentrations of between 10 -100 μM of lipid were used. The minimum concentration which gave maximal SPR shift (20 μM) was used for studies on other SAMs.

The effect of flow rate on liposome deposition on the SAMs was also investigated. Flow rates of between 50 and 200 μl / min were studied. In all these experiments, a stable baseline was obtained prior to the injection of the liposome at the selected concentration and flow rate. A buffer wash was performed at the end of each injection to remove loosely bound material. A liposome concentration of 120 μM was also utilised for experiments to determine the effect of DNA complexation to the liposomes on rate of adsorption to the SAMs. This concentration was chosen as it gave reasonable shifts for adsorption before and after DNA complexation to the liposome without using excessive amounts of complex material.

Investigations utilising DNA were performed at a concentration of 20 μg / ml. The complex dilutions used possessed either an equivalent concentration of DNA (20 μg / ml DNA) or cationic liposomes (120 μM lipid) for comparison of results obtained with the free entities. All dilutions were carried out in Tris buffer (10 mM, pH 8.0). Buffer was flown over the SAMs surface to obtain a stable baseline. After this 1 ml of the materials at

concentrations described above was injected at 100 µl / min to allow for interactions with the SAMs. A buffer wash was allowed after the injection, at the same flow rate to allow removal of loosely bound material, as well as rearrangement of deposited entities.

In cases where the interaction between the components of the complex were to be investigated, the protocol as above was followed, but after the first buffer wash a second injection of either DNA, liposome or complex was undertaken and a second buffer wash then allowed.

6.2.3 : AFM

SAMs for AFM were prepared on template stripped gold (TSG) using a method adapted from Hegner (1993). A small amount of a 1 : 1 (w : w) mixture of Epoteck part A and Epoteck part B (Promatech Ltd, Cirencester, Gloucestershire, U.K.) was applied to the surface of vapour deposited gold, prepared as described by Derose et al. (1991). A fresh glass coverslip (Chance Propper Ltd, Warley, U.K.) was place on top of the resin ensuring that no air bubbles were formed between the gold surface and coverslip and excess glue did not adhere to the mica surface. This was baked in an oven at 120 ±8 °C for 1 h to set the glue. After cooling the mica-gold-glass sandwich was place in a petri dish containing tetrahydrofuran and left for 10 - 20 min depending on the size of the sample. The mica was then removed of using a scalpel and the template gold surface washed with ethanol and a dried under nitrogen. TSG was stored under an Argon atmosphere prior to use.

SAMs were formed on this gold surface by overnight incubation in 1 mM solutions of either, 11-MUA, C12Me, C3Me, or $C2NH_2$ in ethanol. The samples were then washed in ethanol and dried under a nitrogen stream. SAMs were incubated with DNA, liposomes or the complex at concentrations

as used in SPR and then imaged in Tris buffer (pH 8.0, 10 mM) either with or without washing with the same buffer. Imaging was carried out in Tris buffer (pH 8.0, 10 mM) using Digital multimode AFM with Nanoscope IIIa controller. 100 μm long triangular cantilevers with resonant frequencies between 9-12 KHz in water were used in Tapping™ and contact modes.

6.3 : Results and discussion.

6.3.1 : SPR - interactions of cationic liposomes with model SAM surfaces

Table 6.1 summaries the effect of flow rate on the extent of interaction between the liposomes and methyl and carboxyl terminated SAMs. This table shows that at the flow rates investigated no effect on the extent of liposome deposition on the 11-MUA SAM was observed. However, at a flow rate of 200 μl / min a significant decrease in the change in SPR angle from 159 ± 16 mDA to 120 ± 10 mDA on the interaction of the liposomes with the methyl terminated SAM is observed. This suggests that at this high flow rate a complete deposition of the liposome layer on the methyl surface is not obtained. Therefore, all further investigations monitoring the interaction of the gene therapy complexes and their constituent parts with the SAMs surfaces were performed at 100 μl / min.

Table 6.2 summaries the extent of interaction between the liposome, DNA, and complex with the silver SPR slide or SAMs as determined by SPR at nominal flow rate. It was important to determine the level of non-specific interaction of all the systems with the silver SPR substrate before interactions with the specific chemistries of the various SAMs was characterised. This table shows that no interaction was observed between any of the materials and the silver SPR slide. Any initial change in SPR angle that was observed, those

Flow rate (µl / min)	C12Me	11-MUA
50	169 ± 17	241 ± 18
100	159 ± 16	251 ± 17
200	120 ± 10	257 ± 21

Table 6.1 : Effect of flow rate and liposome concentration on liposome coverage as measured by SPR

values = average ± 1 standard deviation (n ≥ 14)

Surface	Liposome	DNA	Complex
Silver slide	0	0	(5-10)
C12Me	120 ± 25	0	(5)
C3Me	116 ± 11	0	0
C2NH2	220 ± 25	31 ± 5	38 ± 6
11-MUA	311 ± 29	(5)	0

Numbers in brackets represent initial shifts which returned to baseline levels after the buffer wash

Table 6.2 : Summary of SPR data for interactions with SAMs

values = average ± 1 standard deviation (n ≥ 27)

numbers in brackets in Table 6.2, were seen to decrease to the same as the baseline after the buffer wash showing that the interaction with the silver surface was weak. These results suggest that any interactions observed between the adsorbing biomaterials and the SAMs coated on the silver film are due to the terminal group of the SAM rather than any exposed areas of the underlying silver SPR slide.

Table 6.2 shows only the liposome material interacted with the hydrophobic methyl terminated SAMs C12Me and C3Me. Figure 6.3 (a) shows a typical trace for the liposomes interacting with a C12Me surface. This trace shows one phase during the injection of the liposomes, but during the buffer wash a secondary increase in the SPR angle is observed. The phase during injection could be attributed to the initial binding of the liposomes to the methyl surface. Whilst subsequent fusing of these to form a hybrid bilayer with the SAM, which would result in an increase in lipid density at the SAM surface and hence SPR angle is attributed to the increase in SPR angle observed during the buffer wash. This hybrid bilayer may form with the lipids hydrophobic tails pointing towards the SAM, maximising their hydrophobic interactions with the methyl terminated surface. This is represented schematically in Figure 6.3 (b). Neither the negatively charged DNA or lipid / DNA complex interacted with the hydrophobic methyl terminated SAMs. This could be attributed to their charge density limiting the potential for hydrophobic interactions.

As can be observed from Table 6.2 the shifts for the adsorption of the cationic liposomes to the carboxyl terminated SAM (311 ± 29 mDA) is significantly larger than that for the adsorption to the hydrophobic surface (120 ± 25 mDA). Figure 6.4 (a) shows a typical trace for the interaction of the liposomes with the carboxyl terminated SAM. It can be observed from this figure that the change in SPR angle is monophasic and significantly larger to

(a)

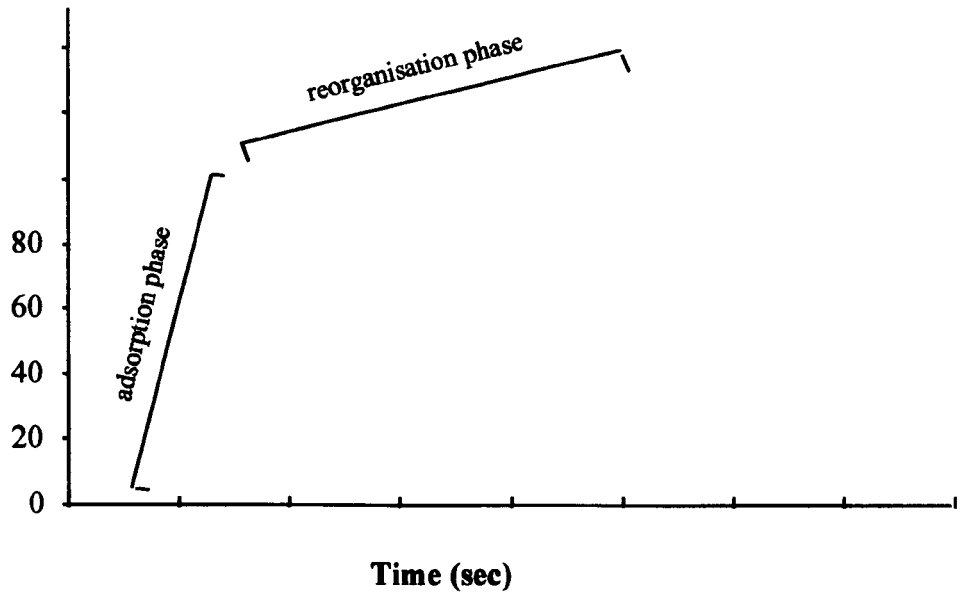

(b)

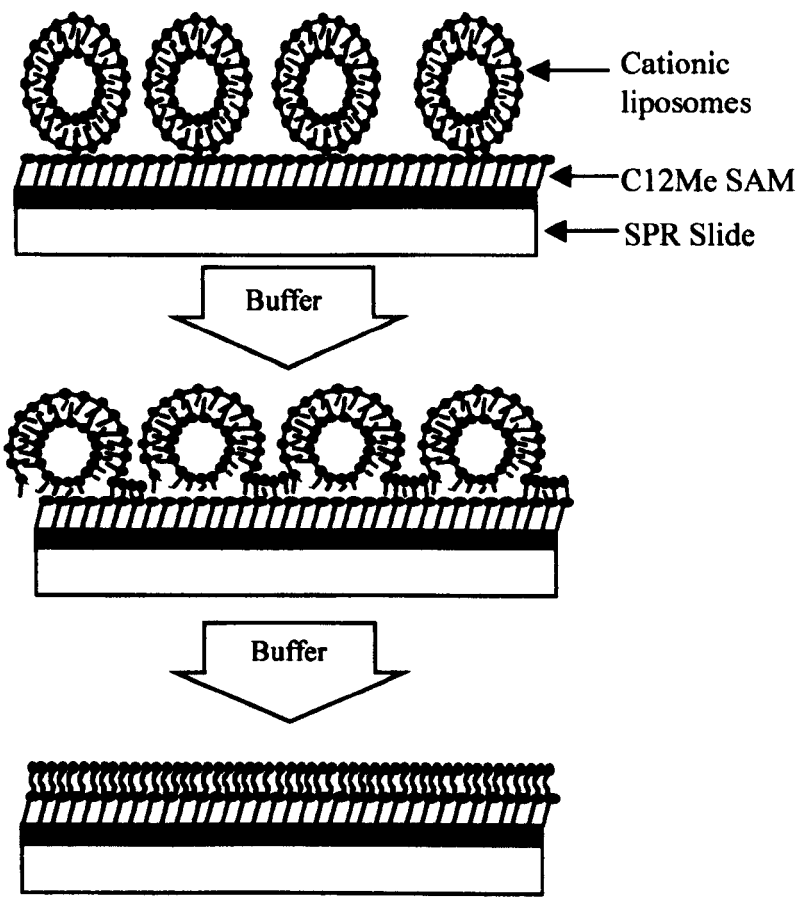

Figure 6.3 : Interaction of cationic liposomes with a C12Me surface

(a) Typical SPR trace

(b) Schematic representation of mechanism of adsorption

(a)

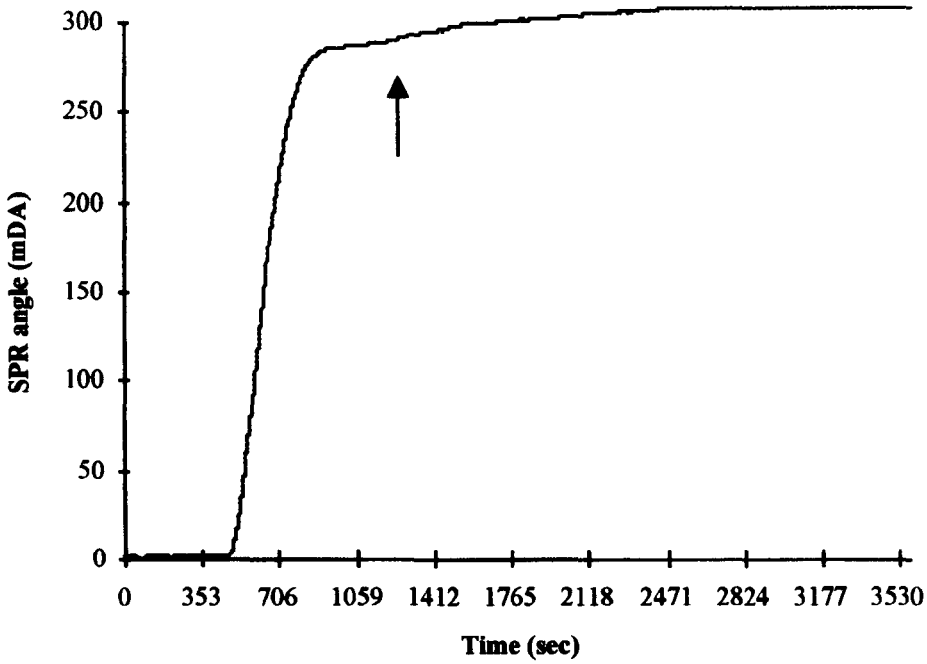

(b)

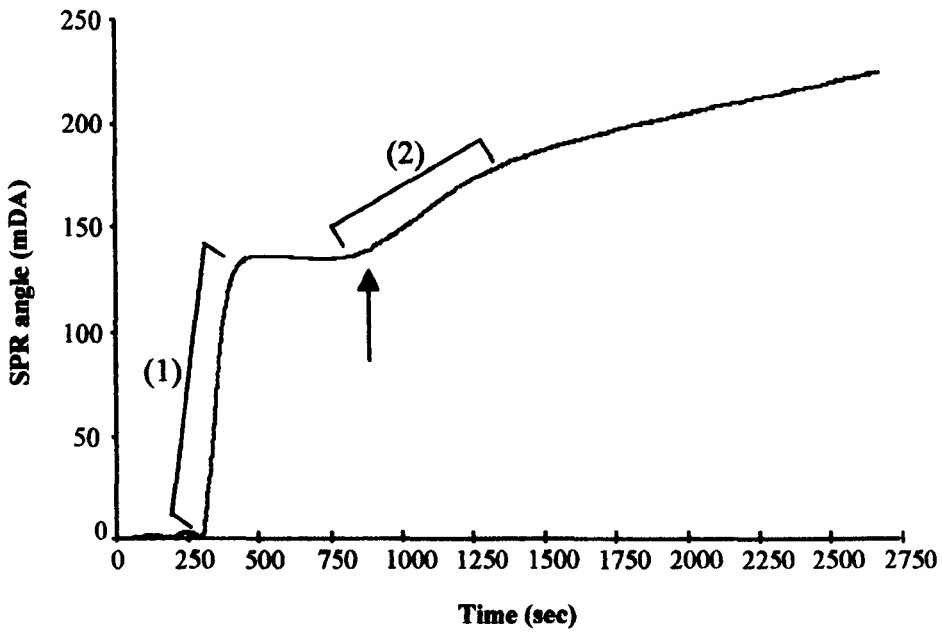

(1) Primary phase (2) Secondary phase

Figure 6.4 : Typical SPR traces for the interaction of cationic liposomes with SAMs

(a) 11-MUA SAM
(b) $C2NH_2$ SAM
(arrow represents beginning of buffer wash)

Interaction of the liposomes with 11-MUA is monophasic, suggesting liposomes adsorb to this surface as stable entities. However, a biphasic shift is observed for the adsorption of the liposomes onto the amino terminated SAM. This suggests that the liposomes conformation changes (2) after initial adsorption (1).

that of the interaction with the hydrophobic surfaces. The fact that the interaction with this charged surfaces promotes a significantly larger change in SPR angle to that seen with the hydrophobic methyl terminated SAM and that the trace is monophasic suggests that the mechanism of interaction for the liposomes with this surface is different. Further evidence for this is shown in Figure 6.5 which depicts the relative rates of interaction for the liposomes with the three surfaces. The rate of change in SPR angle, reflecting the affinity of the molecules for the interface is significantly slower for the hydrophobic SAM when compared to the charged counterparts. The rate of interaction of the liposomes with the 11-MUA SAM is fastest. This would be expected as this positively charged surface possesses an opposite charge to that of the cationic liposome. This shows that the charge attraction between the two surfaces has some role to play in the adsorption mechanism. The monophasic trace suggests that the liposomes remain intact on the surface of the 11-MUA SAM or that the rearrangement process is very rapid as it is charge driven and so can not be distinguished from the adsorption phase. This second theory is felt to be less likely due to the significant increase in the change in SPR angle for the liposome adsorption on the 11-MUA compared to the C12Me. This increase in SPR shift is indicative of either a denser or thicker layer on the SAM surface and in this case is more likely to be associated with the adsorption of intact liposomes.

Some studies have shown that results obtained for experiments depend on the length of carbon chain in the SAM used as this influences the packing and structure of the SAM (Porter (1987)). Shorter chain thiolated hydrocarbons are unable to form such a dense and reproducible surface packing. Since a C11 amino terminated thiol was unavailable, the effect of chain length on the adsorption of the liposomes onto two different length methyl terminated SAMs was investigated to see if any difference was

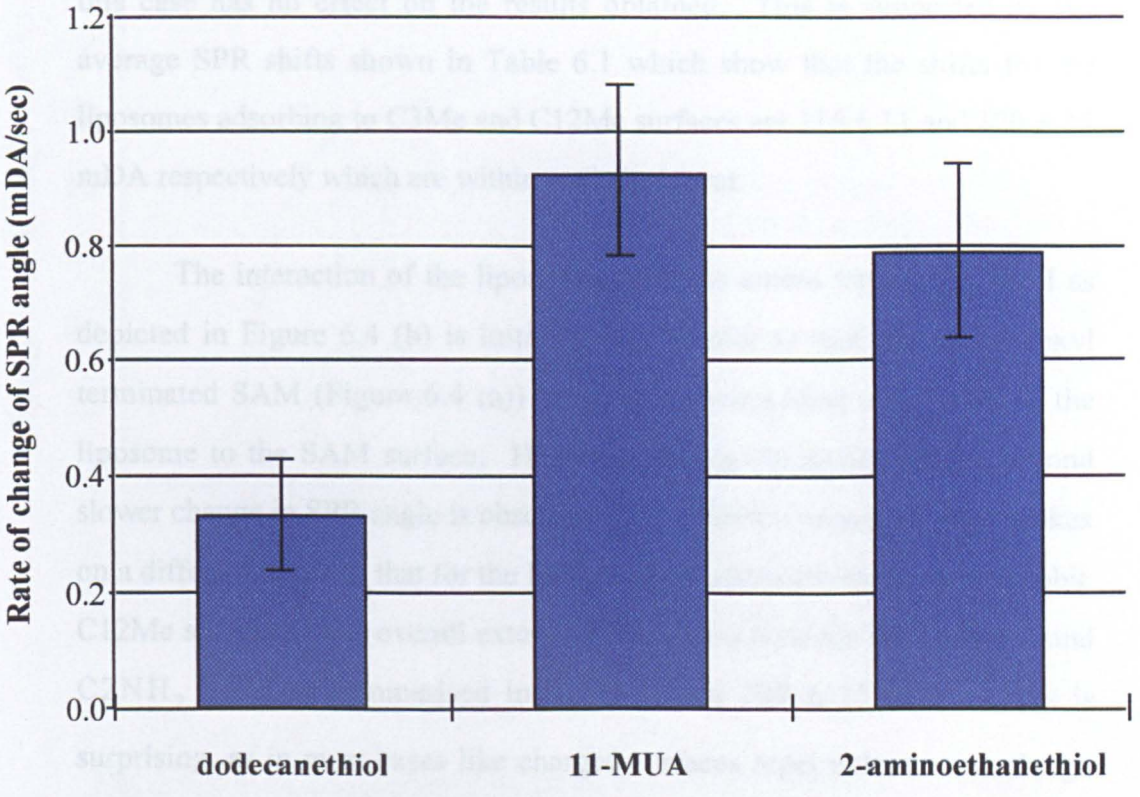

Figure 6.5 : Relative rates of interaction of liposomes with SAMs

The rate of interaction of the liposomes with the SAMs as measured by SPR appears to be not only mediated by charge but also liposome structure

bars = average ± 1 standard deviation ($n \geq 22$)

observed in the adsorption profiles. Figure 6.6 shows two typical SPR traces one for the adsorption if the liposomes to a C3Me surface and one to a C12Me surface. From these traces it is obvious that chain length of SAMs in this case has no effect on the results obtained. This is supported by the average SPR shifts shown in Table 6.1 which show that the shifts for the liposomes adsorbing to C3Me and C12Me surfaces are 116 ± 11 and 120 ± 25 mDA respectively which are within statistical error.

The interaction of the liposomes with the amino terminated SAM as depicted in Figure 6.4 (b) is initially very similar to that for the carboxyl terminated SAM (Figure 6.4 (a)) showing a monophasic adsorption of the liposome to the SAM surface. However, during the buffer wash a second slower change in SPR angle is observed. However this secondary phase takes on a different shape to that for the liposomes interacting with the hydrophobic C12Me substrate. The overall extent of interaction between the liposome and $C2NH_2$ SAM as summarised in Table 6.1, is 220 ± 25 mDA. This is surprising, as in most cases like charged surfaces repel unless some charge coupling can occur. Therefore, it is proposed that this shift could be primarily due to the interaction of the neutral cholesterol present in the liposomes with the SAM surface, which in turn causes an interaction with the cationic lipids. Another possible mechanism for the interaction could be attributed ability of the lipids to move laterally within the liposome construct. This means that the liposomes may become polarised by the surface and interact via dipole interactions, involving counterions from the buffer solution (Thomson (1999)).

The SPR trace for the liposomes interacting with the $C2NH_2$ surface (Figure 6.4 (b)), shows an initial increase and plateau and then during the buffer wash a secondary change in the SPR angle. This suggests that the primary interaction of the liposomes with this surface is not as stable and

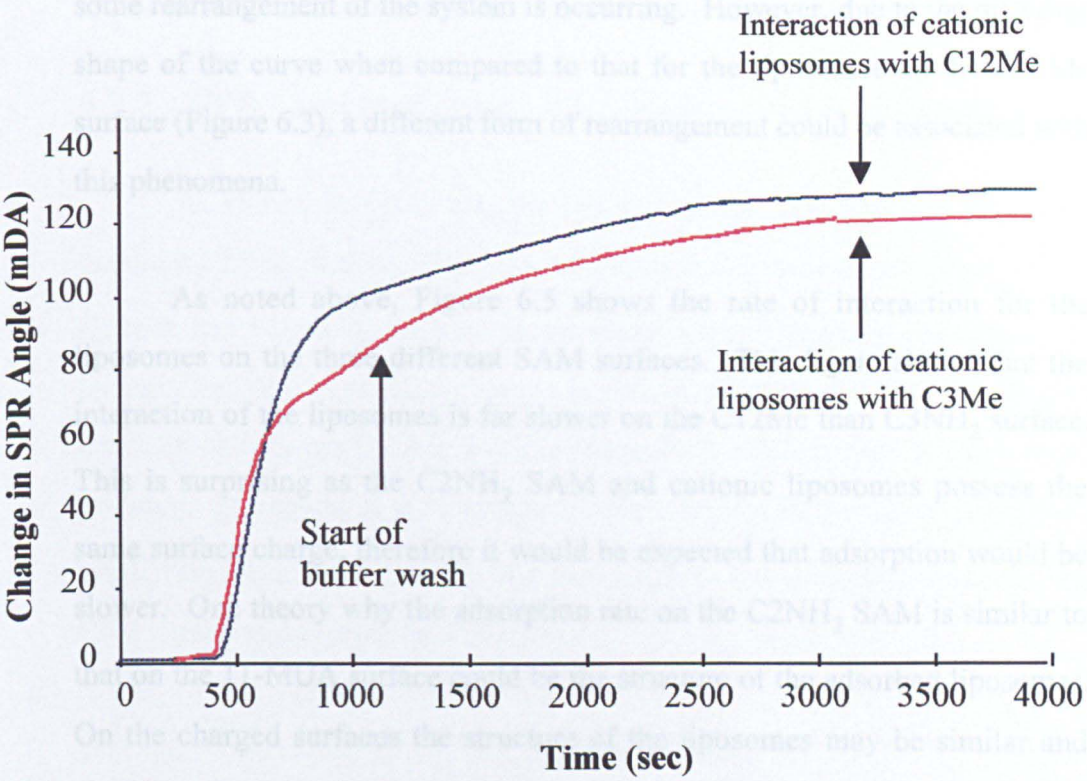

Figure 6.6 : Comparison of SPR traces for cationic liposomes interacting with C12Me and C3Me surfaces

some rearrangement of the system is occurring. However, due to the differing shape of the curve when compared to that for the liposomes on the C12Me surface (Figure 6.3), a different form of rearrangement could be associated with this phenomena.

As noted above, Figure 6.5 shows the rate of interaction for the liposomes on the three different SAM surfaces. This figure shows that the interaction of the liposomes is far slower on the C12Me than $C3NH_2$ surface. This is surprising as the $C2NH_2$ SAM and cationic liposomes possess the same surface charge, therefore it would be expected that adsorption would be slower. One theory why the adsorption rate on the $C2NH_2$ SAM is similar to that on the 11-MUA surface could be the structure of the adsorbed liposomes. On the charged surfaces the structure of the liposomes may be similar and significantly different to that of their structure on the hydrophobic C12Me surface. This change in conformation of the liposome may significantly alter the adsorption rate.

When comparing the overall shifts for the liposomes on the three different SAM surfaces it can be observed from Table 6.2 that they increase from 120 ± 25, to 220 ± 25 and finally 331± 29 mDA in order of the interaction with the C12Me, $C2NH_2$ and 11-MUA surfaces respectively. It was suggested above, that the interaction of the liposomes with the hydrophobic C12Me surface took the form of a hybrid monolayer as depicted in Figure 6.3 (b). The shifts for the other surfaces seem to take on the form of approximate multiples of this. Therefore it could assumed that the liposomes may form a bilayer on the amino surface. Whereas, on the carboxyl terminated SAM, a structure able to produce a greater change in SPR angle, either a denser or thicker surface, possibly intact liposomes is formed. However, these structures can only be hypothesised upon as SPR data provides no

information for structural determination of the liposomes on these surfaces.

6.3.2 : SPR - interactions of DNA with model SAM surfaces

As shown in Table 6.1, the DNA only interacts with the positively charged $C2NH_2$ surface. The lack of interaction between the molecule and C12Me and 11-MUA surface can be attributed to the charge of the DNA. Being a flexible, negatively charged molecule, the potential for hydrophobic interactions with the C12Me and like charged 11-MUA surface is likely to be minimal. The extent of the interaction of the DNA with the $C2NH_2$ surface is small, only 31 ± 5 mDA suggesting only a thin or low density coverage of the DNA on the amino terminated surface.

6.3.3 : SPR - interactions of cationic liposome / DNA complex with model SAM surfaces

The negatively charged complex only interacts with the positively charged $C2NH_2$ surface, producing a change in SPR angle of 38 ± 6 mDA see Table 6.2. The reason why no interaction is observed with the C12Me and 11-MUA surfaces can be attributed to the negative surface charge of the complex. This will be repelled by the 11-MUAs carboxyl surface and reduce the potential for hydrophobic interactions with the C12Me. The fact that no interactions are observed for the complex on the 11-MUA surface suggests that it is acting like DNA and this may suggest the DNA is located at the surface of the gene therapy construct. These theory is corroborated by previous phase analysis light scattering (PALS) and photon correlation spectroscopy (PCS) which suggested that the DNA is located on the surface of the liposome (Bristol Colloid Centre (1998)). It can also be observed from Table 6.2 that the weak interaction between the DNA and 11-MUA surface

which is washed off during the buffer wash does not occur when the DNA is complexed to the liposome. This suggests that complexation of the DNA to the liposome changes the DNA conformation to reduce its potential for non-specific interactions.

Figure 6.7 shows the relative rates of adsorption of the DNA and complex (a), and liposome and complex (b) to the $C2NH_2$ surface. The lipid concentration in Figure 6.7 (a) is the same in both the liposome and complex (120 μM EDMPC), whereas in Figure 6.7 (b) an equivalent concentration of DNA (20 μg / ml) both free and associated with the liposome, were utilised. From Figure 6.7 (a) it can be observed that the rate of interaction for the complex is significantly faster than that for the liposome with the amino terminated SAM surface when they are present at the same lipid content. This can be attributed to a surface charge of the liposome and complex. The liposome is positively charged in the region of + 26 mV as determined by PALS (Bristol Colloid Centre (1998)) and therefore has the same charge as the surface, whereas the complex is negatively charged (~ -51 mV) as determined by PALS, Bristol Colloid Centre (1998)) and hence possess an opposite charge to the surface. As oppositely charged surfaces attract and like charged surfaces repel, the rate of interaction between the complex and amino surface will be faster.

Figure 6.7 (b) shows the effect of complexation of the DNA to the cationic liposome on the rate of interaction with the amino terminated SAM surface. This figure shows that the rate of interaction of the complex is significantly slower than that for the free DNA. This suggests that the charge density on the complex surface is less than that of the free DNA. However PALS showed that the average surface charge of DNA was - 32 mV whereas the complex was -51 mV. Therefore the lower rate of interaction with the

(a)

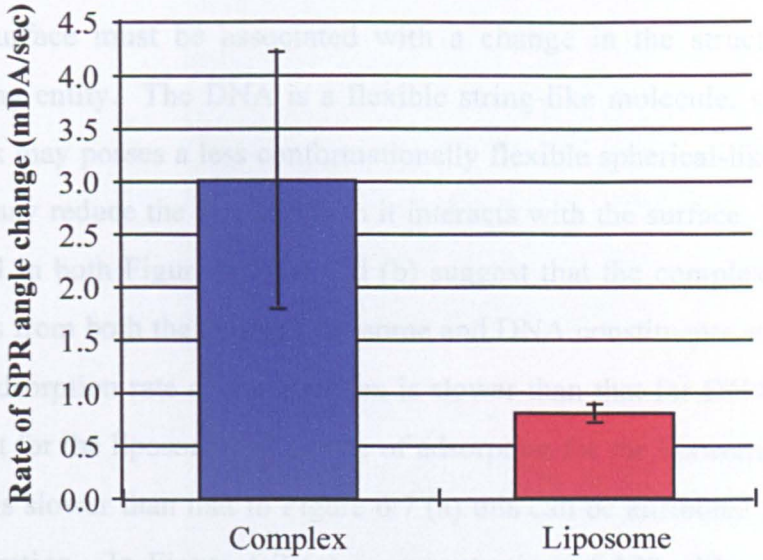

(b)

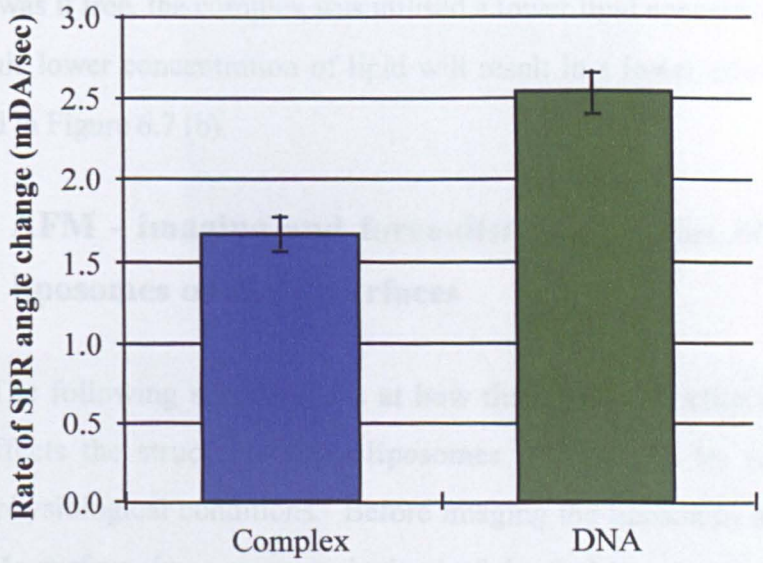

Figure 6.7 : Relative rates of adsorption of liposomes, DNA and complex on $C2NH_2$ SAM

(a) Concentration of lipid is 120 μM in both liposome and complex
(b) Concentration of DNA 20 μg / ml for both DNA and complex (lipid concentration 6.7 μM)

bars = average ± 1 standard deviation ($n \geq 14$)

SAM surface must be associated with a change in the structure of the adsorbing entity. The DNA is a flexible string-like molecule, whereas the complex may posses a less conformationally flexible spherical-like structure, which may reduce the rate at which it interacts with the surface. The results depicted in both Figure 6.7 (a) and (b) suggest that the complex possesses qualities from both the cationic liposome and DNA constituents at its surface as the adsorption rate of the complex is slower than that for DNA but faster than that for the liposome. The rate of adsorption for the liposome in Figure 6.7 (b) is slower than that in Figure 6.7 (a) this can be attributed to the lipid concentration. In Figure 6.7 (a) a concentration of 120 μM was utilised, however to obtain a concentration of DNA in the complex the same as that when it was it free, the complex was utilised a lower lipid concentration of 6.7 μM. This lower concentration of lipid will result in a lower adsorption rate observed in Figure 6.7 (b).

6.3.4 : AFM - imaging and force-distance studies of cationic liposomes on SAM surfaces

The following section looks at how the surface functionality of the SAM effects the structure of the liposomes as observed by AFM under pseudo-physiological conditions. Before imaging the liposomes adsorbed to the SAMs surface, images were obtained of the SAM surfaces as controls. These are depicted in Figure 6.8. It can be observed from these images that no significant differences in topology are observed after SAM formation on the gold. The only significant topological feature in all these images is the underlying crystal structure of the gold.

Representative images of the liposomes adsorbed on the different SAM surfaces are shown in Figure 6.9. Significant differences in the surface topology is observed in these three figures which represent the liposomes on

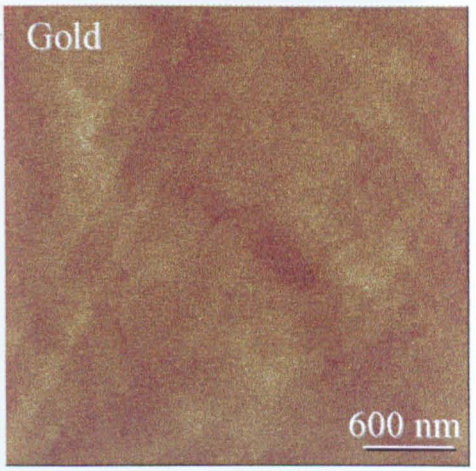

z scale = 5nm

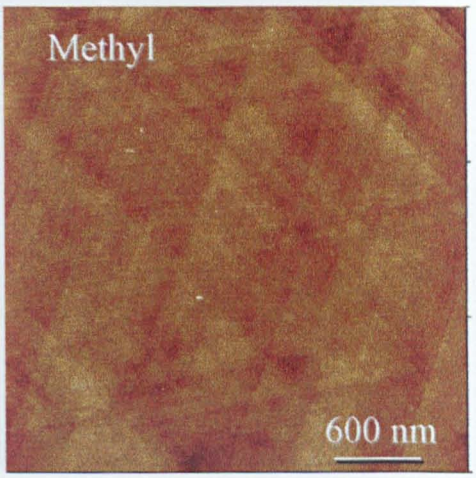

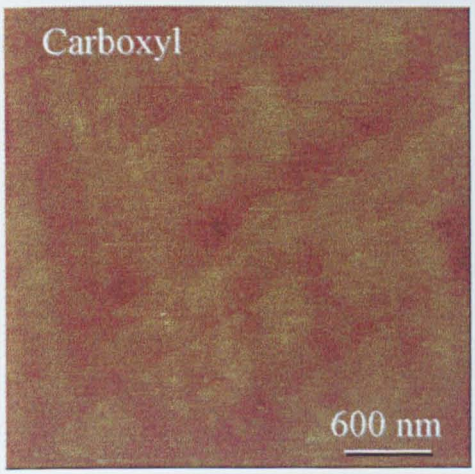

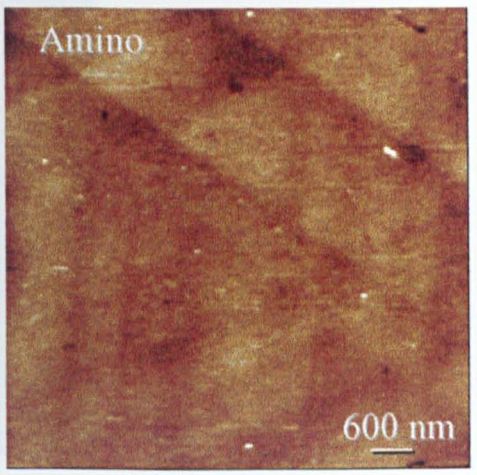

Images taken in Tris buffer in Tapping™ mode.
z scale = 8nm unless otherwise stated

Figure 6.8 : AFM images of template stripped gold and SAMs

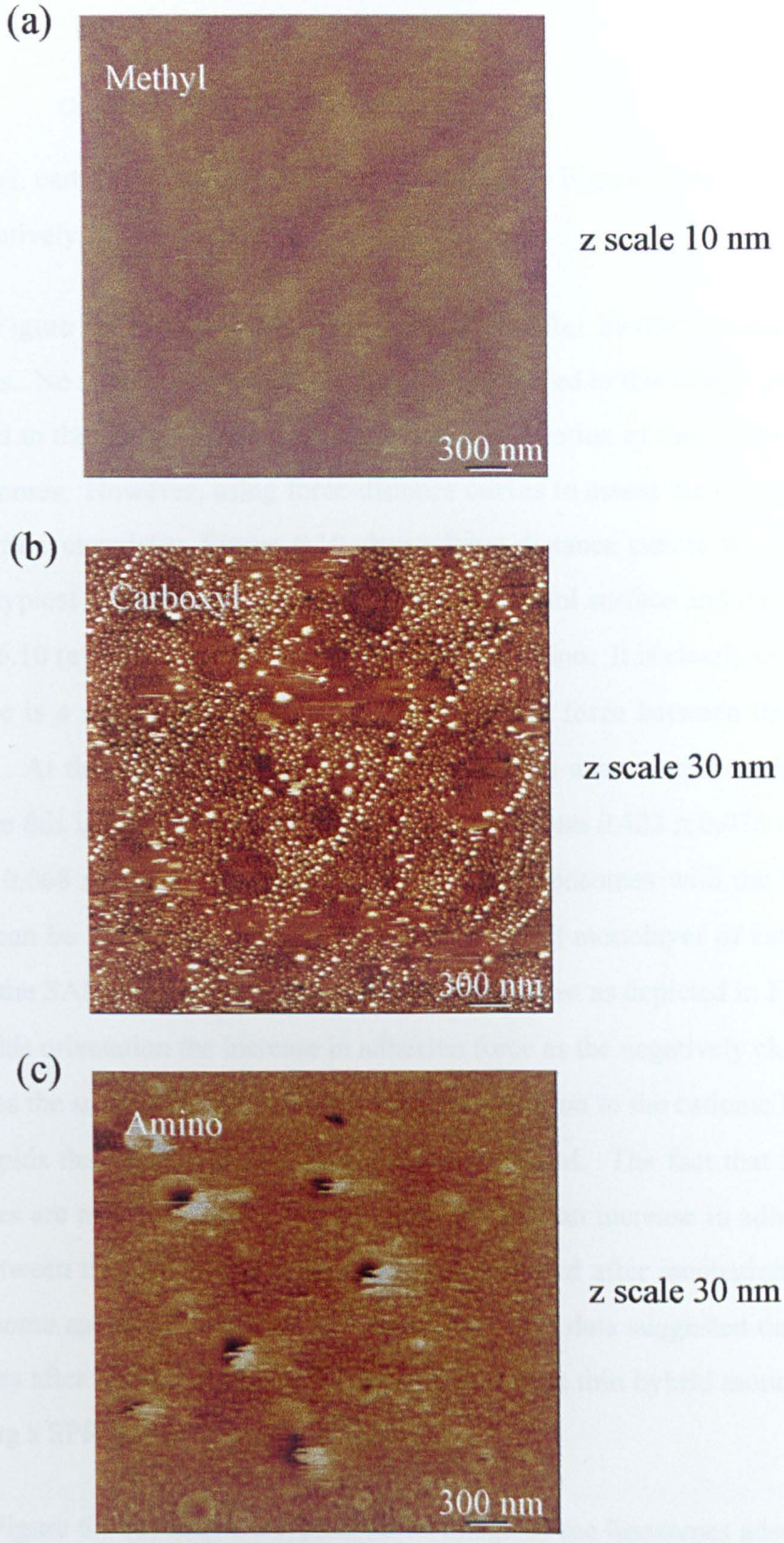

Images taken in Tris buffer in Tapping™ mode.

Figure 6.9 : AFM images of liposomes adsorbed to SAMs
(a) Methyl terminated
(b) Carboxyl terminated
(c) Amino terminated

the methyl, carboxyl and amino terminated surfaces in Figures 6.9 (a), (b) and (c) respectively.

Figure 6.9 (a) depicts the C12Me surface after incubation with the liposomes. No significant change in topology is observed in this image when compared to the control images obtained before incubation of the SAMs with the liposomes. However, using force-distance curves to assess the changes in local surface chemistry, Figure 6.10 shows force-distance curves which are entirely typical of those seen between the dodecanethiol surface and AFM tip before (6.10 (a)) and after (6.10 (b)) liposome deposition. It is clearly evident that there is a significant difference in the adhesion force between the two surfaces. At this pH the silicon nitride tip possesses a net negative charge. Therefore this increase in maximum adhesion force from 0.423 ± 0.075 nN to 0.690 ± 0.068 nN after incubation of the cationic liposomes with the SAM surface can be attributed to the formation of a hybrid monolayer of cationic lipid on the SAM surface with cationic heads uppermost as depicted in Figure 6.3. In this orientation the increase in adhesion force as the negatively charged tip probes the surface, would reflect a stronger attraction to the cationic heads of the lipids than the hydrophobic surface of the SAM. The fact that intact liposomes are not observed in AFM images and that an increase in adhesion force between the AFM tip and the surface is observed after incubation with the liposome appears to confirm SPR data. This SPR data suggested that the liposomes after binding to the SAM collapse to form a thin hybrid monolayer producing a SPR angle shift of 120 ± 25 mDA.

Figure 6.9 (b) shows a typical AFM image of the liposomes adsorbed to the 11-MUA SAM. Individual spherical entities with a diameter of 67 ± 8 nm, this corresponds well to sizes obtained from previous PCS studies of these entities which were between 75-77 nm (Bristol Colloid Centre (1998)). A size distribution of the liposomes adsorbed to this surface is shown in

a)

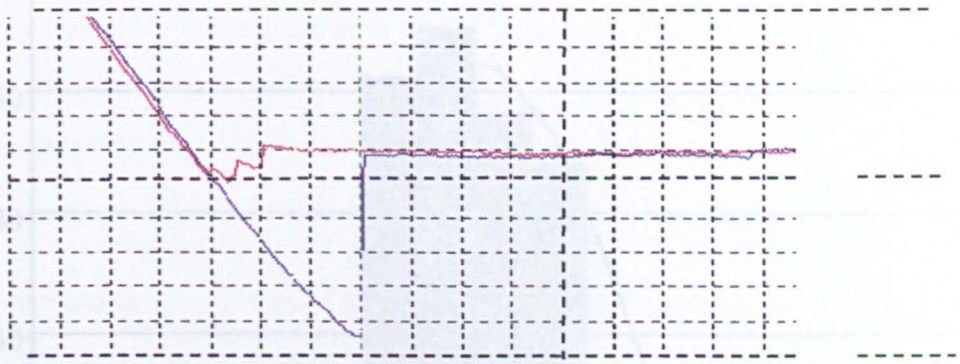

Maximum adhesion = 0.423 ± 0.075 nN
Energy = 7.347 ± 2.646 aJ

b)

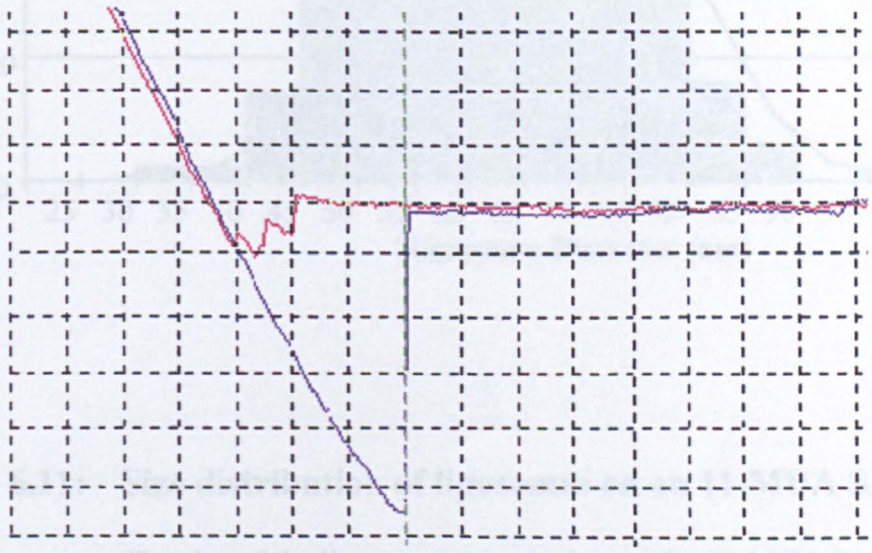

Maximum adhesion = 0.690 ± 0.068 nN
Energy = 30.33 ± 4.95 aJ

x scale = 5.00 nm / division in both cases

Figure 6.10 : Typical force-distance curves of a dodecanethiol surface :
(a) before cationic liposome deposition
(b) after cationic liposome deposition

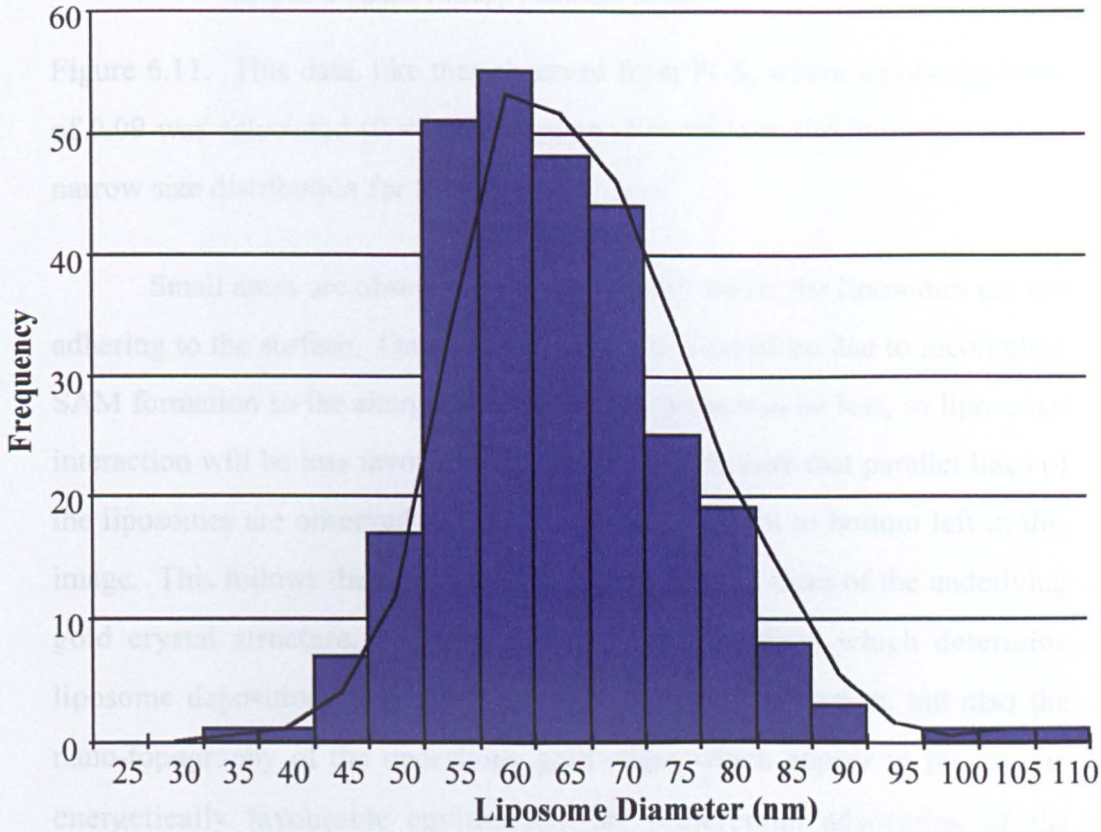

Figure 6.11: Size distribution of liposomes on an 11-MUA SAM

The size of the liposomes adsorbed on to the 11-MUA SAM correlates well to solution values obtained from zeta sizing which gave a diameter of between 75 - 77 nm for the cationic liposomes

Figure 6.11. This data, like that observed from PCS, where a polydispersity of 0.09 was calculated (0 = no dispersion, 1 = random distribution) shows a narrow size distribution for these entities.

Small areas are observed in Figure 6.9 (b) where the liposomes are not adhering to the surface. One explanation for this could be due to incomplete SAM formation so the charge density in these areas will be less, so liposomal interaction will be less favoured. It is interesting to note that parallel lines of the liposomes are observed in the direction of top right to bottom left in this image. This follows the direction of one of the crystal faces of the underlying gold crystal structure. This suggests that contributions which determine liposome deposition, not only arise from the SAM formation, but also the nano-topography of the underlying gold edges which appear to provide an energetically favourable environment for preferential adsorption of the liposomes.

Reproducible and clear images of the liposomes on the amino terminated SAM were difficult to obtain in tapping or contact mode due to sweeping of the entities on the surface as can be observed from Figure 6.9 (c) and Figure 6.12. This suggests that the interaction between the cationic liposomes and the amino terminated SAM are weak, allowing the lateral forces of the imaging AFM tip to displace the liposome structure. The images obtained of the liposomes on this surface also appear to change with time. Initially, spherical entities of 71 ± 12 nm which correlate well with data obtained from PCS (75 - 77 nm) are observed as shown in Figure 6.12 (a). After approximately 5 - 10 min images such as those in Figure 6.9 (c) and Figure 6.12 (b) were obtained. These entities have a size distribution of 175 ± 96 nm as shown in Figure 6.13. The liposome mean diameters observed after 5 - 10 min incubation period on the $C2NH_2$ surface are significantly larger than

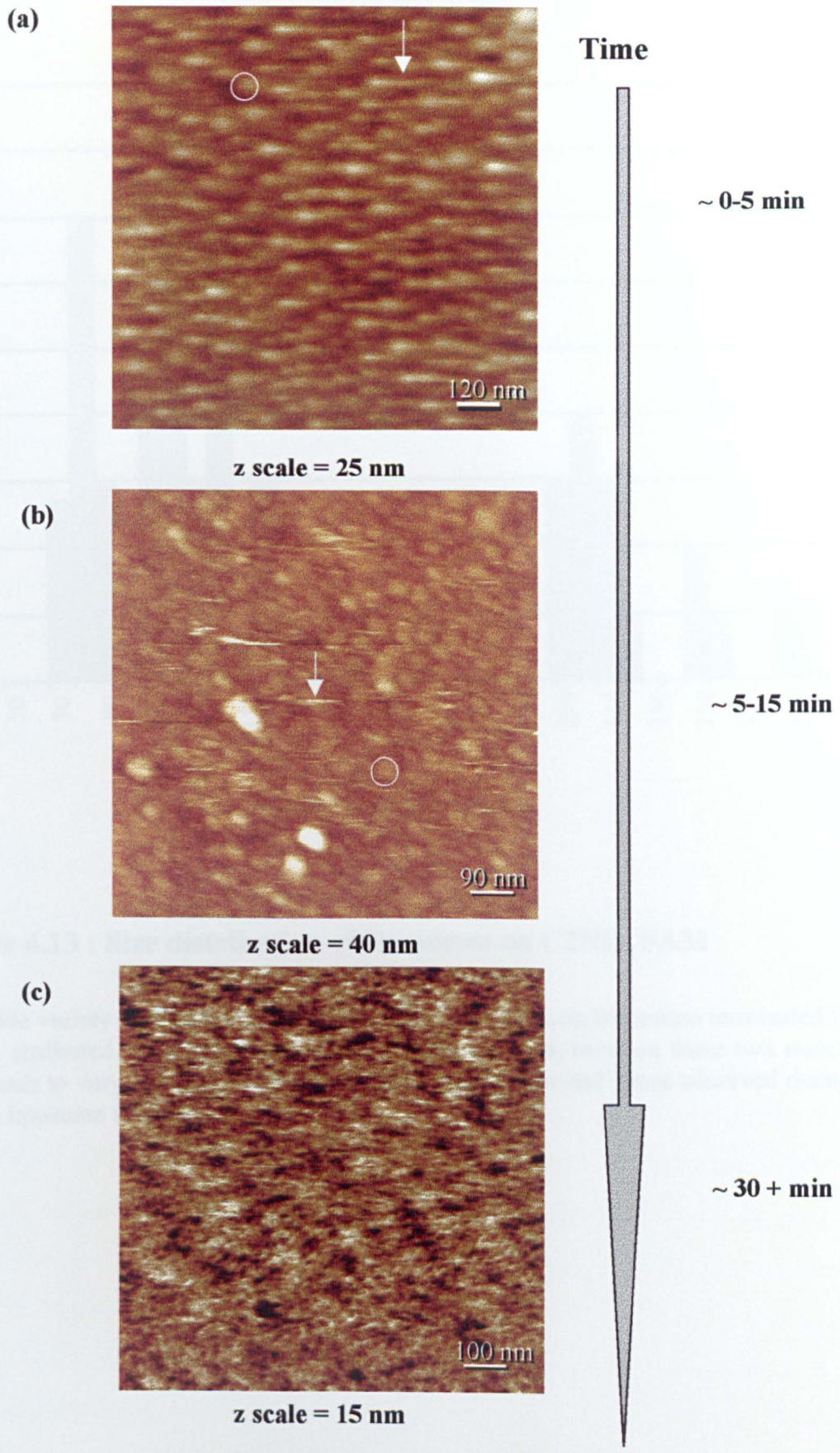

Figure 6.12 : Images of liposomes on amino terminated SAM. Effect of time on structure observed

Images taken in Tapping™ mode in liquid

○ Liposome structure

→ Sweeping caused by weak interaction

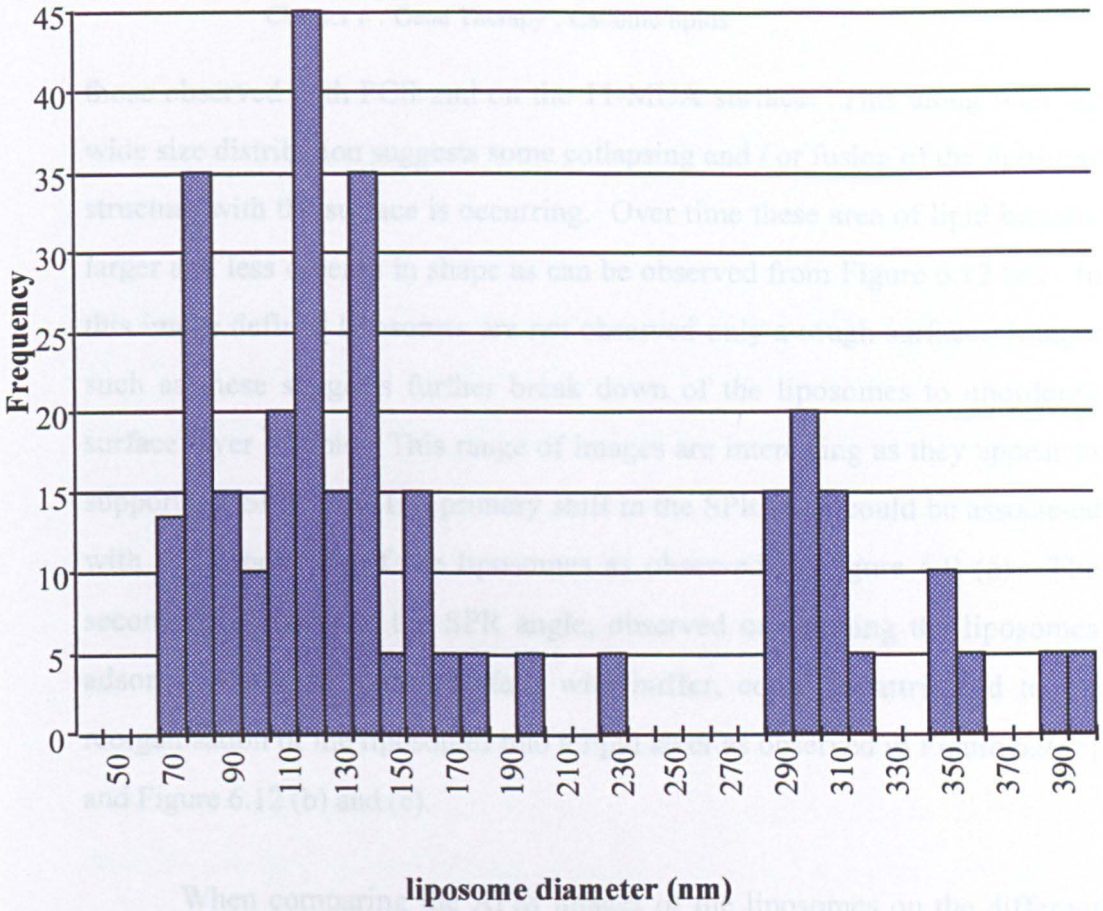

Figure 6.13 : Size distribution of liposomes on $C2NH_2$ SAM

The wide variety of diameters observed for the liposomes on the amino terminated SAM maybe attributed to the unstable nature of the interaction between these two materials. This leads to varying degrees of collapse of the liposomes and hence observed diameters for the liposome structures.

those observed with PCS and on the 11-MUA surface. This along with the wide size distribution suggests some collapsing and / or fusion of the liposome structure with the surface is occurring. Over time these area of lipid became larger and less ordered in shape as can be observed from Figure 6.12 (c). In this image defined liposomes are not observed only a rough surface. Images such as these suggests further break down of the liposomes to unordered surface layer of lipid. This range of images are interesting as they appear to support the SPR data. The primary shift in the SPR trace could be associated with the deposition of the liposomes as observed in Figure 6.9 (a). The secondary increase in the SPR angle, observed on washing the liposomes adsorbed onto the amino surface with buffer, could be attributed to the reorganisation of the liposomes into a lipid layer as observed in Figure 6.9 (c) and Figure 6.12 (b) and (c).

When comparing the AFM images of the liposomes on the different SAM surfaces, their coverage and integrity appears to correlate with the change in SPR angle observed for the adsorption of the entities to the three different surface types. The lowest SPR shift is for the interaction of the cationic liposomes on the C12Me surface. The liposomes on this surface seem to form a hybrid monolayer, which although relatively dense will produce the thinnest layer giving rise to the relatively low SPR shift of 120 ± 25 mDA. A shift of 220 ± 25 was obtained for the liposome on the $C2NH_2$ surface. This will correspond to the thicker layer formed by the collapsed lipid structures observed at later time point images on the AFM (Figure 6.9 (c) and 6.12 (b)). The further increase in change of SPR angle to 311 ± 29 mDA for the 11-MUA surface can be attributed to the densely packed, thick layer of complete liposomes.

6.3.5 : AFM - imaging and force-distance studies of DNA on SAM surfaces

As well as investigating the structure of the liposomes prior to complexation with the DNA, the structure of DNA was also investigated prior to its formulation with the liposomes. The visualisation of DNA was only investigated on the $C2NH_2$ surface as this was the only surface from SPR which showed an interaction with the DNA. As can be observed in Figure 6.14 it was difficult to obtain clear images of the DNA on the $C2NH_2$ surface, when imaged in either tapping or contact modes under liquid. In some images, as observed in Figure 6.14 string and globular-like entities (marked with arrows) which could be the supercoiled plasmid DNA in the are observed, which were not present on control images of this surface as can be observed from Figure 6.8. However, due to sweeping, which occurred even at low contact forces, this could not be confirmed. The observed sweeping suggests that DNA is bound to the $C2NH_2$ surface but the interaction is weak. Further evidence in the form of force distance curves also suggest that DNA was interacting with the $C2NH_2$ SAM. Figure 6.15 shows typical force-distance curves on the $C2NH_2$ surface before (a) and after (b) DNA deposition. In (a) an interactive force with an average of 7.3 ± 2.9 nN can be observed. At this pH the SiN AFM tip is negatively charged and the amino SAM surface is positively charged, promoting a strong attractive force. However, after DNA deposition the retract curve significantly changes its shape. The whole retract curve hysteresis is longer and multiple pull-offs are observed. This is attributed to the DNA acting like a polymer and stretching and rupturing between the surface and tip in a similar manner to that described by Ortiz and Hadziioannou for poly(methacrylic acid) strands (Ortiz (1999)).

The images obtained of DNA on the amino SAM surface are not of

(a)

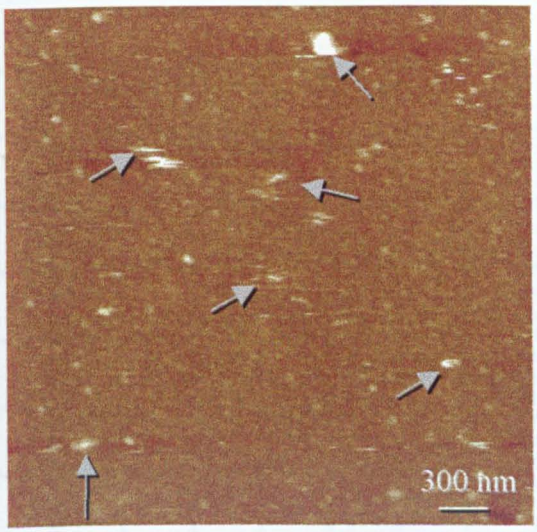

z scale 15 nm

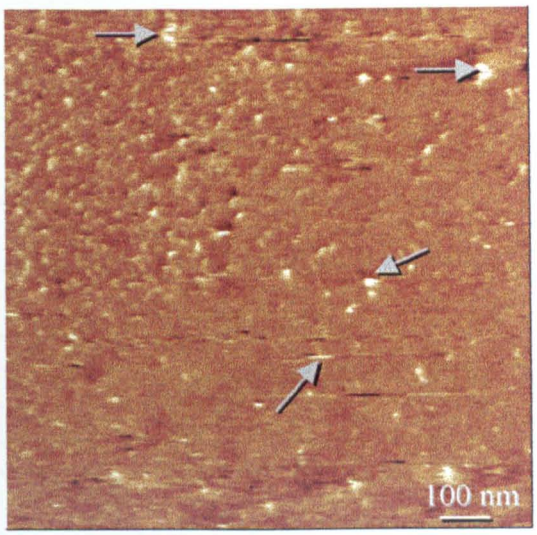

z scale 10 nm

(b)

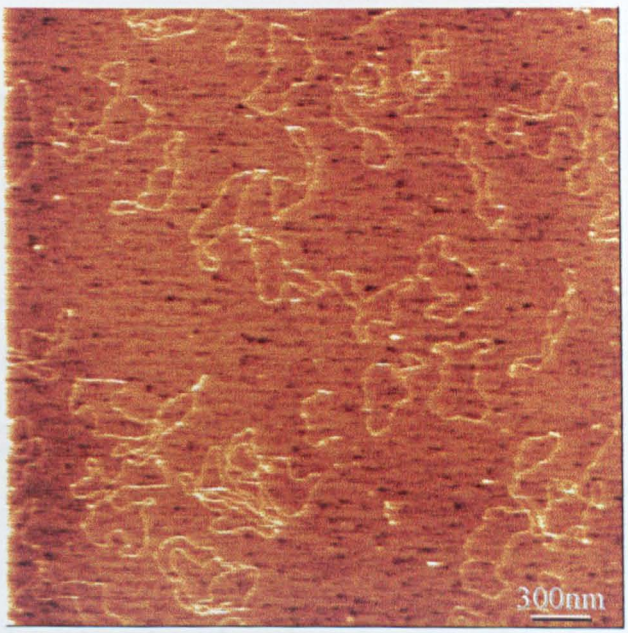

z scale 4 nm

Figure 6.14 : Images of DNA

(a) adsorbed to $C2NH_2$ surface
(b) on mica in 20 mM Tris, 2.5 mM MgCL2 (pH 8.0)

arrows in Figure 7.13 (a) represent entities in image which could be associated with DNA

(a)

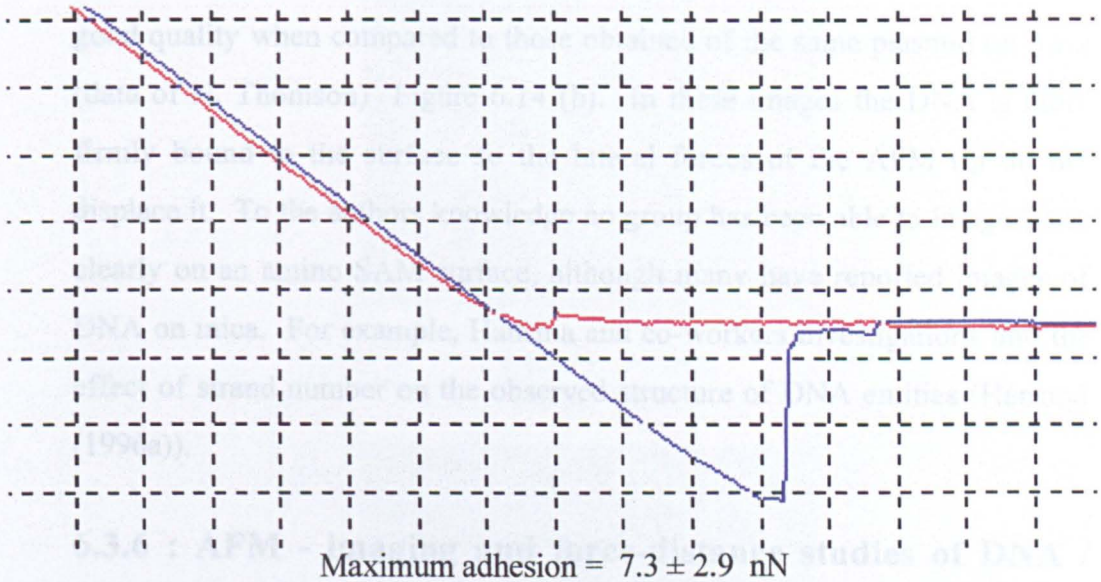

Maximum adhesion = 7.3 ± 2.9 nN
z scale =10 nm / division

(b)

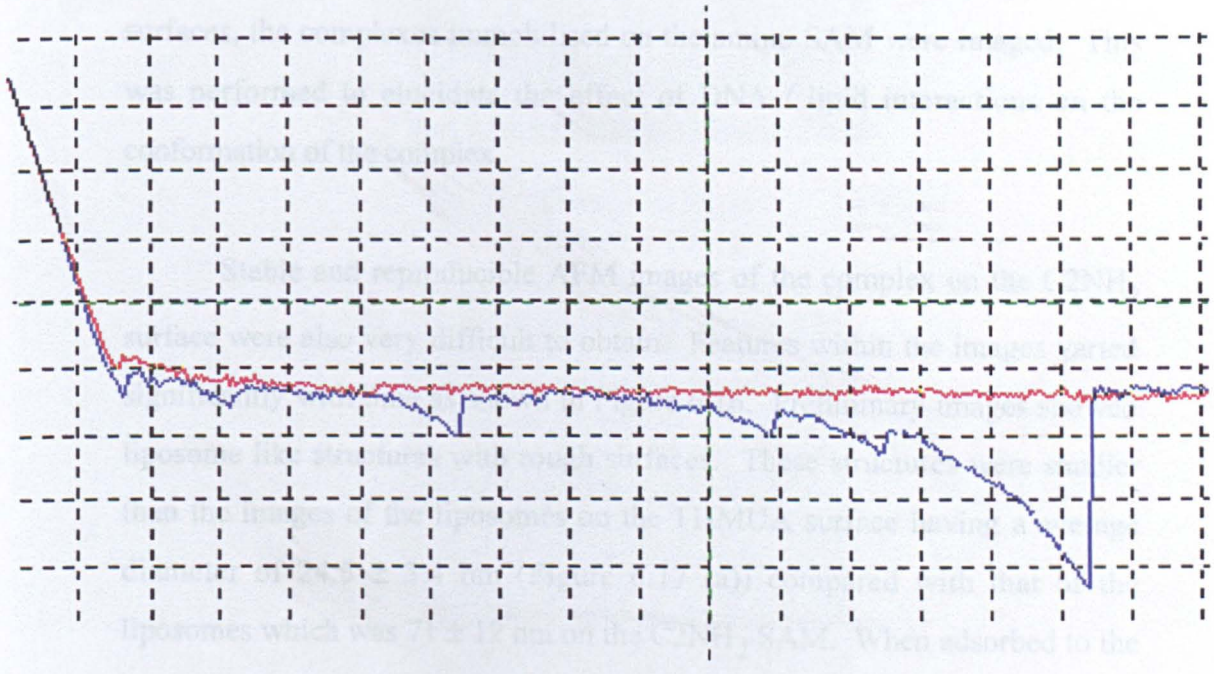

x scale = 5.00 nm / division

Figure 6.15 : Force-distance curves of a 2-aminoethanthiol surface :
(a) before DNA deposition
(b) after DNA deposition

good quality when compared to those obtained of the same plasmid on mica (data of N. Thomson) Figure 6.14 (b). In these images the DNA is more firmly bound to the surface so the lateral forces of the AFM tip do not displace it. To the authors knowledge no group has been able to image DNA clearly on an amino SAM surface, although many have reported images of DNA on mica. For example, Hansma and co-workers investigations into the effect of strand number on the observed structure of DNA entities (Hansma (1996a)).

6.3.6 : AFM - imaging and force-distance studies of DNA / cationic lipid complex on amino SAM surface

After obtaining control images of the liposome and DNA on the SAM surfaces, the complexes immobilised on the amino SAM were imaged. This was performed to elucidate the effect of DNA / lipid interactions on the conformation of the complex.

Stable and reproducible AFM images of the complex on the $C2NH_2$ surface were also very difficult to obtain. Features within the images varied significantly with time as shown in Figure 6.16. Preliminary images showed liposome like structures with rough surfaces. These structures were smaller than the images of the liposomes on the 11-MUA surface having a average diameter of 24.5 ± 3.4 nm (Figure 6.17 (a)) compared with that of the liposomes which was 71 ± 12 nm on the $C2NH_2$ SAM. When adsorbed to the $C2NH_2$ surface however this structure does not appear to be stable. As time passes the structures loose their surface roughness and their diameter increases to 71.8 ± 5.6 nm (Figure 6.17 (b)) which is in close correlation to that of the free liposomes but slightly smaller than PCS size of the complex in solution of 117 nm (polydispersity = 0.25) (Bristol Colloid Centre (1998)).

(a)

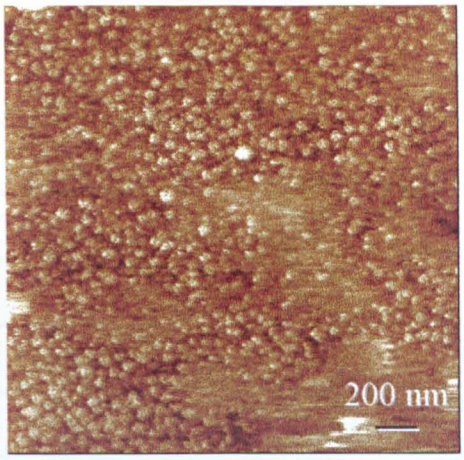

Size of complex =
24.49 ± 3.37 nm

Time ~ 2-5 min
z scale = 40 nm

(b)

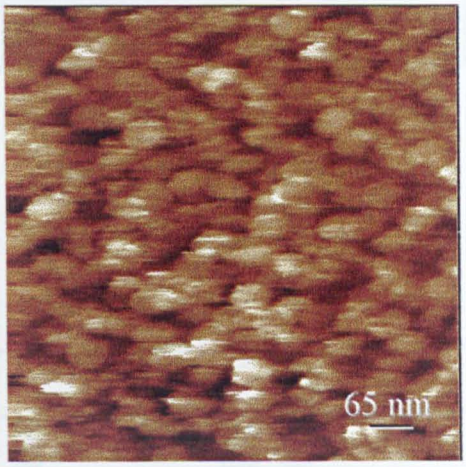

Size of complex =
71.84 ± 5.60 nm

Time ~ 5-15 min
z scale = 40 nm

(c)

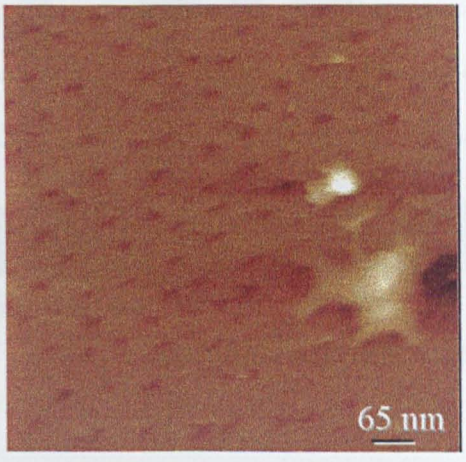

Time ~ 15-30 min
z scale = 20 nm

Figure 6.16 : Images of the complex on the 2-aminoethanethiol surface after varying periods of time.

Images taken in contact and Tapping™ mode under Tris buffer

(a)

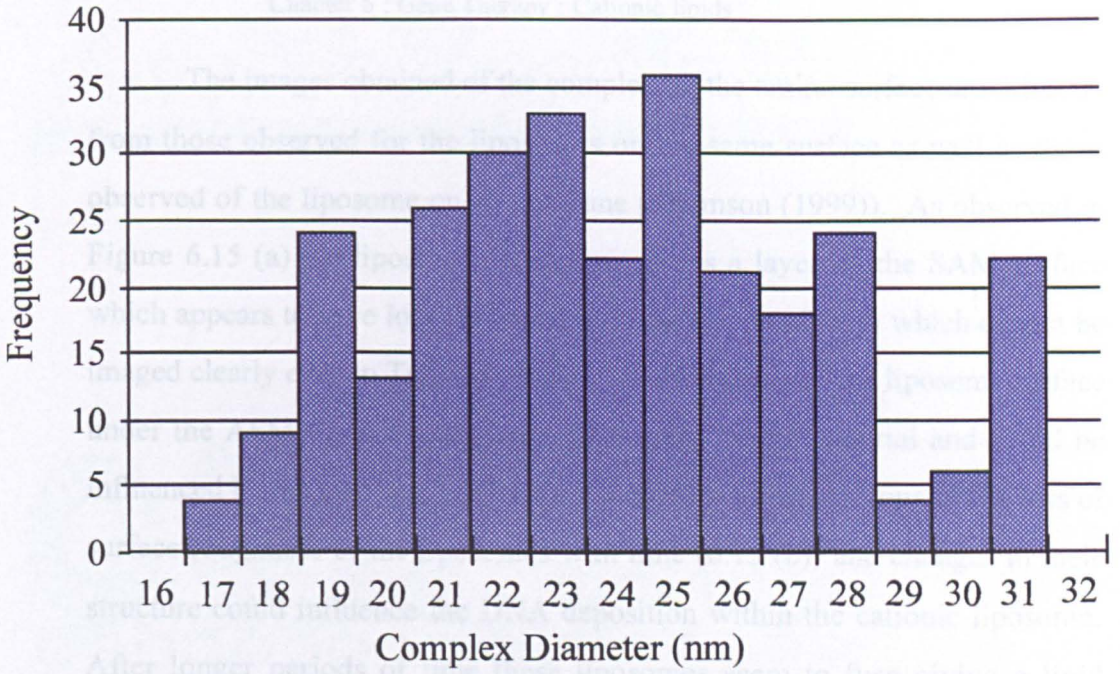

(b)

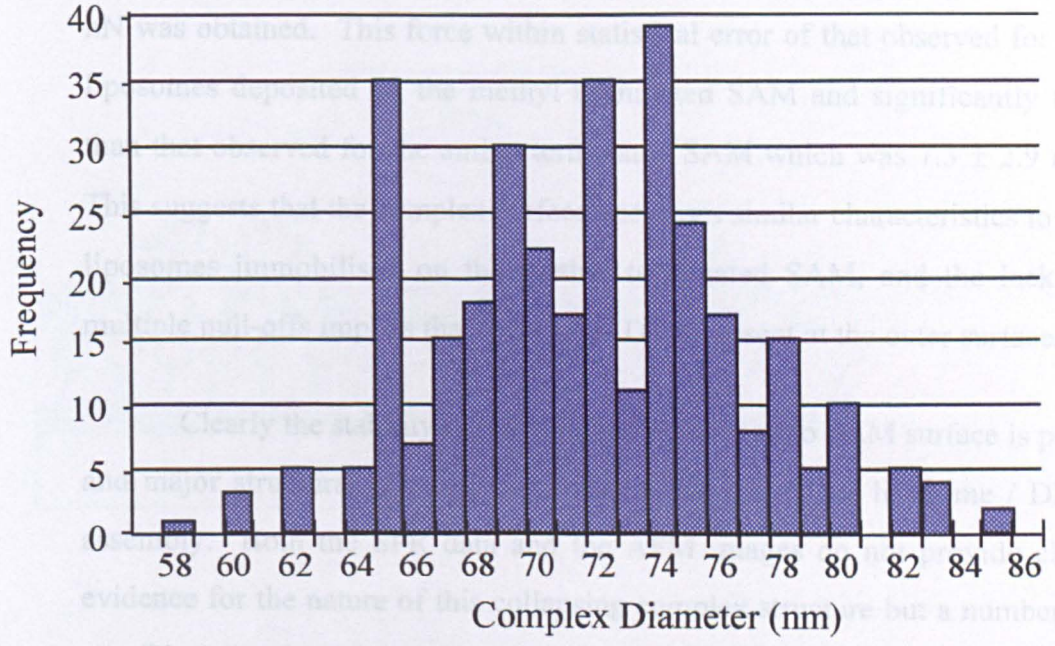

Figure 6.17 : Size distribution for complex structures from early time point images
(a) Distribution from images as Figure 6.16 (a)
(b) Distribution from images as Figure 6.16 (b)

The images obtained of the complex on the amino surface are different from those observed for the liposomes on the same surface as well as those observed of the liposome on aminosilane (Thomson (1999)). As observed in Figure 6.15 (a) the liposome component forms a layer on the SAM surface which appears to have loosely bound material on top of them which cannot be imaged clearly even in Tapping™ mode. This blurring of the liposome surface under the AFM tip is characteristic of loosely bound material and could be influenced by the presence of DNA at the surface of the liposome. The loss of surface roughness of the liposomes with time (6.15 (b)) and changes in their structure could influence the DNA deposition within the cationic liposome. After longer periods of time these liposomes seem to fuse giving a lipid covered SAM surface (Figure 6.15 (c)). On performing force-distance curves on this surface a single pull-off with maximal adhesion force of 0.835 ± 0.098 nN was obtained. This force within statistical error of that observed for the liposomes deposited on the methyl terminated SAM and significantly less than that observed for the amino terminated SAM which was 7.3 ± 2.9 nN. This suggests that the complex surface possesses similar characteristics to the liposomes immobilised on the methyl terminated SAM, and the lack of multiple pull-offs implies that there is no DNA present at the outer surface.

Clearly the stability of the complex on the amino SAM surface is poor and major structural rearrangements are occurring in the liposome / DNA assembly. Both the SPR data and the AFM images do not provide clear evidence for the nature of this collapsing complex structure but a number of possible scenarios may exist. Figure 6.18 shows schematic representation of the one potential explanations, this figure shows that on binding to the surface the DNA which may be associated with the surface of the complex, preferentially binds to the SAM altering the conformation of the liposome, which in turn is destabilised by this and rearranges to form a lipid layer on top

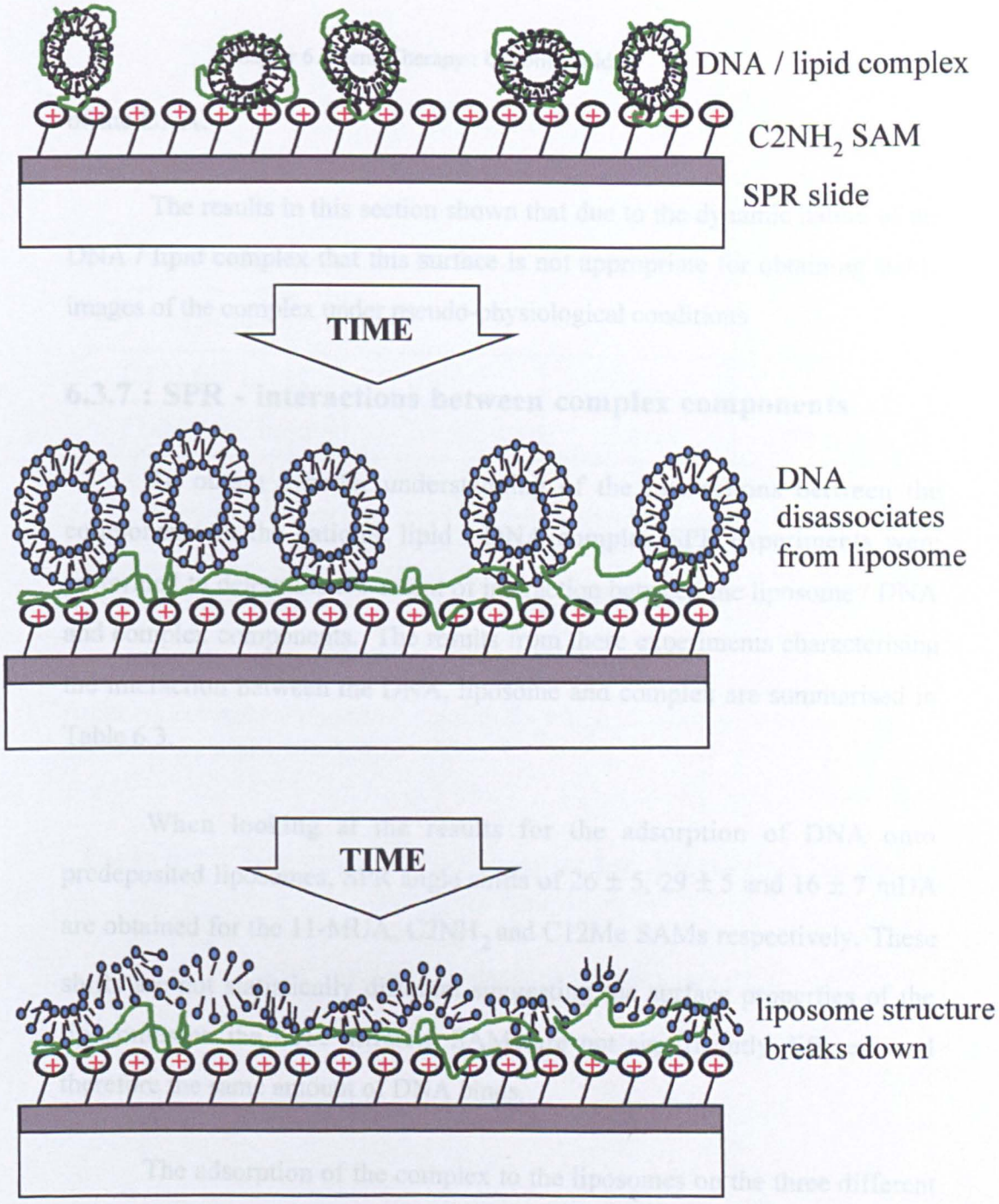

Figure 6.18 : Schematic representation of proposed interaction of complex with 2-aminoethanethiol surface over time

of the DNA.

The results in this section shown that due to the dynamic nature of the DNA / lipid complex that this surface is not appropriate for obtaining stable images of the complex under pseudo-physiological conditions

6.3.7 : SPR - interactions between complex components

To obtain a better understanding of the interactions between the components in the cationic lipid / DNA complex SPR experiments were performed to determine the extent of interaction between the liposome / DNA and complex components. The results from these experiments characterising the interaction between the DNA, liposome and complex are summarised in Table 6.3.

When looking at the results for the adsorption of DNA onto predeposited liposomes, SPR angle shifts of 26 ± 5, 29 ± 5 and 16 ± 7 mDA are obtained for the 11-MUA, $C2NH_2$ and C12Me SAMs respectively. These shifts are not statistically different suggesting the surface properties of the liposomes on the three different SAMs are not significantly different and therefore the same amount of DNA binds.

The adsorption of the complex to the liposomes on the three different surface types produces significantly different SPR shifts dependant on surface type to which the liposomes are adsorbed. The lowest shift is obtained on the C12Me surface of 14 ± 1 mDA and higher shifts of 44 ± 5 and 38 ± 5 mDA were observed on the 11-MUA and $C2NH_2$ surfaces respectively. These shifts could be accounted for by the topography of the liposomes adsorbed on the different SAMs as discussed in section 6.3.4. The topology of the liposomes on the C12Me surface produces a planar surface with lower surface

Solution Species --- Surface	DNA	Liposome	Complex
C12Me / Lipid	16 ± 7	N/A	14 ± 1
11-MUA / lipid	26 ± 5	N/A	44 ± 5
$C2NH_2$ / lipid	29 ± 5	N/A	38 ± 5
$C2NH_2$ / DNA	N/A	365 ± 30	(4)
$C2NH_2$ / complex	0	302 ± 22	N/A

Numbers in brackets represent initial shifts which returned to baseline levels on washing surface with buffer

Table 6.3 : Summary of SPR results for interaction between complex fractions

values = average ± 1 standard deviation ($n \geq 27$)

area to that of the liposomes adsorbed on the other two SAMs, where the liposomes are bound as either complete or partially fused entities. Therefore there will not be such an opportunity for the complex to bind to the lipid coated C12Me surface so the observed change in SPR angle will be lower than that for the other two surfaces.

A small interaction of the complex is observed on the $C2NH_2$ SAM coated in DNA (~ 4 mDA). However, during the buffer wash this is seen to decrease to baseline levels. This suggests that only a weak interaction exists between the DNA and complex structure.

Results for liposome deposition on both the DNA and complex surface produce similar shifts of 365 ± 30 and 302 ± 22 mDA respectively. These shifts are similar to those obtained for the adsorption of the liposomes onto the 11-MUA surface which gave a shift of 311 ± 29 mDA. This suggests that the liposomes are adsorbing to these surfaces as complete entities.

6.4 : Conclusions

6.4.1 : Imaging of gene therapy constructs under pseudo-physiological conditions

As introduced in section 6.1.4, there were two main aims to the work in this chapter. The first of these was to find a method by utilising SAMs as model surfaces to successfully image the intact liposomes, DNA and complex under physiological conditions. The success of these investigations varied depending on the entity and surfaces used.

When imaging the complex and DNA none of the SAM surfaces used were able to act as surfaces for immobilising the entities to obtain reproducible images. In the case of the DNA, where imaging was performed on the amino SAM only, the DNA was swept by the lateral forces of the tip scanning. It was suggested that this sweeping was due to weak interactions between the DNA and amino terminated SAM.

In the case of the complex, images of spherical entities with diameters of similar magnitude to those obtained form PCS were observed. However, these images were not stable over relatively short time periods. This suggested that the interaction between the complex and the amino terminated SAM destabilised the interactions between the lipids in the liposome and the liposome and DNA which resulted in the collapse of the complex and hence lead to the unstable images obtained.

A more positive result was obtained for imaging of the liposomes on the SAM surfaces. In this case, when utilising a carboxyl terminated SAM, reproducible images of the liposomes with diameters in close correlation to those obtained from PCS data were obtained. These structures were stable over time. It was interesting to note that the liposome appear to preferentially adsorbed to areas of the SAM located on crystal edges of the underlying gold. This suggests that surface topography plays an important role in the adsorption of these entities to surfaces.

6.4.2 : Investigations into interactions with model surfaces

The second aim of this chapter was to utilise SAMs to investigate the interaction of the complex and its component parts with a range of model surfaces, and hence obtain preliminary knowledge of how these structures may

interact with the cell membrane. This could in turn provide information of the processes by which cells may internalise these gene therapy vectors. This aim was more successfully achieved.

When considering the liposomes interactions three statistically different results as measured by SPR on the three SAMs surfaces were obtained for their overall extent of interaction. The least interaction was observed for the methyl terminated SAM followed by the amino with the largest interaction being for the carboxyl terminated SAM. In the case of the methyl and amino terminated SAMs the change in SPR angle was biphasic. This suggests more than one process was occurring at the surface on the introduction of the liposomes to the system. SPR results were consolidated by AFM imaging and force distance measurements.

AFM images of the methyl terminated surface appeared to look the same before and after liposome deposition. However, AFM force-distance curves taken after the liposome deposition showed a significantly higher adhesion to the surface than those obtained before. This, along with the small SPR shift for liposome deposition on this surface lead to the conclusion that a hybrid monolayer had been formed with the cationic heads of the lipid being uppermost. This would promote the larger adhesion force observed with the negatively charged AFM tip after liposome deposition, and the biphasic SPR trace which could associated with initial binding then fusing of the liposomes on the methyl terminated surface.

The increased magnitude of the SPR shift on the amino terminated SAM was associated with the initial absorption of liposomes onto the SAM surface but as observed from AFM images these adsorbed entities were not stable and degraded possibly forming a lipid bilayer on the surface of the

SAM. This degradation process was associated with the secondary increase in SPR angle on washing buffer over the liposomes surface in SPR experiments.

As discussed above, liposomes on the adsorbed as complete entities on the carboxyl terminated SAM. This would account for the large monophasic SPR shift observed for the interaction of the liposomes with this surface.

The complex and DNA were only observed to interact with the amino terminated SAM. This shows that their surface charge and conformation limits the extent of their hydrophobic interactions. The rate at which these two entities, as well as the liposomes adsorbed to this surface were different. The complex rate being between that for the DNA and liposomes. This suggested that the complex possessed surface characteristic drawn from both its DNA and liposome constituents.

In summary, although clear images of all the entities investigated were not obtained, significant information on their surface interactions was gleaned and results obtained from two different techniques, namely SPR and AFM produced complementary results. The results obtained in the investigations performed in this chapter provide a basis for understanding this systems interactions with more complicated surfaces such as that of the cell membrane.

Chapter 7 : Polymers as drug delivery vehicles - dendrimers

7.1 : Introduction

The class of polymers termed as not only dendrimers but also starburst polymers, molecular trees, arborols and cauliflowers has developed into a major new group of polymeric materials since their first synthesis in 1978 by Vögtle (Buhlein (1978)). However, their familiar name dendrimer was not coined until 1984 by Tomalia. Its origins come from the Greek *dendri*tic or dendron, meaning tree and the suffix from oligo*mer* representing the smallest structural repeat unit of the macromolecule (Tomalia (1984)). Unlike previously known groups of polymeric materials as summarised in Figure 7.1, dendrimeric polymers can be viewed as defined polymers with molecular architectures in which molecular information is transferred between generations (sets of monomer units) which emanate from a central core or germ (seed). This molecular information includes factors concerned with flexibility, shape, size, topology and surface characteristics, such that this family of polymers can be manipulated to form discrete nanoscopic entities (Tomalia (1994)).

This fourth class of dendrimeric polymers as depicted in Figure 7.1 gave rise to a new philosophy of macromolecular isomerism, where the macromolecular architecture is viewed as a third element of polymeric structure with the first two being elemental composition and molecular weight distribution (Dvornic (1996)). For example, polymers may have the same repeat units and molecular weight but if their molecular architecture is different they will possess different properties and behave differently on the macroscopic scale. When considering a dendrimer's molecular architecture three main factors need to be considered. The core, or seed from which the dendrimer will grow, the type of monomer unit and degree of branching or generation number. The core molecule defines the number of primary branches. The monomer defines the bulk and surface characteristics of the dendrimer. The degree of branching or generation of the dendrimer defines its size, flexibility and shape. These factors are depicted schematically in Figure 7.2.

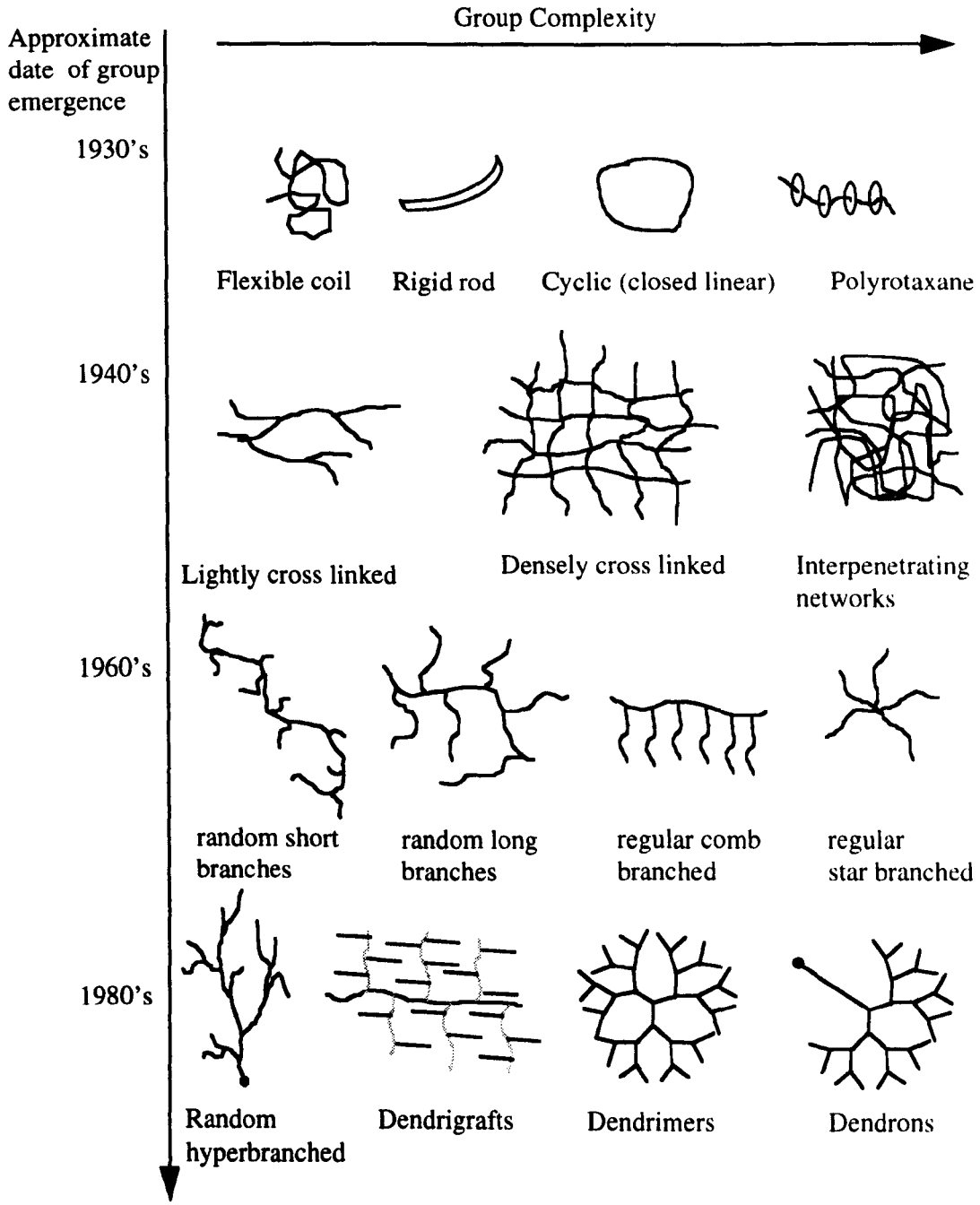

Figure 7.1 : Summary of polymer groups (adapted from Dvornic (1996))

Degree of branching or generation number

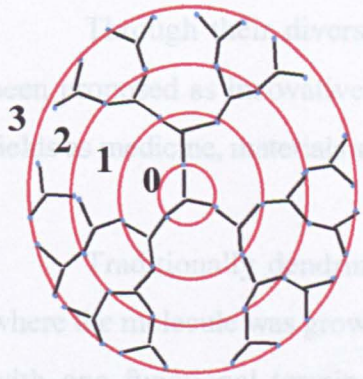

Numbers represent generation number which is representative of the number of sets of monomer units added to the core molecule

core functionality

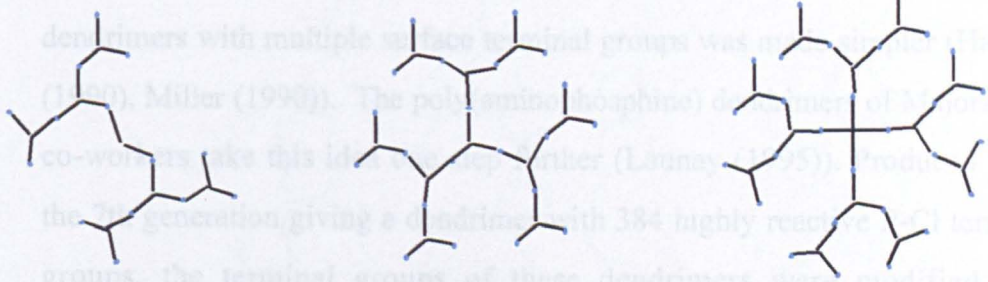

Two pronged core Three pronged core Four pronged core

Monomer type

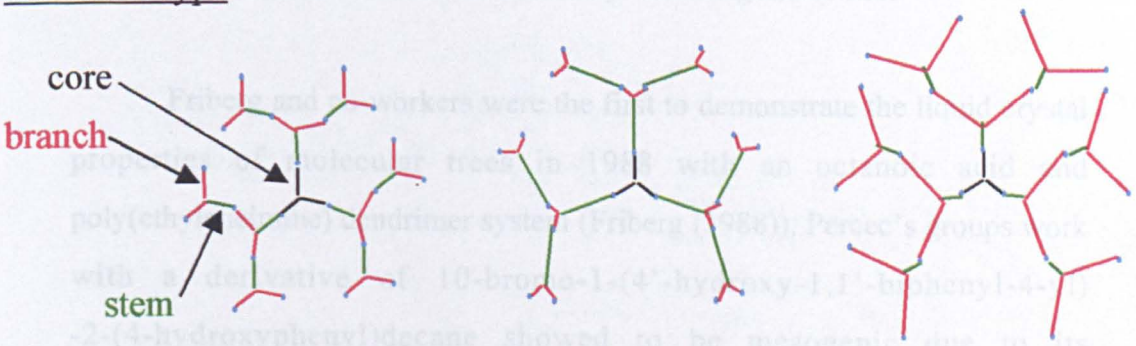

Equal length branches and stem Short branches and long stem Long branches and short stem

Figure 7.2 : The effect of core repeat group and generation number on the architecture of dendrimers

7.1.1 : Dendrimer synthesis and uses

Through their diverse, yet distinct characteristics, dendrimers have been proposed as innovative molecules for solving problems in such diverse fields as medicine, materials science, agrochemistry and electronics.

Traditionally dendrimers were synthesised by the divergent method where the molecule was grown from the core. This led to dendrimers primarily with one functional terminal group type. However, with the convergent method of synthesis, first published by Frèchet and Miller's groups in 1990 where dendrimers were grown from the outside in, the opportunity to produce dendrimers with multiple surface terminal groups was made simpler (Hawker (1990), Miller (1990)). The poly(aminophosphine) dendrimers of Majoral and co-workers take this idea one step further (Launay (1995)). Produced up to the 7th generation giving a dendrimer with 384 highly reactive P-Cl terminal groups, the terminal groups of these dendrimers were modified with *bis*-allylamine to give the first dendrimer possessing two different functional groups at each terminal site. These types of dendrimers have the potential for differing chemistries to be performed on their terminal groups giving complex entities which will mimic intricate naturally occurring molecules.

Friberg and co-workers were the first to demonstrate the liquid crystal properties of molecular trees in 1988 with an octanoic acid and poly(ethyleneimine) dendrimer system (Friberg (1988)). Percec's groups work with a derivative of 10-bromo-1-(4'-hydroxy-1,1'-biphenyl-4-yl) -2-(4-hydroxyphenyl)decane showed to be mesogenic due to its conformational isomerism (as shown in Figure 7.3) Transitions between its nematic and isotropic states is in the region of 20 - 50 °C dependent on the R group, which makes it an interesting candidate for a variety of applications (Percec (1992)).

Various research groups have seen the advantages of the use of

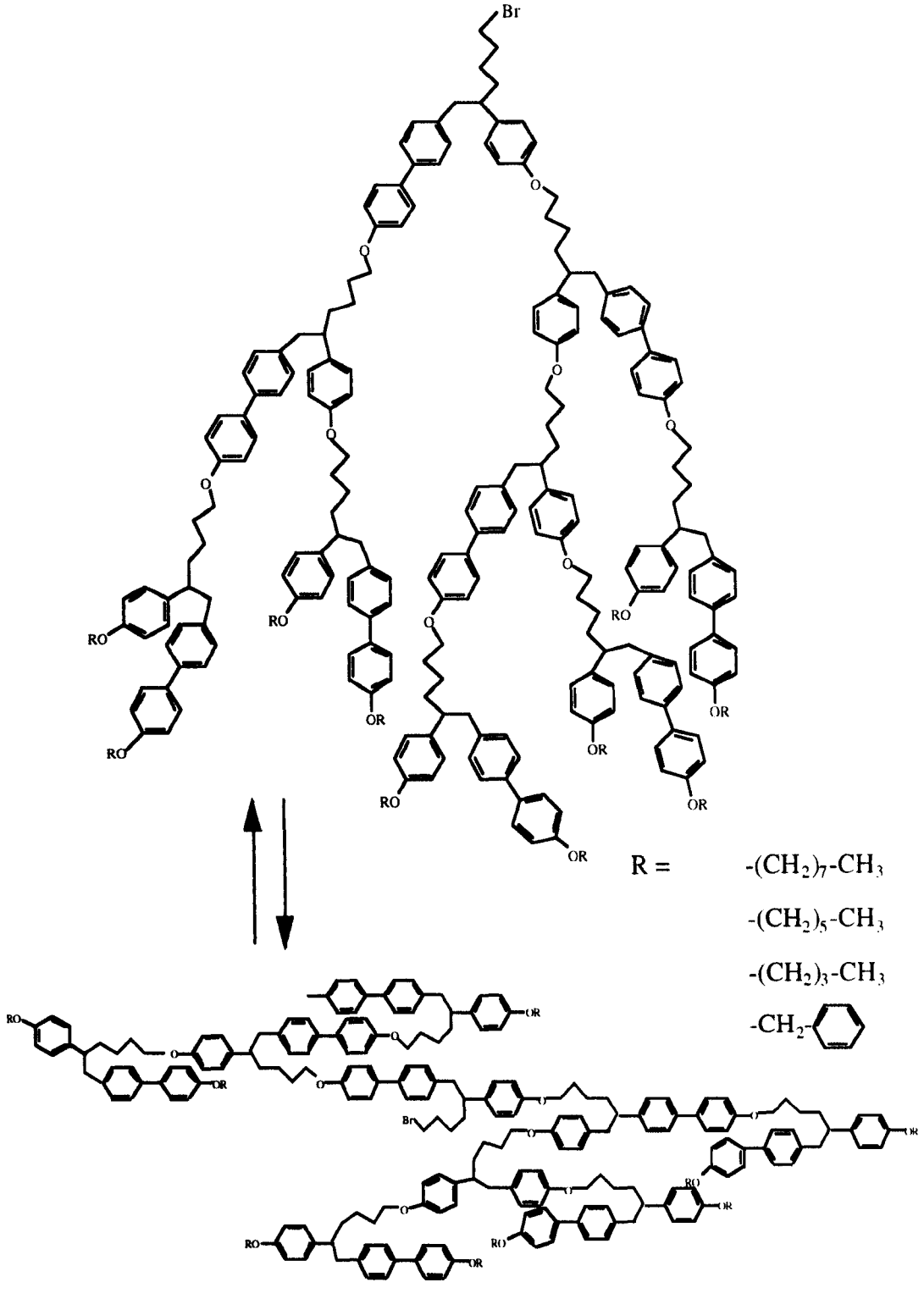

Figure 7.3 : Conformational isomerism of dendimers

dendrimeric catalysts for chemical reactions (Schlenk (1999)). Dendrimers have the advantage over conventional catalysts in better presentation of the catalytically active surface groups and the ease of removal for the product mixture by ultrafiltration (Knapen (1994)). Dendrimeric catalysis have shown their use not only in organic synthesis but in redox-reactions (Van Der Made (1992))

Groups such as Newkome and coworkers, Seebach et al. and McGrath (1998) have reported the production of chiral dendrimers (Newkome (1991), Seebach (1994a), (1994b)). Their use as enantiospecific catalysis has already been demonstrated by Brunner and co-workers amongst others (Brunner (1994a), (1995)). It is hoped that the development of such groups of dendrimers may in the future lead to entities which will possess a chiral shape, or, lead to dendrimeric hosts which will recognise only specific entantiomers of molecules as guests into their internal cavities for use within the biological field (Newkome (1991), Seebach (1994a), (1994b)).

As well as significant research into the synthesis and applications of dendrimers, the use of dendron blocks is also of interest. Dendron blocks connected by a linear polymer have been shown by various groups including Frèchet and co-workers to posses different solution properties, dependent on solvent, due to their amphiphilic nature. It has been suggested that this type of dendritic molecule may be useful as nanoscopic reactors, being able to perform functions not usually associated with molecules of this size (Gitsov (1996)), as well as environmentally sensitive delivery vehicles (Choi (1999)).

As well as being synthesised in solution, solid-phase synthesis of dendrimers has been developed to enable a higher percentage yield of full generations and easier separation of the final product. The solid-phase synthesised glycodendrimers (dendrimers with carbohydrate termini) of Roy and co-workers have been shown to produce chemical entities possessing protein binding properties, whilst seemingly not initiating immunogenic side

effects (Toyokuni (1995)). This makes them potentially useful therapeutic agents for the prevention of infections by bacteria and viruses. Preliminary work by the same group has shown that influenza A strain can be inhibited from infecting human erythrocytes and inhibition of leucocyte adhesion molecules can be achieved by the utilisation of these glycodendrimers (Roy (1996)).

Dendrimers possessing metal ligand complexation sites have not only sparked interest in the electronics field, where they can be used for the spatial manipulating excited energy states and / or charges by utilising a convergent molecular antenna effect (Xu, Z. (1994)), but also in the biological field where dendrimers with porphyrin cores have been proposed as synthetic models for globular haem proteins (Dandliker (1997)).

As alluded to above, the dendrimer structure, which emanates from a core or seed, has been liked to many biological entities such as liposomes and viruses. This biomimicry had lead to the hope that dendrimer polymers may act as important components in synthetic mimics of naturally occurring systems, such as photosynthesis (Issberner (1994)).

The use of dendrimers as polymeric boxes has been exemplified by the work of Meijer and co-workers. Amino acid surface modified dendrimers known as dendritic boxes have been shown to induce a unimolecular encapsulation behaviour. The highly hydrogen bonded and hence almost solid state surface of these entities has been shown to hold 'guest' molecules within the construct even after extensive dialysis to remove them. However, the guest molecules could be released under certain conditions where the surface modification was broken down by partial or full hydrolysis releasing the small and large guest molecules respectively unharmed (Jansen (1995)). The type and number of guest molecule which can be held within dendrimeric constructs depend on the internal volume of the dendrimeric cavity which in turn depends on the macromolecular architecture of the dendritic box. Suggestions for guest

molecules for dendrimer hosts have included inks, as the dendrimer/ink complex will possess a higher viscosity making it a better material for permanent printing, lithography and coating paints, and fluorescent markers and imaging contrast agents for medical imaging techniques such as MRI (Dendritec (1999), (Wiener (1994)). A large research interest has centred on drugs and biological molecules as guest molecules. Wallimann et al. (1996) report the synthesis of water-soluble dendritic cyclophanes termed dendrophanes. These molecules can act as complexing agents for steroids such as progesterone, cortisone and testosterone with binding constants similar to those observed for the free cyclophane core. Other dendrimer families which possess pH-dependent release of the guest molecules have the potential to be used as drug carriers for the endosomal release of drugs (Pistolis (1999)).

As stated above the use of dendrimers within the medical field has a wide variety of applications. The main two are in medical imaging techniques such as MRI as carriers of dyes to increase contrast and as therapeutic agent carriers for not only small molecule drugs such as the use of poly(amidoamine) (PAMAM) dendrimers as carriers of 4-hydroxybenzoate used against coughs (Kuzdzal (1994)) and zinc porphyrin deuterated dendrimers for vitamin K_3 (Jin (1993)), but also carrying agents for radiotherapy (Barth (1994)), cancer chemotherapy (Malik (1999)) and peptide and gene delivery (Bielinska (1996)). Smaller but equally important areas of research in the medical field including the development of immunoassays using dendrimers for increased sensitivity and biotinylated dendrimers as antibody pretargets to improve the selectiveness of radiotherapy in cancer patients, have also been reported lately (Wilbur (1998), Kricka (1999)).

7.1.2 : Characterisation of PAMAM dendrimers

Many reviews such as Dvornic (1996a) and Ardoin (1995) show that a wide variety of both organic and inorganic based dendrimers exist. However, the most widely known and studied are the starburst or PAMAM dendrimers

of Tomalia. The structure of these dendrimers is shown schematically in Figure 7.4. Many investigations have been carried out to determine the solution structure of these molecules such as the series of papers by Tomalia and co-workers using electroparamagnetic resonance (EPR). Results from these investigations showed that the amino terminated or full generation dendrimers bound with copper (II) ions both internally and externally. The amount bound to the terminal amino groups decreases from pH 3.5 until, at pH 6 and above. The only copper ions bound to the dendrimer were present as the internal Cu-N_4 complex (Ottaviani (1997a)).

With the half generation or carboxyl terminated dendrimers, structural information was also gleaned from studies with Cu (II). These studies showed three different complexing states for the Cu (II) to the dendrimer. The presence of these were defined by pH, temperature and dendrimer generation. Results show that the dendrimer posses different conformations below and above generation 3.0. However, later papers and investigations by other experimental and theoretical groups quote that this conformational change from open, flexible, discoid structure to rigid and less penetrable spheres occurs anywhere between generation 3.0 and 4.5 (Ottaviani (1994), Naylor (1989)).

Mn (II) ions were only seen to complex to the carboxyl terminated PAMAMs. Information on dendrimer structure was again obtained. This showed the PAMAMs to be more flexible below generation 4.5 and as rigid spheres above. The effect of the high charge density on the surface of the larger generation dendrimers was also noted by the distortion from cubic symmetry of the Mn (II) environment (Ottaviani (1996)).

The aggregation profile of the positively charged surfactants and the anionic carboxyl terminated dendrimers has also been studied by EPR. The surfactants are seen to aggregate at lower concentration in the presence of the dendrimers. The extent of decrease in the concentration where aggregation occurs was observed to be related to dendrimer generation. The form of the

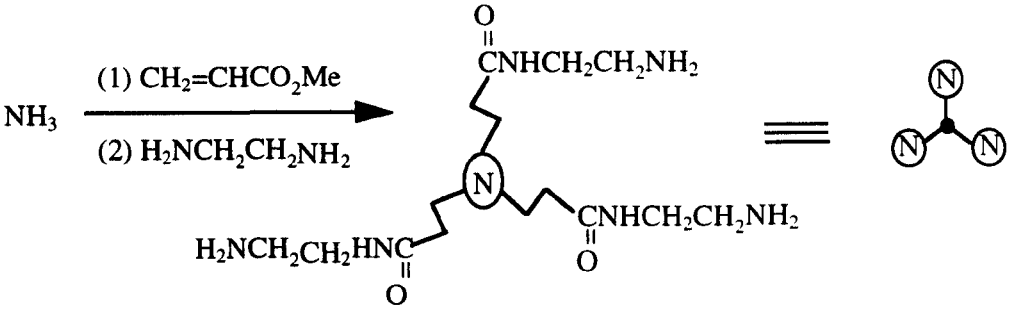

Generation 0 or the core

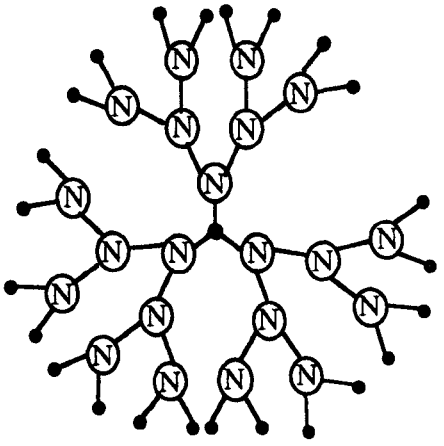

Schematic representation of a genration
3.0 or 3.5 PAMAM dendrimer

= N-CH_2-CO-NH-CH_2-CH_2-N

Full generation (n.0) = N-H

Half generation (n.5) =N-CH_2-CH_2-CO_2- Na^+

Figure 7.4 : Schematic representation of the PAMAM dendrimer

surfactant micelle interacting with the dendrimer also depends on the dendrimer generation and solution concentration (Ottaviani (1997b)).

Work with 4-ammonio-2,2,6,6,tetramethylpiperidine-*N*-oxyl iodide derivatives, known as the CAT surfactants, showed that the half generation carboxyl terminated dendrimers possess the ability to interact by both charge and hydrophobic mechanisms (Ottaviani (1995)).

Using potentiometry, tubidimetry and quasi-elastic light scattering techniques, Zhang (1996) showed that binding of poly(diallydimethylammonium chloride) to the carboxyl terminated dendrimers was affected by pH and ionic strength, showing the ionic nature of the interaction. The dendrimer generation and hence surface charge density was also seen to have an effect.

7.1.3 : Applications of the PAMAM dendrimers

As well as their aqueous structure being investigated, PAMAM dendrimers have been probed for their suitability for a range of applications. PAMAM dendrimer films have been prepared by chemical immobilisation to a surface. These PAMAM films can distinguish between volatile organic compounds possessing different functionalities. The system shows a rapid response to the analyst which is reversible on the analytes removal and it has a high signal-to-noise ratio showing the potential of this type of system for uses as chemical sensors and environmental monitoring devices. (Wells (1996)).

As *in vivo* carriers the PAMAM dendrimers, both alone and conjugated to antibodies, have been shown to produce no or minimal cytotoxicity in *in vitro* and *in vivo* testing and were shown to target biological agents to specific cells (Malik (1999), Barth (1994)).

As highlighted earlier, in Chapters five and six, the area of gene therapy

could provide solutions to a number of current clinical problems. PAMAM dendrimers have been shown as effective carries for antisense, oligonucleotides and antisense expression plasmids, producing *in vitro* gene expression (Bielinska (1996)) as well as producing expression from plasmid DNA in eukaryotic cells *in vitro* (Kukowska-Latallo (1996)).

The delivery of peptides and proteins as well as their use in immunoassays is another area where dendrimers could be of advantage. The PAMAMs terminal groups show a high chemical reactivity when compared to the presence of the same groups within other macromolecules (Frèchet (1994)). This allows the conjugation of peptides or proteins in relatively mild conditions so reducing the chances of inactivating them (Singh (1996), (1998)).

By reacting the terminal amino groups of full generation PAMAM dendrimers with epoxyalkanes, reverse micelle type entities have been produced and their potential as carriers of hydrophillic molecules into organic solvents is shown by utilising Cu (II) ions (Sayed-Sweet (1997)).

7.1.4 : Aims of this chapter

The aim of the work presented in this Chapter is to understand the factors effecting the PAMAM dendrimers interactions with surfaces. These factors have wide ranging implications on all biomedical applications of these polymers. The work is biased toward gaining a better insight into the factors which specifically effect the dendrimers interaction with the cell membrane due to the interest in using PAMAM dendrimers not only as gene therapy vectors, but also as hosts for guest drugs such as cisplatin (Malik (1999)). Interactions with the cell membrane are of particular interest as *in vitro* and *in vivo* studies have shown increased benefits in using PAMAM dendrimers as drug carriers and conjugates, but no insight into their cellular uptake mechanism has been demonstrated. The cell membrane is a complex surface, so the work presented here is only a first step towards understanding the

factors effecting interactions with this complex surface. Both carboxyl and amino terminated dendrimers between generation 1.0 and 10.0 were investigated during the course of this work so the effect terminal group, size and flexibility on the interaction with the surfaces could be determined. As described in Chapter 6.1 the model surfaces also utilised in this work were SAMs, due to their ability to provide reproducible and well characterised interfaces. Three different SAMs were utilised namely a carboxyl, amino and methyl terminated SAM. A range of pH's and ionic strengths were investigated so the contribution of both hydrophobic and ionic charge contributions could be quantified. The results from work on the SAMs and preliminary data from work with protein and membrane fraction layers not only give us a basis for a more detailed understanding of the cellular uptake mechanisms of the PAMAM dendrimers, but also provides us with information to improve our chemical synthesis of these molecules to make them better entities for the chosen application.

7.2 : Materials and methods

7.2.1 : SPR

7.2.1.1. : Interactions with SAMs

SAM's of dodecanethiol, 2-aminoethanethiol and 11-mercaptoundecanoic acid were formed as described in 6.2.2. Polymer brush SAM's were prepared from compounds provided by E.Schacht's group at the University of Gent. Denoted by the terms Lan-1 and Lan-2, these products are co-polymers, Lan-1 of dimethylaminoethyl methacrylate and methylthioethyl methacrylate and Lan-2 of methacrylic acid : methylthioethyl methacrylate, both in a 9 : 1 ratio (Figure 7.5). The SPR slides were incubated overnight in a 1 mg / ml solution of either Lan-1 or Lan-2 in HEPES buffer, 250 mM, pH 7.0, washed in buffer and allowed to air dry. PAMAM dendrimer samples were obtained from either Sigma Chemical Company (Poole, Dorset,

a

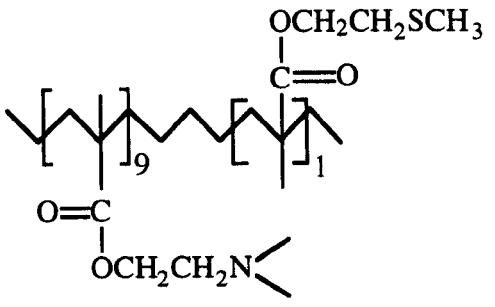

b

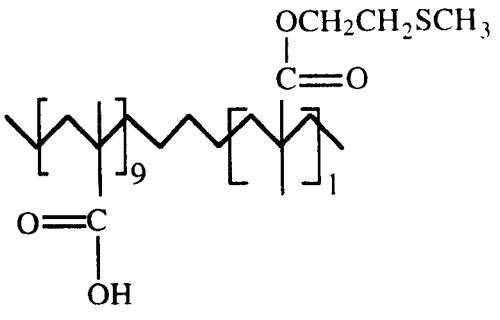

c

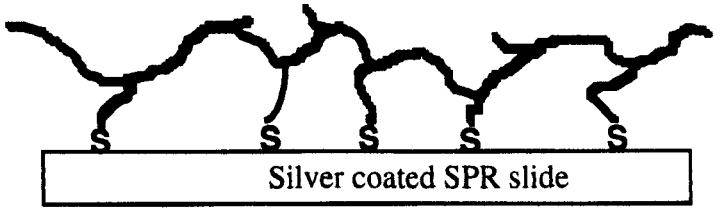

Figure 7.5 : Structure of Lan-1 and Lan-2

a : Lan-1 structure
b : Lan-2 structure
c : Idealised surface structure of Lan-1 and Lan-2 when bound to silver SPR slide

UK.) or Dendritec (Midland, MI, 48642, USA) as methanol solutions. Methanol was removed by blowing nitrogen over the samples. Dendrimer stocks were stored as 10 mg / ml solutions in deionised water at 2-5 °C under a nitrogen atmosphere.

SPR experiments were performed to determine the extent of dendrimer interaction with the models surfaces. A stable baseline was obtained by buffer flow over the chosen SAM prior to a 1 ml injection of the dendrimers (0.1 mg/ml in HEPES pH 7.0, 250 mM). The normal 300 sec buffer wash followed to remove any loosely bound dendrimers from the SAM surface.

7.2.1.2. : Characterisation and interactions with cell membranes

The best deposition criteria for the cell membrane fraction (Élan, Dublin, Ireland), (preparation see Appendix 2) was determined by investigating a variety of factors, namely SAM carbon chain length, membrane fraction protein concentration and flow rate.

Experiments to determine the optimal flow rate for depositing the Caco2 cell membranes were performed utilising dodecanethiol SAMs and the membrane fraction at 1 mg / ml protein concentration. Flow rates of between 10 -250 µl / ml were utilised in experiments where 1 ml of the lipid membrane was injected over the SAM to determine the extent of interaction.

Where the optimal concentration of membrane fraction was to be determined, both dodecanethiol and 11-MUA SAMs were utilised. 1 ml of the CACO2 cell membrane fractions were injected at protein concentrations of between 0.1 -1.75 mg / ml and a flow rate of 0.1 ml / min. The change in SPR angle, indicative of the amount of membrane fraction deposited was measured at the end of the injection and buffer wash.

The last factor investigated was the effect of thiol chain length and hence, hydrophobicity and packing of the SAM. SAMs of octanethiol, dodecanethiol and hexadecanethiol, prepared as section 6.2.1, were utilised. The extent of interaction of the CACO2 cell membrane fraction with these surfaces was determined by injecting 1 ml of the membrane fraction (1 mg / ml) over the their surfaces. The change in SPR angle was measured at the end of the buffer wash.

Prior to performing experiments to determine the dendrimers interactions with CACO2 cell membrane fractions, experiments were performed to model the deposition profile of the membrane fraction onto the SAMs surface as observed from SPR. Phosphatidylcholine (PC) was utilised as a model lipid and human serum albumin (HSA), IgG and fibrinogen were utilised as model proteins. The PC was provided as a chloroform \ methanol solution which was blown under a nitrogen stream to dryness and resuspended in Tris buffered saline (TBS) (10 mM Tris, 150 mM NaCl, pH 7.4) to give the required concentration (0.1 - 4.0 mg / ml). All samples were sonicated for 15 min to ensure a uniform distribution of the lipid. Protein samples of either HSA (1 mg / ml), fibrinogen (1 mg / ml) and IgG (0.5 mg / ml) were prepared as solutions in TBS. A range of lipid / protein mixed solutions were also investigated. These solutions were prepared by forming lipid dispersions at a concentration of 2 mg / ml and adding enough fibrinogen to give ratios of lipid to protein of 4 : 1 to 1 : 3. The interaction of all these was investigated with SAMs of dodecanethiol or 11-MUA prepared as in 6.2.1 utilising SPR.

In all SPR experiments a stable baseline was obtained prior to injection of the lipid, protein or lipid / protein mixtures, prepared as described above. Buffer washes were performed after the sample injection to remove loosely bound material. Both the sample injection and buffer wash as performed at 0.1 ml / min.

For experiments to determine the dendrimer interaction with a lipidic

membrane, 1 ml of CACO2 fractionated cell membranes at a 1 mg / ml protein concentration in TBS (10 mM pH 7.4) was injected at a flow rate of 0.1 ml / min over a 11-MUA or dodecanethiol SAM, prepared as in 6.2.1. A buffer wash (0.1 ml / min, 600 s) was then performed prior to a 1 ml dendrimer injection (0.1 mg / ml in TBS, 10 mM pH 7.4). The dendrimer injection and following 300 s buffer wash were performed at 0.24 ml / min.

7.2.1.3. : Interactions with DNA

Where the extent of DNA binding to PAMAM dendrimers was to be determined, experiments were performed on SAMs of dodecanethiol prepared as in 6.2.1. After obtaining a stable baseline, 1 ml of the dendrimers (0.1 mg / ml in HEPES, pH 7.4, 10 mM) was injected. After the normal buffer wash period 1 ml of pGal plasmid DNA (5 μg / ml in HEPES, pH 7.4, 10 mM) (5.2.1) was injected at a flow rate of 0.1 ml / min to allow binding to the dendrimers. A final buffer wash was performed to remove any loosely bound DNA.

7.2.2 : AFM imaging

SAMs of 11-MUA, 2-aminoethanethiol and dodecanethiol for AFM were prepared on vapour deposited gold on mica as described in 6.2.3. SAMs of Lan-1 and Lan-2 were prepared by overnight incubation of vapour deposited gold on mica in a 1 mg / ml solution of the polymers in HEPES buffer (250 mM, pH 7.0). The polymer SAMs were then washed in buffer and dried under a nitrogen stream.

For air imaging SAMs were incubated with the dendrimers (0.1μg / ml in HEPES 250 mM pH 7.0) for 15 min, rinsed in deionised water and dried under a nitrogen stream. Samples were imaged utilising single beam TESP silicon nitride cantilevers with resonance frequencies between 250-278 KHz.

For liquid imaging samples were prepared as above but after washing with buffer were not allowed to dry, but instead were imaged in HEPES buffer using silicon nitride, 100 μm long triangular cantilevers with resonant frequencies in water between 9-12 KHz.

7.2.3 : AFM force-distance studies

Force-distance experiments were performed to determine the strength of the interaction between the dendrimers and the SAMs, lipidic and DNA surfaces used in the SPR experiments described in 7.2.1. For immobilisation of the dendrimers a protocol was required which would allow both carboxyl and amino terminated PAMAMs to be attached by the same strength to the tip. This reduced the variables which needed to be taken into consideration when experiments were performed. Chemically modifying the dendrimers with biotin was the preferred route. As discussed in Chapter 4 the streptavidin-biotin bond is the strongest naturally occurring non-covalent bond. Also a well established method is known for immobilising active streptavidin to silicon nitride tips (Allen (1997)).

7.2.3.1 : Dendrimer biotinylation

All dendrimers were obtained from either Sigma Chemical Company (Poole, Dorset, UK.) or Dendritec (Midland, MI, USA) as a methanol solution. The solvent was removed under a nitrogen stream prior to conjugation of the biotin. Biotin conjugation was carried out by two methods depending on the terminal group of the dendrimer.

Carboxyl terminated dendrimers were redissolved in deionized water to a concentration of 10 mg / ml and acidified to pH 3.5 ± 0.2 using concentrated hydrochloric acid. They were then spun in centripreps against deionised water for 20 min. This was performed to desalt the dendrimers so the majority of terminal groups would be present in the free acid form. Dialysis in centripreps

(Pierce, Rockford, Illinois, USA.) against deionised water was repeated twice. The desalted dendrimer solution was added to an amount of carboxydiimide (10 mg / ml in DMF) which provided a theoretical 10% labelling of the dendrimers terminal groups. After 1 h of stirring at room temperature biotin hydrazide (10 mg / ml in DMF) was added at concentrations theoretically labelling 10% of surface functional groups. The mixture was left to stir at room temperature for 48 h. After this period, the reaction mixture was reduced to dryness on a rotary evaporator. The resultant solid was redissolved in 5 ml of water and transferred to Spectra-por dialysis tubing with 1,000 Da cut off. The biotinylated-dendrimer was dialysed against deionized water and the product freeze dried. The resultant yellow / white solid product was stored under vacuum until use.

The amino terminated dendrimers were redissolved in deionized water. The pH was adjusted to 7.0 ± 0.2 using 0.5 M hydrochloric acid and 0.5 M sodium hydroxide giving a final concentration of the dendrimers of 10 mg/ml. EZ-link NHS-biotin (Pierce, Rockford, Illinois, USA.) was made to a stock solution concentration of 10 mg / ml in DMSO. An amount of EZ-link NHS-biotin was added which would theoretically label 10% of the dendrimer terminal groups and the mixture stirred at room temperature overnight. The resultant mixture was dialysed against water two times using Spectra-por dialysis tubing with 1,000 Da cut off and then freeze dried. The resultant white solid product was stored under vacuum until use.

To check if dendrimers had been biotinylated, SPR experiments were performed on biotinylated SAMs. SPR slides were prepared by overnight incubation in a 2.7 mg / ml solution of biotin-HPDP (Pierce, Rockford, Illinois, USA.) in trifluoroethanol (TFE) under a desiccated atmosphere. After incubation, the slides were washed with excess TFE and dried under a nitrogen stream. After a stable baseline had been obtained, 1 ml of streptavidin (50 μg / ml HEPES, 250 mM, pH 7.0) was injected over a biotin-HPDP coated SPR slide. After a buffer wash, 1 ml of either the biotinylated or non-biotinylated

dendrimer was injected (0.1 μg / ml in HEPES, 250 mM, pH 7.0) to determine binding levels. Finally a buffer wash was performed to remove any loosely bound dendrimers.

7.2.3.2 : Experimental procedure for interactions between dendrimers and SAMs

Force-distance experiments were carried out between dendrimer coated AFM tips and the model SAM surfaces. The latter were prepared as described in 6.2.2 and streptavidin coated triangular silicon nitride cantilevers as outlined in 4.2.6. Prior to immobilising the dendrimers onto the tip, force measurements were performed on all SAM surfaces with the streptavidin coated tips to determine background levels of interaction. To immobilise the dendrimers, the AFM tip was incubated in a 0.1 mg / ml solution of the dendrimer in buffer without removal of the tip from the LS-AFM to ensure the contact region remained the same. After 1 h, the tip was washed in buffer and force-distance cycles repeated on the same SAM surfaces as before the incubation.

Preliminary experiments to determine the effect of dendrimer generation on the strength of interaction with the SAM surfaces were carried out in 250 mM HEPES buffer pH 7.0, so comparisons could be made with previous SPR and AFM imaging studies. The experiments to determine the effect of buffer pH and ion strength were carried out in buffers composed of boric and citric acid and trisodium phosphate as taken from "Buffers for pH and metal ion control" (Perrin (1974)). The tip was washed with deionised water between each pH and tips checked to ensure that extreme pH's were not effecting protein structure and hence dendrimer immobilisation. These controls were performed by carrying out force-distance curves on the dodecanethiol surfaces at pH 7.4. The protein was deemed to be undamaged if the same force observed at the beginning of the experiment was repeated at test periods throughout the investigation.

7.2.3.3 : Experimental procedure for interactions between dendrimers and cell membranes

So comparisons could be made with previous SPR work, experiments to quantify the interaction with lipidic membrane systems and DNA were performed in 10 mM TBS, pH 7.4 and 10 mM HEPES, pH 7.4 respectively.

In the case of the interactions with lipidic surfaces, streptavidin coated tips and carboxyl SAMs were used and prepared as described in sections 4.2.6 and 6.2.2 respectively. The integrity of the AFM tips was confirmed by measuring their interaction with streptavidin coated surfaces prepared as in 4.2.6. Force-distance experiments were performed on the carboxyl SAM prior to depositing the cell membrane fraction to determine background levels of interaction with the SAM. The SAM was then incubated in a solution of the CACO2 cell membranes at a concentration of 1 mg / ml protein in TBS (10 mM, pH 7.4) for 30 min. After this period the samples was washed in excess TBS buffer and force-distance experiments repeated to quantify the interaction between the streptavidin coated tip and lipidic surface. After reaffirmed tip integrity, the AFM tip was incubated in a 0.1 mg / ml solution of the dendrimer in TBS (10 mM, pH 7.4) without removal of the tip from the LS-AFM to ensure the contact region was not significantly altered. After 1 h, the tip was washed in buffer and force-distance cycles repeated to determine the extent of interaction between the dendrimers and the immobilised cell membrane fractions.

4.2.3.4 : Experimental procedure for interactions between dendrimers and DNA

Where the interaction between the DNA and dendrimers was to be quantified, streptavidin coated tips and surfaces were prepared as described in section 4.2.6. To ensure tips were coated in streptavidin, force-distance

curves were performed on like coated surfaces. After ensuring minimal interaction was observed, the streptavidin coated surfaces were incubated with pGal plasmid DNA (5 μg / ml in HEPES pH 7.4, 10 mM) for 30 min. After this period, the samples was washed in excess HEPES buffer and force-distance experiments repeated to quantify the extent of the interaction between the streptavidin coated tip and immobilised DNA. After reaffirming integrity of the AFM tip, it was incubated in a 0.1 mg / ml solution of the dendrimer in HEPES (pH 7.4, 10 mM) without removal of the tip from the LS-AFM to ensure the contact region remained the same. After 1 h, the tip was washed in buffer and force-distance cycles repeated to determine the extent of interaction between the dendrimers and immobilised DNA.

7.3 : Results and discussion

7.3.1 : SPR

All SPR experiments were carried out at a pH where both the dendrimer and SAMs terminal groups are charged. This allowed the effect of surface charge, both of the dendrimer and surface, as well as dendrimer size and SAM surface roughness could be investigated. The discussion of the results will be divided into interactions with different SAM types.

7.3.1.1 : Interaction with Dodecanethiol SAM

A typical SPR trace for the interaction of the PAMAM dendrimers with the hydrophobic dodecanethiol SAM is seen in Figure 7.6. After the injection of the dendrimer solution, a rapid increase in SPR angle, followed by a stable plateau region throughout the buffer wash, was observed for all PAMAM dendrimers, independent of terminal group and generation. The rapid change in SPR angle and swift plateauing to the final level is indicative of a rapid interaction with the hydrophobic surface. As no decrease in the plateau level is observed during the buffer wash, it can be concluded that the

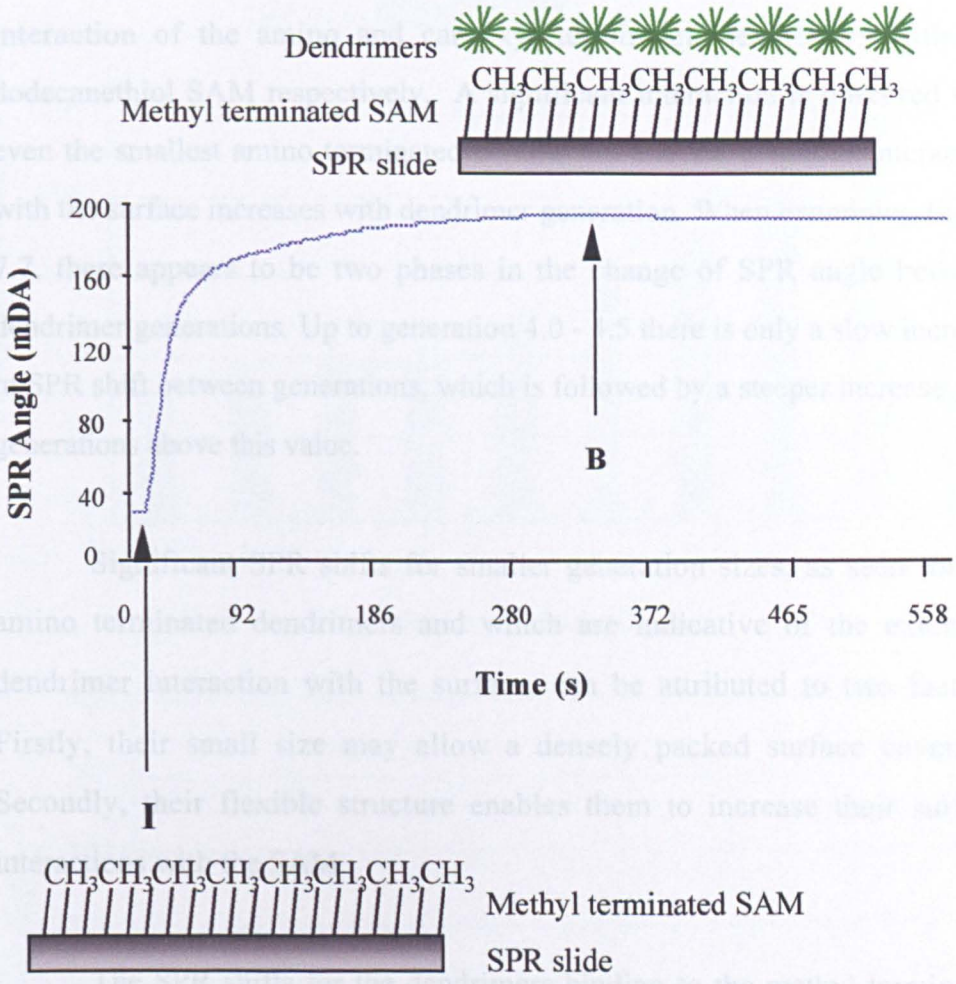

Figure 7.6 : A typical SPR trace for the interaction between generation 8.0 PAMAM dendrimers and a dodecanethiol SAM

I : Injection of dendrimers
B: Start of buffer wash

interaction between the dendrimer and surface is relatively stable.

Figure 7.7 (a) and (b) shows the SPR angle shifts obtained for the interaction of the amino and carboxyl terminated dendrimers with the dodecanethiol SAM respectively. A significant interaction is observed with even the smallest amino terminated dendrimers and the extent of interaction with the surface increases with dendrimer generation. When examining Figure 7.7, there appears to be two phases in the change of SPR angle between dendrimer generations. Up to generation 4.0 - 4.5 there is only a slow increase in SPR shift between generations, which is followed by a steeper increase with generations above this value.

Significant SPR shifts for smaller generation sizes, as seen for the amino terminated dendrimers and which are indicative of the extent of dendrimer interaction with the surface, can be attributed to two factors. Firstly, their small size may allow a densely packed surface coverage. Secondly, their flexible structure enables them to increase their surface interactions with the SAM.

The SPR shifts for the dendrimers binding to the methyl terminated SAM are seen to increase within the two dendrimer groups, ie. carboxyl or amino terminated, with increasing generation. For example, the generation 6.0 dendrimer gives rise to an SPR shift of 145 ± 10 mDA whereas a shift of 178 ± 17 mDA is observed for generation 7.0. This can be explained by the increasing size and density of the dendrimer branches with dendrimer generation, which will produce a thicker surface layer.

It is interesting to speculate on the origin of the two distinct phases for the positively charged dendrimers interacting with the methyl terminated SAM (Figure 7.7 (a)) as noted above. This may be explained by the structure of the dendrimers and hence how they interact with the surface. Below generation 3.0 - 5.0, the dendrimers are flexible, non-spheroidal moieties, whereas above this

(a)

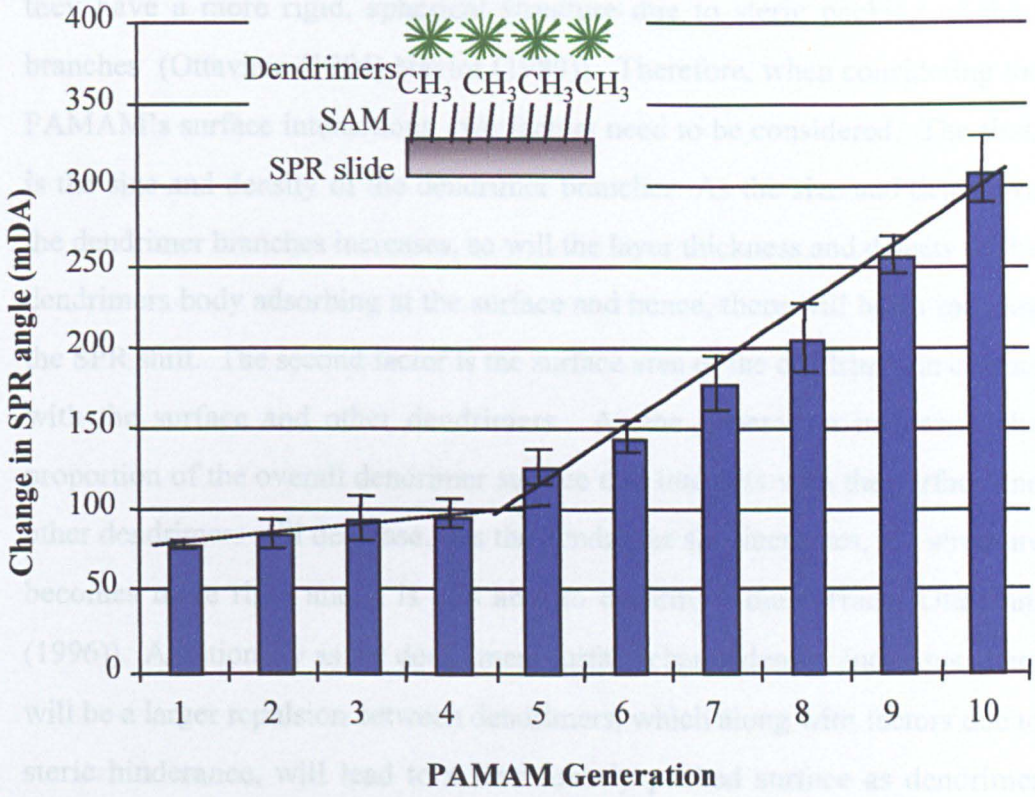

(b)

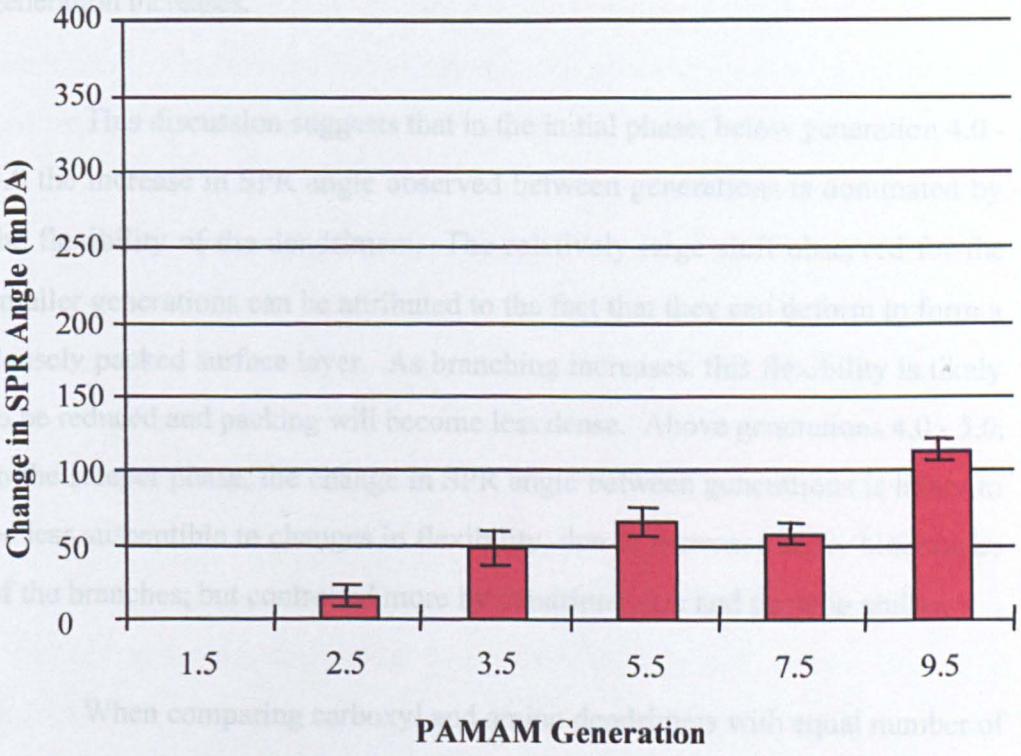

Figure 7.7 : (a) Interaction of amino terminated dendrimers with a dodecanethiol SAM
(b) Interaction of carboxyl terminated dendrimers with a dodecanethiol SAM

bars = average ± 1 standard deviation ($n \geq 14$)

they have a more rigid, spherical structure due to steric packing of their branches (Ottaviani (1994) Naylor (1989)). Therefore, when considering the PAMAM's surface interactions, two factors need to be considered. The first, is the size and density of the dendrimer branches. As the size and density of the dendrimer branches increases, so will the layer thickness and density of the dendrimers body adsorbing at the surface and hence, there will be an increase the SPR shift. The second factor is the surface area of the dendrimer in contact with the surface and other dendrimers. As the generation increases, the proportion of the overall dendrimer surface that interacts with the surface and other dendrimers will decrease. As the dendrimer size increases, it's structure becomes more rigid and it is less able to deform to the surface (Ottaviani (1996)). Additionally as the dendrimers surface charge density increases, there will be a larger repulsion between dendrimers, which along with factors due to steric hinderance, will lead to a less densely packed surface as dendrimer generation increases.

This discussion suggests that in the initial phase, below generation 4.0 - 5.0 the increase in SPR angle observed between generations is dominated by the flexibility of the dendrimers. The relatively large shift observed for the smaller generations can be attributed to the fact that they can deform to form a densely packed surface layer. As branching increases, this flexibility is likely to be reduced and packing will become less dense. Above generations 4.0 - 5.0, in the steeper phase, the change in SPR angle between generations is likely to be less susceptible to changes in flexibility, due to increased steric hinderance of the branches, but controlled more by dendrimer size and packing ability.

When comparing carboxyl and amino dendrimers with equal number of terminal groups ie. generations 4.0 and 3.5, Figure 7.7 shows that the interactions for the positive charged (amino terminated) dendrimers is much greater than the negative (carboxyl terminated) ones with this particular surface.

7.3.1.2 : Interaction with 11-MUA SAM

Figure 7.8 (a) and (b) shows the interactions of the PAMAM dendrimers with an 11-MUA SAM. At pH 7.0, this surface has a negative charge. From this figure it can be observed that interactions for both dendrimer types increases with generation. When compared with Figure 7.7, interactions for the small carboxyl dendrimers are less than those for the same generation on the hydrophobic surface. For the amino dendrimers, the smaller generations, up to generation 4.0, show less binding, but above this show a comparable level to that of the interactions with the hydrophobic SAM.

The smaller interaction of the carboxyl dendrimers with the 11-MUA SAM when compared with the dodecanethiol SAM could be attributed to repulsion between the two like charged negative surfaces. However, an interaction is observed with the larger negatively charged carboxyl terminated dendrimers. This may be due to dimerisation between the dendrimer terminal carboxyl groups and the SAM's terminal carboxyl functions.

When considering the interactions of the amino terminated dendrimers with the 11-MUA surface, two types of binding need to be taken into consideration; ionic and hydrophobic. A lower SPR shift for the low generation dendrimers is observed with the 11-MUA surface when compared to that for the dodecanethiol SAM. It can be proposed that these small dendrimers form a pancake-like structure at this interface. With the hydrophobic dodecanethiol SAM a large proportion of the flexible dendrimers relatively hydrophobic interior will be attracted to the surface forming a densely packed surface coverage. However, on the 11-MUA SAM the interaction will be predominately between the negatively charged SAM surface and the dendrimers positively charged functional groups. This may provide a surface coverage which is less dense and may be the reason why a lower SPR shift is observed compared to the hydrophobic SAM. This hypothesis is visualised in Figure 7.9 Above generation 4.0 - 5.0, it could be proposed the

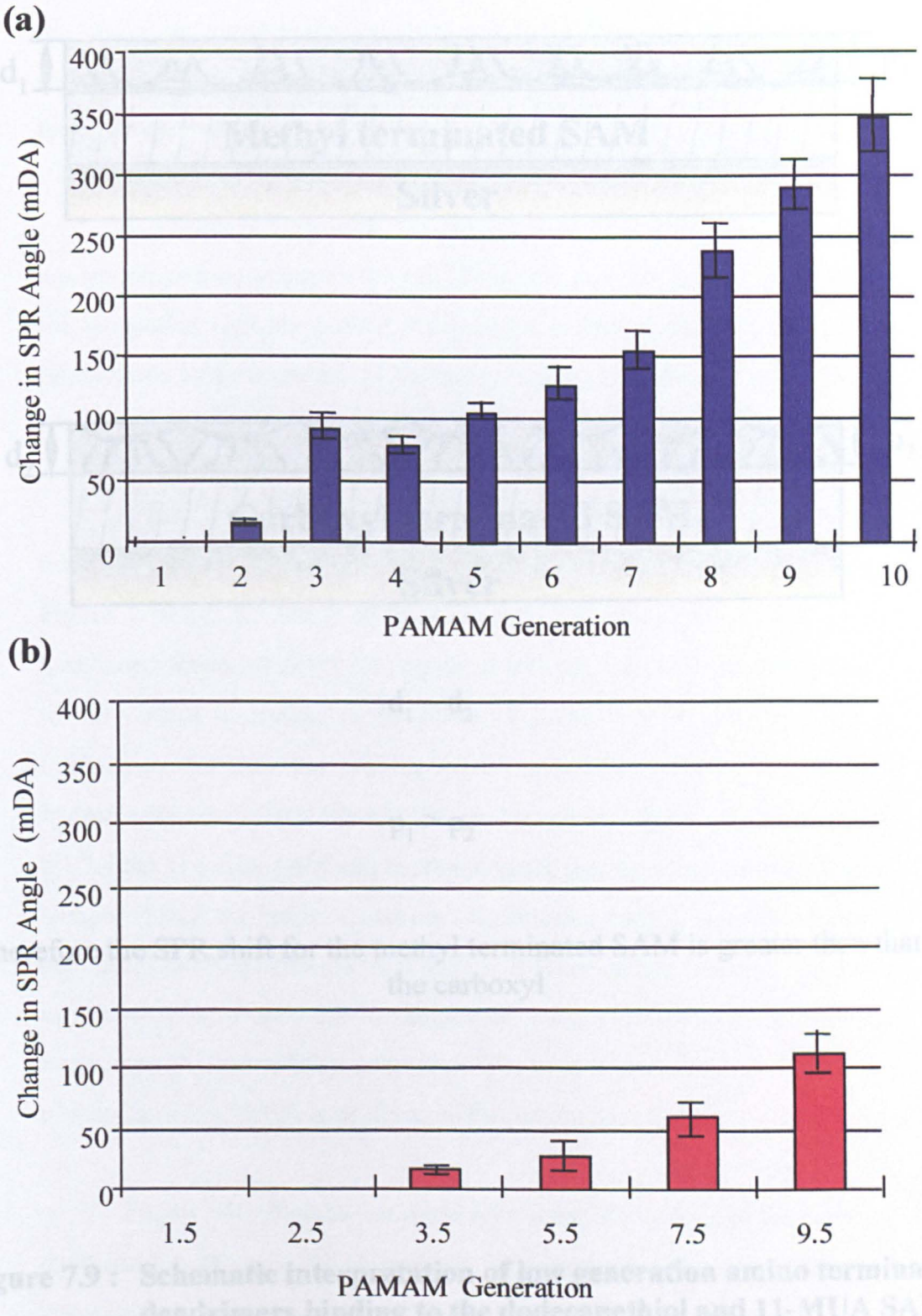

Figure 7.8 : (a) Interaction of amino terminated dendrimers with an 11-MUA SAM
(b) Interaction of carboxyl terminated dendrimers with an 11-MUA SAM

bars = average ± 1 standard deviation ($n \geq 25$)

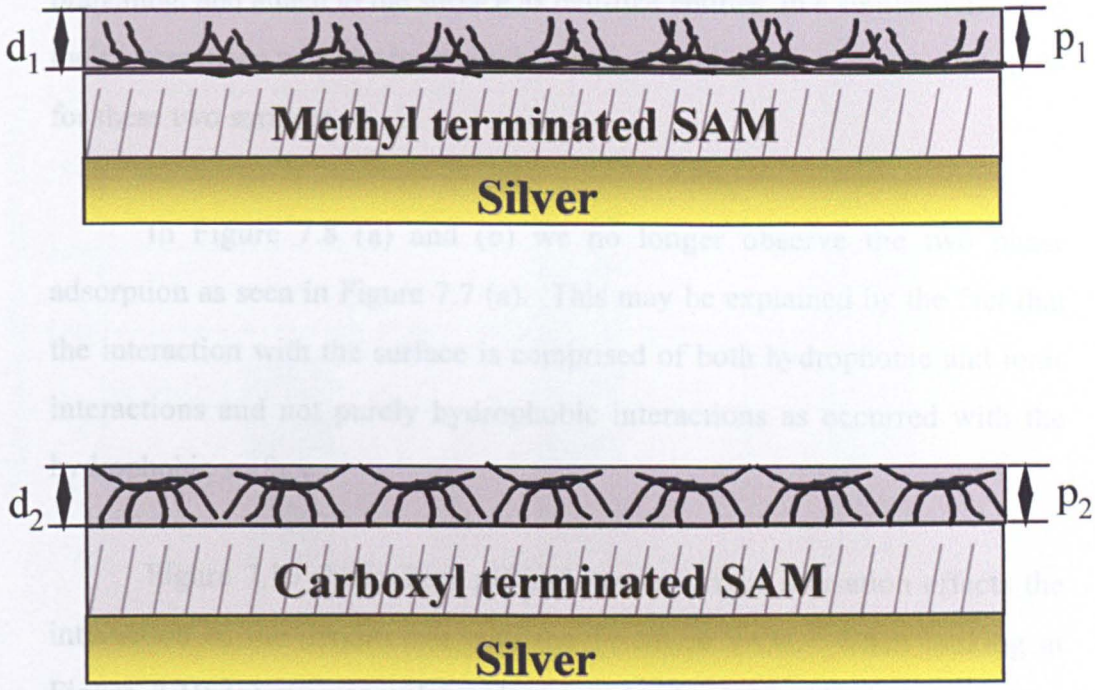

$d_1 \sim d_2$

$p_1 > p_2$

Therefore the SPR shift for the methyl terminated SAM is greater than that of the carboxyl

Figure 7.9 : Schematic interpretation of low generation amino terminated dendrimers binding to the dodecanethiol and 11-MUA SAMs

larger spheroidal generations are sterically constrained by the degree of branching, and attach to the surface as ball-like entities, in a similar manner to their interactions with the hydrophobic surface, giving rise to the similar shifts for these two surfaces.

In Figure 7.8 (a) and (b) we no longer observe the two phase adsorption as seen in Figure 7.7 (a). This may be explained by the fact that the interaction with the surface is comprised of both hydrophobic and ionic interactions and not purely hydrophobic interactions as occurred with the hydrophobic surface.

Figure 7.10 shows how pH and hence surface ionisation effects the interaction of the dendrimers with the 11-MUA SAM. When looking at Figure 7.10 (a) we see a large increase in the interaction of the amino terminated dendrimer at pH 7.4 compared with pH 3.0. This can be attributed to the surface ionisation of the 11-MUA SAM. At pH 3.0 the SAM is uncharged, therefore the binding of the dendrimers will be due to only hydrophobic interactions between the dendrimers and the SAM. However, at pH 7.4 the 11-MUA SAM will be deprotonated and therefore carry a negative charge. Since the amino terminated dendrimers carry a positive charge a significant increase in the extent of binding is observed due to charge attraction. In is interesting to note that the degree of charge interaction is significantly larger than the hydrophobic interaction. An overall increase in the interaction of between 225 - 293 % is observed on decreasing the pH.

Figure 7.10 (b) shows how pH effects the interactions of the carboxyl dendrimers with the 11-MUA surface. No significant difference is observed between the binding levels at pH 7.4 and pH 3.0. This is surprising, it would be expected that less binding would occur at pH 7.4, as both the dendrimer and SAM posses the same charge and therefore they will repel each, whereas at pH 3.0 the dendrimer terminal groups and carboxyl surface are both uncharged, so both hydrogen bonding and hydrophobic interactions could occur. A

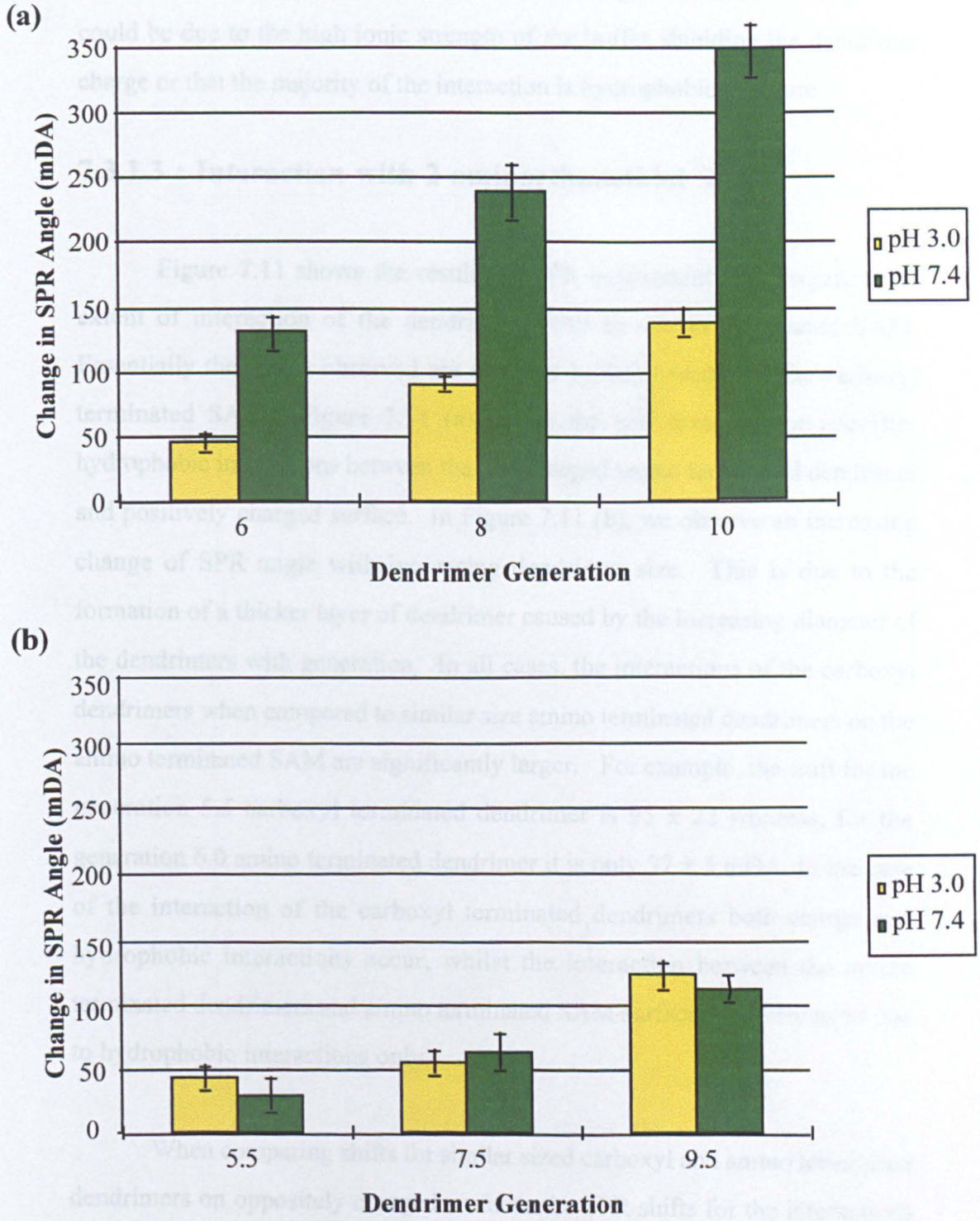

Figure 7.10 : Effect of pH on interaction of dendrimers with an 11-MUA SAM
(a) amino terminated dendrimers
(b) carboxyl terminated dendrimers

bars = average ± 1 standard deviation ($n \geq 11$)

possible explanation why a lower level of binding is not observed at pH 7.4 could be due to the high ionic strength of the buffer shielding the dendrimer charge or that the majority of the interaction is hydrophobic in nature.

7.3.1.3 : Interaction with 2-aminoethanethiol SAM

Figure 7.11 shows the results of SPR experiments investigating the extent of interaction of the dendrimers with an amino terminated SAM. Essentially the trends observed are opposite to those seen with the carboxyl terminated SAM. Figure 7.11 (a) shows the low level of non-specific, hydrophobic interactions between the like charged amino terminated dendrimer and positively charged surface. In Figure 7.11 (b), we observe an increasing change of SPR angle with increasing dendrimer size. This is due to the formation of a thicker layer of dendrimer caused by the increasing diameter of the dendrimers with generation. In all cases, the interactions of the carboxyl dendrimers when compared to similar size amino terminated dendrimers on the amino terminated SAM are significantly larger. For example, the shift for the generation 5.5 carboxyl terminated dendrimer is 95 ± 22 whereas, for the generation 6.0 amino terminated dendrimer it is only 37 ± 5 mDA. In the case of the interaction of the carboxyl terminated dendrimers both charge and hydrophobic interactions occur, whilst the interaction between the amino terminated dendrimers and amino terminated SAM surface are likely to be due to hydrophobic interactions only.

When comparing shifts for similar sized carboxyl and amino terminated dendrimers on oppositely charged surfaces the SPR shifts for the interactions on the carboxyl SAM are larger. For example the generation 10.0 dendrimer produces a SPR shift of 350 ± 30 mDA on the carboxyl SAM whereas the generation 9.5 dendrimers shift on the amino terminated surface is lower at 212 ± 22 mDA. This could be attributed to the structure of the SAM. The shorter carbon chain amino terminated SAM produces a surface which is less well packed and contains more and larger molecular defects than SAMs formed

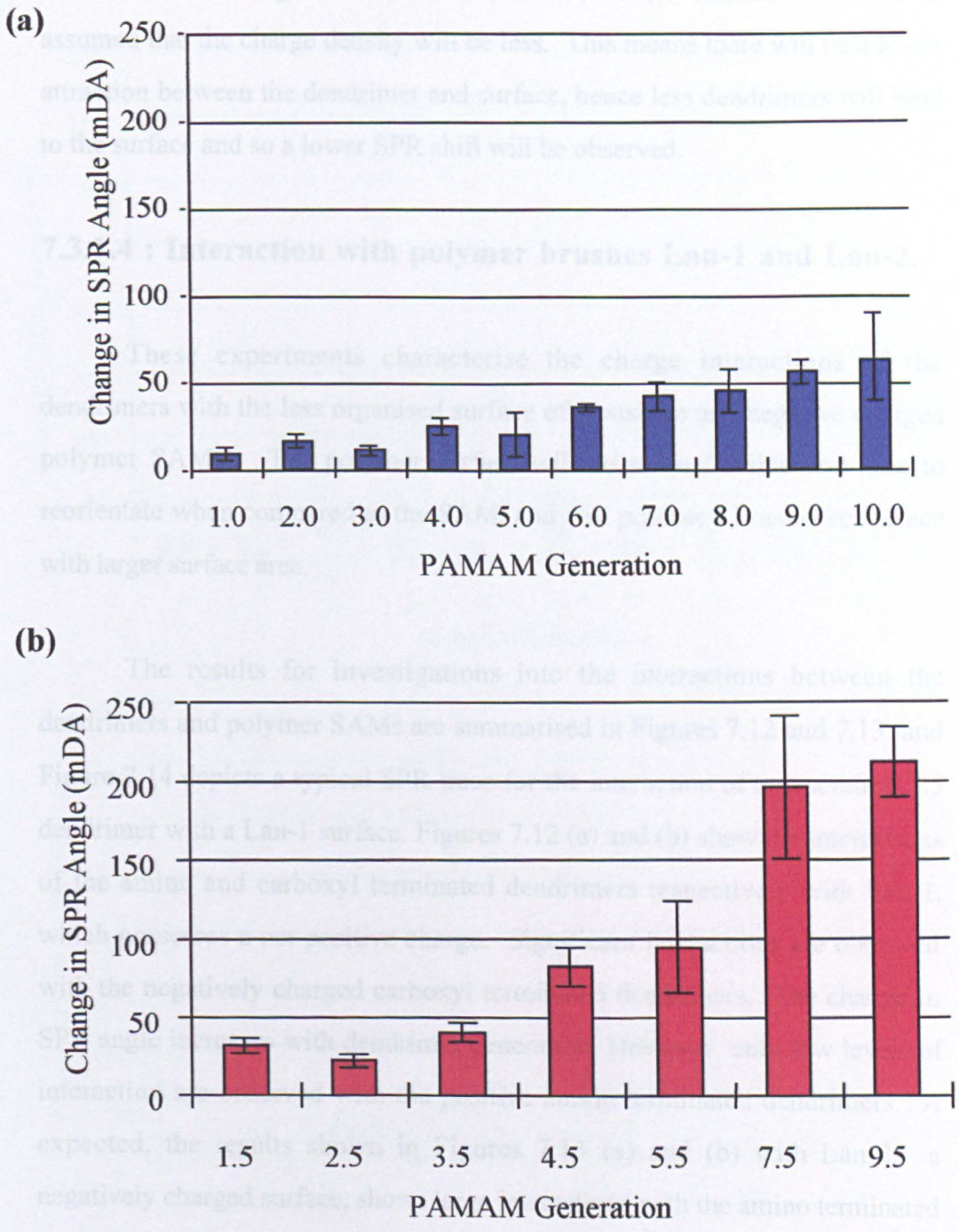

Figure 7.11 : (a) Interaction of amino terminated dendrimers with a 2-aminoethanethiol SAM
(b) Interaction of carboxyl terminated dendrimers with a 2-aminoethanethiol SAM

bars = average ± 1 standard deviation ($n \geq 18$)

from thiols with longer carbon chains (Porter (1987)). Therefore, it could be assumed that the charge density will be less. This means there will be a lower attraction between the dendrimer and surface, hence less dendrimers will bind to the surface and so a lower SPR shift will be observed.

7.3.1.4 : Interaction with polymer brushes Lan-1 and Lan-2.

These experiments characterise the charge interactions of the dendrimers with the less organised surface of a positive and negative charged polymer SAM. The polymer surface will be more flexible and able to reorientate when compared to the SAM, and will possess a brush-like surface with larger surface area.

The results for investigations into the interactions between the dendrimers and polymer SAMs are summarised in Figures 7.12 and 7.13 and Figure 7.14 depicts a typical SPR trace for the interaction of a generation 7.5 dendrimer with a Lan-1 surface. Figures 7.12 (a) and (b) show the interactions of the amino and carboxyl terminated dendrimers respectively with Lan-1, which possesses a net positive charge. Significant interactions are observed with the negatively charged carboxyl terminated dendrimers. The change in SPR angle increases with dendrimer generation. However, only low levels of interaction are observed with the positive amino terminated dendrimers. A expected, the results shown in Figures 7.13 (a) and (b) with Lan-2, a negatively charged surface, shows large interactions with the amino terminated dendrimers but only minimal interaction with the carboxyl terminated dendrimers.

In both cases, as can be observed from Figure 7.14, the specific charge interaction between the oppositely charged SAM surface and dendrimer is rapid, completed within 2 min and is stable to a 5 min buffer wash. This suggests that the interaction between dendrimer and surface is strong.

(a)

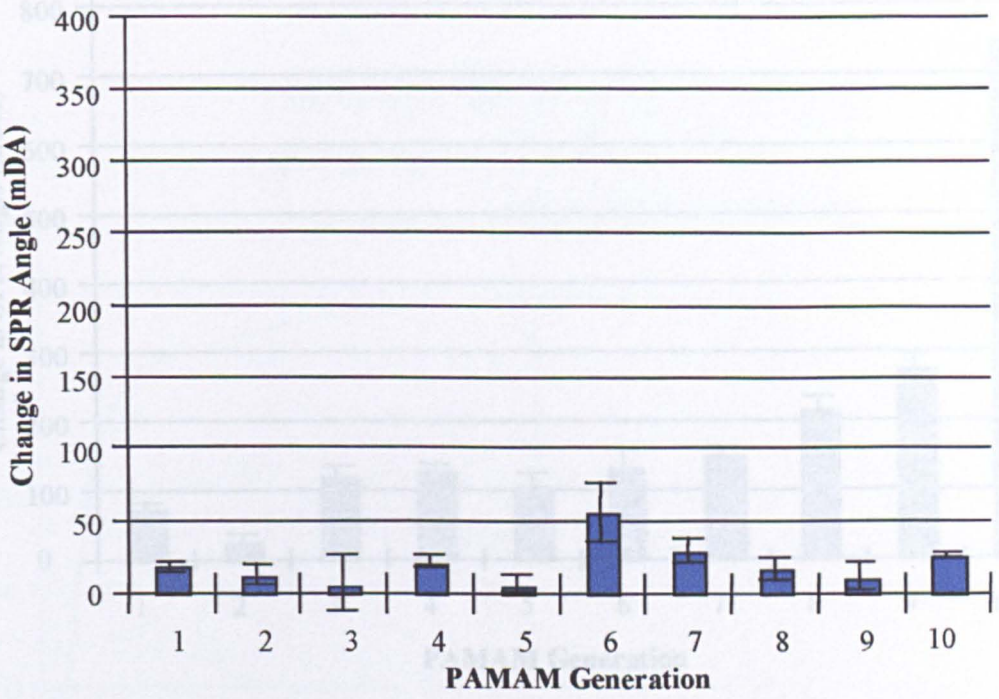

(b)

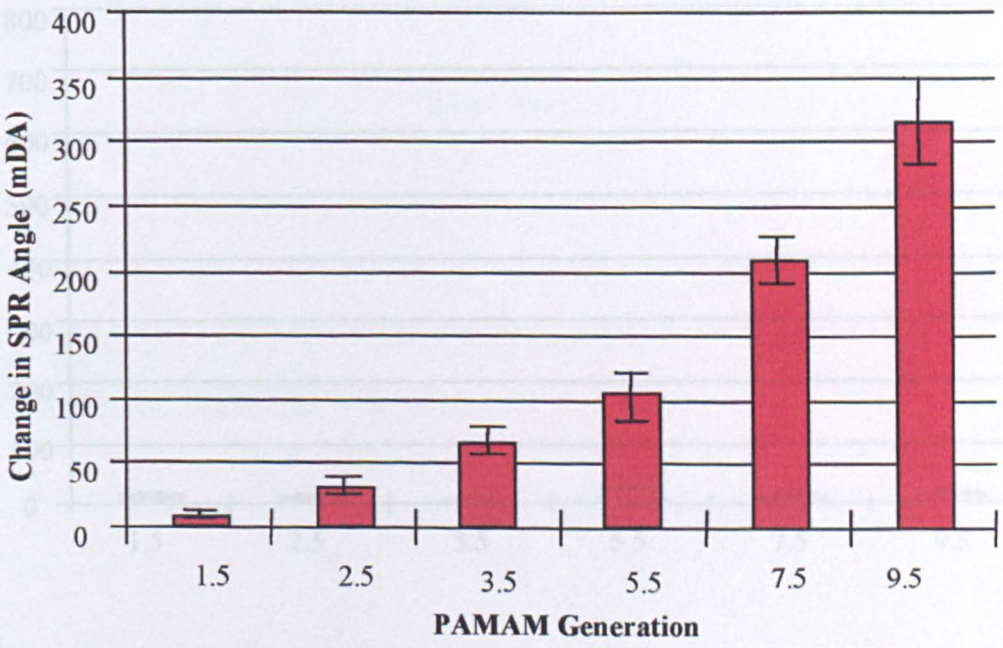

Figure 7.12 : (a) Interaction of amino terminated dendrimers with Lan-1
(b) Interaction of carboxyl terminated dendrimers with Lan-1

bars = average ± 1 standard deviation ($n \geq 17$)

(a)

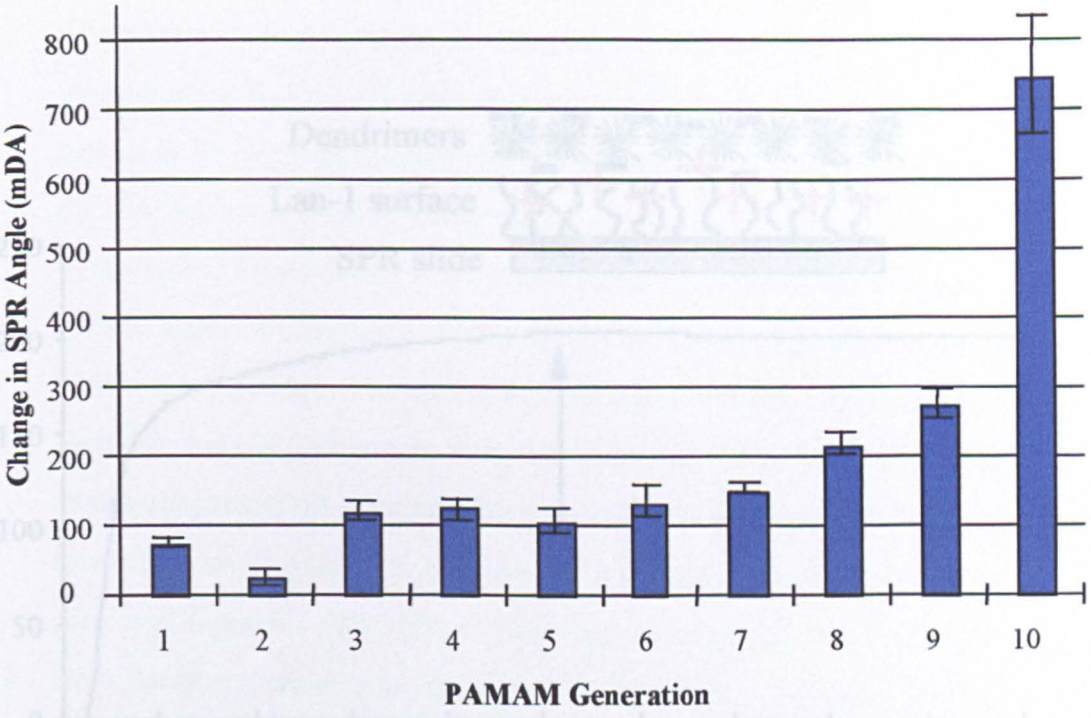

(b)

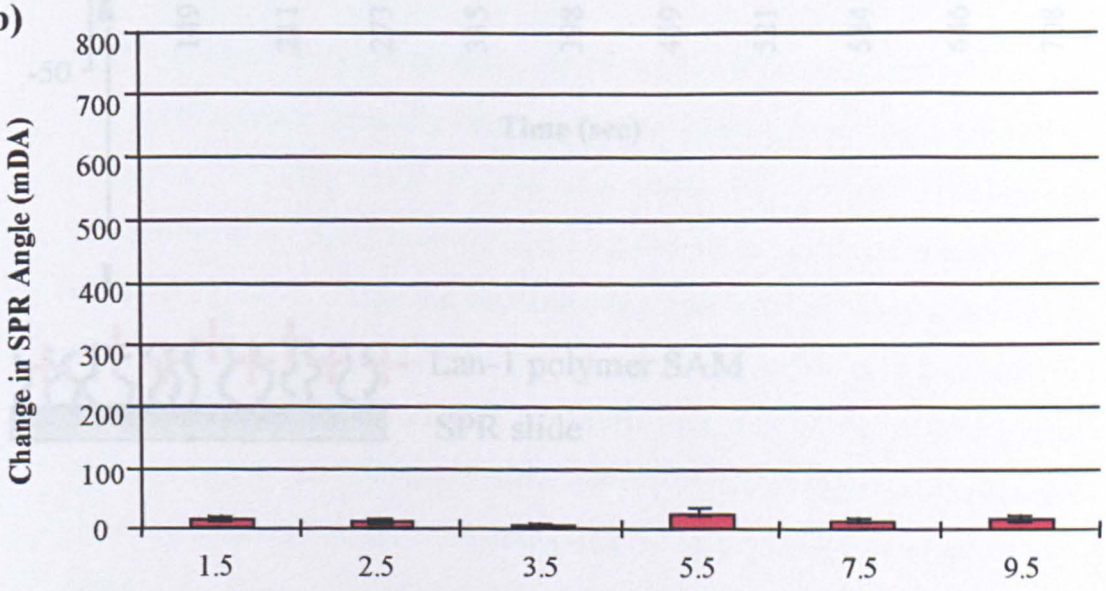

Figure 7.13 : (a) Interaction of amino terminated dendrimers with Lan-2
(b) Interaction of carboxyl terminated dendrimers with Lan-2

bars = average ± 1 standard deviation ($n \geq 18$)

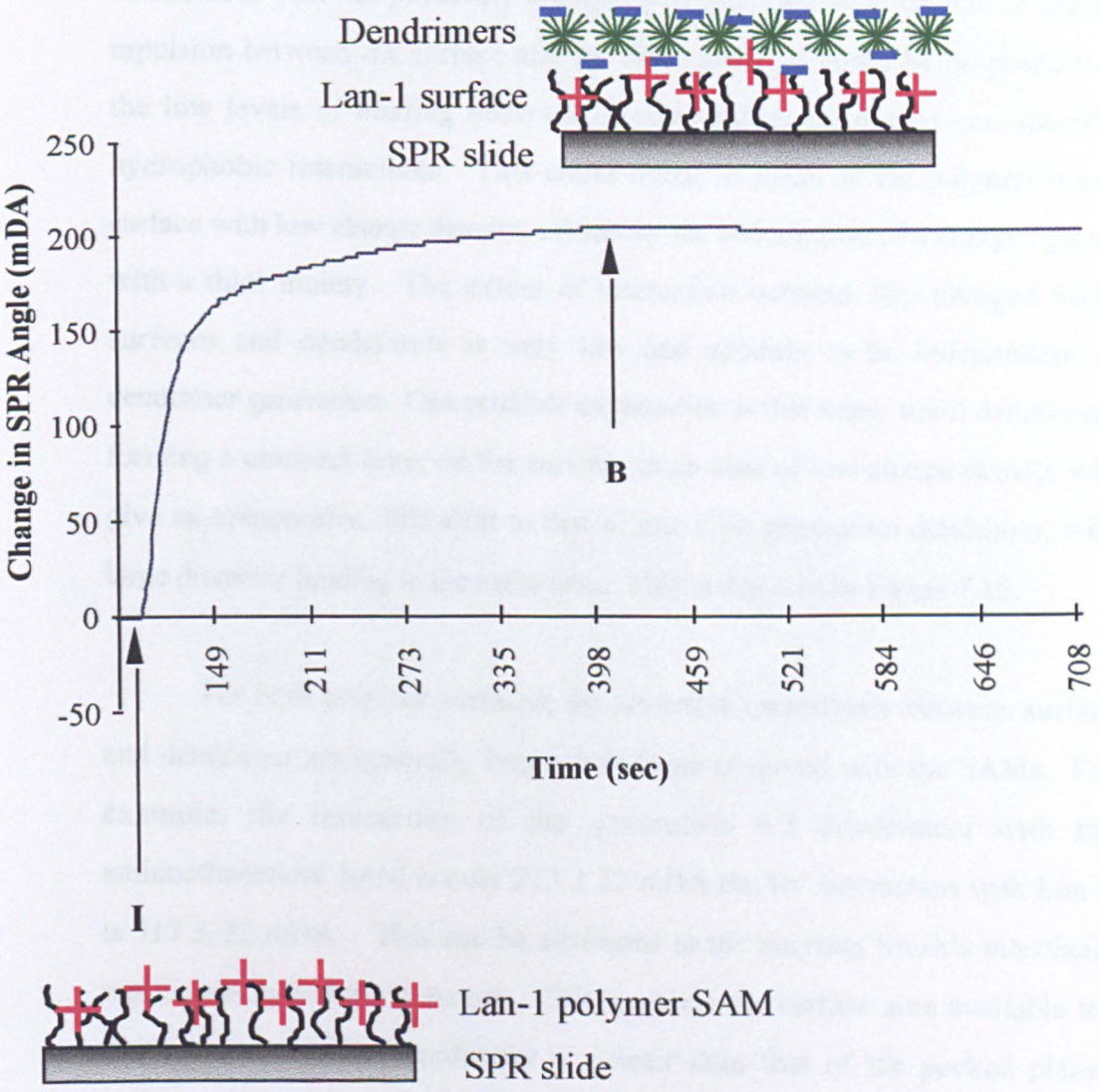

Figure 7.14 : A typical SPR trace for the generation 7.5 dendrimer interacting with a Lan-1 surface

I : Injection of dendrimers
B : Start of buffer wash

The low levels of interactions between the carboxyl terminated dendrimers with the negatively charged polymer and the amino terminated dendrimers with the positively charged polymer, can be attributed to charge repulsion between the surface and the dendrimers. It could be proposed that the low levels of binding observed in these cases are due to non-specific, hydrophobic interactions. This could occur in areas of the polymer brush surface with low change density, caused by the substitution of a charged group with a thiol moiety. The extent of interaction between like charged SAM surfaces and dendrimers is very low and appears to be independent of dendrimer generation. One possible explanation is that many small dendrimers forming a compact layer on the surface, in an area of low charge density will give an comparable SPR shift to that of one high generation dendrimer, with large diameter binding to the same area. This is depicted in Figure 7.15.

For both polymer surfaces, the attractive interactions between surface and dendrimer are generally larger than those observed with the SAMs. For example, the interaction of the generation 9.5 dendrimers with the aminoethanethiol SAM is only 212 ± 22 mDA but its' interaction with Lan-1 is 317 ± 22 mDA. This can be attributed to the polymer brush's interfacial region which is fluid in nature. This suggests the surface area available for interactions with the dendrimer is greater than that of the packed planar surface of the SAM. The larger surface area provides a larger binding area for the dendrimers to interact with, promoting the larger change in observed SPR angle.

7.3.1.5 : Characterisation of lipid surface

Before studies were performed characterising the interaction of the dendrimers with the Caco2 membrane fraction, experiments were performed to determine optimum conditions for the membrane fraction deposition on the SPR slides and to characterise its deposition profile. TBS was used for these experiments as previous work by Kalb (1992), Brian (1984) and Plant (1995) showed that this buffer gave a more reproducible and stable surface.

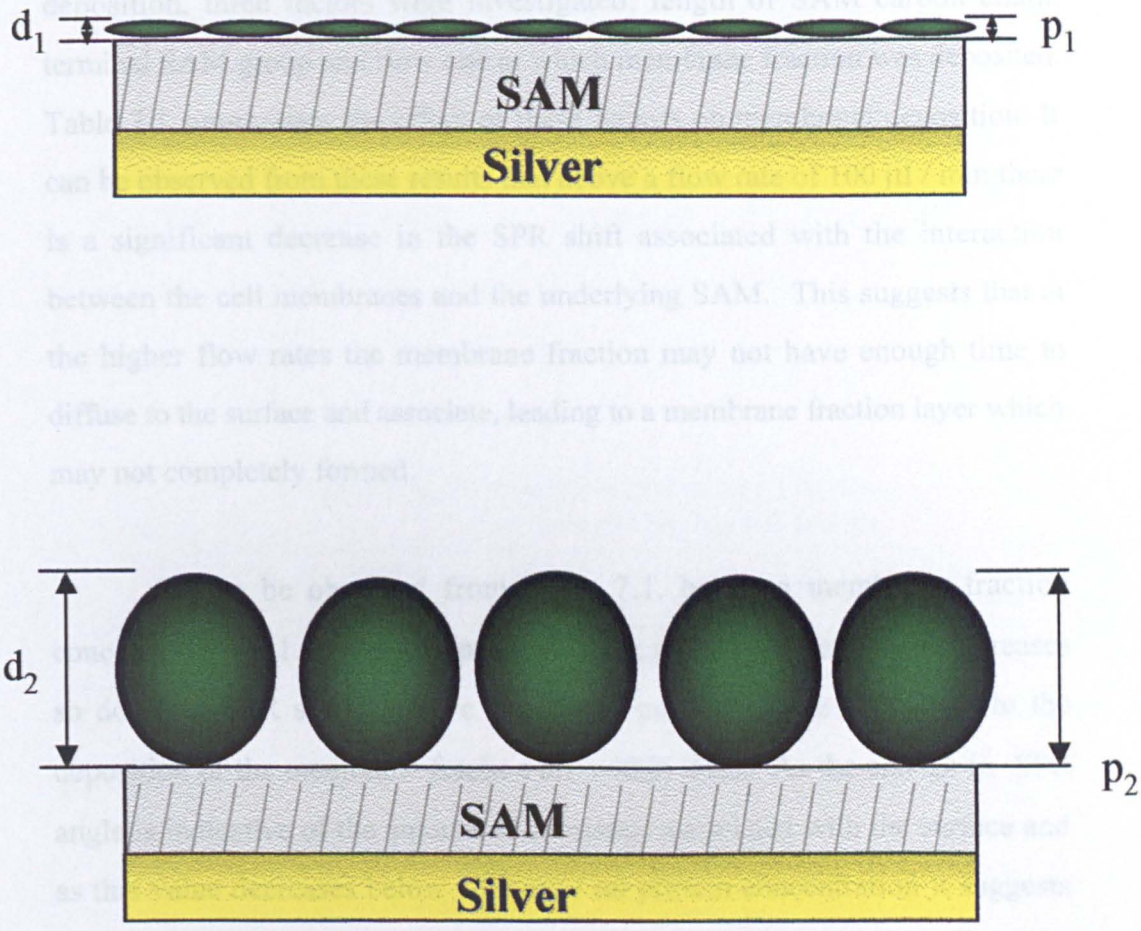

$d_2 > d_1$ but $p_1 > p_2$

therefore shifts $\approx$ the same

Figure 7.15 : Effect of dendrimer generation on depth and density of adsorbed layer

To determine the conditions for optimum membrane fraction deposition, three factors were investigated; length of SAM carbon chain, terminal SAM group and flow rate at which membrane fraction was deposited. Table 7.1 summarises the effect of these factors on membrane deposition. It can be observed from these results that above a flow rate of 100 µl / min there is a significant decrease in the SPR shift associated with the interaction between the cell membranes and the underlying SAM. This suggests that at the higher flow rates the membrane fraction may not have enough time to diffuse to the surface and associate, leading to a membrane fraction layer which may not completely formed.

As can be observed from Table 7.1, below a membrane fraction concentration of 1.00 mg / ml protein, as the protein concentration decreases so does the SPR shift. Above 1.00 mg / ml protein the shifts due to the deposition of the membrane fraction are within error. As the change in SPR angle is indicative of the amount of substance associated with the surface and as this value decreases below 1.00 mg / ml protein concentration it suggests that a complete layer of the membrane fraction is not being formed on the SAM surface below this concentration.

When observing the results for the effect of chain length on membrane fraction deposition it can be seen that increasing the chain length over C12 has no significant effect on the membrane fraction adsorption (Table 7.1). However, below this level, less adsorption is observed, suggesting incomplete monolayer coverage. This may in part be attributed to the structure of the SAM. At shorter carbon chain lengths, the SAM surface is not as well formed or organised so adsorption to the hydrophobic methyl surface will be less (Porter (1987)). When comparing values of the membrane fraction adsorption to the 11-MUA and dodecanethiol SAMs, it can be seen that the adsorption to the 11-MUA is just under twice that observed for the dodecanethiol SAM. For example, at a protein concentration of 1.00 mg / ml protein, the change in SPR angle associated with the interaction of the membrane fraction and the

SAM	FLOW RATE (µl / min) (n = min 8) Sample concentration 1 mg / ml protein			
	10	50	100	250
dodecanethiol	1044 ± 169	1035 ± 38	1074 ±148	832 ± 68
11-MUA	1756 ± 113	1639 ± 67	1775 ± 142	1528 ± 127

SAM	MEMBRANE FRACTION CONCENTRATION (mg protein / ml) (n = min 8) Flow rate 100 µl / min						
	0.10	0.25	0.50	1.00	1.25	1.50	1.75
Dodecane-thiol	591 ± 22	664± 45	795 ± 91	1074 ± 148	1092 ± 183	N / P	N / P
11-MUA	450 ± 45	803 ± 53	1278 ± 138	1775 ± 142	2001 ± 176	2147 ± 211	2167 ± 189

N/P = not probed

SAM	No. OF CARBONS IN THIOL CHAIN (protein conc 1mg / ml, flow rate 0.100 m l / min)		
	8	12	18
dodecanethiol	673 ± 101	1074 ± 148	1158 ± 172

Table 7.1 : Summary of lipid membrane SPR characterisation studies

SAMs are 1074 ± 148 and 1775 ± 142 mDA for the methyl and carboxyl terminated SAMs respectively. This could be attributed to the membrane fraction forming a bilayer rather than a monolayer on the SAM surface, as depicted in Figure 7.16. One possible reason for the value of the proposed bi-layer not being double of that for the dodecanethiol SAM is because of the protein content of the layer. The protein molecules will be significantly larger than the lipids therefore will traverse across the lipid bilayer, so on deposition of the second lipid layer of the bilayer a smaller surface area will need to be filled by the membrane fraction, hence leading to a shift which is not twice that observed for the monolayer on the methyl terminated surface.

For adsorption of the membrane fraction on both surfaces a biphasic shift is observed. To illustrate this, a typical trace for an SPR experiment investigating the interaction of the membrane fraction with a 11-MUA SAM is shown in Figure 7.17. To explain the biphasic interaction observed, two hypotheses are proposed. Firstly, that the lipid / protein structures, possibly present as micelles, may primarily associate with the SAM surface and then rearrange to form the final membrane-like surface, or secondly, that the interaction of the protein and lipids with the SAMs occurs at varying rates. Experiments were performed to determine which of the two hypotheses was correct. Preliminary experiments were performed to investigate the effect of lipid concentration and protein type on the extent and rate of interaction of the materials with the dodecanethiol and 11-MUA surfaces. After this mixtures of proteins and lipids were investigated. Ratios of between 4 : 1 and 1 : 3 lipid to protein were studied since the ratio of lipid to protein in cell membranes can vary between 4 :1 to 1 : 4 (Stryer (1988)). The protocol for these experiments are described in section 7.2.1.2 of this chapter. A summary of the results from these investigations are shown in Table 7.2 and Figure 7.18 shows typical SPR traces for adsorption of the phosphatidylcholine and proteins to the SAM surfaces.

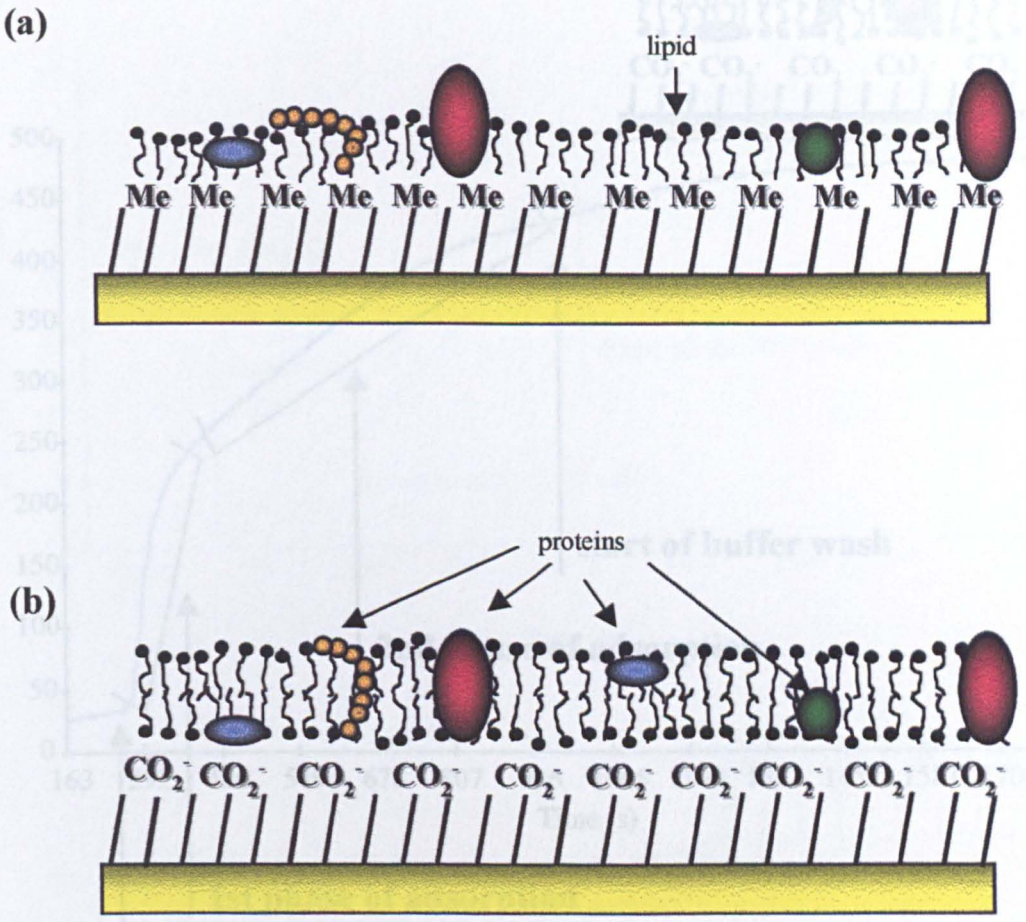

Figure 7.16 : Schematic representation of the membrane fraction adsorbed to dodecanethiol and 11-MUA SAMs

(a) : Methyl terminated SAM

(b) : Carboxyl terminated SAM

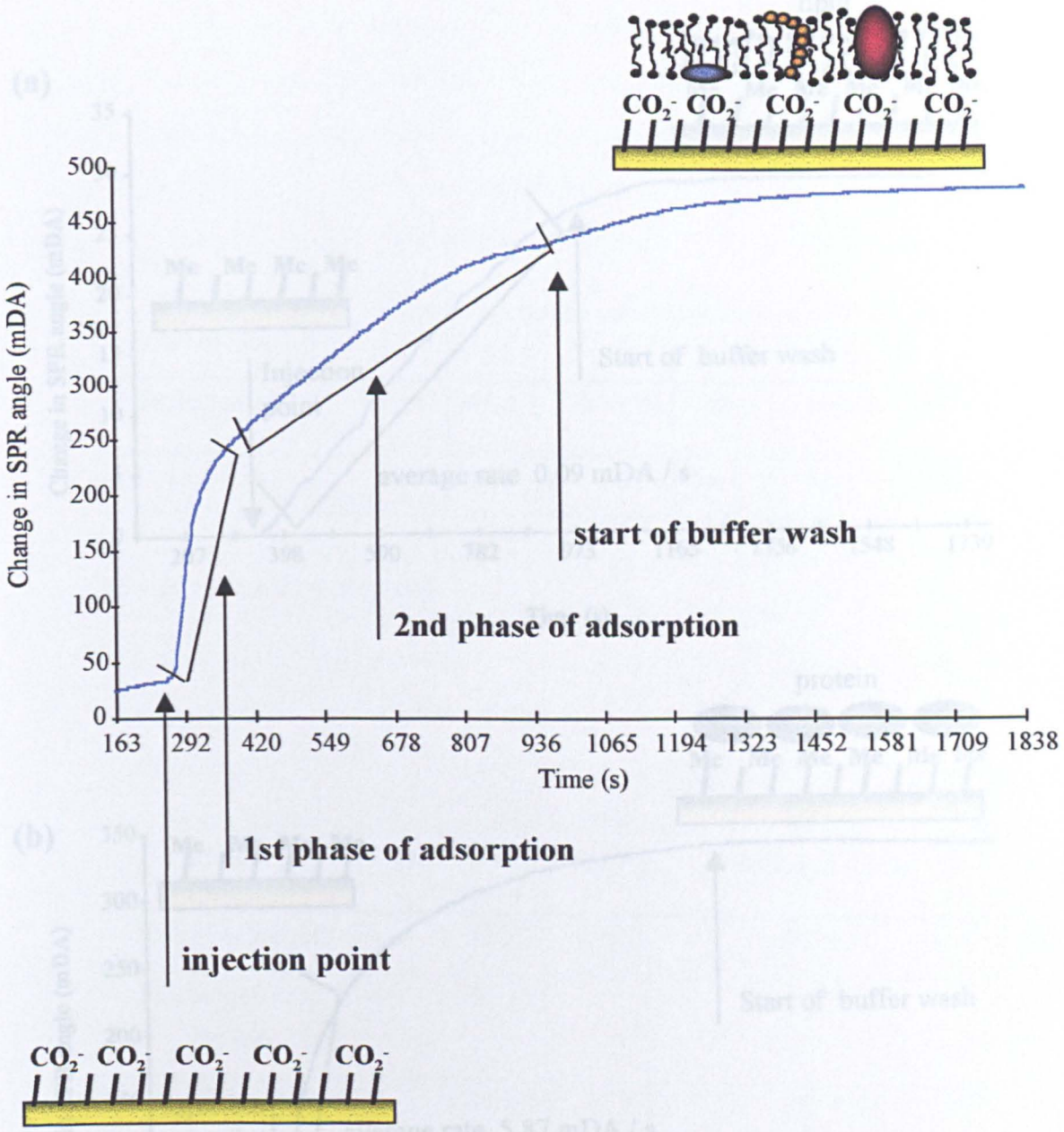

Figure 7.17 : Typical SPR trace for the adsorption of the cell membrane fraction to an 11-MUA SAM (0.1 mg / ml protein)

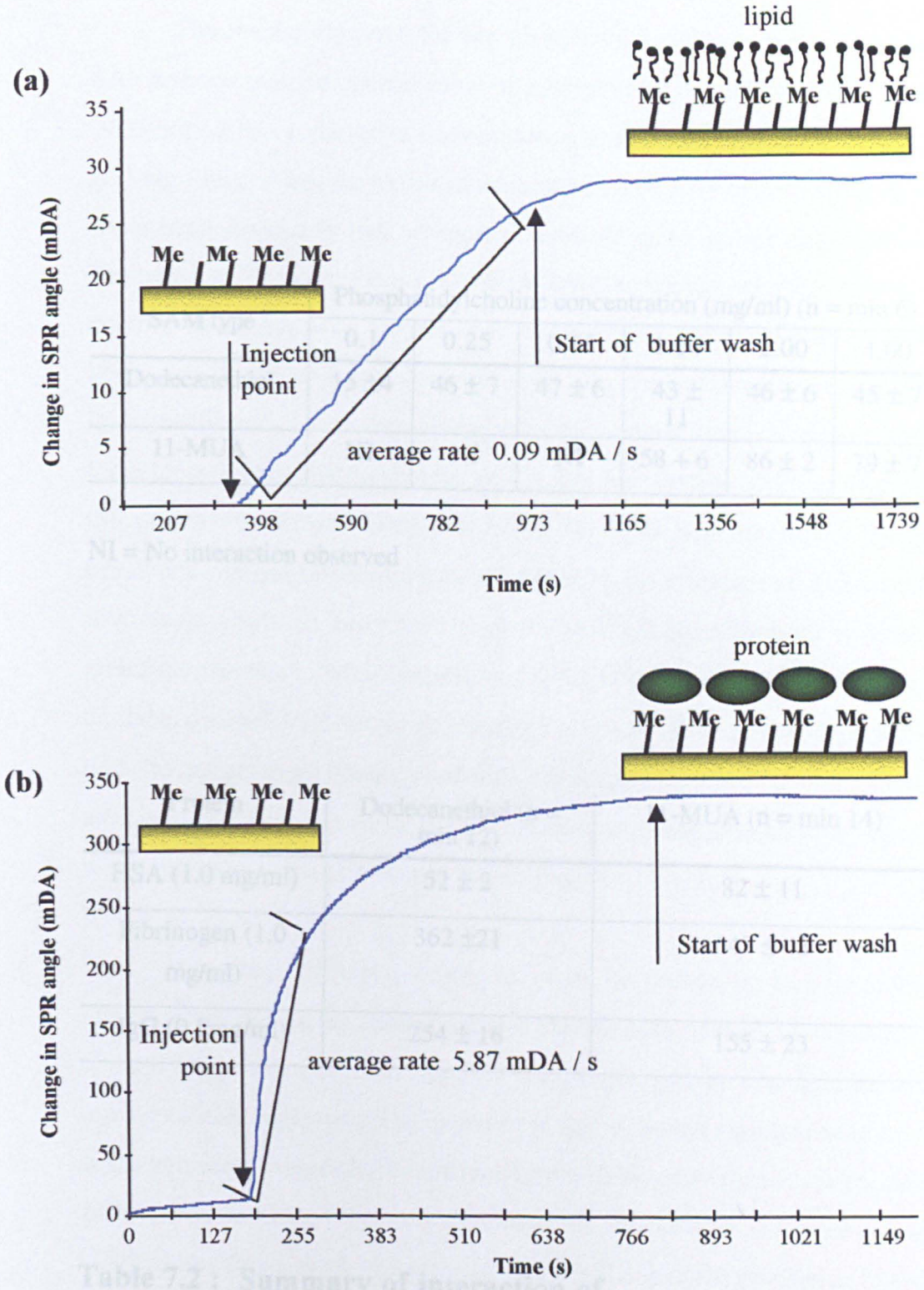

Figure 7.18 : Typical adsorption profiles for PC (a) and fibrinogen (b) to the dodecanethiol SAM

(a) 5 mg / ml PC

(b) 1 mg / ml fibrinogen

SAM type	Phosphatidylcholine concentration (mg/ml) (n = min 6)					
	0.1	0.25	0.75	1.00	2.00	4.00
Dodecanethiol	15 ±4	46 ± 7	47 ± 6	43 ± 11	46 ± 6	45 ± 7
11-MUA	NI	NI	NI	58 + 6	86 ± 2	79 ± 7

NI = No interaction observed

Protein	Dodecanethiol (n = min 12)	11-MUA (n = min 14)
HSA (1.0 mg/ml)	52 ± 2	82 ± 11
Fibrinogen (1.0 mg/ml)	362 ±21	547 ± 43
IgG (0.5mg/ml)	254 ± 16	155 ± 23

Table 7.2 : Summary of interaction of phosphatidylcholine, HSA, IgG and fibrinogen with the dodecanethiol and 11-MUA surfaces

The results obtained for the phosphatidylcholine adsorption to the SAMs shows that the plateau value of adsorption to the dodecanethiol SAM (0.25 mg / ml) is achieved at a lower concentration than that of the 11-MUA (2.0 mg / ml). Also, the extent of adsorption taken from the change in SPR angle is approximately half, at approximately 45 mDA for the dodecanethiol compared to 79 mDA for the 11-MUA SAM at 4 mg / ml PC. This may possibly be explained by the nature of the layer structure of the lipid on these surfaces. On the dodecanethiol, the lipid may form a monolayer with the hydrophobic tails directly associating with the terminal hydrophobic groups of the SAM and their charged headgroups at the outer surface. On the 11-MUA, the positively charged head groups of the lipid may interact with the negatively charged 11-MUA surface. Therefore, the increase in the change in SPR angle could be associated with the charged lipid forming a denser monolayer on the 11-MUA surface of the SAM compared with that formed on the dodecanethiol SAM or alternatively a bilayer of the lipid being formed with the charged head groups outermost. The higher plateau SPR shift may be attributed to either a denser layer or a thicker layer being formed, with respect to the charge and bilayer scenarios respectively.

These two proposed structures could be probed by two methods. Firstly, by measuring the contact angle of the two lipid surfaces against water. If the hydrophobic chains of the lipid were at the interface, a significantly smaller contact angle would be observed to that if the hydrophilic heads were at the interface. Secondly, by interacting the lipid layers formed on the two different SAMs with a negatively charged probe. If a bi-layer is formed on the 11-MUA surface, a similar increase in SPR angle due to the interaction of the negative probe with the lipid should be observed as the lipid layers on both the dodecanethiol and 11-MUA surfaces would have the charged heads of the lipid at the interface. If the increase in SPR angle due to the deposition of the lipid on the 11-MUA surface was due to a denser layer forming with the hydrophobic tails of the lipid at the interface, significantly less binding of the negatively charged probe would be expected when compared to its binding

levels on the lipid surface immobilised on the dodecanethiol surface.

The degree of adsorption of the proteins on the SAMs vary widely. This is due to their different molecular weights, packing abilities and surface charge distributions as previously described by Green et al. (Green (1997)). The adsorption of the protein to the SAMs occurred at a significantly faster rate to that of the lipid (Figure 7.18). This may provide some evidence to suggest that the biphasic shift is due to the different deposition rates of different components of the cell membrane fraction, rather than binding and rearrangement of the lipid component. Further evidence for this hypothesis is that the phosphatidylcholine binding is monophasic rather than biphasic as can also be observed from Figure 7.18. Fibrinogen, gave shifts closest to those observed for the first phase of binding of the cell membrane fraction. Therefore, this protein was used in experiments where the adsorption of a phosphatidylcholine / protein mix was investigated. The results from these experiments are shown in Table 7.3. It can be seen from this table that a ratio of at least 1 : 2.5 lipid to protein is needed to produce a bi-phasic increase in the SPR shift. This suggests that in the cell membrane fraction there must be a mass excess of protein of at least 2.5.

Results from these experiments produced an overall shift of only approximately half of that seen with the cell membrane fraction. This can be rationalised by the facts that the membrane fraction is far more complex than one lipid and one protein mixture, the proteins utilised in the investigation were not membrane proteins and components of the membrane fraction may cause synergistic binding of other components producing the larger observed shift. However, this work has provided an interesting insight into the binding mechanism of the cell membrane fraction to the SPR slide surface and hence supplied a greater understanding of the surface characteristics of the membrane layer. This work could form the foundation for further investigations to probe the cell membrane structure and interactions with this complicated system.

Ratio of lipid to protein	Overall SPR angle shift	Phase 1 SPR angle shift	Phase 2 SPR angle shift
4 : 1	304 ± 7 (n = 5)	304 ± 7	N/O
1 : 1	311 ± 26 (n = 7)	311 ± 26	N/O
1 : 2.5	394 ± 47 (n = 7)	317 ± 21	75 ± 18
1 : 3	476 : 38 (n = 6)	329 ± 17	128 +32

N/O Not observed

Table 7.3 : Effect of lipid : protein ratio on adsorption profile observed on dodecanethiol SAM with SPR

7.3.1.6 : Interaction with model membrane surface

Figure 7.19 shows the binding of the PAMAM dendrimers as measured by SPR to the Caco2 cell membrane fraction. There is a significant difference observed between the carboxyl (generation n.5) and amino terminated (generation n.0) dendrimers.

For the carboxyl terminated dendrimers, only a very low level of binding is observed, independent of generation size with the membrane surface. This can be attributed to their negative surface charge and the cell membrane composition. The cell membrane is a complex system comprised of lipids, both charged and neutral, proteins which may be integral or peripheral, as well as carbohydrates which are attached to other membrane constituents (Darnell (1990)). This complicated structure and the fact that the components overall percentage in the cell membrane can vary significantly, means that its interactions with this material are also complicated. However, a few generalization can be made about the cell membrane. The lipid portion of the membrane forms a bilayer with the polar heads outermost. At a neutral pH, the majority of the lipid portion of the membrane posses a neutral or negative charge (Ganong (1993)). Attached to this lipid bilayer are the proteins. These bind by either hydrophobic interactions with the lipid acyl chain or by protein-protein interactions. Overall, the cell membrane possess a net negative charge at both of its surfaces (Ganong (1993)). Therefore, the low level of interaction between the carboxyl terminated dendrimers and the membrane surface can be attributed to charge repulsion between the two negatively charged entities. The small extent of interaction observed between the membrane layer and the carboxyl terminated dendrimers is probably due to non-specific interactions between the surface exposed protein portion of the membrane layer or the neutral lipids and the dendrimers.

When considering the data for the amino terminated dendrimers, the extent of interaction increases with dendrimer generation. This can be

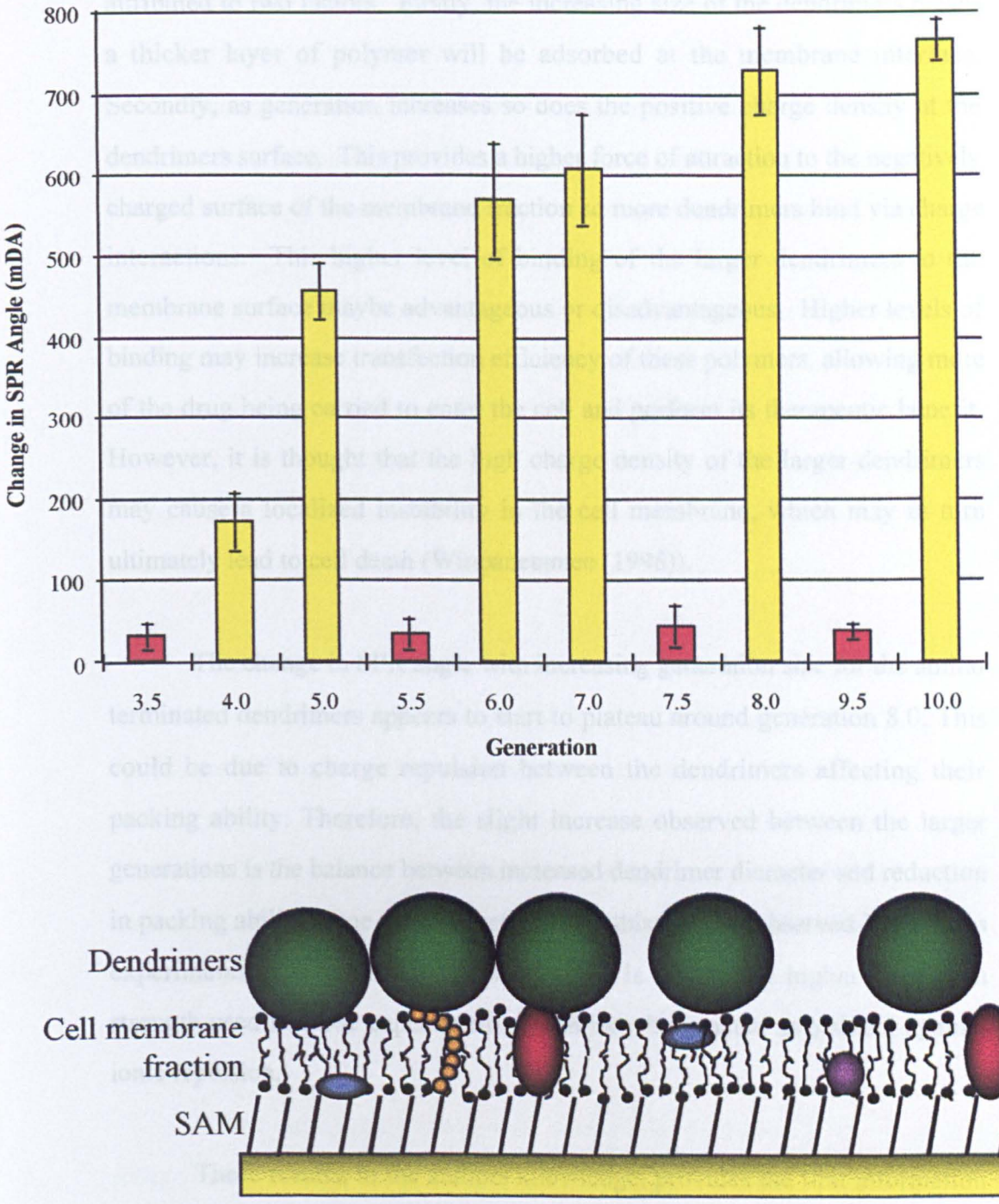

Figure 7.19 : Interaction between PAMAM dendrimers and CACO2 cell membrane fraction

Bars = average ± 1 standard deviation ($n \geq 20$)

attributed to two factors. Firstly, the increasing size of the dendrimers means a thicker layer of polymer will be adsorbed at the membrane interface. Secondly, as generation increases so does the positive charge density at the dendrimers surface. This provides a higher force of attraction to the negatively charged surface of the membrane fraction so more dendrimers bind via charge interactions. This higher level of binding of the larger dendrimers to the membrane surface maybe advantageous or disadvantageous. Higher levels of binding may increase transfection efficiency of these polymers, allowing more of the drug being carried to enter the cell and perform its therapeutic benefit. However, it is thought that the high charge density of the larger dendrimers may cause a localized instability in the cell membrane, which may in turn ultimately lead to cell death (Winpanetantee (1998)).

The change in SPR angle with increasing generation size for the amino terminated dendrimers appears to start to plateau around generation 8.0. This could be due to charge repulsion between the dendrimers affecting their packing ability. Therefore, the slight increase observed between the larger generations is the balance between increased dendrimer diameter and reduction in packing ability. One possible reason why this was not observed in previous experiments with the model SAM surfaces is due to the higher buffer ion strength used in those experiments which may have acted as a shield against ionic repulsion.

These results, to the authors knowledge, provides the first information on the effect of dendrimer charge and generation on the degree of interaction with immobilised cell membrane fractions. It is encouraging to note that this data agrees with work performed by Dr. R. Winpanetantee on the inverted gut sac model which measures the ability of materials to traverse the gut wall. In her studies, she showed significantly more transport across the gut wall for the amino terminated dendrimers when compared to the carboxyl ones, as well as a generation dependance for the transport levels of amino terminated dendrimers (Winpanetantee (1998)).

7.3.1.7 : Dendrimer interactions with DNA

The interaction of DNA with dendrimers adsorbed onto SAMs by hydrophobic (dodecanethiol) and charge interactions (11-MUA or 2-aminoethanethiol) were investigated to determine factors which may contribute to the loading of these polymers with DNA. Control experiments were performed to ascertain the binding level of DNA to the uncoated SAMs, to check that levels of DNA interaction with any uncovered areas of the SAM were minimal. An average shift of 15 ± 7 mDA was obtained for DNA adsorption to the dodecanethiol SAM. This is only a small interaction and can be attributed to hydrophobic interactions between the DNA and SAM interface.

Figure 7.20 summarises the extent of interaction of the DNA with the dendrimers. Three dendrimers were chosen for this investigation. Firstly two dendrimers of similar size, but oppositely charged (generation 8.0 and 9.5) where chosen to investigate the effect of the dendrimers surface charge on the extent of interaction with the DNA, and secondly, two dendrimers of the same charge but differing sizes (generation 8.0 and 4.0), were chosen to investigate the effect of charge density and polymer conformation on the interaction of the dendrimers with DNA.

When considering the results concerned with the effect of surface charge on the interaction of the dendrimers with DNA, it can be observed that the binding of DNA to the generation 8.0 dendrimer is significantly higher than that for the generation 9.5 dendrimer. Binding of DNA to the 9.5 dendrimer is likely to be primarily due to hydrophobic interactions. However, binding to the 8.0 dendrimer will have contributions not only from hydrophobic interactions but also charge interactions, as it possesses an opposite charge to the DNA at this pH. It can be observed from Figure 7.20 that the interaction between the generation 9.5 dendrimer and the DNA is less than that observed for its interaction with the hydrophobic methyl terminated SAM. This may

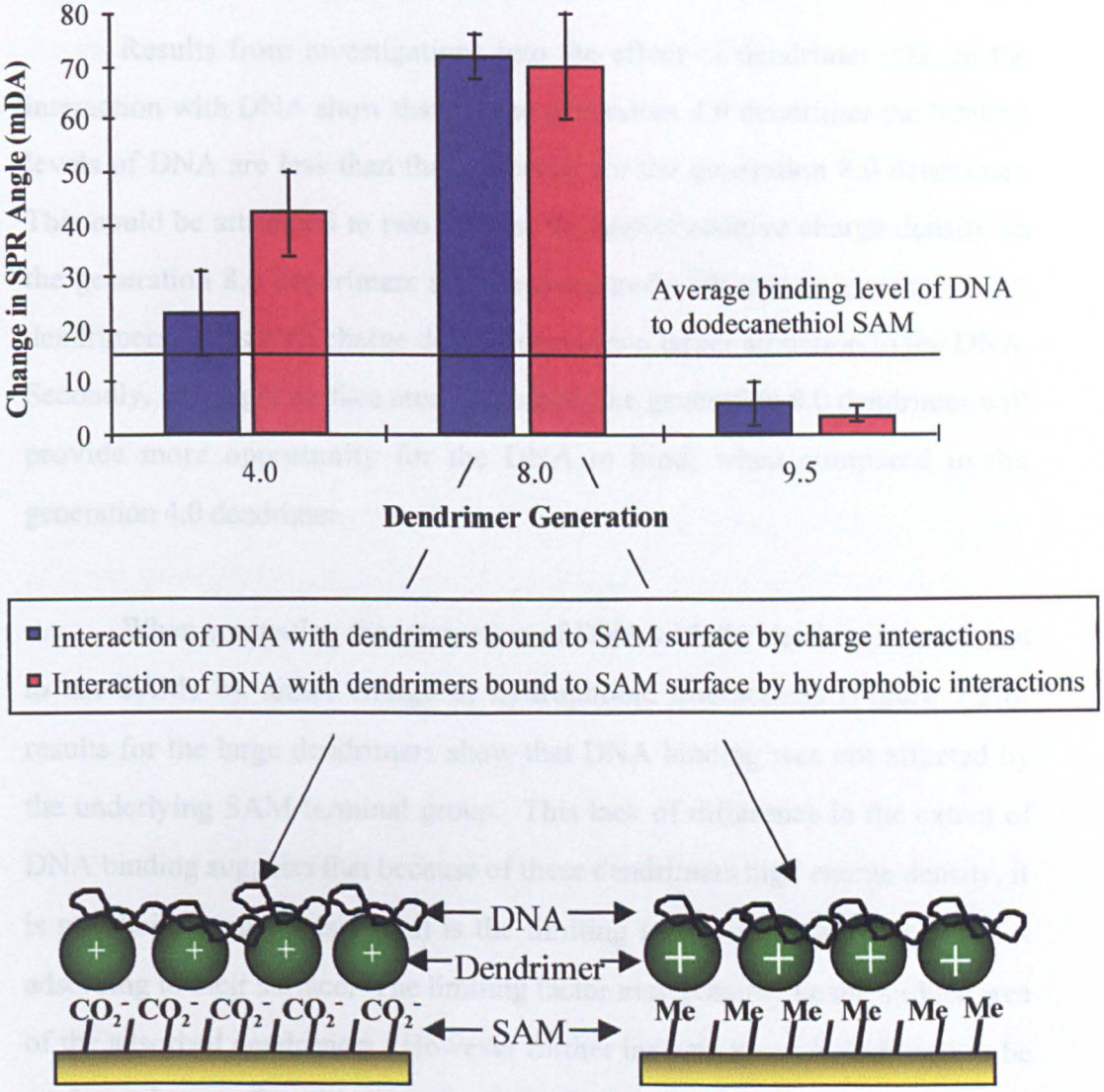

Figure 7.20 : Interaction between PAMAM dendrimers and DNA

bars = average ± 1 standard deviation (n ≥ 18)

be attributed to the dendrimers negative surface charge which will repel the like-charged DNA reducing the opportunity for hydrophobic interactions.

Results from investigations into the effect of dendrimer size on the interaction with DNA show that for the generation 4.0 dendrimer the binding levels of DNA are less than that observed for the generation 8.0 dendrimer. This could be attributed to two factors; the higher positive charge density on the generation 8.0 dendrimers surface compared with that on generation 4.0 dendrimers. This high charge density provides a larger attraction to the DNA. Secondly, the larger surface area of the ball like generation 8.0 dendrimer will provide more opportunity for the DNA to bind, when compared to the generation 4.0 dendrimer.

When comparing the interaction of DNA with the dendrimers adsorbed to the SAMs by either charge or hydrophobic interactions (Figure 7.20), results for the large dendrimers show that DNA binding was not affected by the underlying SAM terminal group. This lack of difference in the extent of DNA binding suggests that because of these dendrimers high charge density, it is not their charge density that is the limiting factor to the amount of DNA adsorbing to their surface. The limiting factor may possibly be the surface area of the adsorbed dendrimers. However further investigations would have to be performed to confirm this hypothesis.

Results for the generation 4.0 dendrimer show a significant decrease in the amount of DNA binding to the dendrimer surface when the dendrimer is adsorbed to the SAMs by a charge interaction compared to when it is adsorbed due to hydrophobic interactions. This can be attributed the surface charge density of the dendrimer in these two different cases. On the methyl terminated SAM the dendrimer binds to the surface via hydrophobic interactions so all its surface charge will be available to bind to DNA. However, on the charged SAM surface, since the generation 4.0 dendrimer only possesses 24 charged terminal groups, after interacting with the

oppositely charged SAM, the number of positive charges left on the dendrimer to bind DNA will be minimal. Therefore less DNA will bind, resulting in the significantly lower change in SPR angle observed. It should also be noted that the extent of interaction with the generation 4.0 dendrimer on the charged surface is not significantly different from that of the DNA interacting with the methyl terminated SAM. This could suggest that the majority of the DNA binding to the dendrimer in this case is due to hydrophobic interactions.

7.3.2 AFM imaging

The SPR studies described above provided information on the effect of dendrimer surface charge and size on the extent of their interaction with a range of model surfaces. However, it is unable to provide direct information on the packing density and structure of the dendrimers on the model surfaces. For this reason AFM was employed to provide high resolution images of the dendrimers and hopefully glean more information on how dendrimer charge and size influences their interaction with surfaces.

8.3.2.1 : AFM imaging in air

Preliminary AFM imaging studies to obtain information on the dendrimers structure when adsorbed to the model surfaces were performed in air. Figure 7.21 shows typical images of the SAM on a gold surface as well as images of various dendrimer generations adsorbed onto this interfaces. Figure 7.21 (a) depicts a methyl terminated SAM on gold. This images shows a relatively flat surface, where the only features observed are the gold islets and small spaces between these which are the underlying mica. However, in Figure 7.21 (c) and (d) which depict images of the SAM after incubation with the generation 9.5 and 6.0 dendrimers respectively, a variety of spheroidal entities are observed.

The mean size of the generation 9.5 and 6.0 dendrimers are 11.90 ± 1.92 and 8.26 ± 1.36 nm respectively. These values are significantly larger

than the theoretical values of 9.5 and 6.0 nm for the generation 9.5 and generation 6.0 dendrimers (Malik (1999)). These discrepancies may be due to two facts. Firstly, broadening of the dendrimer features due to tip deconvolution (Vesenka (1996), Williams (1994)) and secondly, the drying of the dendrimer samples for air imaging, which may cause some degree of collapse and spreading of the dendrimers. The relatively wide distribution of dendrimer sizes may be attributed to the drying of the dendrimer sample. Depending on the dendrimers position in the sample, for example its number of nearest neighbours and its position on the gold surface, (ie. if it is at the edge or middle of an islet), it will have different forces acting on it as the liquid front recedes on drying the sample. These differing degrees of force will change the conformation of the dendrimer to different extents producing the variety of dimensions observed for the dried dendrimers.

Only dendrimers of generation 5.0 or larger could be imaged clearly. Below this value a rough surface was observed with oval entities of varying sizes. The clarity of these entities decreased with dendrimer generation. However, even with the smallest dendrimers, a significant difference was observed between the surface structure of the SAM before and after deposition of the dendrimers. These dendrimer entities are depicted in Figure 7.21 (b) which shows a typical image of the generation 4.0 dendrimers on the methyl terminated SAM, and are attributed to areas of aggregated dendrimers. This aggregation can be attributed to the dendrimers increased flexibility below generation 5.0, which allows interpenetration of branches of neighboring dendrimers producing a denser and less defined surface layer.

This image may provide some evidence to support the results obtained from the SPR investigations into the adsorption of the small dendrimers onto the methyl terminated SAM surface. A relatively large SPR shift was observed for these small entities when considering their diameter. For example, the generation 4.0 PAMAM has a diameter of only 4 nm. However, these AFM images show that the dendrimers form a dense interpenetrating

(a)

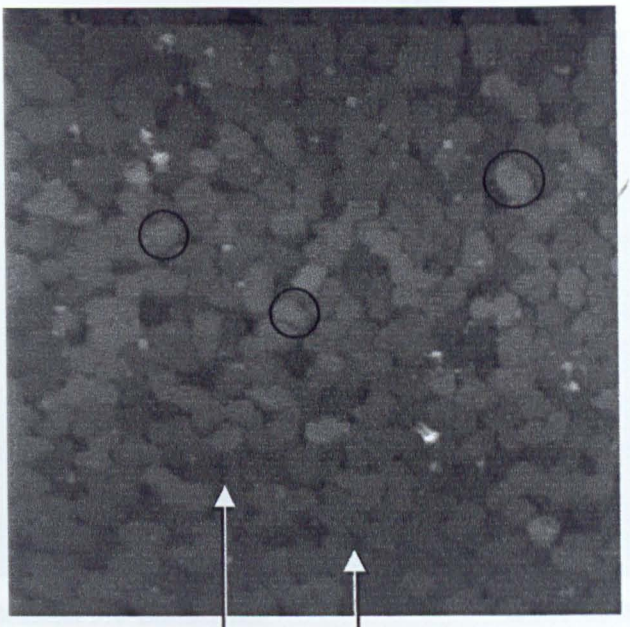

Methyl SAM
4.00 x 4.00 µm image
z scale = 5 nm

Rings circle
individual gold islets

Holes between gold islets

(b)

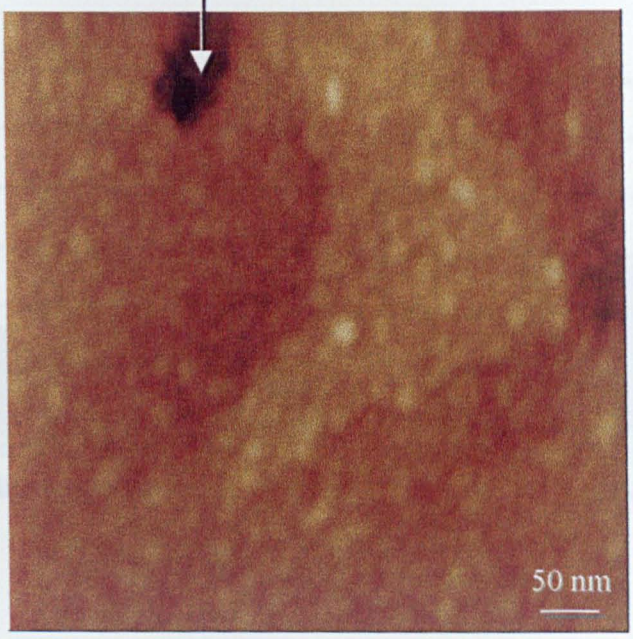

Generation 4.0
500 x 500 nm image
z scale = 5 nm

Figure 7.21 : AFM images of dendrimer in air
(a) Methyl SAM on gold
(b) Generation 4.0 dendrimer

(c)

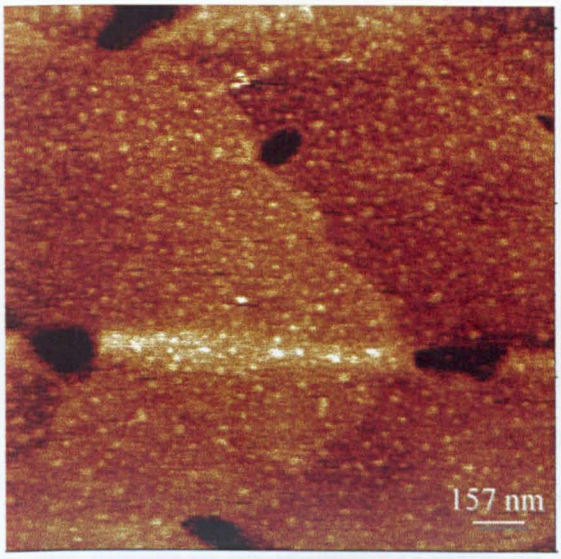

Generation 9.5 dendrimer
1.57 x 1.57 μm image, z scale = 12 nm

(d)

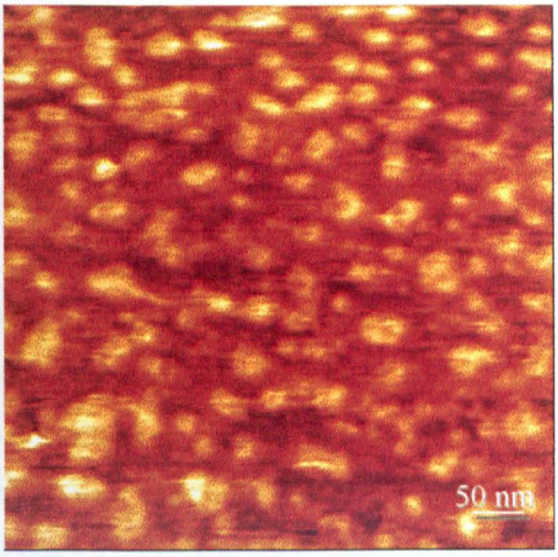

Generation 6.0 dendrimer
500 x 500 nm image, z scale = 8 nm

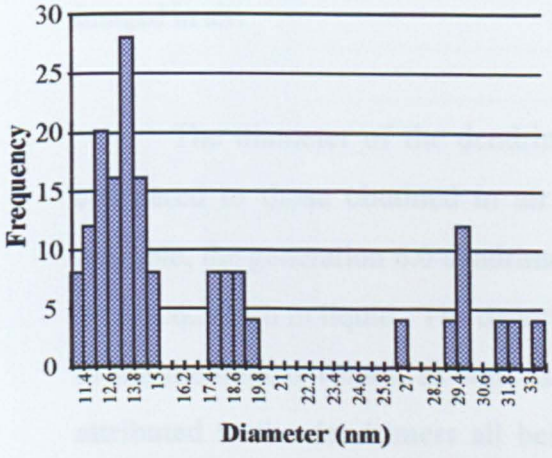

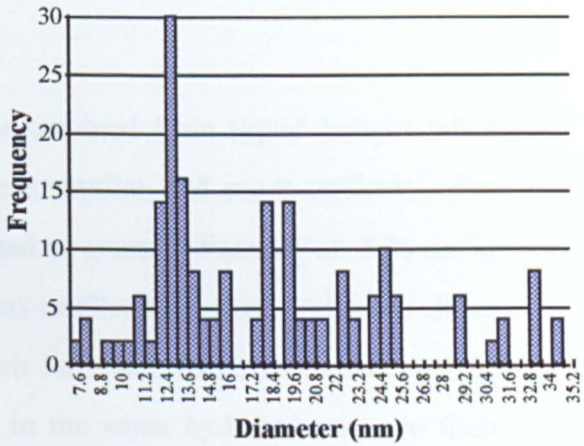

Figure 7.21 : AFM images of dendrimers in air
(c) generation 9.5 dendrimer
(d) generation 6.0 dendrimer

layer on the surface and this high density of the thin dendrimer film may indeed account for the relatively large SPR shift observed for these dendrimers in comparison to their diameter.

7.3.2.2 : AFM liquid imaging - effect of generation

Figure 7.22 depicts images of the generation 10 and generation 6.0 dendrimers adsorbed on a 11-MUA SAM, and the size distribution of these dendrimers when measured in an aqueous environment. The surface structure of these dendrimers is not as well defined in these images when compared to the images of the dendrimers taken air (Figure 7.21). The appearance of the dendrimers under liquid can be attributed to the fact that under an aqueous environment the dendrimers will be hydrated and hence their structure will be softer and easier to deform when compared to its dehydrated state when imaged in air.

The diameter of the dendrimers obtained from liquid images when compared to those obtained in air were smaller and more uniform. For example, the generation 6.0 dendrimer had an average diameter of 8.26 nm in air and 6.26 nm in liquid. The dendrimers smaller diameters, which are closer to the theoretical values, as well as their narrower size distribution may be attributed to the dendrimers all being in the same hydrated state, so their structural dimensions should all be the same.

As observed in air imaging, when imaging dendrimers of generations less than 5.0, individual dendrimers were difficult to distinguish. This is attributed to their flexible nature, allowing interpenetration of the dendrimer branches to form molecular aggregates. These aggregates varied in size and their surface structure was poorly resolved when imaged in liquid due to the flexible nature of these small dendrimers, indicating they were easy to deform.

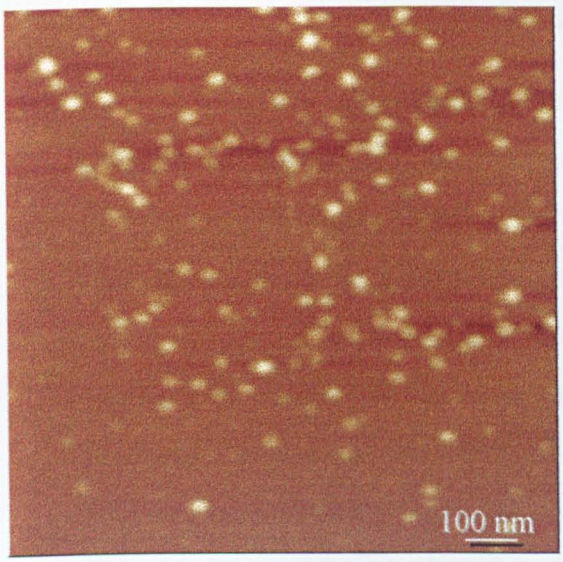

Generation 10.0 PAMAM imaged in buffer
image = 1.00 x 1.00 μm z scale = 9 nm

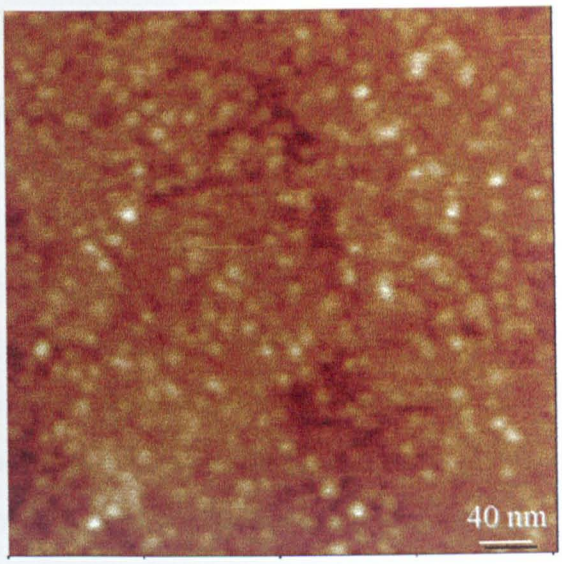

Generation 6.0 PAMAM imaged in buffer
image = 400 x 400 μ^2 z scale = 4 nm

Size distribution in liquid for generation 10.0 PAMAM dendrimer

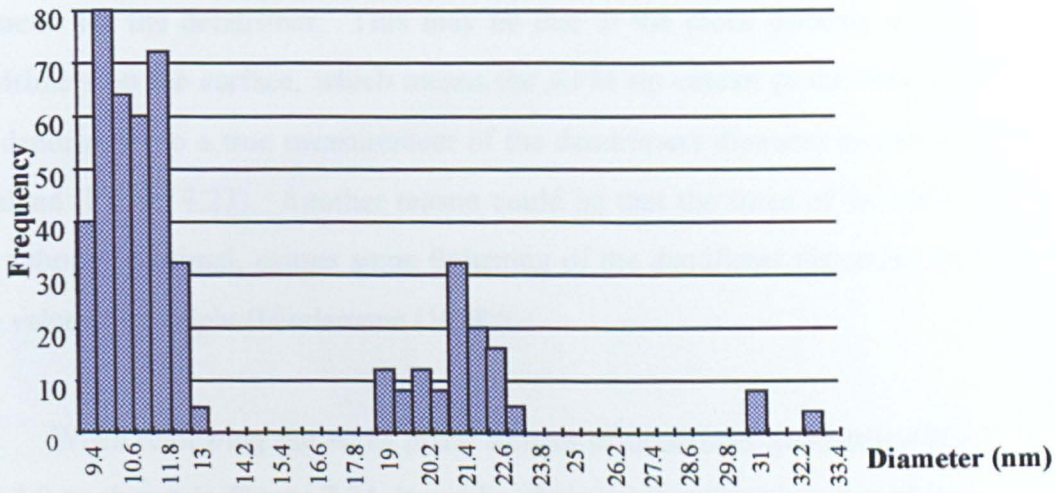

Size distribution in liquid for generation 6.0 PAMAM dendrimer

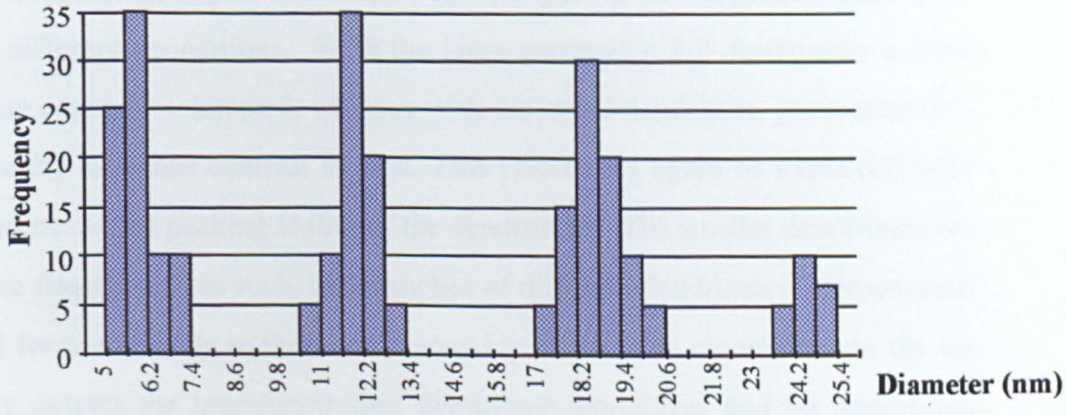

Figure 7.22 : AFM images in buffer

Figure 7.23 shows the distribution of height measurements taken for generation 7.0 dendrimers both in liquid and air with contact forces no greater than 0.17 nN different of each other. Firstly, it can be observed that the most common height value in air is less than that in liquid. This may attributed to the flattening of the dendrimers during the drying process, as well as the capillary forces on the tip during imaging. Secondly, the distribution of dendrimer heights measured from air samples, as can be observed from Figure 7.23 are greater than those obtained from images of the dendrimer under liquid. This again may be attributed to the many different conformations the dendrimers collapse into due to the different forces acting on them as the sample was dried. The narrower spread for the hydrated sample may be attributed to the fact that all the dendrimers should be in the same hydrated state. In both sets of data the height measurements are less than the theoretical diameter for the dendrimer. This may be due to the close packing of the dendrimers on the surface, which means the AFM tip cannot probe between the dendrimers so a true measurement of the dendrimers diameter cannot be obtained (Figure 7.23). Another reason could be that the force of the AFM tip, although minimal, causes some flattening of the dendrimer distorting the true value of its height (Hierlemann (1998)).

When reviewing the AFM phase images of dendrimer generations 8.0 and 4.0 as shown in Figure 7.24, it can be observed that there is a significant difference in the degree of contrast when comparing the images produced from the different generations. With the large generation 8.0 dendrimers a large phase contrast is detected, whereas with the small dendrimer, generation 4.0, virtually no phase contrast is seen. This effect may again be explained with reference to the packing ability of the dendrimers. The smaller dendrimers are more flexible and as such, the branches of different dendrimers interpenetrate and form a densely packed continuous layer. In such circumstances the tip only detects the interpenetrating dendrimer monolayer and no underlying substrate and so little phase contrast is observed. With the large ball-like dendrimers which maintain their spherical structure the packing is not as dense

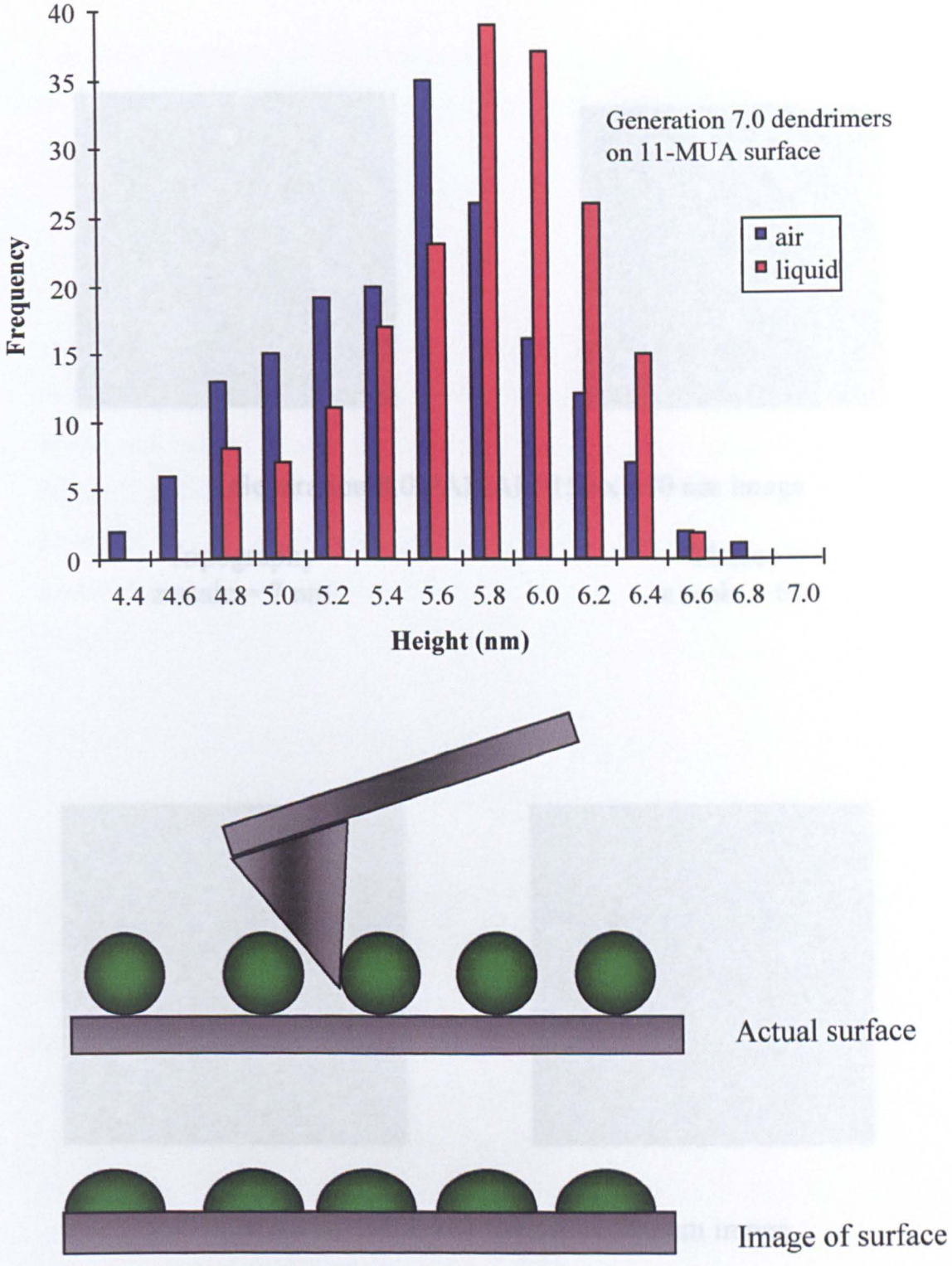

Figure 7.23 : Height distribution taken from both liquid and air images of dendrimers

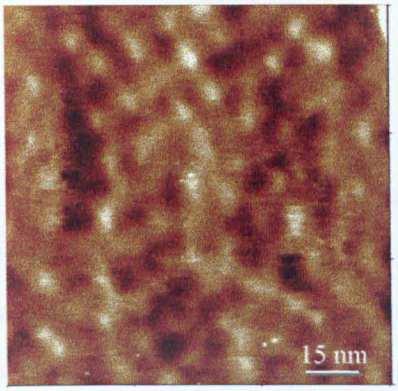

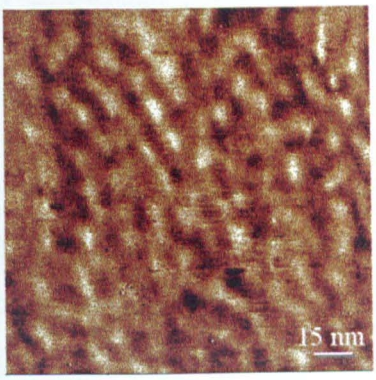

Generation 8.0 PAMAM 150 x 150 nm image

Topography
z scale = 7 nm

Phase
z scale = 6°

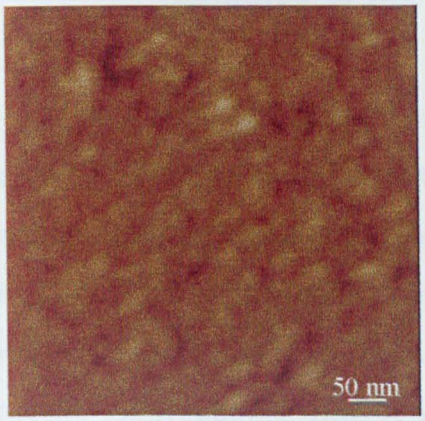

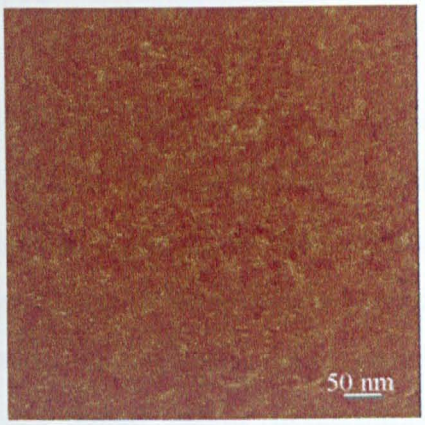

Generation 3.0 PAMAM 500 x 500 nm image

Topography
z scale = 6 nm

Phase
z scale = 6°

Figure 7.24 : Effect of dendrimer generation on packing as observed from phase images

and interpenetrating. It is likely in such a case that the tip would sense both the dendrimer monolayer and the underlying SAM, so a larger phase contrast is observed.

Images in Figure 7.21 and 7.22 were obtained using dendrimer concentrations of 0.1 μg / ml to try to obtain images of individual dendrimers, although most formed monolayers. When images were obtained of the dendrimers using the same concentration as used in SPR (0.1 mg / ml), the dendrimers took on a more closely packed surface arrangement as shown in Figure 7.25 showing generation 8.0 dendrimers on a 11-MUA surface. It is proposed that the dendrimers take on this pseudo-crystalline molecular packing to minimise the unfavourable charge repulsion interaction felt between them.

7.3.2.3 : Effect of SAM terminal group on the images obtained of the dendrimers

No significant difference was observed between the size or shape of the dendrimers when adsorbed onto the SAMs with carboxyl, amino or methyl terminal groups. However, when imaging the larger sized dendrimers, generations 6.0 and upwards, very low imaging forces were needed on the methyl terminated SAM to obtain clear pictures. This suggests that the non-specific hydrophobic interactions between these larger dendrimers (irrespective of surface charge) and the methyl terminated SAM surface is weak. This is depicted in Figure 7.26. The same phenomena was observed with the carboxyl and amino SAM surfaces when dendrimers of the same charge were adsorbed to the surface. In this case repulsive forces between the dendrimer and SAM will be predominant. However this 'sweeping' did not occur in cases where the dendrimers and SAM possessed opposite charges and attractive forces were dominant. This suggests that the charge attraction forces between the oppositely charged dendrimers and surfaces promotes a significant interaction.

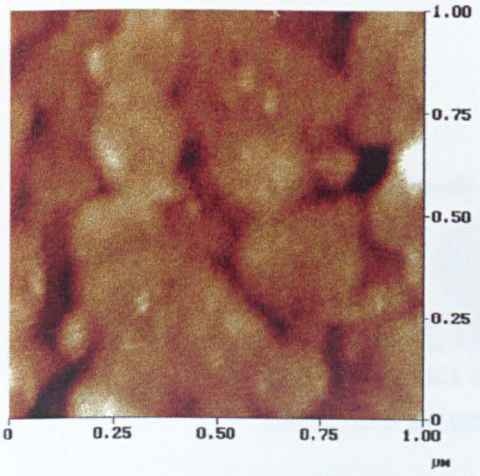

1.00 x 1.00 µm image
z scale =15 nm

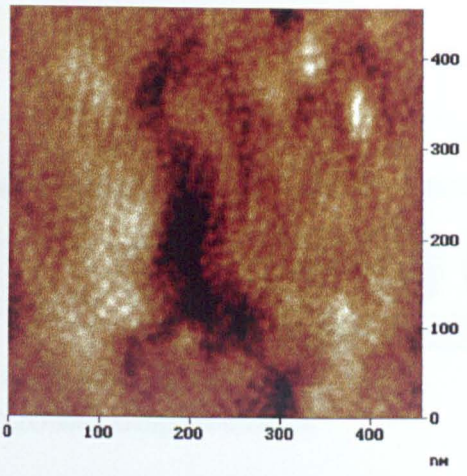

450 x 450 nm image
z scale =15 nm

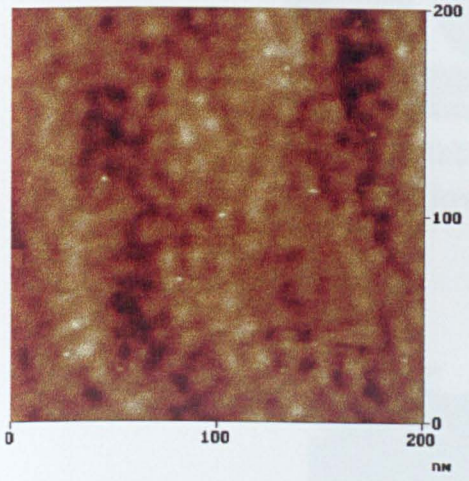

200 x 200 nm image
z scale = 7 nm

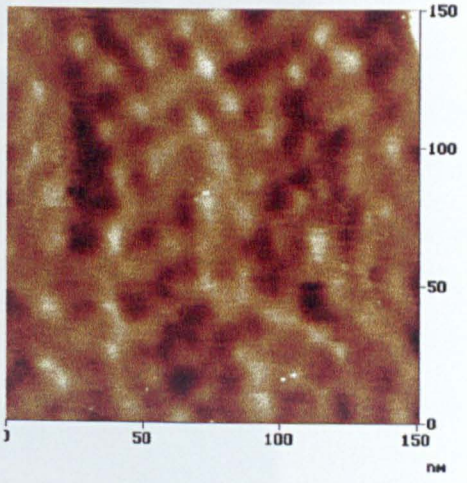

150 x 150 nm image
z scale = 6 nm

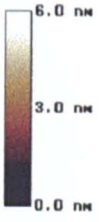

Figure 7.25 : Close packed generation 8.0 dendrimers observed by AFM

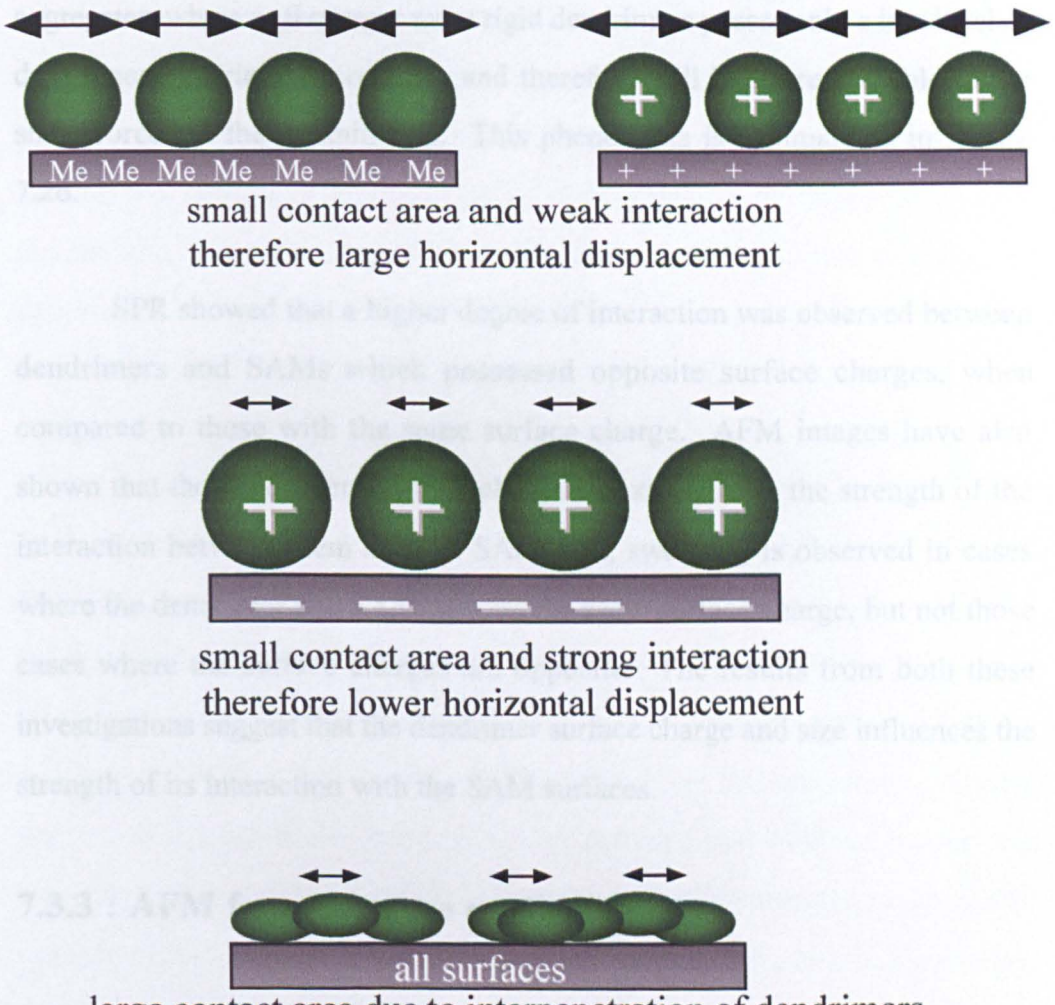

Figure 7.26 : Schematic representation of the effect of dendrimer-surface interactions on the degree of sweeping

The 'sweeping' phenomena was reduced significantly or not observed at all with dendrimers of generation 5.0 or less. This suggests that these smaller dendrimer monolayers are stabilised by forming interpenetrating aggregates, where as the larger more rigid dendrimers posses only a low level of dendrimer-dendrimer association and therefore will be more unstable to the shear forces of the scanning tip. This phenomena is summarised in Figure 7.26.

SPR showed that a higher degree of interaction was observed between dendrimers and SAMs which possessed opposite surface charges, when compared to those with the same surface charge. AFM images have also shown that the dendrimers surface charge and size effects the strength of the interaction between them and the SAMs, ie., sweeping is observed in cases where the dendrimer and SAM possess the same surface charge, but not those cases where the surface charges are opposite. The results from both these investigations suggest that the dendrimer surface charge and size influences the strength of its interaction with the SAM surfaces.

7.3.3 : AFM force-distance studies

AFM force-distance experiments were performed to quantify the strength of the dendrimer's interactions with the different surfaces. AFM imaging conditions suggested that differing degrees of force existed between the dendrimers and surfaces, but no quantitative value could be obtained. As well as quantifying the effect of dendrimer terminal group and degree of branching on the strength of the interaction, pH and ionic strength of the buffer were also investigated to determine the role of charge versus hydrophobicity on the overall interactions.

7.3.3.1 : Biotinylation of dendrimers and characterisation

To measure the strength of interaction between the dendrimers and SAM surfaces a method needed to be developed to immobilise the dendrimers firmly onto the AFM tip. It was decided that an avidin-biotin immobilisation strategy, as introduced in Chapter 4 would be utilised. Therefore, the dendrimers needed to biotinylated to allow them to be immobilised to a streptavidin coated tip. It was important that enough biotin was added to the dendrimers to allow effective immobilisation, but not so much that the surface properties of the dendrimers were significantly altered.

To check that the dendrimers had been biotinylated SPR experiments as described in 7.2.3.1 were utilised. Before labelling all the dendrimers, investigations were performed on the generation 3.5 dendrimers to determine the minimum amount of biotin groups which would give maximum levels of binding to a streptavidin monolayer. Results from this experiment are shown in Figure 7.27 (a). It can be observed from this figure that the non-biotinylated generation 3.5 dendrimer has a low level of interaction with the streptavidin monolayer (9 ± 4 mDA) prior to biotinylation. This is attributed to the charge attraction between the positively charged dendrimer and the negatively charged protein monolayer. For the biotinylated dendrimers the interaction with the monolayer of streptavidin increases as the degree of biotinylation increases up to a level of 10% substitution where the SPR shift is 45 ± 12 mDA, above this level there is no significant increase in the extent of dendrimer binding to the streptavidin monolayer. Therefore a 10 % substitution of the surface groups was utilised to biotinylate all other dendrimer generations as this level of biotinylation provided maximum binding to the streptavidin surface with minimal alteration to the dendrimers surface characteristics.

Figure 7.27 (b) shows the effect of the spacer length of the biotinylating agent on the extent of binding of the biotinylated dendrimer to the streptavidin monolayer. The binding of the generation 5.5 dendrimer to the

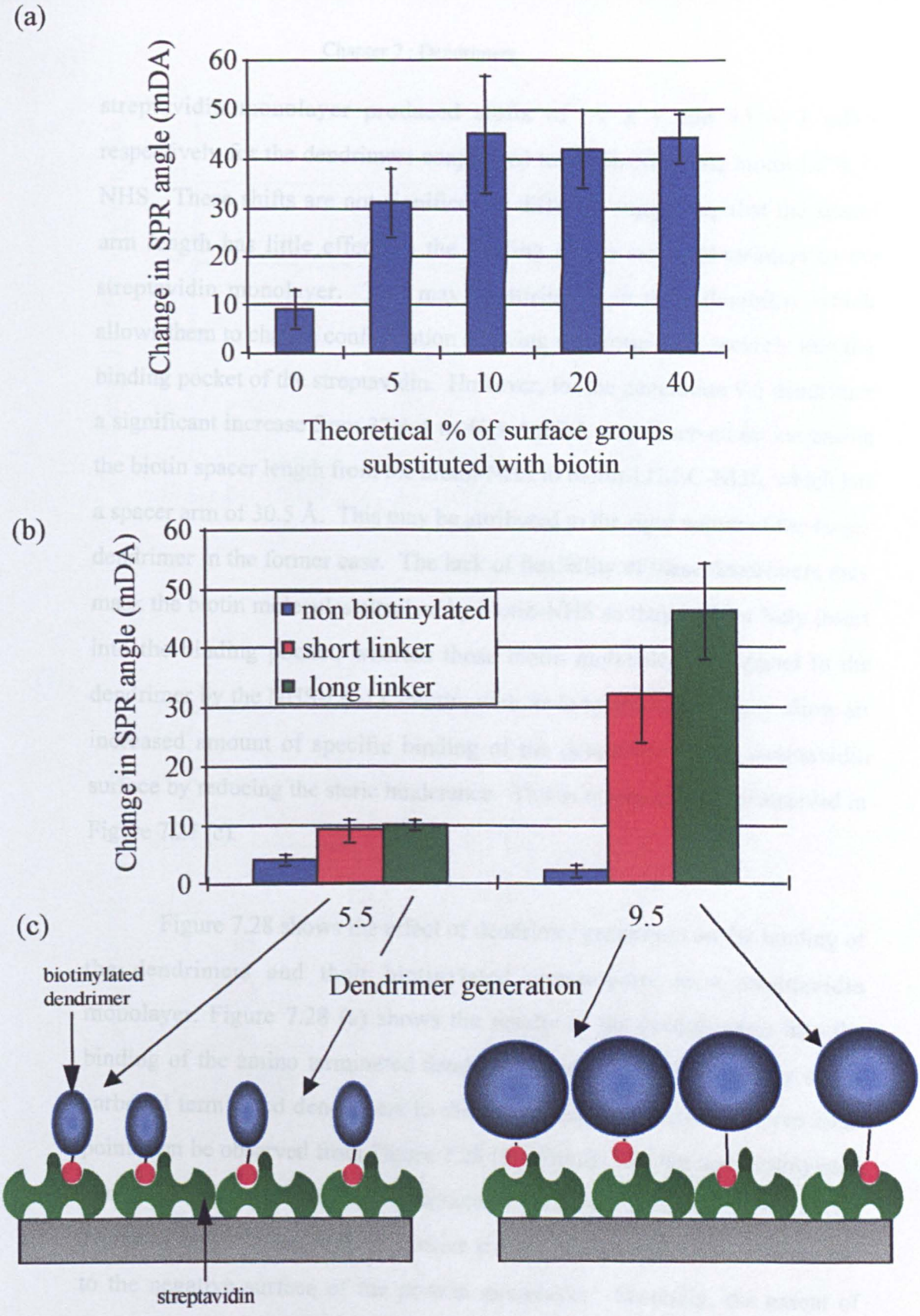

Figure 7.27 : Effect of biotinylation on interaction of dendrimers with streptavidin (1)

(a) Effect of degree of substitution
(b) Effect of linker length
(c) Schematic representation of effect of linker length

bars = average ± 1 standard deviation (n ≥ 15)

streptavidin monolayer produced shifts of 9 ± 1 and 15 ± 3 mDA respectively for the dendrimers conjugated to biotin-NHS and biotin-LC-LC-NHS. These shifts are not significantly different suggesting that the spacer arm length has little effect on the binding of the small dendrimers to the streptavidin monolayer. This may be attributed to their flexibility which allows them to change conformation allowing the biotin to fit securely into the binding pocket of the streptavidin. However, for the generation 9.5 dendrimer a significant increase from 32 ± 4 to 46 ± 6 mDA was observed on increasing the biotin spacer length from the biotin-NHS to biotin-LC-LC-NHS, which has a spacer arm of 30.5 Å. This may be attributed to the rigid nature of the larger dendrimer in the former case. The lack of flexibility of these dendrimers may mask the biotin molecules attached by biotin-NHS so they can not fully insert into the binding pocket, whereas those biotin molecules conjugated to the dendrimer by the NHS-LC-LC-biotin, with its long spacer arm, may allow an increased amount of specific binding of the dendrimer to the streptavidin surface by reducing the steric hinderance. This is schematically represented in Figure 7.27 (c).

Figure 7.28 shows the effect of dendrimer generation on the binding of the dendrimers and their biotinylated counterparts to a streptavidin monolayer. Figure 7.28 (a) shows the results of the investigation into the binding of the amino terminated dendrimers and 7.28 (b) the binding of the carboxyl terminated dendrimers to the streptavidin monolayer. Three main points can be observed from Figure 7.28 (a). Firstly, that the non-biotinylated dendrimers show a significant interaction with the streptavidin monolayer. This may be attributed to their positive surface charge which will be attracted to the negative surface of the protein monolayer. Secondly, the extent of interaction is observed to increase with dendrimer generation. This can be attributed to two factors. Primarily, the increase in dendrimer diameter with increasing generation which will lead to a thicker layer of dendrimers being formed on the surface, but also, as the dendrimer generation increases so will the positive charge density at its surface providing a greater potential for

(a)

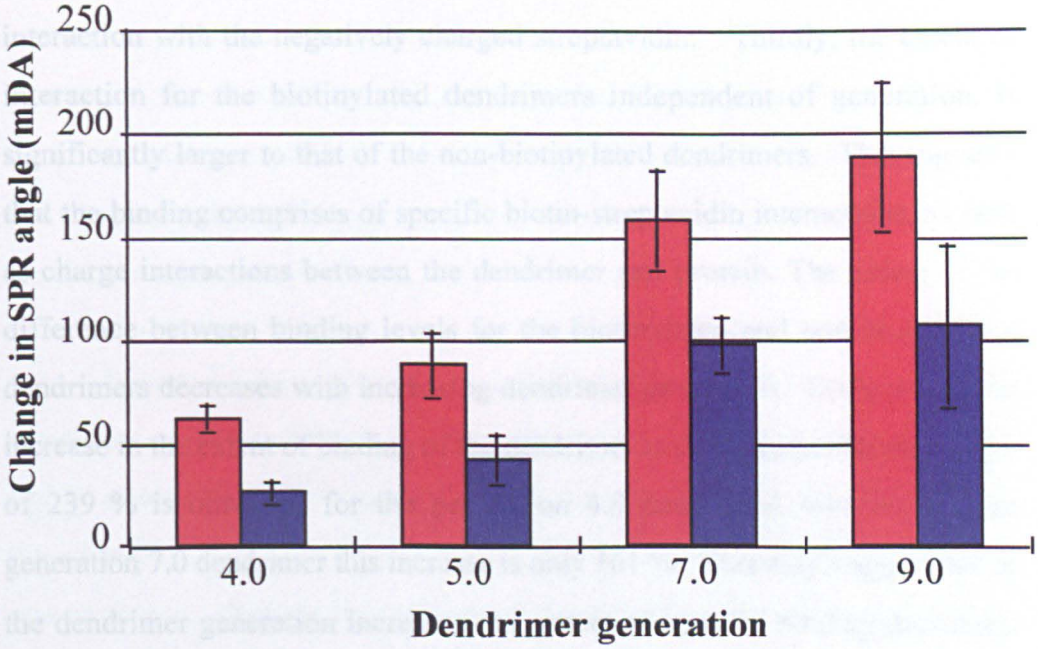

(b)

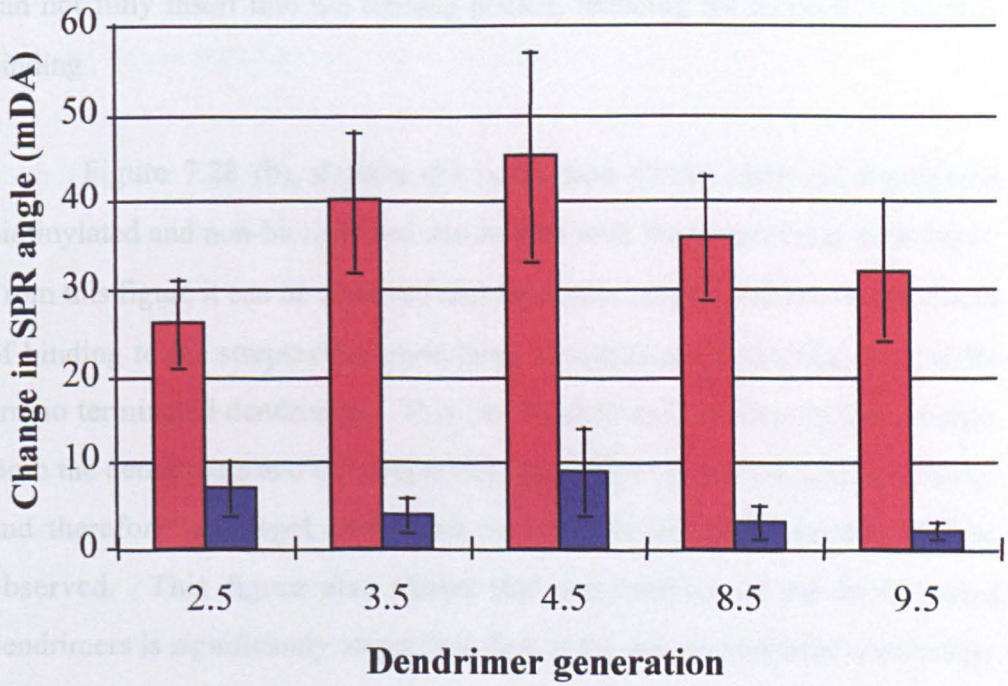

Figure 7.28 : Effect of biotinylation on interaction of dendrimers with streptavidin (2)
(a) Amino terminated dendrimers
(b) Carboxyl terminated dendrimers

bars = average ± 1 standard deviation (n ≥ 19)

interaction with the negatively charged streptavidin. Thirdly, the extent of interaction for the biotinylated dendrimers independent of generation, is significantly larger to that of the non-biotinylated dendrimers. This suggests that the binding comprises of specific biotin-streptavidin interactions, as well as charge interactions between the dendrimer and protein. The extent of the difference between binding levels for the biotinylated and non-biotinylated dendrimers decreases with increasing dendrimer generation. For example, an increase in the extent of binding of the dendrimer to the streptavidin monolayer of 239 % is observed for the generation 4.0 dendrimer, whereas for the generation 7.0 dendrimer this increase is only 161 %. This may suggest that as the dendrimer generation increases, the extent of specific binding decreases. The reason for this effect may be many-fold, but it may possibly be attributed to the lack of flexibility in the larger dendrimers, which mask the biotin so it can not fully insert into the binding pocket, reducing the amount of specific binding .

Figure 7.28 (b), depicts the interaction of the carboxyl terminated biotinylated and non-biotinylated dendrimers with the streptavidin monolayer. From this figure it can be observed that for similar sized dendrimers, the extent of binding to the streptavidin monolayer is significantly less than that of the amino terminated dendrimers. This can be attributed to their surface charge. Both the dendrimers and the streptavidin monolayer possess a negative charge and therefore will repel each other so lower levels of interaction will be observed. This figure also shows that the binding of the biotinylated dendrimers is significantly larger than that of the non-biotinylated dendrimers. For example the interaction of the generation 3.5 non-biotinylated dendrimers to the streptavidin monolayer gives rise to an SPR shift of 8 ± 2 whereas for the biotinylated version 40 ± 4 mDA is observed. The extent of the interaction between the streptavidin and the biotinylated carboxyl terminated dendrimers is relatively constant, independent of dendrimer generation. This can be attributed to the dendrimers surface charge. The smaller dendrimers will have only a low charge density so many of them will bind to the protein

surface as the charge repulsion is not great. As dendrimer generation increases so will the charge density on their surface, therefore less will bind because of the greater charge repulsion. However, as their size is significantly larger they will produce a shift of similar magnitude to the denser but thinner layer of the smaller biotinylated dendrimers.

Figure 7.28 (c) shows the effect of biotinylation on the rate of interaction of the dendrimers with the streptavidin surface. From this graph it can be observed that the rate of binding for the biotinylated dendrimers is significantly larger than for the non-biotinylated dendrimers independent of size or charge. This can be attributed to the fact that the major mechanism of interaction is different ie specific rather than non-specific. When comparing the carboxyl and amino terminated dendrimers it can be observed that the rate of interaction for the carboxyl terminated dendrimers is significantly slower. This can be attributed to the carboxyl dendrimers negative surface charge. As they possess the same charge as the surface, their desire to interact with the surface will be significantly less. When comparing the different generations of carboxyl terminated dendrimers, it can be observed from Figure 7.28 (c) that although the rate of binding of the biotinylated species are within error, as both dendrimer generations are binding by the same mechanism (via the avidin-biotin interaction), the non-specific binding rate for the smaller non-biotinylated dendrimers is significantly faster than that of the larger dendrimers. This can be attributed to the surface charge density. As the dendrimer generation increases the dendrimer surface negative charge density increases. Therefore, there will be a larger charge repulsion between it and the like-charged protein surface, so the rate of interaction will be slower.

(c)

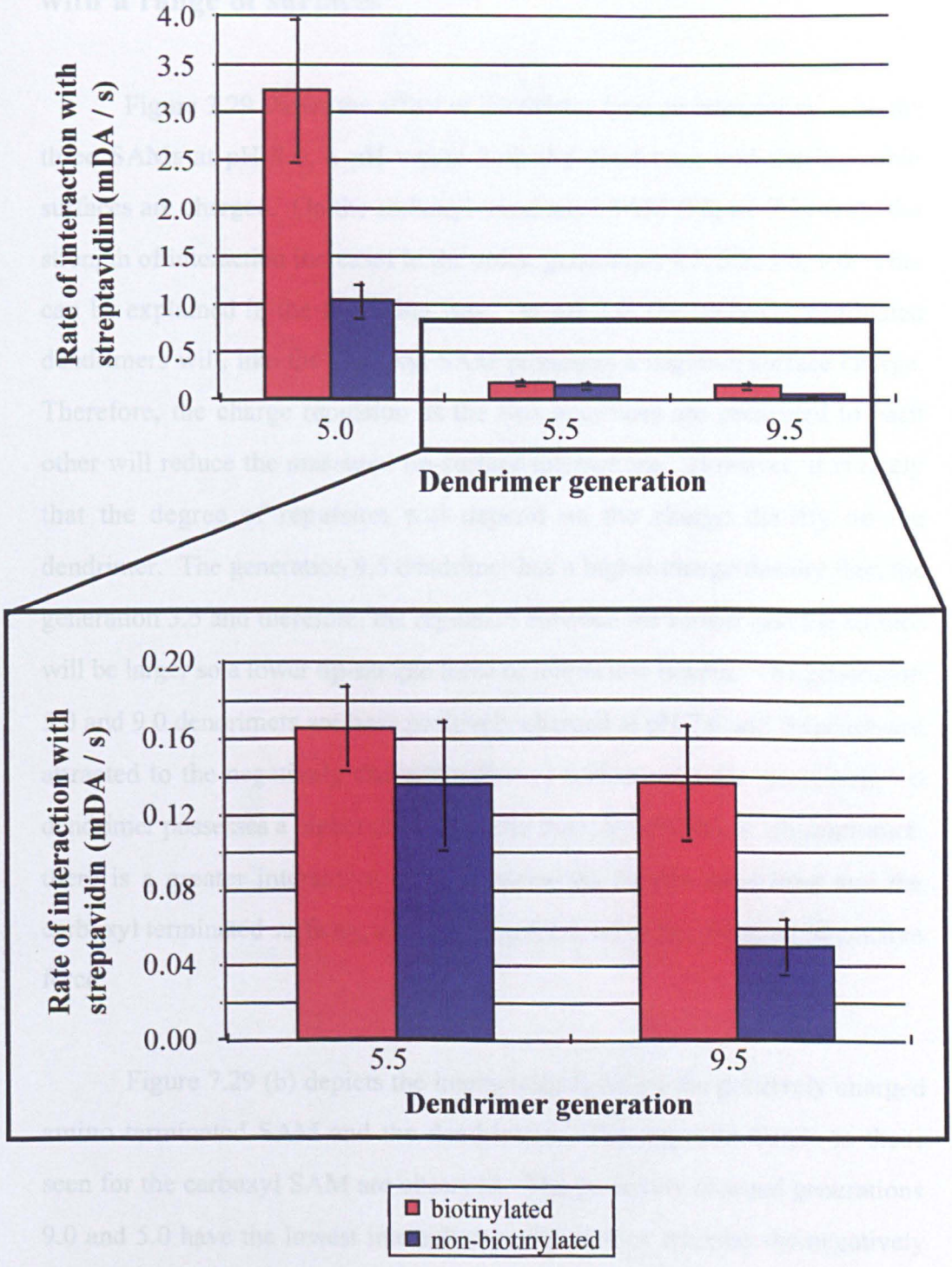

Figure 7.28 (cont) : Effect of biotinylation on interaction of dendrimers with streptavidin (2)
(c) Rate

bars = average ± 1 standard deviation (n ≥ 19)

7.3.3.2 : Effect of dendrimer type on the force of interaction with a range of surfaces

Figure 7.29 shows the effect of dendrimer type on interactions with the three SAMs at pH 7.0, a pH where both the dendrimer and the ionizable surfaces are charged. On the carboxyl terminated SAM (Figure 7.29 (a)), the strength of interaction increases in the order, generation 9.5, 3.5, 5.0, 9.0. This can be explained in the following way. At pH 7.0, the carboxyl terminated dendrimers will, like the carboxyl SAM possesses a negative surface charge. Therefore, the charge repulsion as the two interfaces are presented to each other will reduce the measured tip-surface interactions. However, it is likely that the degree of repulsion will depend on the charge density on the dendrimer. The generation 9.5 dendrimer has a higher charge density than the generation 3.5 and therefore, the repulsion between the former and the surface will be larger so a lower tip-sample force of interaction is seen. The generation 5.0 and 9.0 dendrimers are both positively charged at pH 7.0 and therefore are attracted to the negatively charged carboxyl surface. As the generation 9.0 dendrimer possesses a higher charge density than the generation 5.0 dendrimer, there is a greater interactive force between the former dendrimer and the carboxyl terminated surfaces, so increasing the level of the observed interactive force.

Figure 7.29 (b) depicts the interactions between the positively charged amino terminated SAM and the dendrimers. The opposite trends to those seen for the carboxyl SAM are observed. The positively charged generations 9.0 and 5.0 have the lowest interaction to the surface whereas the negatively charged generations 3.5 and 9.5 have the higher interactive force with the amino terminated SAM surface. This is explained firstly by the repulsion between the positively charged amino terminated dendrimers (generations 9.0 and 5.0) and positive amino surface. The repulsion is greater for the generation 9.0 dendrimer when compared with the generation 5.0 due to its greater charge density. This results in the small measured interaction forces for the AFM

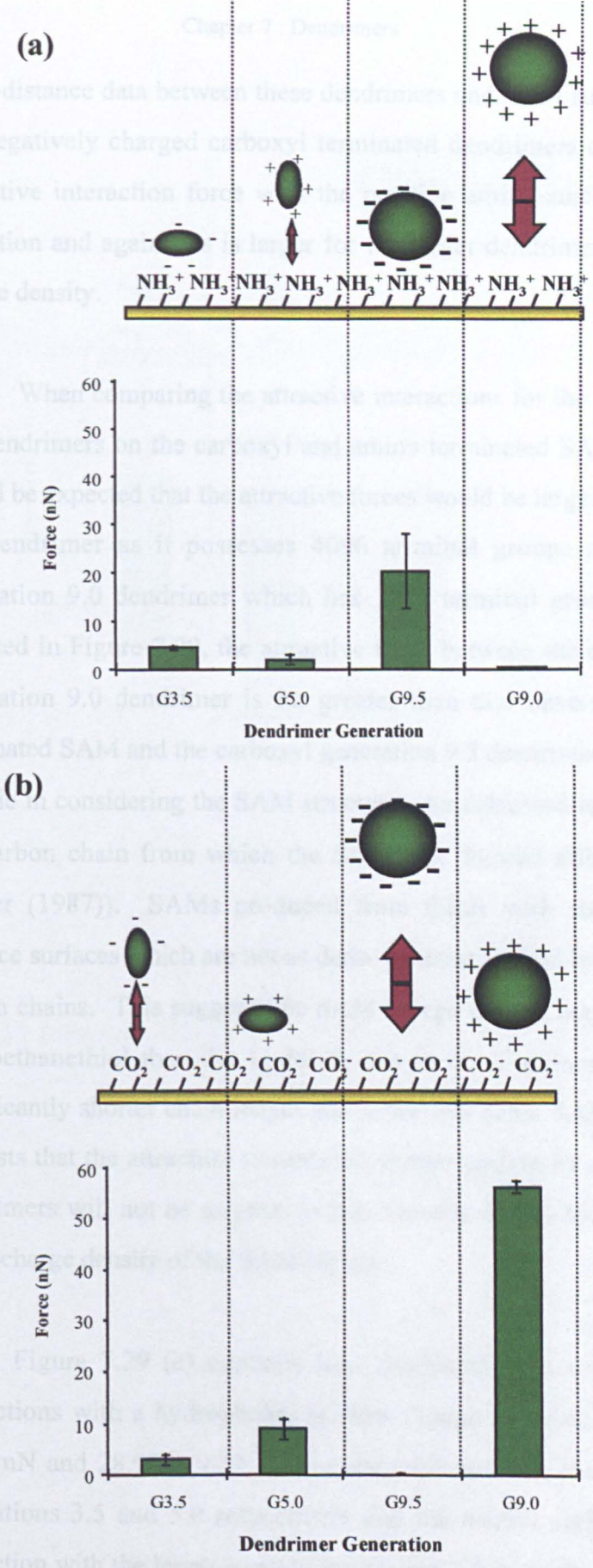

Figure 7.29 : Effect of dendrimer type on the interaction with model surfaces

(a) amino terminated surface (b) carboxyl terminated surface
bars = average ± 1 standard deviation (n ≥ 58)

force-distance data between these dendrimers and SAM surface. Conversely, the negatively charged carboxyl terminated dendrimers demonstrate a high attractive interaction force with the positive amino surface, due to charge attraction and again this is larger for the larger dendrimer due to its greater charge density.

When comparing the attractive interactions for the generation 9.0 and 9.5 dendrimers on the carboxyl and amino terminated SAMs respectively, it would be expected that the attractive forces would be larger for the generation 9.5 dendrimer as it possesses 4096 terminal groups as opposed to the generation 9.0 dendrimer which has 2048 terminal groups. However, as depicted in Figure 7.29, the attractive force between the carboxyl SAM and generation 9.0 dendrimer is far greater than that observed for the amino terminated SAM and the carboxyl generation 9.5 dendrimer. One explanation may lie in considering the SAM structure. As discussed earlier, the length of the carbon chain from which the SAMs are formed affects their structure (Porter (1987)). SAMs produced from thiols with short carbon chains produce surfaces which are not as dense as those formed by thiols with longer carbon chains. This suggests the SAM charge density may be less on the 2-aminoethanethiol than the 11-MUA due to the 2-aminoethanethiol having significantly shorter chain length and hence less dense SAM formation. This suggests that the attraction towards the former surface by oppositely charged dendrimers will not be as great as that towards the 11-MUA because of the lower charge density of the SAM surface.

Figure 7.29 (c) explains how dendrimer type effects the force of interactions with a hydrophobic surface. Large adhesive forces of 34.67 ± 10.62 nN and 28.99 ± 9.59 nN are observed between the small dendrimers generations 3.5 and 5.0 respectively and the methyl surfaces, whereas the interaction with the larger generations 9.0 and 9.5 is smaller, only 9.88 ± 3.36 nN and 9.11 ± 6.14 nN respectively. This can be rationalised by the flexibility of these dendrimers. Below generation 4.0-5.0, the dendrimers are flexible non-

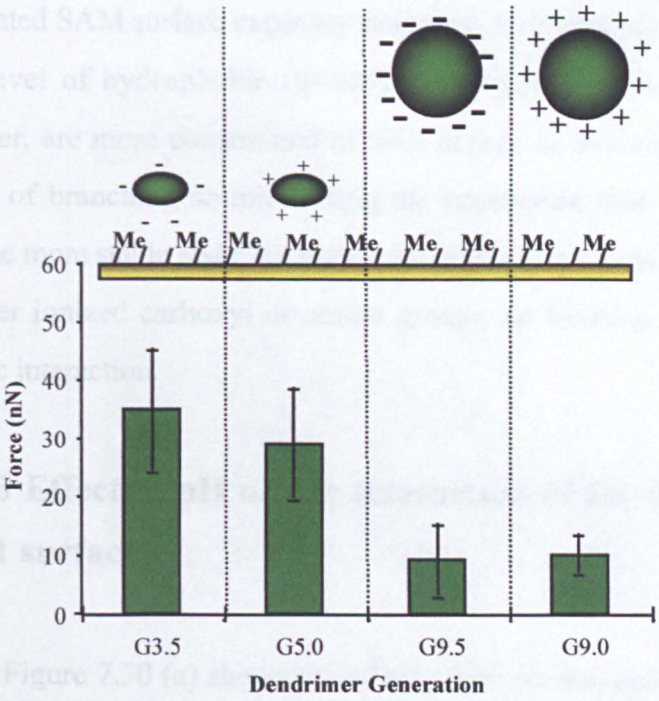

Figure 7.29 (cont) : Effect of dendrimer type on the interaction with model surfaces

(c) methyl terminated surface

bars = average ± 1 standard deviation ($n \geq 55$)

spheroidal structures, as such they can deform on contact with the methyl terminated SAM surface exposing their more hydrophobic interior, leading to a high level of hydrophobic tip-surface interaction. The larger dendrimers however, are more constrained in their degree of movement due to the high degree of branching so minimising the interaction with the methyl surface. Also the more stable and rigid higher dendrimer generation surfaces are covered in either ionized carboxyl or amino groups, so limiting the amount of non-specific interaction.

7.3.3.3 Effect of pH on the interaction of the dendrimers with model surfaces

Figure 7.30 (a) shows the effect of pH on the measured force distance interactions between the carboxyl terminated 11-MUA SAM and the large carboxyl terminated generation 9.5. From this graph it can be seen that below pH 4, there is a high level of binding, approximately 10 nN, which does not change with pH. The force of interaction decreases between pH 4 and 5 to 2.27 ± 0.20 nN and again between pH 5 and 7 to 1.83 ± 0.14 nN. Above pH 7 there are no more significant changes in the interactive force between the dendrimer and the surface, and the measured interactive force remains low. This may be explained by considering the respective charges on the dendrimer and the SAM surfaces. Below pH 4, both the dendrimer and the SAM are uncharged so a high degree of hydrogen bonding and non-specific interactions are observed between the terminal carboxyl groups of the dendrimer and those of the SAM. Between pH 4 and 5 the dendrimer surface carboxyl groups become ionized so the extent of interaction between the dendrimer and 11-MUA SAM is reduced. Between pH 5 and 7, the carboxyl SAM becomes deprotonated. Since both the dendrimer and carboxyl terminated SAM possess a negative charge, they repel each other and only a small level of interaction is observed, due to the high charge density on both surfaces.

(a)

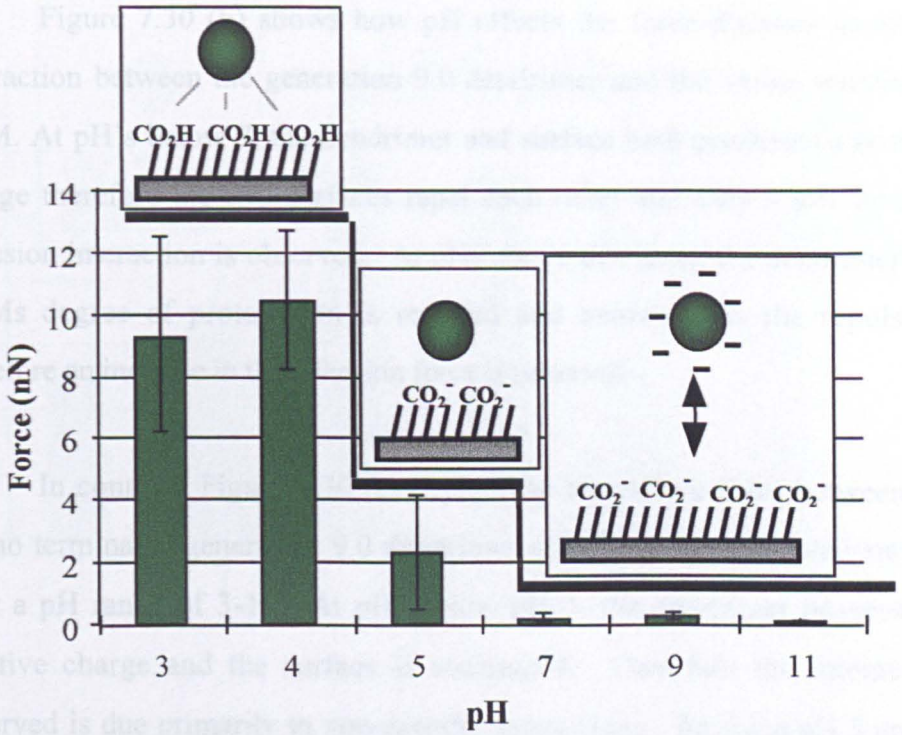

(b)

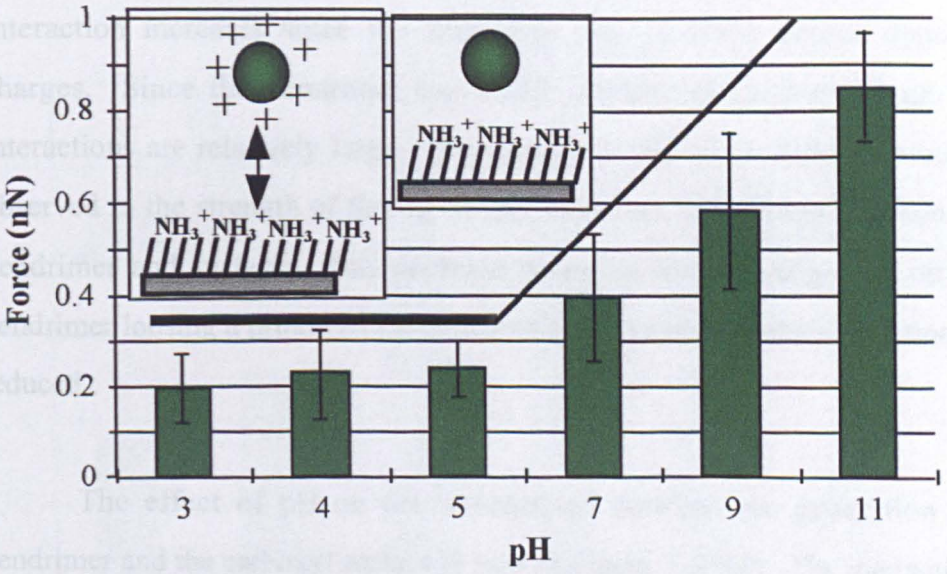

Figure 7.30 : Effect of pH on the interaction of PAMAM dendrimers with model surfaces
(a) Interaction between 11-MUA and the generation 9.5 dendrimers
(b) Interaction between 2-aminoethanethiol and the generation 9.0 dendrimers

bars = average ± 1 standard deviation ($n \geq 59$)

Figure 7.30 (b) shows how pH effects the force-distance measured interaction between the generation 9.0 dendrimer and the amino terminated SAM. At pH's below 7, the dendrimer and surface both possesses a positive charge therefore the two surfaces repel each other and only a low level of adhesion interaction is observed. At pHs above this level, the dendrimer and SAMs degree of protonation is reduced and hence, so is the repulsion, therefore an increase in the adhesion force is observed.

In contrast, Figure 7.30 (c) depicts the interactive force between the amino terminated generation 9.0 dendrimer and carboxyl terminated surface over a pH range of 3-11. At pHs below pH 5, the dendrimer possesses a positive charge and the surface is uncharged. Therefore the interaction observed is due primarily to non-specific interactions. Between pH 5 and 7, the 11-MUA is also deprotonated so the extent of tip-surface adhesion interaction increases since the dendrimer and 11-MUA posses opposite charges. Since the dendrimer has a high density of surface charge, the interactions are relatively large. Between pH 9 and 11, a slight decrease is observed in the strength of the tip-surface adhesion interactions between the dendrimer and surface. This decrease is due to the amino groups on the dendrimer loosing a proton so the contribution of charge-charge interactions is reduced.

The effect of pH on the interactions between the generation 5.0 dendrimer and the carboxyl surface is seen in Figure 7.30 (d). The interactions at pH 3 and 4 are constant. This may be due to the fact that the surface characteristics of the dendrimer and SAM remain the same at these pH values, the former is positively charged and the latter is uncharged. At pH 7, there is a slight increase in the level of binding from 4.8 ± 2.4 to 8.9 ± 3.3 nN. This is due to the 11-MUA becoming deprotonated so there is a greater affinity between the dendrimer and surface as they possess opposite charges. At pHs 9 and 11, a decrease in the extent of interaction is observed as the dendrimers terminal amino groups loose their positive charge and hence the attraction

(c)

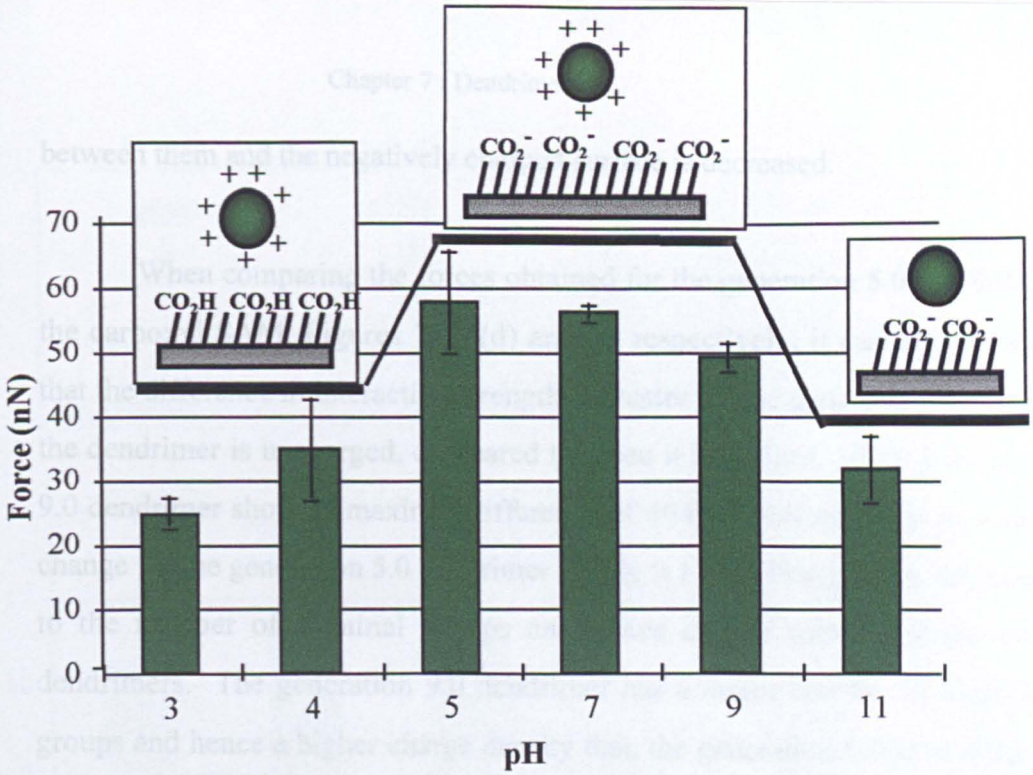

(d)

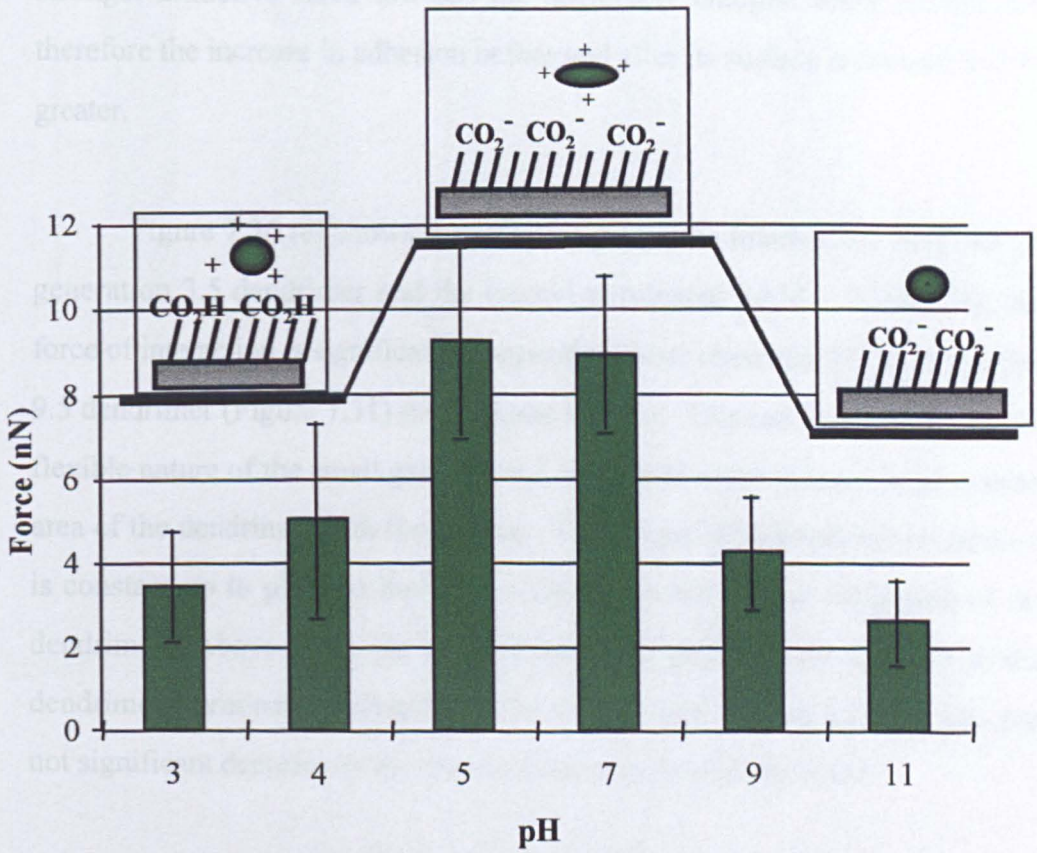

Figure 7.30(cont.) : Effect of pH on the interaction of PAMAM dendrimers with model surfaces
(c) Interaction between 11-MUA and the generation 9.0 dendrimers
(d) Interaction between 11-MUA and the generation 5.0 dendrimers

bars = average ± 1 standard deviation ($n \geq 67$)

between them and the negatively charged surface is decreased.

When comparing the forces obtained for the generation 5.0 and 9.0 on the carboxyl SAM, Figures 7.30 (d) and (c) respectively, it can be observed that the difference in interaction strength is greater for the generation 9.0 when the dendrimer is uncharged, compared to when it is ionized. The generation 9.0 dendrimer shows a maximal difference of 40.0 nN where as the maximal change for the generation 5.0 dendrimer is only 9.1 nN. This may be attributed to the number of terminal groups and hence charge density of the two dendrimers. The generation 9.0 dendrimer has a larger number of terminal groups and hence a higher charge density than the generation 5.0 promoting a stronger attractive force towards the negatively charged SAM surface and therefore the increase in adhesion before and after its surface is ionized will be greater.

Figure 7.30 (e) shows the effect of pH on the interactions between the generation 3.5 dendrimer and the methyl terminated SAM. Generally, the force of interaction is significantly larger than those observed for the generation 9.5 dendrimer (Figure 7.31) on the same surface. This can be attributed to the flexible nature of the small generation 3.5 dendrimer providing a large contact area of the dendrimer with the surface. The extent of hydrophobic interaction is constant up to pH 5 as there is no change in the surface ionisation of the dendrimer. Above pH 5, the terminal carboxyl groups loose a proton so the dendrimers terminal functionalities become charged leading to the slight, but not significant decrease in the observed interaction with the SAM.

7.3.3.4 : Effect of ionic strength on the interaction of the dendrimers with model surfaces

The effect of ionic strength on the interaction of the dendrimers with the model surfaces was investigated to determine the contribution of charge interactions to the overall adhesive force as measured by AFM force-distance

(e)

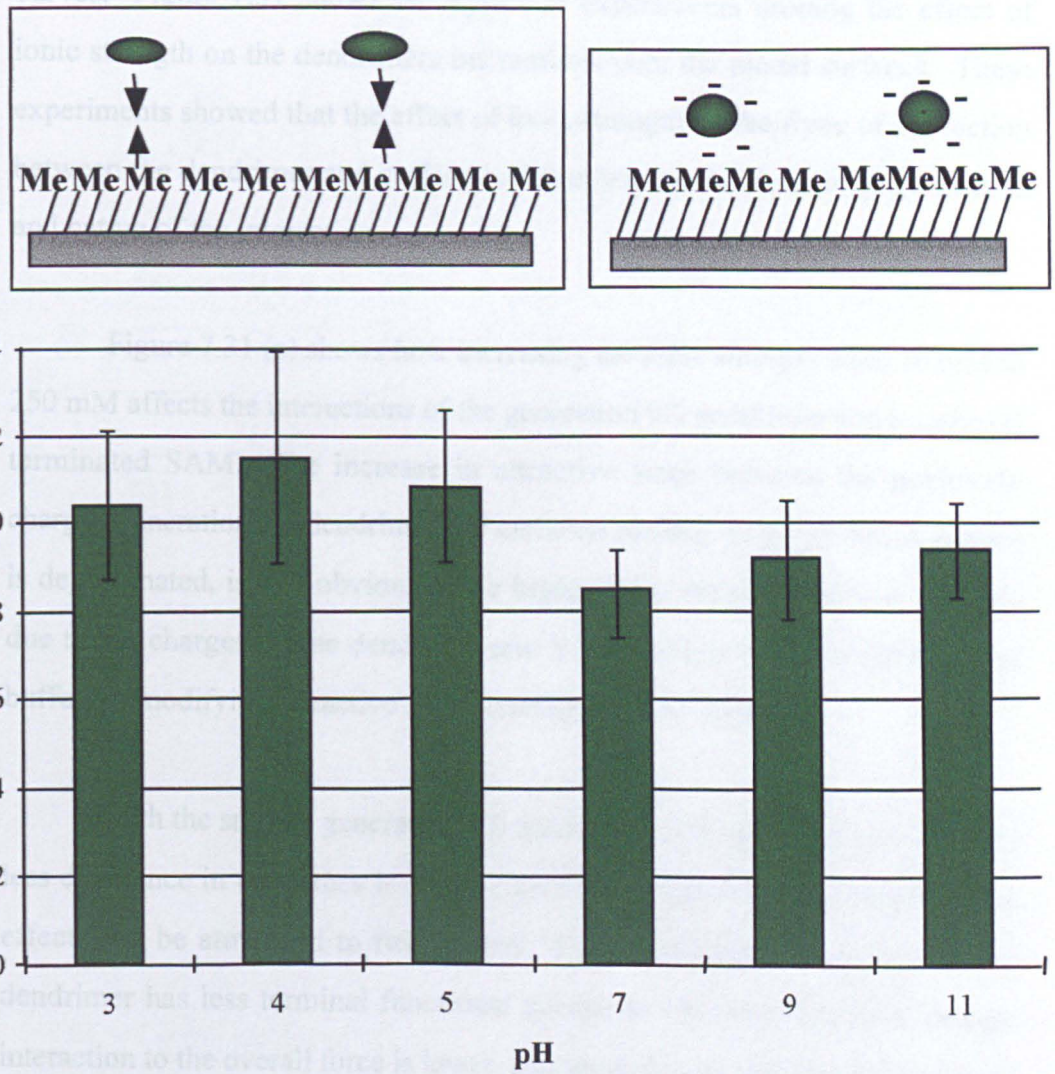

Figure 7.30(cont.) : Effect of pH on the interaction of PAMAM dendrimers with model surfaces
(e) Interaction between dodecanethiol and the generation 3.5 dendrimers

bars = average ± 1 standard deviation ($n \geq 66$)

curves. Figure 7.31 shows the results of experiments probing the effect of ionic strength on the dendrimers interactions with the model surfaces. These experiments showed that the effect of ionic strength on the force of interaction between the dendrimer and surface is dependent on the dendrimer generation and nature of the interaction.

Figure 7.31 (a) shows how increasing the ionic strength from 10 mM to 250 mM affects the interactions of the generation 9.0 dendrimer and a carboxyl terminated SAM. The increase in attractive force between the positively charged generation 9.0 dendrimer and carboxyl surface, as the 11-MUA surface is deprotonated, is less obvious at the higher ionic strength. This is possibly due to the charges on the dendrimer and SAM surface being shielded by the buffer, so modifying attractive force between the two entities.

With the smaller generation 5.0 dendrimer, as shown in Figure 7.31 (b) less difference in the forces is observed for the range of ionic strengths. This effect may be attributed to two factors. Firstly, the smaller generation 5.0 dendrimer has less terminal functional groups so the contribution of charge interaction to the overall force is lower, and secondly, its high flexibility means the dendrimer can expose its more hydrophobic core so obtaining a larger surface area with the SAM surface, increasing the extent of hydrophobic interactions which are less effected by pH.

Overall, it can be observed from studies investigating the effect of pH and ionic strength on the interactions between the generation 5.0 and 9.0 dendrimers and the carboxyl surface, that charge interactions have a more significant contribution to the latter dendrimers overall interaction than the former. This can be attributed to the large excess of terminal groups the generation 9.0 dendrimer has over the generation 5.0 dendrimer.

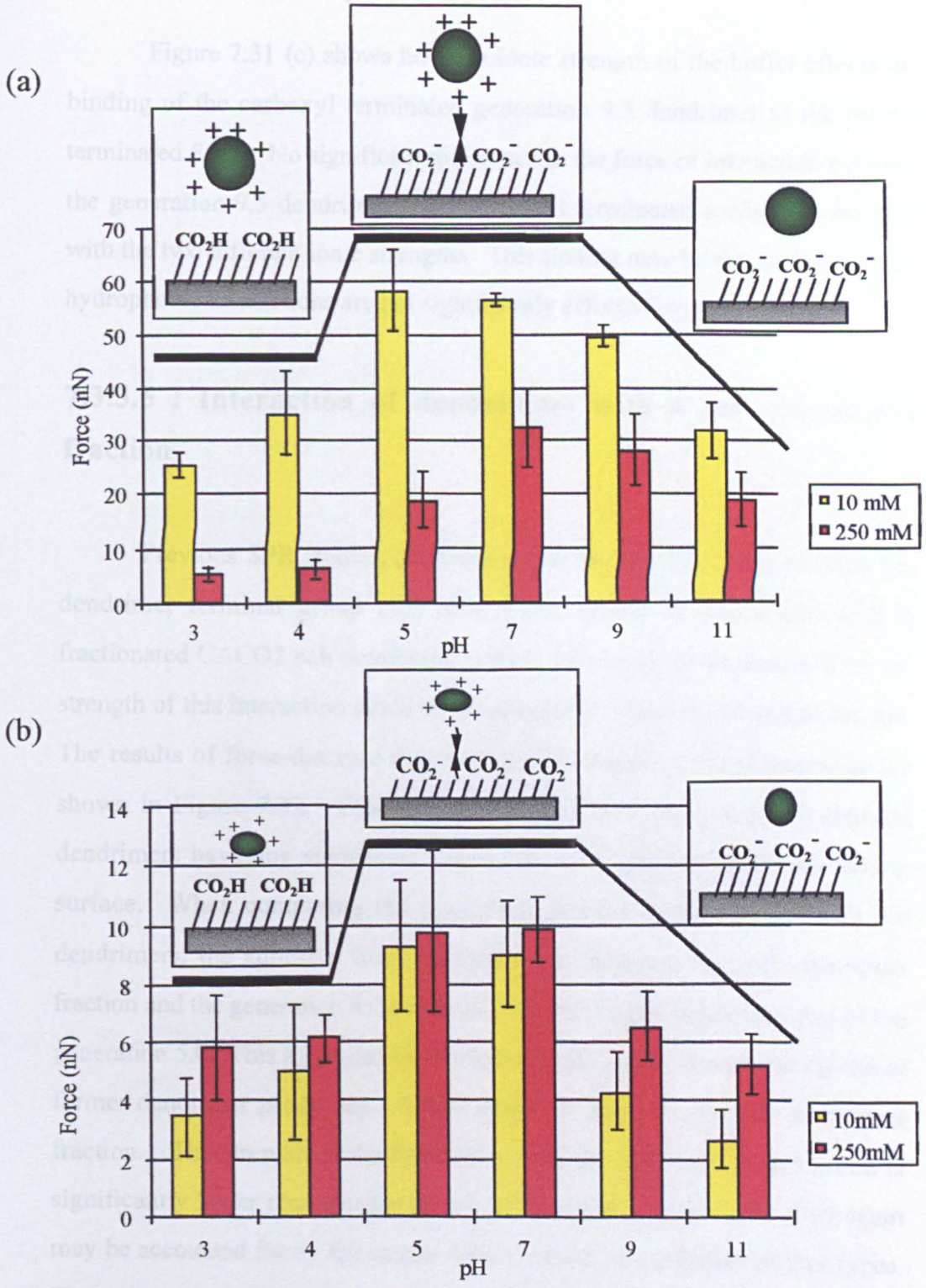

Figure 7.31 : Effect of ionic strength on interactions between dendrimers and model surfaces
(a) Interaction between 11-MUA and the generation 9.0 dendrimers
(b) Interaction between 11-MUA and the generation 5.0 dendrimers

bars = average ± 1 standard deviation ($n \geq 56$)

Figure 7.31 (c) shows how the ionic strength of the buffer effects the binding of the carboxyl terminated generation 9.5 dendrimer to the methyl terminated SAM. No significant difference in the force of interaction between the generation 9.5 dendrimer and the methyl terminated surface is observed with the two different ionic strengths. This finding may be due to the fact that hydrophobic interactions are not significantly effected by ionic strength.

7.3.3.5 : Interaction of dendrimers with a cell membrane fraction

Previous SPR studies, as discussed in section 7.3.1, showed that the dendrimer terminal group type effects the extent of interaction with a fractionated CACO2 cell membrane surface. However, no information on the strength of this interaction could be obtained from that data set and technique. The results of force-distance experiments investigating this phenomena are shown in Figure 7.32. This data reveals that only the positively charged dendrimers have any significant interaction with the membrane mimicking surface. When comparing the positively charged generation 9.0 and 5.0 dendrimers, the adhesive force of interaction between the cell membrane fraction and the generation 9.0 dendrimer is significantly larger than that of the generation 5.0. This again can be attributed to the higher charge density the of former dendrimer producing a larger attractive force for the cell membrane fraction. The strength of the interaction with the cell membrane fraction is significantly lower than that for the 11-MUA SAM (Figure 7.29). This again may be accounted for by the charge density of the two different surface types. The cell membrane fraction is comprised of a variety of molecules which possess varying degrees of hydrophilicity, which overall provides a negatively charged surface at pH 7.4. Whereas the SAM possesses only negatively charged groups which are ordered into a dense surface layer producing a greater charge density, which in turn leads to a larger adhesive force between the tip and surface.

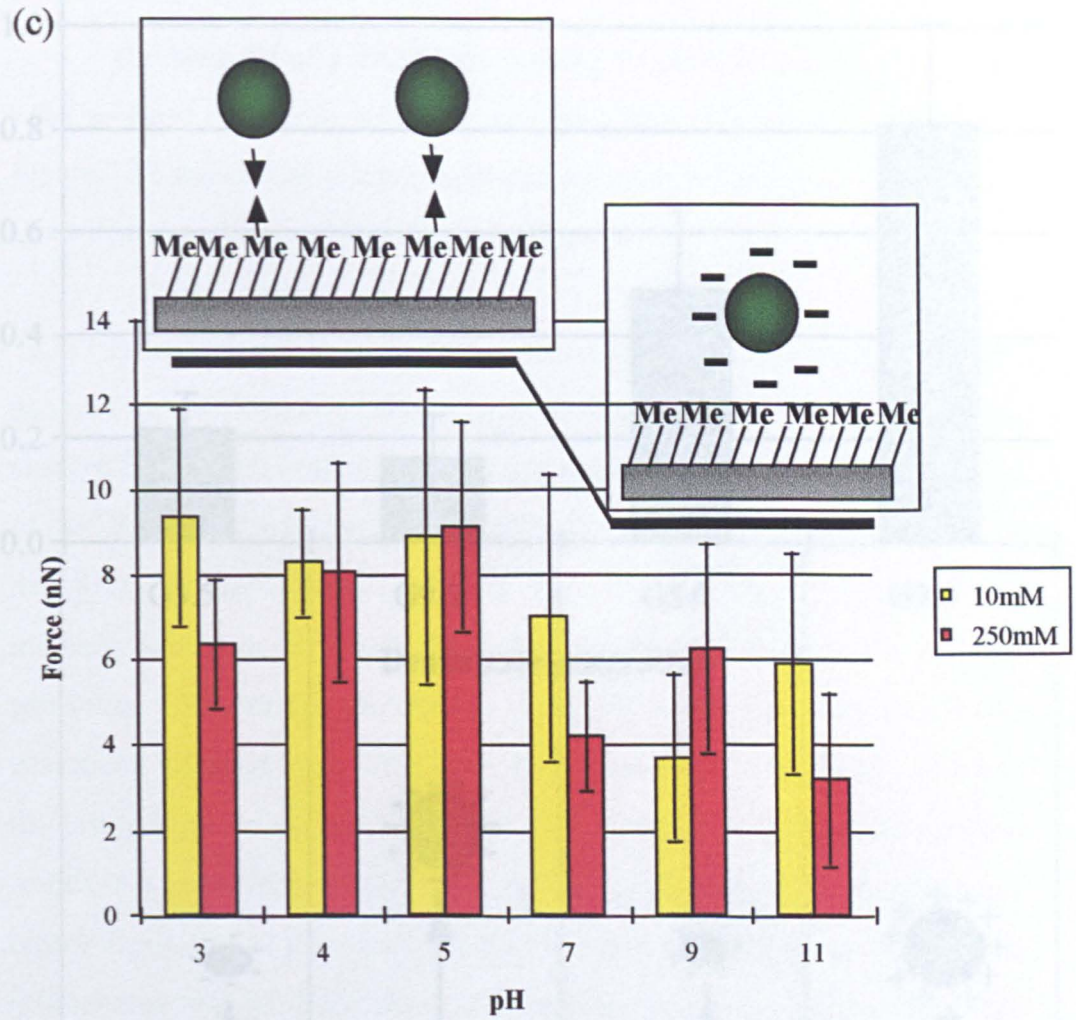

Figure 7.31 : Effect of ionic strength on interactions between dendrimers and model surfaces
(c) Interaction between dodecanethiol and generation 9.5 dendrimers

bars = average ± 1 standard deviation ($n \geq 53$)

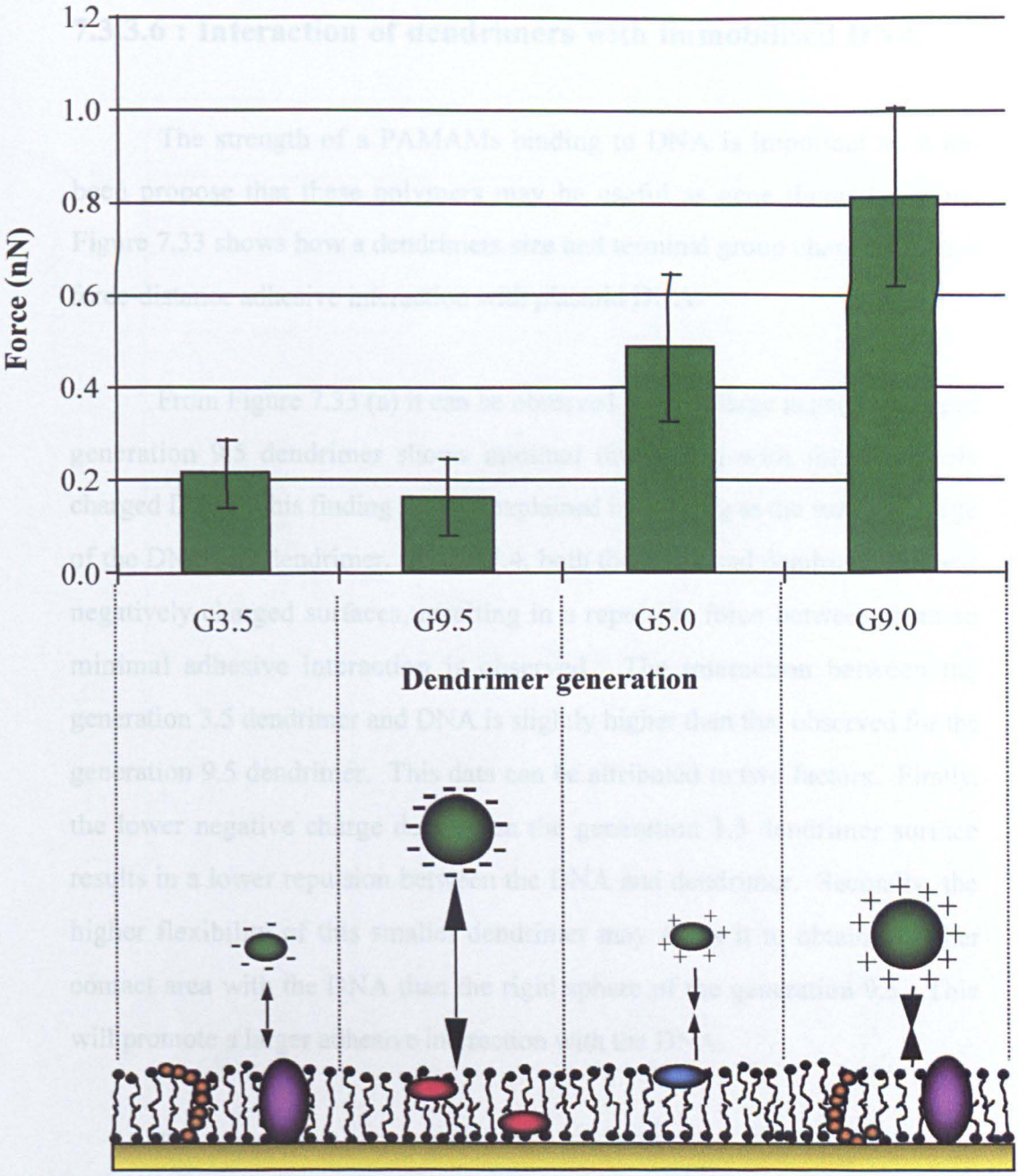

Figure 7.32 : Effect of dendrimer type on the interaction with a membrane mimicking surface

bars = average ± 1 standard deviation (n ≥ 69)

7.3.3.6 : Interaction of dendrimers with immobilised DNA

The strength of a PAMAMs binding to DNA is important as it has been propose that these polymers may be useful as gene therapy vectors. Figure 7.33 shows how a dendrimers size and terminal group charge effects it force-distance adhesive interaction with plasmid DNA.

From Figure 7.33 (a) it can be observed that the large negative charged generation 9.5 dendrimer shows minimal interaction with the negatively charged DNA. This finding may be explained by looking at the surface charge of the DNA and dendrimer. At pH 7.4, both the DNA and dendrimer possess negatively charged surfaces, resulting in a repulsive force between them so minimal adhesive interaction is observed. The interaction between the generation 3.5 dendrimer and DNA is slightly higher than that observed for the generation 9.5 dendrimer. This data can be attributed to two factors. Firstly, the lower negative charge density on the generation 3.5 dendrimer surface results in a lower repulsion between the DNA and dendrimer. Secondly, the higher flexibility of this smaller dendrimer may allow it to obtain a higher contact area with the DNA than the rigid sphere of the generation 9.5. This will promote a larger adhesive interaction with the DNA.

For the positively charged amino terminated dendrimers (generations 5.0 and 9.0), a higher degree of interaction with the DNA is observed than that for the negatively charged ones. This finding again can be explained by reference to the charge attraction between the positively charged dendrimers and the negatively charged DNA. The extent of interaction appears to be dependent on the dendrimers surface charge density. The generation 5.0 dendrimer has less positively charged surface amino groups in comparison to the generation 9.0 dendrimer. This means the generation 5.0 dendrimer has a lower charge density and hence lower attractive force to the DNA. Therefore the AFM force-distance adhesive force measured is significantly less for the generation 5.0 dendrimer (0.24 ± 0.09 nN) than that for the generation 9.0 (

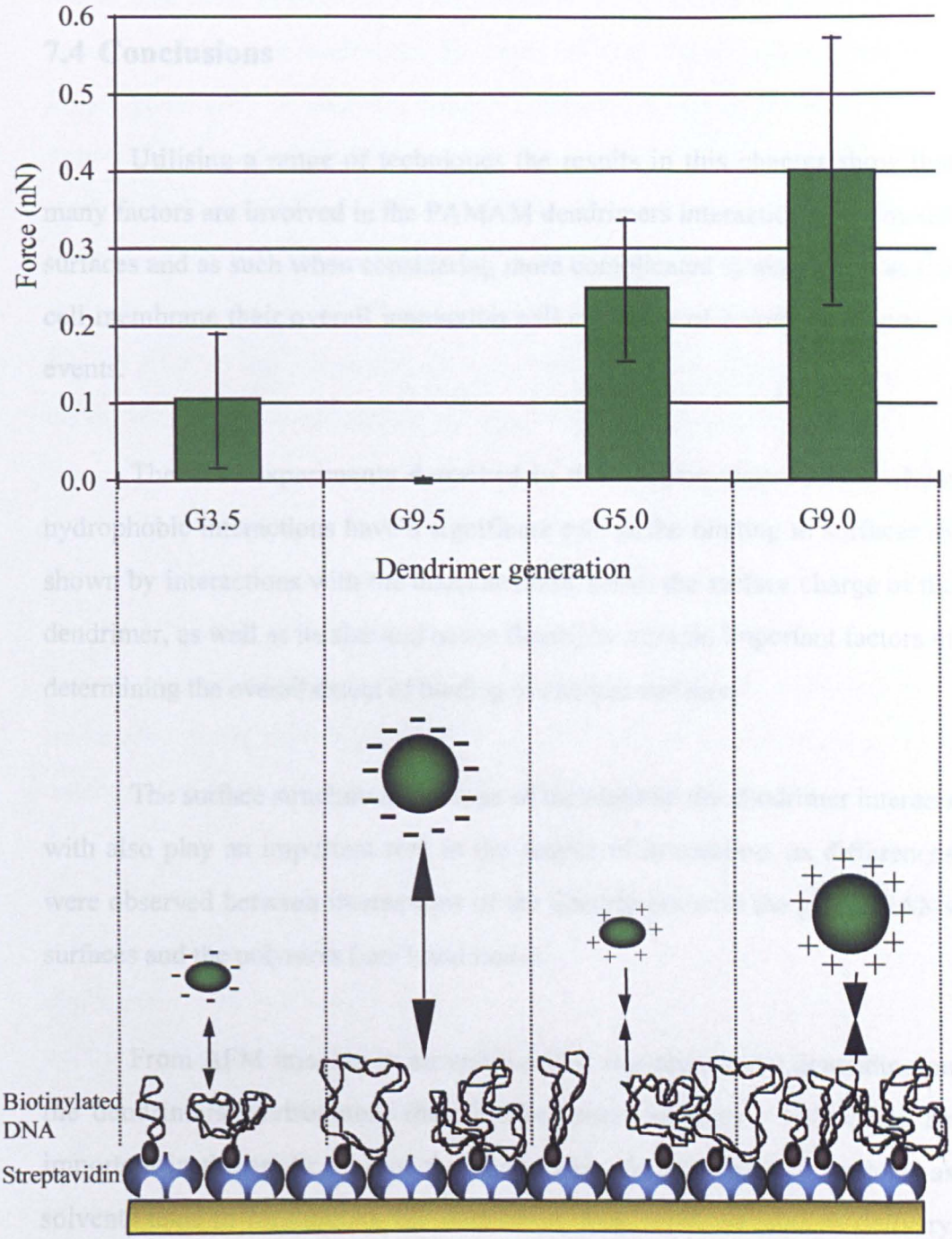

Figure 7.33 : Effect of dendrimer type on the interaction DNA

bars = average ± 1 standard deviation (n ≥73)

0.40 ± 0.17 nN).

7.4 Conclusions

Utilising a range of techniques the results in this chapter show that many factors are involved in the PAMAM dendrimers interactions with model surfaces and as such when considering more complicated systems such as the cell membrane their overall interaction will comprise of a complex series of events.

The SPR experiments described in this chapter showed that whilst hydrophobic interactions have a significant role in the binding to surfaces as shown by interactions with the dodecanethiol SAM, the surface charge of the dendrimer, as well as its size and hence flexibility are also important factors in determining the overall extent of binding to charged surfaces.

The surface structure and charge of the material the dendrimer interacts with also play an important role in the degree of interaction, as differences were observed between interactions of the dendrimers with the planar SAMs surfaces and the polymers Lan-1 and Lan-2.

From AFM imaging in air and liquid it was shown that depending on the dendrimers environment their conformation changes. This could be important in the application of the dendrimers as drug delivery vehicles as solvents used in formulating the dendrimer drug vector as well as delivery routes will have to be carefully controlled to ensure that the dendrimer conformation does not change as this may effect the drug loading of the dendrimers.

AFM force distance experiments provided more information on how dendrimer flexibility and surface charge effects the strength of interaction with the model SAM surfaces. On the methyl terminated surface, the smaller

generation dendrimers were observed to possess a higher degree of interaction due to their more flexible nature which allows the to mould to the surface and hence maximise their interaction. However with the charged SAM surfaces the larger generation dendrimers posses a higher degree of interaction with oppositely charged surfaces due to their larger surface charge density. PH, as well as ionic strength, of the media was observed to effect the extent of interaction between the dendrimer and surfaces due to their effect on surface ionisation and charge shielding respectively. The extent to which these two factors effected the interaction between dendrimer and surface depended on dendrimer generation and surface charge as well as SAM terminal group.

Results obtained on these simple surfaces have provided a basis for understanding the interactions of dendrimers with more complicated systems such as DNA and cell membrane fractions. Preliminary AFM force-distance investigations probing the interactions between the dendrimers and these materials suggest that charge density is the major factor contributing to the extent and strength of interactions with these materials, rather than size.

Further investigations based on the grounding provided by work in this chapter are needed to fully understand the interactions of PAMAM dendrimers with cell membranes and hence, gain an understanding to their cellular uptake mechanisms. However, the results in this chapter show that the application of these surface analytical techniques provides useful information on a these polymers interactions. In turn this provides a basis from which directed chemical synthesis of this type of system can be performed to synthesis materials which are more effective in their chosen application.

Chapter 8 : Overall conclusions

The use of polymers within the field of medicine, as introduced in Chapter 1 has developed into a diverse field of research over the last 50 years. The aim of this thesis was to investigate whether the surface chemistry of a variety of polymeric materials intended for different biomedical applications could be related to their surface interactions and hence their efficacy within a chosen application.

Chapters 3 and 4 concentrated a polymer for tissue engineering applications. The surface analytical techniques of XPS and SIMS were utilised in Chapter 3 to probe the effect of PLA : PEG ratio on the surface composition of a range of PLA-PEG-biotin polymers. These investigations showed that the surface chemistry of these materials was controlled by their molecular structure. Chapter 4 showed that the results on the interfacial chemistry of the PLA-PEG-biotin polymers could be related to their specific and non-specific protein interactions, and hence degree of surface modification by avidin. Future work on this system will probe the effect of these varying degrees of surface modification by avidin and in turn biotinylated cell adhesion molecules, to cell binding and spreading on the polymeric surfaces.

In addition, the effect of surfactants on the surface engineering of these polymer systems was investigated in Chapter 4. It was shown that the degree by which specific avidin binding to the biotin moiety was reduced could be controlled by the choice of surfactant. Cell culture experiment also need to be performed on these surfactant coated polymer systems to investigate the contribution of these surfactants to the cell adhesion and spreading processes.

Chapter 5 showed the effect of PEG molecular weight on the formation profile and resultant structure of DNA \ PLL-PEG complexes under pseudo-physiological conditions. This work provides a basis for future work investigating similar systems where the PLL molecular weight of the polymer is varied in the presence of a constant block of PEG or similar hydrophilic polymer, as well as the interaction of DNA with branched and hyperbranched materials of a similar nature.

The work in Chapter 6 utilised SAMs as model surfaces to immobilise a lipid based gene therapy vector to try and obtain stable images of its structure. However, limited success was ultimately acheived, though the results from these investigations did provided a significant insight into the interaction of the system with model surfaces. The information obtained provides a preliminary basis which can be added to to understand such systems interactions with more complicated interfaces such as the cell membrane. This in turn may provide an insight into the gene therapy vectors macromolecular structure and it's *in vivo* interactions.

The final experimental chapter, Chapter 7 in its investigations with dendrimers shows that although a polymer may be comprised of the same monomers, the number and degree of branching of these can significantly alter the materials interaction with interfaces. In a similar fashion to which the liposome mediated gene therapy complexes interactions with SAMs were investigated in Chapter 6, the factors effecting the interactions of PAMAM dendrimers with such surfaces were probed in this chapter by SPR and AFM in both imaging and force-distance modes. By breaking down and characterising the interactions in terms of the factors which contribute to them,

such as molecular flexibility, the sign and density of the materials surface charge, as well as environmental parameters such as pH and ionic strength, it is hoped that on probing the dendrimers interactions with more complicated systems such as DNA and the cell membrane the factors effecting the extent of interactions can be understood.

Also in chapter 7 the use of fractionated cell membranes as a cell mimicking surface for probing biomaterials interactions was investigated. The use of such systems in conjunction with the surface analytical techniques described provides a multitude of avenues for research. As well as understanding processes involved in the cell membrane itself, such as lipid redistribution and biomolecule transport, the use of such surfaces to probe the uptake mechanisms of drug delivery vehicles, biocompatiblility of materials for medical devices and tissue engineering applications and probing factors effecting resistance in specific cell lines could be probed.

Although many of the investigations documented in this thesis provide only a basic foundation to which many more experiments need to be performed to elucidate the answer to the bigger questions such as.....

What is the perfect surface chemistry for a tissue engineering scaffold?

What is the aqueous structure of cationic polymer or cationic lipid / DNA complexes?

What is the cellular uptake mechanism of polymeric drug delivery systems?

How can this biomaterials chemistry be altered to optimise it for its application?

.....they do show that by using a range of surface analytical techniques in a complementary fashion significant steps towards answering these questions can be made.

"One small step for man, one giant leap for mankind"

Neil Armstrong

Acknowledgements

There are many people without whom this thesis would not exist. They can be divided into two groups, those who thought I could do it and those who didn't. For those who thought I couldn't, thank you, without your doubts I wouldn't have a had the perseverance to keep going when things were tough and prove to you and myself that you were wrong and that I would get this little book written.

For those people who knew I would make it to the end of the last three years, I would firstly like to thank my supervisors Prof. Saul Tendler, Dr Clive Roberts and Dr Phil Williams for their guidance and help in my research. I would especially like to express my gratitude to my main supervisor Prof. Martyn Davies. Thank you for providing me with the opportunities to carry out some interesting research both at Nottingham and at other research institutions, then letting me travel half way round the world to present the results. I also want to apologies; I think you must have dreaded having to read this thesis as much as I dreaded writing it. I think it is as much your hard work as mine that we finally got it finished.

The work in this thesis would not have been possible with out the funding of the EPSRC and the input of many collaborators. I would firstly like to acknowledge Prof. Ruth Duncan for making me feel one-of-the-lab rather than just a visiting student when carrying out work at CPT and for taking me under her wing at the 'Recent Advances in Drug Delivery Systems' conference and the CRS when Martyn had to unfortunately return to Nottingham. Whilst in CPT I worked with a great group of people and wish to thank everyone, but especially Simon, Nav, Dale, Lisa and Sam for not only being there in the lab but also at the many extra-curricular activities and all those Long Island ice teas, they where "all your fault"!

I also wish to acknowledge Prof. Schacht for allowing me to visit his laboratory in Gent and carry out some polymer synthesis, with Veska, Ineka, Katty, Luc and Stefan, a great group of chemists.

Chapter 5, would not have been possible without Glaxo Research and Development and especially Dr. Karen Palin and Dr. Dave Parkins, who provided Neil and I with an interesting system to work with.

Whilst friends and colleagues at other research establishments have been helpful and supportive in my work, the people in the Spacker-suite have been there the most. I would especially like to thank Steph for her tireless discussion on FD work and Chud for getting me started and warning me what I had let myself in for. Harriet, Adam, Joe and Yogi, I think we have all been there through everyones good times and bad tines and survived. Master Clarke, for being well Stu and keeping me and the rest of the 'ceutics lab entertained whilst demonstrating.

In the last few months I have made a new group of friends who have seen me through the worst part of my thesis corrections. So to those people in the 'fishbowl' I apologies, I'm not always so miserable and ratty, honestly. Even when the corrections were complete there still remained the small matter of printing this thesis and without Daves' selfless offer of letting me monopolize his computer for two days it would have taken a lot longer.

Whilst everyone I have mentioned above has put up with me for the last three years which is a feat in itself, two people have served a life sentence having put up with me for the last 25, my parents. Thanks mum and dad for being there even at mad times of the night when I just needed someone to tell how bad my day was. This thesis is mainly a product of your support, belief in me, and dads proof reading. I'll return the favour when you write yours, only joking mum!!

Erratum

Addition to acknowledgments

It's always the same - when you are doing something, the obvious is always the least easy to see. When writing my acknowledgments there was one person whose help and advice I had got so used to over the last three years I forgot to thank. Therefore this note is just to say thank you Kevin, for being an extra supervisor and providing me the opportunity to perform some interesting research on the PLA-PEG-biotin system, which you and Scott developed whilst working with Prof. Langer in MIT.

Thanks

Appendix 1 : Charge ratio calculations

(a) Number of charges per PLL molecule

PLL molecular weight = 20,000 Da

Molecular weight of 1 monomer (bromide salt) =

C x 6	= 72
H x 13	= 13
N x 2	= 28
O x 1	= 16
Br x 1	= 80

	209

But 5% of amine groups are substituted with biotin therefore number of charges per 209 g is actually 0.95 rather than 1.

Therefore 1 charge actually = 209 / 0.95 = **220**

But also need to include contribution from biotin mass =

C x 16	= 192
H x 24	= 24
N x 3	= 42
O x 3	= 48
S x 1	= 32

	= 338
-	
Br x 1	= 80
H x 2	= 2

	= **256** = mass of biotin substitution

therefore mass per charge = mass corrected for substitution + (5% of biotin)
= 220 + (256 x 0.05) = **232.8**

(b) Conversion of mass ratios to charge ratios

Every 313 g of DNA contains 1 negative charge *

Every 232.8 g of PLL contains 1 positive charge

Therefore a 1:1 mass ratio of DNA to PLL corresponds to a charge ratio of 1 : 1.42

Experiments were performed at mass ratios of DNA to PLL	1 : 1 5 : 1 1 : 2
These correspond to charge ratios of	1 : 1.35 1 : 0.27 1 : 2.70

(c) calculation of mass ratios for PLL-PEGs to keep same charge ratios

Number of repeat units of PLL per 20,000 Da polymer = 20,000 / 209
= 96

amount of PEG added to PLL = 5, 12 or 20 k

Therefore mass per charge becomes

PLL-PEG (5k) = 5,000 / 96 = 52.1

= 52.1 + 232.8 = **284.9**

PLL-PEG (12k) = 12,000 / 96 = 125

= 125 + 232.8 = **357.8**

PLL-PEG (20k) = 20,000 / 96 = 208.1

= 208.3 + 232.8 = **441.1**

These correspond to charge ratios of

	Mass ratios		
	(5 k)	(12 k)	(20 k)
1 : 1.35 =	1 : 1.23	1 :1.54	1 : 1.90
1 : 0.27 =	5 : 1.23	5 : 1.54	5 : 1.90
1 : 2.70 =	1 : 2.46	1 : 2.29	1 : 3.81

* average mass of one base of DNA. Value from Dr. L. Pope

Appendix 2 : Preparation of cell membrane fractions

Confluent Caco-2 cell monolayer were washed twice with Dulbecco's phosphate buffered saline (DPBS) and then harvested by treatment with 10 mM EDTA-DPBS. The cell suspension was centrifuged at 1000 rpm and the pellet washed three times with DPBS. The pellet was resuspended in three volumes of HED buffer (20 mM HEPES (pH 7.67), 1 mM EDTA, 0.5 mM dithiothreitol, 1 mM phenylmethylsulphonyl fluoride). After allowing the cells to swell for 5 min on ice they were homogenized for 30 s. The homogenate was centrifuged at 40,000 rpm for 45 min at 4 °C. The pellet comprised of the cell membranes was resuspended in HEDG buffer (20 mM HEPES (pH 7.67), 1 mM EDTA, 0.5 mM dithiothreitol, 1 mM phenylmethylsulphonyl fluoride, 100 mM NaCl, 10% glycerol) and its protein concentration determined using the Bradford assay. The cell membrane fractions were stored at -80 °C and utilised within 2 mth of supply.

References

Absolom, D.R., Zing, W., van Oss, C.J. & Neumann, A.W. (1984) Biomat. Med. Dev. Art. Org. 12:235-241

Advincula R, Aust E, Meyer W, Knoll W. (1996)Langmuir 12: 3536-3540.

Affrossman, S., O'Neill, S.A. & Stamm, M. (1998) Macromol. 31:6280-6288

Albanese, A., Barbucci, R., Belleville, J., Bowry, S., Eloy, R., Lemke, H.D. & Sabatini, L. (1994) Biomaterial 15(2):129-136

Alberts, B. Bray, D., Lewis, J., Raff, M., Roberts, K. & Watson, J.D. (1989) Molecular Biology of the Cell, Chapter 18, 2nd Edition. Garland Publishing, New York, USA

Allen, J.V., Horwell, D.C., Lainton, J.A.H., O'Neill, J.A. & Ratcliffe, G.S. (1998) Lett. Pep.Sci. 5:133-137

Allen, S., Davies, J., Dawkes, A.C.,Davies, M.C., Edwards, J.C., Parker, M.C., Roberts, C.J., Sefton, J., Tendler, S.J.B.T. et al (1996) FEBS Letts. 390(2):161-164

Allen, S. Davies, M.C., Roberts, C.J., Tendler, S.J.B. & Williams, P.M. (1997a) TIBTECH 15:101-105

Allen, S. (1997b) "The study of biomolecular interactions using scanning probe microscopy" PhD thesis, University of Nottingham

Allen, S., Chen, X., Davies, J., Davies, M.C., Dawkes, A.C., Edwards, J.C., Roberts, C.J., Tendler, S.J.B. & Williams, P.M. (1998) Appl. Phys. A - Mater. Sci. Processing, 66(1):S255-S261

Amiji, M. & Park, K. (1993) J. Biomat. Sci. Polym. Edn. 4(3):217-234

Amrein,, M., Durr, R., Gross, H. & Travaglini, G. (1989) Science 243:1708-1711

Anczykowski, B, Kruger, D & Fuchs, H. (1996) Phys Rev B 53:15485-15488

Anderson, J.M. & Shive, M.S. (1997) Adv. Drug Deliv. Rev. 28:5-24

Aoki, H., Tottori, T., Sakurai, F., Fuji, K. & Miyajima, K. (1997) Intl. J. Pharmaceut. 156:163-174

Archiola, C.R., Radin, L., Alvergna, P., Cenni, E. & Pizzoferrato, A. (1993) Biomat. 14(15):1161-1164

Ardoin, N & Astruc, D (1995) Bull. Soc. Chim. Fr. 132:875-909

Atkins, P.W. Physical chemistry 4th Edition (1990) Richard Clay Ltd., Bungay, Suffolk UK

Baker, L.C., Kameneva, M.V., Watach, M.J., Litwak, P.& Wagner, W.R. (1998) Art. Organs 22(9):799-803

Bandara, G., Mueller, G. M., Galea-Lauri Jr., L.,Tindal, M. H., Georgescu, H. I., Suchanek, M.K., Hung, G.L. et al (1993) Proc. Natl. Acad. Sci. USA. 90:10764-10768

Barbucci, R., Maghani, A., Albanese, A. & Tempesti, F. (1991a) Int. J. Artif. Org. 14:499-507

Barbucci, R., Albanese, A., Maghani, A. & Tempesti, F. (1991b) J. Biomed. Mater. Res. 25:1259-1274

Barbucci, R. & Magnani, A. (1994) Biomat. 15(12):955-962

Barham, P.J., Atkins, E.D.T. & Niedoszynski, I.A. (1974) Polymer 15:762-766

Barth, R.F., Adams, D.M., Soloway, A.H., Alam, F. & Darby M.V. (1994) Bioconj Chem 5:58-66

Bates, P.J., Dosanjh, H.S., Kumar, S., Jenkins, T.C., Laughton C.A. & Neidle, S. (1995) Nuc Acid. Res. 23(18):3627-3632

Beamson, G. & Briggs, D. (1992) High resolution XPS of Organic Polymers, The Scient ESCA300 Database. J. Wiley & sons Ltd, Chichester, UK.

Behr, J.-P., Demeneix, B., Loeffler, J.-P. & Perez-Mutcel, J. (1989) Proc. Natl. Acad. Sci. USA 86:6982-6986

Beratan, D.N. & Onuchic, J.N. (1989) Photosynth. Res. 22(3):173-186

Bernstein, F.C., T.F.Koezle, Williams, G.J., Meyer, E.E. Jr., Brice, M.D., Rodgers, J.R., Kennard, O. et al (1997) J. Mol. Biol. 112:535. On web page http://www.rcsb.org/pdb/. Using PDB ID :1STP taken from Weber, P.C., Ohlendorf, D.H., Wendoloski, J.J. & Salemme, F.R. (1989) Science 243:85-8

Bezanilla, M., Drake, B., Nudler, E., Kashlev, M., Hansma, P.K. & Hansma, H.G. (1994) Biophys. J. 67:2454-2459

Bhaduri, A. & Das, K.P. (1998)J. Dispersion Sci. Technol. 19(4):451-464

Bhattacharya, S. & Madel, S.S. (1998) Biochem. 37:7764-7777

Bhushan, B., Israelachvili, J.N. & Landman, U. (1995) Nature 374:607-616

Bielinska, A., Kukowska-Latallo, J.F., Johnson, J., Tomalia, D.A. & Baker Jr., J.A. (1996) Nuc. Acid Res. 24 (11):2176-2182

Binnig, G., Quate, C.F. & Gerber, Ch. (1986) Phys. Rev. Lett. 56(9):930-933

Black, F.E., Hartshorne, M., Davies, M.C., Roberts, C.J., Tendler, S.J.B., Williams, P.M. & Shakesheff, K.M . Langmuir, (1999), 15(9):.3157-3161

Blaese, R. M., Culver, K. W., Miller, A.D., Carter, C. S., Fleisher, T.,Clerici, M., Shearer, G., et al (1995) Science 270:475-479

Boland, T. & Ratner, B.D. (1995) Proc. Natl. Acad. Sci. USA. 92:5297-5301

Bondeson, K., Frostell-Karlsson, A., Fagerstam, L. & Magnisson, G. (1993) Anal Biochem 214: 245-251.

Bordignon, C., Notarangelo, L. D., Nobili, N., Ferrari, G., Casorati, G., Panina, P., Mazzolari, E. et al (1995) Science 270:470-474

Bos, J.C., Grooteman, M.P.C., vanHoute, A.J., Schoorl, M., van Limbeek, J. & Nube, M.J. (1997) Nephrol. Dialysis Transplantation 12(7):1387-1393

Bousquet, Y., Swart, P.J., SchmittColin, N., VelgeRoussel, F., Kuipers, M.E., Meijer, D.K.F., Bru, N., Hoebeke, J. & Breton, P (1999) Pharm. Res. 16(1):141-147

Boussif, O., Lezoualch, F., Zanta, M.A., Mergny, M.D., Scherman, D, Demeneix, B, Behr, JP. (1995) Proc. Natl. Acad. Sci. USA 92(16):7297-7301

Boussif, O., Zanta, M. A.& Behr, J.P. (1996) Gene. Ther. 3:1074-1080

Briggs, D. & Hearn,M.J. (1988) Surf. Interf. Anal. 13:181- et seq

Briggs, D., Brown, A. & Vickerman, J.C. (1989) Handbook of secondary ion mass spectrometry (SIMS) J. Wiley & Sons, Chichester, UK.

Brigham-Burke, M. & O'Shannessy (1993) Chromatographia 35(1/2):45-49

Bristol Colloid Group (1998) Internal and confidential report on gene therapy complex characterisation

Brooks, D.E., Sharp, A. & Stocks, S.J. (1988) Makromol. Chem., Macromol Symp. 17:387

Bruinsma, R. & Mashl, J. (1998) Europhys. Lett. 41(2):165-170

Brunner H. & Furst (1994) Tetrahedron 50:4303

Brunner H, (1995) J. Organomet Chem 500(1-2):39-46

Buckle, M., Williams, R.M., Negroni, M. & Buc, H (1996) Proc. Natl. Acad. Sci. USA. 93:889-894

Buhlein, E., Wehner, W. & V"gtle, F. (1978) Synthesis 155

Bunjes, N., Schmidt, E.K., Jonczyk, A., Rippmann, F., Beyer, D., Ringsdorf, H., Graber, P.,Knoll, W. & Naumann, R. (1997) Langmuir 13:6188-6194

Burns, M.S., File, D.M., Deline, V. & Galle, P. (1986) Scanning Elec. Microsc. 4:1277-1284

Butt, H.J., Wolf, E.K., Gould, S.A.C., Nothern, B.D., Peterson, C.M. & Hansma, P.K. (1991a) J. Struct. Biol. 105, 54-61

Butt, H.J. (1991b) Biophys. J. 60:1438-1444

Butt, H.J., Siedle, K., Siefert, K., Fendler, K., Seeger, T., Baamberg, E., Weisenhorn, A.L., Goldie, K. & Engel, A.(1993) J. Microsc. 69:75-84

Calnan, J. (1970), Proc. R. Soc. Med 63:1115-1118

Cannizzaro, S.M., Padera, R.F., Langer, R., Rogers, R. Black, F.E., Davies, M.C., Tendler, S.J.B. & Shakesheff, K.M.(1998) Biotech. & Bioeng. 58:529-535

Caruso, F., Niikura, K., Furlong, D.N. & Okahata, Y. (1997) Langmuir, 13:3427-3433

Casalini, P., Luison, E., Menard, S., Colnaghi, M.I., Paganelli, G. & Canevari, S. (1997) J. Nuc. Med. 38(9):1378-81

Cazenave, J.P. & Mulvihill, J.N. (1988) Contr. Nephrol. 62:118-127.

Chen, C.H.,Clegg, D.O. & Hansma, H.G.(1998) Biochem. 37:8262-8267

Chen, G. & Hoffman, A.S. (1995) Nature 373:49-53

Chen, G.P., Imanishi, Y. & Ito, Y. (1998) J. Biomed. Mater. Res. 42(1):38-44

Chen, J. & Gardella, J.A. Jr. (1998) Macromol. 31:9328-9336

Chen, X., Shakesheff, K.M., Davies, M.C., et al. (1995) J. Phys. Chem. 99: 11537-11542.

Chen, X., Davies, M.C., Roberts, C.J., Skakesheff, K.M., Tendler, S.J.B. & Williams, P.M. (1996) Anal. Chem. 68:1451-56

Chen, X. McGurk, S.L., Davies, M.C., Roberts, C.J., Shakeheff, K.M., Tendler, S.J.B. & Williams, P.M.(1997) Macromol. 31(7):2278-2283

Chen, X., Davies, M.C., Roberts, C.J., Skakesheff, K.M., Tendler, S.J.B., Williams, P.M., Davies, J., Dawkes, A.C. & Edwards, J.C. (1998) Ultramicros. 75:171-181

Chidsey, C.E.D. & Loiacono, D.N. (1990) Langmuir 6:682-691

Chilkoti, A., Schmierer, A.E., Perez-Luna, V.H. & Ratner, B.D. (1995a) Anal. Chem. 67:2883-2891

Chilkoti, A., Boland, T., Ratner, B.D. & Stayton, P.S. (1995b) Biophys. J. 69:2125-2130

Cima, L.G. & Langer, R. (1993) Chem.Eng. Prog. June 46-54

Claesson, P.M., Ederth, T., Bergeron, V. & Rutland, M.W. (1996) Adv. Colloid. Interf. Sci. 67:119-183

Clery, D. (1992) New Scienctist March 7th 42-46

Cleveland, J.P., Anczykowski, B., Schmid, A.E. & Elings, V.B. (1998) Appl. Phys. Lett.72(20):2613-2615

Cornetta, K. (1992) Br. J. Haem. 80: 421-426

Cotton, C., Glidle, A., Beamson, G. & Cooper, J.M. (1998) Langmuir, 14:5139-5146

Costantino, H., Langer, R. & Klibanov, A.(1994) J. Pharm. Sci. 83:1662-1666

Cramer, K., Wawkushewski, A., Domb, A., Cantow, H.-J. & Magonov, S.N. (1995) Polym. Bull. 32:457-464

Creighton, T.E. (1993) Proteins - Structure and Molecular Properties, 2nd edition. Freeman N.Y. USA.

Culver, K.W., Ram, Z., Wallbridge, S., Ishii, H., Oldfield, E.H. & Blaese R.M. (1992) Science 256:1550-1552

Dai, W.G. & Saltzman, W.M. (1996) Biotech. Bioeng. 50(4)349-56

Dammer, V., Popescu, O., Wagner, P., Anselmetti, D., Guntherodt, H.J. & Miseuic, G. (1995) Science 267:1173-74

Dan, N. (1997) Biophys. J. 73:1842-1846

Dan, N. (1998) Biochim. et Biophys. Acta. 1369:34-38

Dandliker, P.J., Diederich, F., Zingg, A., Gisselbrecht, J-P., Gross, M., Louati, A. & Sanford, E. (1997) Helvetica Chimica Acta 80:1773-1801.

Danesh, A., Davies, M.C., Roberts, C.J., Shakeheff, K.M., Tendler, S.J.B., Williams, P.M. & Wilkins, M. (1999) Langmuir in press

Darnell, J., Lodish, H. & Baltimore, D. (1990) Molecular Cell Biology 2nd Edition. Scientific American Books, New York, USA.

Davies, J. (1994) Nanobiol. 3:5-16

Davies, N.M., Farr, S.J., Hadgraft, J. & Kellaway, I.W. (1992) Pharm. Res.9:1137-1144

Davies, M.C. & Brown A.(1987) in Controlled Release Technology : Pharmaceutical Applications" ACS Symp. Ser. 348:100-112 Washington D.C. USA.

Davies, M.C., Brown, A ., Newton, J.M. & Chapman, S.R. (1988) Surf. Interf. Sci. 11(12):591-595

Davies, M.C., Short, R.D., Khan, M.A., Watts, J.F., Brown, A., Humphrey, P., Vickerman, J.C. & Vert, M. (1989) Surf. Interface Anal. 14:115-120

Davies, M.C. & Lynn, R.A.P. (1990) Crit. Rev. Biocompat. 5(40):297-341

Davies, M.C., Lynn, R.A.P., Watts, J.F. Paul, A.J., Vickerman, J.C. & Heller, J. (1991) Macromol 24 (20):5508-5514

Davies, M.C. (1993) in "Polymer Surfaces and Interfaces II" Ed. Feast, W.J., Munro, H.S. & Richards, R.W. J. Wiley & sons Ltd. Chichester, UK.

Davies, M.C., Lynn, R.A.P., Davis, S.S., Hern, J.,Watts, J.F., Vickerman, J.C. & Johnson, D. (1994) Langmuir 10(5)1399-1409

Davies, M.C., Lynn, R.A.P., Hern, J., Paul, A.J., Vickerman, J.C. & Watts, J.F. (1995) Langmuir 11(11):4313-4322

Davies, M.C., Shakesheff, K.M., Shar, A.G., Domb, A. Roberts, C.J., Tendler, S.J.B. & Williams, P.M. (1996) Macromol. 29:2205-2212

Davies, M.C., Roberts, C.J., Tendler, S.J.B. & Williams, P.M. (1997) Biocompatability Assessment of Medical Devices and Materials. Ed. Braybrook. J. Wiley and son Ltd Chichester UK.

Davies M.C. (1999) 'Wish List' slide from "Polymer Therapeutics" meeting, Lake Shiga, Japan, May 1999

Decho, A.W. (1999) Carbohydrate Res. 315:330-333

Dee, K.C. & Bizios, R. (1996) Biotech. Bioeng.50:438-442

Dendritec Inc. (1999) Web page, c/o Michigan Molecular Institute http.//www.mmi.org/

Derose, J.A., Thundat, T., Nagahara, L.A. & Lindsay, S.M. (1991) Surf. Sci. 256:102-106

Deslandes, Y., Pleizier, G., Alexander, D. & Santerre, P. (1998) Polym. 39(11):2361-2366

Diamandis,E.P. & Christopulos,T.K (1991) Clin. Chem. 37(5):625-636

Digital Instruments Inc. (1996) "User manual for multimode SPM" Santa Barbara CA. USA

Ding, Z.L., Long, C.J., Heyashi, Y., Bulmus, E.U., Hoffman, A.S. & Stayton, P.S. (1999) Bioconj. Chem. 10(3):395-400

Dong, X., Proctor, A. & Hercules, D.M. (1997) Macromol. 30:67-70

Dovek, M.M., Albrecht, T.R., Kuan, S.W.J., Lang, C.A., Emch, R., Grutter, P., Frank, C.W., Pease, R.F.W. & Quate, C.F. (1988) J. Microscopy 152:229-236

Drake, P.A. & Bohn, P.W. (1995) Anal Chem 67: 1766-1771.

Dranoff, G., Jaffee, E., Lazenby, A., Golumbek, P., Levitsky, H., Brose, K., Jackson, V., et al (1993) Proc. Natl. Acad. Sci. USA. 90:3539-3543

Dubois, L.H. & Nuzzo, R.G. (1992) Annu. Rev. Phys. Chem. 43:437-63

Dubois, L.H., Zegarski, B.R. & Nuzzo, R.G. (1993) J. Phys. Chem. 98(1):678-688

Duc, T.M. (1995) Surf. Rev. Lett. 2:833-858

Ducker, W.A., Senden, T.J. & Pashley, R.N. (1991) Nature 353:239-241

Duevel, R.V. & Corn, R.M. (1992) Anal. Chem. 64(4):337-342

Duncan, R., Dimitrijevic, & Evagorou, E.G. (1996) STP Pharma. Sci. 6:237-262

Dunlap, D.D., Maggi, A., Soria, M.R. & Monaco, L. (1997) Nuc. Acid Res. 25:3095-3101

Duschl, C., Liley, M., Lang, H., Ghandi, A., Zakeeruddin, S.M., Stahlberg, H., Dubochet, J. et al (1996) Mat. Sci. Eng. C 4:7-18

Dvornic P.R. & Tomalia, D. A. (1996a) Curr. Op. Colloid and Interface Sci. 1:221-235

Dvornic P.R. & Tomalia, D. A. (1996b) Sci Spectra 32-54

Dzahavakhidze, P.G., Kornyshev, A.A., Tadjeddine, A. & Urbakh, M.I. (1989) Electrchimica Acta 34(12):1677-1680,

Edelman, E., Brown, L. & Langer, R. (1987) J. Biomed. Mater. Res. 21:339-353

Elam, J.H., Nyren, N. & Stenberg, M. (1984) J. Biomed. Mater. Res. 18:953-959.

Elisaf, M.S., Germanos, N.P., Bairaktari, H.T., Pappas, M.B., Koulouridis, E.I. & Siamopoulos, K.C. (1997) Am. J. Nephrol. 17(2):153-157

Elisseeff, J., Anseth, K., Sims, D., McIntosh, W., Randolph, M. & Langer, R. (1999) Proc. Natl. Acad. Sci. USA. 96(6):3104-3107

Eng, L.M., Jandt, K.D., Fuchs, H. & Petermann, J. (1994) Appl. Phys. A. 59:145-150

Engel, A. (1991) Annu. Rev. Biophys. Biophys. Chem. 20:79-108

Erbacher, P., Zou, S.M., Bettinger, T., Steffan, A.M. & Remy, J.S. (1998) Pharm. Res. 15(9):1332-1339

Erbacher, P., Remy, J.S. & Behr, J.P. (1999) Gene Ther. 6(1):138-145

Erdtmann, M., Keller, R. & Baumann, H. (1994) Biomaterials. 15:1043-1048.

Erie, D.A., Yang, G., Schultz, H.C. & Bustamante, C. (1994) Science, 266:1562-1566

Ertel, S.I., Ratner, B.D. & Horbett, T.A. (1990) J. Biomed. Mater. Res. 24:1637-1659

Feast, W.J. & Munro, H.S. (1987) in "Polymer Surfaces and Interfaces" J. Wiley and sons, Chichester, U.K.

Felgner, P. L., Gadek, T.R., Holm, M., Roman, R., Chan, H.W., Wenz, M., Northrop, J.P. *et al* (1987) Proc. Natl. Acad Sci. USA 84:7413-7417

Felgner , J. H., Kumar, R., Sridhar, C. N., Wheeler, C.J., Tsai, Y.J., Border, R., Ramsey, P. *et al* (1994) J. Biol. Chem. 269:2550-2561

Fergusson, W.C. (1973)"Plastics their Contribution to Society and Considerations of their Disposal" Hutchinson Benham Ltd, Colchester UK.

Ferri, G.L., Gaudio, R.M., Castello, F.L., Tirolo, C. & Chiolerio, F. (1999) Appl. Immunohistochemistry 7(1):73-80

Ferruti, P., Domini, I., Barbucci, R. Beni, M.C., Dispensa, E., Sancasciani, S., Marchiso, M.A. & Tanzi, M.C. (1983) Biomaterials 4:218-221.

Ferruti, P., Ranucci, E., Sartore, L., Bignotti, F., Marchisio, M.A., Bianciardi, P. & Veronese, F.M. (1994) Biomaterials. 15:1235-1241.

Fisher, R.J., Fivash, M., Casas-Finet, J., Erickson, J.W., Kondoh, A., Bladen, S.U., Fisher, C., Watson, D.K. & Papas, T. (1994) Protein Sci 3: 257-267.

Florin, E.L., Moy, V.T. & Gaub, E.H. (1994) Science 264:415-417

Florin, E.L Rief, M., Lehmann, H., Ludwig, M., Dornmair, C., Moy, V.T. & Gaub, H.E. (1995) Biosen. Bioelectronics 10:895-901

Flotte,T.R., Barraza-Ortiz, X, Solow, R., Afione, S.A., Cater, B.J. & Guggino, W.B. (1995) Gene Ther. 2:29-37

Folkman, J. & Long, D. (1964) Surg. Res. 4:139-142

Fournier, C., Leonard, M., Le Coq-Leonard, *I. & Dellacherie, E. (1995)* Langmuir 11:2344-2347

Frazier, R.A. (1996) "Macromolecular Interactions at Polysaccharide Surfaces" PhD thesis, University of Nottingham.

Frazier, R.A., Davies, M.C., Matthijs, G, Roberts, C.J., Schacht, E., Tendler, S.J.B.& Williams, P.M. (1997a) Langmuir 13(26):7115-7120

Frazier, R.A., Davies, M.C., Matthijs, G., Roberts, C.J., Schacht, E., Tendler, S.J.B., Williams, P.M. (1997b) Langmuir 13(18):4795-4798

Frèchet, J.M.J. (1994) Science 263:1710-1715

Frèchet, J.M.J. (1999) Talk at Recent Advances in Drug Delivery Systems conference. Salt Lake City, Utah, USA. Feb 1999

Friberg, S.E., Podzimek, M, & Tomalia, D.A. (1998) Mol. Cryst. Liq. Cryst. 164:157-163

Frisbie, C.D., Rozsnyal, L.F., Noy, A., Wrighton, M.S. & Lieber, C.M. (1994) Science 265:2071-2074

Fritz, J., Anselmetti, D., Jarchow, J. & Fernandez-Busquets, X. (1997) J. Struct. Biol. 119:165-171

Fritz, M., Radmacher, M. & Gaub, H.E. (1994) Biophys. J. 66:1328-1334

Fritz, M.C., Hahner, G., Spencer, N.D., Burli, R. & Vasella, A. (1996) Langmuir 12:6074-6082

Furness, E.L., Ross, A., Davis, T.P. & King, G.C. (1998) Biomaterials 19(15)1361-1369

Ganong , W.F. (1993) Review of Medical Physiology 16th Edition. Prentice Hall, London, UK.

Gao, J.M., Niklason, L. & Langer, R. (1998) J. Biomed. Mater. Res. 42(3):417-424

Gao, J.Y., Dubin, P.L. & Muhoberac, B.B. (1997) Anal. Chem. 69:2945-2951

Gao, J.Y. & Dubin, P.L. (1999) Biopolymers, 49(2):185-193

Gardner, T.J., Frisbie, C.D. & Wrighton, M.S. (1995) J. Am. Chem. Soc. 117:6927-6933

Garnett M. C. (1999) Crit. Rev. Therapeutics Drug Carrier Sys. 16(2):147-207

Garrett, Q & Milthorpe, B.K. (1996) Investigative Opthalmology and Visual Sci. 37(13):2594-2602

Gershon, H., Ghirlando, R., Guttmann, S.B. & Minsky, A. (1993) Biochem. 32:7143-7151

Giancarlo, L.C. & Flynn, G.W. (1998) Annu. Rev. Phys. Chem. 49:297-336

Gilding, D.K., Paynter, R.W. & Castle, J.E. (1980) Biomater. 1:163-168

Gitsov, I. & Frèchet J.M.J. (1996) J. Am. Chem. Soc. 118:3785-3786

Goh, M.C. (1995) in 'Advances in Chemical Physics Vol XCI'. Ed Prigogine, I. & Rice, S.A. J. Wiley and Sons Inc.

Goldraich, M. & Kost, J. (1993) Clin. Mater. 13:135-142

Gombotz, W.R., Guanghui, W. & Hoffman, A.S. (1989), J. Appl. Polym. Sci. 37(1):91-107

Gombotz, W.R., Guanghui, W., Horbett, T.A. & Hoffman, A.S. (1991) J. Biomed. Mater. Res 25(12):1547-1562

Good, R.J. (1992) Abs. Papers Am. Chem. Soc. 203(1):2-COLL

Gorman, C. M., Aikawa, M., Fox, B., Fox, E., Lapuz, C., Michaud, B., Nguyen, H. et al (1997) Gene Ther. 4:983-992

Gott, V.L., Whiffen, J.D. & Dutton, R.C. (1963) Science 142:1297-1298

Gould, S.A.C., Drake, B., Prater, C.B., Weisenhorn, A.L., Manne, S., Hansma, H.G., Hansma, P.K., Massie, J. et al (1990) J. Vac. Sci. Technol. A 8:369-373

Graham, N.B. & McNeill, M. E. (1984) Biomater. 5:27-36

Grainger, D.W., Kim, S.W. & Feijen, J. (1988) J. Biomed. Res. 22:231-245

Grainger, D.W., Knuton, K., Kim, S.W. & Feijen, J. (1990) J. Biomed. Res. 24:403-431

Grandbois, M., Beyer, M., Rief, M., ClausenSchaumann, H. & Gaub, H.E. (1999) Science 283(5408):1727-1730

Greaves, J.L. & Wilson, C. G. (1993) Adv. Drug Del. Rev.11(3):349-383

Green, R.J. (1996) Protein / polymer Interactions Investigated by Surface Plasmon Resonance. PhD thesis, University of Nottingham

Green, R.J., Davies, J., Davies, M.C., Roberts, C.J. & Tendler, S.J.B. (1997a) Biomater. 18(5):405-413

Green, R.J., Tasker, S., Davies, J., Davies, M.C., Roberts, C.J. & Tendler, S.J.B. (1997b) Langmuir, 13(24):6510-6515

Green, R.J., Davies, M.C., Roberts, C.J. & Tendler, S.J.B. (1997) J. Biomed. Mater. Res. (1998) 42(2):165-171

Grier, D.G. (1997) Curr. Opin. Colloid Interf. Sci. 2:264-270

Grode, G.A., Anderson, S.J., Grotta, H.M. & Falb, R.D. (1969) Trans. Am. Soc. Artif. Intern. Org. 15:1

Grotenhuis, P.D.J. & van Boeckel, C.A.A. (1991) Jam. Chem. Soc. 113:2743-2747

Gukenberger, R.,Wiegrabe, W., Hillebrand, A., Hartmann, T. & Baumeister, W. (1989) Ultramicroscopy 31:327-332

Haberle, W., Horber, J.K. H. & Binnig, G. (1991) J. Vac. Sci. Technol. B. 9:1210-1213

Haensler, J. & Szoka, F.C. Jr. (1993a) Bioconj. Chem. 4:372-379

Haensler, J. & Szoka, F.C. Jr. (1993b) Bioconj. Chem. 4:85-93

Hanley, S.J., Giasson, J., Revol, J.-F. & Gray, D.G. (1992) Polymer 33:4639-4642

Hansma, H. G. (1996a) J. Vac. Sci. Technol. B 14(2):1390-1394

Hansma, H.G., Revenko, I., Kim, K. & Laney, D. (1996b) Nuc. Acid. Res. 24(4):713-720

Hansma, H.G., Kim, K.J., Laney, D.E., Garcia, R.A., Argaman, M., Allen, M.J. & Parsons, S.M. (1997) J. Struct. Biol. 119:99-108

Hansma, P.K., Salisbury, D. (1989) New Scientist May 27th, 52-56

Hanson, S.R., Harker, L.A., Ratner, B.D. & Hoffman, A.S. (1979) Ann. Biomed. Eng. 7:357-67

Harris, L.D., Kim, B.S. & Mooney, D.J. (1998) J. Biomed. Mater. Res. 42(3):396-402

Hart, S.L., Arancibia-Carcamo, C.V., Wolfert, M.A., Mailhos, C., O'Reilly, N.J., Ali, R.R., Coutelle, C., George, A.J. *et al* (1998) Hum. Gene Ther. 9:575-585

Hawker, C.J. & Frèchet, J.M.J (1990) J. Am. Chem. Soc. 112:7638

Hearn, M.J., Briggs, D., Yoon, S.C. & Ratner, B. D. (1987) Surf. Interf. Anal. 10(8):384-391

Hearn, M.J., Ratner, B.D. & Briggs, D. (1988) Macromol. 21(10):2950-2959

Hegner, M, Wagner, P. & Semenza, G. (1993) Surf. Sci. 291(1-2):39-46

Heller, J. (1997) in Controlled Drug Delivery : Challenges and Strategies. Ed. Park, K. Am. Chem Soc. Washington DC, USA.

Henderson, E., Hayelon, P.G. & Sakaguchi, D.S. (1992) Science, 257:1944-1946

Hierlemann, A., Campbell, J.K., Baker, L.A., Crooks, R.M. & Ricco, A.J. (1998) J. Am. Chem. Soc. 120(21):5323-5324

Himmel, H-J., Weiss, K., Jager, B., Dannenberger, O., Grunze, M. & Woll, C. (1997) Langmuir 13:4943-4947

Hinterdorfer, P., Baumgartner, W., Gruber, H.J., Schilcher, K. & Schindler, H. (1996) Proc. Natl. Acad. Sci. USA, 93(8):3477-3481

Hirsch-Lerner, D. & Barenholz, Y. (1998) Biochim. et Biophys. Acta. 1370:17-30

Hoh, J.H. & Hansma, P.K. (1992) Trends in Cell Biol 2:208-213

Hoh, J.H., Cleveland, J.P., Prater, C.B., Revel, J.P. & Hansma, P.K. (1993) J. Am. Chem. Soc. 114:4917-4919

Hopfield, J.J. (1974) Proc. Natl. Acad. Sci. USA 71:3640

Horbett, T.A. & Brash, J.L. (1995) Proteins at Interfaces II : Fundamentals and Applications. ACS Symp.Ser. 602 Washington DC. USA.

Horwitz, A.F. (1997) Sci. Am., May 46-53

Hufnagel (1968) Ann. NY. Acad. Sci. 146:262-270

Hug, P. & Sleigh, R.G. (1991) Biochim et Biophys. Acta 1097:1-17

Hui, H.W. & Robinson, J.R. (1985) Int. J. Pharm 26:203-213

Humes, H.D., Buffington, D.A., MacKay, S.M., Funke, A.J. & Weitzel, W.F. (1999) Nature Biotech. 17(5)451-455

Hutter, J.L. & Bechhoefer, J. (1994) Rev. Sci. Instrum. 64:1868-1873

Ikai, A., Mitsui, K., Tokuoka, H. & Xu, X.M. (1997) Mater. Sci. Eng. C - Biomimetic Mater. Sensors and Sys. 4(4 SISI):233-240

Illum, L. (1998) Pharm. Res. 15(9):1326-1331

Ingram, A.J., Parbtani, A. & Churchill, D.N. (1998) Nephrol. Dialysis Transplant. 13(6):1452-1457

Irvine, D.J., Mayers, A.M., Satija, S.K., Barker, J.G., SofiaAllgor, S.J. & Griffith, L.G. (1998) J. Biomed. Mater. Res. 40(3):498-509

Ishaug, S.L., Yasemski, M.J., Bizios, R. & Mikos, A.G. (1994) J. Biomed. Mater. Res. 28:1445-1453

Ishida, M., Machida, Y., Nambu, N. & Nagai, T. (1981) Chem. Pharm. Bull. 29:810-816

Issberner, J., Moors, R. & Vögtle, F (1994) Angew Chem. Int. Ed. Engl. 33:2413

Ito, Y. & Imanishi, Y. (1989) CRC Crit. Revs. Biocomp. 5:45-109

Ito, Y. (1998) Mater. Sci. Eng. C. - Biomimietic Mater. Sensors Sys. 6(4):267-274

Izumi, K., Gan, P., Toda, A., Miyaji, H., Hashimoto, M., Miyamoto, Y. & Nakagawa, Y. (1994) Jpn. J. Appl. Phys. 33, L1628-1630

Jacobasch, H-J., Simon, F. & Weidenhammer, P. (1998) Colloid. Polym. Sci. 276:434-442

Jacobs, J.W. & Fodor, S.P.A. (1994) TIBITECH 12:19-26

Jansen, J.F.G.A., Meijer, E.W., & De Brabander-Van Den Berg, E.M.M (1995) J. Am. Chem. Soc. 117:4417-4418

Jaques, L.B. (1982) Trends in Pharmacological Sci. 3:289-291

Jin, R.H., Aida, T. & Inoue, S. J. (1993) Chem. Soc. Chem. Commum. 1260-1262

Johnson, O.L., Cleland, J.L., Lee, H.J., Charnis, M., Duenas, E., Jaworowicz, W., Shepard, D., Shahzamani, A., *et al.* (1996) Nature Med. 2(7):795-799

Jones, E.Y. (1996) Curr. Opin. Cell. Biol 8:602-608

Juliano, R.L. & Haskill, S. (1993) J. Cell Biol. 120:577-85

Kabanov, A.V., Astafieva, I. V., Chikindas, M. L., Rosenblat, G. F., Kiselev, V. I., Severin, E.S. & Kabanov, V. A. (1991) Biopolymers 31:1437-1443.

Kabanov, A.V.Astafieva, I. V., Maksimova, I.V., Lukanidin, E.M., Georgiev, G. P. & Kabanov, V. A. (1993) Bioconj. Chem. 4:448-454

Kabanov, A.V. & Alakhov, V. Yu. (1994) J. Contr. Release. 28:15-35

Kabanov, A. V. & Kabanov, V. A. (1995) Bioconj. Chem. 6:7-20

Kai, E., Sawata, S., Ikebukuro, K., Iida, T., Hona, T. & Karube, I. (1999) Anal. Chem. 71:796-800

Karpovich, D.S. & Blanchard, G.S. (1994) Langmuir 10(9):3315-3322

Kashiwagi, T., Ito, Y. & Imanishi, Y. (1993) Biomater. 14(15):1145-53

Kashlev, M., Martin, E., Polyakov, A., Severinov, K., Nikiforov, V. & Goldfarb, A. (1993) Gene 130:9-14

Kawabata, K., Takakura, Y., Hashida, M. (1995) Pharm. Res. 12(6):825-830

Kawaura, C., Noguchi, A., Furuno, T. & Nakanishi, M. (1998) FEBS Lett. 421:69-72

Keller, D. & Bustamante, C. (1993) Biophys. J. 64:896-897

Kim, Y-T. & Bard, A.J. (1992) Langmuir 8:1096-1102

Knapen, J.W.J., Van der Made, A.W., De Wilde, J.C., Van Leeuwen, P.W.N.M., Wijkens, P. Grove, D.M. & Van Koten, G. (1994) Nature 372:659-663

Koester, K.H., Schwarz, M., Sele, V. & Sindrup, E. (1957) Lancet 262

Kohn, D. B., Weinberg, K. I., Nolta, J.A., Heiss, L. N., Lenarsky, C., Crooks, G. M., Hanley, M. E. *et al* (1995) Nature Med. 1:1017-1023

Koltover, I., Salditt, T., Radler, J.O. & Safinya, C.R. (1998) Science 281:78-81

Komazawa, H. Saiki, I., Igarashi, Y., Azuma, I., Kojika, M., Orikasa, A., Ono, M. and Itoh, I. (1993) J. Bioact. Compat. Pol. 8:258-274

Konak, C., Mrkvickova, L., Nazarova, O., Ulbrich, K. & Seymour, L.W. (1998) Supramolec. Sci. 5:67-74

Kooha, F., Muller, R.H., Davis, S.S. & Davies, M.C. (1989) J.Contr. Rel. 9(2):149-157

Kricka, L.J. (1999) Clin Chem. 45(4):453-455

Kukowska-Latallo, J.F., Bielinska, A., Johnson, J., Tomalia, D.A. & Baker, J.R., (1996) FASEB J. 10(6):884-887

Kuzdzal, S.A., Monning, C.A., Newkome, G.R. & Moorefiled, C.N. (1994) J. Chem Soc. Chem Commun 2139-2140

Kwon, I.C., Bae, H.Y. & Kin, S.W. (1991) Nature 354:291-293

Lai, K.N., Wang, A.Y.M., Ho, K., Szeto, C.C., Li, M., Wong, L.K.S. & Yu, A.W.Y. (1996) Am. J. Kidney Diseases 28(5):721-726

Lal, R. & Joh, S.A. (1994) Am. J. Physiol 266 (cell Physiol. 35) C1-C21

Lang, F.-R., Leonard, D., Mathieu, H.J., Moser, E.M. & Bertrand, P. (1998) Macromol. 31:6177-6183

Lang, H., Dusckl, C. & Vogel, H. (1994) Langmuir 10:197-210

Langer, R. & Vacanti, J.P. (1993) Science 260:920-927

Langer, R. (1998) Nature supp. 392:5-10

Larm, O., Larsson, R.& Olsson, P.(1983) Biomed. Mat. Devices Artif. Org. 11:161-174

Larsson, R., Olsson, P.& Lindahl, U. (1980) Thromb. Res. 26:43-57

Larsson, R., Larm, O. & Olsson, P. (1987) Ann. NY. Acad. Sci. 516:102-115

Launay, N. Caminade, A-M. & Majoral, J.P. (1995) J.Am. Chem. Soc. 117: 3282-3283

Lavon, I. & Kost, J. (1998) J. Contr. Rel 54(1):1-7

Leckband, D.E., Schmitt, F-J., Israelachvili, J.N. & Knoll, W. (1994) Biochem. 33:4611-4624

Ledley, F. D. (1996) Pharm. Res. 13:11:1595-1614

Lee, G.U., Kidwell, D.A. & Colton, R.J. (1994a) Langmuir 10(2):354-357

Lee, G.U., Chrisey, L.A. & Colton, R.J. (1994b) Science 266:771-773

Lehman, W.B., Strongwater, A.B., Tunc, D., Kummer, F., Atar, D., Grant, A.D., Kramer, M. & Rohovsky, M.W. (1994) J. Pediat. Orthop. Pt. B 3:190-193

Lemmouchi, Y., Schacht, E. & Dejardin, S. (1998) J. Bioact. Compat. Polym. 13(1):4-18

Lenk, T.J., Hallmark, V.M., Rabolt, J.F., Haussling, L. & Ringsdorf, H. (1993) 26:1230-1237

Leong, K.W., Brott, B.C. & Langer, R. (1985) J. Biomed. Mater. Res. 19:941-955

Leong, K.W., Mao, H.Q., Truong Le, V.L., Roy, K., Walsh, S.M. & August, J.T. (1998) J. Contr. Rel. 183-193

Leu, J.G., Liou, H.H., Wu, S.C., Yang, W.C., Huang, T.P. & Wu, S.C. (1998) J. Formosan Med. Assoc. 97(1):49-54

Lewis, K. B. & Ratner, B.D. (1993) J.Coll. Interf. Sci. 159:77-83

Liedberg, B., Nylander, C., & Lundstrom, I. (1983) Sensors and Actuators 4:299-304

Lin, J.N., Lea, A.S., Hansma, P.K., & Andrade, J.D. (1990) Langmuir 6:509-511

Liu, F., Yang, J., Huang, L. & Liu, D. (1996) Pharm. Res. 13(12)1856-1860

Lomas, M. (1999) PhD thesis, University of Nottingham

Lopez, G.P., Ratner, B.D., Tidwell, C.D., Haycox, C.L., Rapoza, R.J. & Horbett, T.A. (1992) J. Biomed. Mater.Res. 26:415-439

Lowndes, G.J., Threadgill, M. D. & Pouton, C.W. (1994) Proceed. Intern. Symp. Control. Rel. Bioact. Mater. 21:262-264

Lub, J., van Vroonhoven, F.C.B.M., van Leyen, D. & Benninghoven, A. (1987) J. Polm. Sci. Poly. Phys. Ed. 27:2071

Luck, M., Pistel, K.F., Li, Y.X., Blunk, T., Muller, R.H., Kissel, T. (1998) 55(2-3):107-120

Ma, P.X. & Zhang, R.Y. (1999) J. Biomed. Mater. Res. 46(1):60-72

Macleod, H.A. (1987) SPIE 777:282-286,

Maeda, H. (1991) Adv. Drug. Deliv. Res. 6:181-202

Maganov, S.N., Elings, V. & Whangbo, M.-H, (1997) Surf. Sci 375(2-3)L385-L391

Magnani, A., Busi, E. & Barbucci, R. (1994) J. Mater. Sci.: Mater. Med. 5:839-843.

Maher, J.F., Lapierre, L., Schreiner, G.E., Geiger, M. & Westervelt, F.B. (1963) New Engl. J. Med. 268:451-453

Malik, N., Spindler, R.A., Wiwattanapatapee, R. & Duncan, R. (1999) In preperation

Malliaris, A., Tsiourvas, D. & Paleos, C.M. (1999) Chem. : Euro. J. 5(5)1440-1444

Malmsten, M., Lindman, B., Holmberg, K. & Brink, C. (1991) Langmuir. 7:2412-2414.

Maniatis, T., Fritsch, E.F. & Sambrook, J. (1986) Molecular Cloning : A Laboratory Manual 2nd Ed., Cold Harbour Spring Press, NY. USA

Mantus, D.S., Ratner, B.D., Carlson, B.A. & Moulder, J.F. (1993), Anal. Chem. 65:1431-1438

Marchisio, M.A., Longo, T. & Ferruti, P. (1973) Experientia; 39:93-96

Marchisio, M.A., Ferruti, P., Bertoli, S., Belgiojoso, B., Samour, C.M., Wolter, K.D. (1988) A Novel Approach to the Problems of Heparin in Haemodialysis, in Polymers in Medicine III, Elseviers Science Publishers, Amsterdam.

Marti, O., Ribi, H.O., Drake, B., Albrecht, T.R., Quate, C.F. & Hansma, P.K. (1988) Science 239:50-53

Martin, P. (1997) Science 276:75-80

Massia, S.P. & Hubbell, J.A. (1991) J.Cell Biol., 114(5):1089-1100

Matsumura, Y. & Maeda, H. (1986) Cancer Res. 6:6387-6392

Matthews, S.E., Pouton, C.W. & Threadgill, M.D. (1996) Adv. Drug. Delivery Rev. 18(2):219-267

Mattiason, B. (1983) Methods. Enzymol. 92:498-514

McGrath, D.V. & McElhanon, J.R. (1998) J. Am. Chem. Soc. 120(8):1647-1656

McGrath, M.H. & Burkhardt, B.R. (1984) Plast. Reconstrutive Surg. 74:550-560

McGurk, S.M. (1998) "Surface Analysis of Novel Biomaterials" PhD thesis, University of Nottingham

McKay, R. (1997) Science 276:66-71

McPherson, T., Kidane, A., Szleifer, I. & Park, K. (1998) Langmuir 14(1):176-186

Meiners, J.C., Quintel-Ritzi, A., Mlynek, J., Elbs, H. & Krausch, G. (1997) 30:4945-4951

Mejdoub, H., Le Ret, M., Boulanger, Y., Maman, M., Choay, J. & Reinbolt, J. (1991) J. Prot. Chem. 10:205-212

Meredith, J.E., Babak, F. & Schwartz, M.A. (1993) Molec. Biol. of the Cell 4:953-961

Merle, H.J. Alberti, B. Schwendler, M. & Peterson, I.R. (1992) J. Phys. Appl. Phys. 25:1556-1558

Merrill, E.W., Salzman, E.W., Wong, P.S.L., Ashford, T.P., Brown, A.H. & Austen, W.G. (1970) J. Appl. Physiol. 29:723-30

Meyer, E., (1992) Prog. Surf. Sci. 41:3-49

Michalopoulos, G.K. & DeFrances, M.C. (1997) Science 276:60-66

Migonney, V., Lacroix, M.D., Ratner, B.D. & Jozefowicz, M. (1995) J. Biomater. Sci. Polym. Ed. 7:265-275

Miller, A. D. (1990) Hum. Gene Ther. 1:5-14

Miller, T.M. & Neenan, T.X. (1990) Chem. Mat. 2:346

Minidictionary of Physics (1988), Oxford University Press, Oxford, UK

Misra, G.S. (1993) in "Introductory Polymer Chemistry" J. Wiley & sons Inc. New Dehli, India.

Missirilis, Y.F. & Lemm, W. (1991) Modern Aspects of Protein Adsorption on Biomaterials. Kluwer Academic Publishers, Dordrecht, The Netherlands.

Mittler-Neher, S., Spinke, J., Liley, M., Nelles, G.,Weisser, M., Back, R., Wenz, G & Knoll, W. (1995) Biosens. Bioelectron. 10:903-916

Miyazaki, S., Nakayama, M., Takada, Oda, M. & Attwood, D., (1995) Int. J. Pharm. 118:257-263

Morag, E., Bayer, E.A. & Wilchek, M. (1996) Anal. Biochem. 243(2):257-263

Mori, Y., Nagaoka, S., Tanzawa, H., Kikuchi, T., Yanada, Y., Hagiwara, M. & Idezuki, Y. (1982) J. Biomed. Mater, Res. 16(1):17-30

Motomatsu, M., Nie, H.-Y., Mizutani, W. & Tokumoto H. (1996) Polymer 37:183-185

Mrksich, M., Sigal, G.B. & Whitesides, G.M. (1995) Langmuir 11: 4383-4385.

Mrksich, M. & Whitesides, G.M. (1996a) Annu. Rev. Biophys. Biomol. Struct. 25:55-78

Mrksich, M., Chen, C.S., Xia, Y., Dike, L.E., Ingber, D.E. & Whitsides, G.M. (1996b) Proc. Natl. Acad. Sci. USA. 93:10775-10778

Muller, W., Ringsdorf, H., Rump, E., Wildburd, G., Zhang, X., Angermaier, L., Knoll, W. *et al* (1993) Science 262:1706-1708

Mumper, R.J., Wang, J., Claspell, J.M.& Rolland, A.P (1995) Intern. Symp. Cont. Rel. Bioact. Mater. 22:325-326

Mumper, R.J., Duguid, J. G., Anwer, K., Barron, M. K.,. Nitta, H. & Rolland, A.P. (1996) Pharm. Res. 13:701-709

Munro, H.S. & Singh, S. (1993) in Polymer Characterisation Ed. Hunt, B.J. & James, M.I. Blackie Academic and Proffesional, Glasgow, UK

Murray, P., Frampton, G. & Nelson, P.N. (1999) Brit. Med. J. 319(7206):332-334

Muskal, N., Turyan, I., Shurky, A. & Mandler, D. (1995) J.Am. Chem. Soc. 117:1147-1148

Nagai, T. (1985) J. Contr. Rel. 2:121-126

Nakayama, Y., Nakamata, K., Hirano,Y., Goto, K. & Matsuda, T. (1998) Langmuir 14:3909-3915

Naylor, A.M., Goddard, W.A. III, Kiefer, G.E. & Tomalia, D. A. (1989) J. Am. Chem. Soc. 111:2339-2341

Nelles, G., Schonherr, H., Jaschke, M., Wolf, H., Schaub, M., Kuther, J., Tremel, W. *et al* (1998) Langmuir, 14:808-815

Newkome, G.R., Lin, X. & Weiss C.D. (1991) Tetrahedron Asymmetry 2:957-960

Ng, S.Y., Vandamme, T., Taylor, M.S. & Heller, J. (1997) Macromolec. 30:770-772

Nicolau, C., Le Pape, A., Soriano, P., Fargette, F. & Juhel, M. F. (1983) Proc. Natl. Acad. Sci. USA. 80:1068-1072

Noguchi, A., Furuno, T., Kawaura, C. & Nakanishi, M. (1998) FEBS Lett. 433:169-173

Nuzzo, R., G. & Allara, D. L. (1983) J.Am. Chem. Soc. 105:4481-4483

Nuzzo, R., G., Dubois, L.H. & Allara, D. L.(1990) J. Am. Chem. Soc. 112:558-569

O'Donnell, J. & Honeybourne, C.L. (1991) J. Phys. Condensed Matter 3:S337-S34

Ojaniemi, M., Martin, S.S., Fabrizio, D., Olefsky, J.M. & Vuori, K. (1997) J. Biochem. 272:3780-3787

Opatrny, K., Bouda, M., Kohoutkova, L., Vit, L. & Sefrna, F. (1997) Intl. J. Art. Organs 20(2):112-118

Ortiz, C., & Hadziioannou, G. (1999) Macromolec. 32(3):780-787

Osterberg, E., Bergstrom, K., Holmberg, K., Schuman, T.P., Riggs, J.A., Burns, N.L., van Alstine, J.M. & Harris, J.M. (1995) J. Biomed. Mat. Res. 29:741-747

Ottaviani, M. F., Bossmann, S., Turro, N.J. & Tomalia D.A. (1994) J.Am. Chem. Soc. 116:661-671

Ottaviani, M. F., Cossu, E., Turro, N.J. & Tomalia D.A. (1995) J. Am. Chem. Soc. 117:4387-4398

Ottaviani, M. F., Montalti, F., Romanelli, M., Turro, N.J. & Tomalia D.A. (1996) J. Phys. Chem. 100:11033-11042

Ottaviani, M. F., Montalti, F., Turro, N.J. & Tomalia D.A. (1997a) J. Phys. Chem. B. 101:158-166

Ottaviani, M. F., Andechaga, P.,Turro, N.J., & Tomalia D.A. (1997b) J. Phys Chem.B 101:6057-6065

Pan, J., Tao, N. & Lindsay, S.M. (1993) 9:1556-1560

Pan, S., Castner, D.G. & Ratner, B.D. (1998) Langmuir 14:3545-3550

Park, K. D., Piao, A.Z., Jacobs, H., Okano, T. & Kin, S.W. (1991) J. Polym. Sci. A - Polym. Chem. 29:1725-1737

Patel, N., Davies, M.C., Lomas, M., Roberts, C.J., Tendler, S.J.B. & Williams, P.M. (1997) J. Phys. Chem. B 101:5138-5142

Patel, N., Padera, R., Sanders, G.H.W., Cannizzaro, S.M., Davies, M.C., Langer, R., Roberts, C.J., Tendler, S.J.B., Williams, P.M. & Shakesheff, K.M. (1998) FASEB J. 12:1447-1454

Paynter, R.W., King, M.W., Guidoin, R.G. & Rao, T. (1989) Int. J. Artif. Org.12(3):189-194

Pellequer, J.L. & Van Regenmortel, M.H.V. (1993) J. Immunol. Meth. 166:133-143

Peppas, N.A. & Langer, R. (1994) Science 263:1715-1720

Peppas, N.A. & Sahlin, J.J. (1996) Biomater.17:1553-1561

Percec, V. & Kawasumi, M (1992) Polym Preprints Am Chem Soc Div Polym Chem 33,221

Perrin, D.D. & Dempsey, B. (1974) Buffers for pH and Metal Ion Control : Chapman and Hall laboratory manuals, Chapman and Hall Ltd., London, UK.

Persson , B.N.J. (1987) Chem. Phys. Lett. 141(4):366-368

Perutz, M. (1992) Protien Structure : New Approaches to Disease and Therapy. W.H. Freeman & Co. N.Y. USA.

Peter, S.J., Miller, M.J., Yasko, A.W., Yaszemski, M.J. & Mikos, A.J. (1998) J. Biomed. Mater. Res 43(4):422-427

Peters, T. (1982) Adv. Prot. Chem. 37:161-246.

Petro, M., Gemeiner, P. & Berek, D. (1994) J Chromatogr A. 665:37-45.

Petruzzelli, L., Takami, M. & Humes, H.D. (1999). Am. J. Med. 106(4):467-476

Phizicky, E.M. & Fields, S. (1995) Microbiol. Rev. 59:94-123

Pistolis, G., Malliaris, A., Tsiourvas, D., Paleos, C.M. (1999) Chem. - A Euro. J. 5(5):1440-1444

Plank, C., Zatloukal, K., Cotten, M., Mechtler, K & Wagner, E. (1992) Bioconj. Chem. 3:533-539

Plant, A.L., Brigham-Burke, M., Petrella, E.C. & O'Shannessy, D.J. (1995) Anal. Biochem. 226:342-348

Poirier, G.E. & Pylant, E.D. (1996) Science 272:1145-1148

Pope, L., Davies, M.C., Tendler, S.J.B., Roberts, C.J., Williams, P.M. & Laughton, C.L. (1999) J. Micros. submitted

Porter, C.D., Lukacs, K.V., Box, G., Takeuchi, Y. & Collins, M.K.L. (1998) J. Virol. 72(6):4832-4840

Porter, M.D., Bright, T.B., Allara, D.L. Chidsey, C.E.D. (1987) J. Am. Chem. Soc. 109:3559-3568

Potath, J. & Flodin, P. (1959) Nature 183:1657-1659.

Pouton, C.W., Lucas, P., Thomas, B.J., Uduehi, A.N., Milroy, D.A. & Moss, S.H. (1998a) J. Contr. Rel. 53(1-3):289-299

Pouton, C.W. & Seymour, L.W. (1998b) Adv. Drug. Delivery Rev. 34(1):3-19

Pugliese, L., Coda, A., Malcovati, M. & Bolognesi, M. (1993) J.Mol. Biol. 231:698-710

Putman, D. & Kopecek, J. (1995) Adv. Polym. Sci 122:59-123

Rabke-Clemmer, C.E., Leavitt, A. J. & Beebe, T.P. Jr. (1994) Langmuir, 10:1796-1800

Radler, J.O., Koltover, I., Salditt, T., Safinya, C.R. (1997) Science 275(5301):810-814

Radmacher, M., Fritz, M., Hansma, H.G. & Hansma, P.K. (1994) Science 265:1577-1579

Radmacher, M., Fritz, M. & Hansma, P.K. (1995) Biophys. J. 69:264-270

Ratner, B.D., Yoon, S.C. & Mateo, N.B. (1987a) in "Polymer Surface and Interface" Eds. Feast, W.J. & Munro, H.S. J. Wiley & sons Chitchester

Ratner, B.D., Johnston, A.B. & Lenk, T.J. (1987b) J. Biomed. Mater. Res. Appl. Biomat. 21:59-89.

Ratner, B.D. (1993) J .Biomed. Mater .Res. Appl .Biomat. 27:283-287.

Ratner, B.D. (1995) Surf. Interf. Anal. 23:521-528

Ratner, B.D. & Porter, S.C. (1998) Photocopy of book chapter source not known

Rao, N.M., Plant, A.L., Silin, V., Wight, S. & Hui, S.W. (1997) Biophys. J. 73:3066-3077

Refojo, M. F. (1969) J. Biomed. Mater. Res. 3:333-338

Refojo, M. F. (1971) J. Biomed. Mater. Res. Symp. 1:179-185

Rezania, A., Thomas, C.H., Branger, A.B., Waters, C.M. & Healy, K.E., (1997) J. Biomed. Mater. Res. 37(1):9-19

Rief, M., Gautel, M., Oesterhelt, F., Fernandez, J.M. & Gaub, H.E. (1998) Science 276:1109-1112

Ringsdorf, H. (1975) J. Polym. Sci. Polym. Symp. 51:133-135

Roberts, C.J., Williams, P.M., Davies, M.C., Jackson, D.E. & Tendler, S.J.B. (1994) TIBTECH 12:127-132

Robinson, B. V., Sullivan, F.M., Borzelleca, J.F. & Schwartz (1990) PVP Lewis Publishers, Michigan.

Rosebrough, S.F. & Hartley, D.F. (1996) J. Nuc. Med., 37(8):1380-1384

Rother, R.P., Squinto, S.P. & Rollins, S.A. (1995) Hum. Gene Ther. 6:429-435

Roy, R. (1996) Polymer News 21 7: 226-232

Sackmann, E. (1996) Science 271:43-48

Salamon, Z. & Tollin, G. (1996a) Biophys. J. 71:848-857

Salamon, Z., Wang, Y., Soulages, J.L., Brown, M.F. & Tollin, G. (1996b) Biophys. J. 71:283-294

Salamon, Z. & Tollin, G. (1996c) Biophys. J. 71:858-867

Salamon, Z., Macleod, H. A. & Tollin, G. (1997) Biochim. et Biophys. Acta 1331:131-152

Salditt, T., Koltover, I., Radler, J.O. & Safinya, C.R. (1998) Phys. Rev. E. 58:889-904

Salyer (1969) Art. Heart. Prog. Conf. Proceed. p59

Salzman, E.W.& Merrill, E.W. (1987) Interactions of blood with artificial surfaces, in Haemostasis and Thrombosis. Basic Principles and Clinical Practice. Colman, R.W., Hirsh, J., Marder, V.J., Salzman, E.W. (Eds.), J.B.Lippincott Company, Philadelphia, USA.

Samant, M.G., Brown, C.A. & Gordon II, J.G. (1991) Langmuir 7(3):437-439

Sarid, D. & Elings, V. (1991) J. Vac. Sci. Technol. B 9(2):431-437

Sayed-Sweet, Y., Hedstrand, D.M., Spindler, R & Tomalia, D.A. (1997) J. Mater. Sci. 7(7):1199-1205

Schakenraad, J.M., Busscher, H.J., Wildevuur, Ch. R. & Arends, J. (1986) J. Biomed. Mater. Res. 20:773-784

Scherga, H.A. & Laskowski, M. Jr. (1957) Adv. Prot. Chem. 12:1-131

Scheuring, S., Muller, D.J., Ringler, P., Heymann, J.B. & Engel, A. (1999) J. Microsc. 193(1):28-35

Schlenk, C. & Frey, H. (1999) Monatshefte fur Chemie, 130(1):3-14

Schlenoff, J.B., Li, M. Li, H. (1985) J. Am. Chem. Soc. 117:12528-12536

Schoemaker, W.C. (1976) Crit. Care Med. 4:71-79

Scholes, P.D., Coombes, A.G.A, Illum, L., Davis, S.S., Watts, J.F., Ustariz, C., Vert, M. & Davies, M.C. (1999) J. Contr. Rel., 59(3):261-278

Schuck, P. (1997) Annu. Rev. Biophys. Biomolec. Struct. 26:541-566

Seebach, D., Lapierre, J-M., Greiveldinger, G. & Skobridis, K (1994a) Helv. Chim. Acta 77:1673-1678

Seebach, D., Lapierre, J-M., Skobridis, K & Greiveldinger, G.(1994b) Agnew. Chem. Int. Ed. Engl. 33:440-445

Shaffer, C.B. & Critchfield, F. H. (1947) J. Am. Pharm. Assoc. 36:152

Shakesheff, K.M., Davies, M.C., Jackson, D.E., Leggett, G.J., Roberts, C.J., Tendler, S.J.B. & Williams, P.M. (1994(a)) Nanobiology 3:41-47

Shakesheff, K.M., Davies, M.C., Roberts, C.J., Tendler, S.J.B., Shard, A. & Domb, A. (1994(b)) Langmuir 10:4417-419

Shakesheff, K.M., Davies, M.C., Domb, A., Jackson, D.E., Roberts, C.J., Tendler, S.J.B. & Williams, P.M. (1995) Macromol. 28:1108-1114

Shakesheff, K.M., Davies, M.C., Heller, J., Roberts, C.J.,Tendler, S.J.B., & Williams, P.M. (1995) Langmuir, 11:2547-2553

Shakesheff, K.M., Cannizzaro, S.M. & Langer, R. (1998) J. Biomater. Sci. - polymer Ed. 9(5):507-518

Shao, Z., Mou, J., Czajkowsky, D.M., Yang, J. & Yuan, J.-Y. (1996) Adv. in Phys. 45(1):1-86

Shard, A.G., Sartore, L., Davies, M.C., Ferruti, P., Paul, A.J. & Beamson, G. (1995) Macromol. 28:8259-8271.

Shard, A.G., Volland, C., Davies, M.C. & Kissel, T. (1996a) Macromol. 29:748-754

Shard (1996b) in Handbook of biodegradable polymers (1996) Ed. Domb, A., Kost, J. & Wiseman, J. Harwood Academic, UK.

Sharkey, R.M., Karacay, H., Griffiths, G.L., Behr, T.M., Blumenthal, R.D., Mattes, M.J., Hansen, H.J. & Goldenberg, D.M. (1997) Bioconj. Chem. 8(4):595-604

Shea, L.D., Smiley, E., Bonadio, J. & Mooney, D.J. (1999) Nature Biotech. 17(6):551-554

Sheen, C.W., Shi, J-X., Martensson, J., Parikh, A.N. & Allara, D.L. (1992) J.Am. Chem. Soc. 114:1514-1515

Sheiko, S.S., Gauthier, M. & Moller, M. (1997) Macromol. 30:2343-2349

Sheth, S.R. & Leckband, D. (1997) Proc. Natl. Acad. Sci. USA. 94(16):8399-8404

Sheu, M.S., Hoffman, A.S., Ratner, B.D., Feijen, J. & Harris, J.M. (1993) J. Adhes. Sci. Tech. 7:1065-1076

Shikuma, L.R., Eyer, S.D. & Zaske, D.E. (1988) Drug Intell. Clin. Pharm. 22:211-213

Short, R.D., Khan, M.A., Watts, J.F., Brown, A., Eccles, A.J., Humphrey, P., Vickerman, J.C. & Vert, M. (1989) Surf. Interf. Anal. 14:115-120

Siedlecki, C.A. & Marchant, R.E. (1998) Biomaterials 19:441-454

Silin, V., Weetall, H. & Vanderah, D.J. (1997) J. Colloid Interface Sci. 185(1):94-103

Singh, P., Moll, F.III, Lin, S.H., & Ferzli, C. (1996) Clin. Chem. 42:1567-1569

Singh, P. (1998) Bioconj. Chem. 9:54-63

Smith, D.P.E. (1995) Rev. Sci. Instrum. 66:3191-3195

Smyth, H.F.Jr., Carpenter,C.P., & Weil, C.S. (1950) J. Am. Pharm. Assoc. 39:349-354

Sprik, M., Delamarche, E., Michel, B., Rothlisberger, U., Klein, M.L., Wolf, H. & Ringsdorf, H. (1994) Langmuir 10:4116-4130

Stahl, G. A. (1981) Polymer Science Overview : A Tribute to Herman, Ed F. Mark. ACS, Washington DC, USA.

Stein, P.E., Boodhoo, A., Armstrong, G.D., Cockle, S.A., Klein, M.H. & Read, R.J. (1994) Struct. 2:45-57

Stemmer, A., Hefti, A., Aebi, U., & Engel, A. (1989) Ultramicroscopy 25:171-181

Sternberg, B., Sorgi, F. L. & Huang, L. (1994) FEBS Lett. 356(2-3):361-366

Stoldt, H.S., Aftab, F., Chinol, M., Paganelli, G., Luca, F., Testori, A. & Geraghty, J.G. (1997) Euro. J. Cancer 33(2):186-192

Stryer, L. (1988) Biochemistry 3rd ed. Freeman, New York, USA

Suzuki, A., Yamazaki, M., Kobiki, Y. & Suzuki, H. (1997) Macromol. 30:2350-2354

Svoboda, K. & Block, S.M. (1994) Ann. Rev. Biophys. Biomol. Struct. 23:247-285

Sykes, K.E., McMaster, T.J., Miles, M.J., Barker, P.A., Barham, P.J., Seebach, D., Muller, H.-M. & Lengweiler, U.D. (1995) J. Mater. Sci. 30:623-627

Szleifer, I. (1997) Biophys. J. 72:595-612

Tabor, D. & Winterton, R.H.S. (1969) Proc. R. Soc. Lond. A312:435-450

Takami, T., Delmarche, E., Michel, B., Gerber, C., Wolf, H. & Ringsdorf, H. (1995) Langmuir 11:3876-3881

Tamayo, J. & Garcia, R. (1996) Langmuir, 12(18):4430-4435

Tamm, L.K. & McConnell, H.M. (1985) Biophys. J. 47:105-113

Tang, F., Hughes, J. A. (1998) Biochem. Biophys. Res. Commun. 242:141-145

Tang, M. X., Redemann, C.T. & Szoka, F.C. (1996) Bioconj. Chem. 7:703-714

Tang, M. X. & Szoka, F.C. (1997) Gene Ther. 4:823-832

Tao, N.J., Lindsay, S.M. & Lee, S. (1992) Biophys. J. 63:1165-1168

Temin, H. M., (1990) Hum. Gene Ther. 1:111-123

Thomson, N.H., Miles, M.J., Ring, S.G., Shewry, P.R. & Tatham, A.S. (1994) J. Vac. Sci. Technol B. 12:1565-1568

Thomson, N.H., Fritz, M., Radmacher, M., Cleveland, C.F., Schmidt, C. F. & Hansma, P.K. (1996) 70(5):2421-2431

Thomson, N.H., Collin, I., Davies, M.C., Palin, K., Parkins, D., Roberts, C.J., Tendler, S.J.B. & Williams, P.M. (1999) Biophys. J. submitted

Tomalia D. A. , Dewald, J. R., Hall, M. J., Martin, S. J. & Smith, P. B. (1984) Preprints 1st Society Polymer Science Japan Intl. Polmer Conf. Abstract 65 August 20-24, Kyoto, Japan.

Tomalia D. A. (1994) Adv. Mat 6:529-539

Tomalia, D.A. & Esfand, R. (1997) Chemistry and Industry June 2 416-420

Toncheva, V., Wolfert, M.A., Dash, P.R., Oupicky, D., Ulbrich, K., Seymour, L.W. & Schacht, E.H. (1998) Biochim. Biophys. Acta - Gen Sub. 1380(3):354-368

Toyokuni, T & Singhal A.k. (1995) Chem. Soc. Rev. 231 et seq

Uchida, E. & Ikada, Y. (1997) Macromol. 30:5464-5469

Valtonen, S., Timonen, U., Toivanen, P., Kalimo, H., Kivipelto, L., Heiskanen, O., Unsgaard, G. & Kuurne, T. (1997) Neurosurgery 41(1):44-49

Van Barlingen, H.H.J.J., VanBeek, A., Erkelens, D.W. & DeBruin, T.W.A. (1997) J. Intern. Med. 242(2):125-129

Van den Berg, R., De Groot, H., Van, Dijk, M.A., Denley, D.R.(1994) Polymer, 35:5778-5781

Van Delden, C.J., Lens, J.P., Kooyman, R.P.H., Engbers, G.H.M.& Feijen, J.(1997) Biomaterials 18: 845-852.

Vanden Eynde, X., Bertrand, P. & Jerome, R. (1997) Macromol. 30:6407-6416

Van Der Made, A.W. & Van Leeuwen P.W.N.M. (1992) J. Chem. Soc Commun. 1400-1401

Van der Merwe, P.A. & Barclay, A.N. (1996) Curr. Opin. Immunol. 8:257-261

Van de Wetering, P., Cherng, J.Y., Talsma, H., Crommelin, D.J.A. & Hennink, W.E. (1998) J. Contr. Rel.53:145-153

Van Dijk, M.A. & Van den Borg, R (1995) Macromol. 28:6773-6778

Vann, E.F., Kaloss, M., Broscius & Nienhuis, A.W. (1994) J. Virol. 68:4241-4250

Vansteenkiste, S.O., Davies, M.C., Roberts, C.J., Tendler, S.J.B. & Williams, P.M. (1998) Prog. in Surf. Sci. 57(2):93-136

Veillard, M.M., Longer, M.A., Martens, T.W. & Robinson, J.R. (1987) J. Contr. Rel. 6:123-131

Viera, L., Fabani, M. & AlonsoRomanowski, S. (1998) Biophys. J. 74(2):A12

Vinckier, A., Gervasoni, P., Zangg, F., Ziegler, U., Lindner, P., Groscurth, P., Pluckthun, A. & Semenza, G. (1998) Biophys. J. 74:3256-3263

Wallimann, P., Seiler, P. & Diederich, F. (1996) Helvetica Chimica Acta 79 : 779-788

Wang, C.Y. & Huang, L. (1989) Biochem. 28:9508-9514

Wasan, E.K., Fairchild, A. & Bally, M.B. (1998) J. Pharm. Sci. 87(1):9-14

Wawkushewski, A. Cantow, H.-J. & Magonov, S.N. (1994a) Polymer Bull. 32:235-240

Wawkushewski, A. Cantow, H.-J. & Magonov, S.N. (1994b) Adv. Mater. 6:476-480

Weber, W.H. & McCarthy, S.L. (1975) Phys. Rev. B 12:5643-5650

Weiner, E.C., Brechbiel, M.W., Brothers, H., Magin, R.L., Gansow, O.A., Tomalia, D.A. & Laterbur, P.C. (1994) Magn. Reson. Med. 31:1-8

Weisenhorn, A.L., Hansma, P.K., Albrecht, T.R. & Quate, C.F. (1989) Appl. Phys. Lett. 54:2651-2653

Wells, M. & Crooks, R.M. (1996) J.Am. Chem. Soc. 118:3988-3989

Weng, L.T., Betrand, P. Stone-Masui, J.H. & Stone, W.E.E. (1994) Surf. Interf. Anal. 21:87-93

Weng, L.T., Bertrand, P., Lauer, W., Zimmer, R. & Busetti, S. (1995) Surf. Interf. Anal. 23:(13):879-886

Werner, H.W. (1980) Surf. Interf. Anal. 2:56-62

Whang, K., Thomas, C.H., Healy, K.E., Nuber, G. (1995) Polym. 36:837-842

Wheeler, J.J., Palmer, L., Ossanlou, M., MacLachlan, I., Graham, R.W., Zhang, Y. P. Hope, M.J. *et al.* (1999) Gene Ther. 6(2):271-281

Whitesell, J.K., Chang, H.K. & Whitesell, C.S. (1994) 33:871-873

Wiener, E.C., Brechbiel, M.W., Brothers, H., Magin, R.L., Gansow, O.A., Tomalia, D.A. & Lauterbur, P.C. (1994), Magnetic Res. Med, 31(1):1-8

Wilbur, D.S., Pathare, P.M., Hamlin, D.K., Buhler, K.R. & Vessella, R.L. (1998) Bioconj. Chem., 9(6):.813-825

Wilkinson, I., Jackson, C.J., Lang, T. *et al* (1987) J. Immunol. 139:326-331

Willner, I., Katz, E., Riklin, Z. & Kasher, Z. (1992) J. Am. Chem. Soc. 114:10965-10966

Winpanetantee, R. (1998) Personal communication

Wivel, N.A. & Wilson, J.M. (1998) Hematology / oncology clinics of N. America 12(3):483-503

Wollman, E.W., Kang, D., Frisbie, D., Lorkovic, I.M. & Wrighton, M. S. (1994) J.Am. Chem. Soc. 116:4395-4404

Wright, M.J., Woodrow, G., Umpleby, S., Hull, S., Brownjohn, A.M. & Turney, J.H. (1999) Am. J. Kidney Disease 34(1):36-42

Wu, G. Y. & Wu, C. H. (1988) Biochemistry 27:887-892

Wüthrich,K. (1992) in NMR of Proteins and Nucleic Acids. J. Wiley & Sons N.Y. USA.

Xu, L., Stahl, S.K., Dave, H.P., Schiffmann, R., Correll, P.H., Kessler, S. & Karlsson, S. (1994) Exptl. Hematol. 22:223-230

Xu, Z. & Moore J.S. (1994) Acta Polymer 45:83-87

Yan, L., Marzolin, C., Terfort, A. & Whitsides, G.M. (1997) Lamgmuir 13:6704-6912

Yang, J., Mou, J.X. & Shao, Z.F. (1994) FEBS Lett. 338(1):89-92

Yang, X.L., Dutta, P., Wong, G.K. & Ketterson, J.B. (1992) Thin Solid Films 219:210-214

Yang, X.M., Xiao, D., Xiao, S.J., Lu, Z.H. & Wei, Y. (1994) Physics Lett. A 193(2):195-198

Yei, S., Mittereder, K., Tang, K., O'Sullivan C. & Trapnell, B. C. (1994) Hum. Gene Ther. 1:192-200

Yu, J., Norgman-Montelius, M., Paulsson, M., Gouda, I., Larm, O., Montelius, L. & Ljungh, A. (1994) Biomat. 15(10):805-814

Zabner, J., Fasbender, A.J.,Moninger, T., Poellinger, K. A. & Welsh, M.J. (1995) J. Bio. Chem. 270:18997-19007.

Zalipsky, S. & Lee C. in Poly(ethylene glycol) Chemsitry : Biotechnical and Biomedical Applications (1992) Ed. Harris J.M. Plenum Press, New York, USA

Zamborini, F.P. & Crooks, R.M. (1998) Langmuir, 14(12):3279-3286

Zasadzinski, J.A.N., Helm, C.A., Longo, M.L., Weisenhorm, A.L., Gould, S.A.C. & Hansma, P.K (1991) Biophys. J., 59(3):755-760

Zelphati, O., Uyechi, L.S., Barron, L.G. & Szoka, F.C. Jr. (1998) Biochim. et Biophys. Acta 1390:119-133

Zenhausern, F., Adrian, M. & Descouts, P. (1993) J Electron Microsc 42: 378-388

Zhang, H., Dubin, P.L. Spindler, R. & Tomalia, D. A. (1996) Ber. Bunsenges. Phys. Chem. 100(6):923-928

Zhao, D-D., Watarai, S., Lee, J-T., Kouchi,S., Ohmori, H. & Yasuda, T. (1997) Acta. Med. Okayama 51(3):149-154

Zhong, C-J. & Porter, M.D. (1994) J. Am. Chem. Soc. 116:11616-11617

Zuidam, N. J. & Barenholz, Y. (1997) Biochim. et Biophys. Acta 1329:211-222

Zuidam, N. J. & Barenholz, Y. (1998) Biochim. et Biophys. Acta 1368: 115-128